NASA TECHNICAL MEMORANDUM

NASA TM X-2273

NASA TM X-2273

NASA SPACE SHUTTLE TECHNOLOGY CONFERENCE

Volume II - Structures and Materials

Held at
Langley Research Center
Hampton, Virginia
March 2-4, 1971

NATIONAL AERONAUTICS AND SPACE ADMINISTRATION • WASHINGTON, D. C. • APRIL 197

1. Report No.	2. Government Accession No.	3. Recipient's Catalog No.
NASA TM X-2273		

4. Title and Subtitle	5. Report Date
NASA SPACE SHUTTLE TECHNOLOGY CONFERENCE Volume II - Structures and Materials	April 1971
	6. Performing Organization Code
7. Author(s)	8. Performing Organization Report No. L-7738
9. Performing Organization Name and Address	10. Work Unit No.
	11. Contract or Grant No.
	13. Type of Report and Period Covered Technical Memorandum
12. Sponsoring Agency Name and Address National Aeronautics and Space Administration Washington, D.C. 20546	14. Sponsoring Agency Code

15. Supplementary Notes

Held at the NASA Langley Research Center, March 2-4, 1971.

16. Abstract

The conference encompassed three technology efforts, each published as a separate NASA Technical Memorandum.

Volume I - Aerothermodynamics, Configurations, and Flight Mechanics
(includes aerodynamics; atmospheric operations; and aerodynamic heating).
NASA TM X-2272, 1971.

Volume II - Structures and Materials
(includes structural design technology; thermal protection systems; and materials technology).
NASA TM X-2273, 1971.

Volume III - Dynamics and Aeroelasticity
(includes dynamic loads and response; aeroelasticity; and flight dynamics and environment).
NASA TM X-2274, 1971.

17. Key Words (Suggested by Author(s))	18. Distribution Statement
Space shuttle Aerothermodynamics Dynamics Aeroelasticity Structural design Thermal protection	Unclassified - Unlimited STAR Category 32

19. Security Classif. (of this report)	20. Security Classif. (of this page)	21. No. of Pages	22. Price*
Unclassified	Unclassified	641	$9.00

*For sale by the National Technical Information Service, Springfield, Virginia 22151

FOREWORD

A significant factor in the development of new technology is the timely exchange of information to highlight areas of progress and to establish areas in need of greater emphasis - in short, to provide both program management and technical contributors an opportunity to review their work and plans in the context of the requirements and constraints of the total program.

During the past two years, the Langley Research Center has made a concerted effort to support the NASA objectives for development of a low-cost space transportation system - the space shuttle. The Langley effort covers a broad base of technology including electronics and life support systems, but its primary focus has been in the areas of Aerothermodynamics, Configurations, and Flight Mechanics; Structures and Materials; and Dynamics and Aeroelasticity.

Thus it was in the context of the need for a technology status review and our own active involvement in the aforementioned areas of technology that the Langley Research Center was pleased to host the Shuttle Technology Conference which culminated in this document. As the reader will recognize, the development and presentation of this information was largely achieved by very busy people doing an additional job. Nevertheless, I believe the results of the conference reflect a highly motivated and cooperative effort on the part of industry and NASA centers to provide the best information available for technical review and assessment. This effort is deeply appreciated by those of us involved in the implementation of the conference. Thus, to the authors, session chairmen, and numerous individuals involved in the logistic support of this conference, I offer my thanks both for your effort and for your cooperation. A job well done!

George W. Brooks
General Chairman

CONTENTS

VOLUME II.- STRUCTURES AND MATERIALS

Chairman - R. A. Anderson

GLOSSARY vii

THERMAL PROTECTIONS SYSTEMS AND MATERIALS TECHNOLOGY

Chairman - W. A. Brooks, Jr., LaRC

1. DEVELOPMENT STATUS OF REUSABLE NONMETALLIC THERMAL PROTECTION 1
   by D. Greenshields, G. Strouhal, D. Tillian, and J. Pavlosky (MSC)

2. REUSABLE EXTERNAL INSULATION TPS FOR THE SPACE SHUTTLE 39
   by P. D. Gorsuch, R. A. Tanzilli, and D. E. Florence (GE)

3. METALLIC HEAT-SHIELD MATERIALS FOR SPACE SHUTTLE 95
   by Robert W. Hall (LeRC)

4. CREEP OF METALLIC THERMAL PROTECTION SYSTEMS 119
   by Harry G. Harris and Kenneth N. Morman, Jr. (GAC)

5. ABLATIVE THERMAL PROTECTION SYSTEMS . . . . 15573 . . 163
   by L. F. Vosteen and C. M. Pittman (LaRC)

6. ABLATIVE LEADING-EDGE DESIGN CONCEPTS FOR THE SHUTTLE ORBITER . 15574 195
   by John W. Graham, David A. Mosher (Avco), and Ira Victer (GAC)

7. BOOSTER THERMAL PROTECTION SYSTEM EVALUATION . . . . . . 15575 . 233
   by Allan M. Norton (MMC)

8. THE HEAT SINK CONCEPT FOR THE SPACE SHUTTLE BOOSTER 251
   by Jack Prunty (GD/C)

9. COMPARISON OF ACTIVE AND PASSIVE THERMAL PROTECTION SYSTEM WEIGHTS FOR A DELTA-BODY ORBITER 271
   by H. D. Schultz and F. L. Guard (LMSC)

10. ENVIRONMENTAL TESTING FOR EVALUATION OF SPACE SHUTTLE THERMAL PROTECTION MATERIALS AND SYSTEMS 301
    by Howard K. Larson, Frank J. Centolanzi, Nick S. Vojvodich, Howard Goldstein, M. Alan Covington, and Fred W. Matting (ARC)

STRUCTURES AND MATERIALS DESIGN TECHNOLOGY

Chairman - R. W. Leonard, LaRC

11. COMMENTS ON THE NASA DESIGN CRITERIA DOCUMENT 335
by I. G. Hedrick (GAC)

12. STRUCTURAL ANALYSIS AND AUTOMATED DESIGN 355
by Harvey G. McComb, Jr. (LaRC)

13. CRITICAL STRUCTURAL DESIGN TRADE STUDIES SPACE SHUTTLE SYSTEM 391
by T. P. Brooks (MDAC)

14. APPLICATION OF BERYLLIUM TO ORBITER PRIMARY STRUCTURE 467
by T. J. Harvey and A. E. Trapp (LMSC)

15. DESIGN, MANUFACTURE AND TESTING OF A TD NICKEL-CHROMIUM STRUCTURAL ASSEMBLY 497
by Read Johnson, Jr. (MDAC) and Charles L. Ramsey (AFFDL)

16. DESIGN AND TEST OF ADVANCED STRUCTURAL COMPONENTS AND ASSEMBLIES . . . 527
by E. E. Engler and C. E. Cataldo (MSFC)

17. HIGH TEMPERATURE FASTENER TECHNOLOGY 585
by Frank D. Boensch (AFFDL), William H. Goesch (AFFDL), and Allan M. Norton (MMC)

18. BEARINGS, LUBRICANTS, AND SEALS FOR ACTUATORS AND MECHANISMS 601
by Robert L. Johnson, William R. Loomis, and Lawrence P. Ludwig (LeRC)

GLOSSARY

AC	aerodynamic center
ACLS	air cushion landing system
ACPS	attitude control propulsion system
ADV	advanced
AEM	acoustical emission monitoring
AFFDL	Air Force Flight Dynamics Laboratory
AFML	Air Force Materials Laboratory
APU	auxiliary power unit
ARC	Ames Research Center
ASCEP	Advanced Structural Concepts Experimental Program
ASOP	Automated Structural Optimization Program
AS-REC	as received
ATT	attitude
ATTACH	attachment
BBN	Bolt, Beranek, and Newman
BL	boundary layer
BPR	bypass ratio
BS	body station
BST	booster
CDC	Control Data Corporation
CER	cost estimating relationship
CONT	control
CONV	conventional
CPU	central processing unit
C.R.	cross range

CRIT	critical
CRT	cathode ray tube
CTI	cryogenic insulation
CW	cold worked
DB	dead band
DIA	diameter
DISP	dispersion; displacement
DSM	dispersion-strengthened metals
DW	double wall
EB	electron beam
ECS	environmental control system
ELONG	elongation
EMR	electromagnetic radiation
FLT	flight
FPL	fluctuating pressure level
FSW	flyback system weight
GAC; GAEC	Grumman Aerospace Corporation
GDC; GD/C	General Dynamics/Convair
GDLSWT	General Dynamics low speed wind tunnel
GE	General Electric Co.
GEN	generator; generated
GE-RESD	General Electric Reentry and Environmental Systems Division
HABP	hypersonic arbitrary-body program
HASP	hypersonic aerospace structures program
h. c.	honeycomb
HCF	hardened compacted fibers

HDWE	hardware
HMG	high-modulus graphite
HS	heat sink
HSG	high-strength graphite
HT	high temperature
HX	heat exchanger
HYP	hypersonic
IMU	inertial measurement unit
INSUL	insulation
INT	internal
i. s.	isogrid
IU	instrument unit
L	longitudinal
LaRC; LRC	Langley Research Center
LCR	low cross range
LE	leading edge
LeRC	Lewis Research Center
L. LOAD	limit load
LMSC	Lockheed Missiles and Space Company
LW	left wing
MAC	mean aerodynamic chord
MARL	Mobile Acoustic Research Laboratory
MDAC	McDonnell-Douglas Astronautics Corporation
MDC	McDonnell Douglas Corporation
MEAS	measured
MGMT	management
MIN	minimum

MMC	Martin Marietta Corporation
MRP	moment reference point
MSC	Manned Spacecraft Center
MSFC	Marshall Space Flight Center
MTF	Mississippi Test Facility
NAR; NR	North American Rockwell
NDE	nondestructive evaluation
NDI	nondestructive inspection
NDT	nondestructive testing
NPSH	nominal positive suction head
OA FPL	overall fluctuating pressure level
OA PWL	overall acoustic power level
OART	Office Advanced Research and Technology
OA SPL	overall sound pressure level
OMSF	Office Manned Space Flight
ORB	orbiter
POS	positive
ppm	parts per million
PS	post support
PSD	power spectral density
PWR	power
R_{CR}	cruise range
RCS	reaction control system
RDT&E	Research, Development, Tests, and Engineering
REI	reusable external insulation
REQ'D	required
RT	room temperature

RW	right wing
SAT	Saturn
SBC	single body canard
s/c	skin corrugation
SEP	separated
SF	safety factor
SL	sea level
SLA	spacecraft lunar module adapter
SPL	sound pressure level
SR&T	space research and technology
s.s.	simple support
SSV	space shuttle vehicle
STR	strengthened
SUB	subsonic
SW	single wall
T	transverse
T'COUPLES	thermocouples
TECH	technology
TPS	thermal protection system
TURB	turbulent
TWT	transonic wind tunnel
UB	underbody
u.i.s.	unidirectional
ULT	ultimate
VMSC	Vought Missiles and Space Corporation
WL	water line
WT	wind tunnel

DEVELOPMENT STATUS OF REUSABLE NONMETALLIC THERMAL PROTECTION

By D. Greenshields, G. Strouhal, D. Tillian, and J. Pavlosky
NASA Manned Spacecraft Center, Houston, Texas

INTRODUCTION

The concept of protecting an entry vehicle from the aerothermodynamic environment by the use of refractory ceramic materials is not new; such materials were considered for the first ICBM applications, and a nose cap of cintered zirconia tides was developed for the DYNASOAR program. Likewise, carbon-carbon laminates have been used extensively in missile applications, and were used on the Apollo thermal protection system. However, both the ceramic and carbon systems exhibited severe shortcomings as reusable, thermally, and structurally efficient systems. The ceramics were extremely brittle with high modulus and relatively low strength, and were sensitive to thermal shock. The carbon systems were subject to oxidation although oxidation rates were relatively low.

Within the past few years, approaches to circumventing these two major deficiencies have been developed; as a result both the ceramic and carbon materials were again in a competitive position when serious work on the reusable space shuttle began in 1969. Small but intensive efforts on these two materials began under NASA sponsorship in the Spring of 1970, just one year ago, and system development contracts have been underway since July 1970. The first set of contracts is concluding this month; follow-on efforts will soon be initiated. Because the development programs are only in the preliminary phase, this paper must be considered as only a progress report.

PAPER 1

FIGURE 1

Sufficient progress has been made in the development of oxidation-resistant carbon-carbon laminates and surface insulation materials that both phase B shuttle study contractors have seriously considered the use of these materials for the shuttle orbiter. In addition, the use of these materials on the booster appears promising. Figure 1 is a sketch of the shuttle orbiter showing use of surface insulation, the lightest weight and simplest of the two systems, on the large areas of the vehicle lower surface, and of the carbon materials on the leading edges and nose regions where higher heating and more severe erosion environments are expected. As distributed here, the surface insulation would not encounter temperatures greater than 1400° K (2000° F), and the carbon-carbon material, greater than 1800° K (2800° F).

NONMETALLIC TPS APPLICATIONS

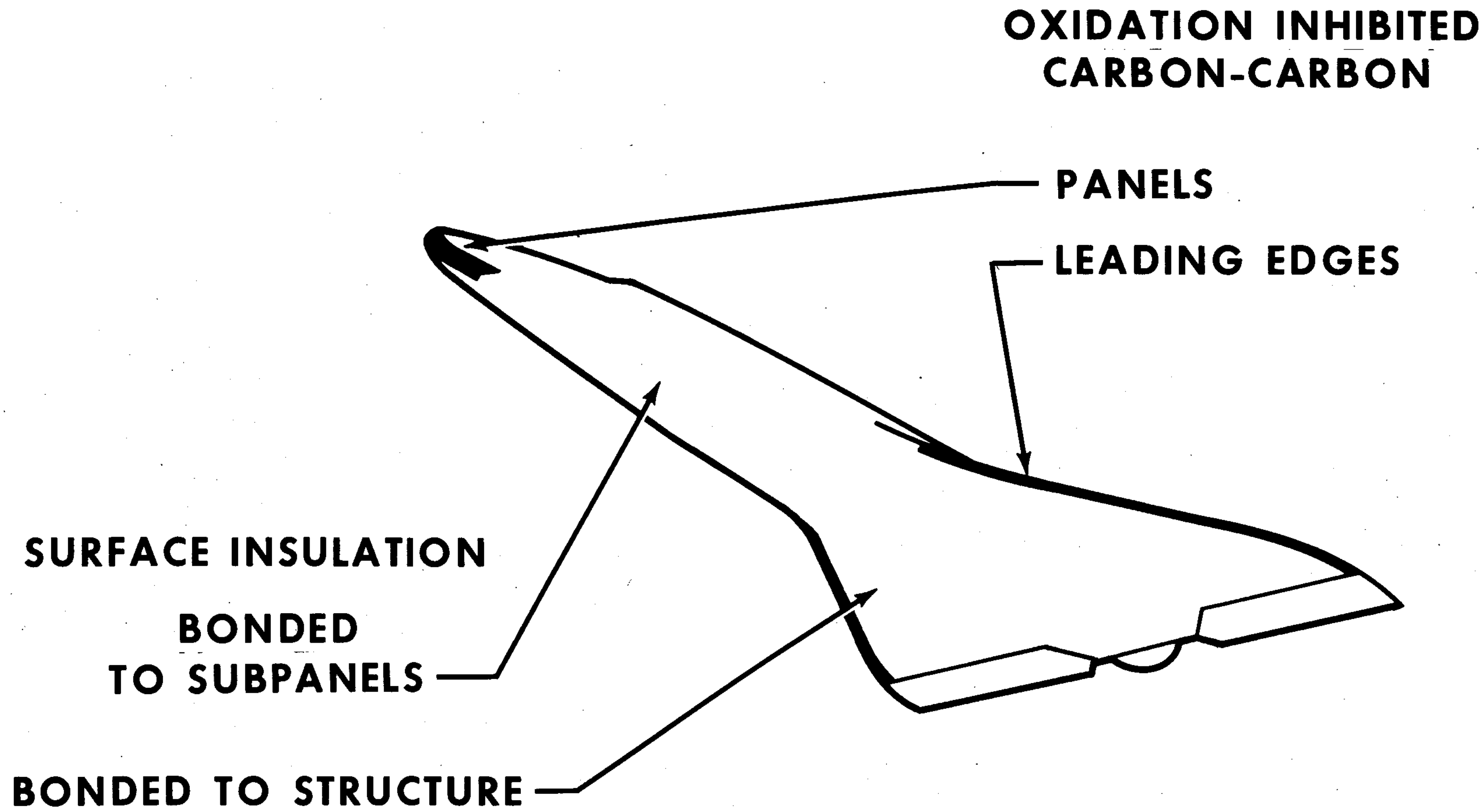

Figure 1

FIGURE 2

The nature of the oxidation-inhibited carbon laminate material is indicated in figure 2. The basic material consists of a carbon cloth laminate bonded with a polymeric resin which has been converted to carbon by pyrolization. This process forms a chemically stable material of high specific strength, which it maintains even at temperatures to 2500° K (4500° F). At the surface of the laminate, the porous carbon matrix has been treated with metals such as silicon and zirconium to form highly stable, although weaker, carbides which resist oxidation at temperatures approaching 1950° K (3000° F). This conversion also decreases the surface porosity to the extent that the oxygen of the entry environment is largely excluded from the interior of the material. To further restrict oxidation of the strong inner matrix, small amounts of the same metals may be included in the basic resin used to form the bond with the fiber prior to pyrolization.

BASIC INHIBITED CARBON-CARBON MATERIAL CONCEPT

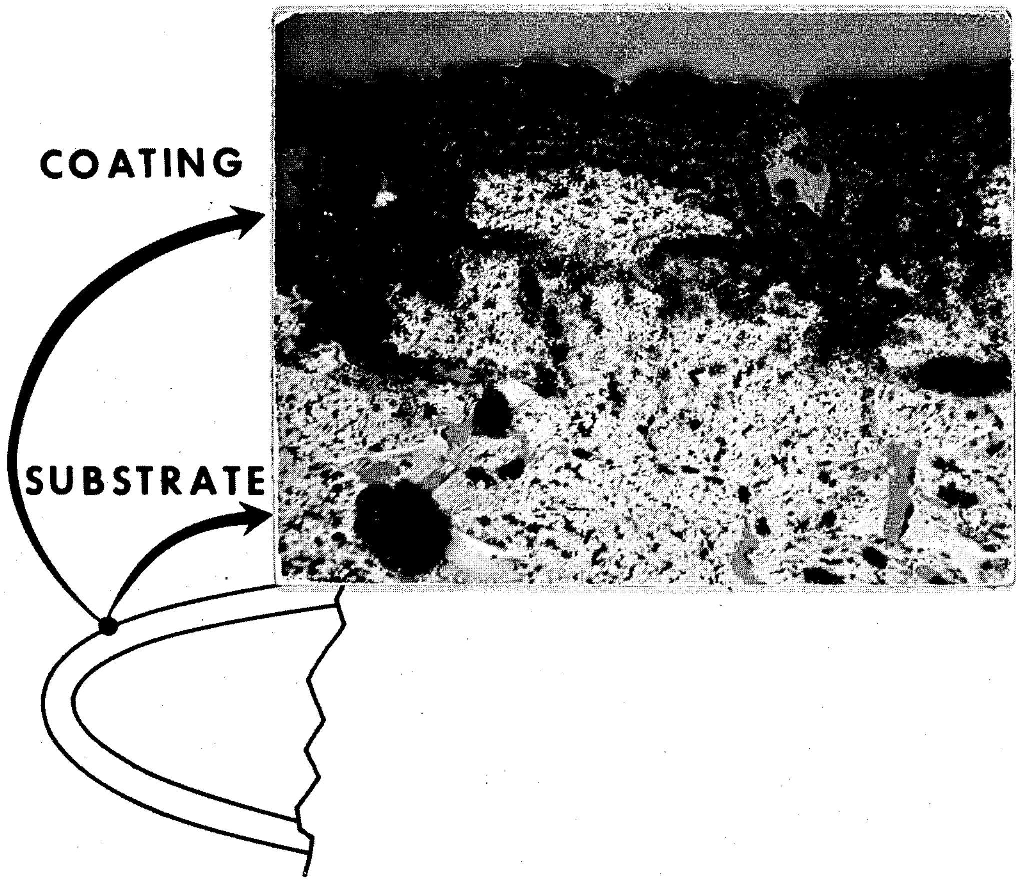

COATING

- OXIDATION RESISTANCE PREVENTS OXYGEN FLOW TO SUBSTRATE

GRAPHITE FIBERS

- PROVIDE HIGH STRENGTH AT HIGH TEMPERATURE
- THERMAL STABILITY

CARBON BINDER

- PROVIDES RIGIDIZATION
- HIGH STRENGTH AT TEMPERATURE
- THERMAL STABILITY
- LOW POROSITY

Figure 2

FIGURE 3

Many combinations of carbon filaments, binder materials, and inhibiting and coating material and techniques have been developed and tested by the two contractors involved in the MSC-sponsored program to date; MDAC and LMSC.* These combinations are indicated in simplified form in figure 4. Both yarns and cloths of carbon and graphite, with phenolic and epoxy used as the initial binders, were evaluated for basic strength properties; further strengthening by the CVD reimpregnation process and by reimpregnation with pitch and furfural alcohol were also evaluated. The various metal and boride oxidation inhibitors were considered as diffused-in coatings and as additives to the initial binders. Overlay coatings of refractory oxides were also tested.

---

*MSC NASA Manned Spacecraft Center.

MDAC McDonnell Douglas Aerospace Corp.

LMSC Lockheed Missiles and Space Corp.

INHIBITED CARBON-CARBON MATERIALS DEVELOPMENT

SUBSTRATES

- GRAPHITE CLOTH
- CARBON CLOTH
- CARBON YARN
- GRAPHITE FILAMENTS
- CARBON FILAMENTS

BINDERS

- PHENOLIC
- EPOXY
- FURFURAL
- PITCH
- CHEMICAL VAPOR DEPOSITION

INHIBITORS

- DIFFUSION
  - SILICON
  - ZrB_2 - SILICON
  - Ta - SILICON
  - Ti - SILICON
  - Zr - SILICON
  - Hf - SILICON
- ADMIXTURE
  - ABOVE MATERIALS MIXED IN BINDER
- COMBINED
  - ABOVE MATERIALS ADDED TO BINDER PLUS DIFFUSION
- OVERLAY
  - LAMINATED OR SPRAYED ON OXIDES

Figure 3

FIGURE 4

Extensive oxidation testing has been performed on these various materials. To determine structural characteristics both before and after thermal exposure, mechanical tests were also conducted. The two best performing materials appear to be the carbon-cloth laminates diffusion-coated with either silicon metal or combinations of zirconium, boron, and silicon.

When these oxidation data are used to predict the number of short cross-range missions which could be sustained by a thermal protection system (TPS) of such materials before significant oxidation occurred, the results are as depicted in figure 4. The rate of oxidation damage to the silicon-metal treated carbon is the lowest; 100 short cross-range missions could be flown at peak temperatures of almost 1900° K (2950° F) before replacement was necessary. For the Zr-B-Si coating system, which shows some mechanical advantages, 100 missions could be flown at 1850° K (2800° F) before replacement. It should be noted that these projections are based on only a few cycles of testing on any one sample, and have been extrapolated on the basis of mass loss as a function of heat-transfer coefficient, a correlation drawn from classical oxidation theory. It should also be noted that approximately 50° K lower temperatures would result if these calculations were made for long cross-range missions.

PREDICTED MISSION CAPABILITY OF DIFFUSION INHIBITED CARBON, SHORT CROSS RANGE LEADING EDGE

BASED UPON
$\dot{M}/h$ CORRELATION

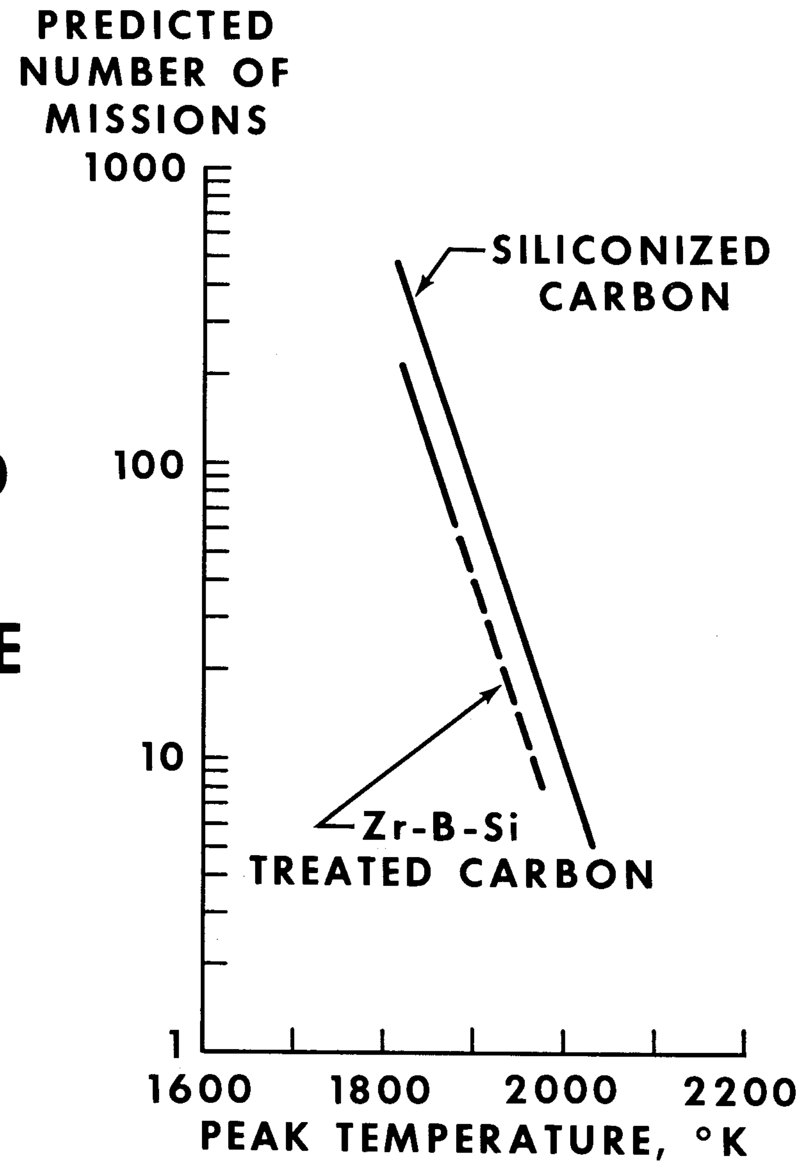

Figure 4

FIGURE 5

Flexure tests were among the many structural-property tests conducted during this initial phase of development. This technique is particularly suited to thin brittle material and is representative of the type of loading anticipated in secondary structure applications. figure 5 indicates some of the data collected on the silicon diffusion-treated system made by VMSC.*

As expected, the strength of this material increases slightly with test temperature. Although the as-fabricated system has high strength, the effects of repeated heating cycles in a furnace environment apparently degrade its strength. However, other tests indicate that inter-laminar strength may increase with such exposure. It is anticipated that the use of an "Admix" system in conjunction with the diffusion system may retard such property changes.

*Vought Missiles and Space Corp.

FLEXURE DATA FOR INHIBITED CARBON-CARBON

SILICONIZED CARBON

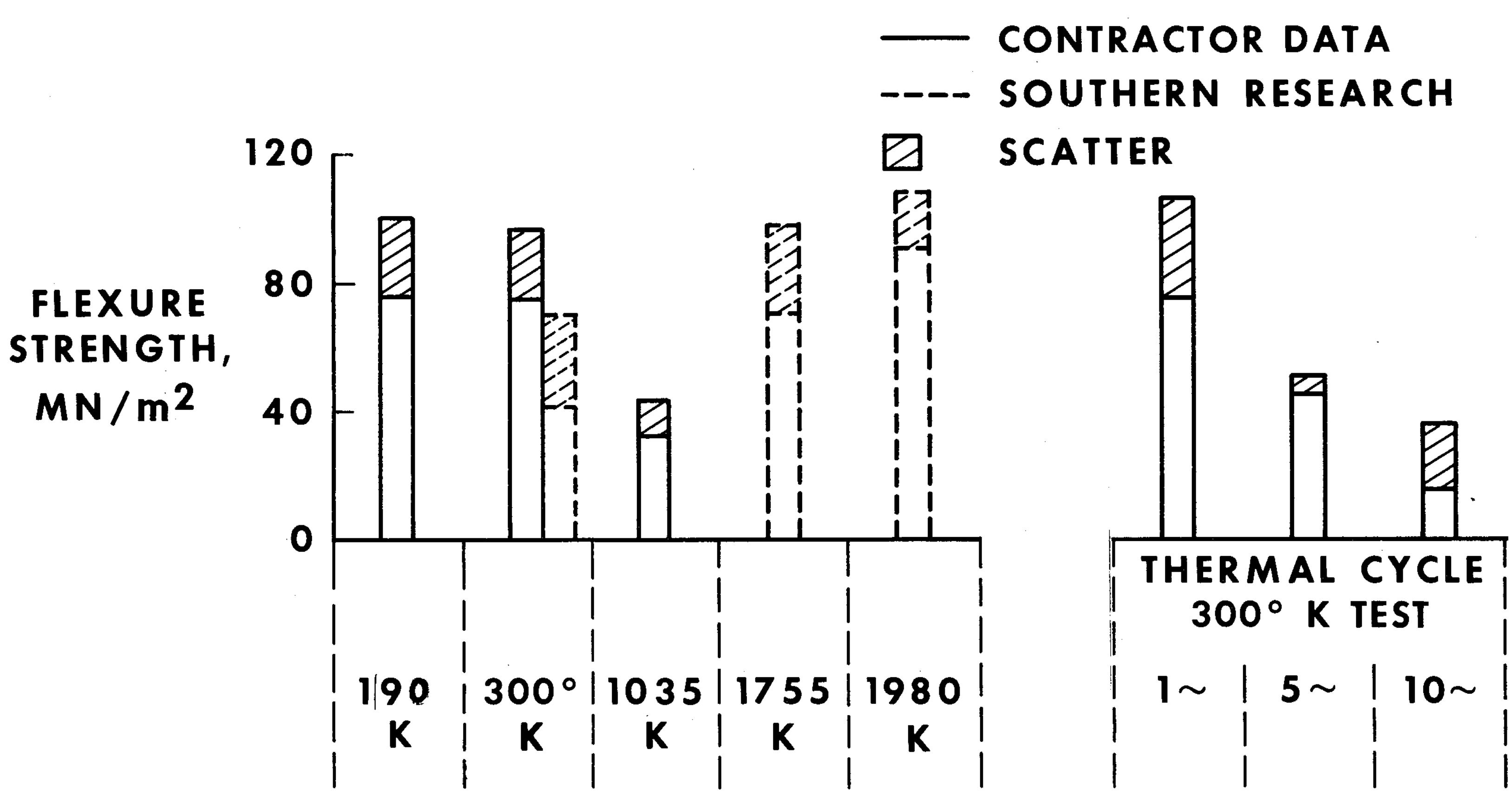

Figure 5

FIGURE 6

Figure 6 indicates data similar to that shown in figure 5, but for the multicomponent Zr-B-Si diffusion-coated system. The initial strengths shown are somewhat lower than those for the silicon-treated system, but do not appear to degrade with thermal exposures. Other tests which have been performed on both materials under repeated loading cycles indicate that mechanical properties do not degrade significantly from mechanical fatigue. Both of these materials appear to justify further testing under realistic heating and loading environments, and further development in processing.

FLEXURE DATA FOR INHIBITED CARBON-CARBON

BORON-ZIRCONIUM-SILICON COATED CARBON

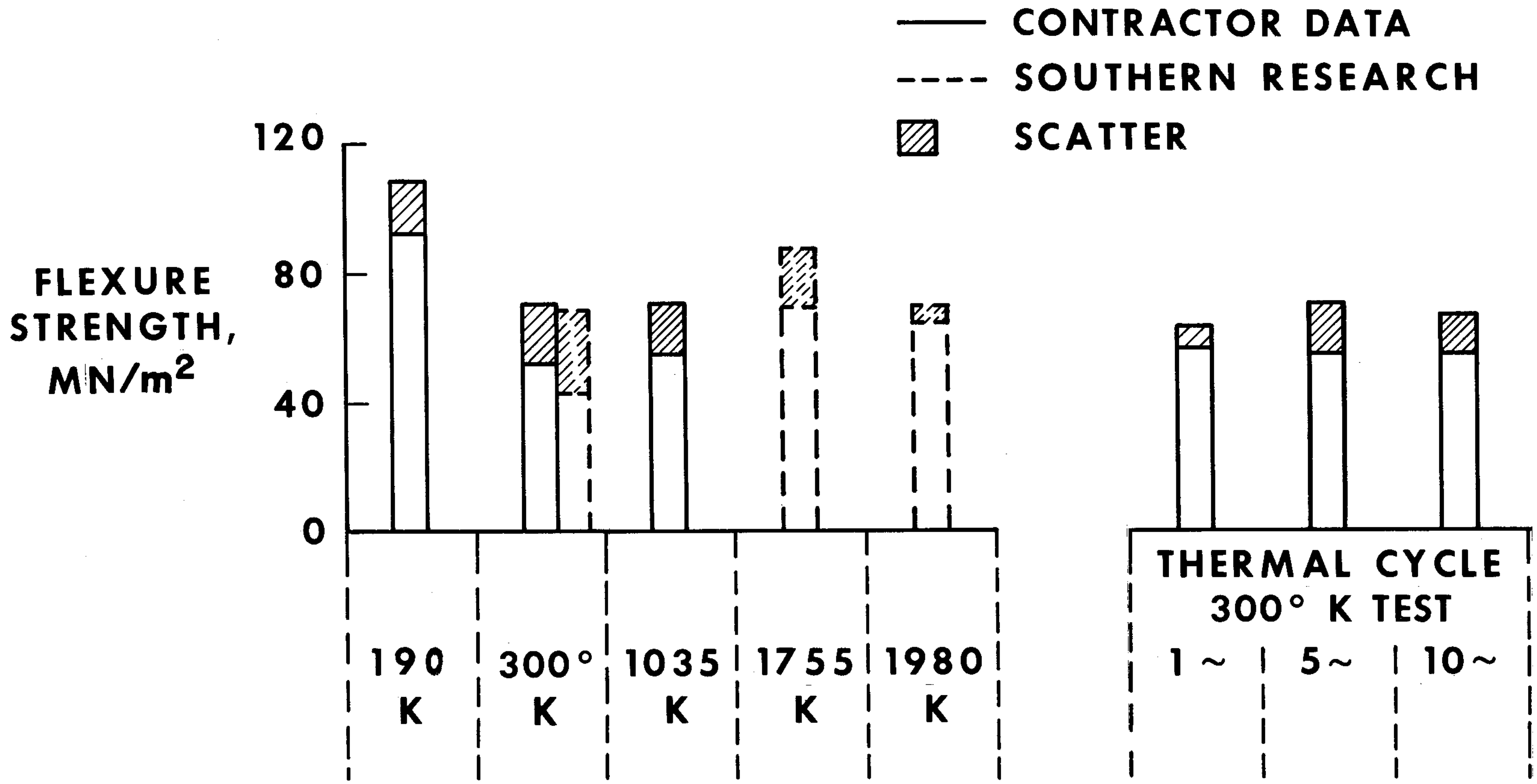

Figure 6

FIGURE 7

The conclusions which can be reached as a result of the initial materials and design efforts are summarized in figure 7. The system, coated by the diffusion process, either with silicon or zirconia-boron-silicon, appears to offer the best thermal and mechanical performance. These systems appear to be useful to near 1900° K for the shuttle reuse requirement. In addition, it has been found that the silicon coating system is noncatalytic and may operate at lower than radiation equilibrium temperatures because peak heating will be suppressed.

The preliminary findings, together with the results of phase B heating studies, indicate that the oxidation inhibited carbon-carbon system can serve as a reusable thermal protection system for the highest heating regions of the space shuttle, and that further evaluation, development of design, and material process development is justified. It should be noted that in addition to this material work, MDAC is presently constructing a full-scale leading-edge section under the phase B test program which will be tested at MSFC.*

*Marshall Space Flight Center.

STATUS OF CARBON-CARBON DEVELOPMENT

- LARGE NUMBER OF CANDIDATES SCREENED
  - BEST THERMAL PERFORMANCE SHOWN BY
    - SILICON AND BORON, ZIRCONIUM, SILICON INHIBITOR SYSTEMS
    - DIFFUSION COATING RATHER THAN ADMIX SYSTEMS
  - SILICONIZED SYSTEMS MOST UNIFORM
  - ZIRCONIUM - BORON - SILICON SYSTEM SHOWS BETTER FLEXURE STRENGTH AFTER REUSE THAN SILICON SYSTEM
  - SILICONIZED SYSTEM IS NONCATALYTIC, LOWERING SURFACE TEMPERATURE
  - PROCESS IMPROVEMENTS IMPROVE STRENGTH

Figure 7

FIGURE 8

Surface insulation systems are being developed for application to the space shuttle by MDAC and LMSC under contract to MSC, and by GE* and GAC* under other sponsorships. The systems being developed under MSC sponsorship are both based on a "rigidized" fiber concept and, in this respect, are similar to the carbon-carbon systems. The use of fibers as a basic building block for the materials makes them much less rigid than typical sintered ceramics, although they must still be classified as brittle materials. These materials also require a coating: in this case to provide a high-emittance surface, to preclude absorption of water, and to resist erosion. The density of the basic material, which consist of rigidized silica or mullite fiber, is sufficiently small to obtain good insulation performance. However, the material has very low strength, and must be continuously supported by either a substrate panel or bonded directly to the airframe of the vehicle. The system under development by LMSC, called LI1500, is basically a silica system. Silica fibers are bonded with silica filler, and silica is used as the carrier for the surface coating. Chromium oxide is added to the coating to provide a high emittance. The MDAC system is based on mullite, a form of aluminum silicate, and is named HCF (hardened compacted fiber). Mullite fibers are bonded with silica, and mixtures of borasilicate glass and phosphates are used as the basis for the coating. Cobalt oxide is used as the high-emittance pigment. The silica system has demonstrated reuse capability to surface temperatures of 1530° K (2300° F), and the mullite system to 1640° K (2500° F).

---

*General Electric Company.
Grumman Aerospace Corp.

BASIC SURFACE INSULATION MATERIAL CONCEPT

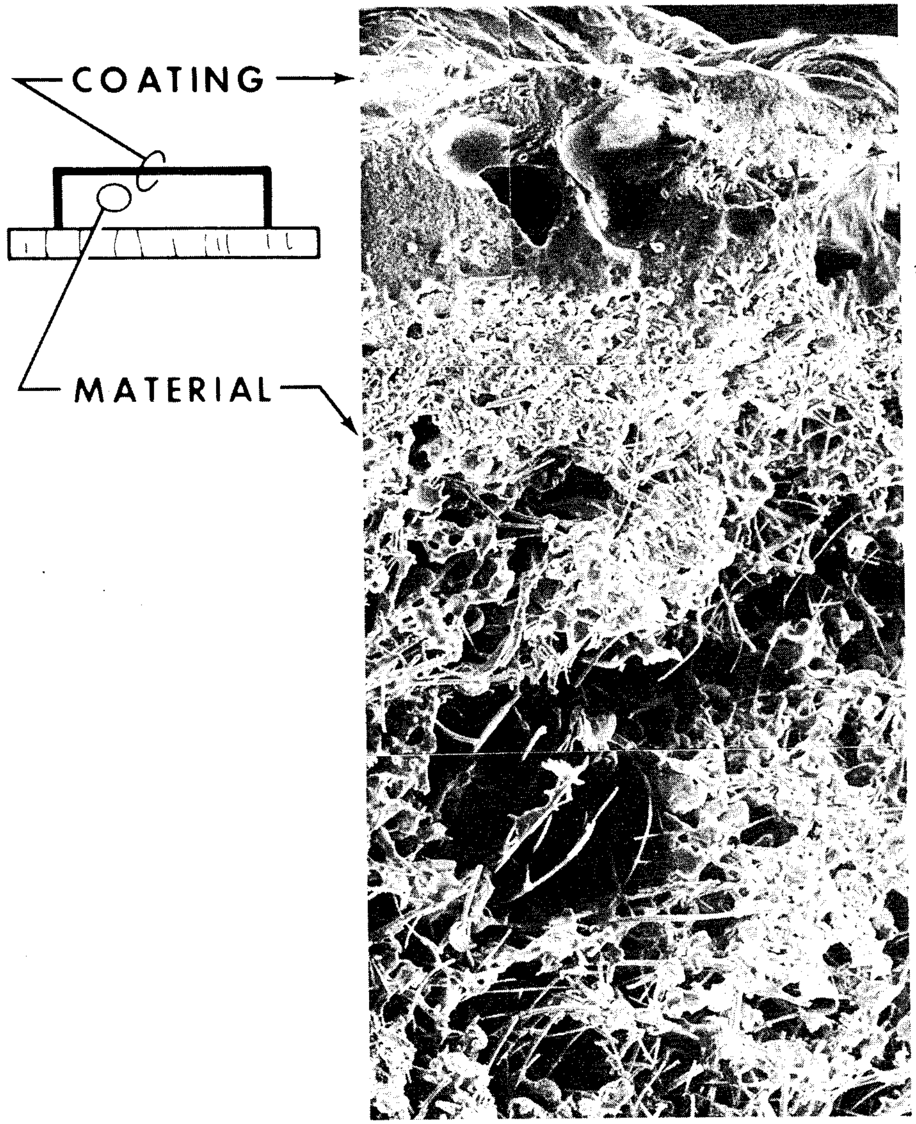

COATING

- HIGH DENSITY SURFACE
- EROSION RESISTANCE
- HIGH EMISSIVITY
- MOISTURE SEAL

CERAMIC FIBERS PROVIDE

- STRENGTH
- LOW DENSITY
- HIGH TEMPERATURE STABILITY
- LOW BULK MODULUS

CERAMIC BINDER PROVIDES

- RIGID STRUCTURE
- HIGH TEMPERATURE STABILITY

Figure 8

FIGURE 9

A summary of the status of the work on surface insulation systems by LMSC and MDAC is indicated in figure 9. Preliminary property measurements have been made on both materials, and a first attempt to develop a simple system using these materials to meet design requirements for typical short cross-range shuttle orbiter applications has been completed. It must be noted that only first-generation versions of the coatings, bonding techniques, and subpanel designs have been developed. Directions for further development and improvement in all these areas, as well as in the basic materials, have become apparent during the program. These first-generation systems have been translated into demonstration hardware. Both contractors are delivering near full-scale examples of both the subpanel and direct structural applications to MSC for testing in the immediate future.

SURFACE INSULATION DEVELOPMENT STATUS

- CONDUCTED PRELIMINARY MECHANICAL, THERMAL, AND PHYSICAL PROPERTY MEASUREMENTS
- DEVELOPED FIRST GENERATION WATER IMPERVIOUS COATINGS
- DEVELOPED FIRST GENERATION SUBPANEL DESIGNS
- DEVELOPED FIRST GENERATION BONDING TECHNIQUES
- COMPLETED DESIGN OF DEMONSTRATION TPS PANELS TYPICAL FOR WING AND FUSELAGE BODY APPLICATIONS
- PREPARED PRELIMINARY PROCESS SPECIFICATIONS AND SMALL SCALE PRODUCTION OF SURFACE INSULATION MATERIALS
- FABRICATION OF DEMONSTRATION TPS PANELS IN PROGRESS
  - BONDED TO SUBPANEL
  - BONDED TO STRUCTURE

Figure 9

FIGURE 10

Since the usefulness of surface insulation depends heavily on its thermal performance, one of the key properties of the material is thermal conductivity. Measurements of the conductivity of both the mullite (HCF) and silica (LI1500) systems were performed by the respective contractors by using the ASTM standard guarded hot-plate technique. The data obtained are shown in figure 10, for both one atmosphere (101.3 kN/m^2) and lower pressures as might be encountered during entry (1.0 kN/m^2). These data indicate that the thermal performance is very similar for the two materials. However, tests under both radiant and convective heating in which temperatures throughout the material were measured indicate inconsistencies with this result. For example, lower conductivities were indicated for the LI-1500 by arc-jet test data. More extensive thermal exposure data will apparently be required before the thermal performance of either material will be known with confidence.

SURFACE INSULATION THERMAL CONDUCTIVITY

STANDARD, GUARDED HOT PLATE MEASUREMENT

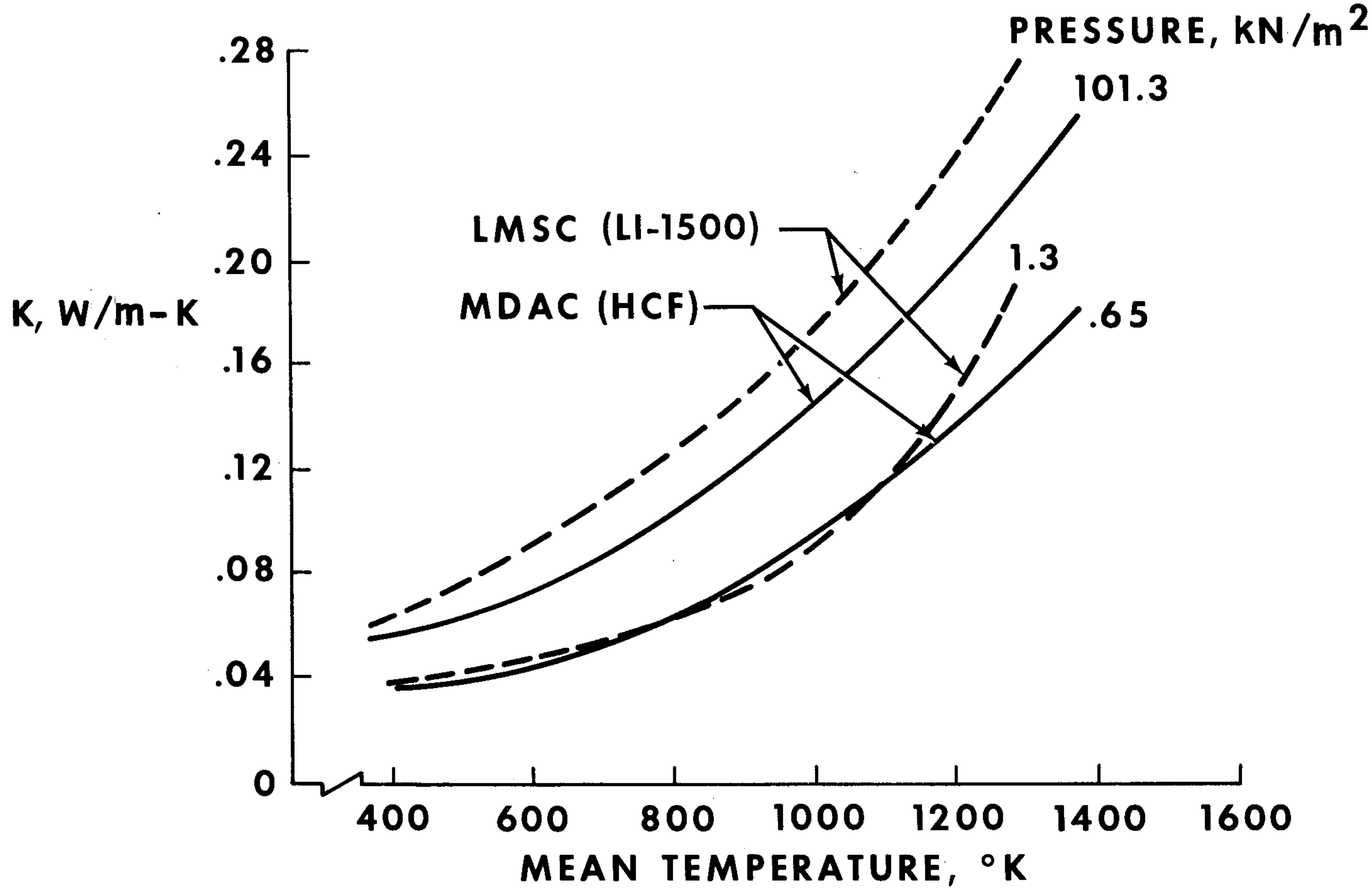

Figure 10

FIGURE 11

Figure 11 indicates some of the mechanical property data collected by MDAC and LMSC during the development program. Properties are different in the plane of the material blocks, and normal to this plane, since the fiber orientation is nonuniform.

Properties for the HCF material were measured on the insulator before and after applying the impervious coating. From these data it was possible to estimate some properties for the high modulus coating. Data were collected for the LI-1500 material only in the coated state; thus, no coating-alone properties are deduced.

It will be noted that the Z-direction properties of the materials are quite similar, and it might be inferred that the properties in the X-Y direction of the LI-1500 shown are controlled by the coating and not the bare material. In both cases, it would appear that the ultimate strain of both systems is limited by the coating, which indicates the coating modulus to be a critical parameter calling for improvement. The next most critical property, as indicated by structural analyses performed by both contractors, is the low shear strength of the materials.

SURFACE INSULATION MECHANICAL PROPERTIES

PROPERTY, kN/m^2 ULTIMATE,	MDAC (HCF) COATING	MDAC (HCF) UNCOATED MATERIAL X-Y	MDAC (HCF) UNCOATED MATERIAL Z	LMSC (LI 1500) COATED MATERIAL X-Y	LMSC (LI 1500) COATED MATERIAL Z
TENSILE STRENGTH	8,618	538	179	621	-
COMPRESSIVE STRENGTH	27,580	800	283	1,076	283
SHEAR STRENGTH	-	172	255	151	-
TENSILE MODULUS	60×10^6	12,963	3,703	272,215	-
COMPRESSIVE MODULUS	-	23,374	46,748	293,451	31,538
SHEAR MODULUS	-	17,927	-	7,585	-

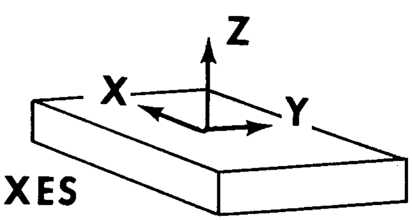

AXES

Figure 11

FIGURE 12

Both contractors are providing MSC with test articles which represent the application of the surface insulators to lightweight subpanels and to load-carrying skins. The designs developed by the contractors for the subpanel application test articles are indicated in figure 12.

Both articles represent a 0.61 m by 0.61 m (2 ft by 2 ft) protected area with an overlay of the substrate to provide for load testing. Both systems consist of four 0.3 m (1 ft) square tiles, with joints between the tiles designed to limit heat in flux. The tiles of the MDAC system are coated on all five sides; whereas the LMSC tiles are coated in the joints only to the step of the joint.

These panels were designed for a peak surface temperature of 1600° K (2300° F) and a short cross-range heating history. The peak bond line temperature specified was 533° K (500° F). The ultimate pressure differential to be applied at peak bond line temperature is 26 600 N/m^2 (4 psi) with the panels simply supported on opposite ends.

The MDAC substrate panel is a titanium honeycomb sandwich with beryllium face sheets. This substrate, built using available material gages, should have a mass of approximately 4.34 kg/m^2 (0.9 lb/ft^2). LMSC selected Z-stiffened beryllium sheet as the subpanel; the weight of this panel is expected to be 1.95 kg/m^2 (0.4 lb/ft^2).

DEMONSTRATION HARDWARE

SURFACE INSULATION BONDED TO SUBPANELS

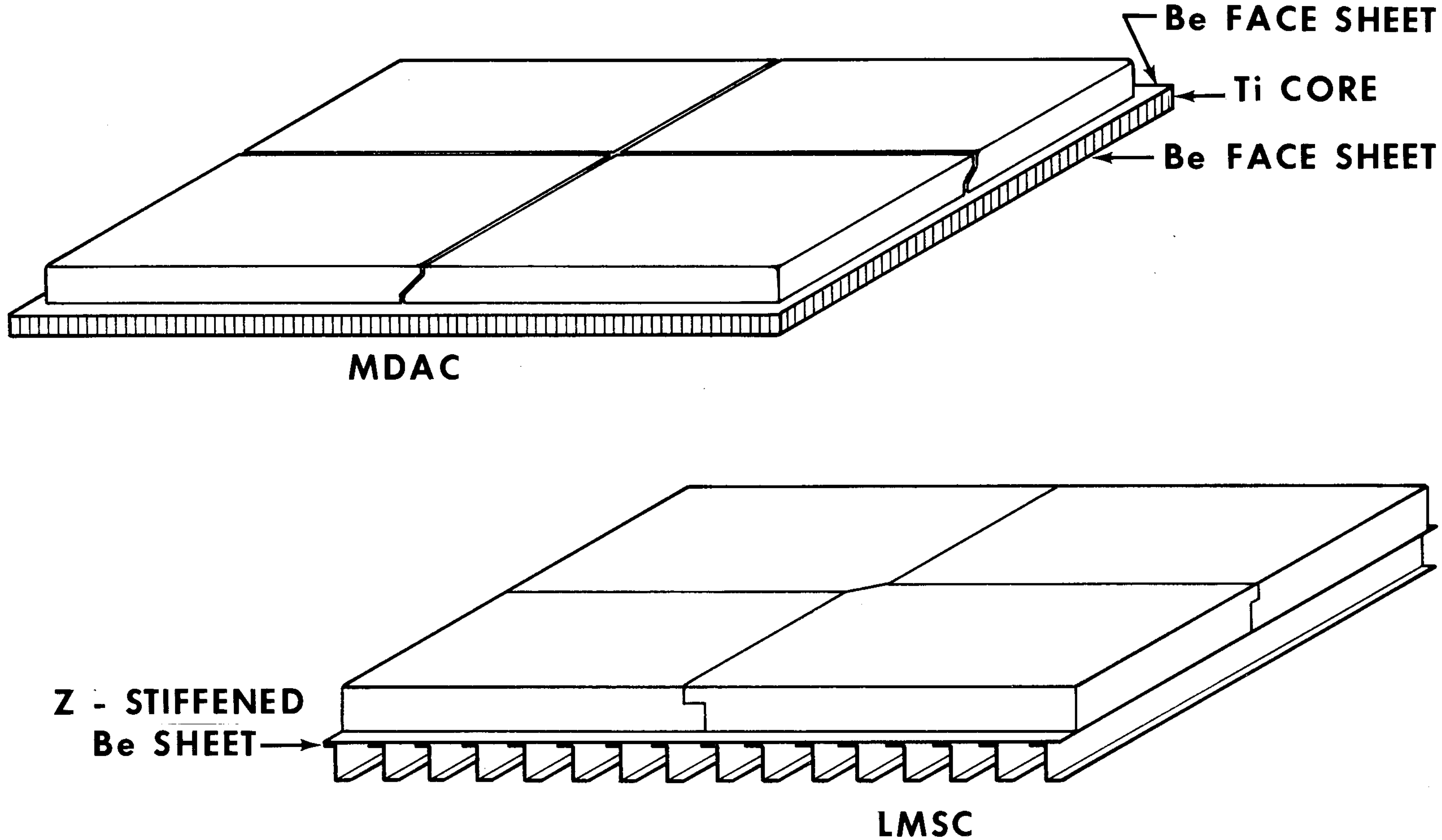

Figure 12

FIGURE 13

Figure 13 is a photograph of the test panel fabricated by LMSC to represent the direct bonding of the LI-1500 material to load-carrying structure. The protected area of this panel, and the similar panel to be supplied by MDAC, is 0.3 m by 0.9 m (1 ft by 3 ft). The titanium structural substrate, with a unit mass of approximately 19.5 kg/m^2 (4 lb/ft^2) extends beyond the protected area at each end to allow imposing significant tensile and bending loads on the system.

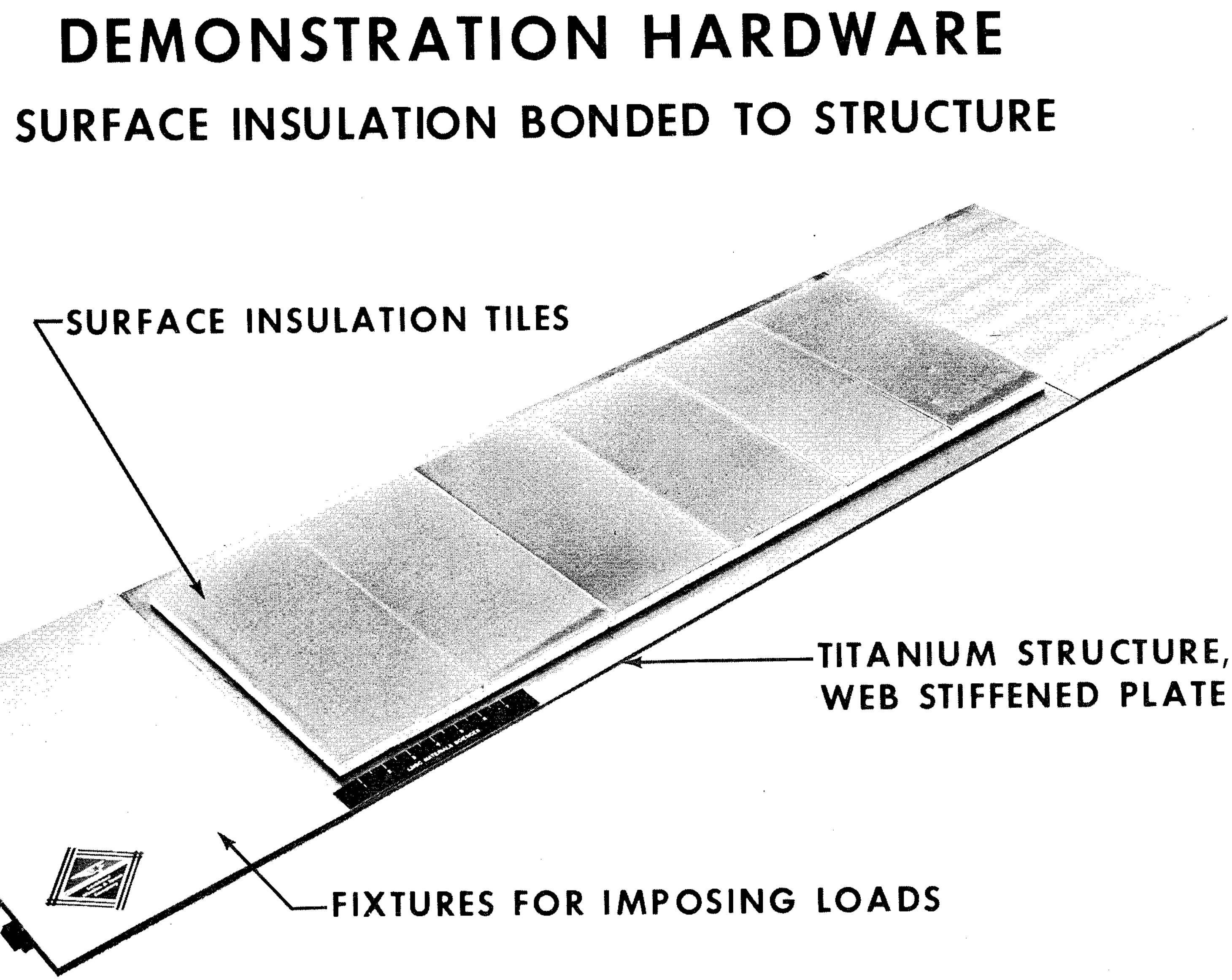
DEMONSTRATION HARDWARE
SURFACE INSULATION BONDED TO STRUCTURE
SURFACE INSULATION TILES
TITANIUM STRUCTURE, WEB STIFFENED PLATE
FIXTURES FOR IMPOSING LOADS

Figure 13

FIGURE 14

The elements which contribute to the weights of the two applications of surface insulation are indicated in figure 14. In concept I, the weight of the TPS includes not only that of the coating, insulation, and bond, but also that of the supporting subpanel. The weights of attachments between the subpanel and the load-carrying structure, and for some cases the weight of insulation below the subpanel, have been included in weight trade studies, but are not included in the demonstration hardware weights.

In the second concept illustrated, the weight of the load-carrying structure is generally not included as part of the TPS.

SURFACE INSULATION DESIGN APPROACHES

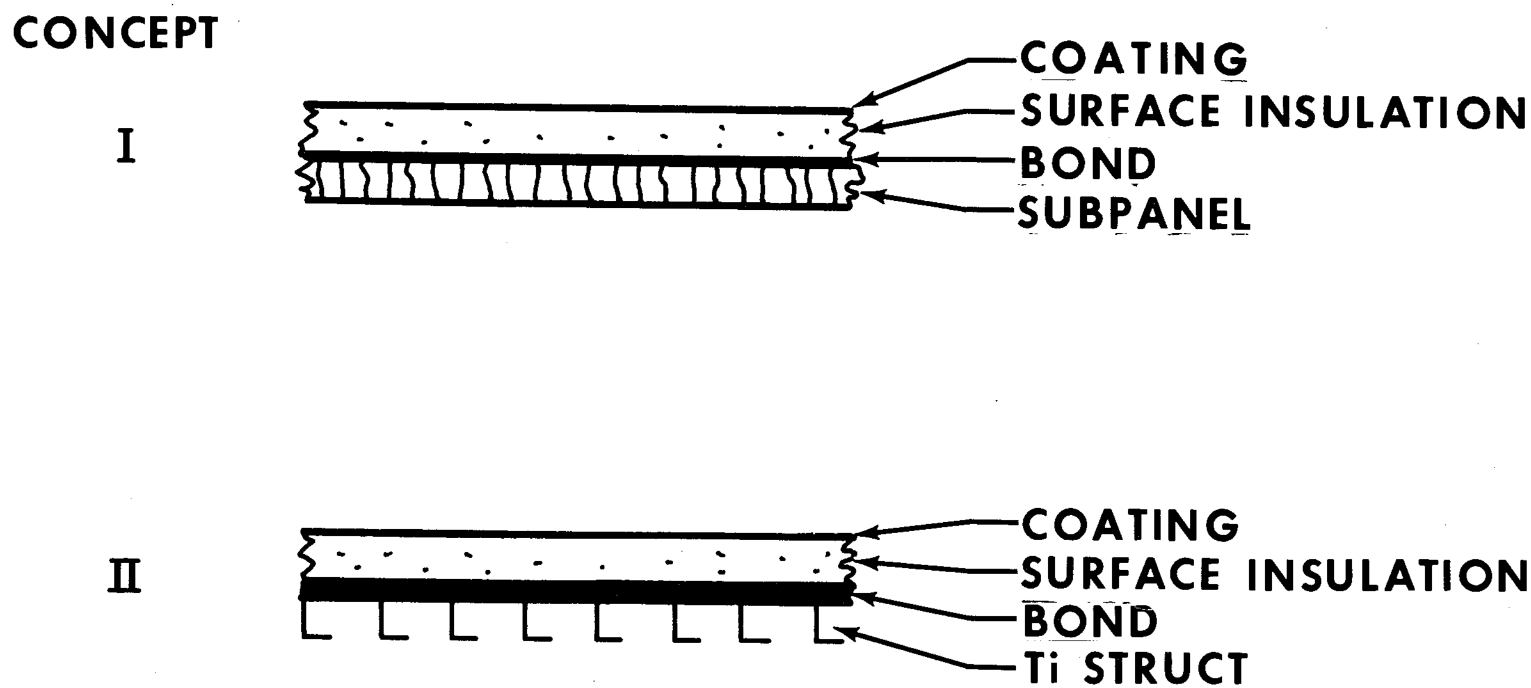

Figure 14

FIGURE 15

Figure 15 shows the weights, calculated from design drawings, of the four types of demonstration hardware being delivered to MSC by LMSC and MDAC. The weight of the MDAC subpanel, as previously discussed, is the primary cause of the weight difference in the concept I hardware. However, it will also be noted that the insulation weights for both concepts are higher in the MDAC designs, although the thermal conductivities of the two materials appear to be similar based on the data of figure 10. Examination of the design analysis performed by the two contractors indicates two contributing factors: First, LMSC included the thermal capacity of the elastomeric bond in the thermal analysis, which was not included by MDAC, and second, MDAC applied a thickness penalty for the higher effective thermal conductivity of the gaps between material tiles on the basis of test data, an effect not accounted for by LMSC.

It is anticipated that the extensive in-house testing of this hardware, as well as of other instrumented samples supplied by both contractors, will determine the accuracy of the thermal designs.

SURFACE INSULATION DEMONSTRATION HARDWARE WEIGHTS

UNIT MASS, kg/m^2

		LMSC	MDAC
I	COATING	.73	1.17
	INSULATION MATERIAL	7.91	9.03
	BOND	.73	1.07
	SUBPANEL	1.95	4.34
	TOTAL	11.32 ($2.32\ LB/FT^2$)	15.61 ($3.20\ LB/FT^2$)
II	COATING	.73	1.17
	INSULATION MATERIAL	4.30	6.44
	BOND	1.27	1.07
	TOTAL	6.30 ($1.29\ LB/FT^2$)	8.68 ($1.78\ LB/FT^2$)

Figure 15

FIGURE 16

Numerous trade studies have been performed to assess the relative merits of the surface insulation, carbon-carbon, and competing metallic systems on the basis of weight. These studies are continually being refined by MSC, and it is of interest to compare the weights of the demonstration hardware with such weight projections.

Figure 16 indicates calculated weights of a superalloy TPS concept and the surface insulation concepts. These calculations are shown for a central location on the lower surface of a delta-wing orbiter as a function of heat load. The heat load at this one location was varied by computer simulations of different cross-range missions: The lower heat loads below 60 MJ/m^2, represent 200 n. mi. missions, whereas, the heat loads between 125 and 160 MJ/m^2, correspond to missions with cross ranges on the order of 1100 to 1500 n. mi. For all the missions simulated, the peak surface temperature at the location considered was between 1150° K (1600° F) and 1350° K (1900° F); thus, a cobalt superalloy panel was used as the metallic reference system. The upper curve for the metallic system is based on a conservative panel design with sufficient insulation to protect an underlying structure to 410° K (300° F). The lower boundary of metallic system weights represents a near-optimum panel weight, and insulation to 615° K (650° F) for the primary structure.

The surface insulation system weights on the upper boundary represent a concept I system with a 278° K (533° F) bondline restriction, and insulation between the subpanel and structure. The lower boundary represents a concept II system with a bondline temperature of 615° K (650° F). The actual weights calculated for the LSMC demonstration hardware agree well with these predictions; however, the

TPS UNIT AREA MASS AS A FUNCTION OF HEAT LOAD, WITH POINT DESIGN COMPARISONS

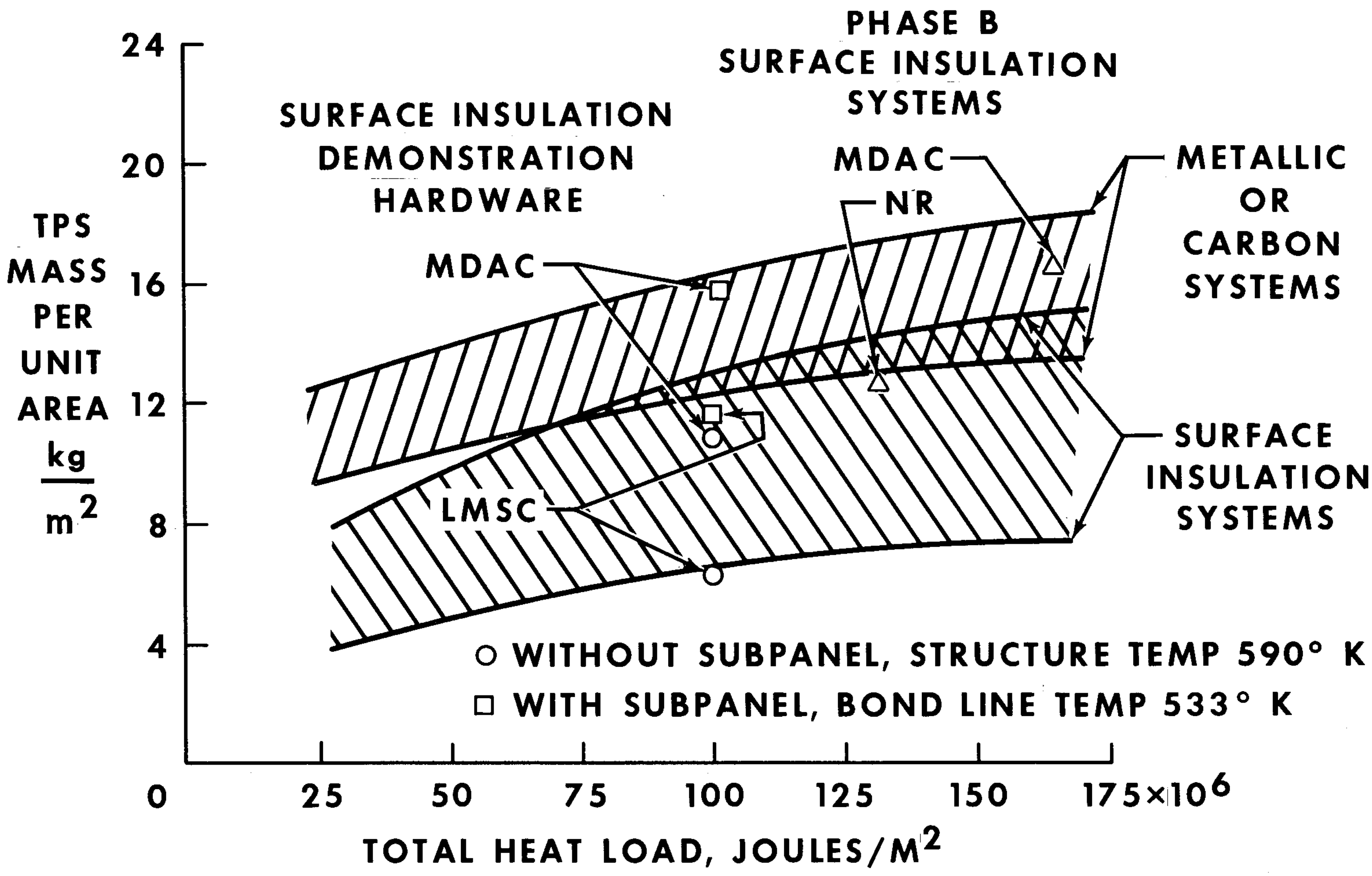

Figure 16

MDAC hardware weights are significantly higher, as has been previously discussed. Also shown for reference are the phase B point designs developed by North American Rockwell (NR) and MDAC as part of the shuttle studies for the surface insulation concept. The NR weights agree with predicted weights; the MDAC phase B calculations are in keeping with the MDAC demonstration hardware weights.

FIGURE 17

An attempt to evaluate the status of surface insulation system development at this time is indicated in figure 17. Six different types of candidate surface insulation materials have been screened by MSC. Of these, only the silica and mullite systems appeared to warrant further development for use in the early operational phase of the shuttle program with its current schedule. For these two systems, typical hardware designs have been fabricated and will be subjected to extensive testing in the immediate future. In addition, the weights of this hardware are commensurate with the weight estimates which initially prompted interest in these systems. However, shortcomings in these early systems are becoming apparent, and direction for improvements in the system have been identified.

SUMMARY OF SURFACE INSULATION EVALUATION

- SCREENING INDICATES ONLY THE SILICA AND MULLITE RIGIDIZED FIBER SYSTEMS ARE PRESENTLY VIABLE
- FIRST-GENERATION SYSTEMS, INCLUDING ALL ELEMENTS REQUIRED TO MEET A TYPICAL REQUIREMENT HAVE BEEN DEVELOPED
- IMPROVEMENTS OVER FIRST GENERATION SYSTEM ARE INDICATED
- EXTENSIVE TESTING OF FIRST GENERATION SYSTEM WILL BE COMPLETE BEFORE JUNE 1971
- CURRENT WEIGHT ESTIMATES AND DEMONSTRATION HARDWARE WEIGHTS ARE LOWER THAN FOR EQUIVALENT METALLIC SYSTEM

Figure 17

CONCLUDING REMARKS

Both inhibited carbon-carbon systems and surface insulation systems have been under intensive development for the past 6 months under MSC sponsorship. A large number of materials have been developed and evaluated, and prime candidates chosen. Early property measurements and design studies indicate that systems satisfying all shuttle requirements can be developed with use of these materials, and that system weights will be lower than those for other system concepts for the same temperature ranges.

As anticipated, problem areas in both systems are becoming evident as test data accumulate; however, directions for further development are likewise evolving. The conclusion reached is that these current efforts have successfully initiated development programs which can establish, within the next year or 18 months, the technological base required for application of the nonmetallic materials to the shuttle thermal protection system.

REUSABLE EXTERNAL INSULATION TPS FOR THE SPACE SHUTTLE

By P.D. Gorsuch, R.A. Tanzilli, and D.E. Florence
General Electric Company, Philadelphia, Pennsylvania

PAPER 2

INTRODUCTION

The General Electric Company's Re-entry and Environmental Systems Division (GE-RESD) has been developing and evaluating a series of high insulative efficiency, rigidized fibrous insulation materials. Thermal protection systems (TPS) based on these materials are much lighter in weight than those using other candidate materials such as coated refractory metals. This weight saving is extremely important since it can be used to increase the payload weight fraction of the space shuttle vehicle. The GE-RESD designation for this class of materials is Reusable External Insulations (REI).

The inherent simplicity, low density, capability for repeatedly surviving the maximum expected surface temperatures during normal entry missions without significant performance degradation and reserve margin are the strong forcing functions (a) for the development of REI materials and (b) for establishing their multimission capability for use in space shuttle TPS. The ultimate goal of the development and evaluation program is an REI TPS with a 100 mission capability.

In this paper the development and evaluation activities at GE-RESD are summarized. Much of the work described was supported through the use of General Electric Company discretionary funds. Application of the REI materials to the shuttle orbiter is being conducted under a purchase order from the North

American Rockwell Corporation (NR) as part of their space shuttle Phase B contract. Other contract activities include (a) fabrication of samples of composite insulation systems utilizing both zirconia and mullite base fibers for the NASA Manned Spacecraft Center and (b) the development of insulation materials for the NASA Langley Research Center. The latter program will emphasize the development of zirconia base insulative composites as well as the development and evaluation of coatings for silica, mullite and zirconia base systems.

SYMBOLS

TPS	-	Thermal Protection System	L	-	Length
NR	-	North American Rockwell Corporation	lb	-	Pound
NDT	-	Nondestructive Testing	mw	-	Megawatt
REI	-	Reusable External Insulation	m	-	Meter
atm	-	Atmosphere	μ	-	Micro
BP	-	Body Point	n	-	Newton
BTU	-	British Thermal Unit	ppm	-	Parts Per Million
C_p	-	Specific Heat	ρ	-	Density
ϵ	-	Total Hemispherical Emittance	sec	-	Second
F_{TY}	-	Failure Tensile Yield Strength	X	-	Distance Along Vehicle
^oF	-	Degrees Fahrenheit	K	-	Thermal Conductivity
G	-	Shear Modulus of Elasticity	t	-	Thickness
in	-	Inch	τ	-	Shear Strength
^oK	-	Degrees Kelvin	M_e	-	Mach Number At Edge of Boundary Layer
kg	-	Kilogram	M_∞	-	Free-Stream Mach Number
kw	-	Kilowatt	RTV	-	Room Temperature Vulcanizing

REUSABLE EXTERNAL INSULATION FOR NR ORBITER

(Slide 1)

The REI class of materials consist of about 5 percent by volume of near randomly oriented silica, mullite, or zirconia fibers rigidized by bonding their points of contact with pyrolyzed silicone, mullite, or zirconia base cements, respectively. The designations REI-Silica, REI-Mullite, or REI-Zirconia have been selected to describe each of these three types of insulative composites. The silica and yttria stabilized zirconia fibers are commercial grades of materials supplied by Johns-Manville Products Corporation and Union Carbide Corporation, respectively. The mullite fibers are alumina rich near stoichiometric ($3\ Al_2O_3$-$2\ SiO_2$) materials supplied by Babcock and Wilcox. The diameter of the fibers are typically 0.5 to 0.75 μm for REI-Silica, 5 μm for REI-Mullite, and 4 to 6 μm for REI-Zirconia. Although made over a range of composite densities, the density range selected to be near optimum for each system, such as 185 kg/m^3 (11.5 lb/ft^3) for REI-Silica, reflects a compromise between mechanical properties such as strength and strain-to-failure and insulative efficiency.

The temperature range of applicability shown in the slide for each REI system is based on considerations relative to the sintering and densification tendencies and phase stability of the fibers and

binders. Although REI-Zirconia would appear to be the most logical candidate system because of its capability for meeting the complete range of expected surface temperatures, other factors must be taken into consideration. These include cost, availability of raw materials, ease of manufacture, properties, thermal-mechanical compatibility with structure and availability of suitable coating systems. Thus it may be both cost and performance effective to use REI-Silica and/or REI-Mullite on the large vehicle surface areas exposed to the lower surface temperatures.

REUSABLE EXTERNAL INSULATION FOR NR ORBITER

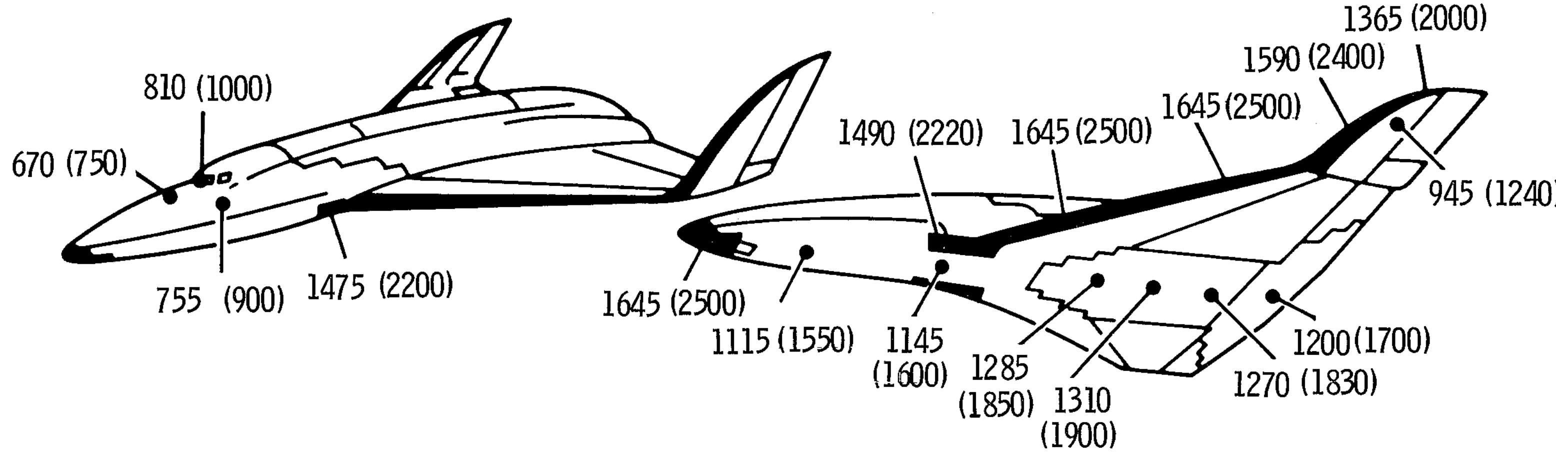

REI MATERIAL CLASS	ESTIMATED MAXIMUM USE TEMPERATURE, ^{o}K (^{o}F)	APPROXIMATE ORBITER AREA COVERED, %
REI - SILICA	1365 (2000)	85 - 90
REI - MULLITE	1700 (2600)	95 - 100
REI - ZIRCONIA	2035 (3200)	100

Slide 1

DESIGN AND SYSTEM REQUIREMENTS

(Slide 2)

The development and effective application of a light weight, high performance surface insulative TPS requires an iterative procedure in which design, system, and mission requirements are defined and translated into material property and behavioral requirements and subsequently into specific test and evaluation criteria. With respect to design, REI materials offer both great flexibility and simplicity since the insulation thickness can be sized to achieve sufficiently low operational backface temperatures to permit the use of adhesive bonds for attaching the panels to the primary structure. However, the limited strength levels of the REI materials, e.g., 689 kN/m^2 (100 lb/in^2) in tension and compression, mandate the use of finite thickness flexible adhesives to reduce both the stress concentrations and the shear and normal stress requirements of the adhesive and insulation.

An important feature of the REI TPS is the need for a multifunctional surface coating to provide environmental protection against handling damage, rain and dust erosion and moisture absorption and to increase heat rejection by radiation. The development of suitable reusable coatings is probably the principal problem which must be solved if REI materials are to be used in the thermal protection system on the shuttle orbiter. The current approaches for developing a coating system involve densifying the outer layers or covering the insulation with a suitable dense refractory inorganic material.

DESIGN AND SYSTEM REQUIREMENTS

COATING

- TEMPERATURE CONTROL
- EROSION RESISTANCE
- IMPACT RESISTANCE
- WATER REPELLANCY
- FUEL COMPATIBILITY
- OXIDATION RESISTANCE

INSULATION

- LOW $\frac{K\rho}{C_P}$
- STRAIN COMPATIBLE
- STRENGTH
- FATIGUE RESISTANCE
- THERMAL STABILITY

ADHESIVE BONDS

- STRENGTH
- STIFFNESS

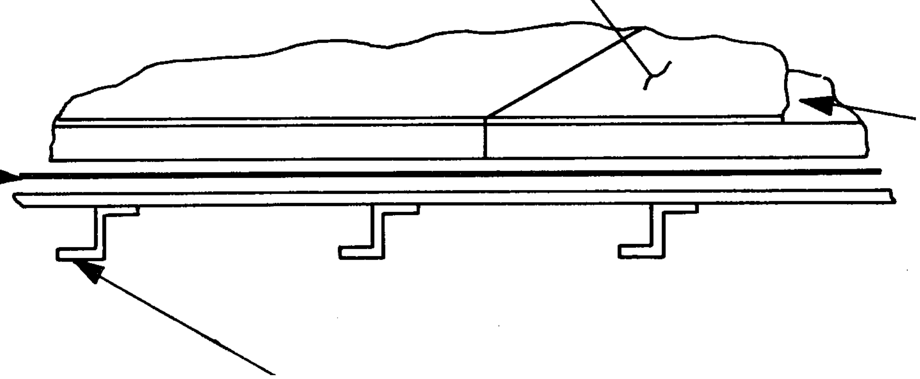

PRIMARY AIRFRAME STRUCTURE

- CONFIGURATION
- LOADS
- HEAT CAPACITANCE
- DEFORMATION

Slide 2

TIME HISTORIES OF AMBIENT PRESSURE AND TYPICAL HEAT FLUX FOR NR ORBITER

(Slide 3)

The insulation efficiency and thermal stability of the REI class of materials depends on both the temperatures and the pressures to which they are exposed. Thus it is necessary, in sizing the REI insulation thickness and predicting its useful operating life, to consider the operational conditions at each stage in entry. Slide 3 shows that the peak heating on typical lower body panels of an orbiter occurs when the local pressure is 10^3 newtons/meter^2 (10^{-2} atmospheres). Assuming that the insulation is vented to the local boundary layer edge pressure, this lower pressure condition would result typically in a 50 percent reduction in the thermal conductivity of the insulation compared with that for atmospheric pressure. Slide 4 shows the magnitude of the TPS weight drop for this increase in insulative efficiency.

TIME HISTORIES OF AMBIENT PRESSURE AND TYPICAL HEAT FLUX FOR NR ORBITER

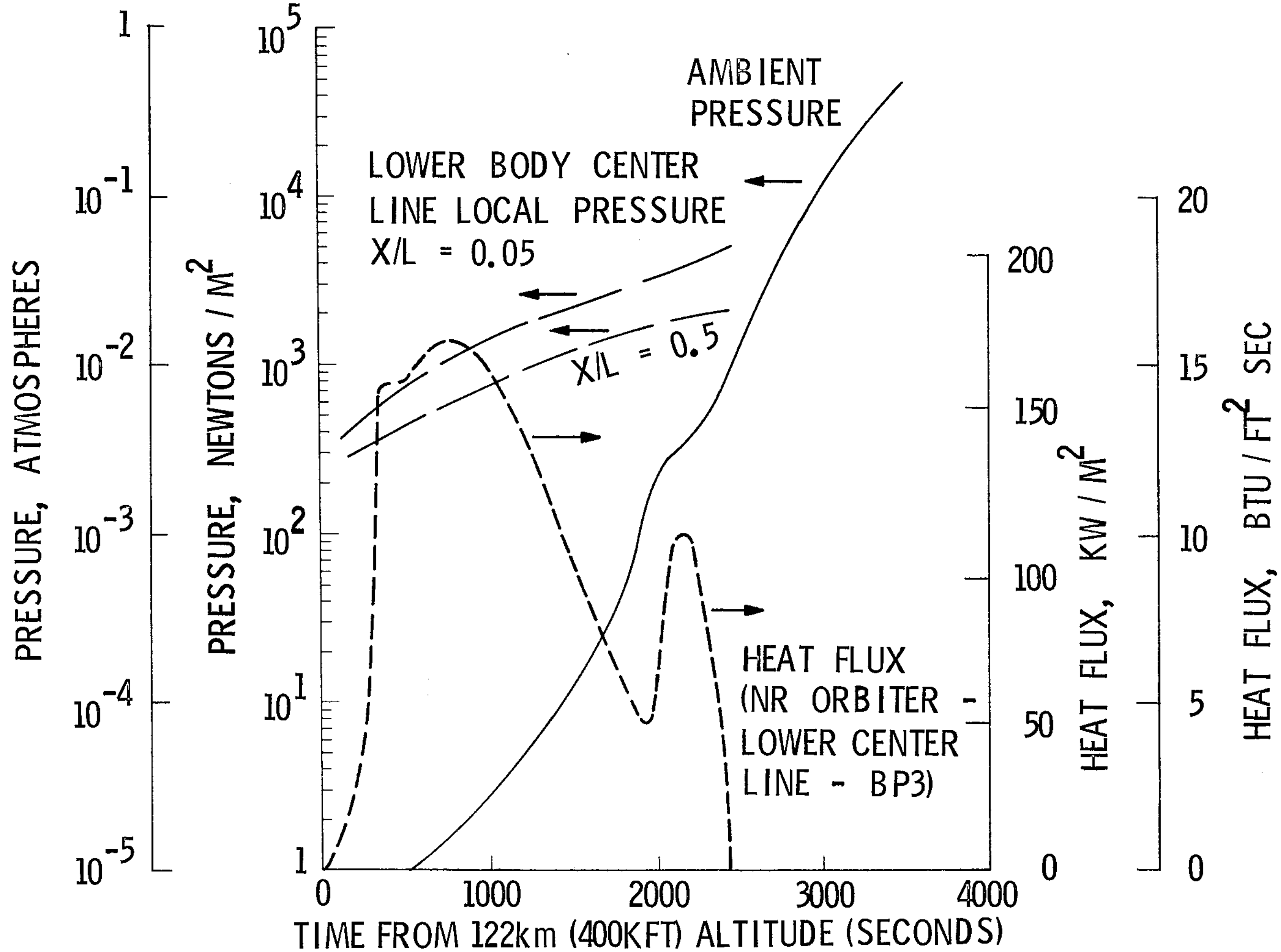

Slide 3

INSULATION WEIGHT DEPENDENCE ON $K\rho / C_p$

(Slide 4)

The weight of the TPS using ceramic insulation systems is minimized when the value of $\frac{K\rho}{C_p}$ is minimized. Thus the designer should select the material system with minimum values of this parameter across the operating temperature range, consistent with the mechanical property requirements. Slide 4 shows that the predicted insulation weight for REI-Silica made from available binders and fibers is quite low. However, there exists the possibility of making marked performance improvement from a weight standpoint through material modifications. Determination of the extent to which this performance gain is realizable would require an extensive study of the relationship between mechanical properties and insulative efficiency and a manufacturing development program to obtain the required fibers and binders in quantities sufficient for detailed evaluation.

The specific approaches which can be used for weight minimizing in each of the three material systems include (a) employing lower density composites, (b) using fibers of the optimum diameter and spacing for their temperature range of operation, (c) introduction of appropriate opacifiers (metallic flakes or fiber coatings) into the composites and (d) operation of the insulations at as low a pressure as possible. Also further reductions in $K\rho / C_p$ can be achieved by interleaving radiation barriers such as sputtered layers within the composites.

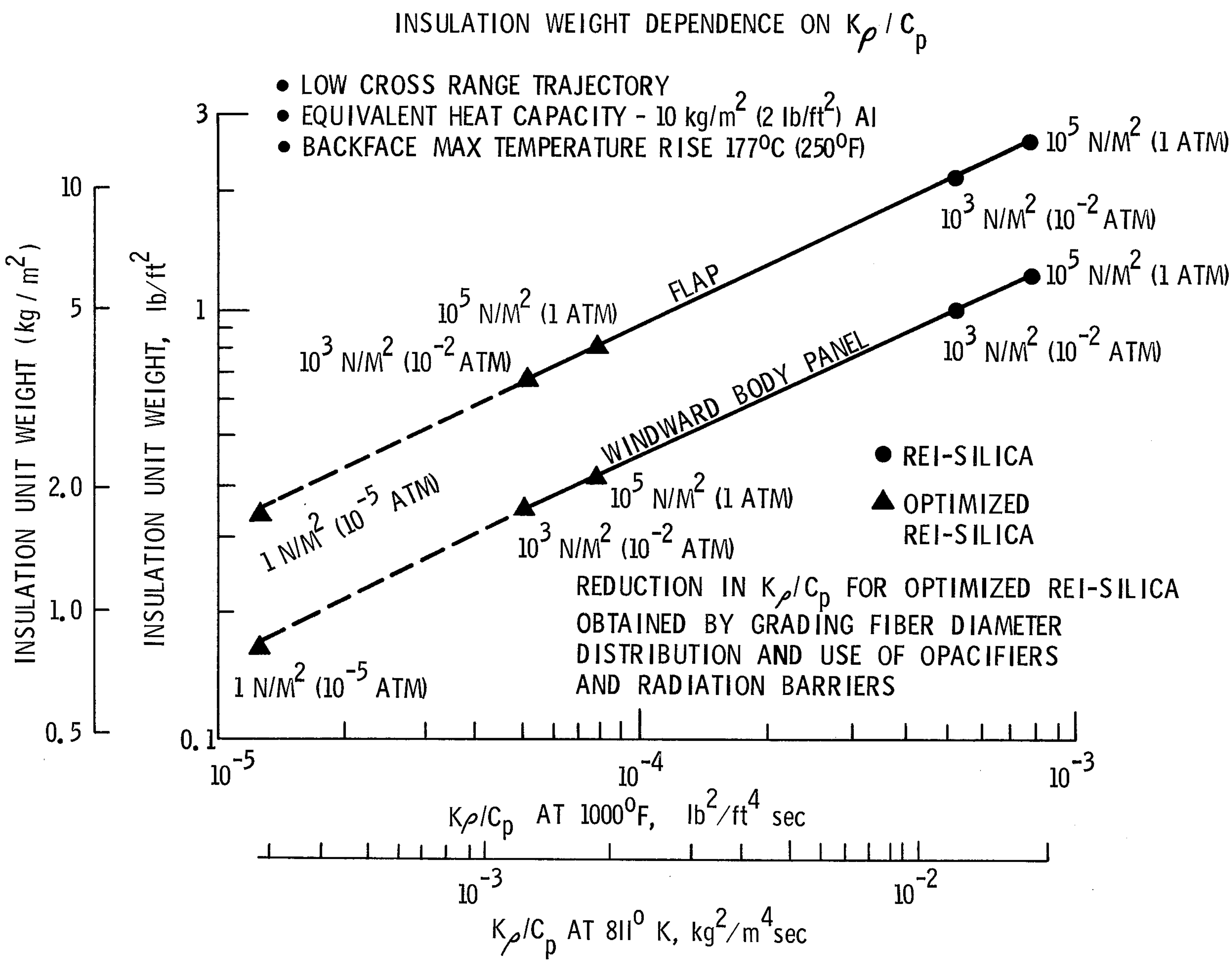
INSULATION WEIGHT DEPENDENCE ON $K\rho / C_p$
• LOW CROSS RANGE TRAJECTORY
• EQUIVALENT HEAT CAPACITY - 10 kg/m^2 (2 lb/ft^2) Al
• BACKFACE MAX TEMPERATURE RISE 177°C (250°F)
INSULATION UNIT WEIGHT (kg / m^2)
10
5
2.0
1.0
0.5
INSULATION UNIT WEIGHT, lb/ft^2
3
1
0.1
FLAP
WINDWARD BODY PANEL
10^5 N/M^2 (1 ATM)
10^3 N/M^2 (10^{-2} ATM)
10^5 N/M^2 (1 ATM)
10^3 N/M^2 (10^{-2} ATM)
10^5 N/M^2 (1 ATM)
10^3 N/M^2 (10^{-2} ATM)
1 N/M^2 (10^{-5} ATM)
10^5 N/M^2 (1 ATM)
10^3 N/M^2 (10^{-2} ATM)
1 N/M^2 (10^{-5} ATM)
● REI-SILICA
▲ OPTIMIZED REI-SILICA
REDUCTION IN $K\rho/C_p$ FOR OPTIMIZED REI-SILICA OBTAINED BY GRADING FIBER DIAMETER DISTRIBUTION AND USE OF OPACIFIERS AND RADIATION BARRIERS
10^{-5}
10^{-4}
10^{-3}
$K\rho/C_p$ AT 1000°F, lb^2/ft^4 sec
10^{-3}
10^{-2}
$K\rho/C_p$ AT 811° K, kg^2/m^4sec

Slide 4

REI STRAIN REQUIREMENTS BASED ON BOTH THERMAL AND STRUCTURAL LOADS

(Slide 5)

REI mechanical property requirements are dependent upon the detailed TPS design as well as the structural materials used in supporting the panels. The coefficients of thermal expansion for all three REI systems are equal to or less than the coefficients of the candidate structural support materials, namely, aluminum and titanium. Slide 5 shows the tensile and compressive strain requirements based on both thermal and structural loads for 2 different designs and the various REI and structure material combinations. Typically strain-to-failure values of at least 0.84% are required when the REI materials are bonded to a continuous air frame stressed skin structure and 0.4% for a design involving non-structural air load carrying panels. Reproducible achievement of these strain-to-failure properties in the materials would greatly simplify their application to shuttle orbiter TPS.

REI STRAIN REQUIREMENTS BASED ON BOTH THERMAL AND STRUCTURAL LOADS

REI MATERIAL SYSTEM	STRUCTURE MATERIAL AND DESIGN CONFIGURATION			
	ALUMINUM		TITANIUM	
	RESTRAINED	FREE	RESTRAINED	FREE
REI - SILICA (AMORPHOUS)	0.70% TENSION 0.50% COMPRESSION	0.40% TENSION 0.34% COMPRESSION	0.83% TENSION 0.60% COMPRESSION	0.40% TENSION 0.15% COMPRESSION
REI - MULLITE	0.70% TENSION 1.45% COMPRESSION	0.40% TENSION 0.62% COMPRESSION	0.84% TENSION 1.48% COMPRESSION	0.40% TENSION 0.50% COMPRESSION
REI - ZIRCONIA	0.70% TENSION 1.76% COMPRESSION	0.40% TENSION 0.80% COMPRESSION	0.84% TENSION 1.78% COMPRESSION	0.40% TENSION 0.60% COMPRESSION
REI - SILICA (CRYSTALLINE)	0.70% TENSION 1.59% COMPRESSION	1.10% TENSION 1.10% COMPRESSION	0.87% TENSION 1.58% COMPRESSION	0.90% TENSION 0.80% COMPRESSION

Slide 5

REI-ADHESIVE INTERFACE SHEAR STRESS REQUIREMENTS

(Slide 6)

To prevent loss of insulation material by delamination, the REI materials and adhesive system utilized for bonding must have an ultimate shear strength capability compatible with the shear stiffness of the adhesive system. Slide 4 shows this general relationship between required insulation shear strength and bond shear stiffness. As indicated, a value of 689 kN/m^2 (100 lb/in^2) for the shear strength of the insulation has been found to be adequate for 2 different types of REI-Silica and REI-Mullite provided the bond shear stiffness was properly tailored.

REI-ADHESIVE INTERFACE SHEAR STRESS REQUIREMENTS

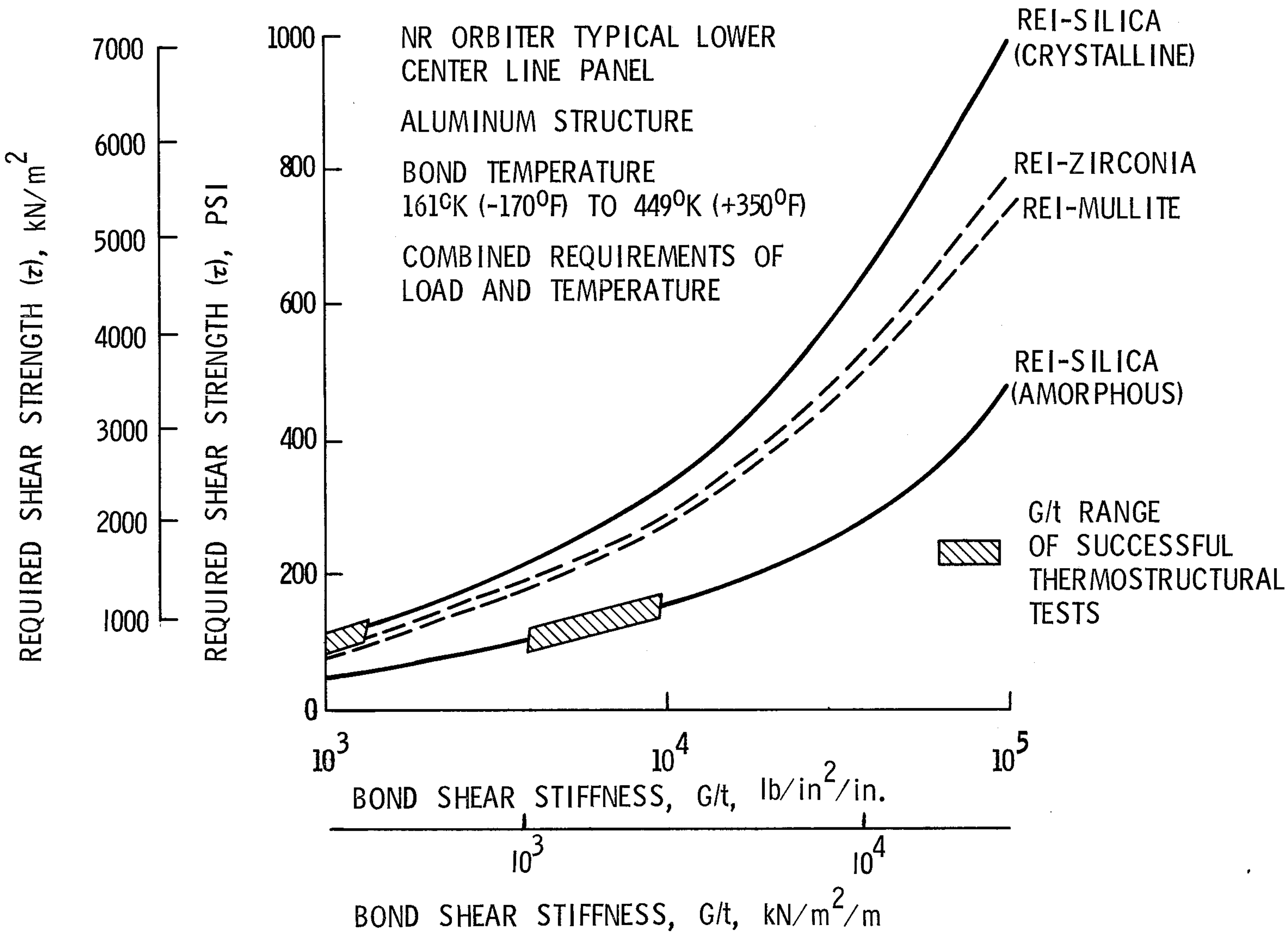

Slide 6

SCANNING ELECTRON PHOTOMICROGRAPH OF REI-SILICA

(Slide 7)

REI-Silica is made by rigidizing silica fibers with high purity silica produced by the pyrolysis of a silicone resin. The silica fibers are first treated and the coated with the silicone resin. The coated fibers are then slurry processed to give a near random distribution in a fiber composite. The composite is subsequently compressed to the required density and fired to reduce the silicone resin to a high purity silica residue which rigidizes the fibers. Impregnation, drying and pyrolysis conditions have been selected to achieve material uniformity and to maximize concentration of the binders at fiber intersections through control of surface tension.

Insulative composites over a wide range of densities from about 160 to 320 kg/m^3 (10 to 20 lb/ft^3) have been reliably and reproducibly fabricated by using pyrolyzed silicone as a rigidizing agent. Currently a density of 185 kg/m^3 (11.5 lb/ft^3) is considered to represent the most effective compromise between mechanical properties and insulation efficiency.

SCANNING ELECTRON PHOTOMICROGRAPH OF REI-SILICA

Slide 7

THERMAL EXPANSION OF THE SILICA MODIFICATIONS

(Slide 8)

REI-Silica is made from binders and fibers which are essentially amorphous in nature after processing. Unfortunately amorphous silica tends to devitrify or crystallize as a result of exposure at temperatures above about $1475^{\circ}K$ ($1800^{\circ}F$) for extended periods of time. The crystal modifications formed are generally quartz, tridymite and cristobalite. Formation of the crystalline material is detrimental because each of the crystalline forms undergoes polymorphic phase transformations when the insulation is cooled. Another bad feature, as shown in Slide 8, is the high coefficients of thermal expansion of the crystalline modifications. These tend to increase the design problems because of greater thermal mechanical strain incompatibility between the insulation and structure as was shown in Slide 6.

The devitrification tendencies of amorphous silica are influenced greatly by fiber and binder purity and test atmosphere as well as the time and temperature of exposure. Because of the known effects of contaminants in promoting devitrification, the fiber pretreatment material and binder system were selected to have high purity. Available data suggest that REI-Silica may have sufficient stability for multi-cycle reuse at temperatures of $1365^{\circ}K$ ($2000^{\circ}F$) and above.

THERMAL EXPANSION OF THE SILICA MODIFICATIONS

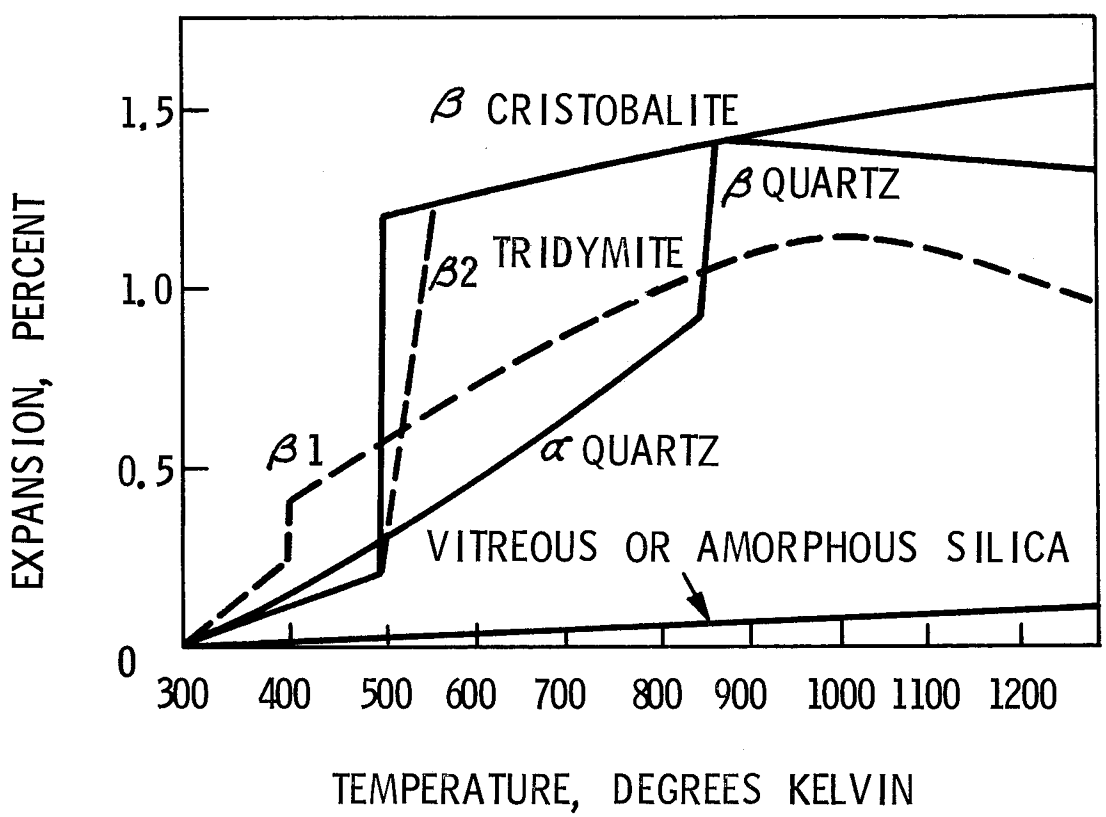

Slide 8

GENERAL TRENDS IN SHRINKAGE AND CRYSTOBALITE FORMATION RATES FOR REI-SILICA

(Slide 9)

In addition to having devitrification tendencies, silica base insulation materials also have a tendency to shrink in dimensions as a result of sintering and surface tension effects during high temperature exposure. However, the magnitude of this shrinkage is the same regardless of temperature of exposure despite marked differences in rates of shrinkage with temperature. An attempt is now being made to accumulate sufficient quantitative data for REI-Silica so that a time, temperature and atmosphere for processing can be adopted which will result in good dimensional stability for the material during service without having unacceptable levels of crystobalite formation.

GENERAL TRENDS IN SHRINKAGE AND CRISTOBALITE
FORMATION RATES FOR REI-SILICA

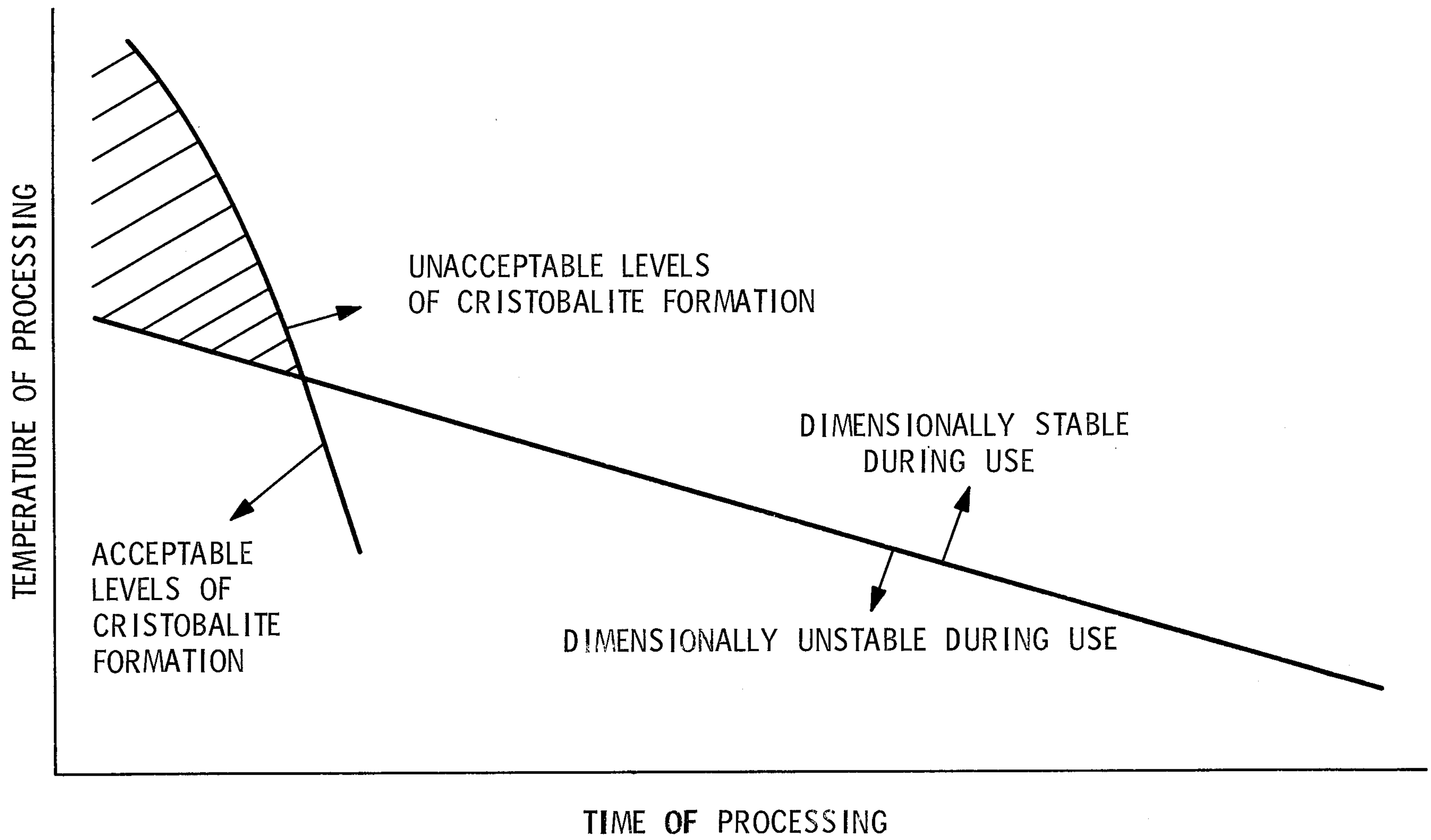

Slide 9

REI-SILICA CHEMICAL ANALYSIS

(Slide 10)

Slide 10 provides confirming evidence of the uniquely high purity level of the REI-Silica binder. In addition, the fiber pre-treatment tends to put a high purity silica coating on the less pure fibers and aids in preventing their devitrification. An additional advantage resulting from the pre-treatment of the fibers is improved mechanical integrity in the composites. This is indicative of better adhesion between the fiber and the binder.

REI-SILICA CHEMICAL ANALYSIS

ELEMENT	IMPURITIES (ppm)	
	J-M STANDARD MICROQUARTZ FIBER	PYROLYZED SILICONE RESIN
ALUMINUM	300	<5
BISMUTH	5	<5
BORON	30	30
CALCIUM	500	3
COBALT	20	<10
COPPER	100	<5
IRON	50	<20
LEAD	500	<20
LITHIUM	1	<1
MAGNESIUM	1000	<1
MANGANESE	10	<5
NICKEL	30	10
POTASSIUM	100	<2
SILVER	2	1
SODIUM	300	<5
STRONTIUM	10	<1
TIN	30	<30
TITANIUM	40	<1
ZIRCONIUM	10	<10

Slide 10

REI-SILICA PROTOTYPE PANEL FABRICATION

(Slide 11)

Slide 11 shows several steps in the fabrication of prototype panels of REI-Silica in finished sizes up to 0.46 by 0.92 meter (18 x 36 inches) with thicknesses up to 0.10 meter (4 inches). A pilot plant for the continuous production of large panels is now being assembled and will go into operation about 1 April 1971.

REI - SILICA PROTOTYPE PANEL FABRICATION

MOLDED REI PANEL

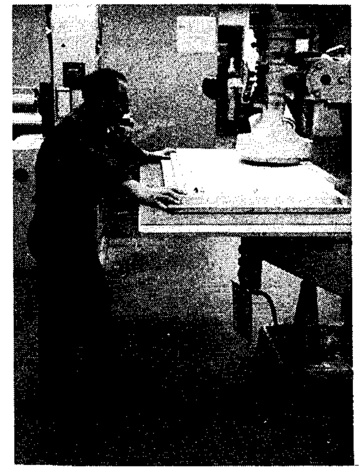

MACHINING REI PANEL

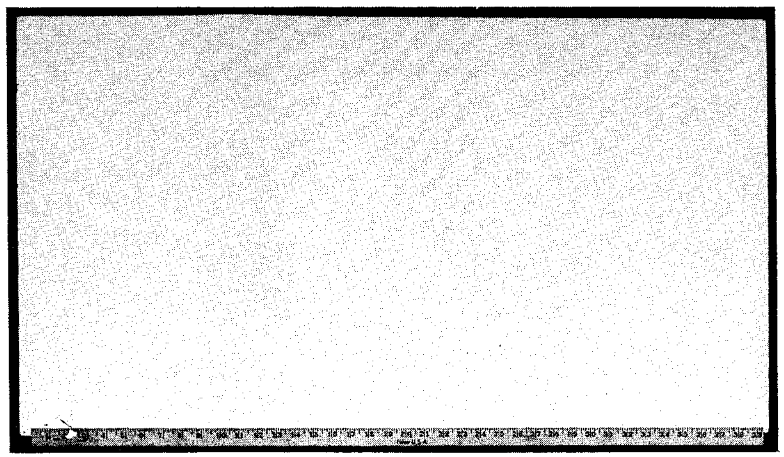

FULLY PROCESSED REI PANEL

Slide 11

REI-MULLITE PROTOTYPE PANELS

(Slide 12)

Mullite fibers produced by Babcock and Wilcox have been rigidized with a synthetic mullite binder and the resulting composites have been shown to be phase and dimensionally stable at temperatures up to at least 1645^{o}K (2500^{o}F) for times ranging up to 64 hours. Panels of this material appear to be strain compatible with aluminum structural support panels during entry simulation testing provided properly tailored adhesive bonds are used for attachment. Development of compatible inorganic coatings for REI-Mullite appears to be much simpler than for REI-Silica because of its higher thermal expansion characteristics.

Slide 12 shows a typical 0.3 x 0.3 x 0.025 meter (12 x 12 x 1 inch) thick panel. Other panels have been fabricated up to 0.46 x 0.92 x 0.025 meter (18 x 36 x 1 inch) thick. The slide also shows the post-entry simulation test appearance of a smaller panel which was adhesively bonded to an aluminum plate.

REI - MULLITE PROTOTYPE PANELS

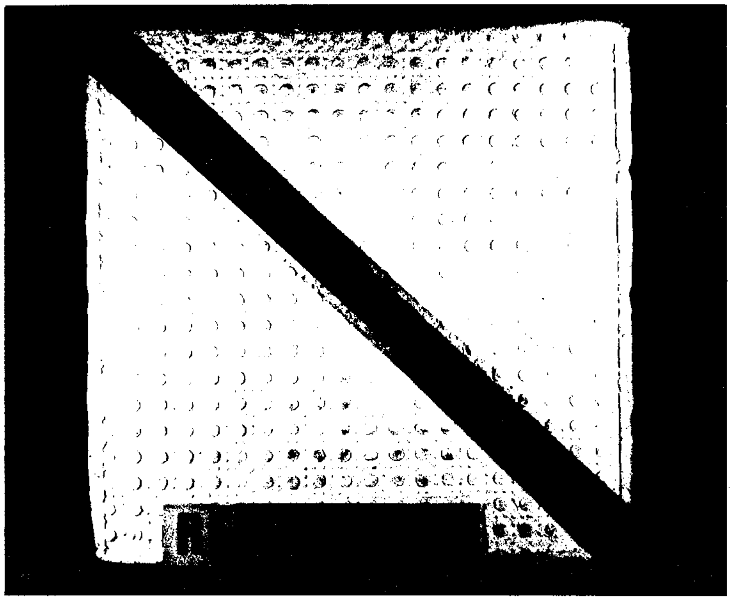

FABRICATED PANEL

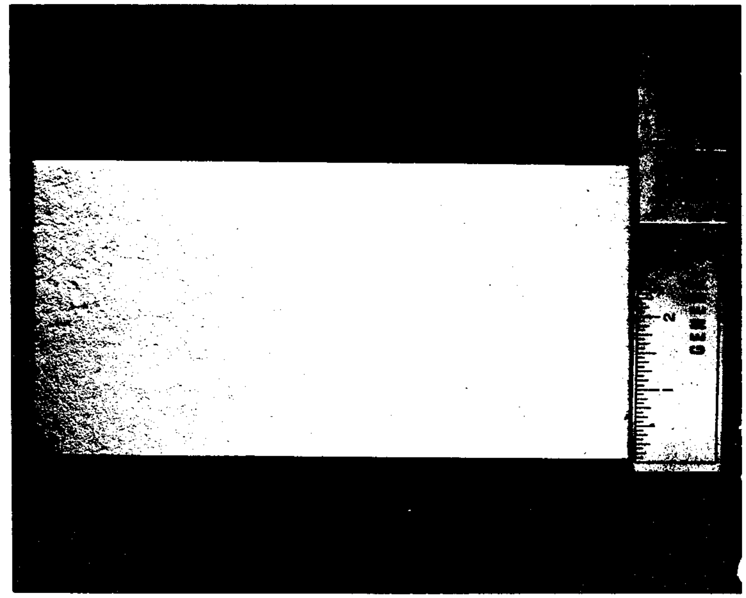

MACHINED AND BONDED PANEL - POST ENTRY SIMULATION TEST

Slide 12

SILICA OMNIWEAVE CONSTRUCTION (UNRIGIDIZED)

(Slide 13)

Much of the material development emphasis reported here has centered around the use of micron-sized fibers, randomly oriented and rigidized into a low density composite. This approach simplifies the composite fabrication cycle but does not necessarily yield a system with optimum mechanical properties. Multi-dimensional reinforcement techniques are being considered as methods for obtaining the most effective compromise between insulation efficiency, mechanical properties and fail-safe characteristics. The approach shown in Slide 13 consists of a multi-dimensional weave of the fiber yarn which is filled during weaving with low density felt mats of the same fibers. Layer interlocking during weaving provides through-the-thickness reinforcement without permitting direct fiber paths for thermal conduction. Also, surface reinforcement can be woven into the basic insulation by omitting the top several layers of low density filler and allowing the yarn to densify at the surface.

SILICA OMNIWEAVE CONSTRUCTION (UNRIGIDIZED)

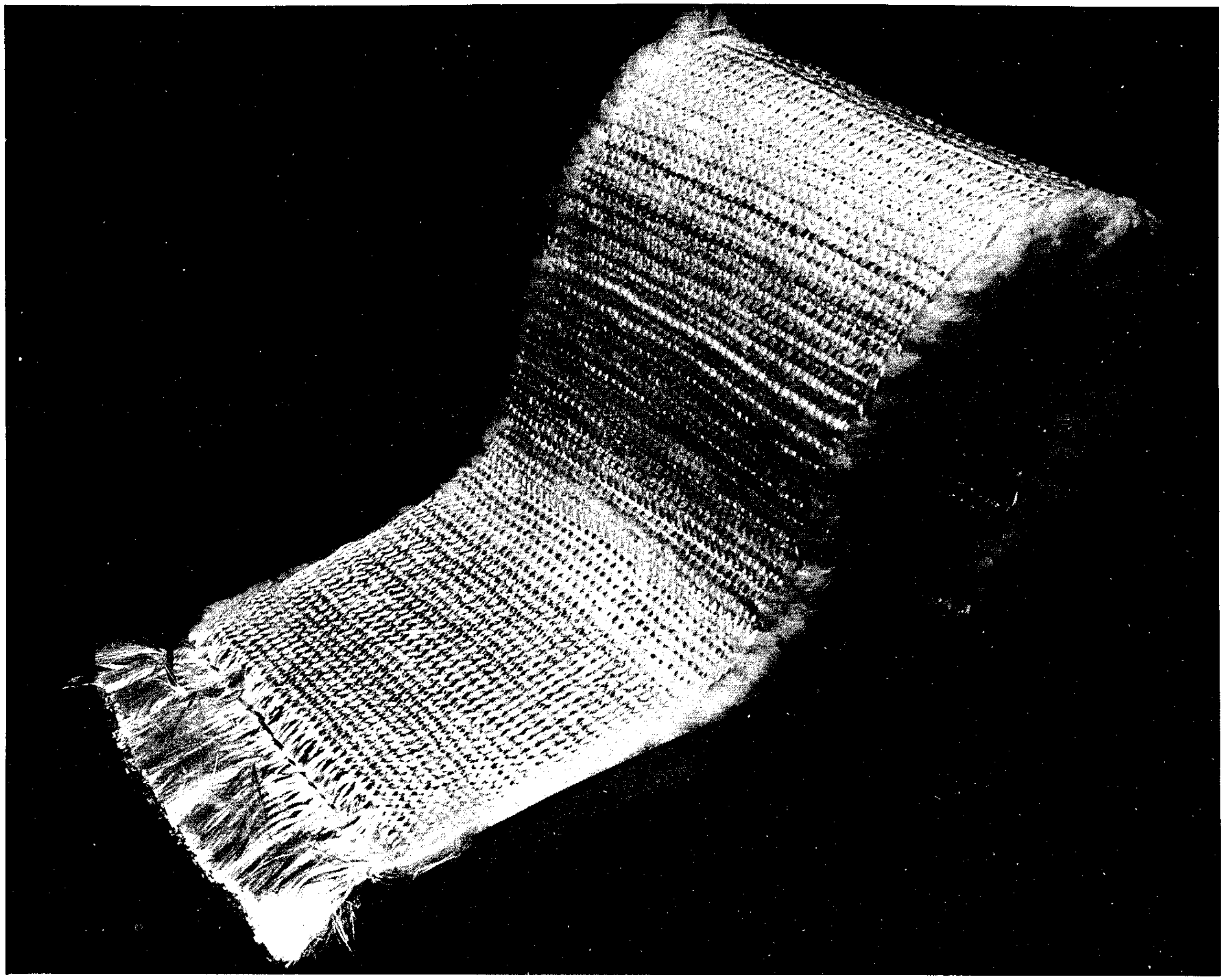

Slide 13

COATINGS

(Slide 14)

Surface coatings are required for REI materials (a) to minimize handling damage, rain and dust erosion and moisture absorption, and (b) to increase heat rejection by radiation. High temperature resistant or refractory viscous glasses applied by conventional enameling techniques and yielding glassy surfaces which are self healing at service temperatures is one approach being evaluated for solving the water absorption and surface erosion problems. An attractive feature of these viscous glass coatings is the relative ease with which their viscosity characteristics and optical properties can be controlled by compositional adjustments to the glass itself or by addition of color pigments to the slurry during initial application. With these types of coatings, a minimum emittance goal of 0.8 is readily obtained.

Slide 14 lists a few of the many complex and interrelated design and operational requirements for the coating systems. Also a few of the more successful coating systems evaluated to date are listed for each REI class of materials. The ductile metal foil tests demonstrated quite conclusively that metal foils bonded to the insulation and properly surface coated do merit consideration for environmental protection of REI thermal protection systems.

COATINGS

REQUIREMENTS

- PROVIDE ENVIRONMENTAL PROTECTION TO BASIC INSULATION
- ENHANCE SYSTEM PERFORMANCE BY PROVIDING HIGHLY RERADIATIVE SURFACES
  - $\epsilon \geqq 0.8$
  - 100 MISSION CAPABILITY
  - PREVENT MOISTURE PICK-UP BY INSULATION
  - RAIN, DUST AND AERODYNAMIC SHEAR FORCE RESISTANT
  - RESISTANT TO VIBRATION, ACOUSTIC NOISE AND DYNAMIC PRESSURE
  - α/ϵ RATIO OF 0.4

DEVELOPMENT STATUS

- REI - SILICA
  - PD198 (PHOSPHATE BASED COATING)
- REI - MULLITE
  - Pt FOIL WITH PLASMA SPRAYED HfO_2
  - OXIDATION RESISTANT VISCOUS GLASSES APPLIED BY ENAMELING TECHNIQUES
- REI - ZIRCONIA
  - Pt FOIL WITH PLASMA SPRAYED HfO_2 (FLIGHT TEST EXPERIMENTS)

Slide 14

NONDESTRUCTIVE TESTING BEING USED ON REI

(Slide 15)

Slide 15 lists some of the NDT techniques being evaluated (a) for in-process inspection and control, (b) for determining flight-worthiness of TPS panels both before and after flight and (c) for use in conjunction with repair or refurbishment of damaged or degraded TPS panels. Radiography, in particular, has been found to be a very effective tool for monitoring the results of efforts to upgrade the manufacturing cycle from a panel uniformity standpoint and in following potential degrading of the panels during entry simulation testing.

Slide 15 shows a radiograph produced by a technique called slit radiography. It was taken on mounted REI-Silica panel which was thermally cycled. Some evidence of the high resolution achieved is given by the sharp line produced by the fine thermocouple wire running across the honeycomb.

NONDESTRUCTIVE TESTING BEING USED ON REI

- RADIOGRAPHY
  - DETECTION OF CRACKS
  - INCLUSION
  - DENSITY VARIATIONS
  - BOND DEFECTS
- DIELECTRIC CONSTANT/LOSS TANGENT
  - MOISTURE CONTENT
  - VARIABILITY COATING THICKNESS
  - DEGREE OF CURE
- MICROWAVE REFLECTOMETRY
  - COATING DEFECTS
- ULTRASONIC (PULSE ECHO)
  - BOND DEFECTS
- ACOUSTIC RESONANCE
  - REI AND BOND DEFECTS
  - PANEL SUBSTRATE UNBONDS

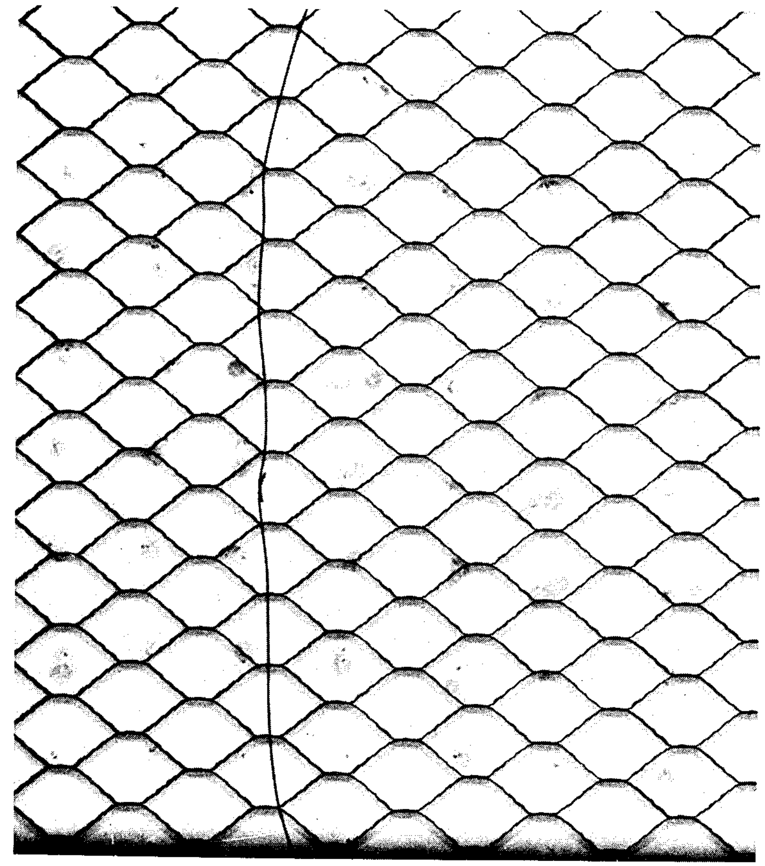

RADIOGRAPH OF THERMALLY CYCLED REI PANEL AND SUBSTRATE BY SLIT RADIOGRAPHY

Slide 15

REI SYSTEMS SCREENING TEST

(Slide 16)

A screening test program was devised to determine the thermal-structural performance of both coated and uncoated panels of the candidate REI materials under simulated shuttle service conditions. The basic specimens tested consisted of 0.1 x 0.2 x 0.025 meter (4 x 8 x 1 inch) REI panels adhesively bonded to aluminum alloy plates. The specimen geometry was selected to analytically simulate the edge conditions which exist in a shuttle panel and also to have sufficient length to achieve plane section geometry in the center of the specimen. Thus this specimen, under thermal and structural loads, simulates the two basic potential failure modes, namely, cracks occurring normal to the insulation surfaces and delaminations parallel to the surfaces.

The screening criteria used in this program are listed in Slide 16. Also the cycle used in the entry simulation tests is contrasted with the surface temperature history for a point on the body of the NR orbiter. The longer exposure to constant peak surface temperatures in the simulated entry tests permits greater definitization of the temperature level effects on material behavior.

REI SYSTEMS SCREENING TEST

- OBJECTIVE
  - DETERMINE IF SELECTED CANDIDATE TPS SYSTEMS MEET CRITICAL SHUTTLE REQUIREMENTS
- SCREENING CRITERIA
  - DEMONSTRATE REI/AIRFRAME COMPATIBILITY
    - ORBITAL COLD SOAK
    - RE-ENTRY HEATING
    - AIRFRAME STRAIN
  - DEMONSTRATE COATING WATER REPELLANCY
- TEST SPECIMENS
  - DESIGNED TO DUPLICATE MID-PANEL STATE OF STRESS OF FULL SIZE PANELS 0.1 x 0.2 x 0.025 m (4 x 8 x 1 in.)
    - BONDED TO 0.003 m (0.125 in.) THICK ALUMINUM ALLOY TEST BAR

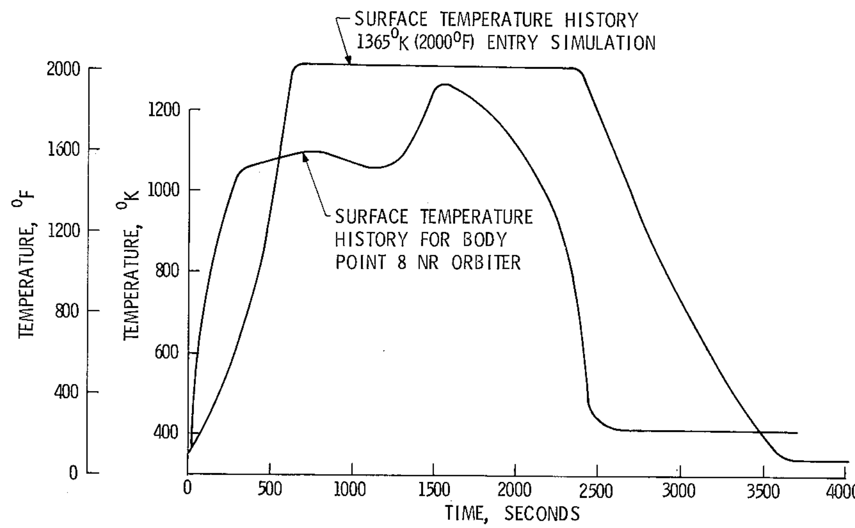

SURFACE TEMPERATURE HISTORY

Slide 16

ENTRY SIMULATION TESTING

(Slide 17)

Slide 17 illustrates the test equipment used in the entry simulation test program. Quartz encapsulated silicon carbide electrodes are used to heat the surface of the specimen to the desired temperature. To achieve the correct temperature distribution through the 0.025 meter (1 inch) thick sample, a water cooled plate is attached to the back of the aluminum support plate. The entire test assembly is then placed in a vacuum chamber so that the test can be carried out at reduced pressure ($10^3 kN/m^2$ or 10^{-2} atmospheres). The last picture in the slide shows a specimen after cyclic testing.

ENTRY SIMULATION TESTING

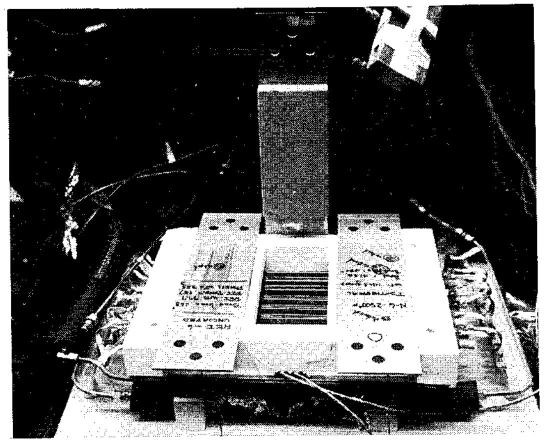

TEST FIXTURE AND SPECIMEN

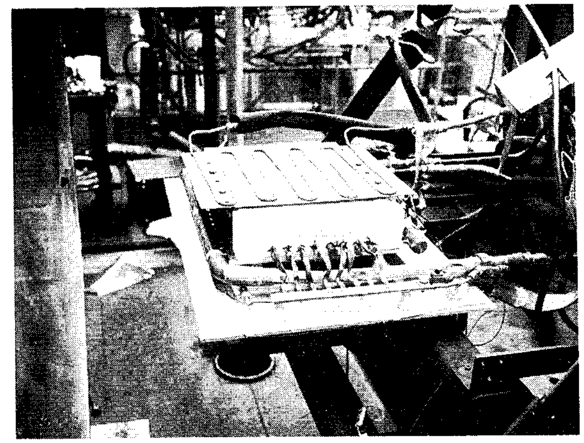

COLD PLATE

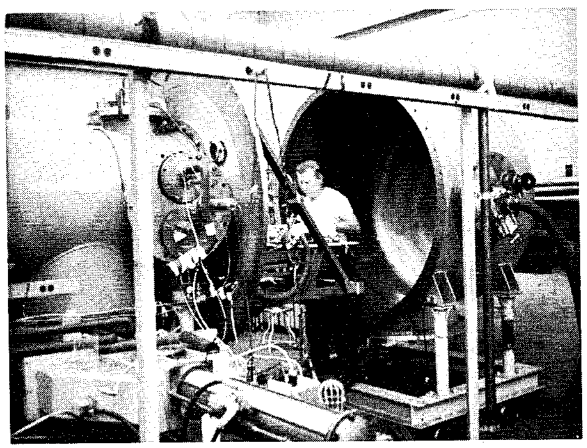

TEST SIMULATOR CHAMBER

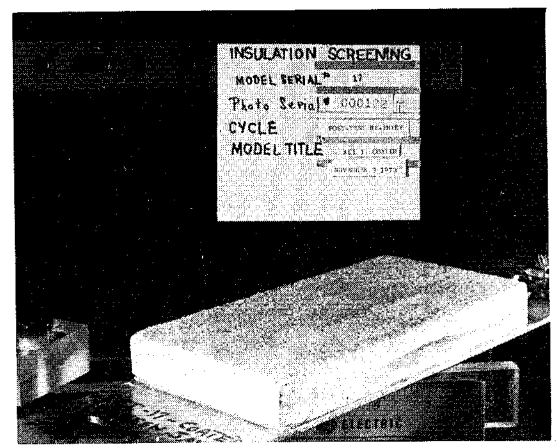

REI SAMPLE - POST TEST

Slide 17

LOAD-STRAIN COMPATIBILITY TEST - REI-SILICA

(Slide 18)

The load-strain compatibility between the bonded insulation panel and aluminum structure was evaluated by testing specimens of the same design as those used for entry simulation testing. The specimen was loaded to levels representative of the limit loads for the aluminum structure and the insulation panel was examined for cracks. The data reported in Slide 18 show that REI-Silica has more than adequate strain-to-failure capability to meet these expected limit loads.

Similar tests are now being conducted on specimens after each 5 cycles of entry simulation testing to determine to what extent the REI-Silica strain capability degrades with cyclic temperature exposure.

LOAD STRAIN COMPATIBILITY TEST

REI - SILICA

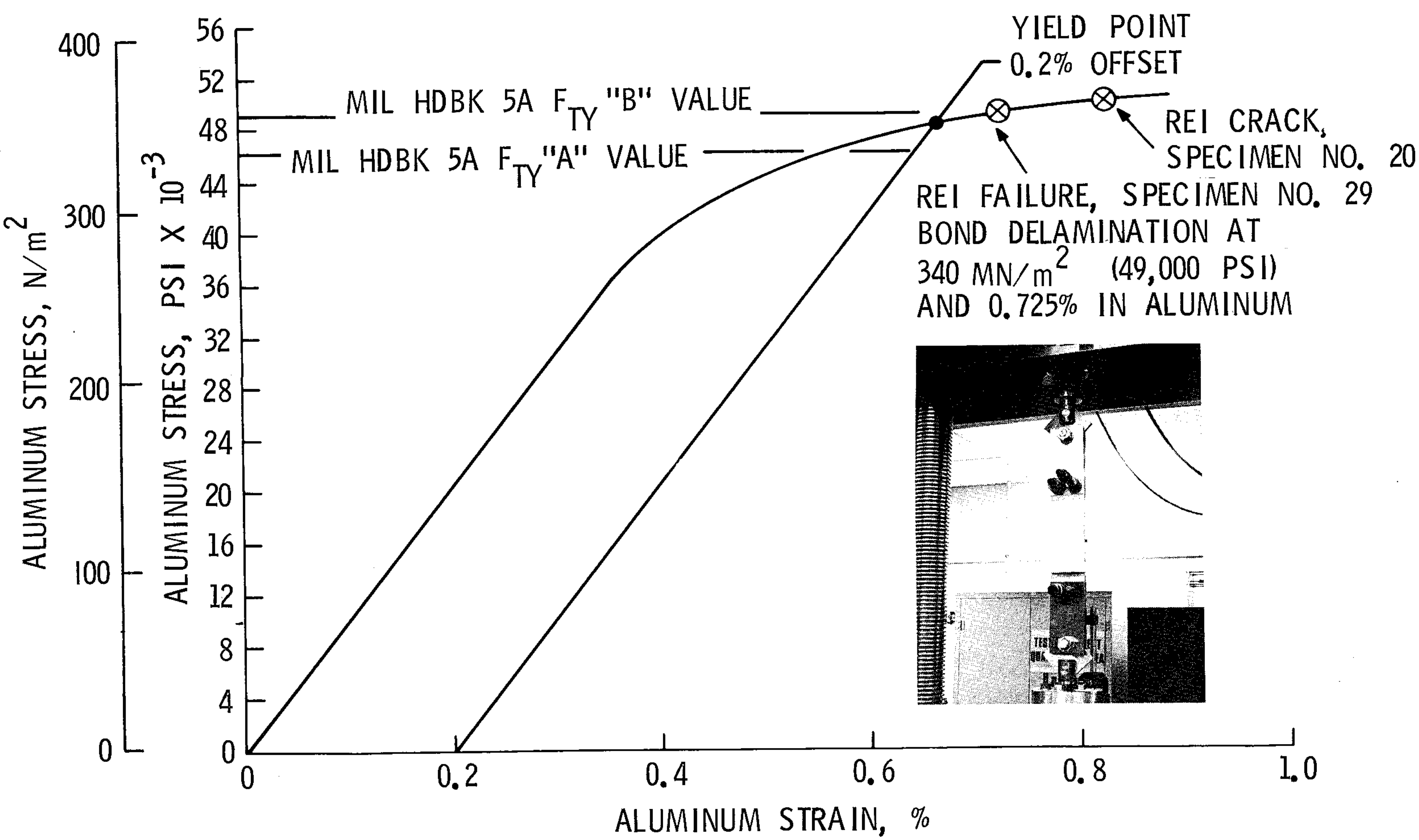

Slide 18

PLASMA ARC TESTS

(Slide 19)

A series of plasma arc ground tests were performed in the GE-RESD 5 MW plasma arc facility to evaluate the ablation performance of coated REI-Silica in a simulated orbiter entry environment. Slide 19 shows the test model configuration and lists the test conditions and test results for three of the tests. These data indicate that the relatively low aerodynamic shear forces of shuttle entry are not an important factor even in an over temperature condition in the design of a REI thermal protection system.

PLASMA ARC TESTS

TEST OBJECTIVE :

EVALUATE PERFORMANCE OF COATED REI-SILICA UNDER SIMULATED RE-ENTRY HEATING CONDITIONS, WITH APPROPRIATE COMBINATIONS OF AERO SHEAR, SURFACE TEMPERATURES, AND AVAILABLE OXYGEN.

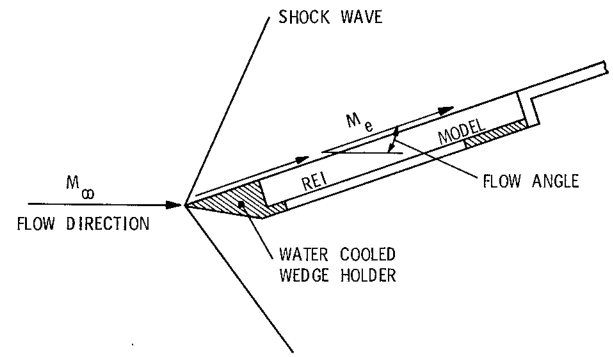

MODEL #	SURFACE TEMPERATURE, ^oK (^oF)	RUN TIME, SECS.	AERO SHEAR N/m^2 (lbs/ft^2)	RESULTS
2	1700 (2600)	120	139 (2.9)	NO EVIDENCE OF COATING REMOVAL
3	1420 -1535 (2100 - 2300)	1200	71.8 (1.5)	COATING WATERPROOF
4	1475 - 1590 (2200 - 2400)	1200	71.8 (1.5)	AFTER 3 CYCLES, COATING PERMITTED H_2O PENETRATION AT MICRO CRACKS

Slide 19

REI TPS PANEL WEIGHT

(Slide 20)

This complete REI thermal protection system will consist of a coated panel which is adhesively bonded to a metal plate. Slide 20 compares typical weights for REI materials with and without coating and bonding for 2000 second entry at body point 8 on the NR delta wing orbiter. Even though coating and bonding does increase the TPS weight to some degree, the TPS weight values indicated for either a titanium or aluminum support structure are still comparatively low compared with other candidate systems.

REI TPS PANEL WEIGHT

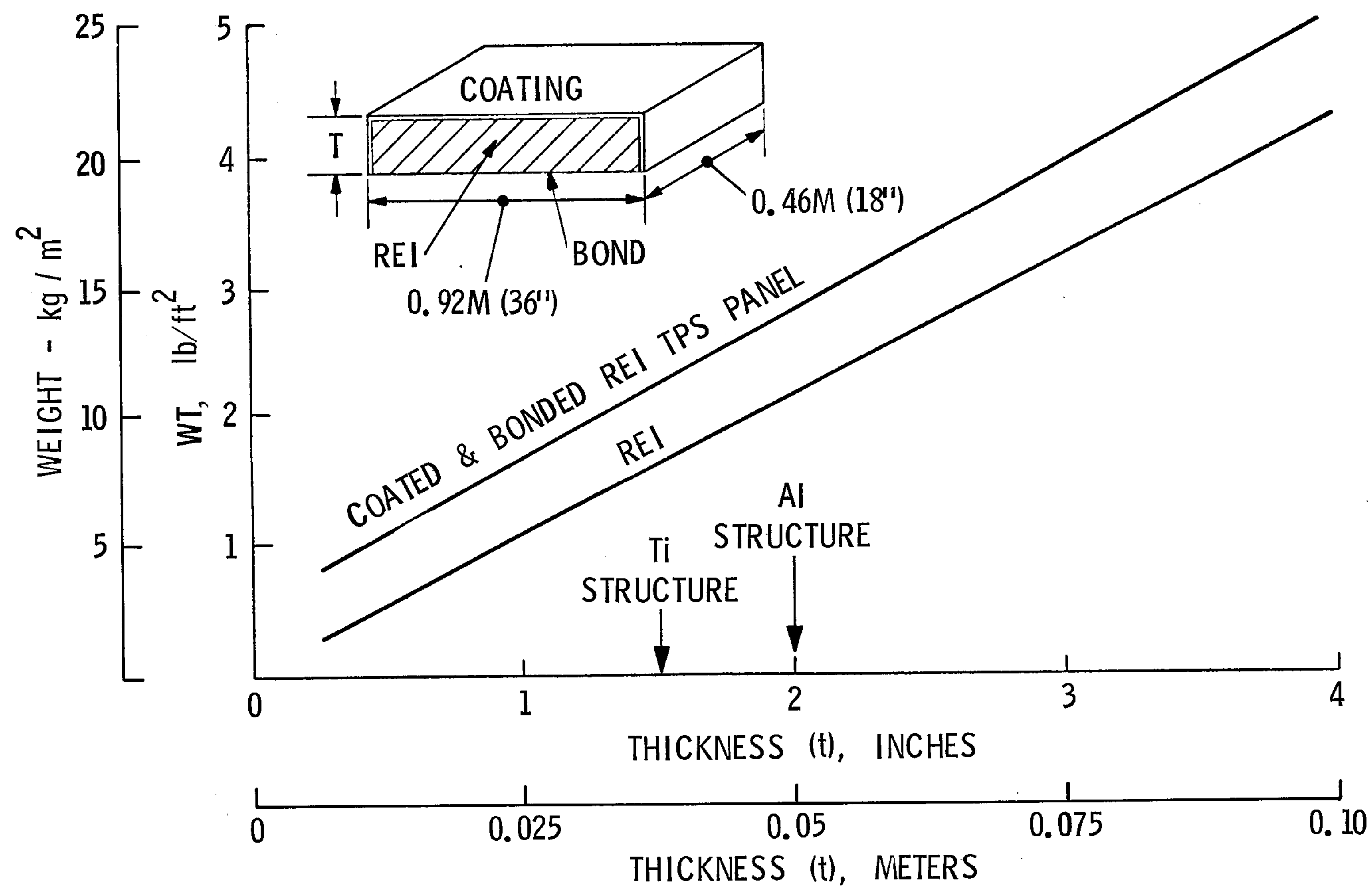

Slide 20

TYPICAL REI THERMAL PROTECTION SYSTEM DESIGNS

(Slide 21)

The two approaches or concepts for attaching coated REI panels to the orbiter vehicle shown in Slide 21 have been considered in detail. The first concept assumes that the air frame construction is conventional with a continuous outer skin to which the REI is attached. In this approach, the coated REI panels are bonded directly to the outer surface of the structure. Although the panel dimensions will be variable and dependent on curvature and geometry constraints, it appears that panels as large as 0.46 by 0.92 meters (18 by 36 inches) are feasible to install.

The second approach involves the use of large modular structural panels. In this design, the coated REI would be attached to the major area of the panel in the same manner as discussed above. However, it would be necessary to make provisions at the periphery of the panels for access to fasteners. A method for providing this access is shown in the drawing.

TYPICAL REI THERMAL PROTECTION SYSTEM DESIGNS

CONCEPT 1

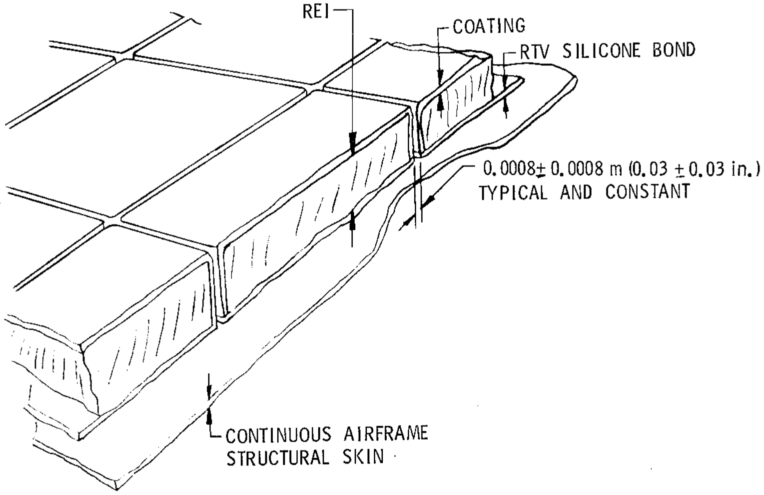

DIRECT BONDING TO
AIRFRAME STRUCTURE

CONCEPT 2

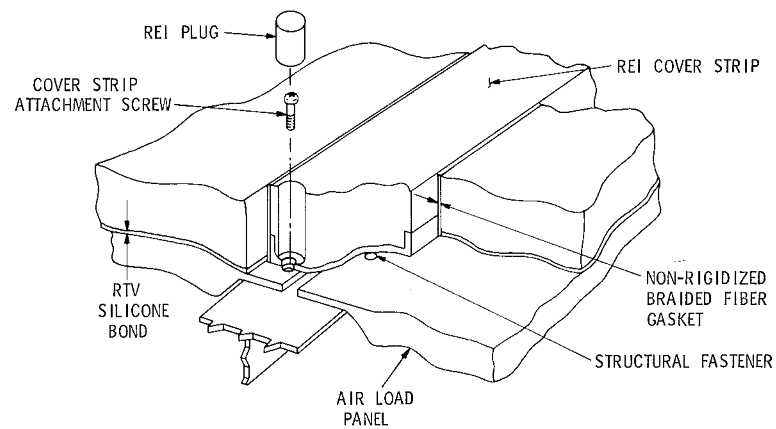

BONDING TO MODULAR
AIR LOAD PANEL

Slide 21

REI USE TEMPERATURE CERTIFICATION

(Slide 22)

Slide 22 shows schematically the approach being used to determine the maximum use temperature capability of the candidate REI materials. Coated and uncoated panels of the type described in Slide 16 are adhesively bonded to aluminum plates. They are then cycled in the entry simulator in the appropriate surface temperature range for a multiple number of cycles. Similar panels unmounted are exposed to constant temperature conditions in the same temperature range for times up to 75 hours. The performance of cyclically tested panels is monitored by subjecting the panels after each 5 cycle exposure to the design limit loads of the aluminum structure and examining the insulation material for tendency to crack. Phase change and shrinkage tendencies are established by X-ray diffraction techniques and dimensional change measurements at appropriate intervals of tests on both types of samples. Comparison of data between panels exposed to both cyclic and isothermal test conditions provides definitive information concerning any potential effects of cyclic testing on property or performance degradation.

Sufficient quantitative data of this type (a) will provide a basis for reliably estimating the maximum service temperature for 100 mission reuse capability for each type of REI material, (b) can be used to estimate service life at higher surface temperatures and (c) will provide information as to compatibility of the coatings and the rigidized insulation materials.

REI USE TEMPERATURE CERTIFICATION

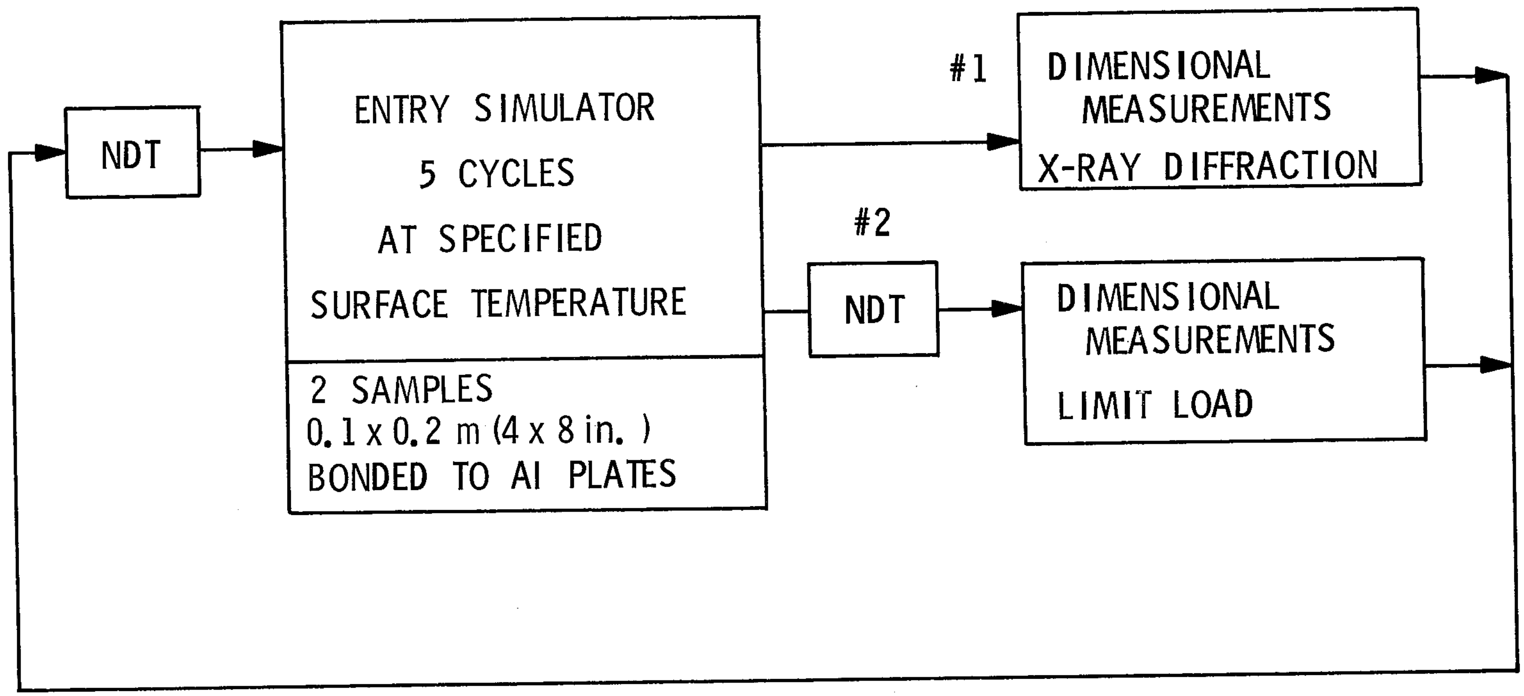

TOTAL CYCLE REPEATED UNTIL
SAMPLE EXPERIENCES STRUCTURAL FAILURE

Slide 22

REI FLIGHT TEST EXPERIMENT

(Slide 23)

The general objective of this activity is to flight test samples of REI materials on USAF experimental flight test vehicles. The specific objectives are (a) to assess the overall performance of REI materials in a representative, transient heat flux, pressure and temperature flight environment and (b) to validate the thermodynamic performance prediction model derived from ground test data for flight environments. Flight test data to be obtained will include both surface and backface temperature response.

Slide 23 shows both a picture of the flight test hardware and a comparison of the aerodynamic heating conditions to be obtained in these flights with those expected for several locations on a shuttle vehicle.

REI FLIGHT TEST EXPERIMENT

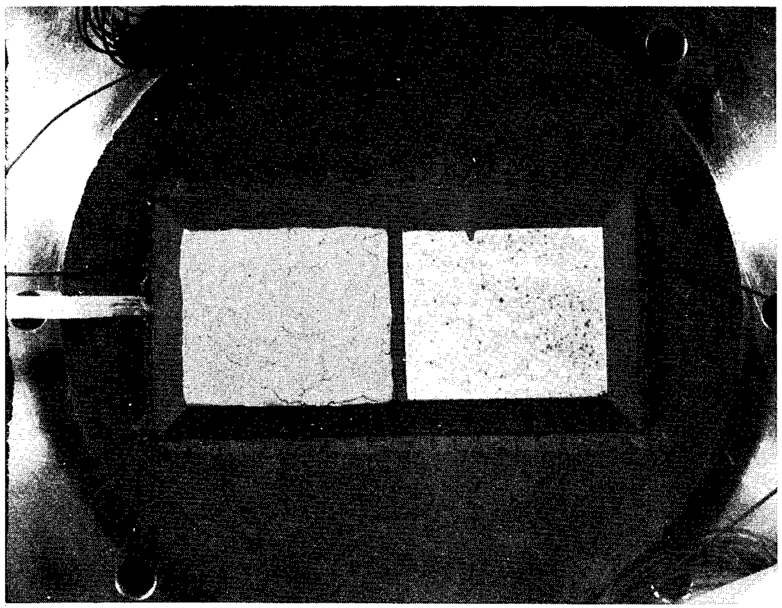

VIBRATION, SHOCK AND ENTRY
TEST HARDWARE

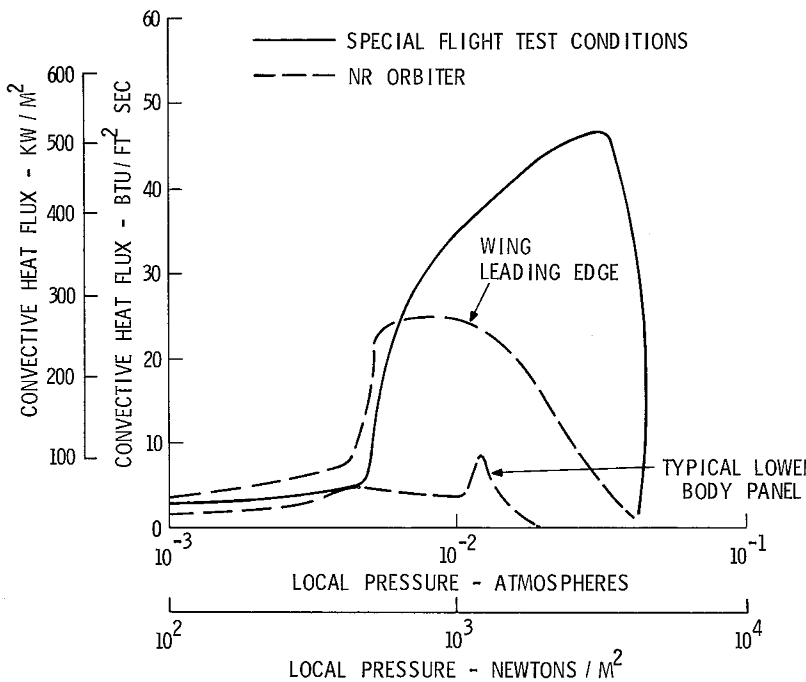

FLIGHT TEST CONDITIONS

Slide 23

SUMMARY OF REI DEVELOPMENT ACCOMPLISHMENTS

(Slide 24)

Much progress has been made toward establishing low density ceramic fiber insulations as viable and competitive candidate thermal protection systems for shuttle orbiter vehicles. REI-Silica and REI-Mullite have been reproducibly fabricated in panel sizes required for full-scale hardware(0.46 x 0.92 meters (18 x 36 inches)). Multimission reuse capability has been demonstrated for both coated and uncoated materials adhesively bonded to representative shuttle structural materials. However, completion of the task of developing these materials to the point where they are fully qualified for use in the thermal protection system on man-rated shuttle orbiter vehicles will require additional development and evaluation activities.

SUMMARY OF REI DEVELOPMENT ACCOMPLISHMENTS

- REI - SILICA
  - REPRODUCIBLE FABRICATION AND COATING OF PANELS UP TO 0.5 X 1.0 METER (18 X 36 INCHES)
  - DEMONSTRATED STRAIN COMPATIBILITY WHEN BONDED TO ALUMINUM
  - MULTI-CYCLE REUSE CAPABILITY TO 1366^{0}K (2000^{0}F) SHOWN (OVER TEMPERATURE CAPABILITY TO 1755^{0}K (2700^{0}F)
  - FLIGHT TEST EXPERIMENT SCHEDULED
- REI - MULLITE
  - REPRODUCIBLE FABRICATION OF PANELS TO 0.5 X 1.0 METER (18 X 36 INCHES)
  - ALL MULLITE SYSTEM WITH COMPATIBLE COATING STABLE TO 1644^{0}K (2500^{0}F)
  - FLIGHT TEST EXPERIMENT SCHEDULED
- REI - ZIRCONIA
  - SELF-SINTERED MATERIAL EVALUATED IN ENTRY SIMULATION TESTS
  - FLIGHT TEST EXPERIMENT SCHEDULED
  - GRADED REI - ZIRCONIA / REI - MULLITE SYSTEMS FABRICATED
- NDT TECHNIQUES FOR IN-PROCESS AND COMPONENT INSPECTION SELECTED
- TAILORED SILICONE ADHESIVE BONDS IN DEVELOPMENT FOR EACH INSULATION SYSTEM
- CONCEPTS FOR APPLYING REI - TPS TO NR ORBITER DEVELOPED

Slide 24

ADDITIONAL REQUIRED PROGRAMS

(Slide 25)

Definition of an REI TPS which is considered to be fully qualified for use on shuttle orbiter vehicles will require additional development and evaluation efforts. These will include (a) establishing the range of applicability of the candidate material system(s) under orbiter entry conditions, with appropriate design constraints, (b) development of improved coatings from an insulation compatibility moisture pickup, rain and dust erosion and emittance standpoint, (c) obtaining adequate statistical property data for design purposes, (d) development of adhesive bonding systems with tailored properties to assure good insulation-structure strain compatibility and (e) demonstration of adequacy of design through testing of full scale coated and bonded panels. The above are required but it would also be appropriate to achieve performance improvements through insulation weight minimization by establishing the best iterative compromise between thermal efficiency, mechanical properties and service life.

To achieve a high degree of cost effectiveness, it will also be necessary to give consideration to simplification of panel fabrication process through automation and/or continuous processing. Also effective repair and refurbishment techniques must be established, and NDT techniques must be selected for evaluation and recertification of the TPS on an orbiter prior to each flight.

ADDITIONAL REQUIRED PROGRAMS

- MAXIMUM USE TEMPERATURE CERTIFICATION FOR 100 MISSIONS WITH BONDED AND COATED PANELS
- COATING MATERIAL IMPROVEMENT AND EVALUATION
- DESIGN APPLICATION AND FULL-SCALE COMPONENT TESTING
- NONDESTRUCTIVE TEST PROCEDURE CERTIFICATION
- GAP SEALANT DEVELOPMENT
- PERFORMANCE IMPROVEMENT THROUGH WEIGHT MINIMIZATION, SUPPLEMENTAL REINFORCEMENT AND / OR GRADING
- REI PANEL PRODUCTION, PROCESS SIMPLIFICATION AND STATISTICAL DESIGN DATA ACCUMULATION

Slide 25

METALLIC HEAT-SHIELD MATERIALS FOR SPACE SHUTTLE

By

Robert W. Hall
NASA Lewis Research Center
Cleveland, Ohio

INTRODUCTION

The purpose of this presentation is to indicate the current status of metallic heat-shield materials being investigated for use on the space shuttle. It is primarily a progress report on the technology program administered by the Space Shuttle Structures and Materials Technology Working Group. Materials for thermal protection systems (TPS) will be emphasized rather than heat-shield design or evaluation because it is in the materials area that the most progress has been made to date.

PAPER 3

METALLIC TPS MATERIALS

(Slide 1)

The metallic materials of interest for the space shuttle's thermal protection system are listed in the first slide, along with an estimate of their maximum-use temperature. For most of these candidate materials, the maximum-use temperature and reuse capability have not yet been firmly established. Generation of the data necessary to establish such limits is an important part of the materials technology program for thermal protection systems.

The column on the right shows an estimate of the orbiter area below the corresponding maximum-use temperature. It is evident that heat shielding for most of the orbiter's surface area could be provided by titanium alloys and nickel- and cobalt-base superalloys. A large background of experience with these materials is available in the aerospace industry.

For temperatures above about 1000°C, less proven materials such as dispersion strengthened NiCr (TD-NiCr) and coated refractory metals are the prime metallic heat-shield material candidates. Some pertinent experience with these materials already exists in the aerospace industry. For example, TD-NiCr has been extensively evaluated for turbine vanes and flame holders in advanced turbojet engines. Coated columbium was successfully used in the Air Force's ASSET reentry vehicle. In this respect, the technology of these alloys is significantly more advanced than that of the non-metallic materials currently baselined for portions of the shuttle TPS. Studies are currently underway to provide the additional property information, fabrication experience, and simulated reentry testing necessary to assess the applicability of these newer metallic materials for use in space shuttle heat shields.

METALLIC TPS MATERIALS

MATERIAL	APPROX MAX-USE TEMP, ^{o}C	APPROX ORBITER AREA BELOW MAX-USE TEMP, %
TITANIUM	480	25-50
SUPERALLOYS	1000	65-90
DISP STR NiCr	1150	85-95
COATED COLUMBIUM	1300	90-98
COATED TANTALUM	1500	95-98

Slide 1

SUPERALLOY TPS TECHNOLOGY PROGRAM
(Slide 2)

Because of the large background of experience with nickel- and cobalt-base superalloys, relatively little additional effort on these materials was deemed necessary in the space shuttle technology program. A limited program is being conducted to provide design data for thin gage sheet of the alloys of prime interest and to establish the reuse capability of these materials for heat shields. Current contractual programs in this area are listed in the slide.

The Battelle program on design allowables has resulted in the compilation of a substantial amount of existing data on properties of Hastelloy X, Inconel 718, L605, and René 41. However, it is apparent that there will be significant gaps in the desired data and that additional testing will be required.

The program on degradation and reuse of radiative TPS materials emphasizes coated refractory metals but lesser attention is being given to the cobalt alloys HS25 and HS188. No definitive results from the superalloy portion of this program are available yet.

SUPERALLOY TPS TECHNOLOGY PROGRAM

DESIGN ALLOWABLE STRENGTH PROPERTIES OF ELEVATED	BATTELLE
TEMPERATURE ALLOYS	NAS8-26325
HASTELLOY X, INCONEL 718, L605, RENÉ 41	
HIGH TEMPERATURE EMISSIVITY MEAS.	LOCKHEED
	NAS8-26304
DEGRADATION & REUSE OF RADIATIVE TPS MATERIALS	BATTELLE
HS25, HS188	NAS8-26205

Slide 2

EFFECTS OF MULTIPLE REENTRY ON CREEP OF RENÉ 41
(Slide 3)

Although this presentation deals primarily with studies funded by NASA as part of the space shuttle technology program, some unpublished results of an in-house funded program conducted by J. W. Davis at the McDonnell Douglas Corporation on the effects of multiple reentry cycling on the reuse of René 41 are included here to illustrate a potentially significant problem area. In his work, Davis subjected thin gage sheet tensile specimens of René 41, HS188, and TD-NiCr to repeated stress-temperature-pressure profiles simulating reentry. He measured the resultant creep deformation and compared this with the creep predicted from the best available data from conventional constant load, constant temperature creep tests. Such a comparison for René 41 specimens which had been aged at 760°C before test is shown on the slide. Similar results were observed for the other two alloys in their proposed use temperature range.

The tests indicated that excessive creep deformation can occur during repeated reentry cycling at loads lower than predicted from available creep data. The reasons for this behavior are not entirely clear at this time. Electron microprobe analysis of the tested specimens indicated, however, that René 41 had experienced a depletion of chromium, aluminum, and titanium. These results indicate the need for simulated service testing as a basis for design of superalloy heat-shield panels which must withstand repeated reentry. Previous estimates of the temperature or stress limits for some materials may need to be revised downward.

EFFECT OF MULTIPLE REENTRY ON CREEP OF RENÉ 41

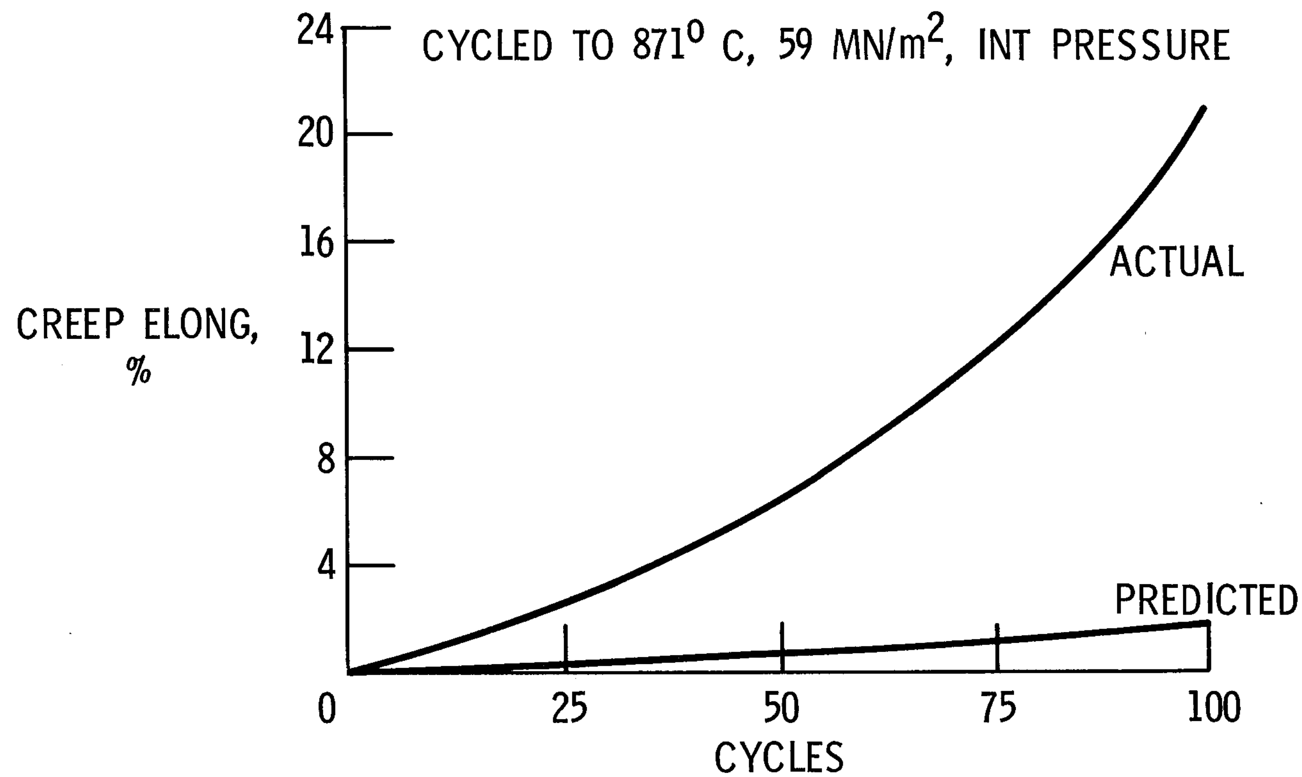

Slide 3

TECHNOLOGY PROGRAM FOR Ni-Cr-ThO_2 SHEET
(Slide 4)

Dispersion strengthened nickel-chromium alloys such as Ni-Cr-2ThO_2 are promising candidates for the temperature range above the maximum limit for superalloys ($\sim 1000^{\circ}C$) and below that where coated refractory metals are required for strength considerations ($\sim 1200^{\circ}C$). The prime advantage of this class of materials over coated columbium for use in this intermediate temperature range is their greatly superior oxidation resistance in the uncoated condition. They also offer good potential for weight and cost savings over coated refractory metals in their applicable temperature range.

Only one Ni-Cr-ThO_2 alloy (Fansteel's TD-NiCr) is commercially available at this time. Although this material holds much promise, its technology was not sufficiently advanced for immediate application to space shuttle heat shields. Therefore a program to develop the required technology has been initiated. Its major elements are shown in the slide.

As will be discussed later, this program also includes an exploration of alloy modifications to improve the properties of this class of materials.

TECHNOLOGY PROGRAM FOR Ni–Cr–ThO_2 SHEET

1. IMPROVE SHEET MANUFACTURING PROCESS
   - THINNER GAGES (0.51 → 0.25 mm)
   - WIDER SHEETS (457 → 610 mm)
   - IMPROVE QUALITY CONTROL & REPRODUCIBILITY
   - IMPROVE HIGH TEMP DUCTILITY
2. DEVELOP ALTERNATE SHEET MANUFACTURING PROCESS
3. DEVELOP IMPROVED PANEL FABRICATION PROCESSES
   - SHEET FORMING
   - JOINING
4. DETERMINE DESIGN ALLOWABLE PROPERTIES
5. DETERMINE EFFECTS OF REENTRY CONDITIONS

Slide 4

PROGRESS IN TD-NiCr PROCESSING PROGRAM

(Slide 5)

Over the last eight months under the NASA-sponsored program, significant progress has been made by the manufacturer of TD-NiCr (Fansteel) in improving both the manufacturing process and the quality of the TD-NiCr supplied. Improvements in the sheet manufacturing process have resulted in higher process yields, better gage control and surface finish and, most importantly, more consistent properties from sheet to sheet. Accompanying these process improvements, a significant improvement in high temperature ductility has been achieved, along with slight increases in strength. These property improvements are due primarily to better control of texture, grain size, etc.

About 200 kilograms of sheet has been delivered to NASA Centers to support their heat-shield fabrication and evaluation programs. These programs will better establish the future role of Ni-Cr-ThO_2 alloys for space shuttle heat shields.

Although the basic Ni-Cr-ThO_2 alloy looks very promising, it is probable that its properties, especially high temperature ductility and oxidation resistance in a high velocity air stream, can be improved by alloying. As part of the technology program at Fansteel, alloy modifications are being explored. A Ni-16Cr-3.5Al-2ThO_2 alloy has been found to possess superior oxidation resistance under simulated reentry conditions and is currently being scaled up for comparison with unmodified TD-NiCr.

PROGRESS IN TD–NiCr PROCESSING PROGRAM

PROCESS IMPROVEMENTS

1. HIGHER YIELDS (~20% → 40%)
2. BETTER GAGE CONTROL (±0.05 mm → ±10%) (±0.002 IN. → ±10%)
3. BETTER SURFACE FINISH (35 RMS → <16 RMS)
4. IMPROVED REPRODUCIBILITY (MORE CONSISTENT PROPERTIES)

PROPERTY IMPROVEMENTS

1. INCREASED HIGH-TEMP DUCTILITY (1% → 4% ELONG - 1093^{0} C)
2. SLIGHT INCREASES IN RT & ELEVATED TEMP STRENGTH

SHEET PRODUCTION

1. 200 kg SHEET DELIVERED TO NASA CENTERS

ALLOY MODIFICATIONS

1. ALLOY SCREENING STUDIES IN PROGRESS
2. SCALE-UP OF Ni-16Cr-3.5 Al-2ThO_2 STARTED

Slide 5

ARC JET OXIDATION TESTS

(Slide 6)

TD-NiCr's reputation for excellent oxidation resistance at high temperatures was based on the results of static furnace tests. Since the protective oxide which forms, Cr_2O_3, has an appreciable vapor pressure above 1000°C, a potential problem of enhanced oxidation under shuttle reentry conditions was recognized. This problem area has been investigated at the Ames, Langley and Lewis Research Centers. The results of arc jet tests at Ames typify the observed behavior.

In a high velocity air stream at 1204°C and 15 torr pressure, TD-NiCr does indeed oxidize much more rapidly than in static furnace tests. The curves shown are based on weight loss measurements. Based on such measurements, the calculated metal recession for TD-NiCr is not excessive; only about 0.017 mm (0.65 mil) after 50 cycles, each of 30-minute duration at 1204°C. However, post test metallographic examination of the Ames specimens at the Lewis Research Center indicated that the actual metal consumption was much greater, approximately 0.05 mm (2.0 mils). For very thin, light weight heat shields, this amount of metal loss might be excessive.

Note that the experimental alloy, TD-NiCrAlY, showed greatly superior oxidation resistance under these test conditions. Its measured surface recession after forty 30-minute cycles was only 0.02 mm (0.8 mil).

ARC JET OXIDATION TESTS

1204° C; 15 TORR; ENTHALPY 6.7 MJ/kg (2900 BTU/LB); MACH 3.6

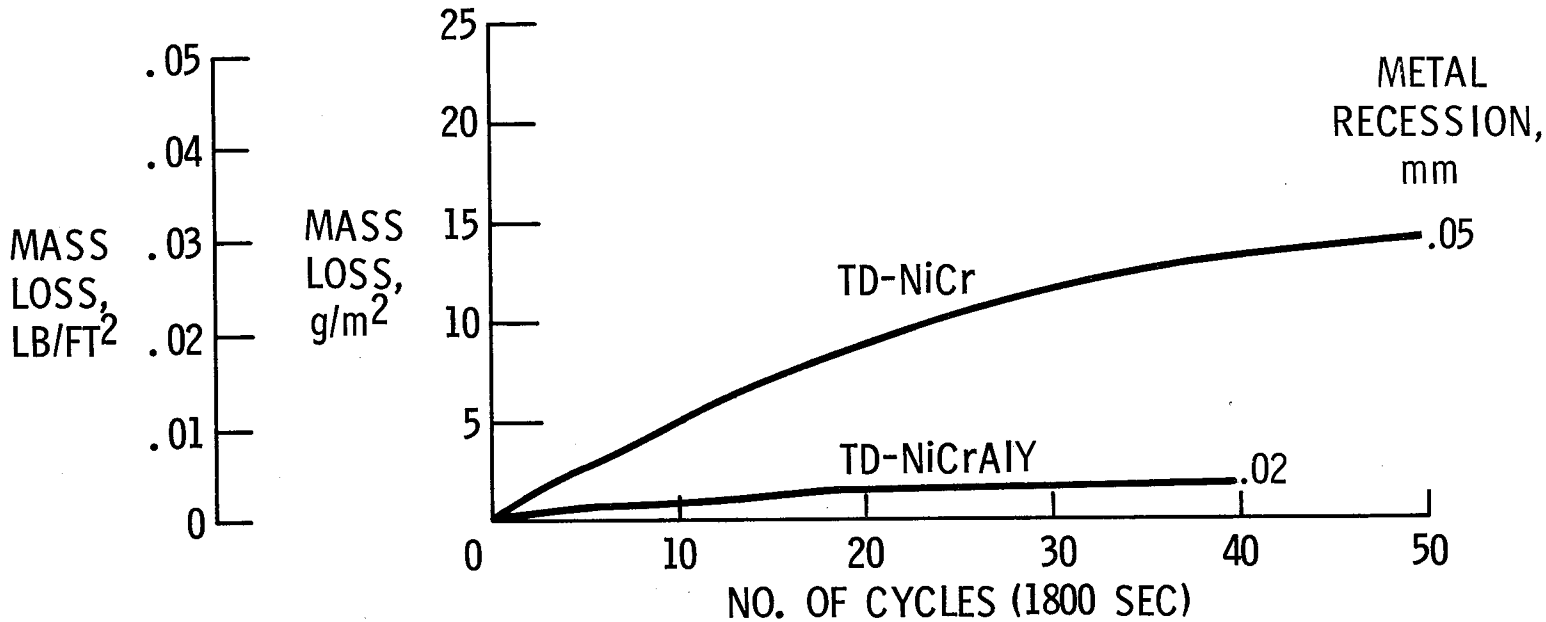

Slide 6

POROSITY IN TD-NiCr AFTER ARC JET TESTS
(Slide 7)

Metallographic examination of 0.30 mm (12 mil) thick sheet specimens of TD-NiCr after 50 one-half hour cycles to 1204°C in the Ames arc jet facility revealed severe porosity through the entire thickness of the sheet. X-ray diffraction measurement of lattice parameters indicated that the chromium content at the surface had been reduced from 20 percent to only 11 percent. This is believed to result from vaporization of CrO_3.

The metallographic results confirmed the superior oxidation resistance of TD-NiCrAlY at 1204°C. Only a few pores developed during forty arc jet cycles. These do not appear to have resulted from surface vaporization. No decrease in Cr content of the surface was indicated by the X-ray analysis. The Al_2O_3 scale which forms during oxidation of this alloy appears to effectively inhibit chromium vaporization.

The effects of the porosity developed in TD-NiCr during simulated reentry heating on the properties of the material must be determined. Arc jet tests of large sheet specimens whose mechanical properties will be measured after exposure are currently underway at the Ames Research Center. However, it appears now that 1200°C is too high a temperature to achieve the desired 100-mission reuse capability with TD-NiCr. A maximum-use temperature of 1150°C may be achievable. In view of the excellent oxidation resistance of TD-NiCrAlY at 1200°C under simulated reentry cycling, increased emphasis on the development and characterization of this alloy appears warranted in the space shuttle technology program.

ARC-JET EXPOSURE OF TWO TPS ALLOYS

1204° C; 15 TORR; 1 CYCLE = 30 MIN AT TEMP

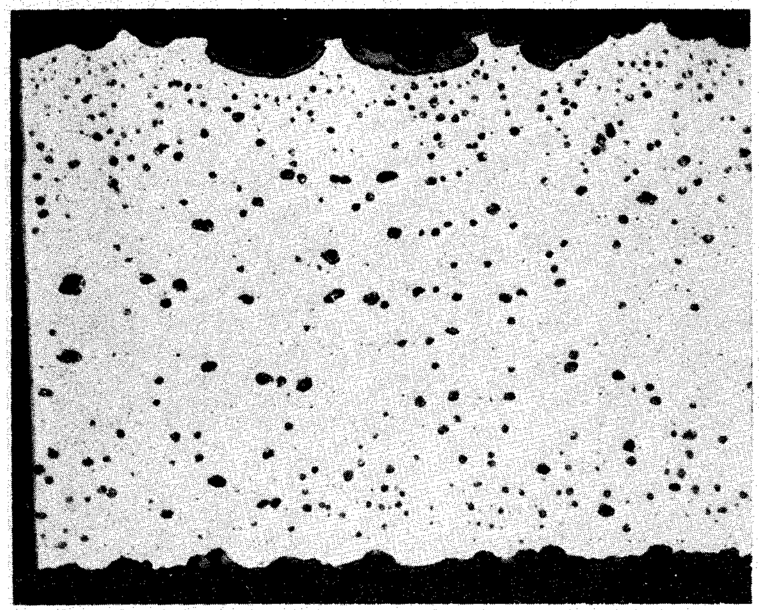

TD-NiCr
50 CYCLES

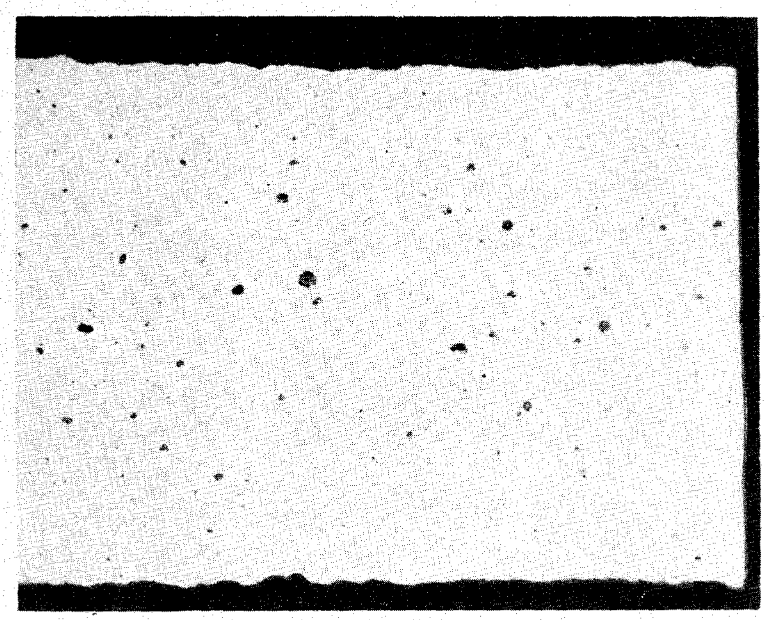

TD-NiCrAlY
40 CYCLES

CS-57737

Slide 7

TECHNOLOGY PROGRAM FOR COATED Cb TPS

(Slide 8)

Fused slurry silicide coated Cb alloys are prime candidates for metallic thermal protection systems for use in the temperature range $1100^{o}C$ to $1300^{o}C$. Two commercial coatings are available with good potential for meeting shuttle requirements: the R512E (Si-20Cr-20Fe) coating developed by Sylvania under Air Force sponsorship, and a proprietary coating, VH109, developed by the Vac Hyd Corporation. The leading columbium alloy candidates include the moderate strength, highly fabricable alloys such as FS85, Cb752, and C129Y.

During the last six months a major in-house and contractual program to provide the required technology to permit the use of coated Cb alloys in space shuttle heat shields has been initiated. The major elements of this program are indicated on the slide. Since the program is still in its early stages, little significant information is available at this time. The initial results of coating evaluation on small test specimens confirms the good oxidation resistance and consistent performance of the fused slurry silicide coatings.

In tests involving repeated thermal cycling of coated test specimens under simulated shuttle reentry conditions, few coating failures have been observed at fewer than 100 simulated reentry cycles. The few failures observed have almost all been located at edges of specimens. This suggests the need for more stringent process control to assure that edges are uniformly coated with a sufficiently thick coating.

TECH PROGRAM FOR COATED Cb TPS

ESTABLISH TPS PERFORMANCE REQUIREMENTS

SELECT & CHARACTERIZE BEST COATING/Cb ALLOY SYSTEM

SCALE-UP COATING PROCESS

DESIGN, FABRICATE, & TEST TPS COMPONENTS & FULL SIZE PANELS IN SIMULATED REENTRY ENVIRONMENT

ESTABLISH REUSE CAPABILITY

DEVELOP NDT & DEFECT REPAIR PROCESSES

PROJECT SYSTEM PERFORMANCE & COSTS

Slide 8

YIELD STRENGTH OF R512E COATED Cb-752
(Slide 9)

For heat-shield design, the effects of the coating on the properties of the substrate must be known. Such data are currently being generated. Initial results from McDonnell Douglas under the NASA sponsored program on fused slurry silicide coatings for columbium are shown on the slide. Yield strength data as a function of temperature are shown for the as-coated system and after 50 to 100 simulated reentry cycles to 1316°C. In addition, defected samples were evaluated.

The results show that some reduction of strength as a result of interdiffusion between the coating and substrate does occur. However, the effect is not unduly large. Elongation measurements indicated no embrittlement resulting from such interdiffusion.

Significantly, specimens which were intentionally defected and then subjected to five or ten reentry cycles showed no catastrophic loss of strength or embrittlement due to oxidation, and none of the tensile failures occurred through the defected areas.

YIELD STRENGTH OF R512E COATED Cb–752

BASED ON ORIGINAL SUBSTRATE CROSS SECTION PRIOR TO COATING

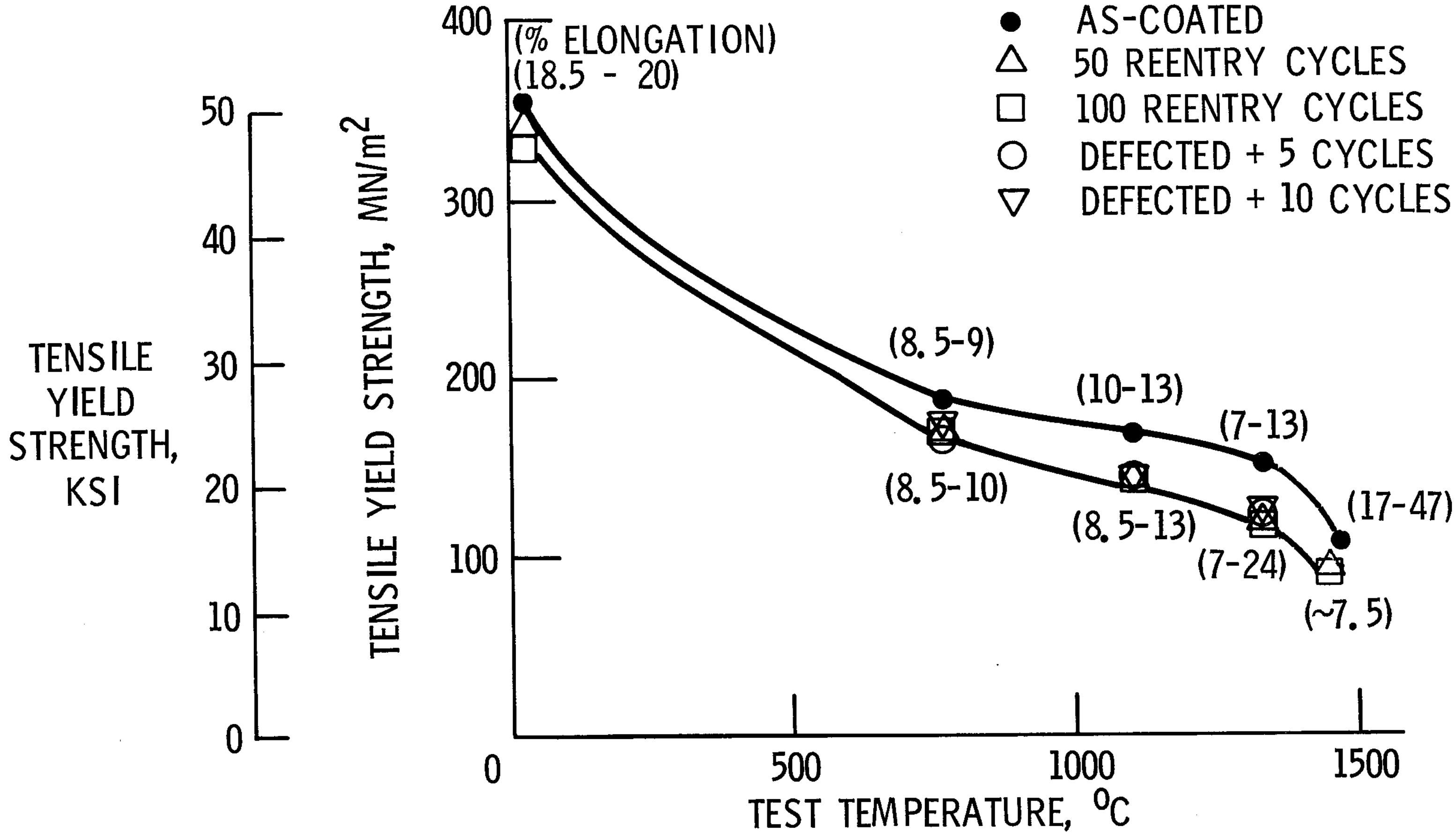

Slide 9

TECHNOLOGY PROGRAM FOR COATED TANTALUM TPS
(Slide 10)

Coated tantalum alloys are of interest for possible use in space shuttle thermal protection systems in the temperature range 1300°C to about 1500°C. Relatively small areas, mainly leading edges and control surfaces, are likely to encounter temperatures in this range during reentry.

Coatings technology for tantalum is much less advanced than for columbium. The best fused slurry silicide coating for tantalum available at the start of the shuttle technology program appeared to have reuse capability for only eight or ten missions under reentry cycling to 1425°C. The purpose of the present technology program is to develop improved coatings, hopefully to meet a goal of 100-mission capability at 1500°C or higher.

Two contractors, Solar (NAS 3-14315) and Lockheed (NAS 3-14316) are about six months into the coating development effort. Although their approaches are somewhat different, both contractors are investigating silicon-rich slurries which depend on the presence of a liquid phase during part of the coating process to assure good coverage.

TECH PROGRAM FOR COATED TANTALUM TPS

OBJECTIVES

DEVELOP IMPROVED COATINGS FOR Ta TPS

ESTABLISH CONTROLLED COATING PROCESS

CONTRACTOR	APPROACH
SOLAR	Si - (Fe, Cr, Ti) EUTECTICS
	Fe - (Mo, W, V, Ti) EUTECTICS + Si
LOCKHEED	METAL EUTECTICS CONTAINING Si

Slide 10

PROGRESS ON TANTALUM COATINGS
(Slide 11)

Both tantalum coating contractors have conducted an extensive screening program in which numerous coating compositions were applied to Ta-10W test specimens. These were subsequently thermally cycled as indicated on the slide. Several coatings have exhibited lives several times longer than the baseline coating, Sylvania's R512C. These preliminary data suggest that a coated tantalum alloy thermal protection system with significant reuse capability in the 1300° to $1500^{\circ}C$ temperature range may be achievable.

Several of the more promising coating systems are currently being more extensively evaluated and their effects on the properties of the substrate determined. If promising results are obtained, one or more coatings will be further optimized and a controlled manufacturing process developed so that full-size Ta heat-shield panels may be coated and evaluated.

PROGRESS ON TANTALUM COATINGS

CYCLE

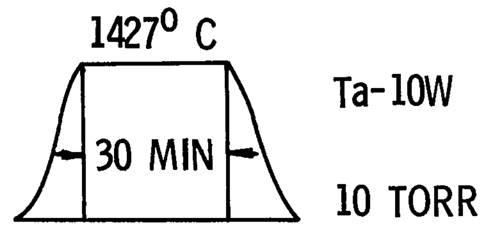

	COATING	CYCLES TO FAILURE
SOLAR	Si-20Fe-10Mo-5Ti-5V	80^+
LOCKHEED	Si-20Mn-27Ti	50, 84, 100^+
	Si-33Co-22Mo	59, 84, 100^+
SYLVANIA	Si-20Ti-10Mo (R512C)	8-10

Slide 11

SUMMARY

In this paper, the current state of the art of metallic materials for space shuttle heat shields is reviewed and recent progress in the space shuttle materials technology program is summarized. The major points of design significance are as follows:

1. Accelerated creep of thin gage sheet of René 41, HS188 and TD-NiCr under multiple reentry cycling conditions has been observed. This effect and the observed degradation in mechanical properties of thin gage sheet under such conditions must be considered in the design of light weight metallic heat shields intended for 100-mission service.
2. Improvements in the manufacturing process for TD-NiCr sheet has made available material with more consistent properties, better gage control and surface finish, and improved high temperature ductility.
3. Severe porosity develops in TD-NiCr sheet when it is cyclically exposed to simulated reentry service in a high velocity heated air stream, as in arc jet testing at 1204°C. An aluminum and yttrium modified alloy, TD-NiCrAlY, exhibits excellent oxidation resistance and develops little porosity under similar conditions.

A major program to further develop and evaluate coated refractory metals for space shuttle heat shields has been initiated. Results of design significance are not yet available from this program.

CREEP OF METALLIC THERMAL PROTECTION SYSTEMS

By Harry G. Harris and Kenneth N. Morman, Jr.

Structural Mechanics Section
Grumman Aerospace Corporation
Bethpage, New York

PAPER 4

SUMMARY

This paper presents the results of an effort to correlate creep analysis with observed creep behavior in Haynes-25 TPS panels under simulated mission environment. An analysis based on the assumption that the TPS material will creep continuously over a total design life of 100 missions (25 hours) without experiencing the effects of the load and temperature interruption of each mission indicated a considerable discrepancy with the test results. An effort to pinpoint the apparent anomaly between theory and experimentation led to a detailed investigation of: 1.) the effect of using different creep theories (the Nadai law and the Pao-Marin theory); 2.) material oxidation during elevated temperature testing; 3.) the effect of residual stresses; 4.) magnitude of biaxial stress effects in the bead; and 5.) the validity of ignoring the effects of periodic loading and heating. The most reasonable correlation with panel test results occurred when the cyclic effect of loading and heating on the material behavior were incorporated into the analysis.

Tests on uniaxial creep coupons indicate that the Haynes-25 material will exhibit nearly the same creep behavior in each mission as the virgin material; for example, there is no memory effect of the temperature and strain history of previous missions. The implications of this cyclic effect, when incorporated into the creep analysis, indicated that the cumulative creep deflections become several times greater than those predicted by an analysis based on a continuous creep time assumption.

The cyclic effect was incorporated into the analysis to predict the cumulative creep deflections of the latest Grumman TPS panel design for Haynes-25. The results show that allowable creep stresses must be limited to levels which accumulate approximately 0.1% creep strain in 25 hours exposure to heat and load in order to meet a maximum 0.5-inch (1.27-cm) permanent deformation per 20 inches (50.8 cm).

INTRODUCTION

The selection of a material for a metallic thermal protection system will be governed by the material's creep properties at elevated temperatures. In order to minimize the penalties due to aerodynamic drag and thermal heating, the successful material must exhibit a minimum amount of permanent creep deformation. Presently, material creep data are obtained under constant stress and temperature conditions. Unfortunately, these experiments yield no information for evaluation of candidate material behavior under cyclic load and temperature environment. What is needed is an extensive test program, supplemented by analytical techniques, to investigate the cyclic behavior of all candidate metallic TPS materials.

A simple engineering analysis which can predict TPS creep deformation subsequent to transient temperature and load application is far from being available. By using a beam model of the TPS panels, two simple digital programs have been formulated. The programs, which utilize beam theory to predict creep deformation and stresses and two different creep theories, yield good correlation with Haynes-25 TPS test panel results. The theory used in one of these programs is capable of predicting the simultaneous action of creep and creep recovery.

A review of metallic TPS technology has recently been presented (ref. 1). In addition, a continuing effort under the Grumman IRAD program has focused on the development of reusable metallic TPS systems for Shuttle Applications (refs. 2 and 3). The present study which is part of this program is the outgrowth of initial attempts to correlate TPS panel creep test data with analysis.

STATEMENT OF THE CREEP PROBLEM (FIGURE 1)

Consideration of the results shown in figure 1 indicates the large discrepancy which was encountered in an attempt to correlate experimental results with a creep analysis. The article tested was an 18 in. (45.72 cm) x 18 in. (45.72 cm) Haynes-25 heat shield which had the accumulated permanent deflections shown in figure 1 under a simulated load and elevated-temperature environment. An analysis was made using available creep data and an assumption that the cyclic behavior of the panel could be approximated by assuming continuous creep behavior through the time span of 100 missions. This procedure implies that 100 15-minute missions are the same as one 1500-minute mission. The discrepancy between the experimental results and the creep analysis based on these assumptions was so great (an order of magnitude) that a more detailed investigation was pursued.

The question arose as to what was the main cause of the differences. Was it the method of analysis? Was it the fact that the creep data were obtained under constant temperature and load conditions, or was it some unknown effect in the experimental panel?

The answer to these questions was found in the method of obtaining and using material creep data. A considerable cyclic effect was discovered to govern the uniaxial creep behavior of the Haynes-25 material. In effect, the material appears to have a recoverable primary creep effect and acts as if it has no memory of previous strain history. When this information was used in the analysis, the correlation of the experimental results with the creep analysis was improved.

HAYNES-25 PANEL NO. 2 @ 1800°F (982°C): COMPARISON OF ANALYTICAL AND EXPERIMENTAL RESULTS

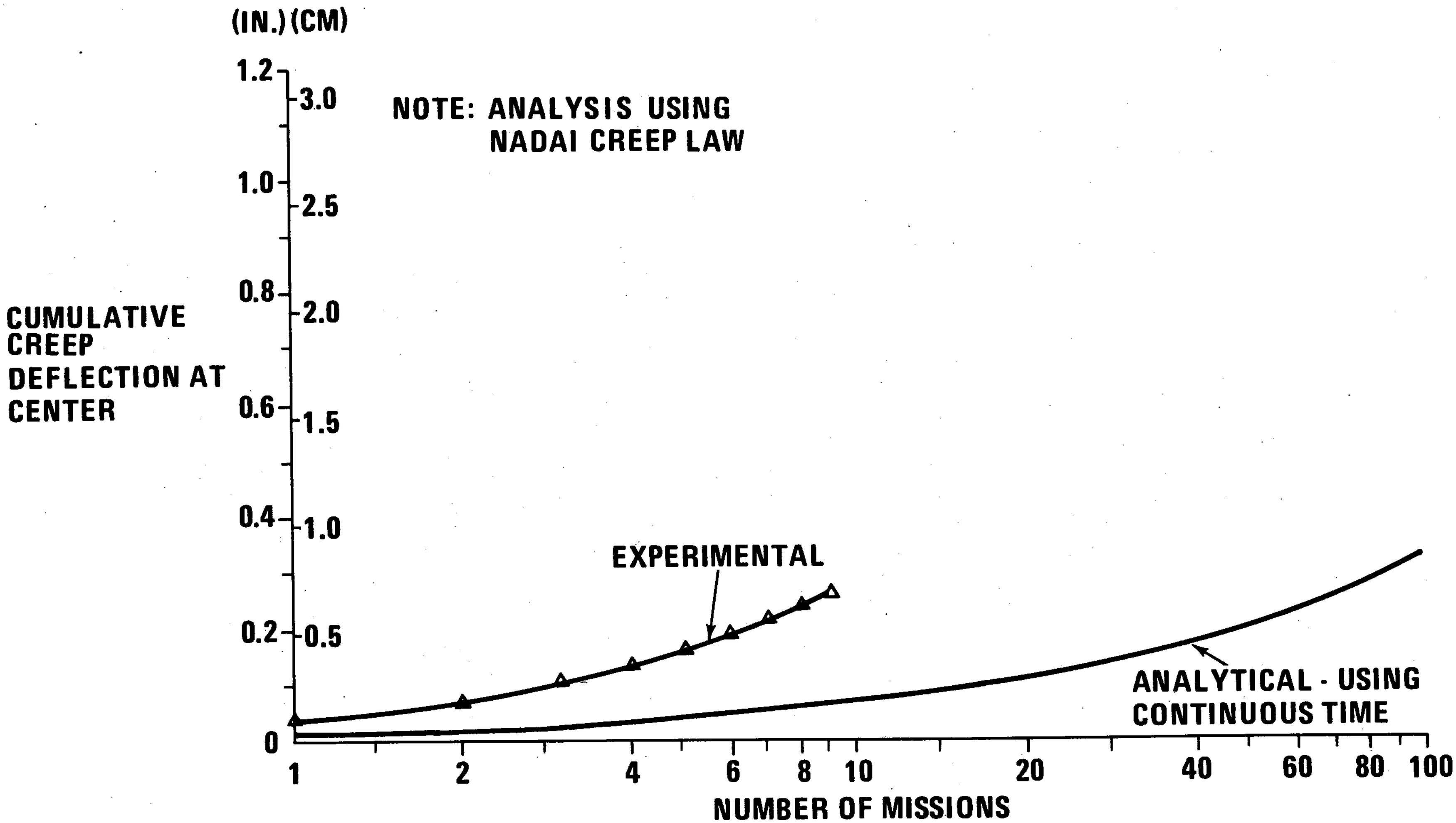

Figure 1

DESCRIPTION OF HAYNES-25 PANELS (FIGURE 2)

The Haynes-25 panel, for which the test results are shown in figure 1, was extensively described in references 2 and 3 and is shown in figure 2. The concept and advantages of the beaded-skin design, stiffened by corrugations in one direction, are shown in figure 2. It can be seen from the picture of panel No. 2, taken after the test, that permanent deformations formed in the beads and were not uniform in the transverse direction. In subsequent designs, the initial height of the bead was increased to prevent yielding and to allow a more uniform distribution of the thermal expansion to take place.

HAYNES-25 PANEL NO. 2

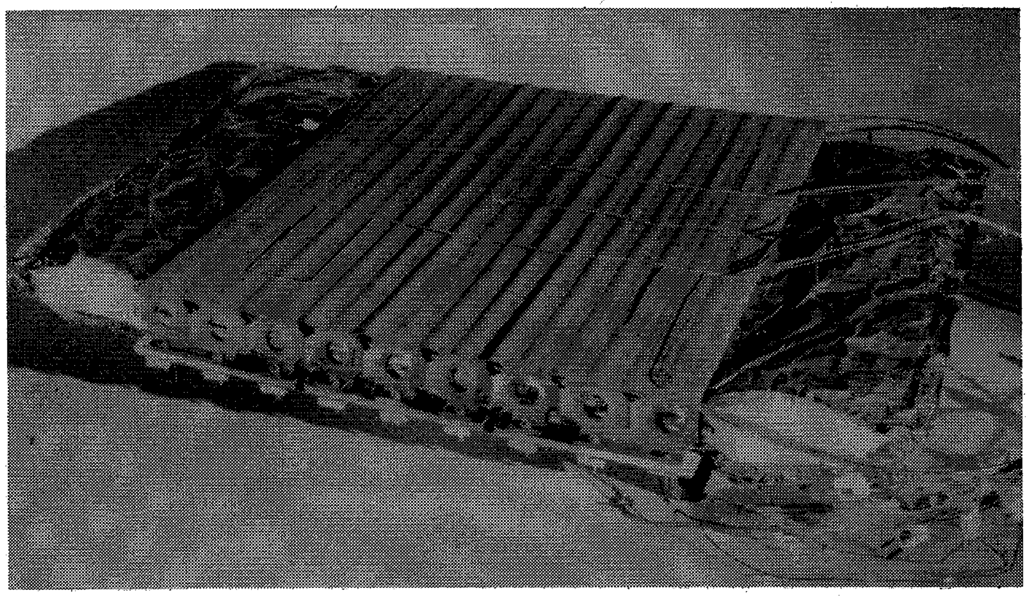

- THERMAL GROWTH IN LONGITUDINAL DIRECTION ONLY
- LATERAL THERMAL EXPANSION ABSORBED BY RISING OF BEADS
- NO SIZE LIMITATIONS IN LATERAL DIRECTION
- EXPANSION JOINTS ON TWO ENDS ONLY
- GOOD FLUTTER RESISTANCE

CONCEPT AND ADVANTAGES OF BEADED-SKIN HEAT SHIELD

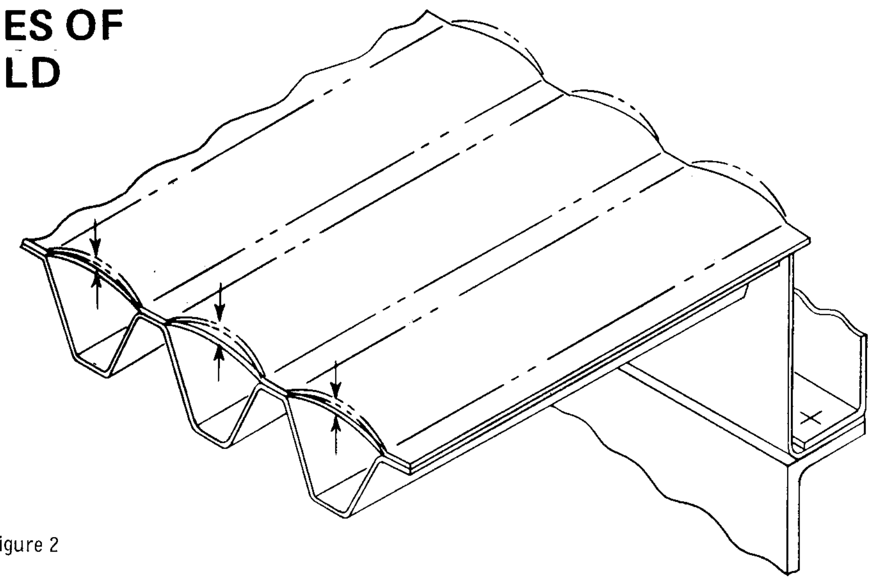

Figure 2

DESIGN CONSIDERATIONS (FIGURE 3)

An analytically derived, 20-minute, temperature-time reentry profile with an 1800°F (982°C) peak was chosen for design. The 1800°F (982°C) is a reasonable maximum temperature at which Haynes-25 and Haynes-188 super alloys could be expected to endure 100 missions. It was decided that the temperature of a protected titanium substructure should not rise above 500°F (260°C) at any time.

The high reentry heating rate is accompanied by varying air pressure normal to the surface. After considering the temperature and pressure profiles, a load of 40 psf (1915 N/m^2) appropriate to the peak temperature was chosen as a critical reentry design condition. For simplicity, this pressure was held constant during test. The temperature and pressure histories are shown in figure 3, together with the assumed 15-minute constant-temperature pulse used in the creep analysis computations.

In the design and analysis of the test panels, the material properties of Haynes-25 were obtained from a military handbook. At high temperatures, the material allowables were chosen as the stresses that create 0.4% creep strain after 25 hours (100 15-minute missions) of heat and load exposure. As will be shown by the present creep analyses, these stresses turned out to be too high to meet a maximum permissible panel surface deflection of 0.5 inch (1.27 cm) per 20 inch (50.8 cm) span. This permanent deformation was established on the basis of aerodynamic drag penalty.

DESIGN CRITERIA

- REUSABILITY: 100 MISSIONS
- MATERIAL ALLOW. STRESS: PER MIL HBK
- CREEP STRAIN: $\leq$ 0.4% @ 25-HR EXPOSURE
- SURFACE DEFLECTIONS: $\leq$ .5 IN. (1.27CM) (AERO LIMIT)/20 IN. (50.8CM) SPAN
- LOCAL & OVERALL STIFFNESS TO PREVENT FLUTTER
- SIMPLY REMOVABLE: INSPECTION
- MINIMUM LEAKAGE AT EDGE SEALS

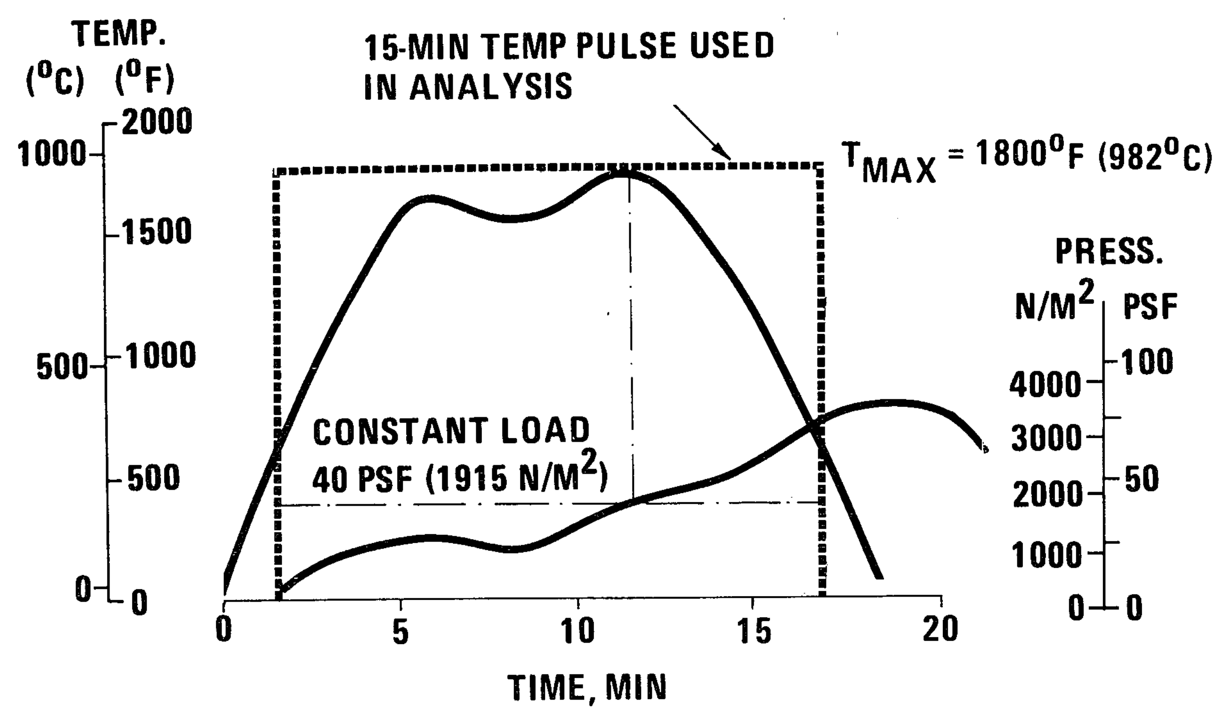

Figure 3

METHOD OF ANALYSIS (FIGURE 4)

General

The creep behavior of the metallic TPS panels during a typical mission will be governed by the complex interactions of such creep mechanisms as strain hardening and softening, creep recovery, loading and temperature history, metallurgical changes in the panel material, and other phenomena. A theoretical approach which attempts to incorporate all of these effects would lead to a highly nonlinear mathematical problem which may not be numerically solvable by modern computational procedures. Under such circumstances, the goal should be to construct a reasonably accurate analysis that limits consideration to those creep mechanisms which lead to a tractable mathematical formulation. With this objective in mind, two theoretical procedures based on simplified versions of the creep laws of Pao and Marin (ref. 4) and Nadai (ref. 5) were formulated and programmed for the IBM 360-75 computer using an idealized beam for the panel structure.

Stress-Strain Relations

It is assumed that the total strain ε in each fiber of the beam is composed of an elastic strain component e and a creep component ϵ:

$$\varepsilon = e+\epsilon \tag{1}$$

The elastic deformation is governed by Hooke's law. Treating the Haynes-25 material from a purely phenomenological viewpoint, the creep strains will be assumed to result from a process of time, temperature, and stress-dependent viscous flow:

$$\epsilon = \phi(t,T)|\sigma|^{m-1}\sigma \tag{2}$$

CREEP THEORIES CONSIDERED IN ANALYSIS

THEORY	LAW	NO. CONSTANTS
NADAI	$\epsilon = Ht^{n} \lvert \sigma \rvert^{m-1} \sigma$	3
PAO–MARIN	$\epsilon = \left[K \left(1-e^{-qt} \right) + Bt \right] \lvert \sigma \rvert^{m-1} \sigma$	4

Figure 4

where m is a positive number, σ is stress, and the function $\phi\ (t, T)$ is determined by experimentation.

The form of $\phi\ (t, T)$ is described in the following discussion of the Pao-Marin and Nadai theories:

Pao-Marin Theory (ref. 4)

According to this theory, total creep strain is composed of a strain-hardening, recoverable component and a viscous, irrecoverable component. For constant stress conditions the function $\phi\ (t, T)$ is of the form $[K(1-e^{-qt})+Bt]$ where K, q, and B are temperature-dependent material constants. Equation (2) yields upon substitution for ϕ:

$$\epsilon = [K(1-e^{-qt}) + Bt]|\sigma|^{m-1}\sigma \tag{3}$$

Through the assumptions of the Pao-Marin theory, equation (3) can easily be extended to describe creep recovery and creep under complex stress systems which vary with time.

Nadai Theory (According to Odqvist, ref. 5)

For a good representation of strain-hardening on the total creep deformation in both the primary and secondary stages, Nadai and his collaborators proposed for constant stress $\phi\ (t, T) = Ht^n$, where H and n are temperature-dependent constants. Equation (2) yields upon substitution for ϕ:

$$\epsilon = Ht^n|\sigma|^{m-1}\sigma \tag{4}$$

This form of the Nadai theory yields good results for slow monotonic changes of the stress with time, but it is not capable of representing the simultaneous action of creep recovery and creep and is therefore inadequate for conditions where the applied loads vary with time.

COMPARISON OF THEORIES WITH EXPERIMENTATION

Using published constant stress creep data for Haynes-25, reference 6, and similar data obtained from a Grumman testing program, constants for the Nadai and Pao-Marin creep laws were calculated for the 1.0 to 8.0 ksi (6.9 to 55.2 MN/m^2) stress range at 1800°F (982°C). Tabulated in table I are the creep constants which represent averaged values of the published data results and the Grumman test results.

TABLE I

ISOTHERMAL CREEP CONSTANTS, T = 1800°F (982°C)

Theory and Constants	English Units (in., kips, hrs.)	S. I. Units (m, Newtons, hrs.)
Nadai:		
m	3.342	3.342
n	0.709	0.709
H	5.19×10^{-6}	7.98×10^{-29}
Pao-Marin:		
m	3.342	3.342
q	1.0	1.0
K	5.92×10^{-6}	9.10×10^{-29}
B	1.94×10^{-6}	2.98×10^{-29}

When plotted against the Grumman constant-stress, constant-temperature data, both theories indicated good correlation in the 3.0 to 8.0 ksi (20.7 to 55.2 MN/m^2) range. In no case, for the indicated stress range, did either law show more than 10% deviation from the experimental results for time values less than one hour. At each stress level the most prominent deviations from experimentation were observed to occur in: 1.) the transient creep stage, where the Nadai theory tended toward over-prediction and the Pao-Marin theory indicated underprediction; and 2.) the secondary or minimum creep rate stage, where the Nadai law underestimates the experimental creep strains.

The difference in the two predictions lies in their curve-fitting capabilities. Characteristically, a mathematical relation such as the Pao-Marin law, which combines the strain-hardening behavior of primary creep with the viscous behavior of secondary creep, will provide a better approximation to steady-state creep deformations. In this sense the Pao-Marin law may be considered to be more accurate. However, the applicability of the phenomenological assumptions of any theory used to predict TPS panel creep behavior under a complex load and temperature environment is a subject that is not considered to be resolved at this time; it is a subject that should be given a more detailed study.

THE APPARENT CUMULATIVE CYCLIC EFFECT (FIGURE 5)

As cited earlier, the results of a creep analysis which ignored the cyclic effect of repeated exposure to the mission environment yielded grossly deficient predictions. Having at hand what appears to be two adequate theories to predict Haynes-25 creep under steady conditions, the question then arose: what deviations from steady-state creep behavior could possibly occur under a cyclic change in stress and temperature environment? Subsequent cyclic load and temperature testing provided some explanation. Figure 5 displays the results of the first nine mission cycles, each of which entailed: 1.) loading an uniaxial specimen to 8 ksi (55.2 MN/m^2) at room temperature; 2.) increasing the temperature to 1800°F (982°C) and maintaining that temperature for 15 minutes; 3.) cooling the specimen to room temperature; and 4.) unloading the specimen. As illustrated, the resultant experimental curve for cumulative creep strain very nearly matches the wavy line which predicts a superposition of the permanent creep which occurs in the virgin material for the first cycle. By contrast, experimental results for a continuous time creep test, on an identical specimen at 1800°F (982°C) and 8 ksi (55.2 MN/m^2) shown in figure 5, indicate less creep strain for the same time duration at peak temperature than in the cyclic test.

CYCLIC CREEP TEST

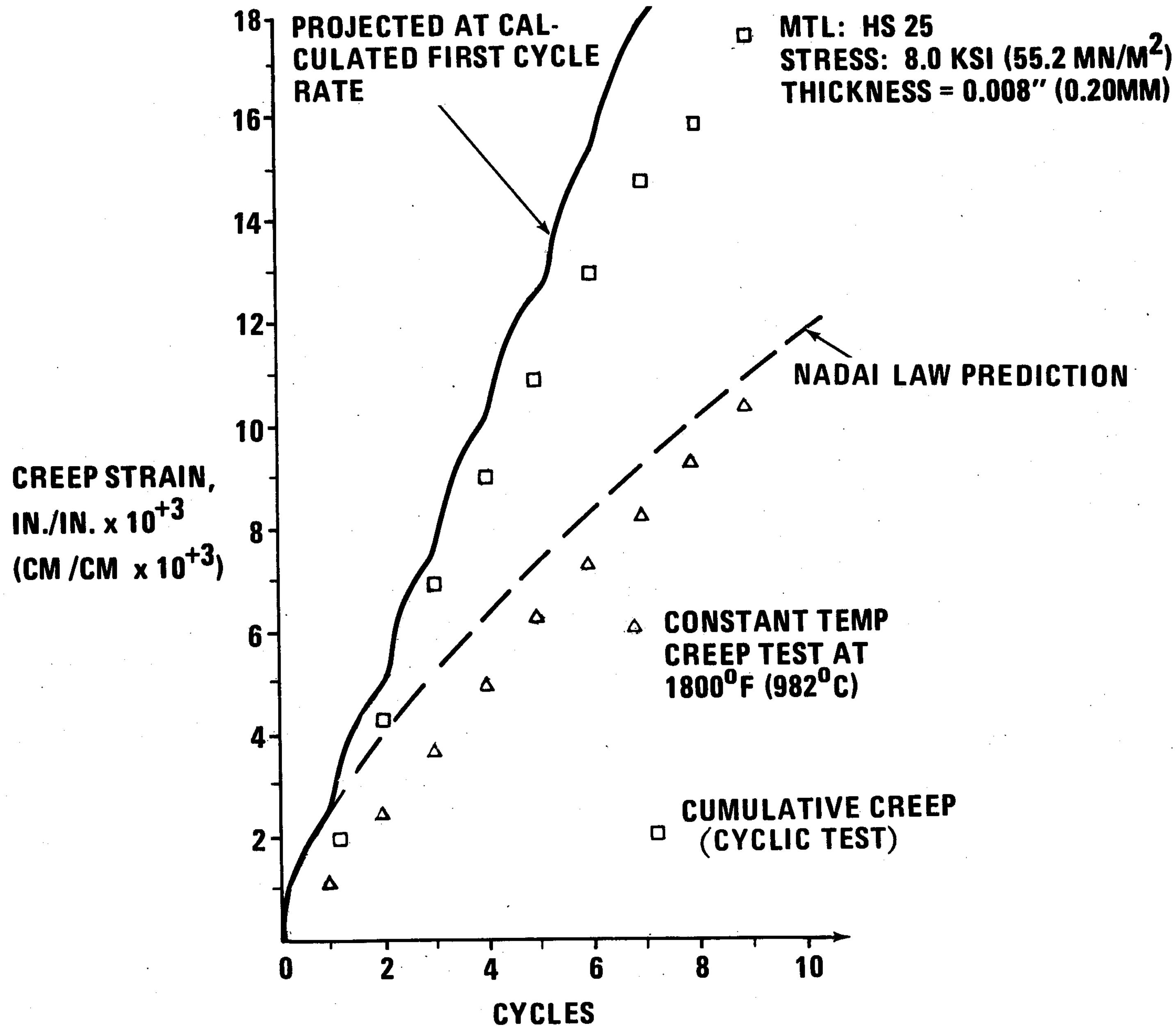

Figure 5

TPS PANEL-IDEALIZATIONS AND METHOD OF SOLUTION (FIGURES 6 AND 7)

For analytical purposes, the TPS panel was idealized as a series of parallel modular beams simply supported, and subjected to constant self-equilibrating end moments M and constant temperature T. The stiffness and area properties of a typical beam module were established by the depth and pitch of a typical panel bead and corrugation element. The bending stress distribution and creep deflection time histories were calculated within two computer programs by use of the creep relations of equations (3) and (4), respectively.

Within each of the two analysis programs the cumulative effects of creep deformation for consecutive Shuttle missions were simulated. The total permanent deflections due to creep were calculated by: 1.) modifying the initial elastic bending stress distribution at the start of each mission by the residual stresses accumulated during the course of prior missions; and 2.) adding to the sum of previously calculated values for creep deflections the deflection quantity computed for the modified load stresses.

The general method by which equations (3) and (4) were employed to account for the effects of stress redistribution is commonly referred to as the "strain-hardening rule." This concept is illustrated in figure 6 in which isochronous creep curves (representing either Pao-Marin or the Nadai laws) are plotted. When the stress σ_1 in the first time interval is changed to σ_2 after a prescribed increment of time Δt_1, the point B moves to C along a constant strain line. In the next time interval creep occurs from C to D.

STRAIN HARDENING RULE

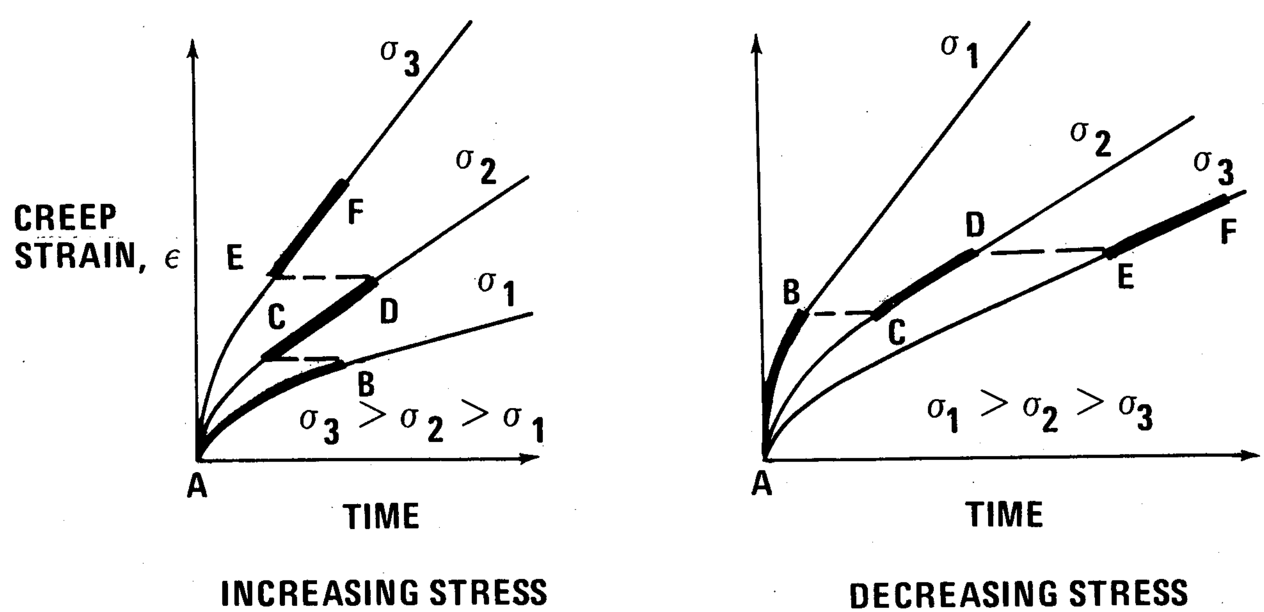

Figure 6

A typical inelastic stress distribution which results from the redistribution of the elastic stresses during each mission is shown in figure 7. The stiffness and cross-sectional properties of the beam were calculated within the analysis programs by idealizing its cross section as illustrated in figure 7. The indicated model represents an eleven-element approximation to one-half of a typical bead and corrugation element. Although the analysis programs are capable of handling more refined models, the preliminary nature of the present study did not warrant a more exact description of the cross section.

INELASTIC STRESS DISTRIBUTION (NO RESIDUAL STRESSES)

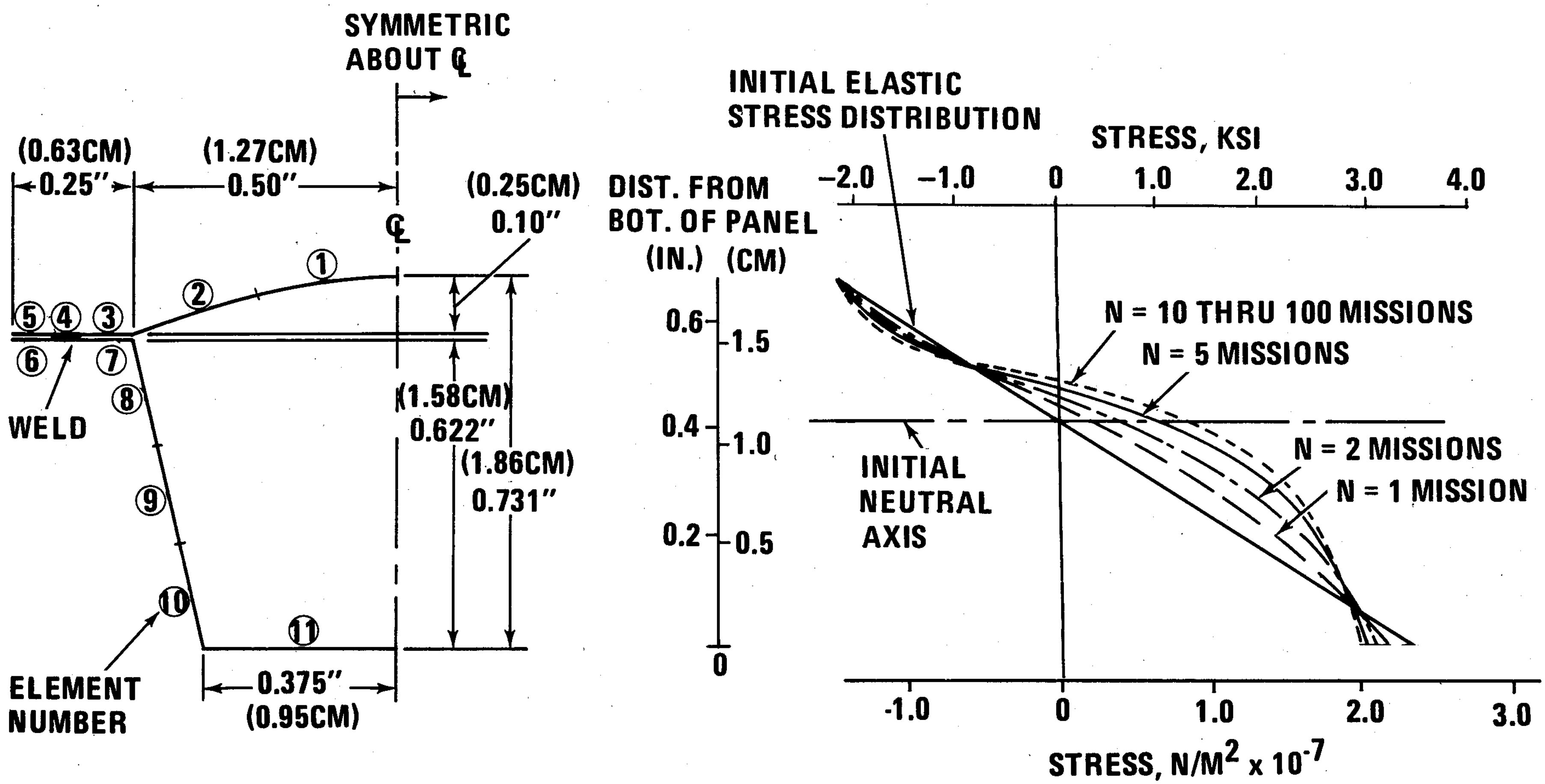

Figure 7

EFFECT OF BIAXIAL STRESSES (FIGURE 8)

A typical corrugation-stiffened bead isolated from the wide simply supported panel and treated as a beam for purposes of a creep analysis cannot take into account the biaxial stresses which exists in the bead. The transverse stresses caused by the thermal expansion were found to be substantial. As the bead deflects, however, there is considerable redistribution of stresses and the bead acts essentially as a flexible membrane but basically in a state of biaxial stress.

In order to evaluate the effect of the biaxial stresses on the creep deformations, the bead effective thickness was varied in a series of computations for panel No. 2 geometry. The results, shown in figure 8, indicate that the reduction in thickness, to account for the bead reduced effectiveness, can have a very large influence on the creep deformations.

The experimental results of panel No. 2 are also shown in figure 8. It should be pointed out that the effect of oxidation would also reduce the bead effectiveness. The best estimates of the effect of oxidation in the case of the Haynes-25 material at the design temperatures would indicate a reduction in the structural thickness of anywhere between 0.0005 to 0.00075 inches (0.0127-0.019 mm).

HAYNES-25 PANEL NO. 2 @ 1800°F (982°C): EFFECT OF BIAXIAL STATE OF STRESS IN BEAD

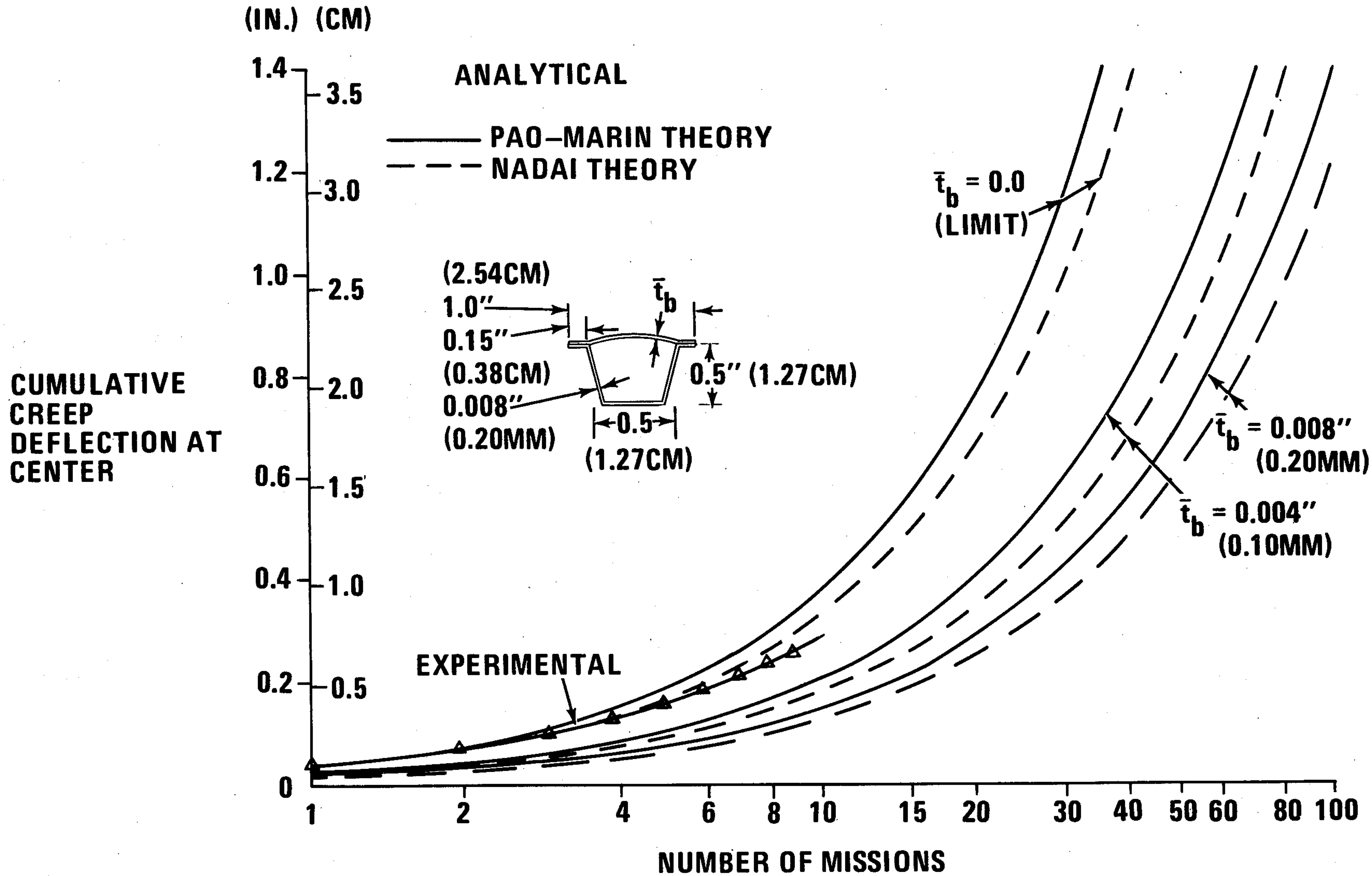

Figure 8

MEASUREMENT OF MANUFACTURING RESIDUAL STRESSES (FIGURE 9)

An examination of the manufacturing residual stresses in the longitudinal direction was made on panel No. 3A. Reference points in the beaded shingle and the corrugated sheet were punched at 8-inch (20.32 cm) gage lengths. The gage lengths marked on the panel were measured before and after welding and the changes in length were converted to stresses. The results, shown in figure 9, indicate that very high residual stresses can exist in the panels prior to testing. The effects of these stresses on the creep deformation were evaluated by use of the average measured results of the seven corrugations shown in figure 9.

The manufacturing stresses can be somewhat reduced by a refinement of forming techniques and the use of intermediate annealing operations for detail parts. However, because of the thin gages of material used, residual stresses would continue to be induced during progress to higher levels of assembly (welding and riveting of details and final installation of TPS). In the higher levels of assembly, the use of annealing would not be practical. In the case of the 10 inch (25.4 cm) x 20 inch (50.80 cm) test article (panel No. 3A), attempts to reduce residual stresses were not employed in order to keep these stresses at a level where their influence could be detected experimentally.

MEASURED FABRICATION RESIDUAL STRESSES

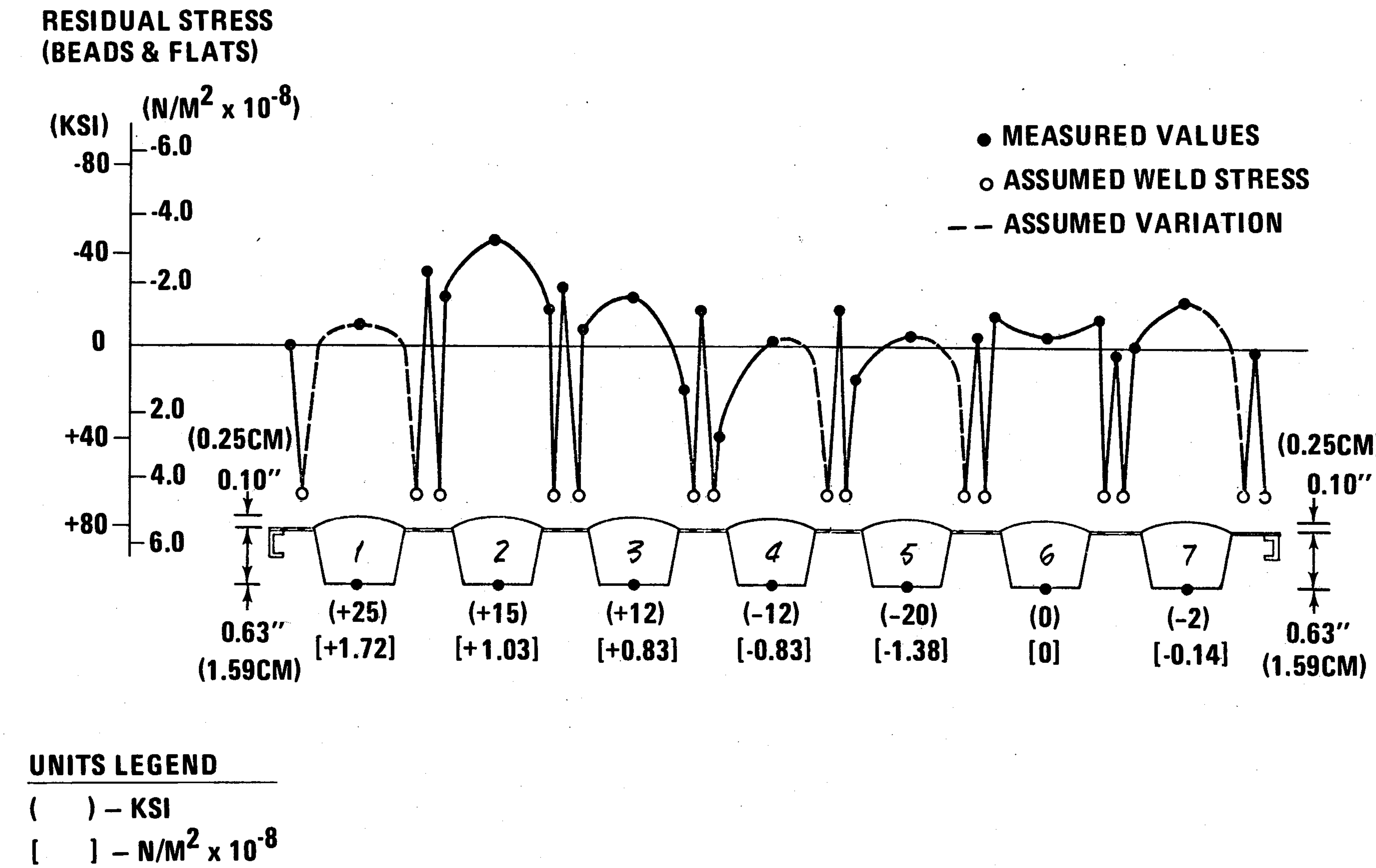

Figure 9

EFFECT OF RESIDUAL STRESSES ON CREEP DEFORMATION (FIGURE 10)

The effect of initial residual stresses on the creep deformations were studied using both creep laws and panel No. 2 geometry. The results, shown in figure 10, indicate that residual stresses which are approximately 10 percent of the average measured values on panel No. 3A have very little effect on the overall cumulative creep deformation. The results for 20-percent residuals (not shown in fig. 10 for clarity) likewise showed no appreciable influence on the deflections.

In the case of panel No. 2 no residual stress measurements were taken. For this panel, which had a shallower bead and a thinner upper skin, it was assumed that the manufacturing residual stresses would be lower than in panel No. 3A. For these reasons a maximum value of 20 percent of the measured residual values on panel No. 3 was assumed. These residuals were self balanced on the cross section of panel No. 2 at zero applied load, and were superimposed on the elastic stresses caused by the 40 psf (1915 N/m^2) constant uniform load.

Figure 10 also shows the combined effects of reduced bead thickness, to account for biaxial effects and oxidation, and initial residual stresses. Both creep laws indicate that a reasonable correlation can be achieved with the experimental results of panel No. 2 provided the cyclic effect of the material is taken into account. The results of the Pao-Marin theory show better agreement with experiment.

HAYNES-25 PANEL NO. 2: COMPARISON OF ANALYTICAL AND EXPERIMENTAL RESULTS @ 1800°F (982°C)

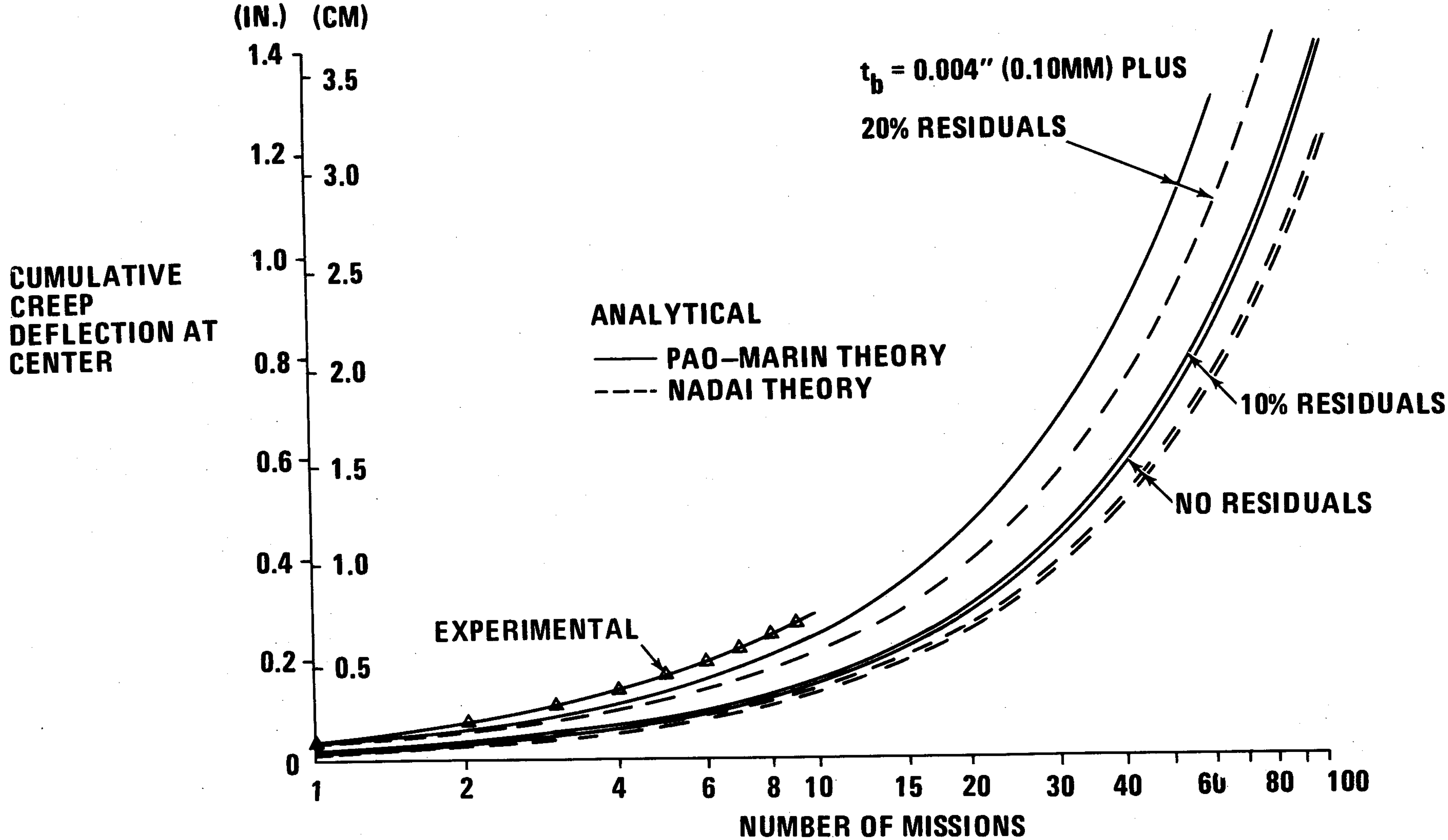

Figure 10

CREEP ANALYSIS OF PANEL NO. 3A (FIGURE 11)

The comparison of the analytical and experimental results for panel No. 3A is shown in figure 11. The permanent deflection obtained in the first cycle was approximately three times the deflection obtained in subsequent cycles. The results up to the tenth cycle indicate a steady behavior with approximately the same permanent deformation obtained in each cycle after the first. The larger deformation obtained on first heating and loading of the panel may be caused by the large initial residual stresses locked in the panel by the manufacturing process. The effect of the pyromarking procedure on the initial residual stresses could not be evaluated quantitatively. However, it is possible that some reduction in residuals did take place during baking of the pyromark coatings.

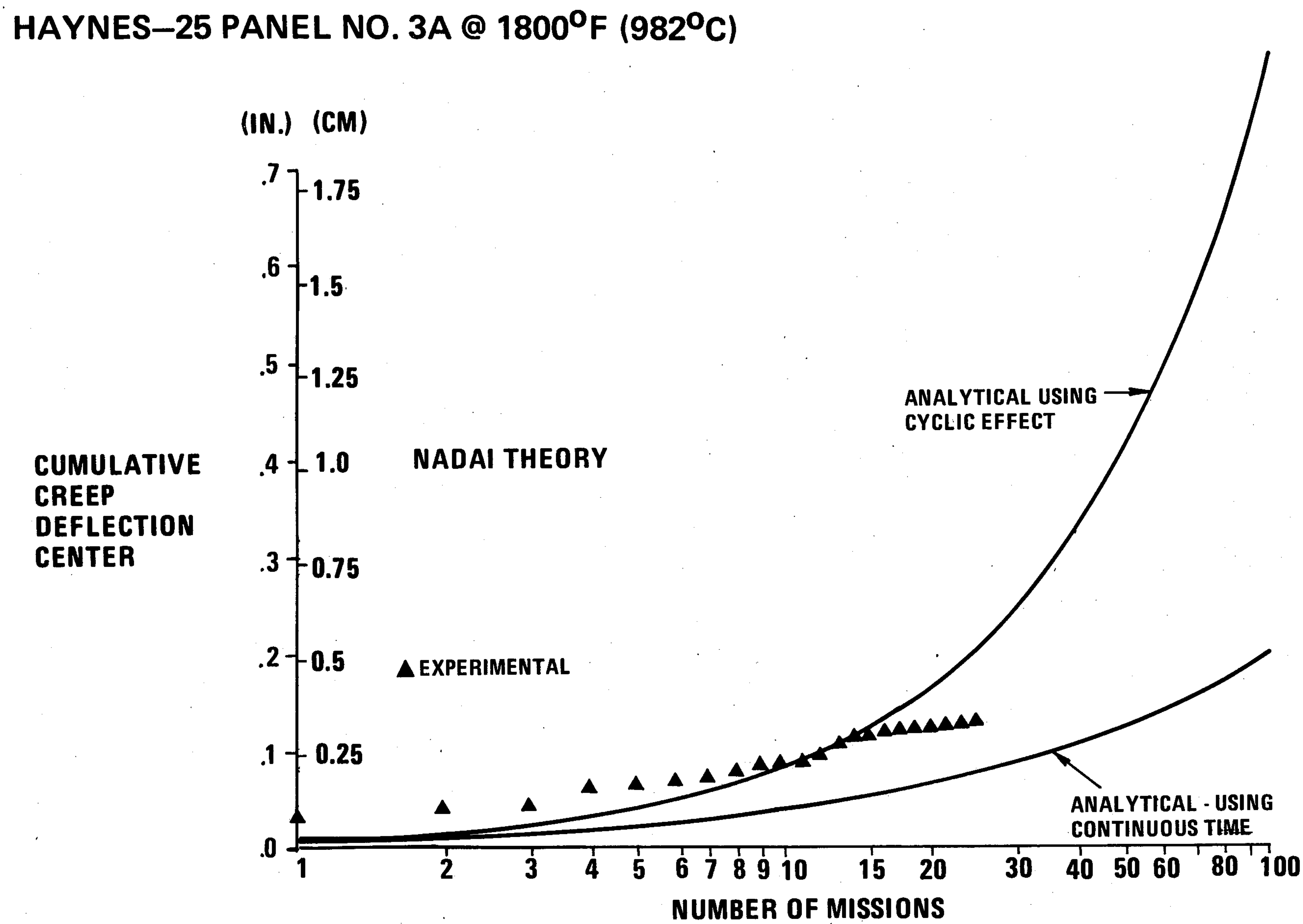
HAYNES–25 PANEL NO. 3A @ 1800°F (982°C)
(IN.) (CM)
.7 1.75
.6 1.5
.5 1.25
.4 1.0
.3 0.75
.2 0.5
.1 0.25
.0
CUMULATIVE
CREEP
DEFLECTION
CENTER
NADAI THEORY
▲ EXPERIMENTAL
ANALYTICAL USING
CYCLIC EFFECT
ANALYTICAL - USING
CONTINUOUS TIME
1 2 3 4 5 6 7 8 9 10 15 20 30 40 50 60 80 100
NUMBER OF MISSIONS

Figure 11

APPLICATION OF CREEP ANALYSIS TO DETERMINE DESIGN STRESS ALLOWABLES (FIGURE 12)

The creep analysis presented is used to evaluate a particular orbiter TPS design having the geometrical details shown subsequently (fig. 15). Both a low cross-range requirement (low L/D vehicle with 100 missions at 15 minutes each) and a high cross-range requirement (high L/D vehicle with 100 missions at 30 minutes each) are considered for a Haynes-25 design at 1800°F (982°C). The results shown in figure 12 indicate the expected cumulative creep deflection as a function of the allowable extreme fiber stress for a perfect panel with no initial residual stresses and no oxidation effects but taking into account the cyclic creep effect of the material.

Using an allowable extreme fiber stress which causes 0.4% creep strain in 25 hours the results of figure 12 clearly indicate that the allowable permanent deformations of both the high L/D and the low L/D vehicle will be exceeded in 100 missions. From this analysis it is seen (fig. 12) that the allowable extreme fiber stresses should be reduced from 3.45 ksi (24 MN/m^2) to 2.7 ksi (18 MN/m^2) (this corresponds to approximately 0.1 percent creep strain) in order to meet the 0.5-inch (1.27 cm) maximum permanent deformation per 20 inches (50.80 cm) for the low L/D vehicle. For the high L/D vehicle the allowable extreme fiber stress for meeting the required 0.25-inch (0.635 cm) permanent deformation per 20 inches (50.80 cm) is only 1.85 ksi (13 MN/m^2).

HAYNES-25 PANEL NO. 3A AT 1800°F (982°C)

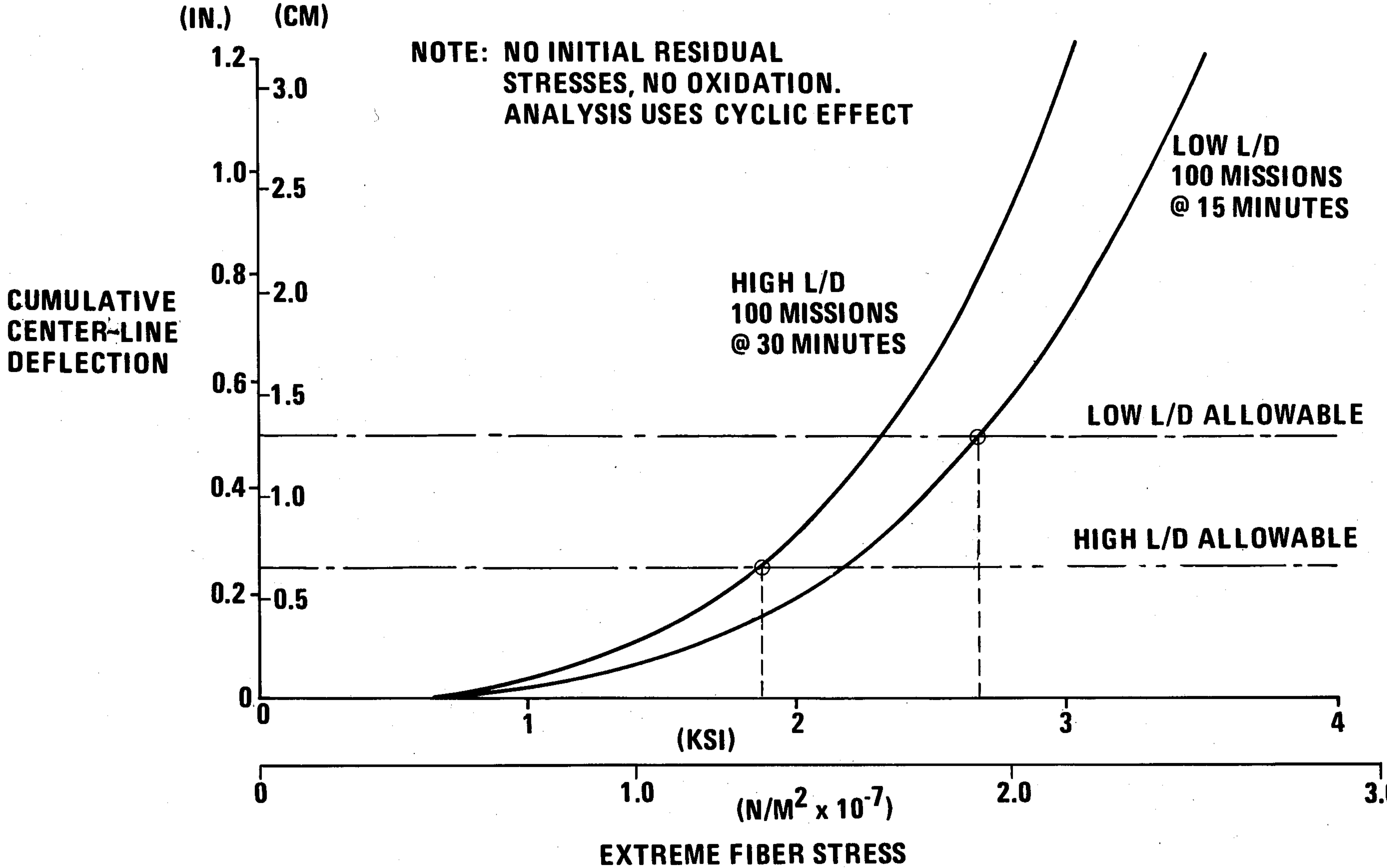

Figure 12

HAYNES-25 MATERIAL ALLOWABLE CREEP STRESS DATA (FIGURE 13)

The available creep data on Haynes-25 material for 25-hour exposure of specimens having thicknesses from 0.005 inches (0.127 mm) to 0.020 inches (0.508 mm) are shown in figure 13. The data shown are the average values for the range of thicknesses given in reference 6. As mentioned earlier, the allowable stresses in the design of panels No. 2 and No. 3A were chosen such that a stress corresponding to 0.4-percent creep strain was chosen from figure 13. After evaluating the results of figure 12, it is seen that an allowable stress closer to the 0.1-percent creep strain might have been more appropriate for the low L/D vehicle.

HAYNES-25 (L-605) MATERIAL CREEP STRESS CURVES

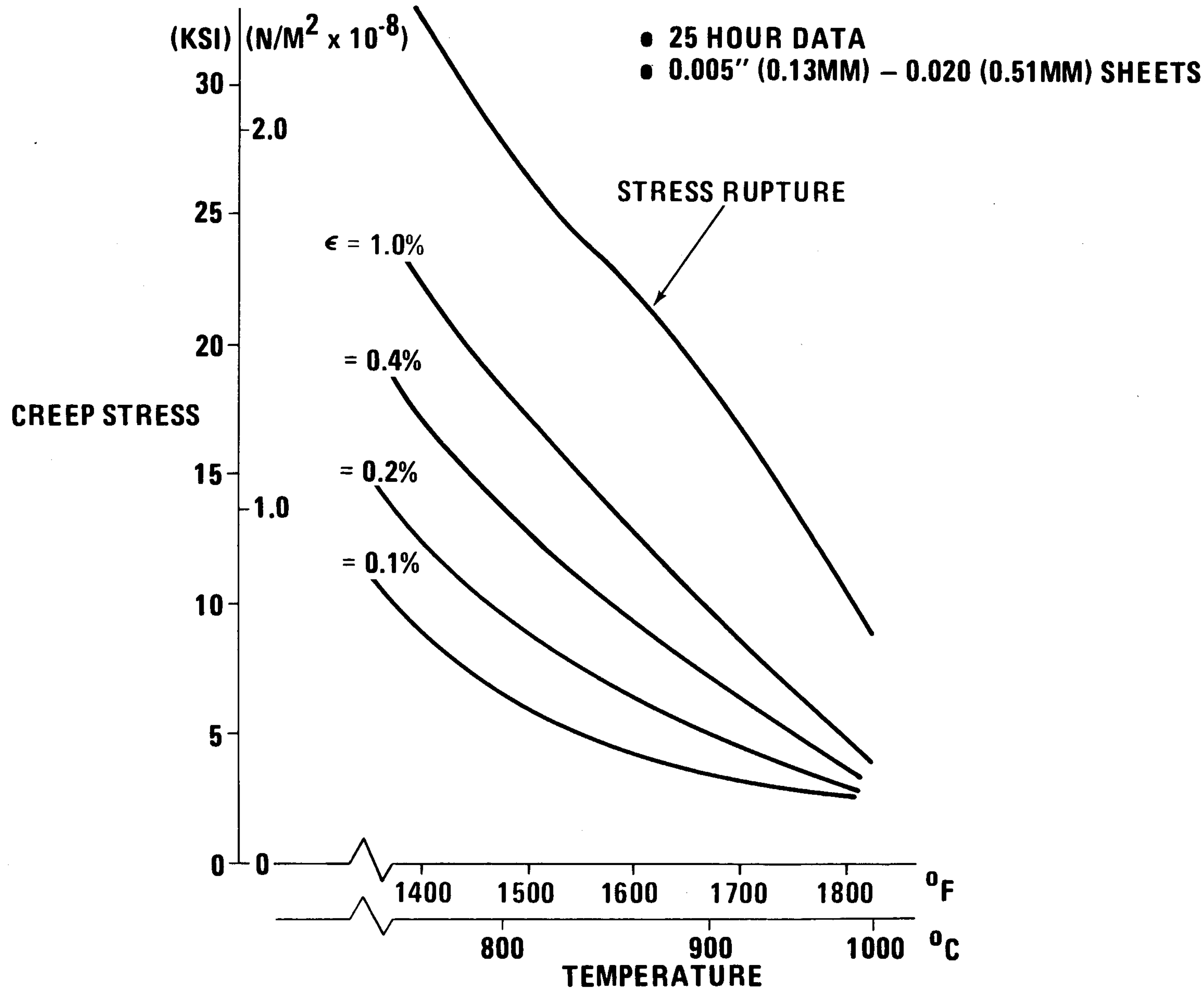

Figure 13

DESCRIPTION OF CREEP COMPONENT PANEL NO. 3A (FIGURE 14)

Test component No. 3A, shown in figure 14, is a 10-inch (25.4 cm) x 20-inch (50.80 cm) Haynes-25 heat shield fabricated especially to evaluate the effects of manufacturing residual stresses and the creep behavior of the panel under simulated reentry conditions.

Unlike panel No. 2 which was preoxidized to give the proper emissivity to the outer skin during heating, panel No. 3A was pyromarked after the thermocouples were installed.

HAYNES-25 PANEL NO. 3A BEFORE TEST

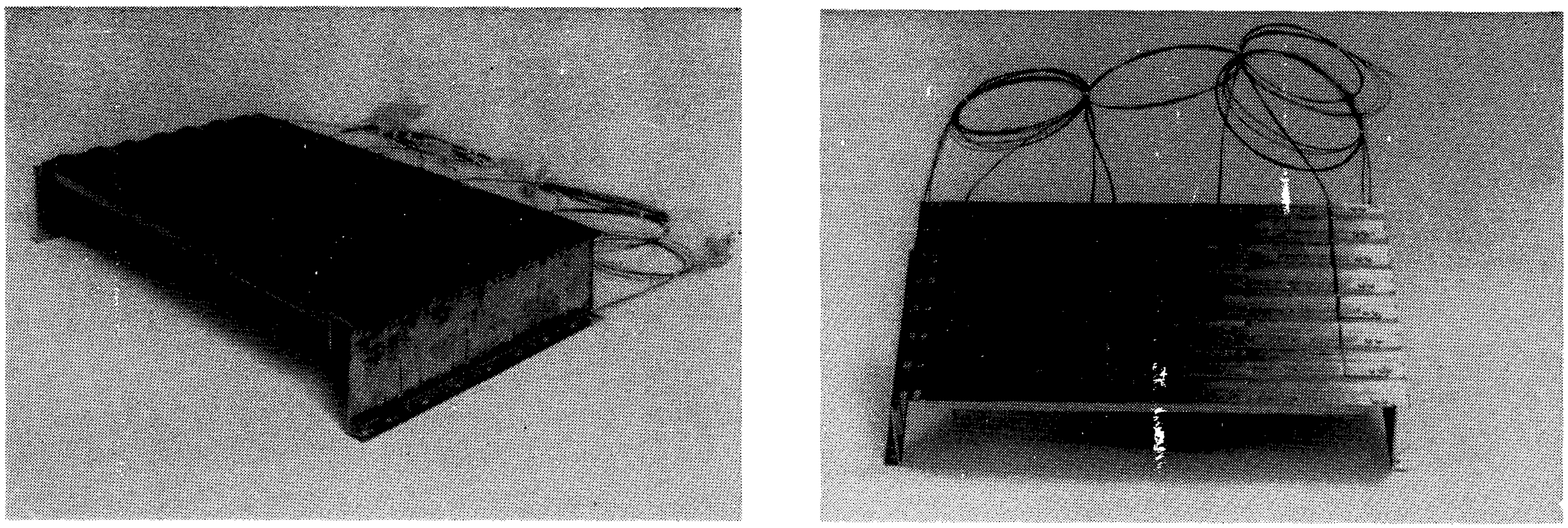

Figure 14

HAYNES-25 PANEL NO. 3A DETAILS (FIGURE 15)

A number of modifications to the design of panel No. 2 were incorporated in panel No. 3A as shown in figures 14 and 15. A wider pitch of 1.5 inches (3.81 cm) was used in the corrugations in order to increase the width of the flats for fastening purposes. An increase in thickness of the upper skin to 0.010 inch (0.254 mm) in order to meet the flutter requirements was necessary. Haynes-25 angle clips 0.060-inch (1.524 mm) thick were used to attach the heat shield to the supports as shown in figure 14. This design eliminated the welding procedure used in panel No. 2.

A bead height to span ratio of 1/10 was used in panel No. 3A. This increased bead height over previous designs allowed a more uniform distribution of the lateral thermal expansion to be taken by the beads and prevented excessive yielding of the beads which occurred in the testing of panel No. 2.

The 1.5-inch (3.81 cm) thick insulation bag used was held to the panel through several stand-offs made of Haynes-188 pins spotwelded to the corrugations as shown in figure 15. The insulation bag consisted of layers of 3/16-inch (0.475-cm) thick fibrous silica quartz felt (Johns-Manville Microquartz) encased in a 0.00125 inch (0.0316 mm) Inconel foil and held in place by 0.010 inch (0.254 mm.) washers.

Panel No. 3A was tied down in the middle by a longitudinal drag brace (fig. 15) which transfers the horizontal shears due to lateral vibration into the supports spaced 20 inches (50.80 cm) apart.

DETAILS OF PANEL NO. 3A

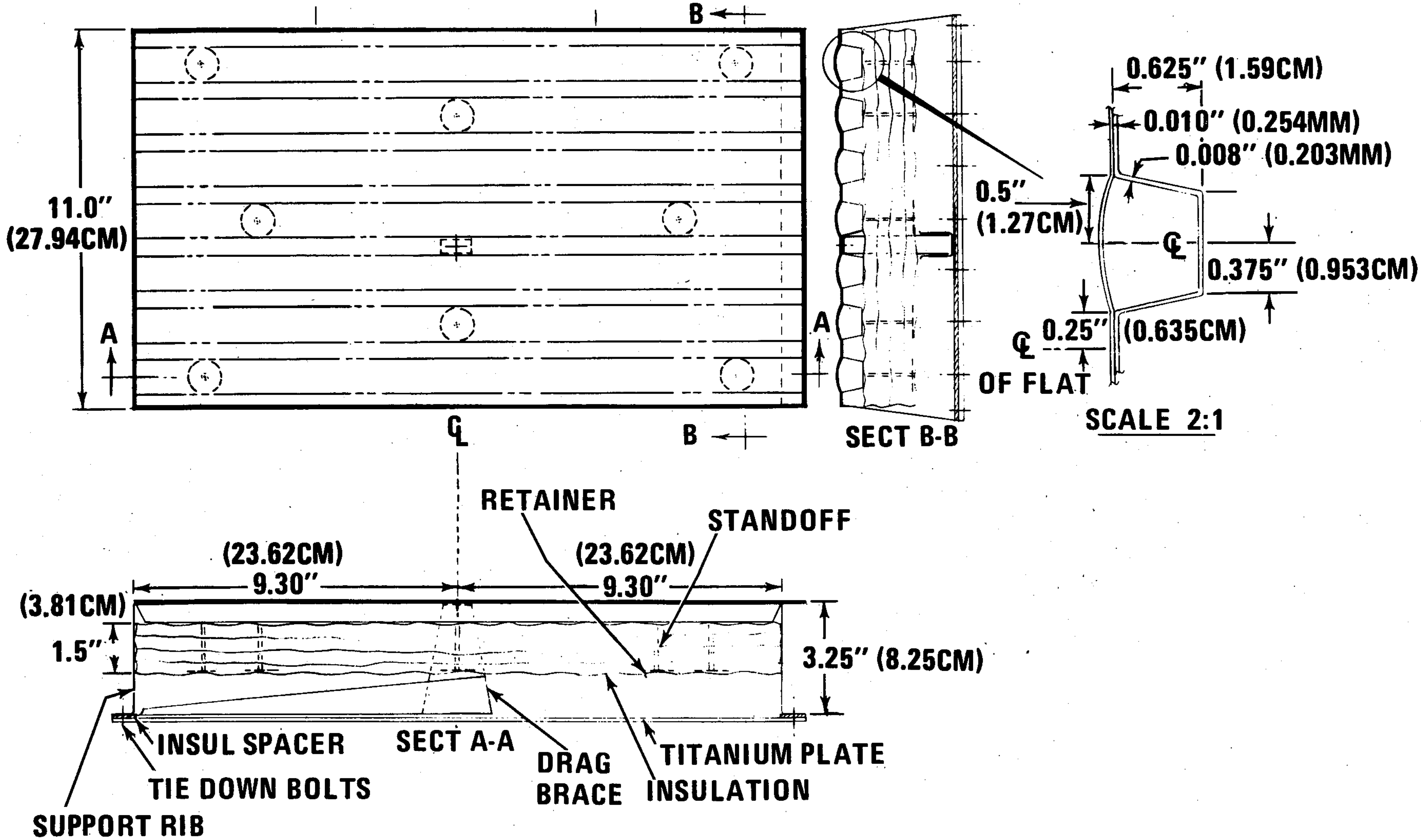

Figure 15

TEST SETUP (FIGURE 16)

The test setup for panel No. 3A is shown in figure 16. The panel and insulation assembly are bolted to a titanium support frame simulating the vehicle structure. A titanium plate 0.1 inch (0.254 cm) is situated below this assembly and it simulates the effective heat sink of the vehicle structure and tankage. The panel, support frame, and plate are tied down to a massive test fixture. This fixture consists of steel "I" sections and is designed as a rigid reference base. Twenty-four weights are suspended in three rows to simulate the parabolic moment distribution caused by the constant pressure of 40 psf (1915 N/m^2) assumed in the analysis. A quartz lamp array is mounted above the skin to simulate reentry heating. The lamps are coupled to a programmed data track which plots TPS skin temperatures against time. Additional insulation is situated off the panel edges and behind the heat sink plate in order to obtain data consistent with the initial assumptions of design.

Instrumentation consists of 40 thermocouples on the panel, frame, and heat sink, and 6 control thermocouples on the skin. The control thermocouples are averaged to yield the proper heating input. In addition, there are 26 deflection probes normal to the panel skin and edges. Linear potentiometers are used to obtain deflection readings.

All thermocouple and deflection probe readings are processed through a "CSC" (Computer Science Corp.) computer which puts the data on magnetic tape. The Grumman Data Systems reduction facility then processes the tapes to yield plots and tabulations of temperatures and deflections against time for each test.

TEST SETUP FOR PANEL NO. 3A

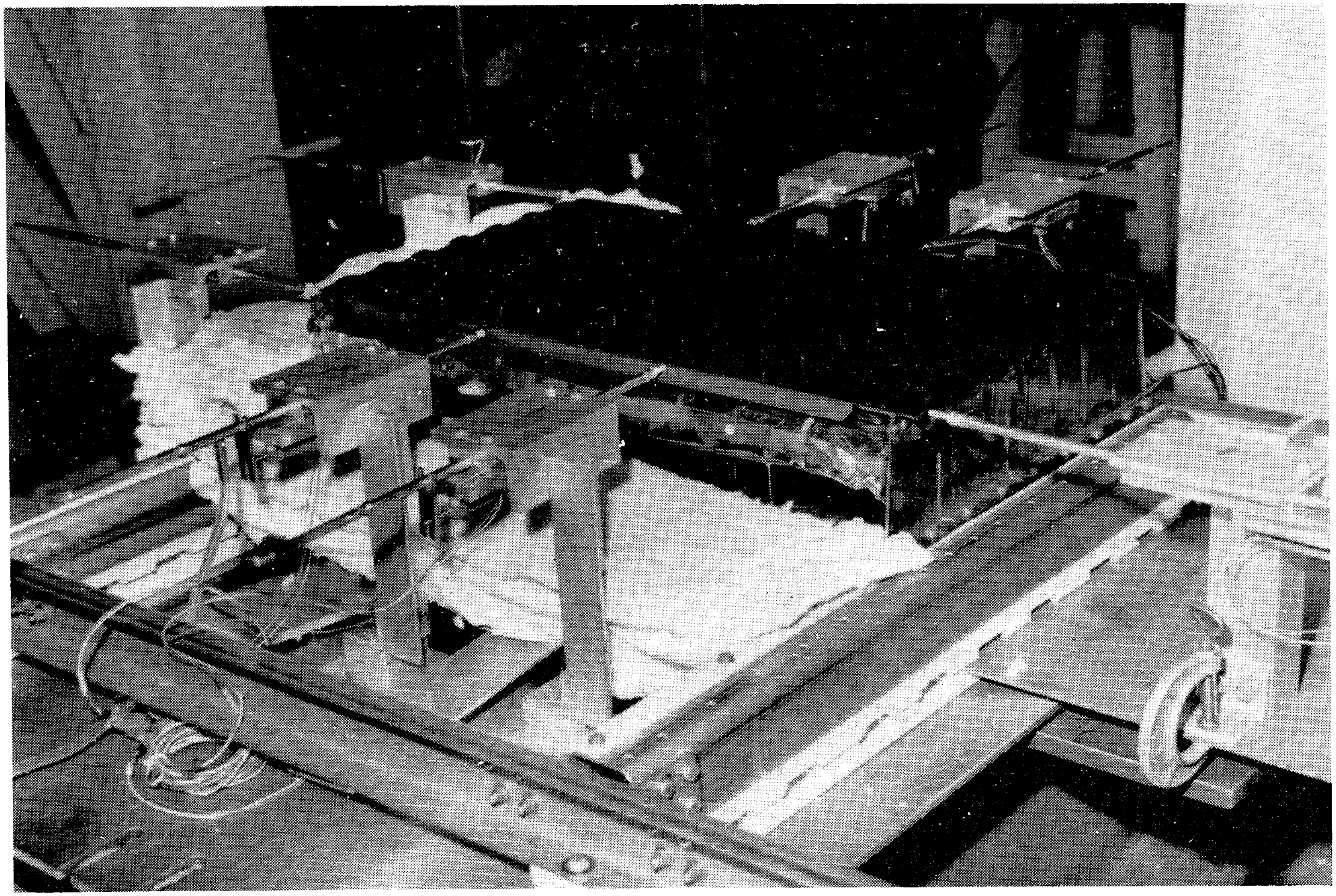

Figure 16

FINITE ELEMENT CREEP ANALYSIS (FIGURE 17)

An independent check of the beam analysis by a finite-element creep and plasticity program was performed. The finite-element representation of a typical beam idealization of the TPS panel is shown in figure 17. The indicated model represents a coarse-grid approximation of one-fourth of the beam idealization. Based on the assumption that the one-dimensional creep theories discussed earlier are applicable to the biaxial state of stress, the finite-element program computes the creep and elastic stresses for every element of the model and the deflections at every node.

The present version of the program (ref. 7) is such that the combined effects of plasticity and creep may be evaluated. The program operations are implemented on the IBM 360/75 computer. The program, having a maximum capacity of 55 planar stress elements, does all the computations in core and is very efficient. A larger version of the program (ref. 8), which uses peripheral storage equipment, has a capacity of 175 elements and 210 nodes and is capable of analyzing a more refined model of the beam structure. Both programs can be modified for computations with any creep theory.

COARSE FINITE-ELEMENT IDEALIZATION

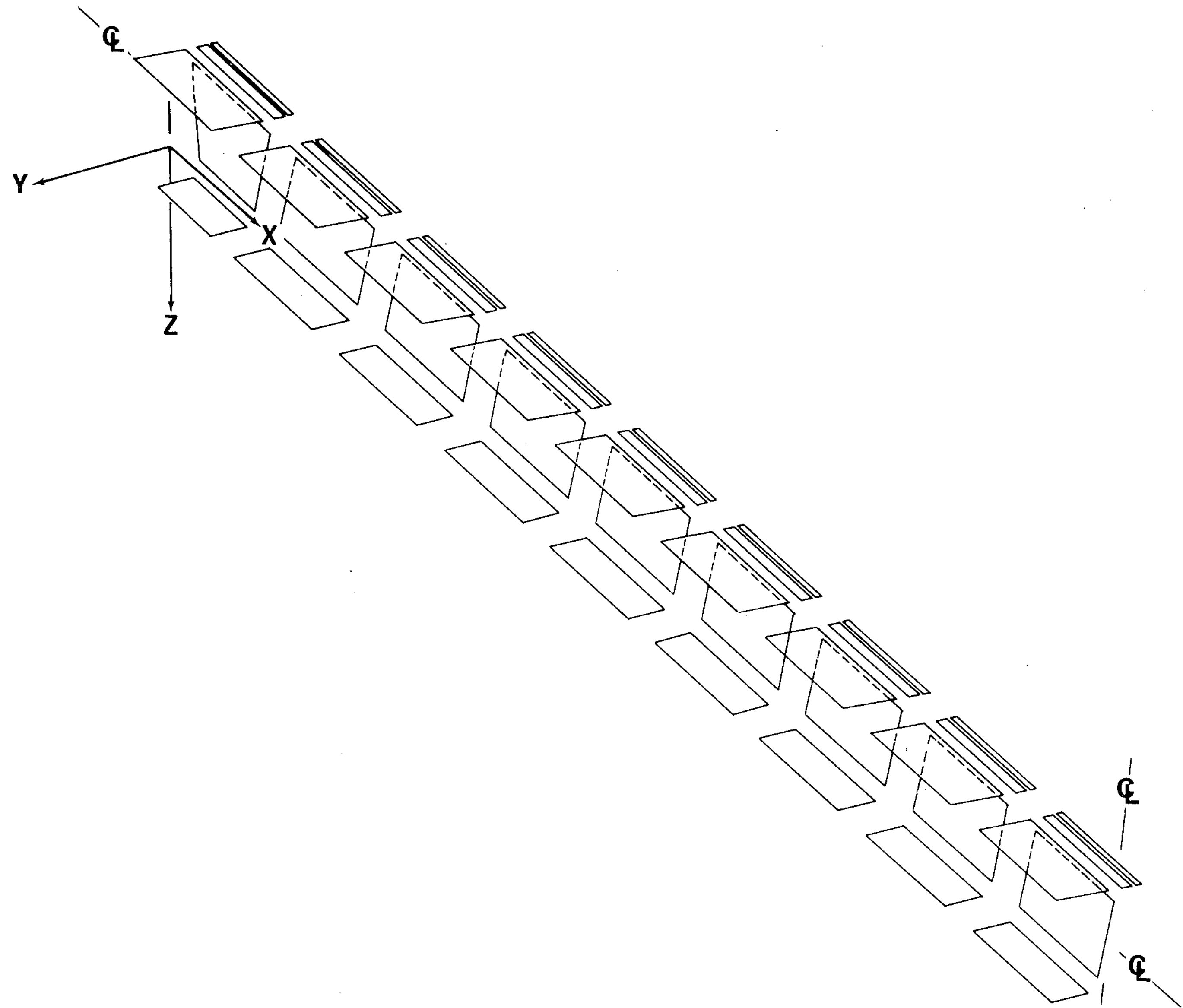

Figure 17

ACKNOWLEDGMENT

The work reported herein was performed under the sponsorship of the Grumman Aerospace Corporation Advanced Development Program, Project No. AD 02-04.

The project was under the general technical direction of Mr. Willy Wolter, TPS Manager on the Earth Orbital Shuttle project. Mr. Robert Micich, Materials and Processes Department, had direct responsibility of the IRAD effort; Mr. David Sharp performed most of the stress analysis and contributed to the beam creep analysis formulation.

A number of people contributed to the overall effort of the project. In particular, the contributions of: A. Varisco, F. Halfen and A. Zier, Structural Design; E. Lesak, Advanced Manufacturing; P. Coschignano, Stress Analysis; A.Fletcher and G. Duckett, Materials and Processes Section; W. Fischer, Environmental Test Section; and H. Paterson, Instrumentation Engineering, are gratefully acknowledged.

REFERENCES

1. Wolter, W. A. and Ratay, R. T., "Superalloy Heat Shield Technology for the Space Shuttle", NASA TM X-52876, 1970, pp. 145-158.

2. Ratay, R. T. and Fischer, W. E., "Development of a Reusable Metallic Thermal Protection System for Lifting Reentry Vehicles", Advanced Development Report No. ADR 02-04-70.1, Grumman Aerospace Corporation, Bethpage, New York, April 1970.

3. Ratay, R. T. and Wolter, W. A., "A Reusable Metallic Thermal Protection System for the Space Shuttle", paper presented at the Second Aerospace Structures Design Conference, Seattle, Washington, September 28, 29, 1970.

4. Pao, Y. H. and Marin, J., "An Analytical Theory of Creep Deformation of Materials", J. Appl. Mech, 20, 245, 1953.

5. Odqvist, F. K., Mathematical Theory of Creep and Creep Rupture, Oxford at the Clarendon Press 1966, Chap III, p. 15.

6. Greene, A., Sieber, H., Wells, D., and Wolfe, T., "Research Investigation to Determine Mechanical Properties of Nickel and Cobalt-Base Alloys for Inclusion in Military Handbook-5", Vol. I, Technical Documentary Report No. ML-TDR-64-116, Air Force Materials Laboratory, Air Force Systems Command, United States Air Force, Wright-Patterson Air Force Base, Ohio, October, 1964.

7. Jensen, W. R., Falby, W. E. and Prince, N., "Matrix Analysis Methods for Anisotropic Inelastic Structures", Advanced Development Report No. ADR 02-11-65.5, Grumman Aerospace Corporation, Bethpage, New York, February 1966.

8. Harris, H. G., Ojalvo, I. U. and Hooson, R. E., "Stress and Deflection Analysis of Mechanically Fastened Joints", Air Force Technical Report AFFDL-TR-70-49, Air Force Flight Dynamics Laboratory, Air Force Systems Command, Wright-Patterson Air Force Base, Ohio, May 1970.

ABLATIVE THERMAL PROTECTION SYSTEMS

By L. F. Vosteen and C. M. Pittman
NASA Langley Research Center
Hampton, Virginia

INTRODUCTION

One of the most difficult space shuttle technology problems is the development of light weight reliable thermal protection systems with a multi-mission life. A need for minimizing weight has been well established and reliability is essential to any manned system. A multi-mission life is desirable to minimize operational costs during the life of the vehicle. Previous papers (papers 1, 2, and 3 of volume II of this compilation) have described such multi-mission systems. As an alternative to a multi-mission life, however, total program costs could be kept to a minimum if the thermal protection system could be made sufficiently inexpensive so that it could be discarded after every flight and replaced. Ablative materials are obviously a prime candidate for such a system. This paper will deal with the rationale for using ablators and the status of a technology program directed at producing inexpensive ablative heat shields. The elements of this program are described in reference 1.

Figure 1 shows some of the advantages of ablative systems and the factors that deter their use as a primary thermal protection system for the shuttle orbiter. Considerable experience exists in the application of ablative materials to reentry vehicles. All of our manned entry systems, Mercury, Gemini, and Apollo used ablative heat shields. Also, the X-15 and the Prime reentry vehicle were covered with ablator. All of this experience, together with the wealth of information obtained from unmanned ballistic entry programs form a sound basis for the application of ablators to the shuttle. Ablators are amenable to simple designs, and their reliability has been proven by the flight vehicles described previously. Ablators are efficient heat rejection systems and weight competitive with other proposed thermal protection systems. Ablators have the added advantage that their performance is not heating-rate limited. Thus, the design of an ablative heat shield is not sensitive to off-nominal trajectories. Ablators tend to be a highly forgiving system and are known to be insensitive to small imperfections. In addition to their thermal advantages, ablators, especially those with an elastomeric resin base, can substantially increase the damping of a structural panel, thus giving an added margin against aeroelastic instability.

The primary objection to the use of ablators on the shuttle is its limited life. At this time, we do not consider ablators as multi-mission thermal protection systems for the shuttle orbiter. The cost of producing ablators for previous manned systems was exceedingly high. Previous design criteria specified a defect free heat shield and, therefore, extensive quality control and defect repair procedures were necessary. Replacement of the ablator after every flight could significantly increase operational costs and could occupy a substantial portion of the time set aside for refurbishment following each flight. The present ablative heat shield technology program is aimed at eliminating the last four barriers so that one mission life is economically acceptable.

SPACE SHUTTLE ABLATIVE HEAT-SHIELD TECHNOLOGY

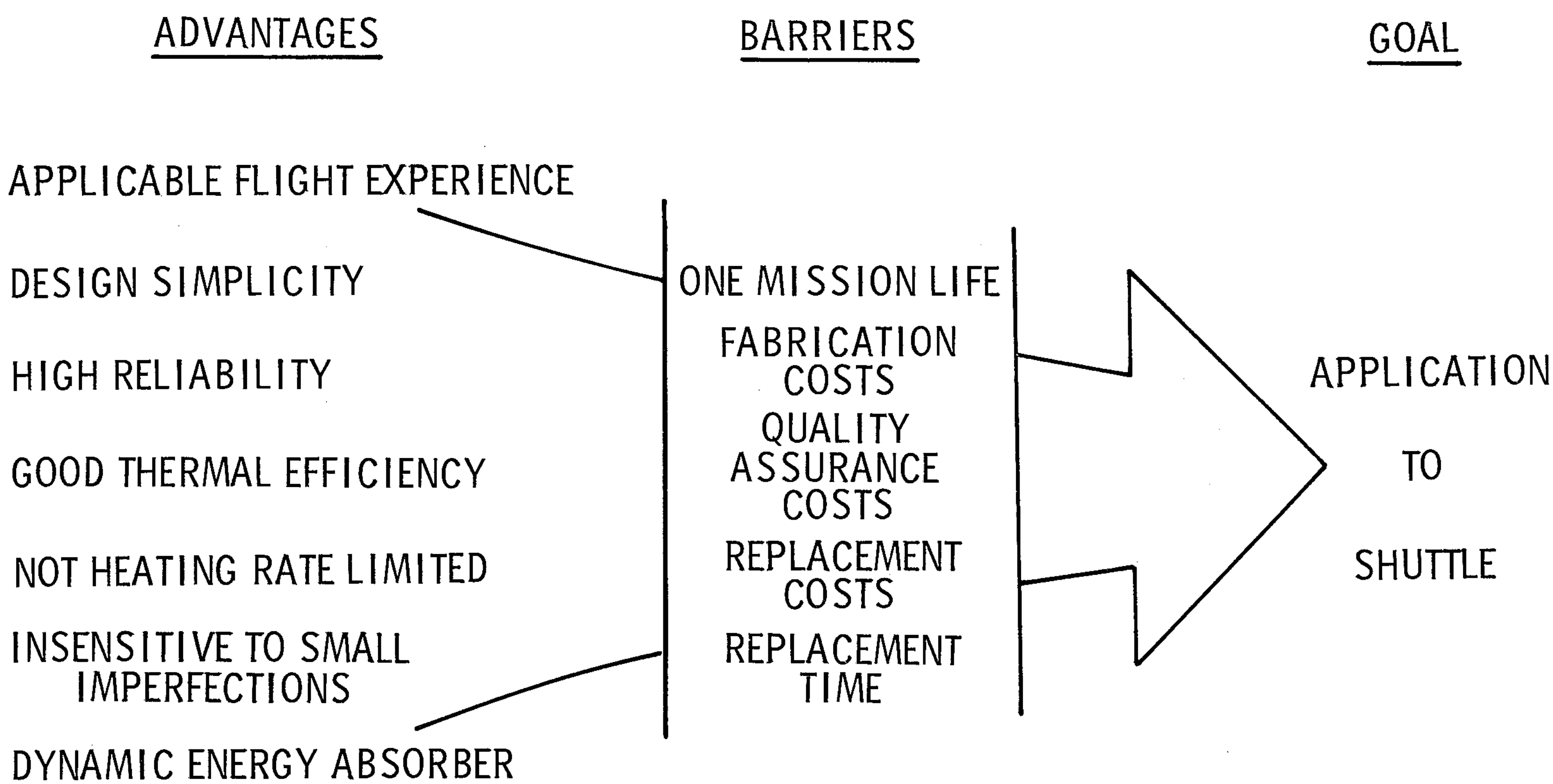

Figure 1

Figure 2a shows a simple replaceable ablative heat shield concept. An ablative material reinforced with honeycomb and bonded to a face sheet is attached with mechanical fasteners to the primary structure. Refurbishment is accomplished by coring out the plugs over the fasteners, removing the spent ablator together with its face sheet and replacing the entire assembly. If the primary structure of the vehicle does not include a structural skin, the ablators could be applied to a load carrying sub-panel. This design would look much the same as that shown for the surface insulation materials discussed in a paper by D. Greenshields (paper no. 1 of volume II of this compilation).

REPLACEABLE ABLATIVE HEAT-SHIELD

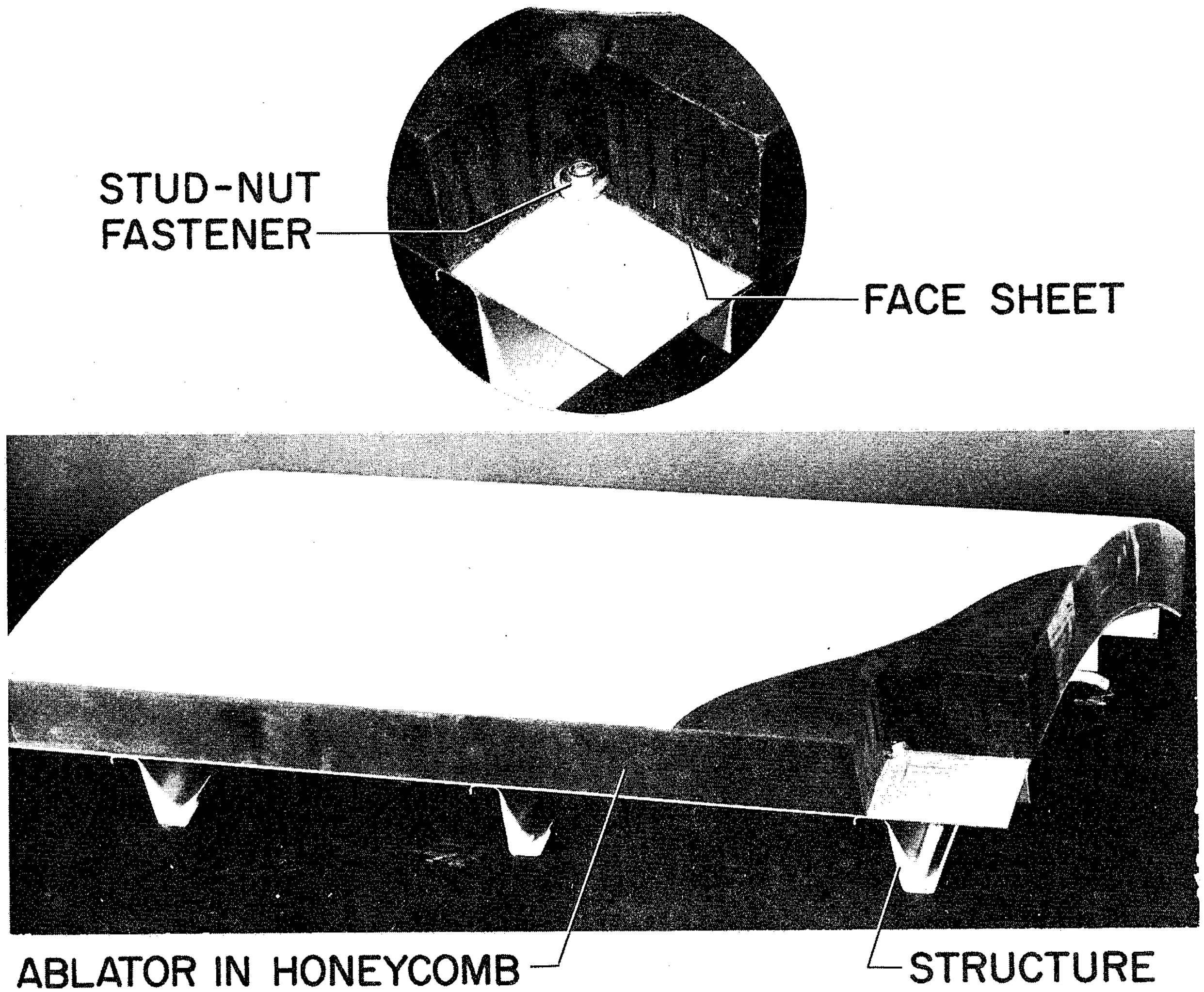

Figure 2(a)

To obtain a good estimate of the cost of ablative panels, parallel contracts were let with five firms to actually fabricate flat and curved panels of specified ablative materials. Typical panels fabricated under these contracts are shown in figure 2b. The material density including face sheet and honeycomb is approximately 15 lbs/cu.ft. Panels fabricated were 0.61m (2 ft.) x 1.22m (4 ft.) x 0.051m (2 in.) thick. Based on the actual costs incurred during the fabrication of eight panels, four flat and four curved, the contractors made cost estimates for various sizes, shapes, and quantities of panels (refs. 2, 3, 4, 5, and a B. F. Goodrich paper that is soon to be published as a NASA Contractor Report).

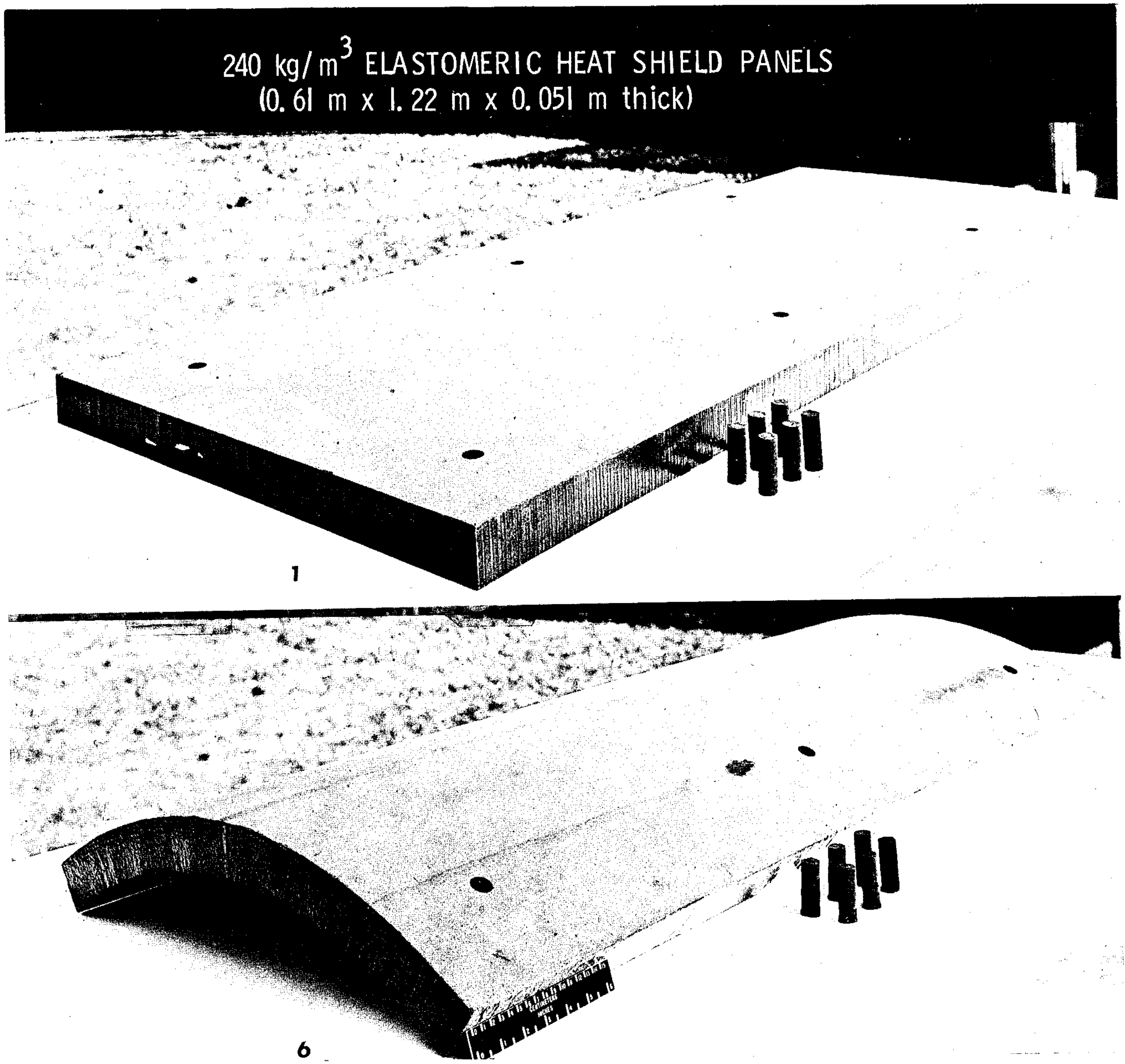

240 kg/m3 ELASTOMERIC HEAT SHIELD PANELS
(0.61 m x 1.22 m x 0.051 m thick)
1
6

Figure 2(b)

The estimated costs of 1.22m (4 ft.) x 1.83m (6 ft.) panels are summarized in figure 3. Two of the contracts were with major aerospace companies. The other three contracts were with companies that frequently work as sub-contractors in the fabrication of flight systems. The cost trends shown are very significant. First it should be noted that the highest estimate for the cost of one panel is an order of magnitude less than the cost of ablators on previous manned entry systems. In general the aerospace companies project costs which are significantly higher than those of the other companies. The only exception is in the fabrication of one panel where the company whose costs are the highest chose to build compression molds to fabricate the panels. It is apparent, however, that this tooling cost is rapidly amortized and costs drop significantly when as few as ten panels are made. Since it is estimated that one vehicle would have approximately 800 ablative panels, many panels of approximately the same size and shape would be required on each vehicle.

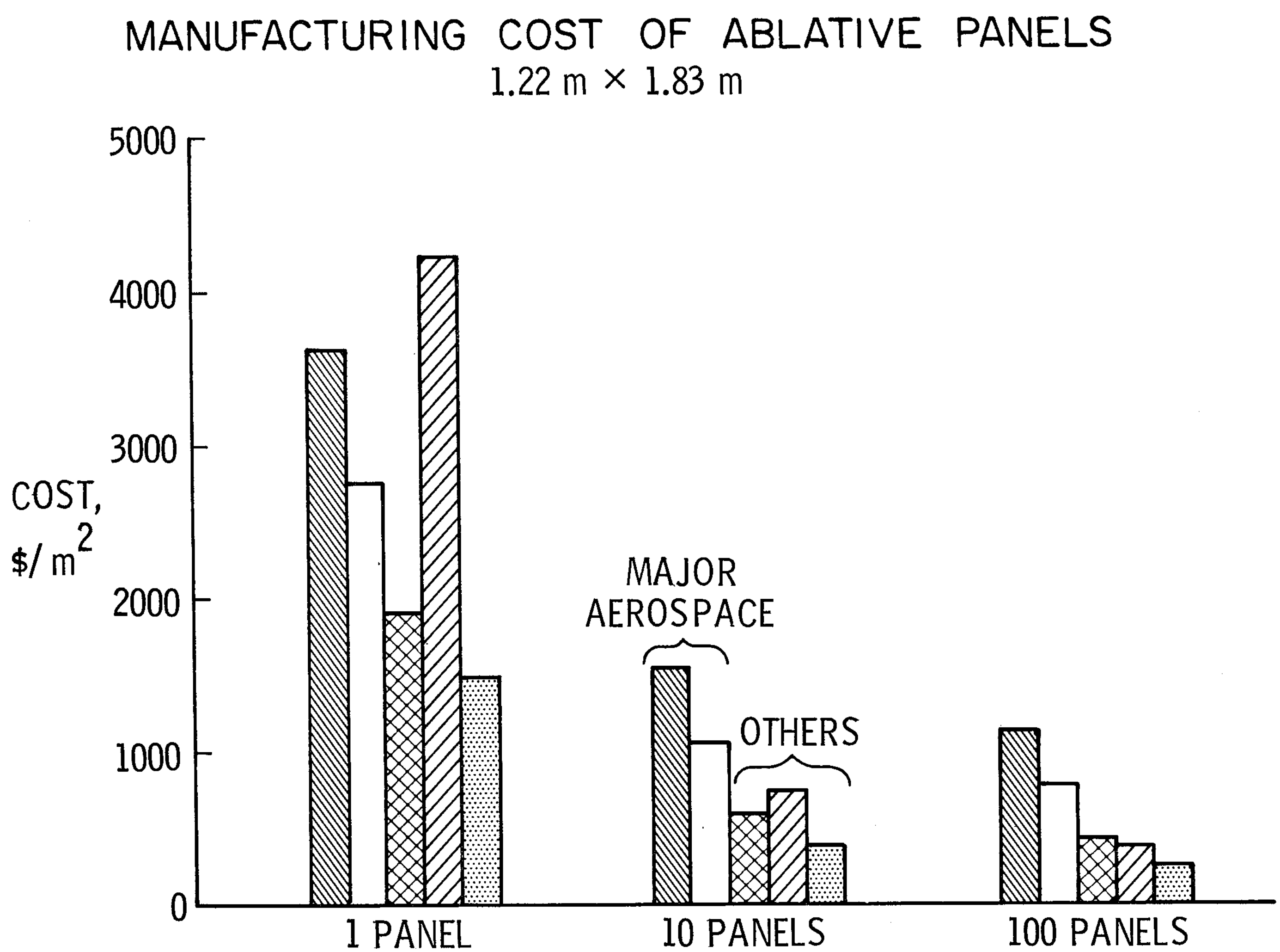
MANUFACTURING COST OF ABLATIVE PANELS
1.22 m × 1.83 m
COST, $/m²
5000
4000
3000
2000
1000
0
MAJOR AEROSPACE
OTHERS
1 PANEL
10 PANELS
100 PANELS

Figure 3

Another significant result from these studies is shown in figure 4. The total fabrication cost has been divided into various cost elements. More than half of the costs are incurred during the manufacturing process. Also, approximately one-half the material costs and 1/3 of the manufacturing costs are attributed to the use of the fiber-glass honeycomb reinforcement. Follow-on studies will consider ways to further reduce both of these costs.

ABLATIVE HEAT-SHIELD PANEL COST DISTRIBUTION

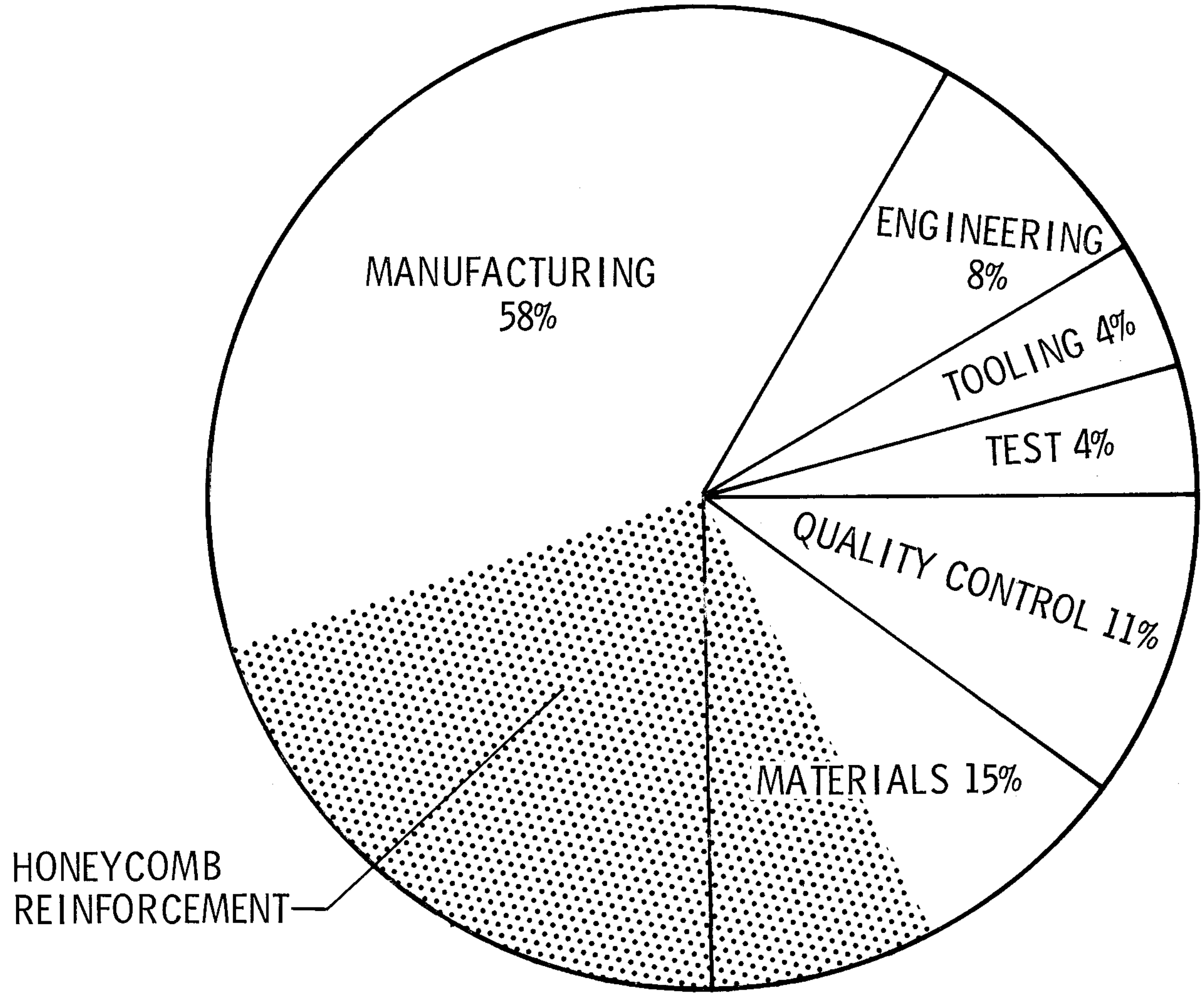

Figure 4

Since the greatest part of the cost is attributed to manufacturing, it is not surprising that the studies also show that increasing the panel size decreases costs substantially. This is shown in figure 5. Increasing the panel area by a factor of three results in about a 1/3 reduction in the unit area costs of the panels. The cost trends are consistent from one fabricator to another and the trends noted in figure 3 for the various types of fabricators are still apparent.

EFFECT OF SIZE ON PANEL COST

240 kg/m^3 ELASTOMER

NO. OF PANELS	PANEL SIZE	COST, $\$/m^2$			
		MARTIN	NORTH AMERICAN	BRUNSWICK	FANSTEEL
1	0.61 m × 1.22m	7621	4295	7244	1701
	1.22m × 1.83m	3595	2734	4209	1475
10	0.61m × 1.22m	2949	1668	1076	624
	1.22m × 1.83m	1550	1044	743	388
100	0.61m × 1.22m	1335	1152	441	344
	1.22m × 1.83m	1109	753	366	237

Figure 5

Tests are currently underway in an arc-heated wind tunnel to determine if the thermal performance of the materials has been compromised by the cheaper fabrication methods employed. Shown in figure 6 are the results that have been obtained to date on specimens taken from the panels fabricated by the two major aerospace companies. Test specimens from each panel were tested under constant stagnation heating rate conditions until a specified back surface temperature rise was obtained. The time required is then used to calculate the comparative efficiencies of the materials tested. The compositions tested included high and low-density phenolic-nylon and filled silicone elastomer. The high density panels were about 450 kg/m^3 (28 lbm/ft^3) and the low density panels were about 240 kg/m^3 (15 lbm/ft^3).

The shaded bars indicate the range of efficiency values obtained from tests of four samples taken from the top and bottom surfaces of both the flat and curved panels. It is apparent that the low-density materials have the highest efficiency at these heating conditions. Specimens from the curved panels were more inconsistent in their performance and this is the primary reason for the scatter in the data. Efficiencies of this magnitude are considered quite acceptable and are comparable to those obtained from tests of material samples made under much more controlled conditions.

THERMAL PERFORMANCE OF PANEL TEST SPECIMENS

HEATING RATE, 220 kW/m^2; 6.35-cm-DIAMETER BLUNT FACE

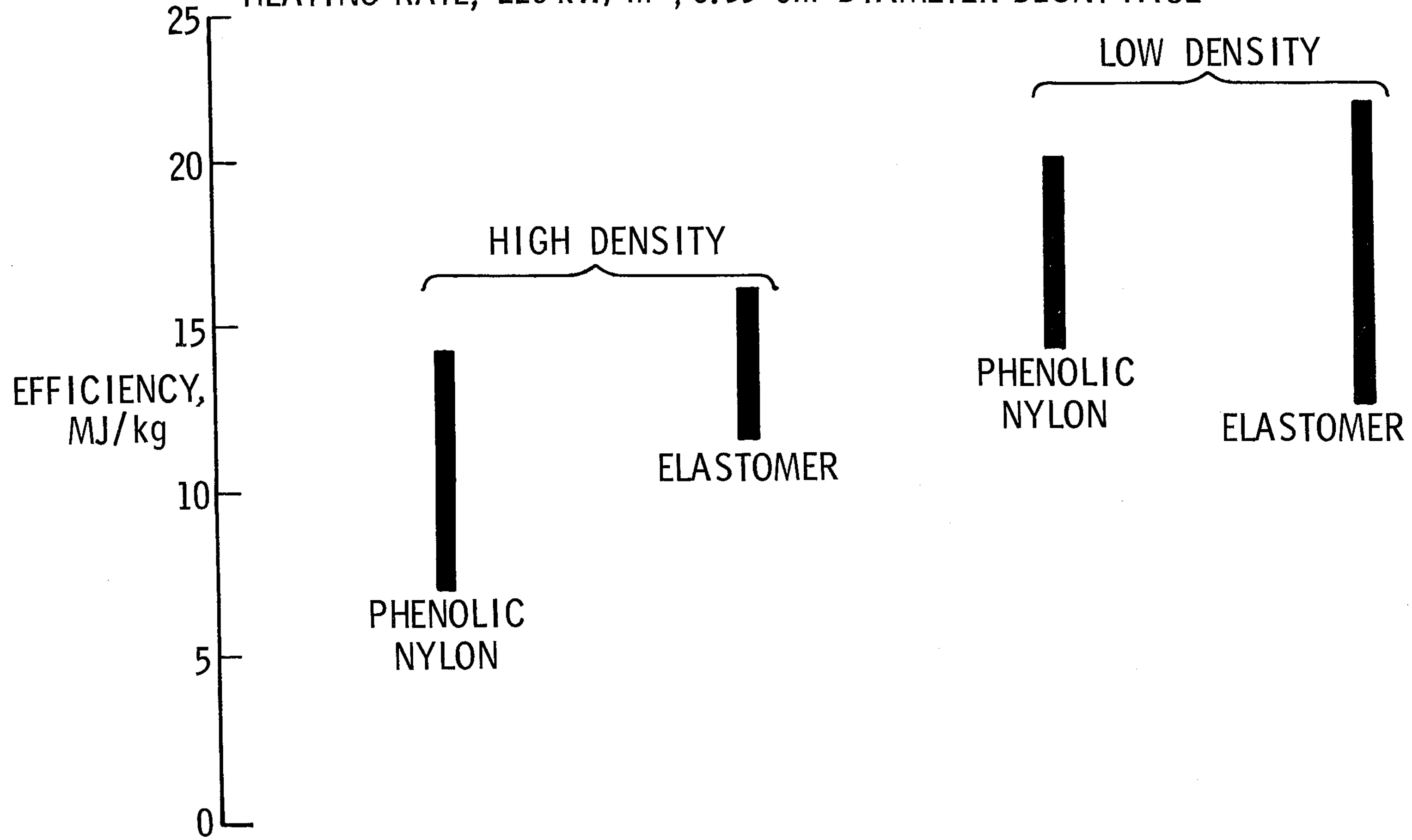

Figure 6

Since an ablative heat shield must be replaced after each flight and other heat shields must be inspected, refurbished, and eventually replaced, TPS refurbishment costs are important. We have two parallel contracts to study this problem (refs. 6 and 7). Some significant results of this effort are shown in figure 7. The contractors studied three types of thermal protection systems: replaceable ablators, low-density ceramics, and metallic heat shields. The results shown are based on an area of $745 m^2$ ($8000 ft^2$) and assumed a fixed material cost of $\$535/m^2$ ($\$50/ft^2$) for ablators, and $\$10400/m^2$ ($\$1000/ft^2$) for low density ceramics. The metallic system was divided into two parts: $280 m^2$ ($3000 ft^2$) of superalloys at $\$2150/m^2$ ($\$200/ft^2$) and $465 m^2$ ($5000 ft^2$) of coated refractory metal at $\$10400/m^2$ ($\$1000/ft^2$). The range of values shown for the various refurbishment items indicates the difference in the estimates of the two contractors. In each case the low estimate was from one contractor and the high estimate from the other. The number of manhours allotted to the removal and replacement of a heat shield panel is approximately the same for the three systems. The cost figures on the next line were obtained by using a labor rate of \$20/hr. The total heat shield refurbishment costs for 100 flights are obtained by assuming that the ablator is replaced after every flight, the low-density ceramic after about 25 flights, and the metallic shields after about 33 flights. The total costs for 100 flights are obtained by including material costs, fabrication costs, and refurbishment costs. It should be noted that the costs shown for low-density ceramics and metallic heat shields do not include between flight inspection and recertification of these systems. This study shows that material costs comprise a major portion of the total costs for all three systems and the wide range of estimates of the manhours required to refurbish systems has only a small effect on the total cost for the ceramic and metallic systems. For the ablative system, a factor of 10 variation in the estimate of refurbishment labor results in a factor of 2 1/2 in the estimates of the total heat shield cost.

THERMAL PROTECTION SYSTEM REFURBISHMENT COST ESTIMATES

ITEM	ABLATORS	LOW-DENSITY CERAMIC	METALLICS
REFURBISHMENT DIRECT LABOR, MAN hr/m^2	4.0 TO 50.7	3.3 TO 40.6	4.4 TO 33.0
REFURBISHMENT DIRECT LABOR COSTS, $/$m^2$	80 TO 1014	66 TO 812	88 TO 660
TOTAL HEAT-SHIELD REFURBISHMENT COSTS FOR 100 FLIGHTS, $/$m^2$	8000 TO 101, 400	264 TO 3248	264 TO 1980
TOTAL HEAT-SHIELD COST FOR 100 FLIGHTS, $(MILLIONS)	45.9 TO 115.4	32.2 TO 34.4	17.0 TO 18.3
TOTAL HEAT-SHIELD COST PER UNIT AREA FOR 100 FLIGHTS, $/$m^2$	61, 800 TO 155, 200	43, 304 TO 46, 288	22, 860 TO 24, 576

DOES NOT INCLUDE BETWEEN FLIGHT INSPECTION AND RECERTIFICATION OF CERAMIC OR METALLIC THERMAL PROTECTION SYSTEM

ASSUMED MFG COSTS: ABLATOR - 540 $/$m^2$, CERAMIC - 10 800 $/$m^2$, METALLIC - 7500 $/$m^2$

Figure 7

Because the cost of ablation material for a single flight is relatively low, ablators could easily be used on the first few flights without a significant increase in total program costs.

Figure 8 shows the cumulative cost of the three systems discussed on the previous figure. The costs shown do not include development and qualification costs or the cost of between flight inspection and recertification. The flat portions of the curves for the low-density ceramic and metallic systems would have a positive slope if between flight inspection and recertification costs were included. Although the estimates show ablators to be the most expensive system for 100 missions, it should be noted that the development costs for an ablative system should be substantially less than for either of the other two systems and ablators could be employed on, say, the first 10 flights without a major impact on total program costs.

HEAT SHIELD CUMULATIVE COST COMPARISON
EXCLUDING DEVELOPMENT AND BETWEEN FLIGHT INSPECTION AND RECERTIFICATION COSTS

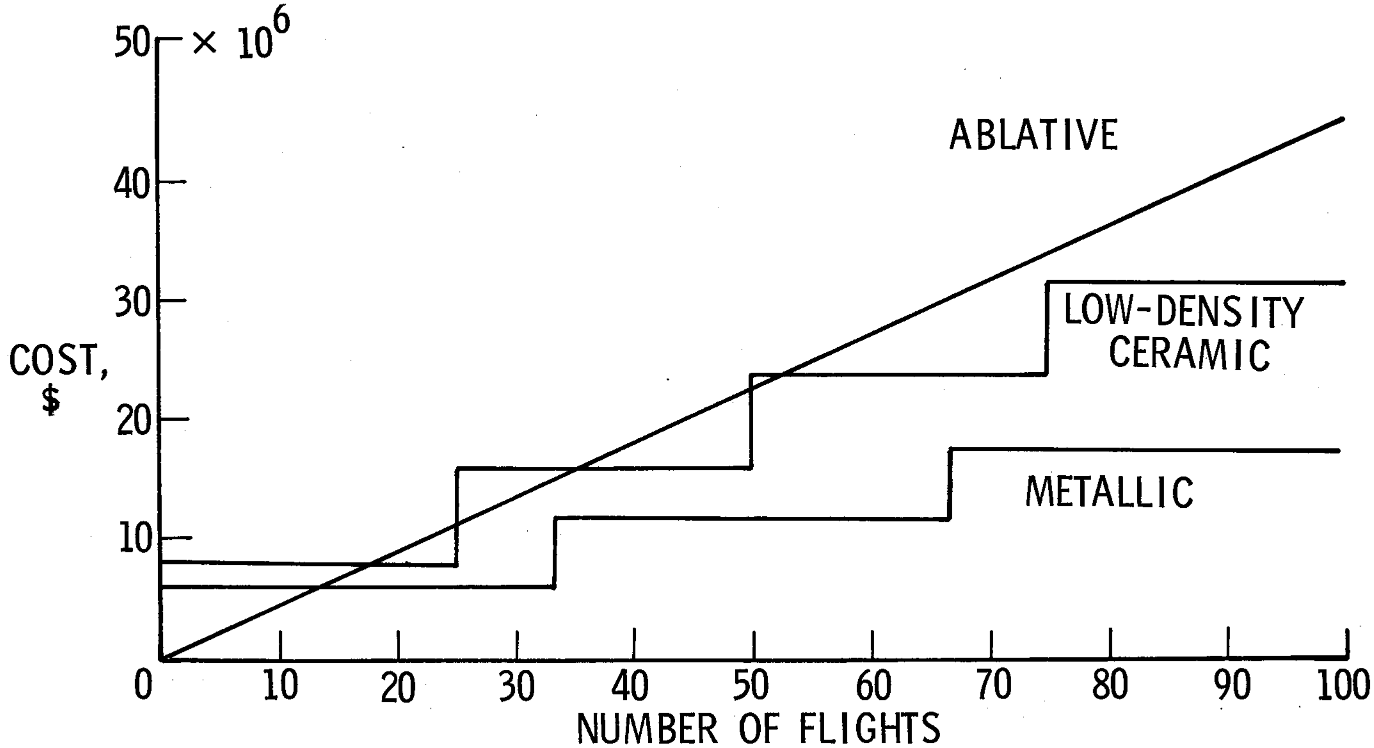

Figure 8

As noted above, the variations in estimates of labor required to refurbish ablative systems results in a substantial difference in the estimated total heat shield cost. To obtain a better estimate of the actual costs associated with refurbishing an ablative system, a follow–on study is planned using the refurbishment mock–up shown in figure 9. The mock–up is a cylindrical segment approximately 3m (10 ft) wide and 6m (20 ft) long and can be positioned by rotating about an axis parallel to the axis of the cylinder. The ring sections are movable and can be used to simulate various ring spacings on the primary structure or to support the heat shield attachment structure.

THERMAL PROTECTION SYSTEM REFURBISHMENT MOCK-UP

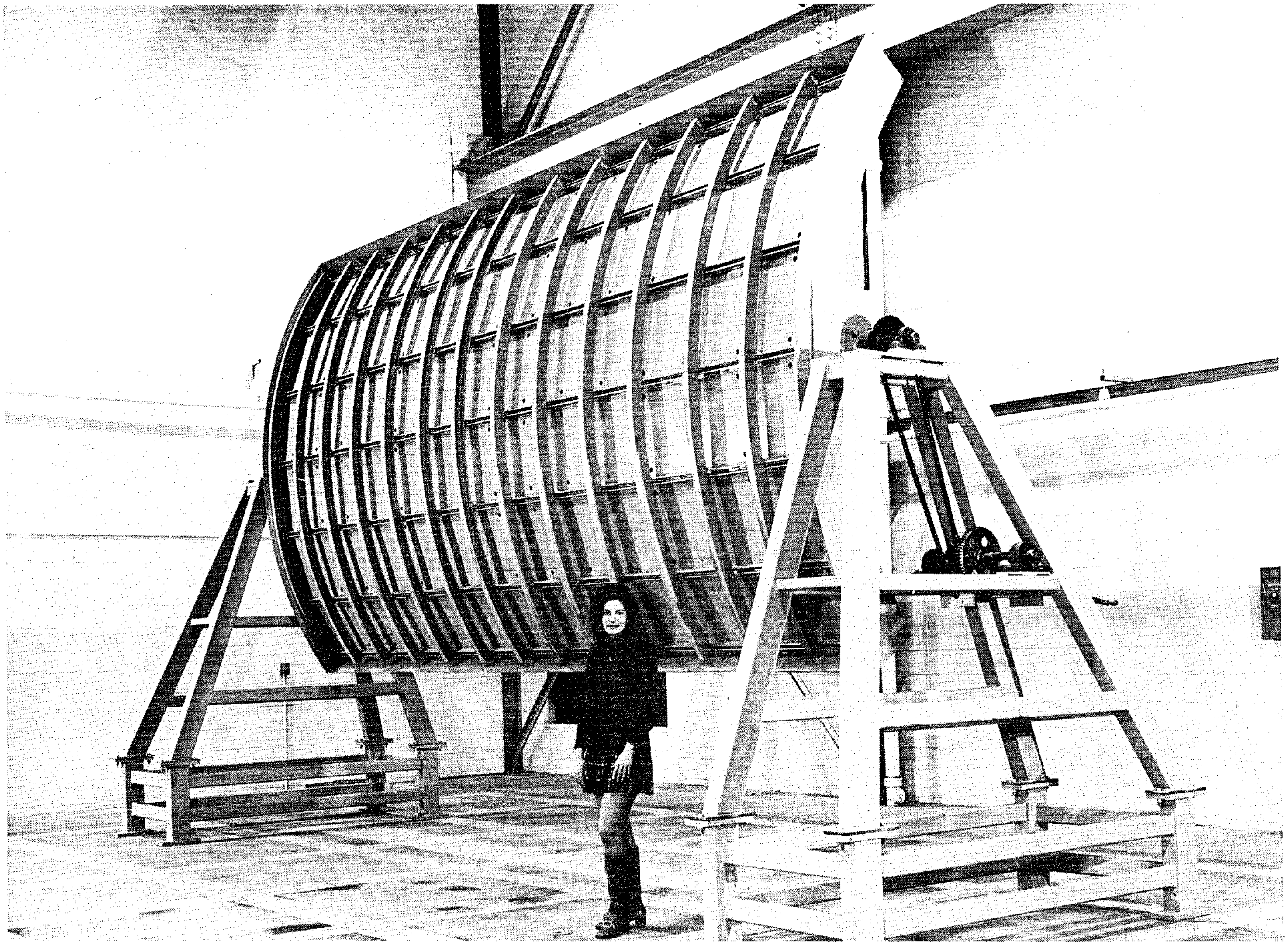

Figure 9

In fabricating thermal protection systems for manned reentry vehicles, great care is taken to insure that the system is free of any flaws or defects that could possibly lead to failure of a mission. Fabrication time and cost could be substantially reduced if it were determined that, over the range of environments of interest, the performance of the heat shield is not critically affected by defects previously considered unacceptable. Some evidence that defects can be accepted was obtained nearly ten years ago in relation to the Apollo program. It was considered necessary at one time to make holes through the Apollo ablative heat shield to accommodate certain external connections. Figure 10 shows a model designed to investigate this problem. This model, about 7.5 cm (3 in.) in diameter, shows a design for an electrical interface through the heat shield. Many of these holes go completely through the ablation material. It was found that the presence of these holes did not significantly affect the thermal performance of this material.

APOLLO ELECTRICAL INTERFACE TEST SPECIMEN

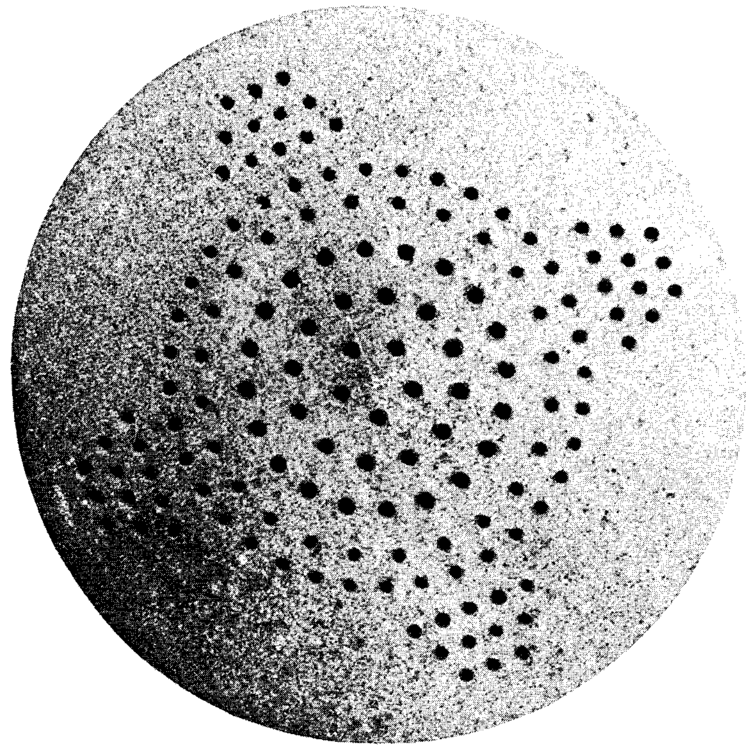

Figure 10

Because of this Apollo experience, a defect study on space shuttle ablation materials was initiated. The objective of this study is to determine what types of defects can be considered non-critical and establish methods for identifying critical defects. The acceptance of certain non-critical defects should lead to relaxed quality control requirements and thus to a further reduction in ablative heat shield costs. The interaction of defects, material performance and cost is illustrated on figure 11. The ablation material being considered is a low-density elastomer in honeycomb. The defects shown here are typical of those that frequently occur in fabricating heat shield panels. The presence of defects such as these may or may not influence the overall material performance through the effect on certain properties of the material such as those shown here. The performance and cost are related through various cost factors as shown here. Whether or not a defect is allowed, of course, depends ultimately on its effect on material performance. In this study,models containing various defects will be tested and their performance compared to that of control models which will be as free of defects as possible. The sensitivity of performance to the presence of defects will be determined and finally the cost impact of allowing defects in shuttle heat shields will be evaluated.

THE INFLUENCE OF DEFECTS ON PERFORMANCE AND COST

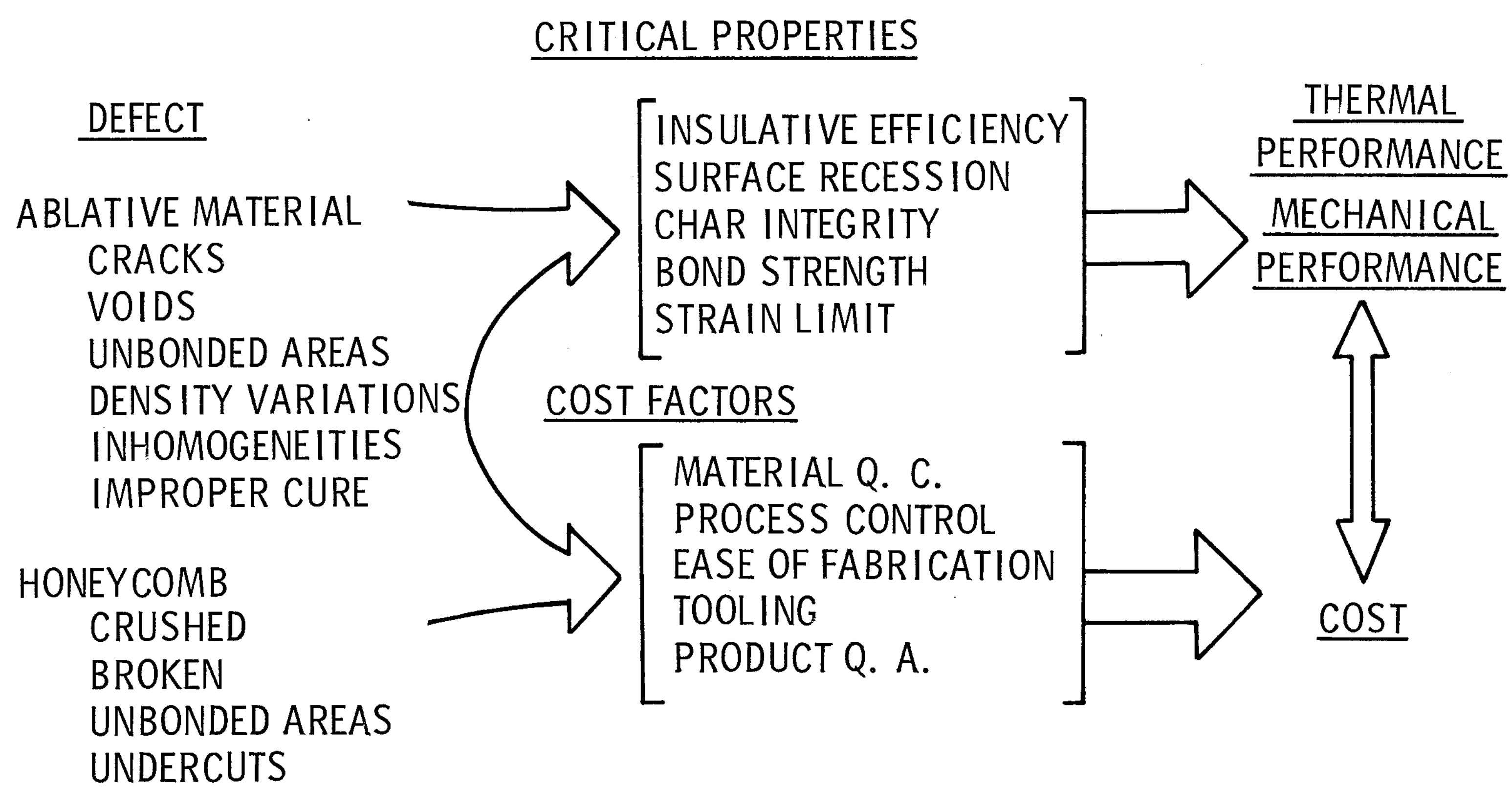

Figure 11

Techniques for detecting critical flaws are also being investigated. Figure 12 shows a typical X-ray radiograph of an ablative panel. Interpretation of such radiographs has always been difficult and time consuming.

X-RAY PHOTOGRAPH OF ABLATIVE PANEL

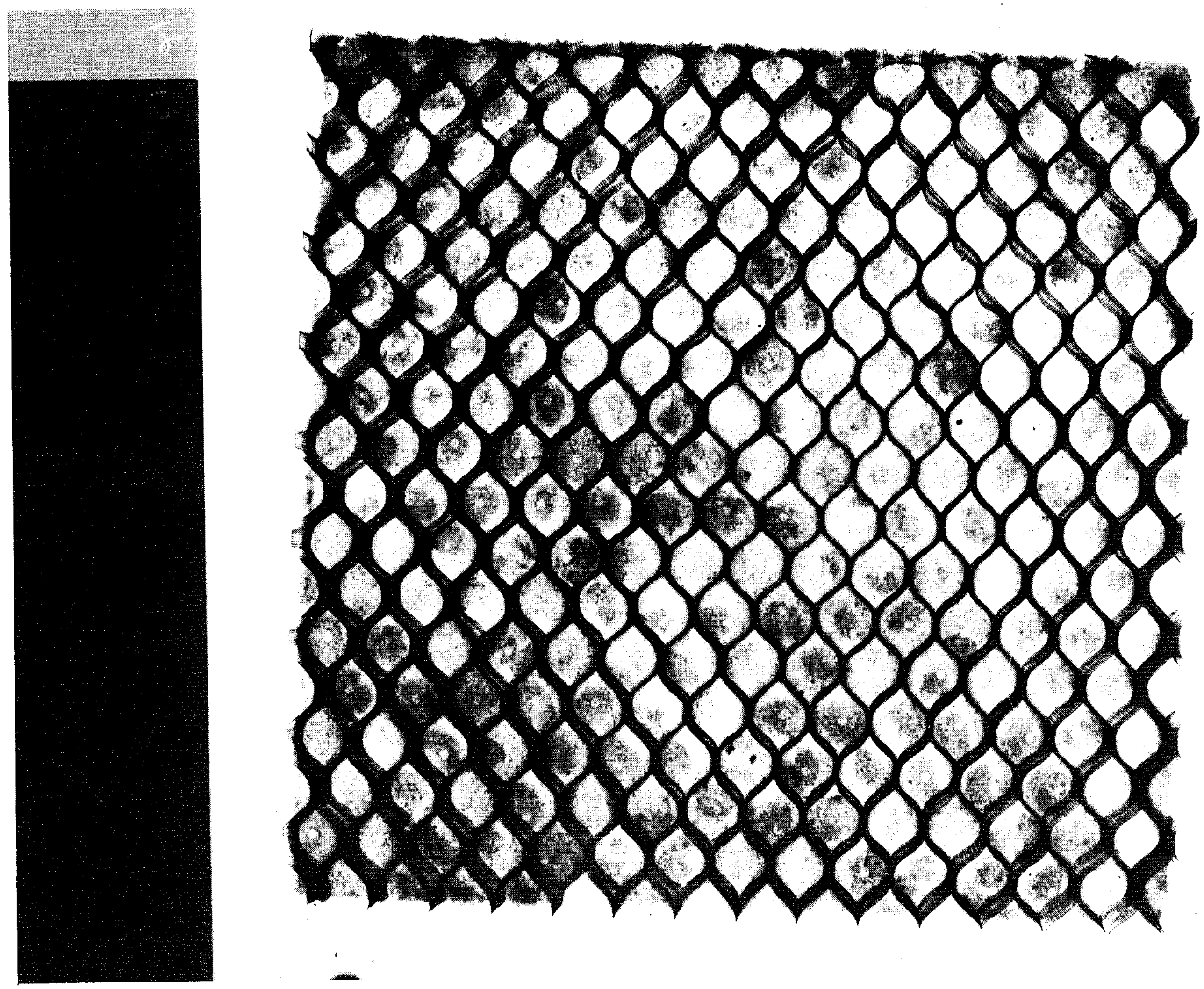

Figure 12

A new technique being developed by the Martin–Marietta Corporation utilizes a television scanner and digitizing system to select various grey bands and convert them to a pseudo color picture as shown on figure 13. Here each color represents a band of densities on the X–ray. The color picture provides a type of enhancement that simplifies the interpretation of the X–ray.

COLOR REPRESENTATION OF X-RAY PHOTO

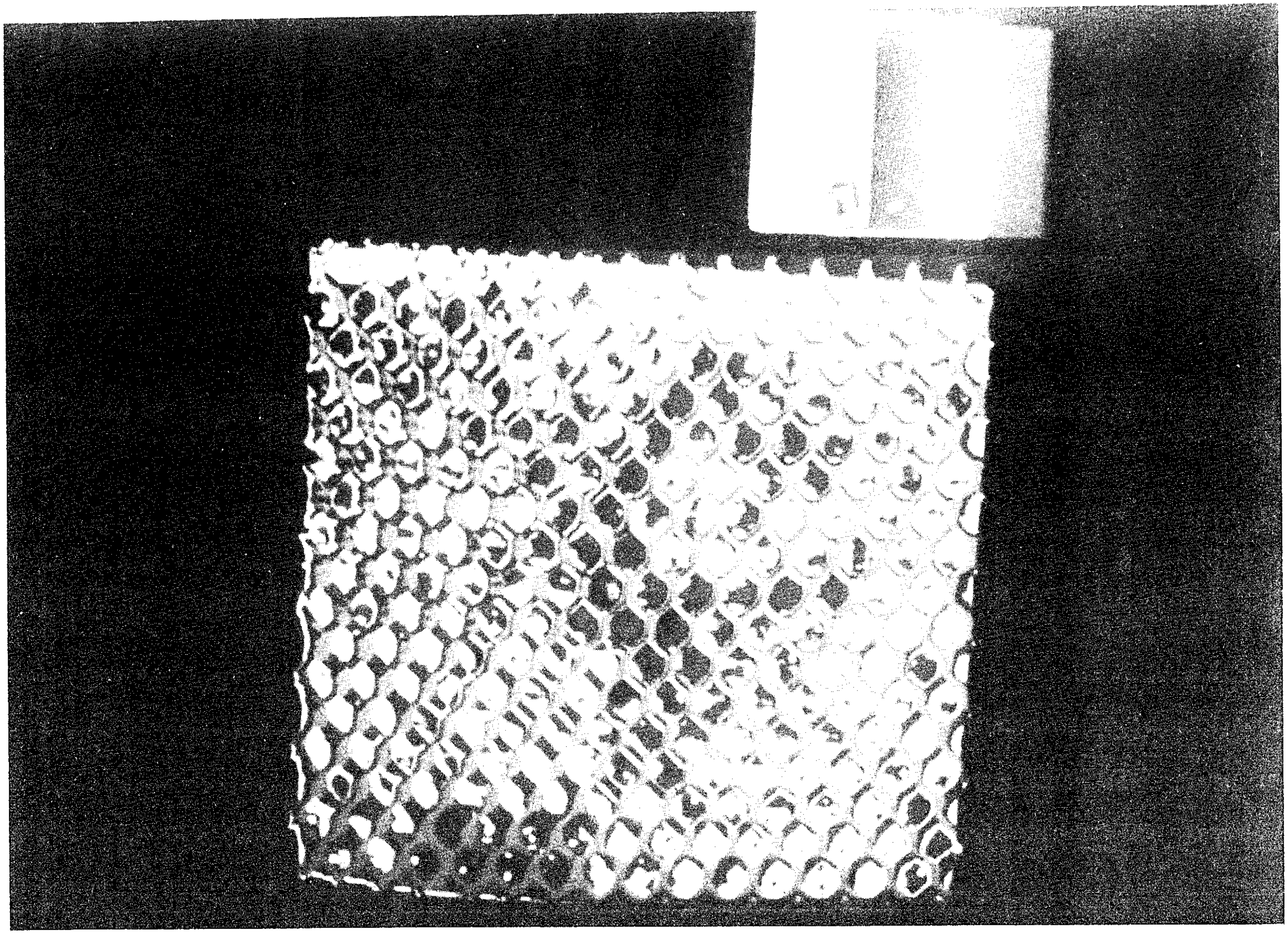

Figure 13

The status of ablative thermal protection systems for application to the shuttle is shown on figure 14. Ablative materials such as those flown on Prime and Apollo could be used now to withstand the shuttle thermal environment. Newer materials, however, which are more efficient for shuttle entry heating conditions, are in an advanced state of development, and, therefore the research, development, and flight qualification costs for these materials should be substantially less than those for any other thermal protection system. Based on the fabrication studies performed to date, it is apparent that ablative heat shields for shuttle should cost an order of magnitude less than those currently being used for flight programs. Costs as low as $\$540/m^2$ ($\$50/ft^2$) appear well within reach. A study of the cost involved in refurbishing thermal protection systems indicates that basic material and manufacturing costs are still the most significant cost factor. Since ablators need not be 100% defect free, in order to function effectively, we believe that quality assurance costs can be significantly reduced by accepting defects which do not substantially degrade thermal or mechanical performance. Because of the extensive experience that has been gained from the use of ablators on reentry systems, ablators are more advanced in their state of development than any other proposed thermal protection system and could be applied to early flight vehicles. The use of ablators on early flight vehicles would not impose a weight penalty and would have little impact on total program cost.

ABLATIVE THERMAL PROTECTION SYSTEM STATUS

- FLIGHT QUALIFIED ABLATIVE MATERIALS ARE AVAILABLE.
- RESEARCH DEVELOPMENT, AND FLIGHT QUALIFICATION COSTS FOR SHUTTLE ABLATORS SHOULD BE SUBSTANTIALLY LESS THAN THOSE ASSOCIATED WITH OTHER THERMAL PROTECTION SYSTEMS.
- SHUTTLE ABLATIVE HEAT SHIELDS SHOULD COST AN ORDER-OF-MAGNITUDE LESS THAN CURRENT ABLATIVE FLIGHT HEAT SHIELDS.
- MANUFACTURING COSTS ARE THE MOST SIGNIFICIENT COST FACTOR
- CURRENT STUDIES SHOULD SHOW THAT Q.A. COSTS CAN BE SIGNIFICANTLY REDUCED.
- ABLATORS FOR SHUTTLE ARE IN AN ADVANCED STATE OF DEVELOPMENT AND COULD BE APPLIED TO EARLY FLIGHT VEHICLES WITHOUT WEIGHT PENALTY AND WITH LITTLE IMPACT ON TOTAL PROGRAM COST.

Figure 14

REFERENCES

1. Swann, R.T.: Low-Cost Ablative Heat Shields. NASA TMX-52876, vol. III, July 1970.
2. Norwood, L.B.: Low-Cost Ablative Heat Shield for Space Shuttles. NASA CR-111795, Nov. 1970.
3. Chandler, Huel H.: Low-Cost Ablative Heat Shields for Space Shuttles. NASA CR-111800, Oct. 1970.
4. Dulak, R.E., and Cecka, A.M.: Low-Cost Ablative Heat Shields for Space Shuttles. NASA CR-111814, Dec. 1970.
5. Abbott, Harry T.: Low-Cost Fabrication Method for Ablative Heat Shield Panels for Space Shuttles. NASA CR-111835, Jan. 1970.
6. Haas, D.W.: Refurbishment Cost Study of the Thermal Protection System of a Space Shuttle Vehicle. NASA CR-111833, Mar. 1970.
7. Peterson, Robert J.: Refurbishment Cost Study of the Thermal Protection System of a Space Shuttle Vehicle. NASA CR-111830, Mar. 1970.

ABLATIVE LEADING-EDGE DESIGN CONCEPTS FOR THE SHUTTLE ORBITER

By

John W. Graham	Avco Systems Division
David A. Mosher	Avco Systems Division
Ira Victer	Grumman Aerospace Corporation

INTRODUCTION

The leading-edge areas of the Space Shuttle Orbiter will experience temperatures of 1365°K (2,000°F) to 1920°K (3,000°F) during entry. For this temperature range, there are four candidate Thermal Protection System (TPS) materials: (1) high temperature coated refractory metals; (2) oxidation resistant carbon/carbon; (3) zirconium diborides, and (4) ablators.

Although the first three materials offer the potential advantage of limited reusability, they are not currently available and will incur higher risks (with inherently higher costs and potential schedule slippages) associated with their development. Furthermore, these materials would raise serious questions about their reliability for the first few flight tests, because of their limited flight test experience and the difficulty in applying rational design margins in their application.

Ablators, on the other hand, are readily available and/or can be developed for specific applications with minimum costs, time, and risk. An ablator leading edge would serve to determine the actual environment during initial shuttle flights. This environment may prove to be different from that predicated and the inherent conservative nature of an ablator material will minimize risks during the early flight test program.

This presentation summarizes the results of preliminary efforts in the design of an ablator leading edge for the shuttle orbiter. Design considerations, refurbishment concepts, analysis and test results are discussed together with the significant conclusions reached during the studies.

PAPER 6

DESIGN OBJECTIVES

Figure 1 shows the goals which must be met in the design of an ablator leading edge. Unless each of these items is accomplished, it will not be possible to satisfy the overall low cost objectives of the space shuttle program.

Although the first four items are self-explanatory, the last one requires some detailed discussions. The ablator can affect the shuttle performance in many ways including:

1. Shape change and surface roughness incurred during entry which will affect subsonic performance

2. Aggravated heating conditions on adjacent TPS caused by differential ablation at joints

3. Degradation of surface of adjacent TPS caused by ablation products flowing downstream

These three factors must be minimized to allow an acceptable ablator leading-edge design.

DESIGN OBJECTIVES

- EASILY REFURBISHABLE
- LOW COST
- LOW WEIGHT
- MINIMUM DEVELOPMENT REQUIREMENTS
- MINIMUM EFFECT ON SHUTTLE PERFORMANCE

Figure 1

TYPICAL LEADING-EDGE CONFIGURATION

It is envisioned that the leading edge of the shuttle will consist of several panels as shown in Figure 2. The span length of each panel depends on the wing rib spacing and ground handling requirements. In addition, thermal growth and interpanel gaps caused by wing deflection must be considered in defining panel span length. Seals will be required between ablator segments and the interfaces between the ablator and adjacent thermal protection system on the windward and leeward sections of the wing.

LEADING-EDGE CONFIGURATION

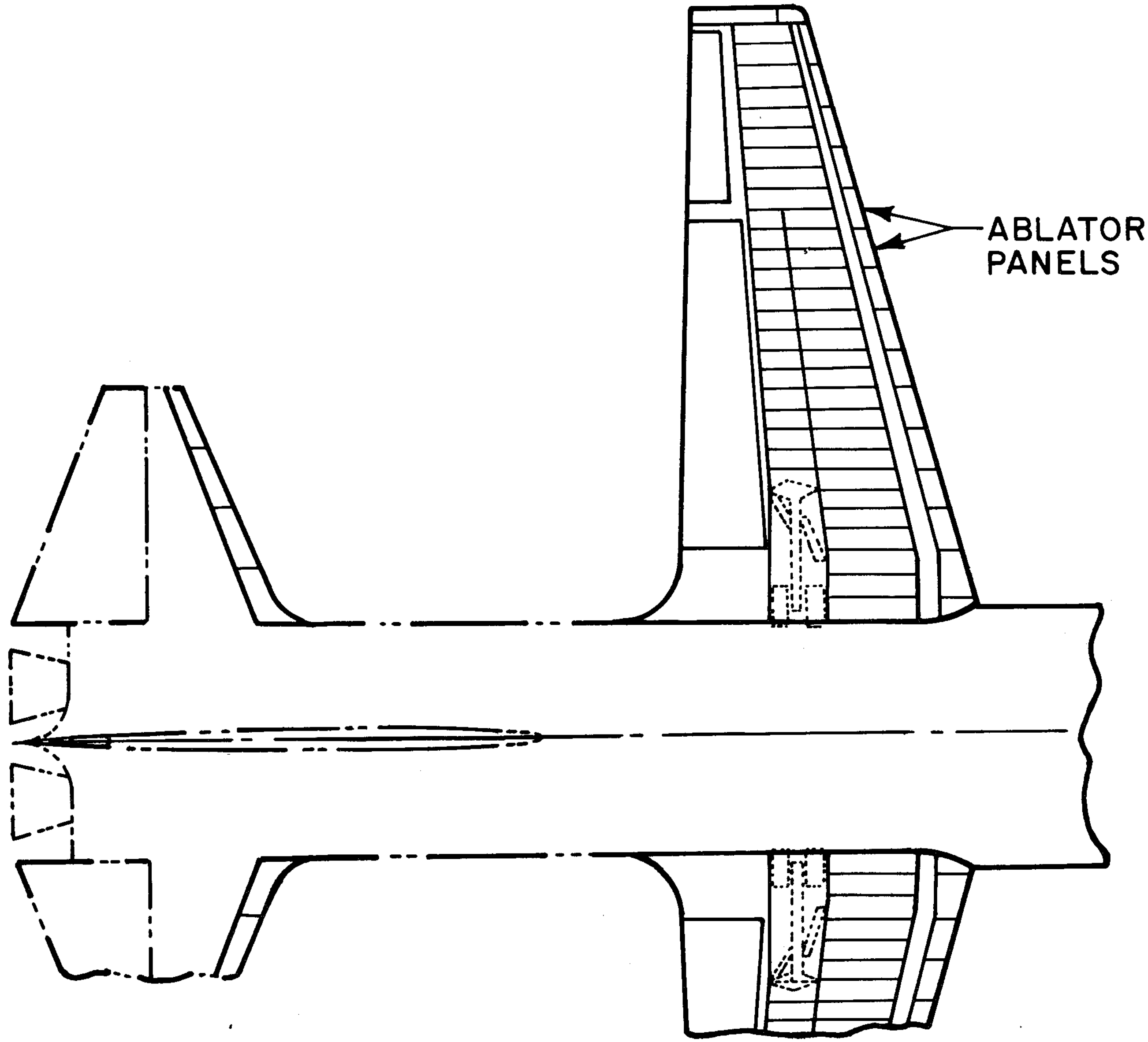

Figure 2

INSTALLATION CONCEPTS

These panels can be installed and refurbished in a number of ways. Figure 3 depicts possible methods for sequential, alternating, and random installation. Although the sequential approach has drawbacks, particularly from the unpredictable damage and replacement standpoint, it does, by providing internal accessibility by means of the end of each panel, present the possibility of eliminating a large number of ablator penetrations (bolt plugs) and reducing refurbishment time through end-actuated or internal attachment design schemes. To remove a leading edge (nose) panel at random, a draft angle along the chord is required to break free and slide along the gap seal. Each panel cannot have positive draft, but every other panel can be wedge shaped and, therefore, be removed or installed as shown in the alternately installed concept. This approach is considered for a number of the concepts for its offers a logical compromise between sequential and random panel removal. Random panel removal requires a solution to the wave seal break-free release problem other than dependence on chordwise panel draft.

INSTALLATION CONCEPTS

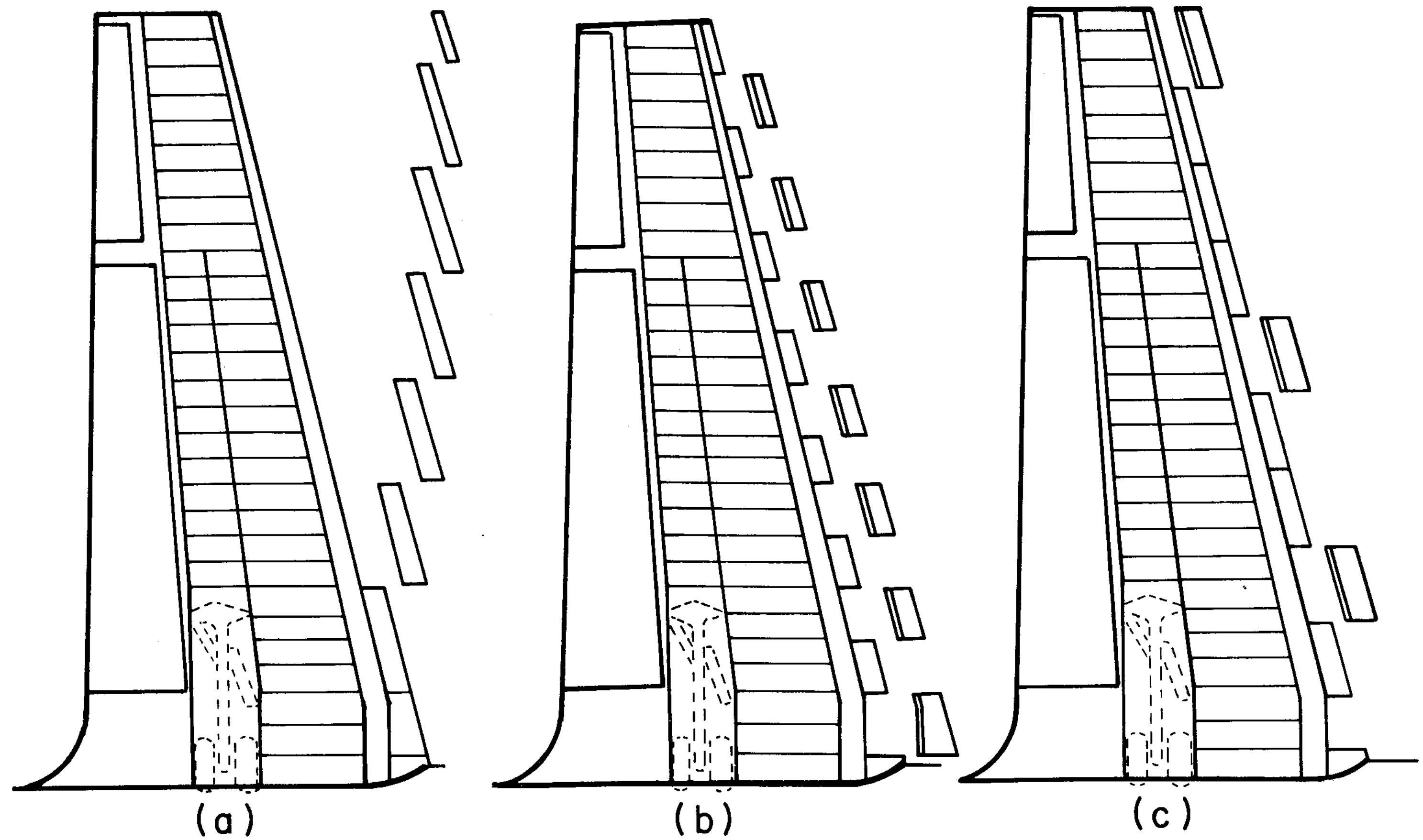

(a) SEQUENTIALLY INSTALLED LEADING EDGE
(b) ALTERNATELY INSTALLED LEADING EDGE
(c) RANDOMLY INSTALLED LEADING EDGE

Figure 3

ABLATOR LEADING-EDGE BOLT-ON DESIGN

Figure 4 depicts an approach whereby standard hardware (bolts) are used as the TPS attachment. The refurbishment sequence is initiated by the removal of the lower panel located between the front spar and the nose section. This removal procedure is initiated by removing the threaded ablator plugs which cover the heads of the panel attachment bolts. Once these bolts are removed, this panel is free to be removed downward to allow the worker access to reach into the wing and to remove the bolts which secure the nose panel. This procedure is repeated for every other panel (spanwise); thus, the remaining panels can then be removed either through an operation similar to the external bolt method or by internal means accessible through the open ends of each remaining panel.

Figure 4 further depicts a throw-away nose structure (i.e. ablator bonded) and a reusable lower panel structure (i.e. ablator mechanically attached). Either approach can be considered for all panels, the final choice being dependent upon the selected substructure cost and the refurbishment time. It is interesting to note that an extra set of substructure panels allows off-site ablator to substructure refurbishment; as a result, improved working and inspection conditions are provided without influencing vehicle turnaround time.

ABLATOR LEADING-EDGE BOLT-ON DESIGN

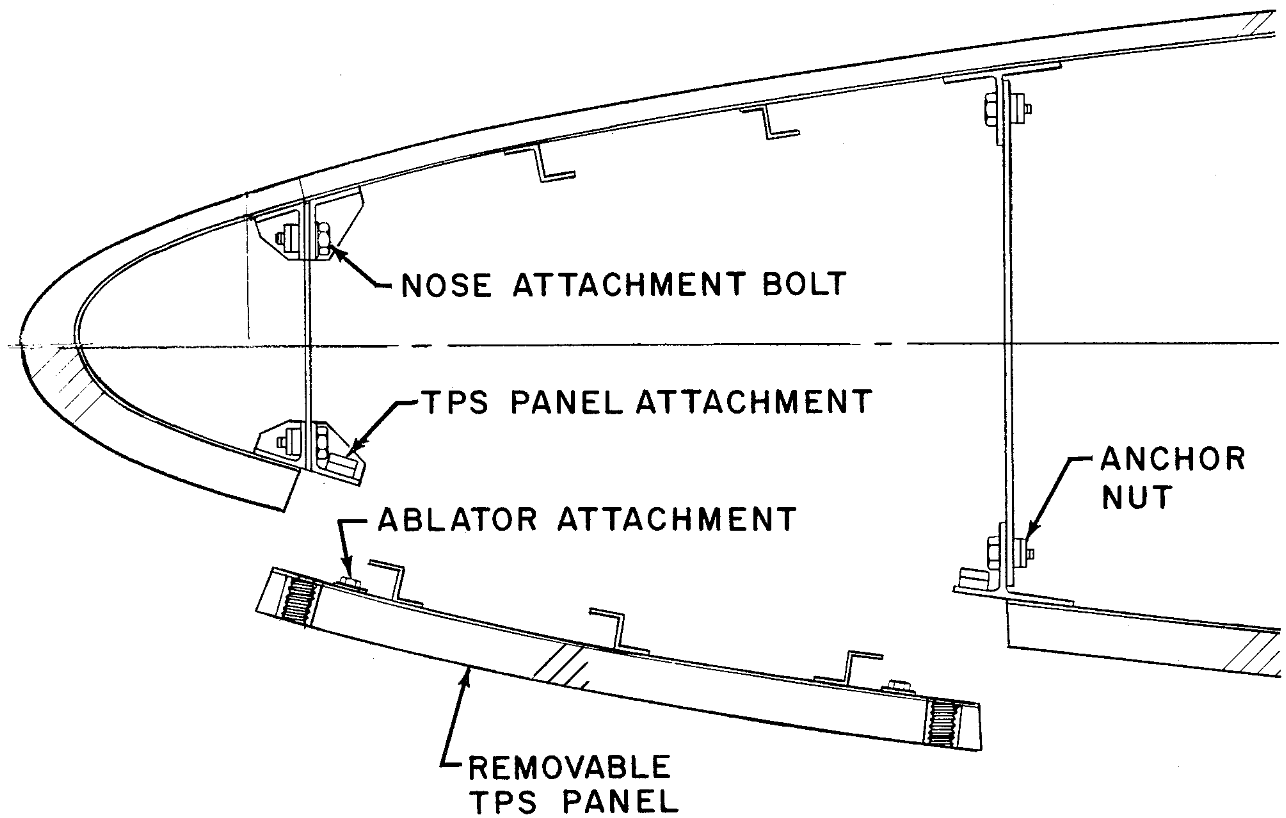

Figure 4

ABLATOR LEADING-EDGE QUICK-RELEASE DESIGN

This concept (Figure 5) presents two excellent advantages with respect to the design objectives for leading-edge thermal protection systems. First leading-edge removal and replacement is extremely rapid. The operation requires the removal of one ablator plug and the rotation of a single drive which operates the remote internal attachments which releases any leading-edge panel. The second advantage is the elimination of all but one external ablator attachment and attachment protection plug. Logistics, cost reduction, and reliability advantages exist for this approach. This concept requires an active program to develop a smooth working internal attachment mechanism which can withstand the entire spectrum of shuttle environments, including vibrations, cold soak, and reentry while maintaining acceptable operating characteristics.

ABLATOR LEADING-EDGE QUICK-RELEASE DESIGN

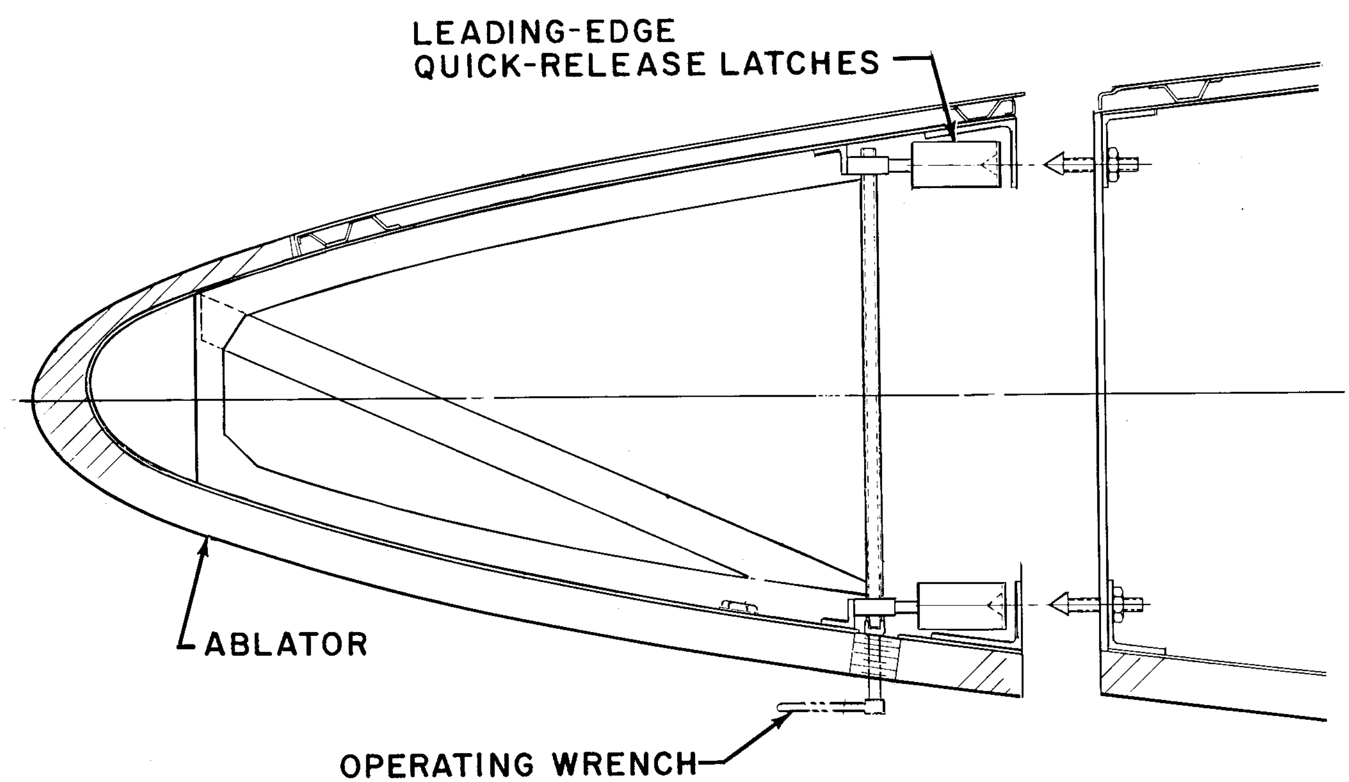

Figure 5

ABLATOR LEADING-EDGE HINGE-PIN DESIGN

Figure 6 shows a sequential panel installation utilizing a continuous piano hinge. The hinge pin is removed from the exposed end of the panel to release the leading edge. This type of hinge offers continuous and lightweight structural continuity as compared with point attachment concepts and totally eliminates ablator penetrations (bolt plugs). The concept would require some development testing in typical shuttle environments to demonstrate design adequacy. The sequential installation aspect of this design inhibits singular replacement of damaged panels. However, this approach could also be used in conjunction with a concept which would allow individual removal of every other panel. A combination system could result in the most efficient design when refurbishment time and ease of access factors are considered.

ABLATOR LEADING-EDGE HINGE-PIN DESIGN

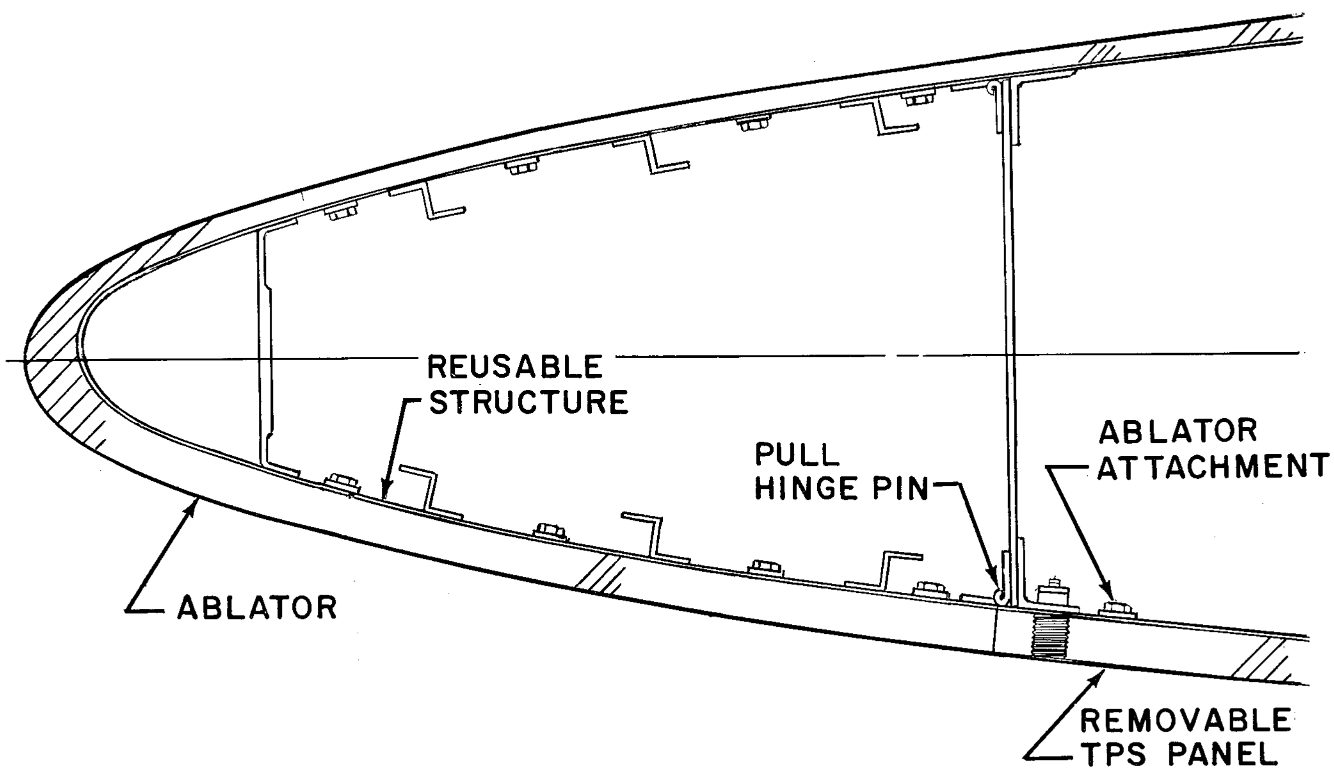

Figure 6

ABLATOR ATTACHMENT -- MOLDED-IN-PLACE INSERT

There are a number of methods of attaching the ablator to its substructure with the final selection influenced by ablator properties, vehicle environment, refurbishment approach, operational cost, as well as a number of other factors. Adhesive bonding and mechanical (bolting) attachment are two of the more practical methods, the latter offering practical substructure reuse and the possibility of higher backface temperatures.

Figure 7 depicts a refurbishable ablator panel which is bolted to a stiffened sheet substructure. This ablator/substructure panel assembly is, in turn, bolted to the vehicle structure on its periphery, access to these bolts being provided by removable ablator plugs. Integrally molded within the ablator are a number of thin-walled inserts containing floating self-locking nuts which provide for the ablator attachment. A thin scrim cloth covers the ablator backface to form a structural tie to resist cracking (loss of free pieces) and enhances the distribution of attachment loads.

ABLATOR ATTACHMENT - MOLDED-IN-PLACE INSERT

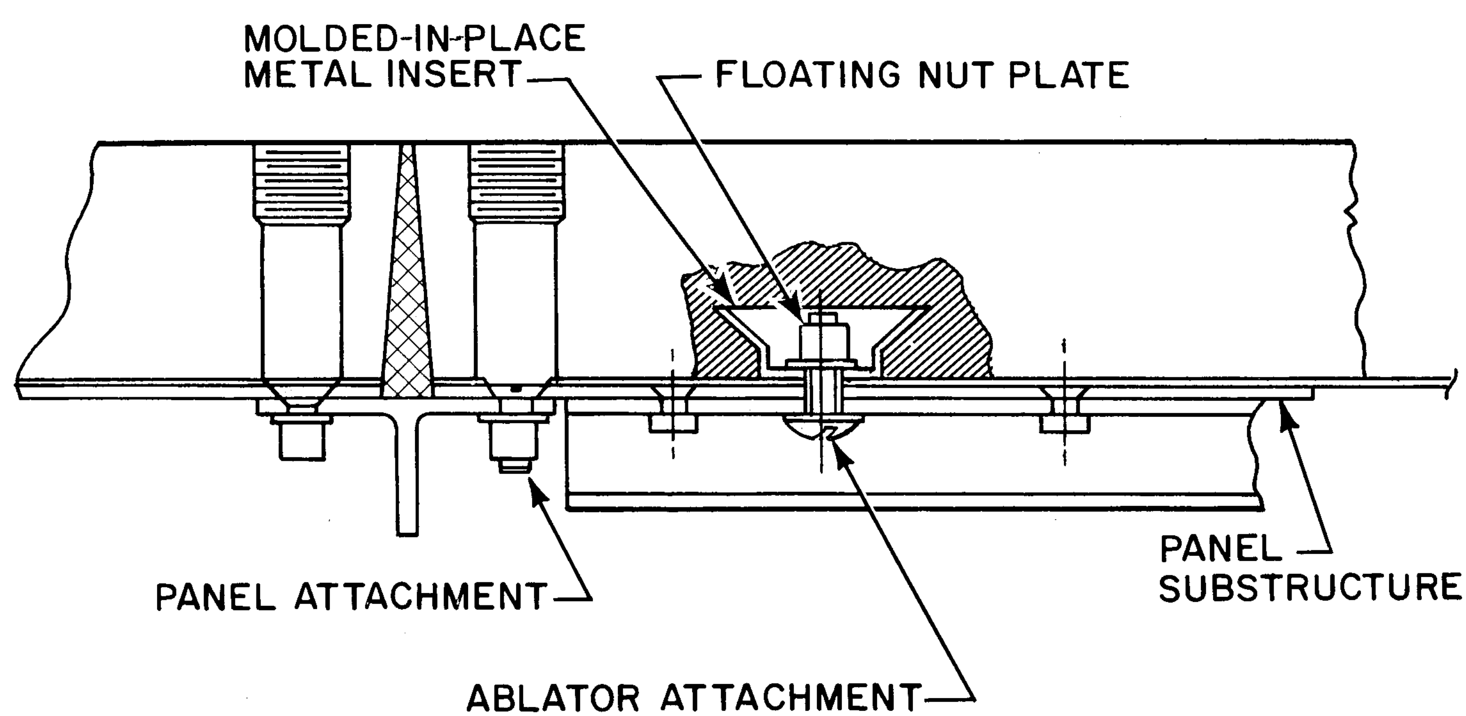

Figure 7

VIBRATION TEST OF LEADING-EDGE ABLATIVE PANEL

Some preliminary experimental studies have already been conducted at Avco and an illustration of the leading-edge test set-up used is shown in Figure 8. The dynamic test environment investigated included both sinusoidal and random inputs.

The response data was measured for all three axes by use of an accelerometer located at the center of the fastener arrangement. At the fundamental frequency of 150 Hertz the peak acceleration (sinusoidal) in the normal direction was 60 g for a 5 g input.

Response PSD* curves were also obtained. An overall acceleration level of 22 g rms* was recorded in the normal direction for the 16 g rms input.

After testing the panel in the vibration environment, inspection around the floating-nut inserts showed no damage to the ablator material. Based on these preliminary test results, the mechanical attachment approach looks promising. Additional test studies are planned to examine different spacings on larger panel sizes and response to higher input vibration levels.

* PSD Power Spectral Density

rms root mean square

VIBRATION TEST OF LEADING-EDGE ABLATIVE PANEL

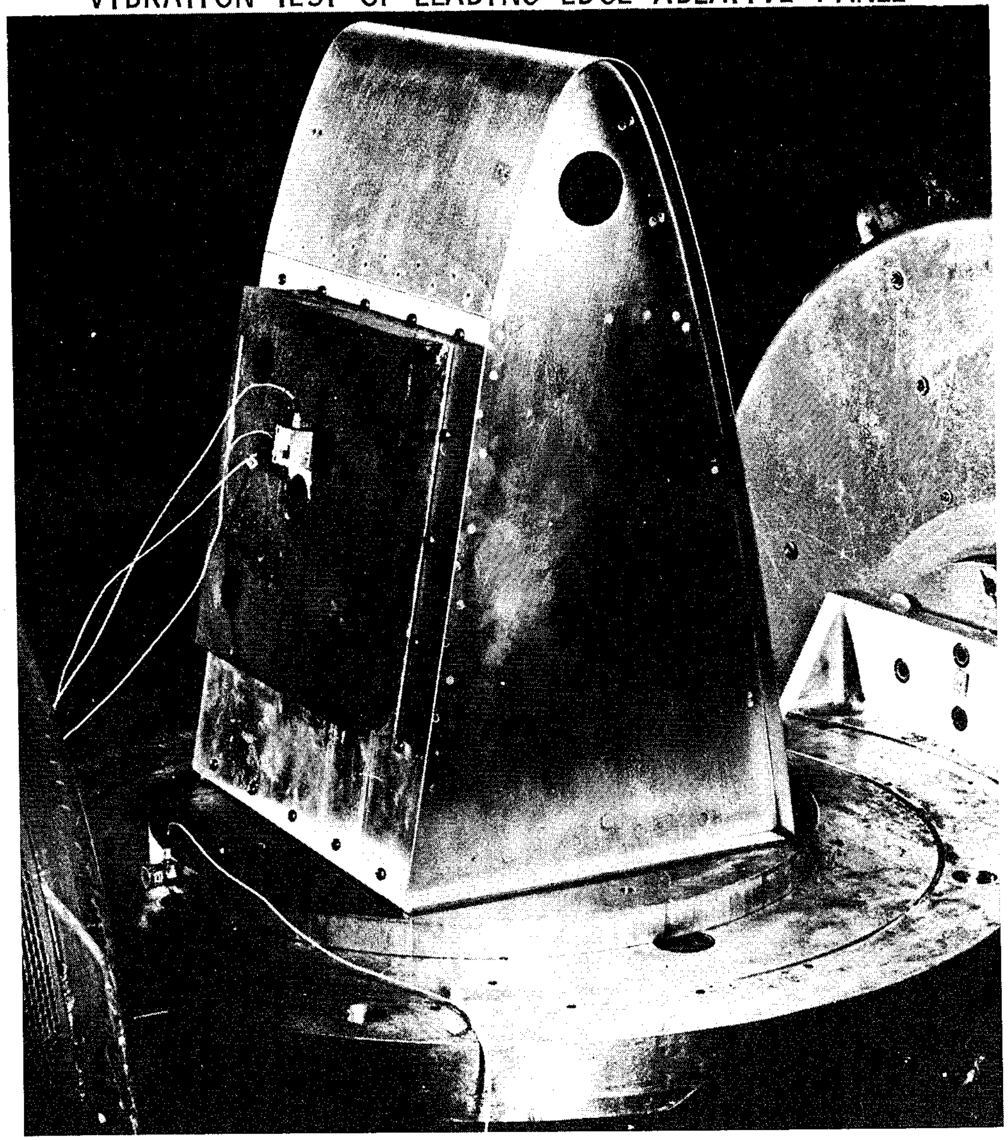

Figure 8

ABLATOR-TO-ABLATOR PANEL SEAL

RTV materials in combination with ablators appear adaptable to the particular requirements (interchangeability and low cost) of the space shuttle. A flexible seal configuration has been developed and is shown in Figure 9. The seal can be precast, cut, and installed faster than by casting in place; and, as a result, costs are reduced. Inspection can be easily accomplished in the factory. The cavity formed by the walls of the abutting panels converges toward the outer surface of the TPS, traps the seal, and prevents flow of hot gases to the vehicle structure.

ABLATOR-TO-ABLATOR PANEL SEAL

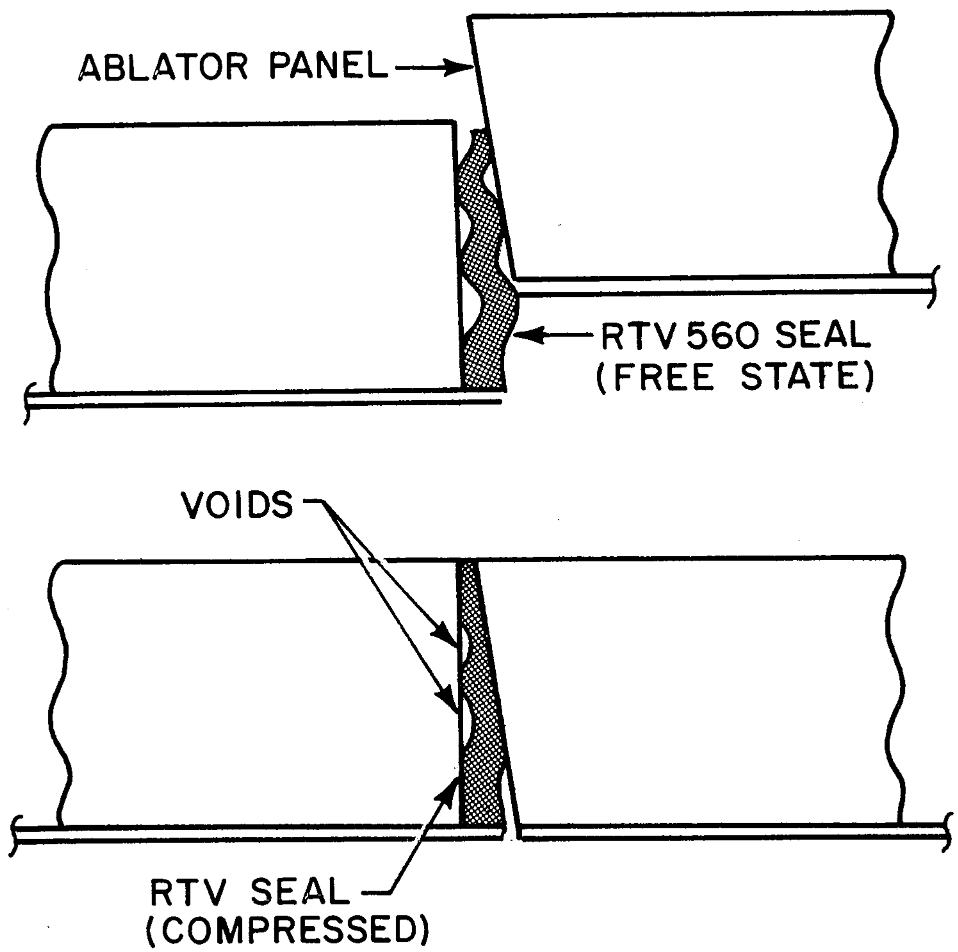

Figure 9

ARC TESTS OF SEALS

Figure 10 shows the results of two arc tests on the corrugated type of seal. As can be seen, these tests were conducted by use of the Avcoat 5026-39 honeycomb material; but similar results should be expected with the molded version of Avcoat 5026-39.

The figure on the right shows the performance of the seal under low heating conditions of 113 kW/m^2-sec (10 Btu/ft^2-sec). In this case the air flow was along the gasket length. The figure on the left shows the results of a test under heating conditions which reached 565 kW/m^2-sec (50 Btu/ft^2-sec) and where the flow was perpendicular to the ablator/gasket surface (splash type).

In both of these tests the temperature data as measured by a thermocouple located on the back surface indicated that no "over-temperature" condition was experienced beneath the seal (i.e., the temperature rise was the same as beneath a sample containing the ablation material only.)

FLEXIBLE-SEAL ARC TEST

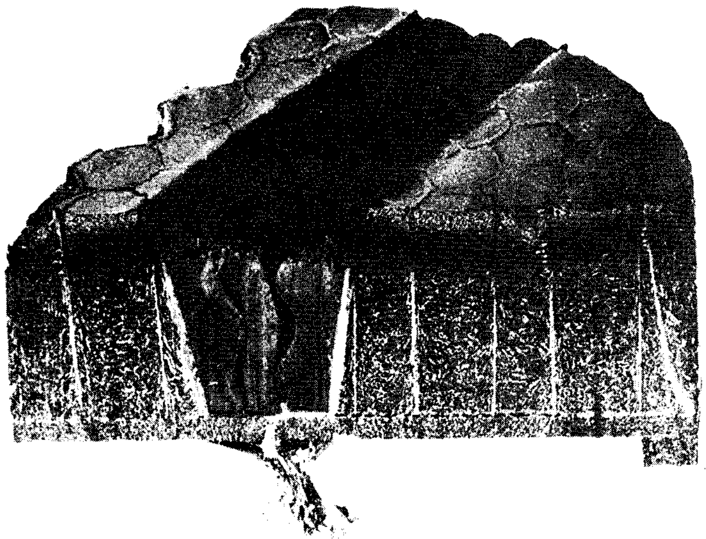

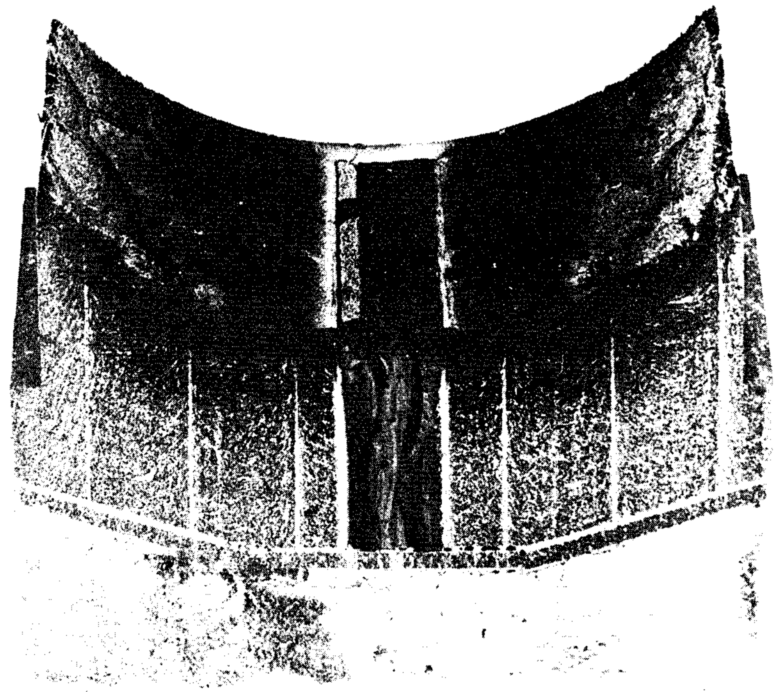

565 kW/m^2
(50 Btu/ft^2-sec)

113 kW/m^2
(10 Btu/ft^2-sec)

Figure 10

ABLATOR TO METALLIC TPS JOINT

Oil flow studies indicate that this joint runs perpendicular to the local flow over most of the wing. Because of the recession of an ablative system forward of the metallic interface, the joint and seal design must prevent the possibility of a forward-facing step after ablation has occurred. The joint can be located at the point where negligible recession takes place, but this approach could result in the use of more ablator than required which introduces additional refurbishment costs and weight. One possible approach to the ablator/metal seal design is shown in Figure 11.

This design utilizes application of a local high-density ablative material immediately upstream of the metallic interface. The high density materials will recede only slightly and, therefore, provide a more gradual transition from ablator to metal TPS. Candidate materials include fiberglass laminates or silica phenolic.

In addition to the design problems, consideration must be given to the effects of ablation product residue or the possible occurrence of transition on the metallic TPS.

ABLATOR TO METALLIC TPS JOINT

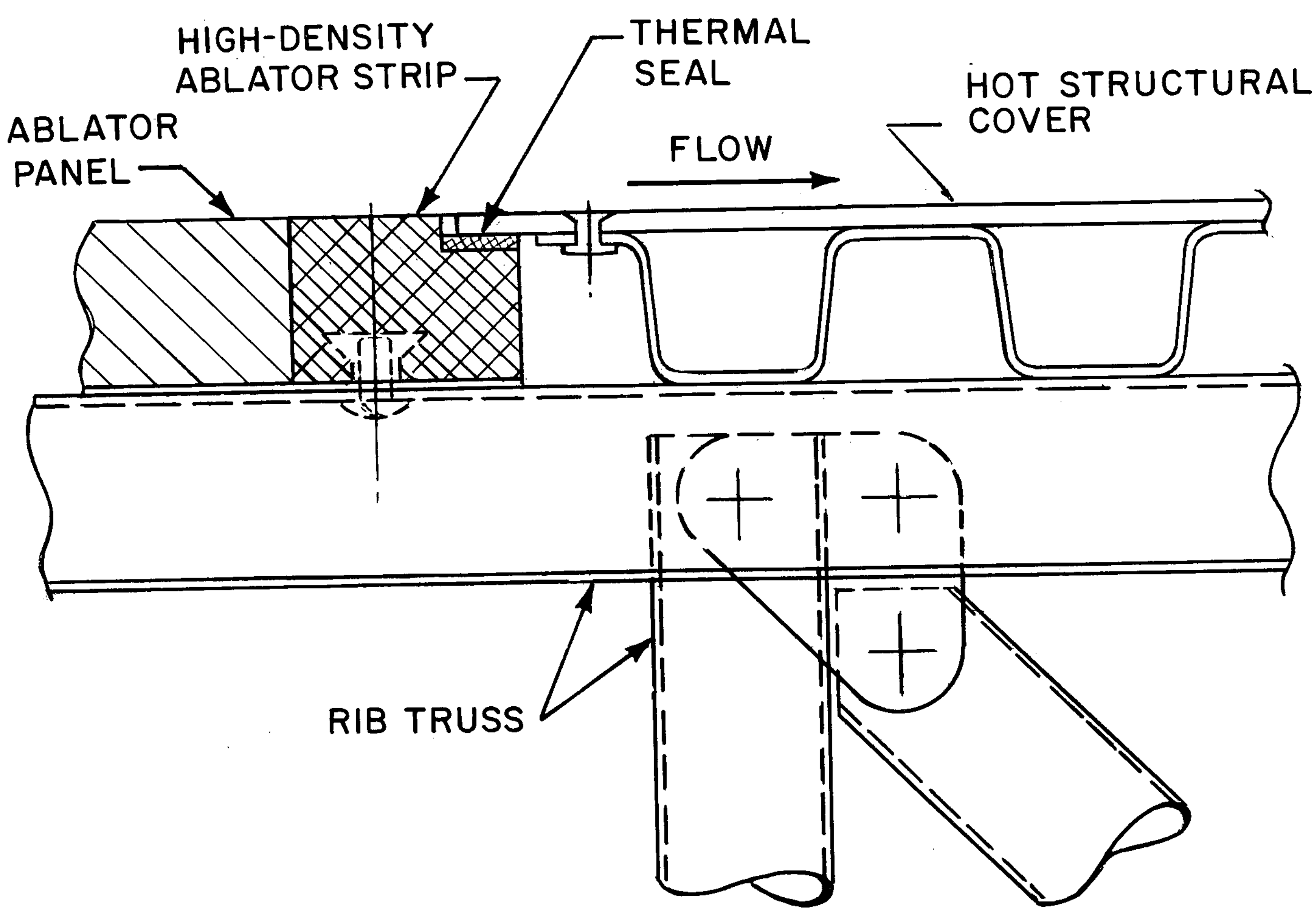

Figure 11

ABLATOR MATERIAL CONSIDERATIONS

The fact that the shuttle must withstand all ascent and reentry environments and still have acceptable subsonic aerodynamic characteristics places many requirements on the selection of the ablator material. Figure 12 shows the main factors that will ultimately affect the choice.

The state of development is important because of the resultant low cost to the program. Surface roughness and recession will, of course, affect the subsonic performance. Char stability is a factor since the leading edge will undergo vibration and other loads after reentry heating but prior to landing; and it is imperative that the leading-edge contour remain stable. Low cost fabrication and inspection procedures are necessary because of the refurbishment requirement. In addition, the material selected should be compatible with the adjacent TPS to insure that the reusability requirement is not sacrificed because of ablator products impinging on the surface.

ABLATOR MATERIAL CONSIDERATIONS

- STATE OF DEVELOPMENT
- SURFACE ROUGHNESS AND RECESSION EFFECTS
- CHAR STABILITY
- LOW COST FABRICATION AND INSPECTION
- COMPATIBILITY WITH ADJACENT TPS

Figure 12

ABLATOR CANDIDATES

Figure 13 shows some of the leading material candidates for the ablator leading edge. The materials are classified in three density categories. The lowest density candidates would probably have to be placed in honeycomb to insure char retention and thereby result in high cost. The moderate density materials have the advantage of increased char strength in the non-honeycomb version and also some of these materials are man-rated (Avcoat 5026-39 and DC 325). The highest density materials have strong char characteristics, would cost about the same as the moderate density materials but would add significant weight to the leading edge. The silica phenolic and carbon phenolic materials have been flown in several ballistic missiles and, therefore, are considered in the well-developed category.

ABLATOR CANDIDATES

- LOW DENSITY - $\rho = 256\ kg/m^3 (16\ lb/ft^3)$
  - NASA/LRC ELASTOMER
  - SLA 561
  - AVCO 480-2
- MODERATE DENSITY - $\rho = 561\ kg/m^3 (35\ lb/ft^3)$
  - AVCOAT 5026-39 (Honeycomb)
  - AVCOAT 5026-39 (Molded)
  - NYLON PHENOLIC
  - ESA 3560 (Prime)
  - PURPLE BLEND MOD 7
  - DC 325 $\rho = 881\ kg/m^3 (55\ lb/ft^3)$
- HIGH DENSITY - $\rho = 1602\ kg/m^3 (100\ lb/ft^3)$
  - SILICA PHENOLIC
  - CARBON PHENOLIC

Figure 13

ABLATOR PERFORMANCE

Figure 14 shows a weight comparison of the various materials under consideration for a structure temperature of $589^{\circ}K$ ($600^{\circ}F$). As would be expected, the low-density ablator MOD 480-2 is more efficient at the lower heating levels than the other materials. However, the weaker char stability and larger surface recession of this material offer significant disadvantages.

The bottom figure shows the surface recession of the candidate materials for the range of heating possible over the leading edge (including interference effects).

This analysis shows that there is insignificant difference in the thermal performance of Avcoat 5026-39 and Purple Blend whereas a severe weight penalty would occur with the use of silica phenolic. The primary difference between the Avcoat 5026-39 and MOD 7 material is, of course, in their state of development.

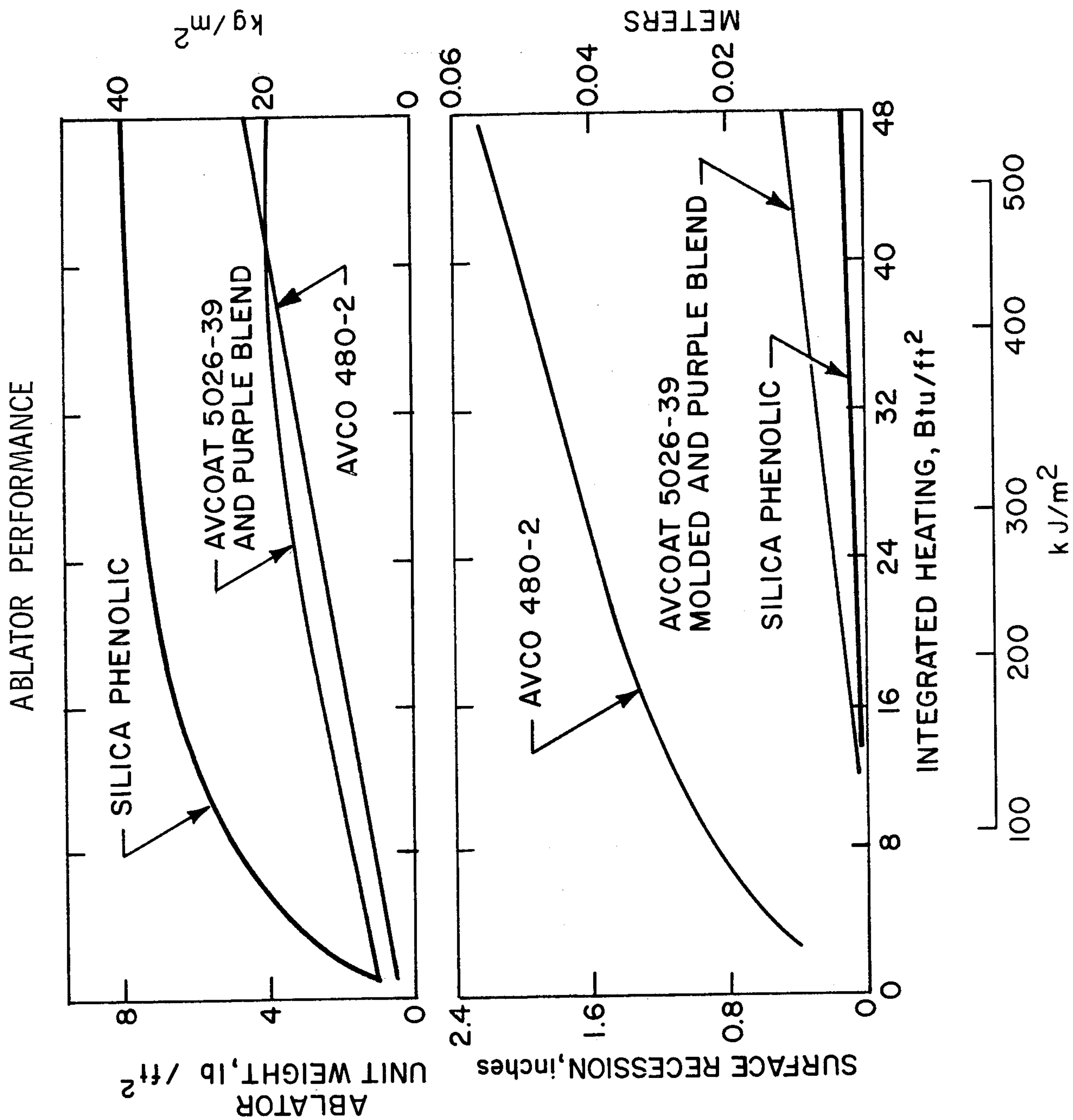
ABLATOR PERFORMANCE
SILICA PHENOLIC
AVCOAT 5026-39
AND PURPLE BLEND
AVCO 480-2
ABLATOR
UNIT WEIGHT, lb /ft^2
kg /m^2
0
4
8
0
20
40
AVCO 480-2
AVCOAT 5026-39
MOLDED AND PURPLE BLEND
SILICA PHENOLIC
SURFACE RECESSION, inches
METERS
0
0.8
1.6
2.4
0.02
0.04
0.06
0
8
16
24
32
40
48
INTEGRATED HEATING, Btu/ft^2
100
200
300
400
500
k J/m^2

Figure 14

ROVERS TEST RESULTS

In order to develop realistic ablator leading-edge weight estimates, tests were conducted at the Avco ROVERS* facility under representative shuttle reentry heating conditions. Typical results of these tests are shown in Figure 15 for Avcoat 5026-39 and Purple Blend MOD 7. The comparison between predicted and measured temperature and recession are seen to be quite good. These data indicate that the analytical tools used to calculate the ablator thickness and surface recession distribution around the leading edge are adequate.

* ROVERS (Radiation Orbital Vehicle Reentry Simulator)

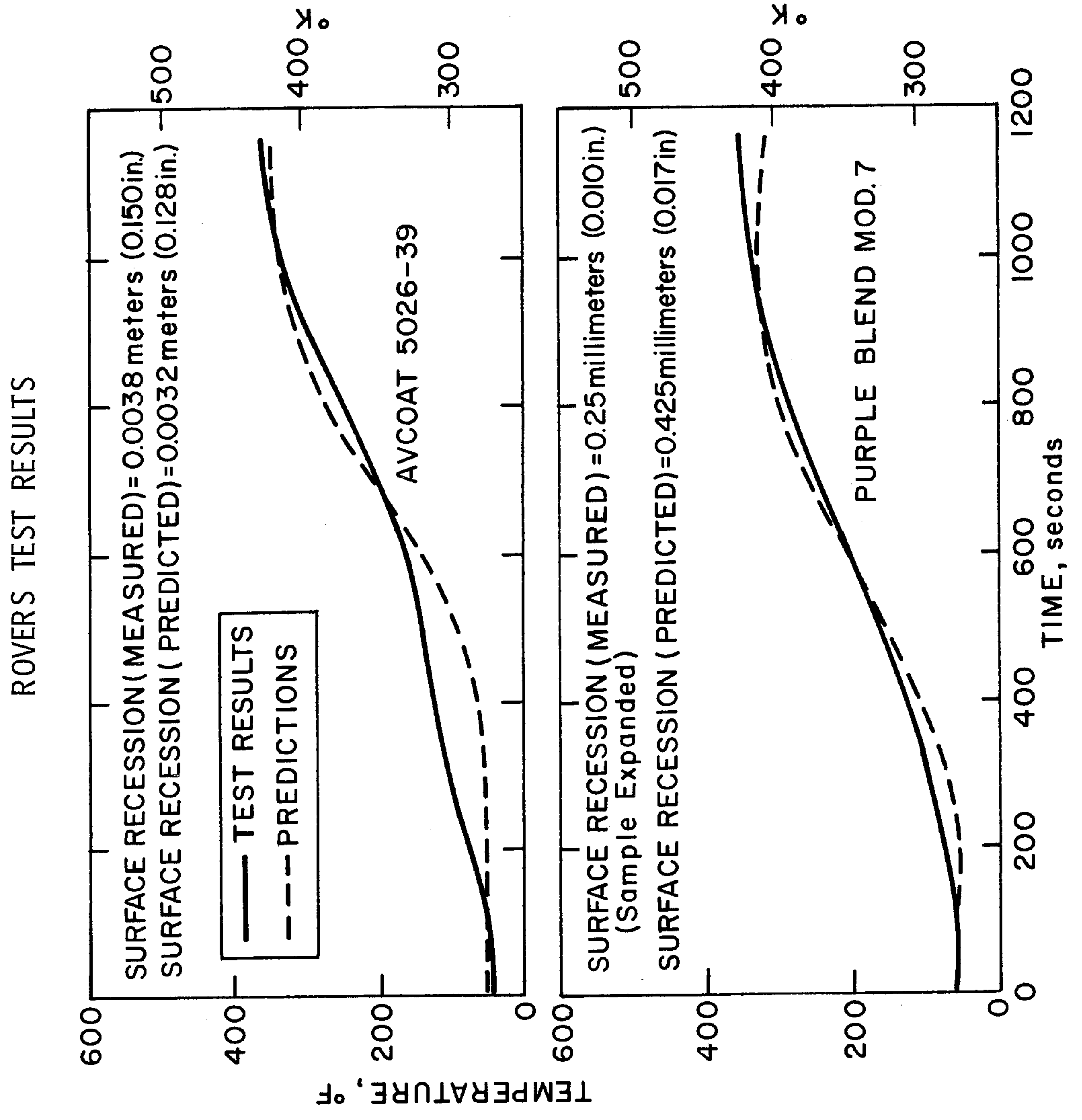
ROVERS TEST RESULTS
SURFACE RECESSION (MEASURED) = 0.0038 meters (0.150 in.)
SURFACE RECESSION (PREDICTED) = 0.0032 meters (0.128 in.)
TEST RESULTS
PREDICTIONS
AVCOAT 5026-39
SURFACE RECESSION (MEASURED) = 0.25 millimeters (0.010 in.)
(Sample Expanded)
SURFACE RECESSION (PREDICTED) = 0.425 millimeters (0.017 in)
PURPLE BLEND MOD. 7
TEMPERATURE, °F
°K
TIME, seconds
0
200
400
600
800
1000
1200
300
400
500

Figure 15

ABLATOR FABRICATION

Studies to date indicate a practical spanwise dimension of 1.22 meters (4.0 feet) for the leading-edge panels considering the influence of wing flexure and ground handling. In conjunction with the mock-ups fabricated in support of in-house studies simple plaster tooling was utilized and leading-edge nose sections 1.02 meters long were molded in an autoclave to a final inner mold line (IML) as seen in the upper photograph (Figure 16). These ablator parts were subsequently cut into smaller segments such that spanwise panel joints (seals) could be incorporated on engineering mock-ups. The lower photograph depicts a large flat panel also molded to IML using the same autoclave process.

The autoclave process was investigated in an attempt to reduce costs involved in utilizing match metal dies (as on Apollo) preliminary density checks on the autoclave process indicate that acceptable values are obtained.

ABLATOR FABRICATION

1.02 METER (40 INCH) MOLDED AVCOAT 5026-39 LEADING EDGE

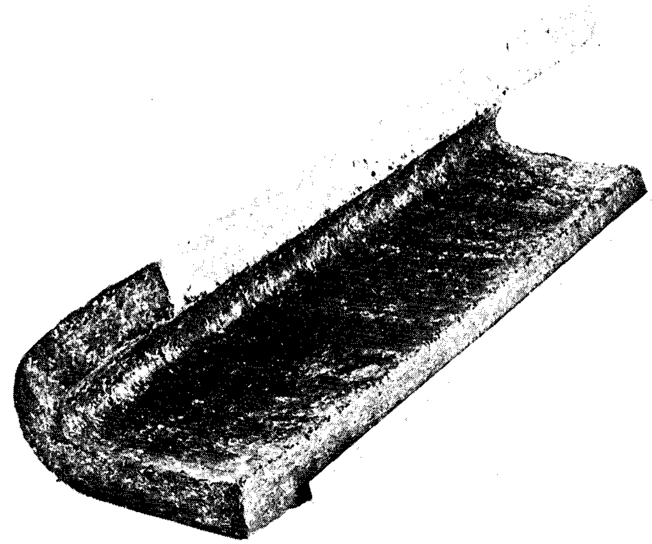

0.81 METER (32 INCH) MOLDED AVCOAT 5026-39 FLAT PANEL

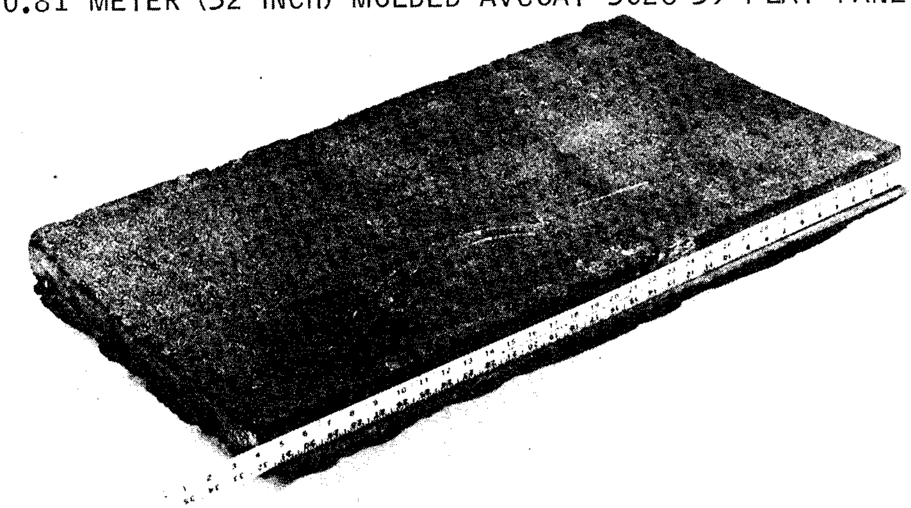

Figure 16

FULL-SCALE LEADING-EDGE MOCKUP

Figure 17 shows an ablative leading-edge mock-up which was fabricated at the Avco Systems Division. This model consisting of actual ablator sections includes several refurbishment techniques, with the emphasis on quick-release mechanisms. These mock-ups have been used to demonstrate feasibility as well as to conduct preliminary cost and maintainability.

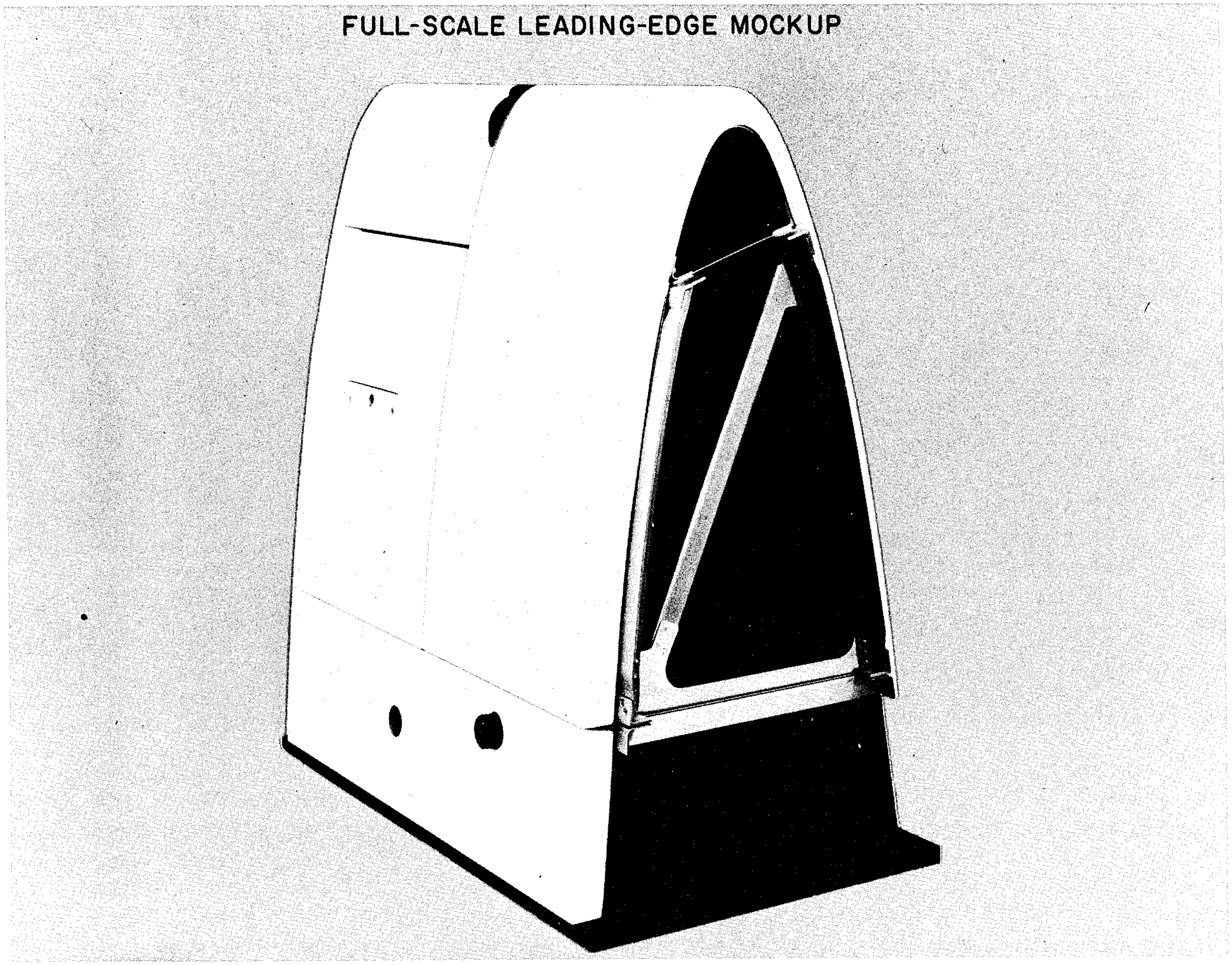

Figure 17

CONCLUSIONS

Figure 18 summarizes the main conclusions reached during the efforts on the ablator leading edge. While the refurbishment time and weight are important, the most significant factor is that man-rated ablators are currently in existence and can be utilized on the shuttle with a relatively small development program. The Avcoat 5026-39 molded material is recommended for use due to its performance on the Apollo flights and the indications from preliminary tests that the material can perform well in the wide range of shuttle environments.

CONCLUSIONS

- LEADING EDGES CAN BE REFURBISHED FOR 4.30 MAN HOURS/m^2 (0.40 man hours/ft^2)
- LEADING EDGE WEIGHT (ABLATOR, STRUCTURE, ATTACHMENTS) AVERAGES 15kg/m^2 (3.0 lb/ft^2) (STRAIGHT WING ORBITER)
- MODERATE DENSITY ABLATORS (ρ = 561 kg/m^3 OR 35 lb/ft^3) SEEM TO BE THE BEST COMPROMISE CONSIDERING WEIGHT, SURFACE RECESSION AND DEVELOPMENT STATUS
- COST OF MOLDED ABLATORS APPROXIMATES 645 DOLLARS/m^2 (60 dollars/ft^2)
- USE OF MAN-RATED APOLLO MATERIAL (AVCOAT 5026-39) WOULD MINIMIZE DEVELOPMENT COSTS
- PRELIMINARY TESTS INDICATE RELATIVELY SIMPLE SEAL AND ATTACHMENT CONCEPTS CAN BE USED

Figure 18

BOOSTER THERMAL PROTECTION SYSTEM EVALUATION

By

Allan M. Norton

Martin-Marietta Corporation, Denver, Colorado

PAPER 7

THE BOOSTER TPS EVALUATION PROCESS
(Figure 1)

The basis for the evaluation of the thermal protection system (TPS) candidates for the booster was to develop design charts of the response of the various TPS candidates to the flight environment. The maximum levels of the thermal and pressure distributions over the booster exposed surface were derived from the aerothermal environment. Then, the design charts were utilized in conjunction with the environmental distribution maps to obtain the total weight of each TPS candidate. In addition, the costs of the various TPS candidates were estimated so that the final selection of the booster TPS could be obtained by optimizing both cost and weight. This is extremely important because the TPS represents approximately 13% of the booster's inert weight and 37% of the maintenance and turnaround cost for the booster.

THE BOOSTER TPS EVALUATION PROCESS

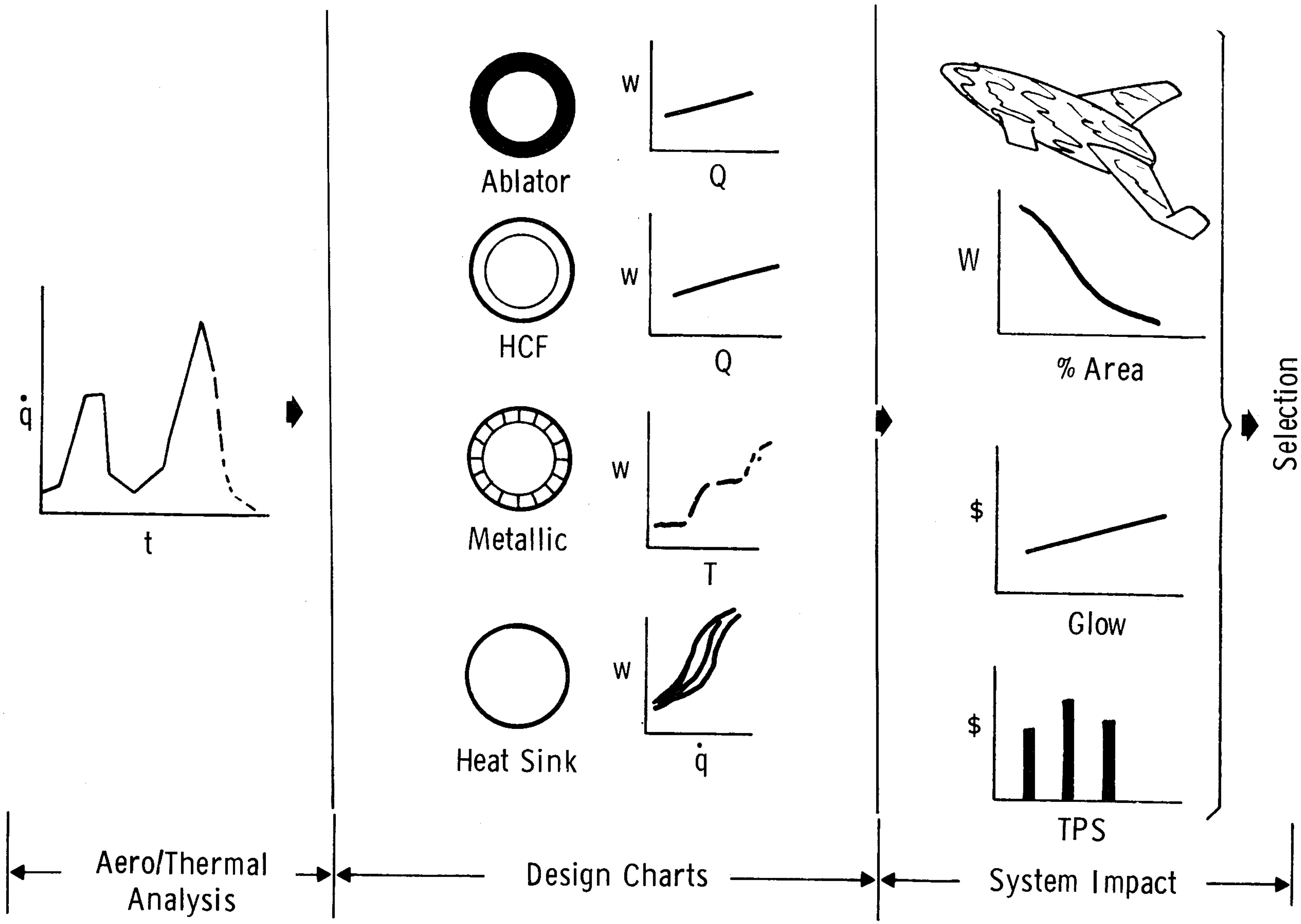

Figure 1

BOOSTER TPS EVALUATION OPTIONS
(Figure 2)

Of the four basic TPS families that were considered in this study and the multitude of derivatives within each TPS family, a total of 279 TPS combinations were evaluated for cost and weight. In the metallic family, five different heat shield panel and/or support arrangements were analyzed for five different materials. In the ablator family, two different design approaches for three materials were assessed. For the reusable non-metallic family, two different designs for one material were evaluated. The heat sink TPS approach was analyzed for one design. By considering that all of these TPS alternatives potentially could be mixed on one vehicle, a total of 279 possible combinations were obtained.

It should be recognized that more than five metallic design approaches, three ablative materials and one reusable, non-metallic material are possible. However, an initial elimination was accomplished to obtain the final design and material alternatives for this study.

BOOSTER TPS EVALUATION OPTIONS

	Metallic Shielding	Ablative Shielding	HCF Shielding	Heak Sink
Metallic (5 Material x 5 Designs)	25	150	50	25
Ablator (3 Material x 2 Designs)	--	6	12	6
HCF (2 Designs)	--	--	2	2
Heat Sink (1 Design)	--	--	--	1
	25	156	64	34 = 279

∴ There are 279 Possible Combinations of TPS for the Booster

Figure 2

THE BOOSTER TPS CANDIDATES - METALLIC
(Figure 3)

The five metallic heat shield designs were obtained by utilizing two basic panel concepts, isotropic and anisotropic, with two support arrangements, simple (S.S.) and post (P.S.). The anisotropic panels were skin/corrugation (s/c) and unidirectional integrally stiffened (u.i.s.) which were considered to be representative of built-up and totally machined construction techniques, respectively. These two extremes were selected primarily because it was thought that the skin corrugation would be more weight effective and the integrally stiffened would be more cost effective. The same type of reasoning was used to select the honeycomb (h.c.) and isogrid (i.s.) constructions for the isotropic heat shields.

The simple support system was selected because it is the most weight efficient support for the anisotropic heat shields while the post support is the most efficient for the isotropic panels.

The five materials that each of these metallic designs were evaluated for were 6Al-4V Titanium, Inconel 718, Rene 41, L-605 and FS-85 Columbium.

The results of the metallic portion of the study was that the post supported honeycomb heat shield was the most weight/cost effective concept for the booster. The individual rankings were:

	Configuration														
	(s/c - S.S.)			(h.c. - P S.)			(h.c. - S.S.)			(u.i.s. - S.S.)			(i.s. - P.S.)		
Material	W	$	$/W	W	$	$/W	W	$	$/W	W	$	$/W	W	$	$/W
Titanium	1	3	3	3	2	2	2	4	4	5	5	5	4	1	1
Inconel	1	3	3	3	2	1	2	5	4	5	4	5	4	1	2
Rene	2	3	3	1	1	1	4	4	4	5	5	5	3	2	2
L-605	3	3	3	1	1	1	2	4	4	4	5	5	2	2	2
Columbium	1	3	2		*			*		3	1	3	2	2	1

*Was not evaluated

THE BOOSTER TPS CANDIDATES - METALLIC

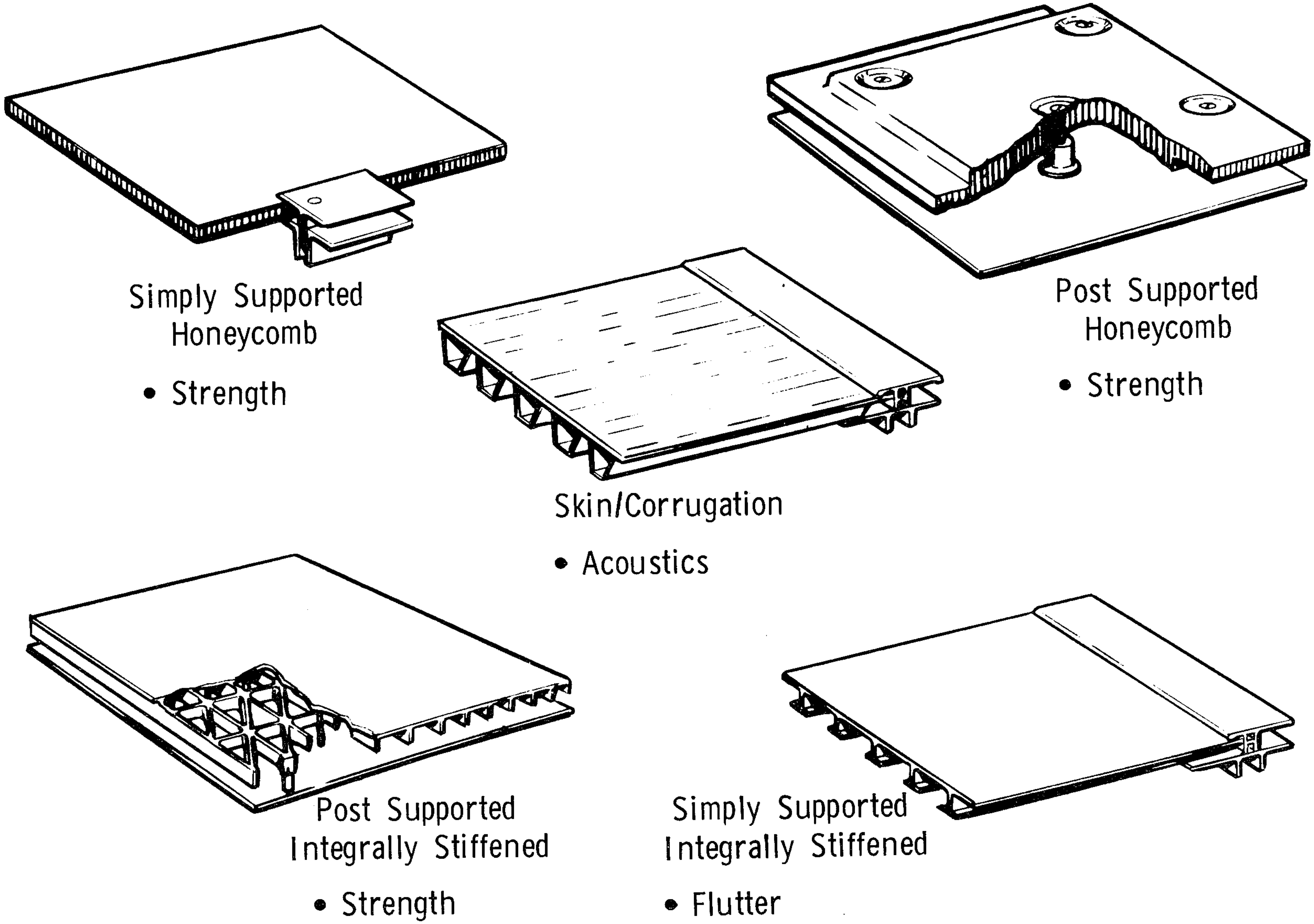

Figure 3

THE BOOSTER TPS CANDIDATES - NON-METALLIC
(Figure 4)

For the reusable non-metallic concepts, two design concepts were applied with the hardened compacted fiber (HCF) material. One approach was to apply the HCF directly to the structure and the other was to bond the HCF to a subpanel which was mechanically attached to the structure. Although the directly applied HCF is theoretically lighter than the subpaneled approach, the strain compatibility between the structure and the HCF system prevents this technique from being practical. Whenever the structure would strain from applied loads or filling the propellant tanks, the HCF would tend to spall. In addition, the cryogenic temperatures in the propellant tank regions would pose a moisture problem in the HCF (most of the moisture preventive coatings will allow water vapor to penetrate but not solid water). Consequently, a subpaneled HCF approach was selected. However, if the strain compatibility and moisture problems can be solved, the direct application approach is approximately 9500 kg lighter.

Three ablative materials applied to two design approaches similar to the HCF designs were investigated. The three materials were 242,(SLA 561) 322 (S 20T) and 402 (MA 25S) kg/m^3 densities. Of these, the MA 25S material was significantly cheaper and not that much heavier when installed. In addition, it has been flight proven on the X-15. Although the direct application technique was again lighter, the refurbishment of the ablator could not be accomplished within the required two week turnaround time. Therefore, the direct application technique was not considered further.

THE BOOSTER TPS CANDIDATES - NON-METALLIC

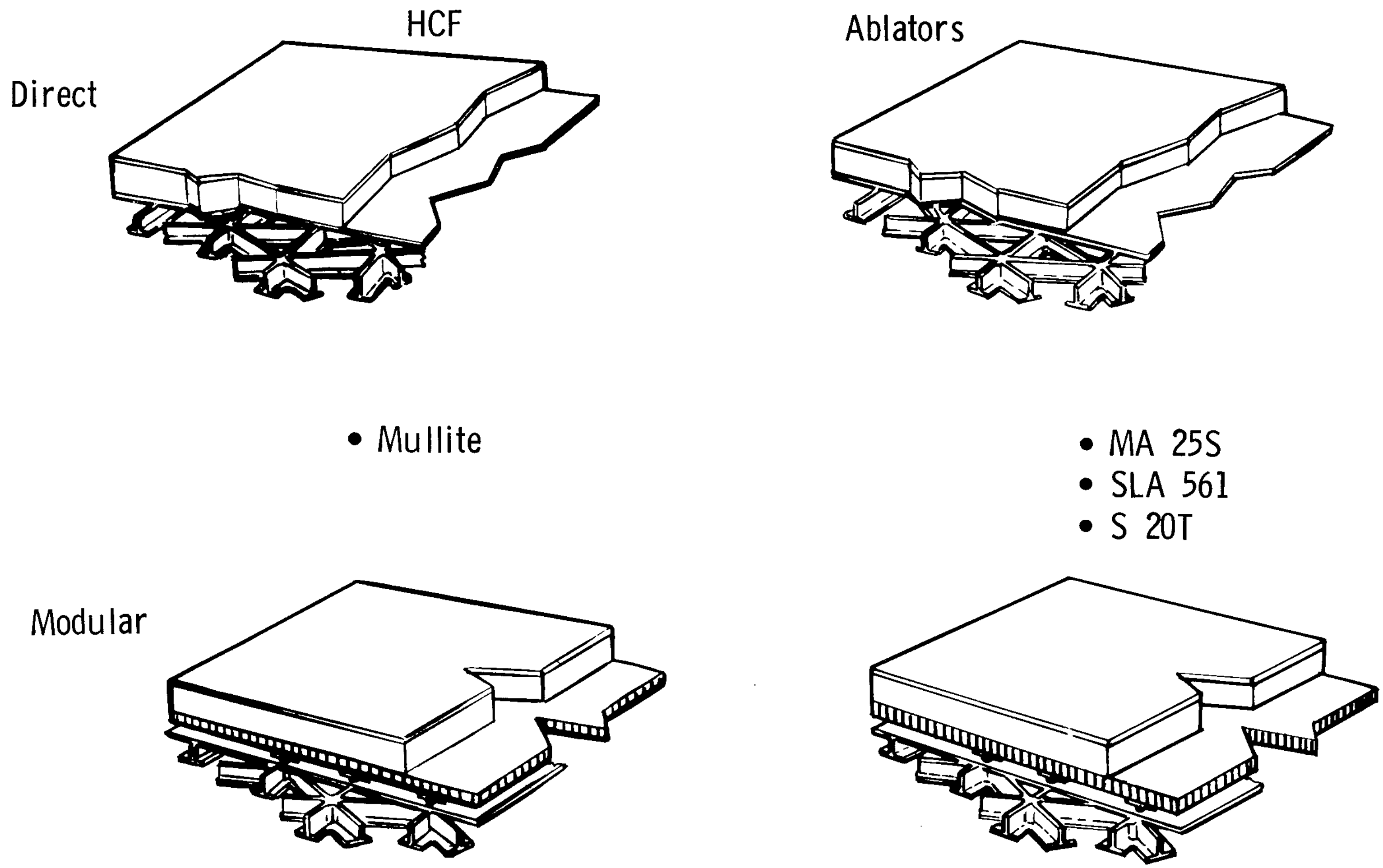

Figure 4

BOOSTER TPS AREAS
(Figure 5)

A low cross range space shuttle system was used to describe the baseline booster vehicle for this study. The Single Body Canard (SBC) booster - Model 14 had 3252 m^2 of exposed surface area and a dry weight of 182,000 kg. To determine the weights of the various TPS candidates, one half of the booster surface area was divided into 107 distinct subareas. These subareas were determined from the heating patterns and geometric shape of the booster (symmetry was assumed).

BOOSTER TPS AREAS

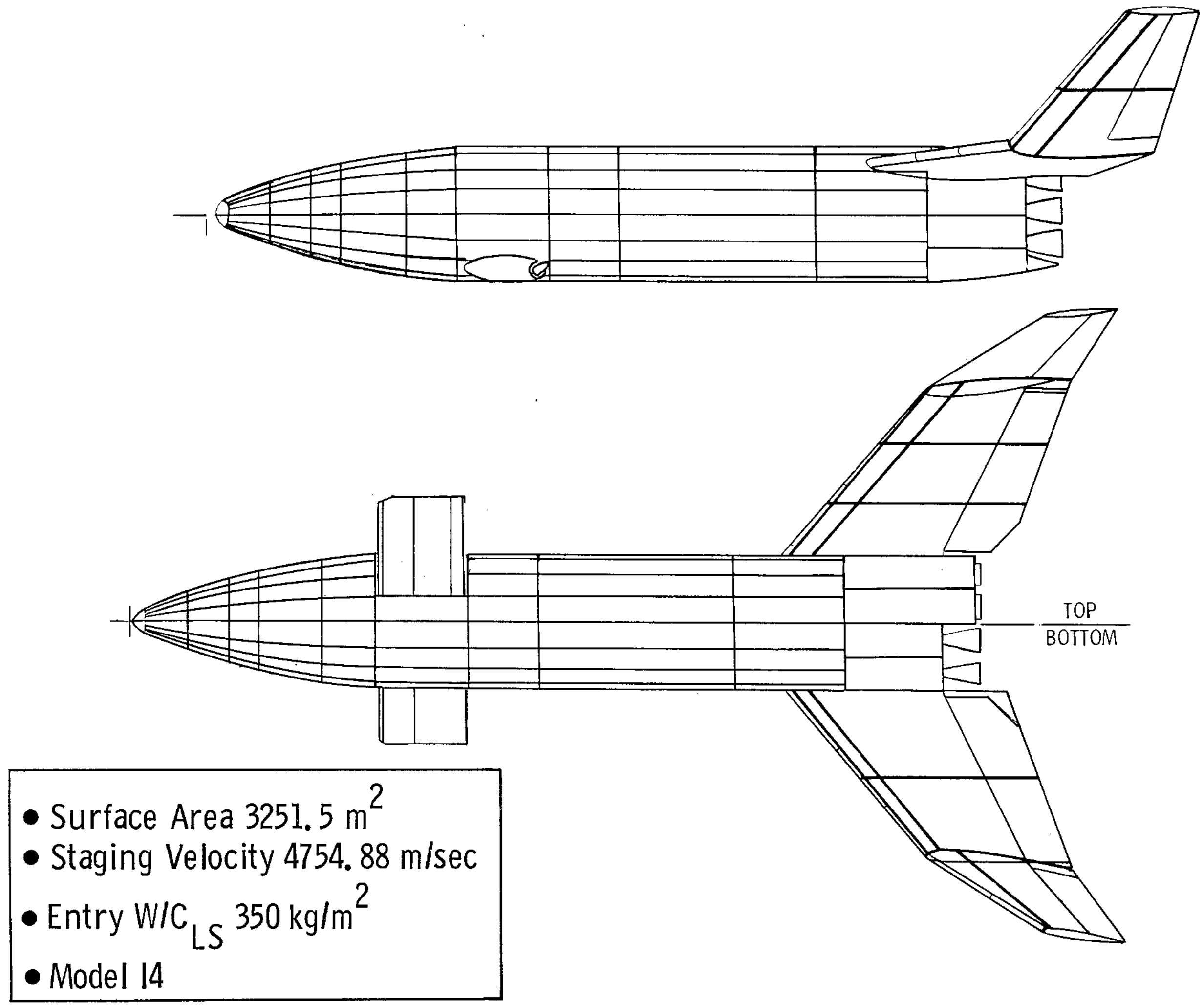

Figure 5

TPS APPLICATION TO BOOSTER
(Figure 6)

Each of the 107 subareas was characterized as to geometry (area), maximum heating environment ($\dot{q}$, Q, T) and primary structure ($\bar{\tau}$). In addition, the tankage areas were further described by assessments for purge, cryogenic insulation (CTI) and frost. Each of the surviving TPS candidates was applied to the booster to obtain a total weight for all of the elements of weight that could discriminate between the candidates.

TPS APPLICATION TO BOOSTER

BASIC DATA

ZONE	LOCATION	AREA (m^2)	$\dot{q}_1$ (KW/m^2)	$\dot{q}_2$ (KW/m^2)	Q_1 (megajoules/m^2)	Q_2 (megajoules/m^2)	Q_T (megajoules/m^2)	T_1 (°C)	T_2 (°C)	$\bar{\tau}_{AL}$ (cm)	ω_{ST} (kg/m^2)	W_{STR} (kg)
1	NOSE CAP	2.32	58.9	152.4	3.46	11.89	15.35	760	943	.25	7.03	16.3
2												
3												
4												
5												
6												
7												
8												
9												
10												
11												

MODULAR HCF

ZONE	τ_{AL} EFF (cm)	ω_{HCF} (Kg/m^2)	COAT (Kg/m^2)	BOND (Kg/m^2)	SUBPANEL (Kg/m^2)	PURGE (Kg/m^2)	FROST (Kg/m^2)	CTI (Kg/m^2)	Σ (Kg/m^2)	W (Kg)
1	.152	3.42	1.17	.488	3.32	0	0	0	8.40	19.5
2										
3										
4										
5										
6										
7										
8										

MODULAR MA25S

ZONE	τ_{AL} EFF (cm)	ω_{MA} (Kg/m^2)	COAT (Kg/m^2)	BOND (Kg/m^2)	SUBPANEL (Kg/m^2)	PURGE (Kg/m^2)	FROST (Kg/m^2)	CTI (Kg/m^2)	Σ (Kg/m^2)	W (Kg)
1	.152	5.96	.39	0	3.32	0	0	0	9.67	38.5
2										
3										
4										
5										
6										

HEAT SINK

ZONE	$\bar{\tau}_{AL}$ REQ (cm)	$\bar{\tau}_{AL}$ BASIC (cm)	$\Delta\bar{\tau}_{AL}$	$\Delta\omega_{AL}$ (Kg/m^2)	FROST (Kg/m^2)	CTI (Kg/m^2)	STRESS (Kg/m^2)	Σ (Kg/m^2)	W (Kg)
1	5.59	.25	5.34	151.9	0	0	0	151.9	352.8
2									
3									

METALLIC

ZONE	T_{MAX} (°C)	MATL	ω_{TPS} (Kg/m^2)	ω_{SUP} (Kg/m^2)	ω_{INS} (Kg/m^2)	PURGE (Kg/m^2)	CTI (Kg/m^2)	Σ (Kg/m^2)	W (Kg)
1	943	L605	7.96	4.93	2.15	0	0	15.04	34.9
2	777	RENE	5.32	3.97	1.76				
3	799	RENE	5.32	3.97					

Figure 6

BOOSTER TPS EVALUATION RESULTS
(Figure 7)

As can be seen from the results of the study on the opposite page, the modular (subpanel) HCF is the lightest and cheapest reusable TPS concept. The ablator costs were based on a 100% replacement per flight. Recent data has indicated that a 50% replacement per flight may be possible which would put the relative total program cost for the ablator system at 1.08. The all metallic approach is considerably heavier than the non-metallic and consequently the resizing cost penalty made this TPS approach less competitive than the subpaneled HCF design. The total heat sink booster was shown to be extremely heavy if not unfeasible. However, there are areas on the leeward side of the body and aero surfaces where the heat sink approach is very competitive from both weight and cost standpoints. However, several important questions regarding the partial application of heat sink remain unanswered. Namely, how much frost/ice penalty is realistic (some sources quote 590 kg/m^2 as the penalty and 12.3 kg/m^2 was used for this study)? Are the heating environment predictions accurate enough for such an unforgiving concept? How is the transition between the heat sink and shielded concept handled? What are the cost penalties for a back-up TPS if the heating predictions are unconservative? Because these questions could not be reasonably answered at this time, any use of heat sink was not further considered.

BOOSTER TPS EVALUATION RESULTS

PURE CONCEPTS	TOTAL TPS WEIGHT*	FIRST UNIT BUILD COST	OPS COST	RESIZ. COST	TOTAL PROG. COST
HCF: Modular	23,850	1.0	1.0	1.0	1.0
ABLATOR: Modular MA25S	23,700	.16	2.93	0.99	1.58
METALLIC: Post Supported Honeycomb	37,400	1.03	0.68	1.56	1.15
HEAT SINK: Total	159,000	--	--	--	--

*Includes Heat Shield + Supports + HT Insulation + Purge + Frost + Cryo Insulation ~ kg

Figure 7

FEATURES OF SELECTED BOOSTER TPS
(Figure 8)

The selected TPS approach for the booster was the modular HCF with a temporary use of an interchangeable MA 25S ablator TPS for the initial flights. The most important advantage of this approach is that the permanent TPS can be tailored to the actual environment after the vehicle has flown. By using the relatively inexpensive and forgiving ablator TPS for just a few flights, the permanent HCF TPS can be sized and installed on the operational vehicles with minimal time delay and cost expense. In addition, if a "hotter" mission is encountered after the design has been committed, the most drastic impact would be on the TPS and the non-metallic approach will allow a relatively easy design change for substantial increases in performance. The metallic approach does not have this flexibility because it is dependent on heating rate and requires a change in materials to effect any substantial change in performance.

Another important advantage is that the non-metallic approach will not require a separate thermal conditioning subsystem for the propellant tanks during ground-hold to prevent moisture accumulation whereas the metallic TPS does.

The primary disadvantage of the HCF TPS is that the HCF material is not current state-of-the-art. Considerable development is required to bring this material to the same technological status as the metallics, but the obvious weight and cost advantages of the HCF system make this a worthwhile investment.

FEATURES OF SELECTED BOOSTER TPS

SELECTED APPROACH:

- Modular HCF As Permanent TPS With Temporary Use Of Modular MA 25S Ablator

ADVANTAGES:

- Flexibility To Tailor TPS
- Less Sensitive To Staging Velocity
- Less Expensive Than Metallics
- Relatively Simple To Integrate Into Vehicle Design
- Minimizes Purge Impact
- Lighter Than Metallics
- Interchangeable With Proven Ablator TPS

DISADVANTAGES:

- Permanent TPS Material Requires Development

Figure 8

THE HEAT SINK CONCEPT FOR THE SPACE SHUTTLE BOOSTER

By Jack Prunty
Convair Aerospace Division of General Dynamics, San Diego, California

INTRODUCTION

This paper presents current findings of an investigation of a heat sink structural concept applied to the Space Shuttle booster. The concept is compared with the more generally accepted thermally protected arrangement, and comparative weight and cost data are presented. Since the characteristics of the latter concept are generally understood, substantiating data and problem discussions presented are confined to the heat sink concept. It will be recognized that the limited effort accomplished to date on the heat sink concept probably implies a lesser understanding of the associated problems compared to those of the thermal protection system (TPS) concept, and that, conversely, the heat sink approach may be amenable to improvement when given further consideration in certain areas. The following outline of this paper includes some suggestions for additional investigation.

Ground rules applicable to the latest phase of the study are presented first. They are subject to review, particularly in the case of staging velocity and other trajectory parameters. The need for a launch capability under severe icing conditions also requires reconsideration. A brief description of the two competing concepts applied to an essentially identical vehicle configuration is presented next. This approach is valid since the body thermostructural concept does not appear to be a configuration driver. The heat sink thickness requirement based upon present ground rules is shown. These values could be reduced if the temperature limitation of 394°K (250°F) for the cryogenic insulation and bonding system could be increased. Next, a significant difficulty with the heat sink concept is discussed; that is, sensitivity to total heat input — a problem aggravated by current uncertainties with respect to the value of this parameter. The problem will be resolved in part when final mission requirements are established and overall vehicle system optimization and trajectory shaping have been completed. There remains the problem of uncertainties in predicting heating rates, a problem that may be largely resolved by wind tunnel test. Also, if the band of uncertainty could be assessed, a suitable margin of heat sink thickness may be acceptable. The problem of ice accumulation on exposed cryogenic tanks requires correlation of the data with actual launch site conditions and associated launch restrictions. The data presented indicate that further investigation may prove that some degree of ice accumulation is tolerable. Comparative weights for the TPS vehicle and several heat sink vehicles with and without allowances for the ice problem or aeroheating uncertainties are presented. These vehicles are synthesized on the basis that current ground rules and all other relevant criteria are held constant. Conclusions reached at this point are presented with a recommended course for future action.

PAPER 8

GROUND RULES
(Figure 1)

A comparison was made of the heat sink concept and the more familiar and highly competitive thermally protected concept. The baseline booster selected by Convair Aerospace for the Space Shuttle study features a thermally protected concept and was therefore used as the basis for the comparative study. The comparison was constrained to the major portion of the body only. A previous study of staging conditions led to the selection of the values given in Item 3 on the basis of minimum program costs for both the heat sink and TPS concepts. The initial entry angle of attack was 60°, but modulation to maintain the specified maximum 4g load factor gave a value of approximately 40° at peak heating.

Aluminum alloy 2219-T87 was selected since peak temperatures were determined by the limitations of the cryogenic insulation. The high specific heat of aluminum provides good heat sink performance compared to other cost competitive materials. The initial temperatures of the LO_2 tank and the LH_2 tank at liftoff are noted, as determined for the most adverse warm day conditions and assuming 7.6cm (3 inches) of internal insulation on the LH_2 tank. Peak temperature limitations for recovery were established as 422°K (300°F), generally to avoid overaging the aluminum, and 394°K (250°F) for the LH_2 tank consistent with reusability of the internal cryogenic insulation and its bonding system.

GROUND RULES

1. OVERALL VEHICLE COMPARISON WITH A TPS BOOSTER ON A CONSISTENT BASIS
2. HEAT SINK VERSUS TPS COMPARISON FOR BODY ONLY
3. STAGING CONDITIONS, VELOCITY = 3.17 km/s (10,388 fps)
   DYNAMIC PRESSURE = 718.5 N/m^2 (15 psf)
4. ENTRY ANGLE OF ATTACK = 40° AT PEAK HEATING
5. HEAT SINK MATERIAL: 2219-T87 ALUMINUM
6. HEAT SINK STARTING TEMPERATURES — 100°K (-280°F) BARE LO_2 TANK, 294°K (70°F) REMAINDER
7. HEAT SINK PEAK TEMPERATURES — 422°K (300°F) BARE LO_2 TANK 394°K (250°F) LH_2 TANK 422°K (300°F) REMAINDER
8. CONSIDER ALL-WEATHER LAUNCH CAPABILITY WITH RESPECT TO ICE ACCUMULATION PROBLEM

Figure 1

COMPARATIVE CONCEPTS
(Figure 2)

This figure illustrates the delta wing booster configuration used in the heat sink investigation and shows the essential difference between the two thermostructural concepts. The heat sink investigation was limited to the fuselage aft of the nose section and forward of the thrust section. This constitutes the area in which the heat sink approach is most attractive, since it consists mainly of relatively thick-walled cryogenic tankage, which, when combined with the additional thickness to attain the heat sink requirement, is very competitive with the double-walled thermally protected concept. The lightly loaded nose section forward of the propellant tanks is a highly efficient single-wall hot structure on the thermally protected vehicle and was retained for the heat sink booster. The thrust skirt is a titanium heat sink for both concepts and involved no changes in the study. Similarly, the hot wing and vertical stabilizer structures were used without modification for the heat sink vehicle.

The thermally protected concept features aluminum 2219-T87 propellant tanks, which with the intertank adapter and the thrust skirt comprise the primary load-carrying structure of the fuselage. This aluminum structure is protected from the thermal environment by a secondary outer shell structure of superalloy materials. The outer shell is supported from the aluminum structure at a few discrete points which feature slip devices to permit relative expansion/contraction between the two structures. Conventional semimonocoque construction is adopted for the tank shells, except that frames and stringers are external to simplify the internal cryogenic insulation of the liquid hydrogen tank.

The heat sink concept dispenses with the outer protective shell, and the aluminum primary structure is thickened where required to provide the heat capacitance required to obtain the specified temperature limits. Since the structural shell is now exposed to the airstream, the shell stiffening must be internal as opposed to the external arrangement used on the thermally protected concept. In the case of the LH_2 tank, the stiffening is changed from frame/stringers to a waffle concept to avoid undue compromise to the cryogenic insulation. Unfortunately, some compromise is necessary since large support rings for the orbiter and wing attachments must be located inside the tank. Detail "A" illustrates the basic differences between the two concepts.

COMPARATIVE CONCEPTS

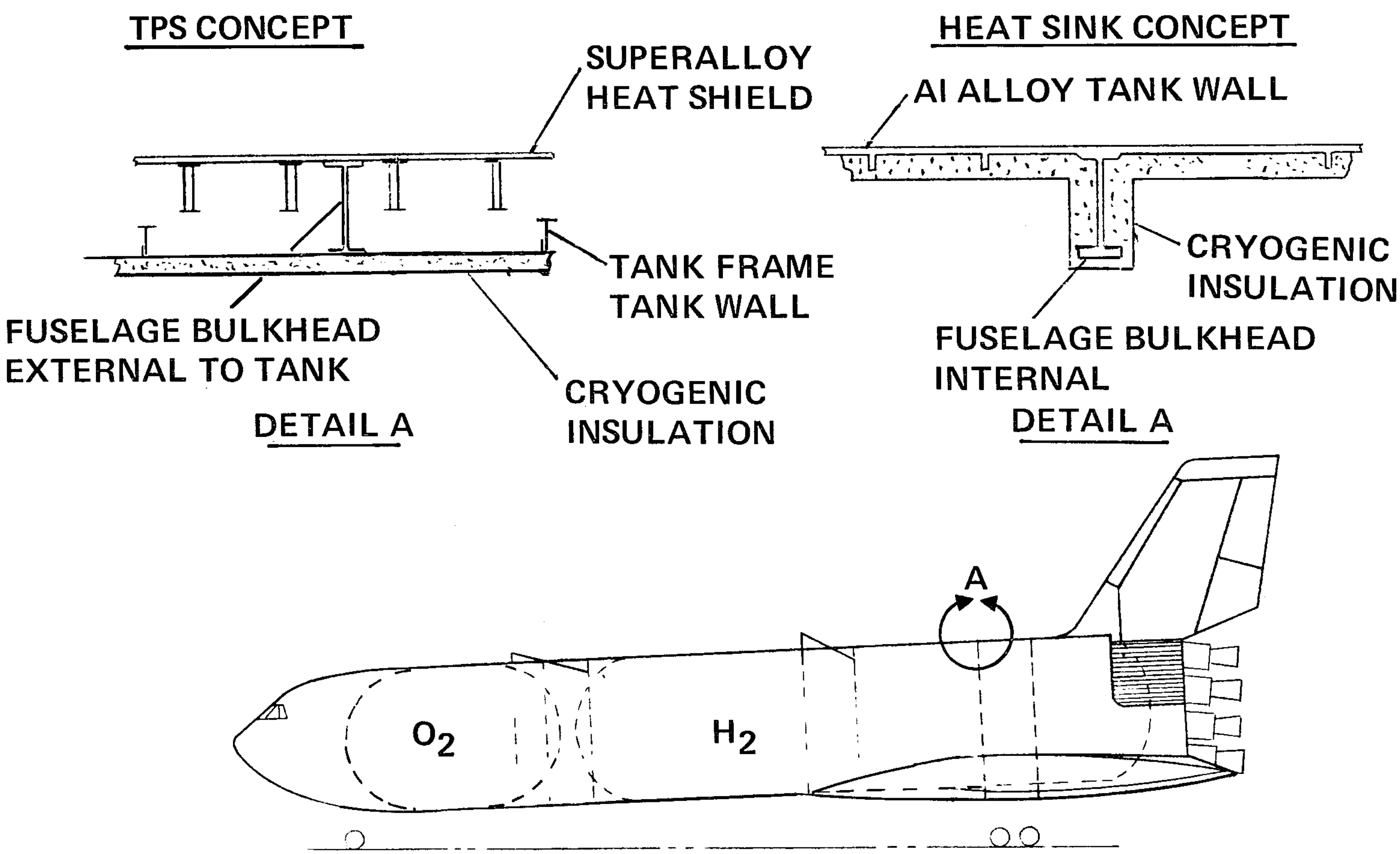

Figure 2

HEAT SINK REQUIREMENTS
(Figure 3)

The total heat sink thickness requirement for 2219 aluminum was computed around the periphery of several stations in the LO_2 tank, the intertank section, and in the LH_2 tank. The figure illustrates a typical distribution in the area of the LH_2 tank.

Plotted are the total wall thickness requirements versus points around the body periphery from the bottom center line to the top center line. The basic strength requirement for overall body loads and propellant containment is also plotted. Note that additional material for heat sink is needed only from the bottom center line around to approximately the 60° point.

The heat sink requirements for a range of staging velocities are shown. These values were obtained from an initial study that varied staging parameters to select the best conditions for both the heat sink and the thermally protected concept. As noted, the 3.17-km/s (10,388-fps) velocity was selected as the most favorable for both concepts from the total vehicle systems cost aspect. This results in a lower centerline thickness of 3.35 cm (1.32 inches).

Areas under the heat sink curves for this staging velocity above the basic structural requirements were used to compute the item "Heat Sink" in the weight tabulations presented later.

The plots shown are for a nominal trajectory with no allowance for heating uncertainties.

LH_2 TANK WALL THICKNESS REQUIREMENTS

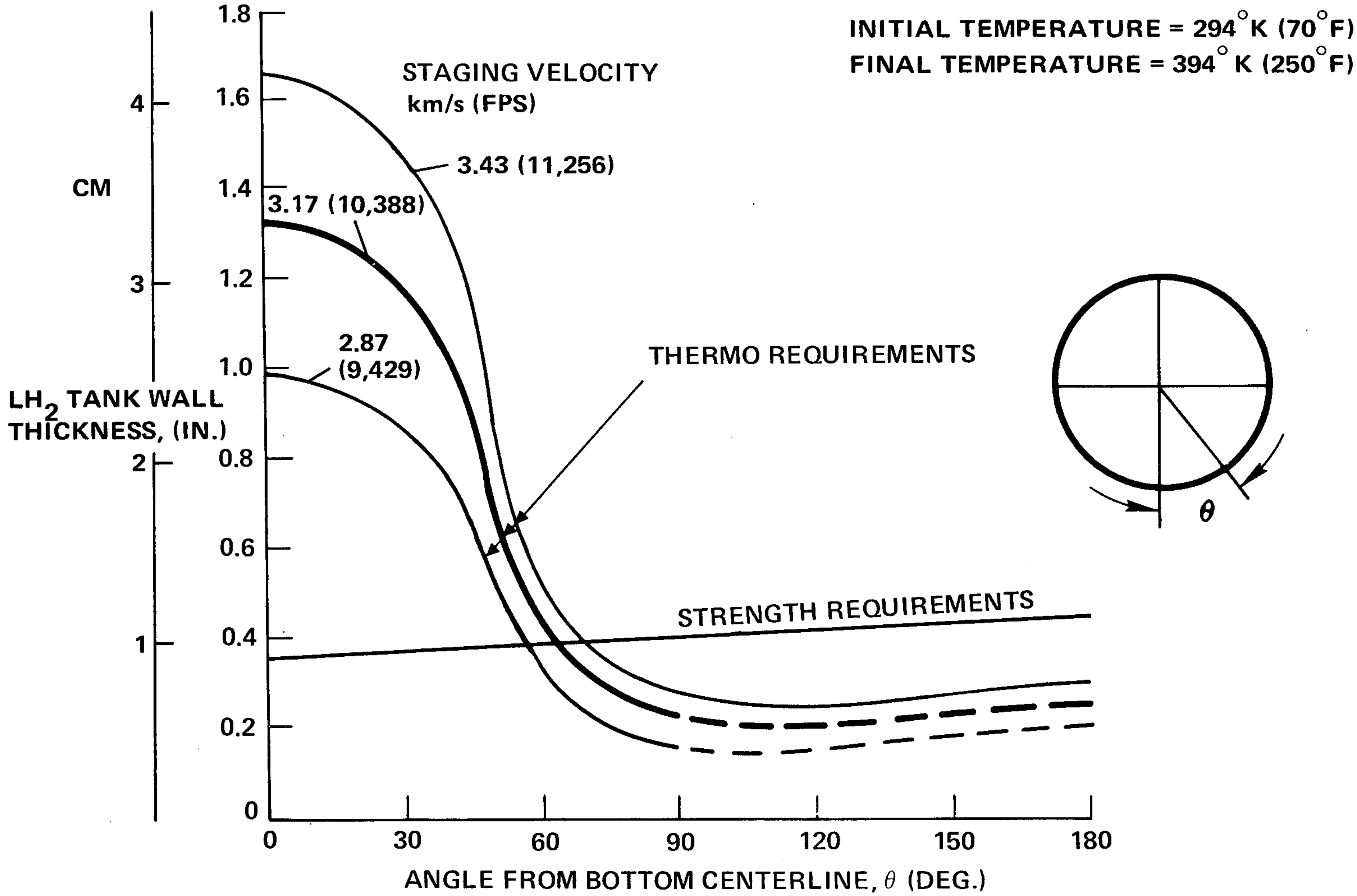

Figure 3

UNCERTAINTIES
(Figure 4)

Perhaps the most important consideration affecting the assessment of the viability of the heat sink concept falls in the area of aeroheating uncertainties. The figure illustrates this problem. The nominal line showing heat sink thickness requirements is based on a given staging condition and entry trajectory; the staging velocity is 3.17 km/s (10,388 fps). As noted, staging velocity may vary with engine thrust level which, in turn, depends upon the final specified thrust per engine and the number of engines required for an acceptable thrust to weight ratio. Mission requirements may also cause variation and trajectories may change, depending upon final vehicle systems optimization. Uncertainties also occur in turbulent heating prediction techniques and in predicting transition. Wind tunnel tests require completion to assist in prediction, particularly in areas of interference, and additional confidence is required in scale-up techniques to apply wind tunnel model data to the full-scale vehicle.

The uncertainty band shown on the figure represents a variation in staging velocity from 2.87 to 3.43 km/s (9,429 to 11,256 fps) and a margin on turbulent heating rate predictions of ±25%. The remaining causes of uncertainty are currently undetermined. A recent study of staging parameters indicated that the nominal heat sink booster, without margin for uncertainties and with no consideration of the ice accumulation problem, is competitive with respect to weight and cost with the thermally protected concept up to a staging velocity of 3.35 km/s (11,000 fps). Allowance for the ice problem and margins for uncertainties would reduce this break-even point. Some indication of the weight variation is given in the subsequent weight tabulation.

HEAT SINK UNCERTAINTY
LH_2 Tank

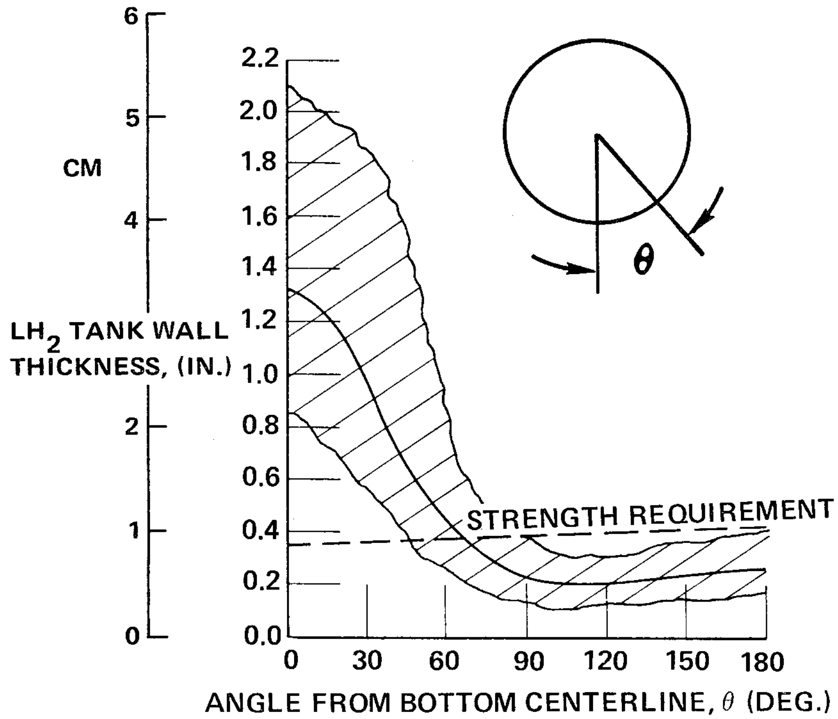

UNCERTAINTY BAND
(NOT FULLY DEFINED)

- PERFORMANCE VARIATIONS
  - STAGING VELOCITY
    - ENGINE THRUST LEVEL
    - MISSION REQUIREMENTS
  - TRAJECTORY
- ANALYTICAL VARIATIONS
  - TURBULENT HEATING RATES
  - TRANSITION CRITERION
- ENVIRONMENT UNCERTAINTIES
  - WIND TUNNEL TESTS
  - FLOW AROUND TANKS
    - WING/CANARD INTERFERENCE
    - ORBITER INTERFERENCE
  - FULL SCALE VEHICLE EFFECTS

Figure 4

ICE ACCUMULATION ON EXPOSED PROPELLANT TANKS

(Figure 5)

If an all-weather launch capability is considered for the heat sink booster, the problem of ice accumulation on exposed cyrogenic tanks must be addressed. Two considerations are involved: obviously the increase in gross liftoff weight, and the possibility of damage to aerodynamic surfaces by impingement of falling ice during the boost phase. As the data indicate, the situation is most critical on the LO_2 tank, which involves an exposed area of some 269.7 m^2 (2,900 square feet). Under the most adverse conditions, 21,338 kg (47,000 pounds) of ice approximately 8.6 cm (3.4 inches) thick might accumulate. In the case of the LH_2 tank for the vehicle considered in this study, the tank is partially shrouded by the delta wing and the large wing-to-fuselage fairing. The net exposed area is approximately 595.2 m^2 (6,400 square feet) which would accumulate some 3651.9 kg (8,044 pounds) of ice during a two-hour ground hold under the most adverse weather conditions. These data were calculated for the Space Shuttle using 7.12 cm (3 inches) of internal cryogenic insulation, the thickness being required to cover the internal grid stiffening of the hydrogen tank. The LO_2 tank in the test was uninsulated.

ICE ACCUMULATION ON EXPOSED PROPELLANT TANKS

TANK	TEMPERATURE		WIND SPEED		ICE THICKNESS		ICE ACCUMULATION	
	°K	°F	m/s	mph	cm	in.	kg/m^2	psf
LO_2 (ATLAS TEST DATA)	275	36	0	0	8.6	3.4	78.9	16.15
			13.5	30	6.1	2.4	55.5	11.40
			26.8	60	3.2	1.25	29.0	5.94
LH_2 (CALCULATED)	272	29	2.25	5	0.69	0.27	6.1	1.25

FOR 2 HOUR GROUND HOLD IN RAIN.

Figure 5

DOUBLE-WALL TANK

(Figure 6)

Several concepts for alleviating the ice accumulation problem are under consideration. The LO_2 tank may be protected on the launch pad by a wraparound blanket, either insulated and sealed or purged by dry nitrogen. The blanket would be retracted from the vehicle by a power-operated boom and cable system immediately before liftoff. The unfurled size of this blanket, however, would be 10.7 by 32 m (35 by 105 feet) and would involve complications in the wrap-around areas of the orbiter attachment and the canard. Uncertainties exist with respect to the reliability of the retraction of this arrangement and the possibility of damage to the oribiter windward thermal protection system, which would be very close to the free edges of the shroud. The problem requires further investigation, but at this point the only effective and reliable approach appears to be provision of an external shell over the LO_2 tank and the use of a dry nitrogen purge in the resulting cavity. A tradeoff study readily indicated that the heat sink approach is now not competitive in this area since the advantage of the capacitance of the basic structure is lost. The most efficient arrangement is illustrated. A superalloy radiative heat shield shell is attached around the periphery of an external frame at the aft end of the LO_2 tank and extends forward to support the nose structure. Thermal expansion relative to the cold tank is accommodated by forward translation of the outer shell which is permitted by link supports from the tank structure. A dry nitrogen purge is provided. As shown later, a weight penalty on dry structure of 4,154 kg (9,151 pounds) is involved in adding the outer shell.

Concepts for protecting the LH_2 tank are also being considered including hot water spray and heat lamp arrays. Pending complete evaluation of such approaches, the penalty for carrying a two-hour ice accumulation is indicated later in the tabulated comparison of vehicle weights.

DOUBLE-WALL TANK

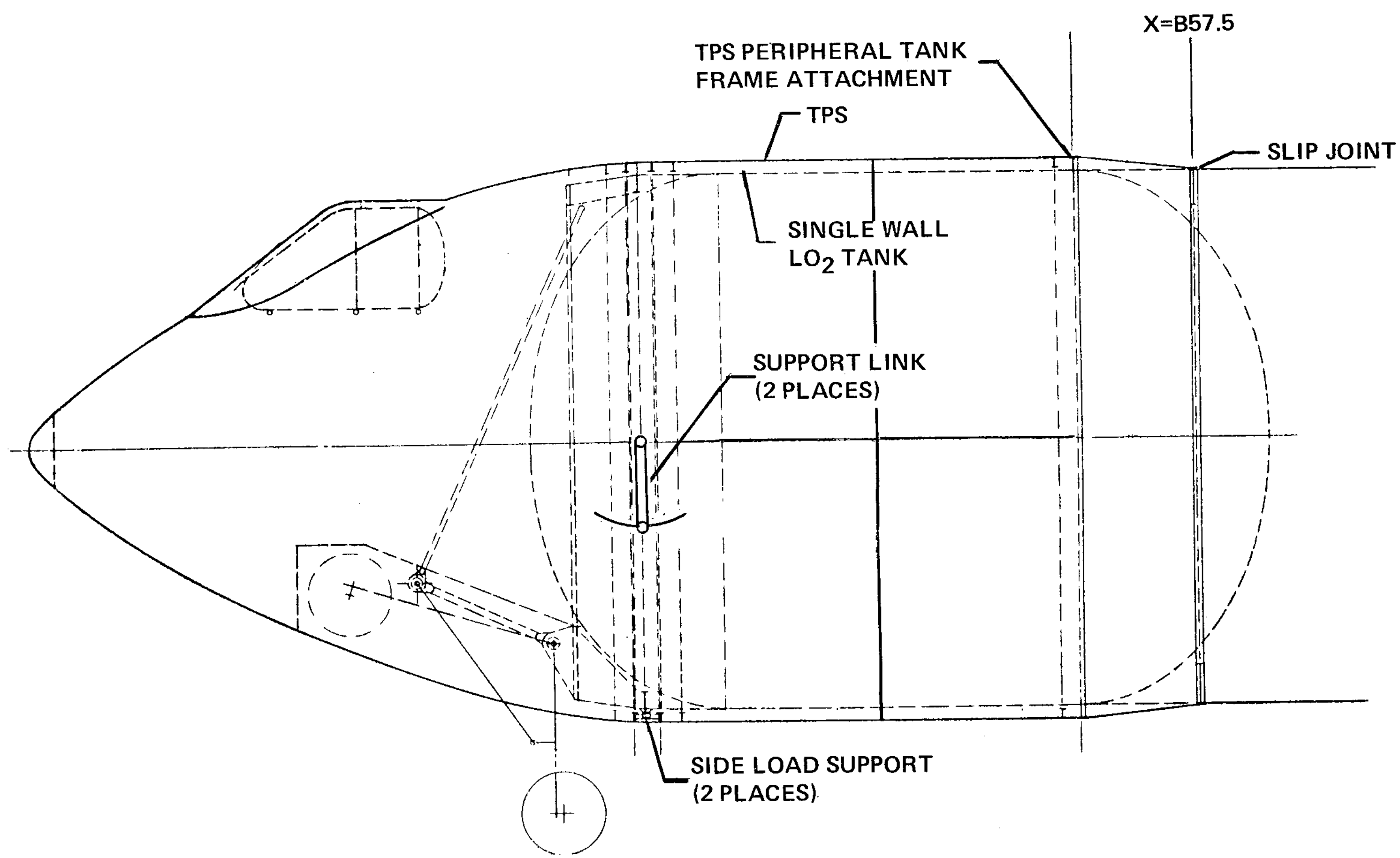

Figure 6

SUMMARY
HEAT SINK VS. TPS BOOSTER WEIGHTS

(Figure 7)

Weight comparisons of a thermally protected booster and various versions of the heat sink booster are presented. The first column is a tabulation for the TPS version. Next is the heat sink booster with a nominal heat sink requirement reflecting no provisions for trajectory dispersions or heating uncertainties. This version provides no alleviation of the ice accumulation problem, only a bare (single wall) LO_2 tank is used for example. The third column includes provision for a double-wall LO_2 tank with an "on pad" dry nitrogen purge to eliminate ice accumulation in this area. The fourth column represents a heat sink booster with the double-wall LO_2 tank and allowance for ice on the LH_2 tank consistent with a two-hour ground hold during the most adverse weather conditions. The final column, in addition to the provisions of the fourth column allows for a 25% increase in heat sink mass, representing a 25% margin over the nominal heat load prediction.

Item 1, the liquid hydrogen tank, reflects an increase for the heat sink booster due to compromise to the internal stiffening elements required to avoid undue complexity of the internal cryogenic insulation. In Item 2, the LO_2 tank weight is reduced since the heat sink booster features a cylindrical tank as opposed to a conical tank. The cylindrical tank, however, requires a larger nose structure, the increased weight of which is reflected in Item 3, which comprises all components of the body primary structure other than the propellant tanks. Item 4, Heat Sink, represents the additional material added to the body for thermal capacitance over the basic structural requirement. The entry against Item 5, TPS, for the heat sink booster represents the TPS panels across the lower surface of the body in the area of the low delta wing. The increase in the remaining columns reflects the local radiative heat shield shell which provides the outer wall of the "double-wall" LO_2 tank. Item 6 reflects the large fairings required between the delta wing and the bare cylindrical tank on the heat sink booster plus allowance for fairing of subsystem line routing along the body. The LH_2 insulation, Item 7, is heavier for the heat sink vehicle due to the necessity for covering the internal stiffening elements. Item 8 varies with the volume of the cavities which require a nitrogen purge around the propellant tanks. The orbiter attachment weight reflects the load differences due to the variation in orbiter offset from the booster with and without a TPS. Item 10, Remainder, contains all items not directly affected by the TPS versus heat sink arrangement, Item 11 is the ice accumulation on the hydrogen tank after a two-hour ground hold.

SUMMARY, HEAT SINK VS. TPS BOOSTER WEIGHTS

CONCEPT	TPS	H.S. (SW)	H.S. (DW)	H.S. (DW) + ICE	H.S. (D.W) + 25% + ICE
1. LH_2 TANK	29,853* 65,756**	33,428 73,630	33,863 74,589	34,145 75,210	34,392 75,753
2. LO_2 TANK ***	8,041 17,711	6,633 14,610	6,726 14,815	6,786 14,947	6,838 15,062
3. BASIC BODY ***	16,237 35,765	17,248 37,991	17,387 38,302	17,480 38,502	17.560 38,678
4. HEAT SINK		15,715 34,614	12,516 27,568	12,576 27,700	15,798 34,798
5. TPS	27,648 60,898	3,203 7,056	8,695 19,251	8,740 19,251	8,780 19,339
6. FAIRINGS	271 597	4,177 9,200	4,177 9,200	4,177 9,200	4,177 9,200
7. LH_2 INSULATION	2,550 5,617	3,965 8,733	3,999 8,809	4,022 8,858	4,041 8,900
8. PURGE SYSTEM	836 1,842	421 928	614 1,352	621 1,367	627 1,381
9. ORBITER ATTACH.	10,488 23,101	9,120 20,088	9,554 21,000	9,534 21,000	9,535 21,002
10. REMAINDER	135,356 298,142	135,645 298,778	136,197 299,993	139,331 306,896	142,073 312,937
11. ICE AND FROST				3,652 8,044	3,652 8,044
DRY STRUCTURE	231,281 509,429	229,555 505,628	233,709 514,779	241,063 530,975	247,473 545,094
GLOW (M)	1.9236 4.237	1.9122 4.212	1.9345 4.261	1.9567 4.31	1.9735 4,347

NOTES

* Kilograms

** Pounds

*** Taper tank on TPS booster. Cylindrical tank on heat sink booster.

Figure 7

CONCLUSIONS
(Figure 8)

The heat sink concept does indicate a potential cost reduction. Preliminary estimates indicate total program cost saving for body of heat sink booster of $222 million versus the thermally protected body. This is for the nominal heat sink booster per Column 2 of Figure 7; that is, without provision for a double wall LO_2 tank or accumulation of ice on the LH_2 tank. Adding these provisions per Column 4 of Figure 7 reduces this saving to $147 million. The saving realized by eliminating the heat shield shell is partially offset by increased costs of forming, machining, and multiple-pass welding of the thick heat sink body segments.

Some additional advantages accrue to the heat sink booster since extensive areas are fully exposed for inspection and maintenance. Safety is enhanced since leakage from large areas of the liquid hydrogen tank is open to the atmosphere and readily detectable.

A serious disadvantage with the heat sink concept concerns extreme sensitivity to the heating environment, compared with the thermally protected concept. The latter concept is relatively insensitive to heating rate and total heat load since most of the thermal energy is rejected by radiation. Increases can be accommodated by changes in surface materials and/or insulation thickness. The heat sink design, on the other hand, is relatively inflexible. Within the shuttle ground rules which currently eliminate consideration of extensive use of ablatives, increased heat load can be compensated only by increased structural shell thickness, a change which would be difficult to accomplish late in the program.

CONCLUSIONS

HEAT SINK BOOSTER INDICATES POTENTIAL FOR COST REDUCTION & EASE OF MANUFACTURING, INSPECTION & MAINTENANCE

BUT

HEAT SINK BOOSTER IS LESS TOLERANT TO ENVIRONMENTAL UNCERTAINTIES (WHICH WILL NOT BE RESOLVED UNTIL LATE IN PROGRAM)

AND

HEAT SINK BOOSTER REQUIRES MORE PRECISE DEFINITION OF "MAXIMUM" PERFORMANCE REQUIREMENTS

Figure 8

RECOMMENDATIONS
(Figure 9)

Largely due to uncertainties in aerodynamic heating predictions to which the heat sink concept is most sensitive, the thermally protected booster is still considered to be the most viable concept at this point in time. However, the potential advantages of the heat sink arrangement are so attractive that additional study and supporting experimental work should be pursued. A changeover to the heat sink concept for the body, should it prove desirable, might be accomplished later on in the program.

In view of this possibility, the concept should be retained as an alternative design approach and effort should be expended to define the necessary design criteria. A better definition of the maximum mission requirements has been obtained since the production of this study material. There remains a need for wind tunnel test results and an evaluation of heating uncertainties. When these data are available, the comparison between the heat sink and the thermally protected concept should be completely reassessed.

RECOMMENDATIONS

- RETAIN TPS BOOSTER FOR CURRENT BASELINE VEHICLE
- PURSUE DEFINITION OF PARAMETERS REQUIRED TO DESIGN HEAT SINK BOOSTER
- RETAIN HEAT SINK CONCEPT AS ALTERNATIVE DESIGN APPROACH
- UPDATE COMPARISON UPON RECEIPT OF
  - UNCERTAINTY ANALYSIS RESULTS
  - MAXIMUM MISSION REQUIREMENTS
  - WIND TUNNEL TEST RESULTS

Figure 9

COMPARISON OF ACTIVE AND PASSIVE THERMAL PROTECTION SYSTEM WEIGHTS FOR A DELTA-BODY ORBITER

By H. D. Schultz and F. L. Guard
Lockheed Missiles & Space Company
Sunnyvale, California

SUMMARY

A study was accomplished which compares active and passive Thermal Protection System (TPS) weights for a delta-body orbiter for crossrange up to 1500 nautical miles (NM). Two heat shield designs were considered: a clip-supported metallic heat shield with 96-kg/m^3 (6-lb/ft^3) Dyna-Flex insulation, and LI-1500, an all-silica, rigid insulation being developed by Lockheed. In all cases, an aluminum primary structure with 370°K (200°F) temperature limit was assumed. For the passive systems, insulation was sized as a function of crossrange. For the active systems, TPS insulation thickness and hardware were optimized for minimum weight at 1500 NM. The reduction in expendable coolant and auxiliary power unit (APU) fuel weights was then computed for shorter crossrange. The active TPS is a redundant, indirect active cooling system which uses water-glycol as the transport fluid, and water and ammonia as expendable coolants.

Principal conclusions resulting from this study are as follows: (1) Regardless of crossrange an active TPS with LI-1500 heat shield is the lightest weight of the four TPS concepts analyzed, (2) an active TPS is roughly one-half as weight sensitive to crossrange as a passive TPS, and (3) for both LI-1500 and metallic heat shields, the passive TPS is about 1225 kg (2700 lb) heavier than the active TPS at 200 NM crossrange and about 2500 kg (5500 lb) heavier at 1500 NM.

INTRODUCTION

The selection of the Space Shuttle orbiter Thermal Protection System (TPS) will have a major impact on the ability of the shuttle to meet its goal of low cost orbital payload delivery. This is particularly true for those configurations capable of achieving large aerodynamic crossrange since the entry duration, and therefore heat input, increases significantly with crossrange. For a passive TPS, several thousand kilograms of additional TPS weight are required as the crossrange is increased from 200 to 1500 NM. One method to reduce TPS weight sensitivity to crossrange, and thereby avoid most of the payload penalty associated with a passive TPS, is to employ an indirect active cooling system.

OBJECTIVE/APPROACH

(Figure 1)

A thermal protection system trade study was performed to determine the minimum weight system for a delta-body orbiter as a function of entry crossrange. Both LI-1500 (a 240-kg/m^3 [15-lb/ft^3] all-silica, rigid insulator being developed by Lockheed) and metallic (columbium/Dyna-Flex) heat shields were considered. The passive TPS utilizes sufficient insulation to prevent excessive structure temperatures. The active TPS is a redundant, indirect active cooling system which uses water-glycol as the transport fluid, and water and ammonia as expendable coolants.

An outline of the study approach is shown. Whereas the passive TPS is sized as a function of crossrange, the active TPS is optimized for minimum weight at a crossrange of 1500 NM. The resulting active TPS is therefore capable of operation at any crossrange up to 1500 NM by varying the amount of expendable coolant and APU fuel carried.

OBJECTIVE/APPROACH

OBJECTIVE:

- COMPARE ACTIVE AND PASSIVE THERMAL PROTECTION SYSTEM WEIGHTS FOR A DELTA-BODY ORBITER FOR ENTRY CROSSRANGE UP TO 1500 NM.

APPROACH:

- ESTABLISH VARIATION IN THERMAL ENVIRONMENT WITH CROSS-RANGE.
- SIZE PASSIVE TPS INSULATION FOR EACH CROSSRANGE.
- OPTIMIZE ACTIVE TPS INSULATION AND HARDWARE FOR 1500 NM CROSSRANGE. COMPUTE REDUCTION IN EXPENDABLE COOLANT AND APU FUEL FOR SHORTER CROSSRANGE.
- COMPARE RESULTING TPS WEIGHTS.

Figure 1

DELTA-BODY ORBITER CONFIGURATION

(Figure 2)

The orbiter configuration is characterized by a 78° leading-edge-sweep delta-lifting body. For the present study the orbiter was sized as the spacecraft of a stage-and-one-half system which resulted in a reentry planform wing loading of 239 kg/m^2 (49 psf). The orbiter aerodynamic characteristics are such that maximum hypersonic lift-drag ratio and lift coefficient occur at angles of attack of 20° and 55°, respectively.

Previous Lockheed comparisons of active/passive TPS have shown a passive upper surface to be lighter for crossrange up to at least 1500 NM. As a result, the present study considers an actively cooled windward surface area of 414 m^2 (4455 ft^2), which represents about 36 percent of the total surface area. The actively cooled area includes the entire lower surface aft of the nose cap skirt and inboard of the leading-edge geometric stagnation line.

DELTA-BODY ORBITER CONFIGURATION

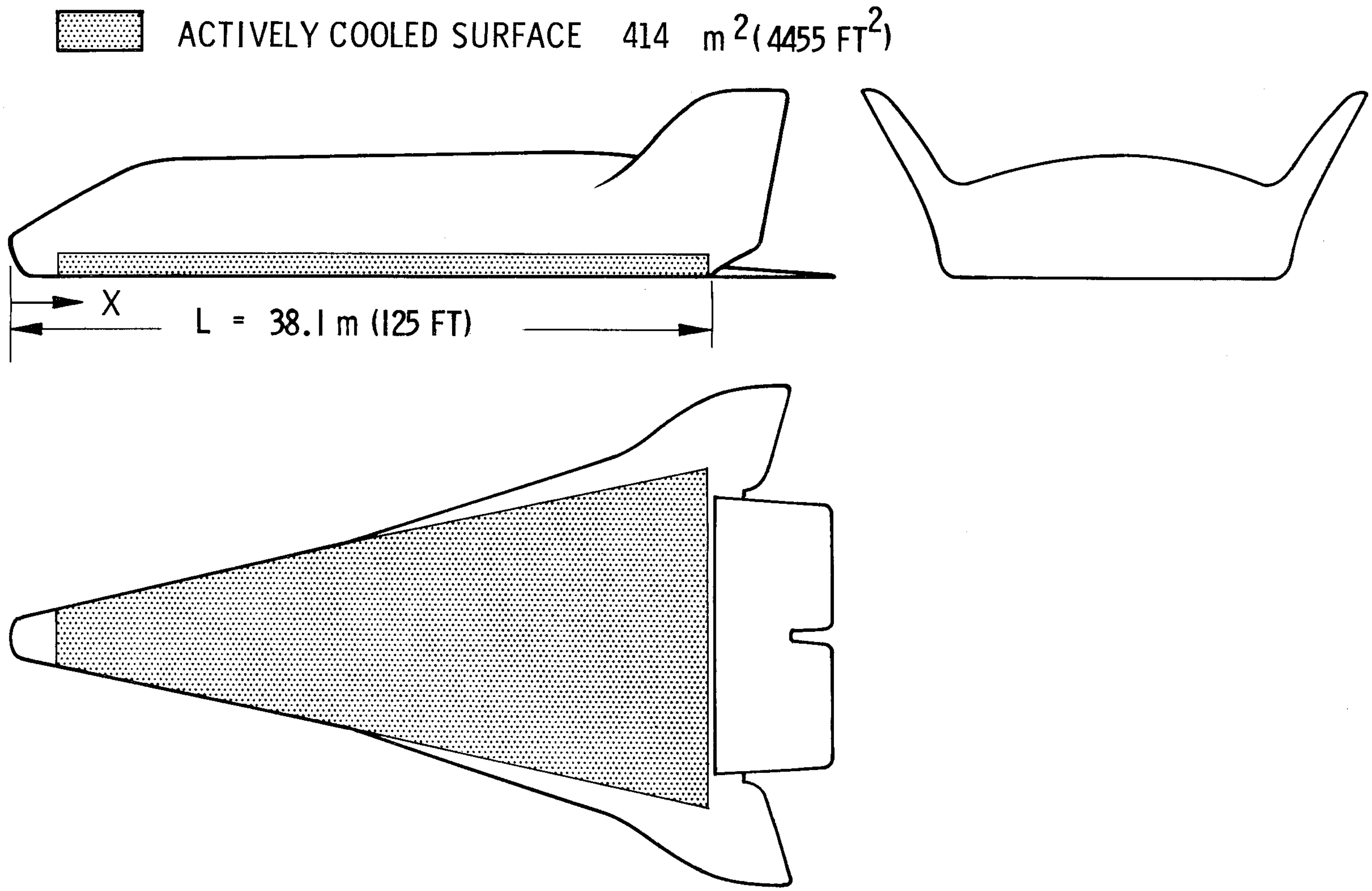

Figure 2

LOWER SURFACE TPS/STRUCTURAL ARRANGEMENT

(Figure 3)

This figure shows the four TPS concepts analyzed. The nonmetallic TPS consists of 240 kg/m^3 (15 lb/ft^3) LI-1500 bonded directly to the aluminum primary structure. The metallic TPS consists of a clip-supported columbium heat shield with 96 kg/m^3 (6 lb/ft^3) Dyna-Flex used to insulate the structure. For increased stiffness the columbium outer panel is formed with circular-arc corrugations, using a pitch of 35.6 mm (1.4 in.) and a height of 3.56 mm (0.14 in.). Consequently, although the entry trajectories are constrained to produce a smooth-panel peak temperature of 1530°K (2300°F), local temperatures as high as 1590°K (2400°F) occur on the corrugations.

For the passive systems, insulation is sized for a 370°K (200°F) backface temperature. For the active systems, insulation thickness is optimized for minimum TPS weight and the structure is cooled by flowing water-glycol through aluminum tubes which are attached to the interior surface.

LOWER SURFACE TPS/STRUCTURAL ARRANGEMENT

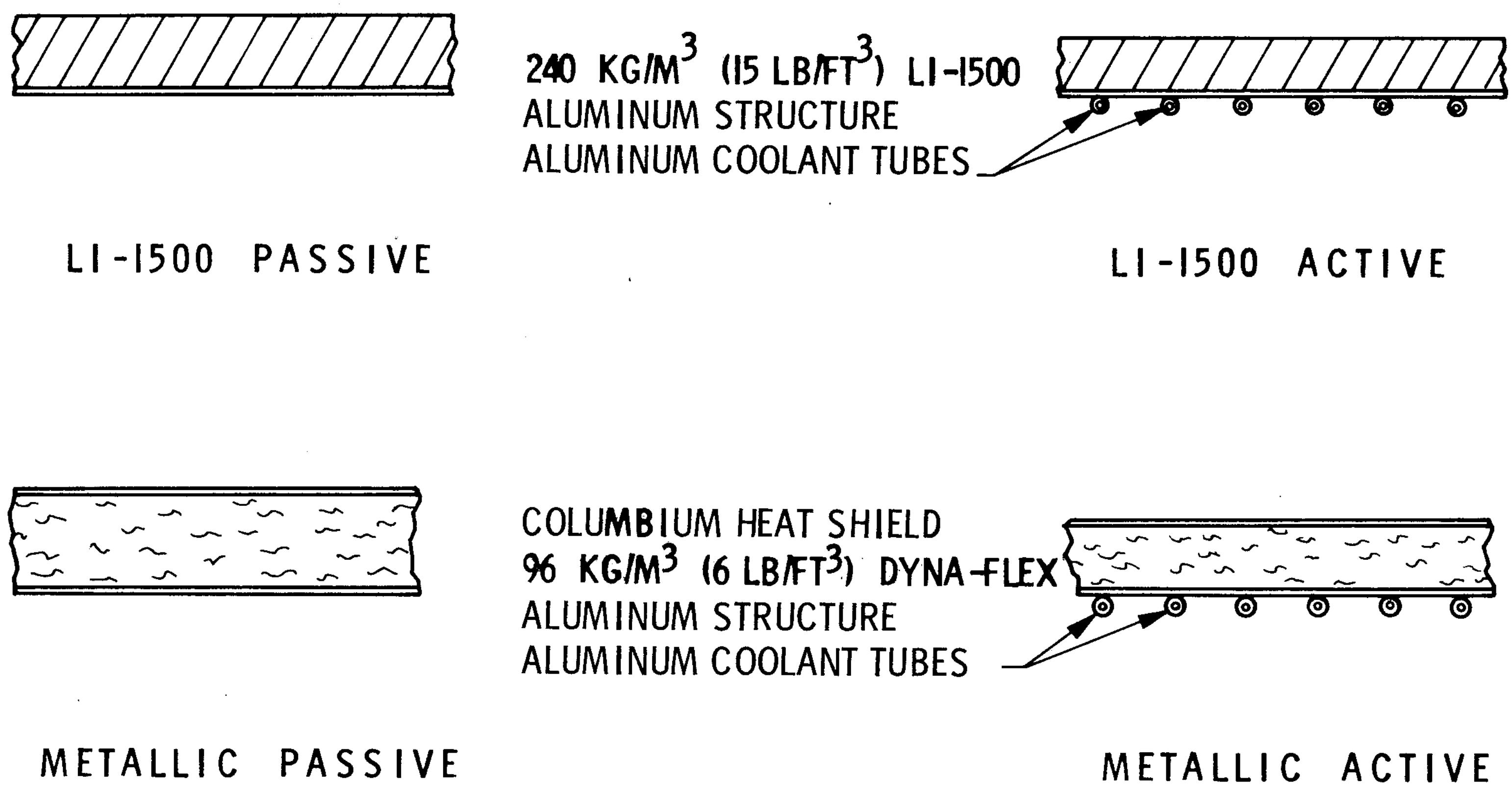

Figure 3

ENTRY THERMAL ENVIRONMENT

(Figure 4)

The variation in thermal environment as a function of crossrange was established by generating temperature-constrained, minimum-duration entry trajectories for the nominal crossranges shown. To minimize entry time, and thereby TPS weight, the vehicle is banked as much as possible without exceeding heating, dynamic pressure, or g-load limits. A lower-surface/leading-edge temperature limit of 1530°K (2300°F) was used for this study.

The trajectories are based on entry, turning East, from a 270 NM, 55° inclination orbit. Approximately 500 NM crossrange is obtained for entry at maximum lift coefficient, i.e., $\alpha = 55^{\circ}$. If desired, this crossrange could be reduced by bank reversal; however, no reduction in entry time or TPS weight would be achieved compared to the weight for 500 NM.

Due to the small variation in insulation requirements with lower-surface location, the TPS weights are based on the thermal environment at two locations, namely, the lower centerline at 25 and 75 percent of the vehicle reference length. Surface temperature histories at these two locations are shown for each of the three entry trajectories. The effect of increased crossrange is a large increase in entry duration since all three trajectories are constrained to the same lower surface peak temperature.

ENTRY THERMAL ENVIRONMENT

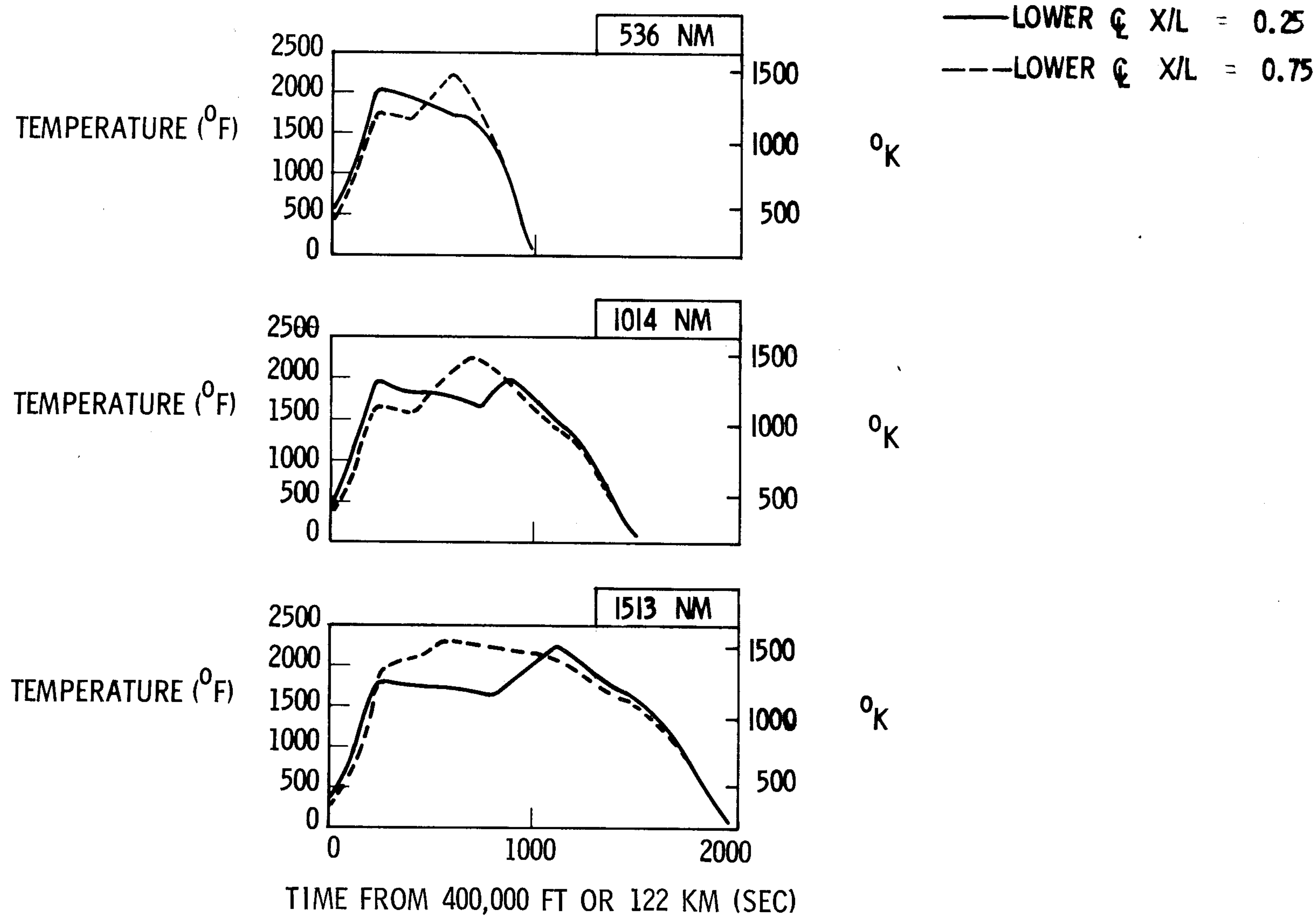

Figure 4

PASSIVE INSULATION THICKNESS AND UNIT WEIGHTS

(Figure 5)

This figure shows the required insulation thickness versus crossrange, based on a $370^{\circ}K$ ($200^{\circ}F$) structure temperature limit. The calculations account for the variation of thermal properties with temperature, and include parallel conduction through the Dyna-Flex insulation and columbium clips for the metallic TPS. To minimize insulation weight the structure is assumed to be cooled with air supplied by a ground cart, starting 10 minutes after touchdown.

TPS unit weights are based on Lockheed in-house studies and include the heat shield, insulation, clips and attachments, i.e., everything external to the structure:

$$(W/A)_{\text{LI-1500 TPS}} = 1.17 + 2.51\ t \quad (\text{kg/m}^2)$$

$$(W/A)_{\text{Columbium TPS}} = 6.35 + 1.18\ t \quad (\text{kg/m}^2)$$

where t is the required insulation thickness in centimeters.

PASSIVE INSULATION THICKNESS AND UNIT WEIGHTS

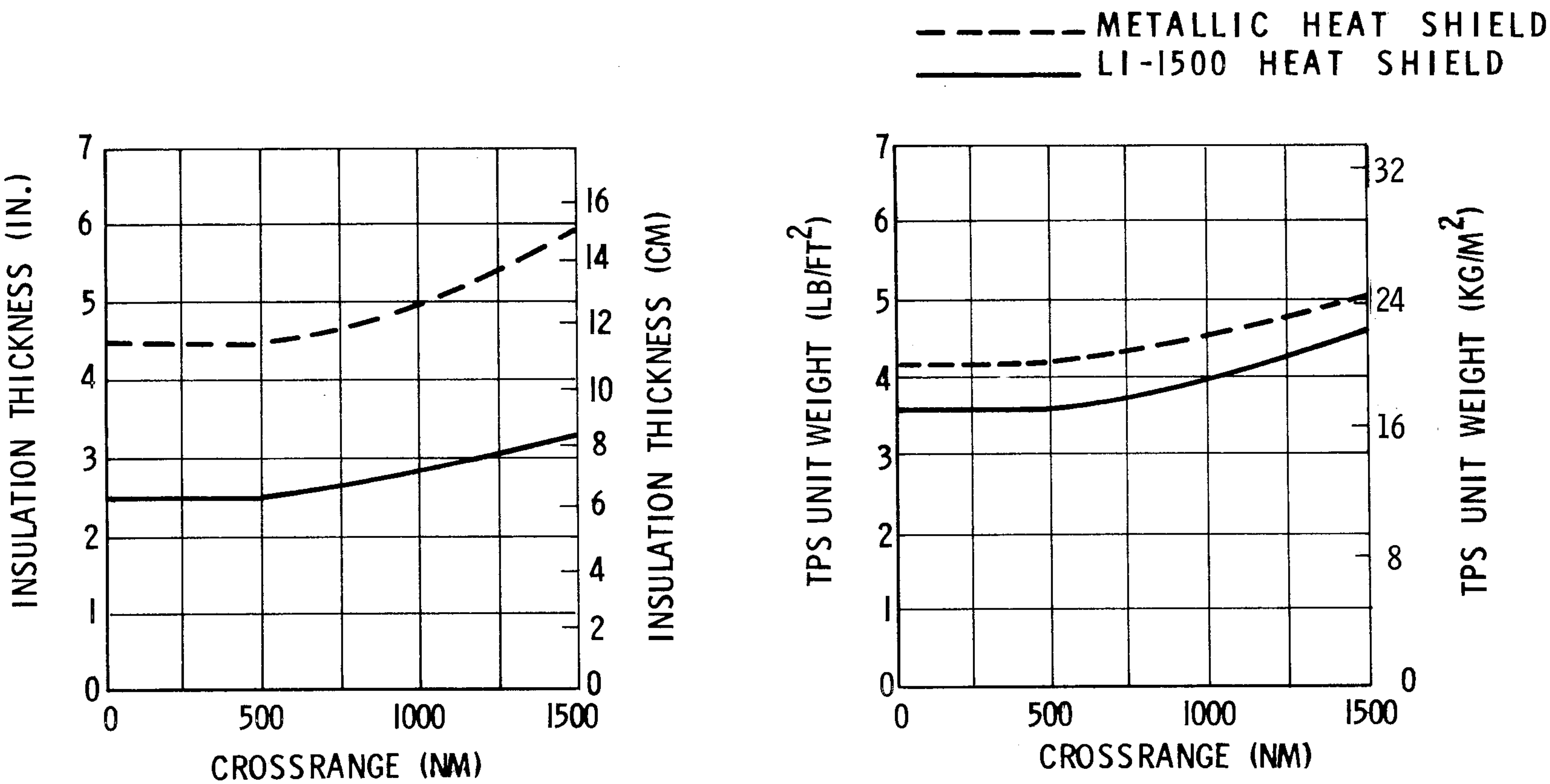

INSULATION THICKNESS

TPS UNIT WEIGHT

Figure 5

ACTIVE COOLING SCHEMATIC

(Figure 6)

This figure is a schematic of the indirect active cooling system. To minimize the possibility of a catastrophic structural failure the system is completely redundant, with the exception of the expendable water and ammonia tanks, and their pressurizing source. Ammonia replaces water as the expendable coolant when the altitude drops below 30.5 km (100,000 ft).

Panel coolant passages are 3.55 mm (0.14 in.) outside diameter by 0.51 mm (0.020 in.) thick aluminum tubes which are attached to the structure at 25.4 mm (1.0 in.) intervals for the LI-1500 TPS and 30.50 mm (1.2 in.) intervals for the metallic TPS. The tube length is 0.914 m (3 ft), which corresponds to the distance between frames. The water-glycol flow rate, based on a 17°K (30°F) temperature rise as it passes through the 0.914 m (3 ft) coolant passage, is 55 kg/sec (121 lb/sec) for the LI-1500 TPS and 42 kg/sec (92 lb/sec) for the metallic TPS.

In the event of failure of one cooling leg, the system is sized such that the remaining leg would provide sufficient cooling capacity to limit the structure temperature to 370°K (200°F). In this case the flow through alternate tubes would be zero and the heat load would be absorbed by tubes spaced at 51 mm (2.0 in.) intervals with a flow rate of 27.4 kg/sec (60.5 lb/sec) (using the LI-1500 TPS as an example).

ACTIVE COOLING SCHEMATIC

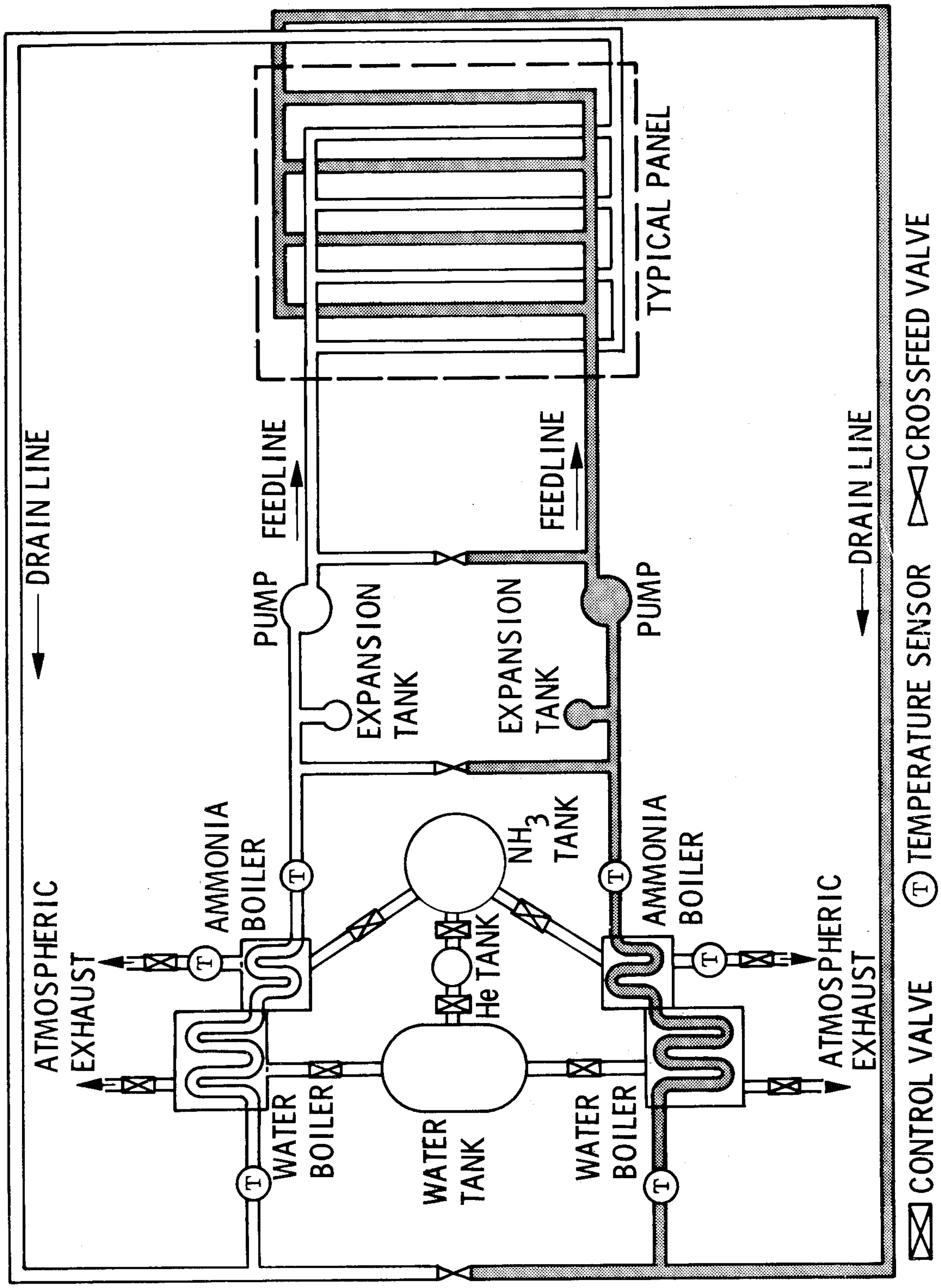

Figure 6

WATER-GLYCOL DISTRIBUTION SYSTEM

(Figure 7)

To minimize pumping requirements and variations in vehicle C.G., the expendable coolants, heat exchangers, APU's, pumps and motors are located at the centroid of the area to be actively cooled. The distribution system is divided into two parts with separate distribution lines serving the areas forward and aft of the centroid. After the water-glycol leaves the pump it passes through a main feedline manifold which runs along the vehicle lower centerline. The water-glycol then enters the panel feedline manifold, passes through the panel cooling passages, is collected in the panel drain line, and returned to the heat exchangers through the secondary and main return lines. Since the active cooling system is redundant, two identical distribution systems like the one shown are required.

WATER-GLYCOL DISTRIBUTION SYSTEM

- LOCATION OF EQUIPMENT (PUMPS, HEAT EXCHANGERS, ETC.)
  ARROWS INDICATE DIRECTION OF FLOW

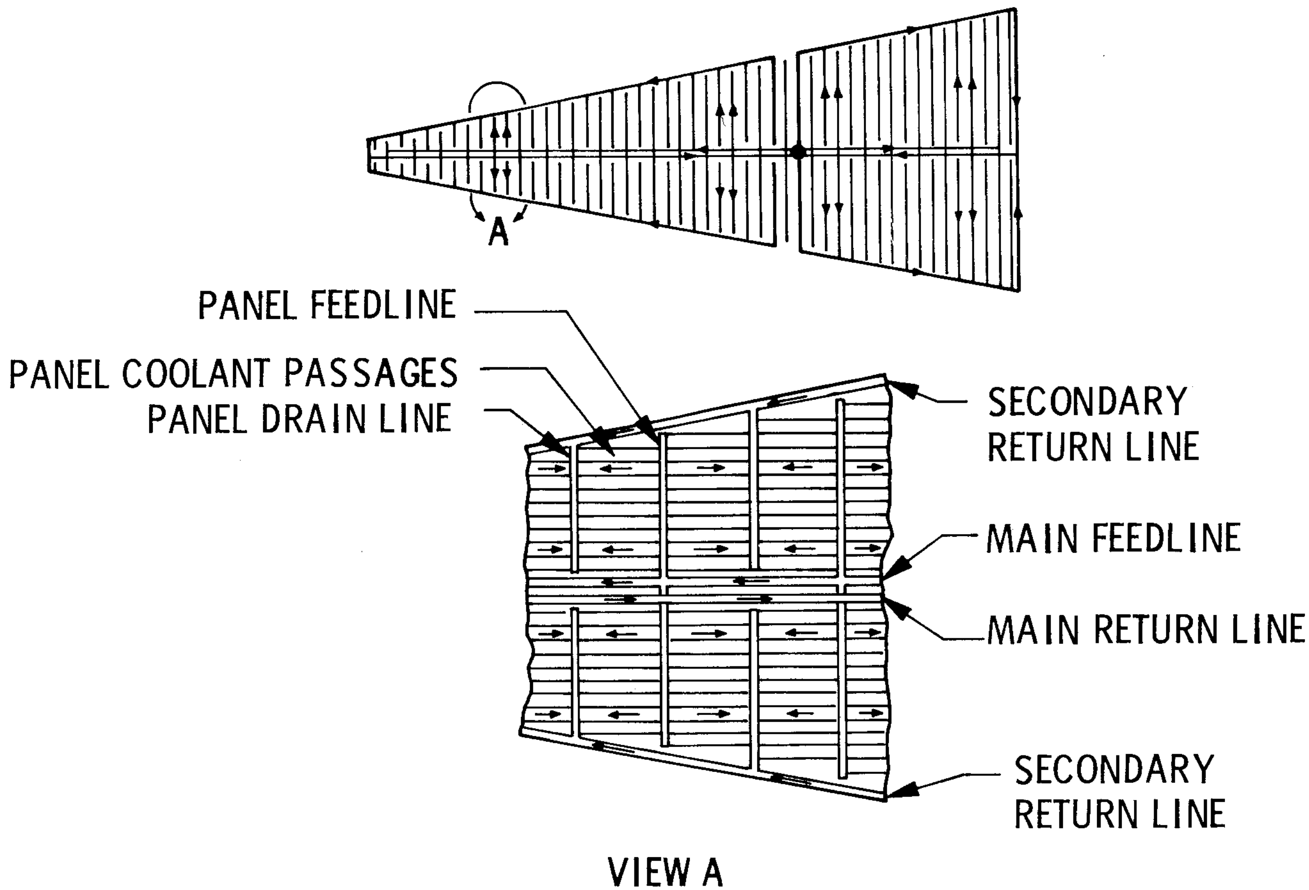

Figure 7

DISTRIBUTION LINE WEIGHT OPTIMIZATION

(Figure 8)

Distribution system tube sizes are based on weight and pressure loss considerations. This figure illustrates the rationale for selecting tube diameter, using the main return line of the LI-1500 TPS forward distribution system as an example. Weights of the tube, trapped water-glycol, and APU fuel expended to pump the water-glycol through the tube are all plotted versus the tube diameter and then summed to determine the total weight versus diameter. The minimum total weight for this line occurs at a diameter of 43 mm (1.7 in.). However, the pressure loss through the tube is extremely sensitive to diameter (roughly to the fifth power) and a sizable reduction in pressure loss can be achieved at minor weight penalty.

In this case a tube diameter of 51 mm (2.0 in.) was selected, which results in a 5.89 kg (13 lb) weight penalty compared to the weight-optimized diameter of 43 mm (1.7 in.). System reliability is increased, however, because the pressure loss is reduced from 462 to 207 kN/m^2 (67 to 30 psi).

DISTRIBUTION LINE WEIGHT OPTIMIZATION

LI-1500 HEAT SHIELD, FORWARD MAIN RETURN LINE

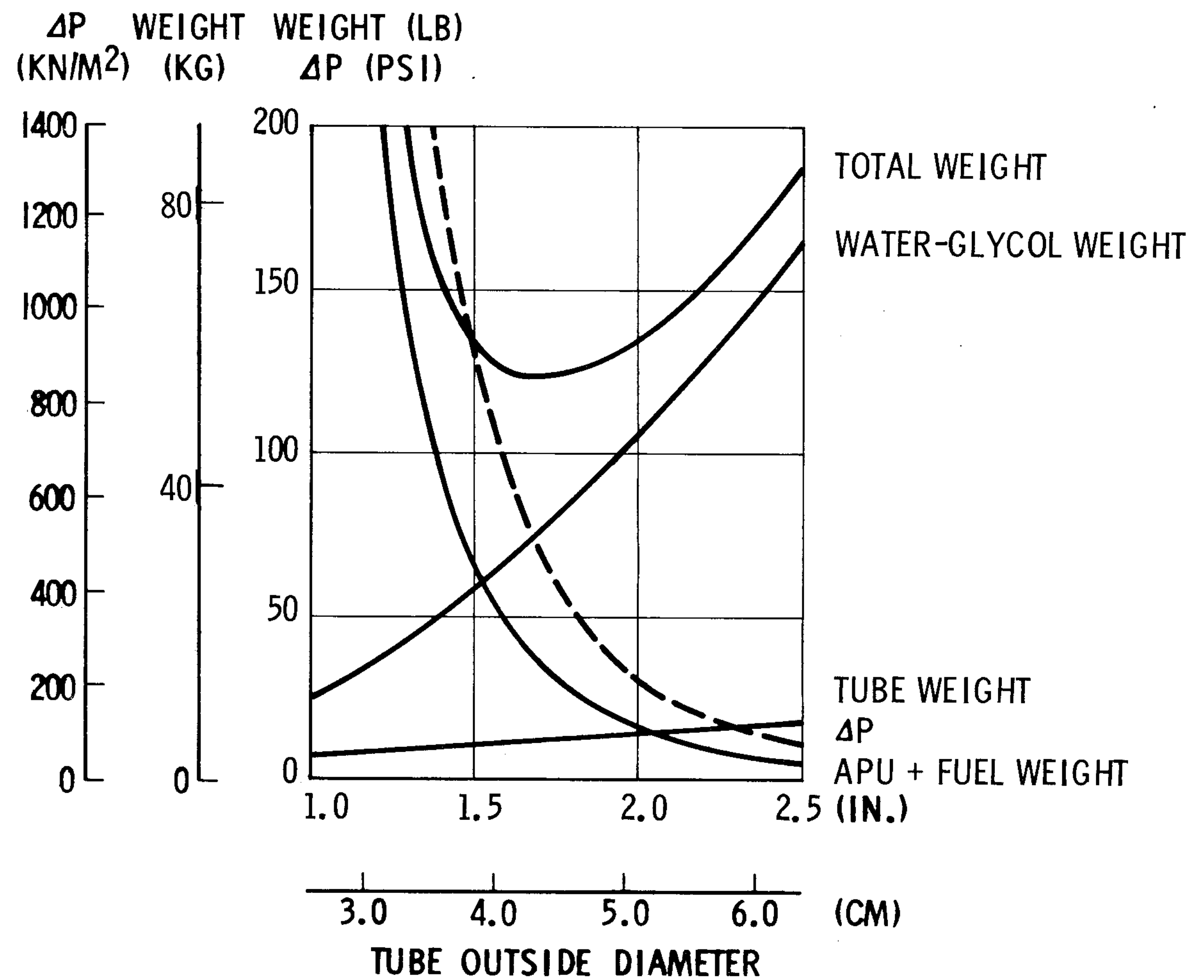

Figure 8

ACTIVE COOLING TPS WEIGHT OPTIMIZATION

(Figure 9)

As stated previously, the active cooling system insulation and hardware are optimized for operation at 1500 NM crossrange. This figure shows the unit weight of insulation, heat exchangers (HX) and expendable coolant as a function of insulation thickness for the LI-1500 and metallic heat shields. These weights are summed to determine, approximately, the insulation thickness which results in minimum active cooling system weight. Optimum insulation thicknesses are 19 mm (0.75 in.) for the LI-1500 TPS and 38 mm (1.50 in.) for the metallic TPS. These optimized thicknesses are considerably different, despite the identical thermal environment, because active cooling system weights are traded against 240 kg/m^3 (15 lb/ft^3) insulation for the LI-1500 TPS and 96 kg/m^3 (6 lb/ft^3) insulation for the metallic TPS.

ACTIVE COOLING TPS WEIGHT OPTIMIZATION

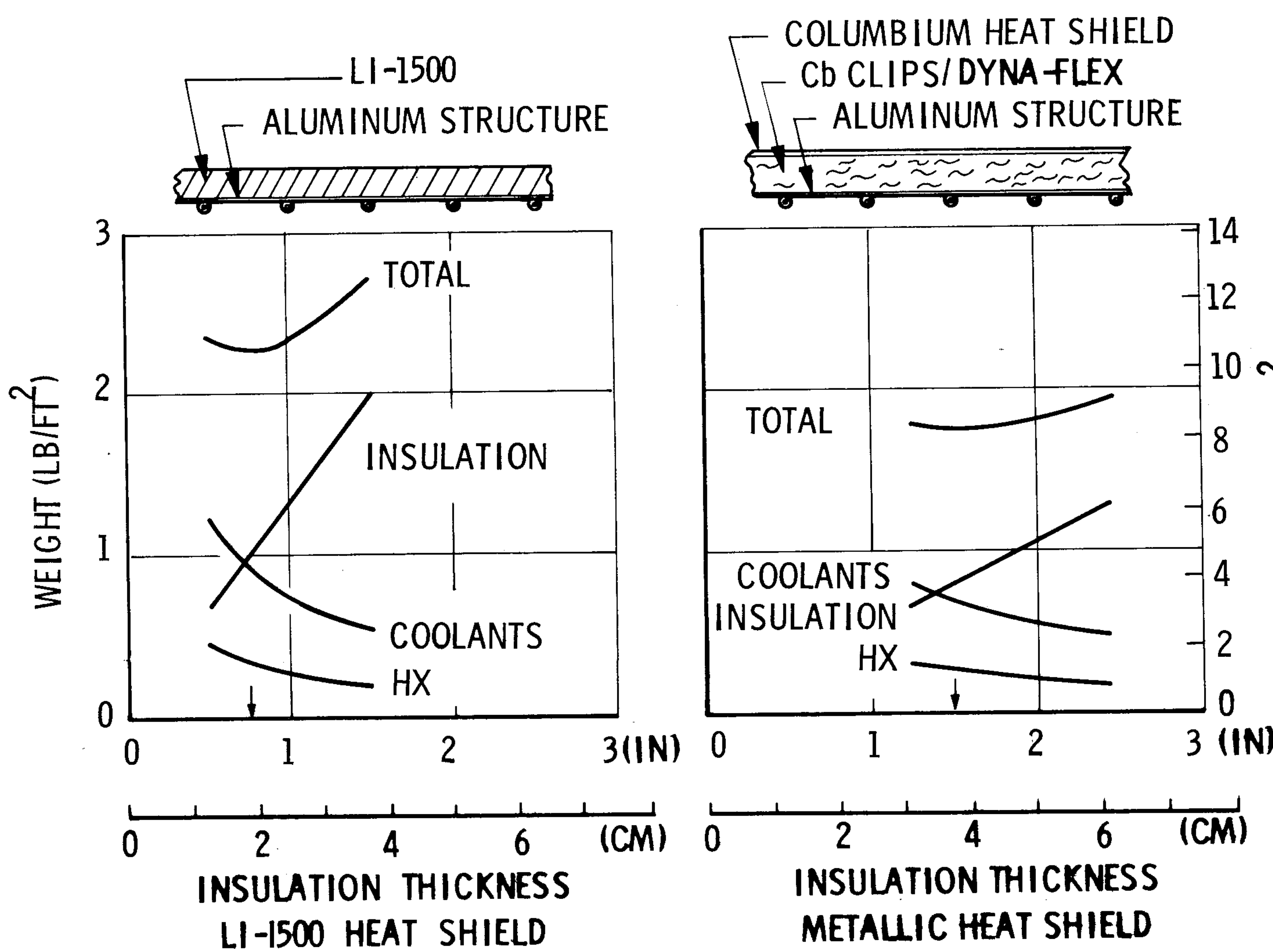

Figure 9

ACTIVE TPS WEIGHT STATEMENT

(Figure 10)

This table shows a weight breakdown for the LI-1500 and metallic TPS for each of the three entry trajectories. Because active cooling system components are optimized for 1500 NM, only the expendable coolant and APU fuel weights vary with crossrange. Water-glycol distribution system weights are based on a detailed analysis, with all lines sized by the procedure outlined previously. Tubing weights include a nonoptimum factor of 1.5 to account for fittings, attachments, and an expansion tank. Included with the distribution system weights is an estimate of 23 kg (50 lb) for flow meters, valves, and control devices. Heat exchangers are of the shell-and-tube type with the expendable coolant located outside the tubes and the water-glycol passing through the tubes. The tubes are 6.35 mm (0.25 in.) outside diameter and 0.635 mm (0.025 in.) thick. The heat exchanger weights include a 20 percent nonoptimum factor, applied to metallic components, to account for attachments and vapor exhaust ducting. Also included are weights for trapped expendable coolant based on the assumption that the heat exchangers are full of coolant when their operation is terminated.

Weights of expendable coolants were computed by dividing the integrated structure heating rate by a heat of vaporization of 2.32×10^{6} J/kg (1000 Btu/lb) for water and 1.16×10^{6} J/kg (500 Btu/lb) for ammonia. Coolant tanks and supports were taken as 12 percent of the coolant weight. Power to pump the water-glycol is supplied by an APU, which is assumed to weigh 6.08×10^{-4} kg/W (1.0 lb/hp). The APU fuel weight is estimated at 1.22×10^{-3} kg/W-hr (2.0 lb/hp-hr). The weight of the water-glycol pump and motor was obtained from Figure 29 of Reference 1.

Although not shown, the weight penalty associated with the use of a redundant cooling system is 1190 kg (2632 lb) for the LI-1500 TPS and 950 kg (2086 lb) for the metallic TPS.

ACTIVE TPS WEIGHT STATEMENT

ITEM	LI-1500 HEAT SHIELD			METALLIC HEAT SHIELD		
	536 NM	1014 NM	1513 NM	536 NM	1014 NM	1513 NM
Heat Shield	5,453	5,453	5,453	9,921	9,921	9,921
Water-Glycol Distribution System	1,572	1,572	1,572	1,235	1,235	1,235
Panel Coolant Passages	921	921	921	768	768	768
Valves, Flow Meters, Sensors	50	50	50	50	50	50
Heat Exchangers (Water Boilers)	1,786	1,786	1,786	1,348	1,348	1,348
Heat Exchangers (Ammonia Boilers)	422	422	422	281	281	281
Expendable Water	1,091	1,782	2,900	686	1,198	2,036
Expendable Ammonia	334	321	368	356	294	321
Water Tanks and Supports	487	487	487	350	350	350
Ammonia Tanks and Supports	61	61	61	49	49	49
Water-Glycol Pump and Motor	140	140	140	110	110	110
APU + Fuel	224	242	262	224	242	262
TOTAL WEIGHT (lb; 1 lb = 0.453 kg)	12,541	13,237	14,442	15,378	15,846	16,731
UNIT WEIGHT (lb/ft^2; 1 lb/ft^2 = 4.88 kg/m^2)	2.82	2.97	3.24	3.45	3.56	3.75

Figure 10

COMPARISON OF ACTIVE TPS WEIGHTS

(Figure 11)

This table compares the metallic TPS active cooling system weight breakdown for 1513 NM crossrange with values computed by weight factors reported in Reference 1. The total TPS weights differ by only 96 kg (212 lb). These are significant differences, however, in heat exchanger and APU fuel weights. The heat exchanger weights used during the present study are relatively large due to the assumption that they are filled with trapped coolant when their operation is terminated. The APU fuel weight from Reference 1 is based only on surface area ($0.488\ kg/m^2$, $0.10\ lb/ft^2$), and consequently, is only a rough estimate. The present analysis, which accounts for APU power and operating time, is believed to be more accurate.

COMPARISON OF ACTIVE TPS WEIGHTS

METALLIC TPS; 1513 NM CROSS-RANGE

ITEM	WEIGHT FROM PRESENT STUDY (LB)	WEIGHT FROM AFFDL-TR-65-124 (LB)
Heat Shield	9,921	9,921
Water-Glycol Distribution System	1,235	1,337
Panel Coolant Passages	768	768
Valves, Flow Meters, Sensors	50	50
Heat Exchangers (Water Boilers)	1,348	852
Heat Exchangers (Ammonia Boilers)	281	258
Expendable Water	2,036	2,036
Expendable Ammonia	321	321
Water Tanks and Supports	350	350
Ammonia Tanks and Supports	49	49
Water-Glycol Pump and Motor	110	110
APU + APU Fuel	262	891
TOTAL WEIGHT (lb, 1 lb = 0.453 kg)	16,731	16,943

Figure 11

LOWER SURFACE TPS WEIGHT COMPARISON

(Figure 12)

This figure shows passive and active TPS weights as a function of crossrange for the LI-1500 and metallic heat shields. Regardless of crossrange, the LI-1500 active TPS is the lightest of the four systems analyzed. For both LI-1500 and metallic heat shields, the active system weighs about 1225 kg (2700 lb) less than the passive at low crossrange and about 2500 kg (5500 lb) less at high crossrange.

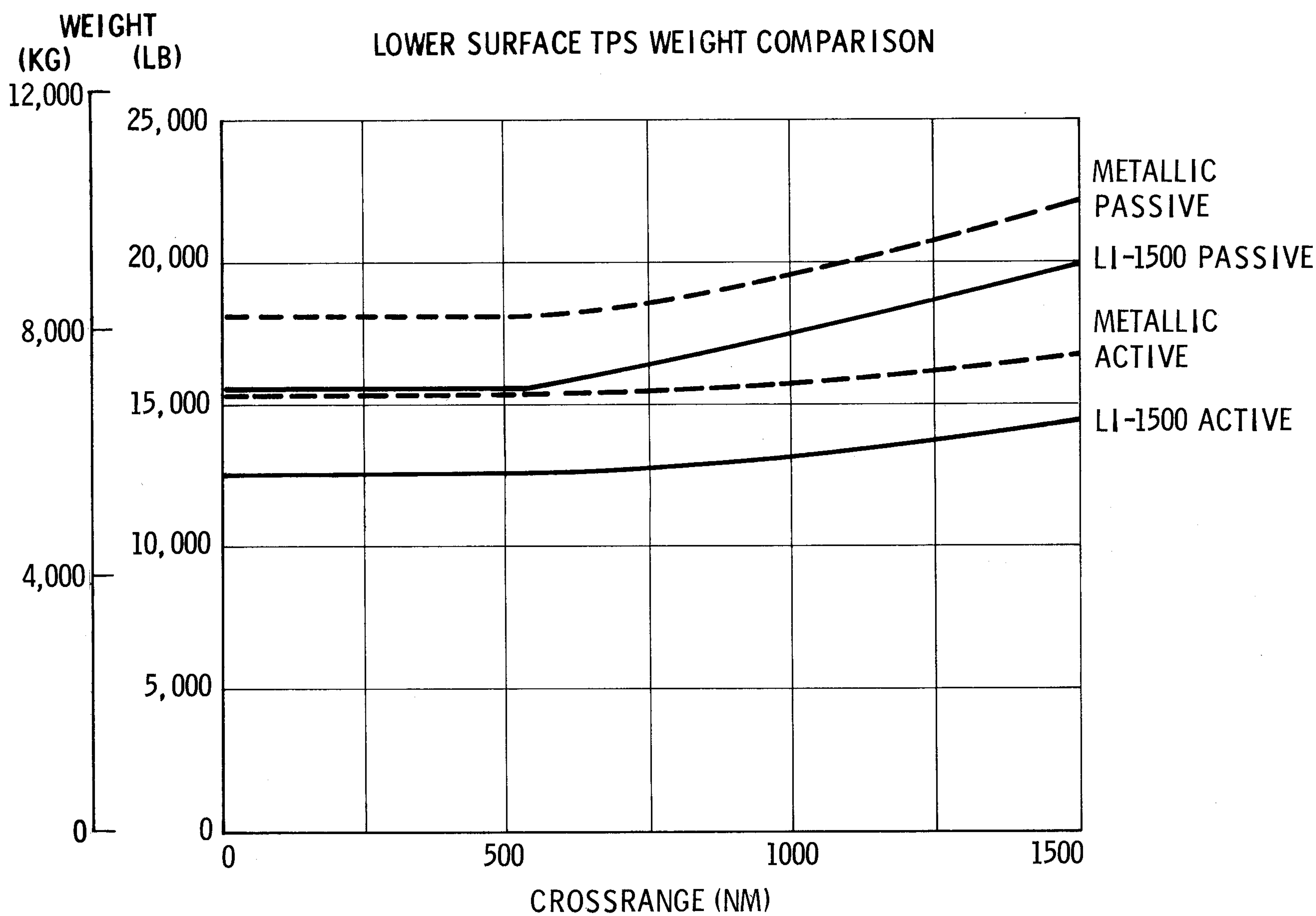

LOWER SURFACE TPS WEIGHT COMPARISON
WEIGHT
(KG)
(LB)
12,000
8,000
4,000
0
25,000
20,000
15,000
10,000
5,000
0
0
500
1000
1500
CROSSRANGE (NM)
METALLIC PASSIVE
LI-1500 PASSIVE
METALLIC ACTIVE
LI-1500 ACTIVE

Figure 12

TPS WEIGHT DISTRIBUTION

(Figure 13)

This figure shows the contribution of various items to the total TPS weight. As shown, the weight advantage of an LI-1500 active TPS is due to the exceptionally lightweight heat shield 2470 kg or 5.95 kg/m^2 (5453 lb or 1.22 lb/ft^2) which results from the weight-optimized LI-1500 thickness of 19.05 mm (0.75 in.). For the metallic active TPS the heat shield weight is 4500 kg (9,921 lb), of which 2630 kg (5,805 lb) is a "fixed" portion, independent of insulation thickness, consisting of the columbium outer panel, clips and attachments.

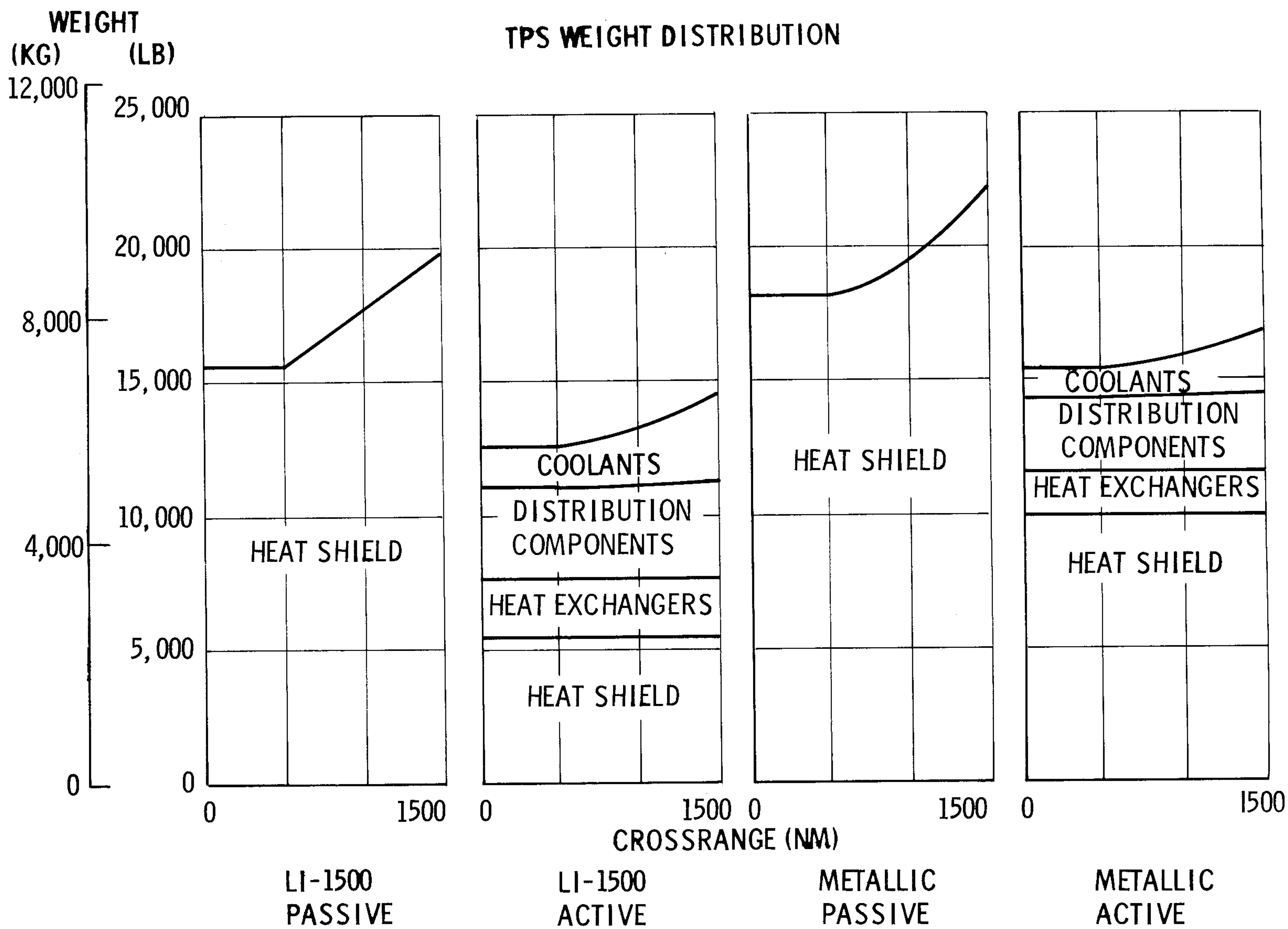

TPS WEIGHT DISTRIBUTION
WEIGHT
(KG)
(LB)
12,000
8,000
4,000
0
25,000
20,000
15,000
10,000
5,000
0
HEAT SHIELD
COOLANTS
DISTRIBUTION COMPONENTS
HEAT EXCHANGERS
HEAT SHIELD
HEAT SHIELD
COOLANTS
DISTRIBUTION COMPONENTS
HEAT EXCHANGERS
HEAT SHIELD
0
1500
0
1500
0
1500
0
1500
CROSSRANGE (NM)
LI-1500 PASSIVE
LI-1500 ACTIVE
METALLIC PASSIVE
METALLIC ACTIVE

Figure 13

CONCLUSIONS

(Figure 14)

Study conclusions are summarized on the attached chart. In general, the actively cooled TPS offers a significant weight reduction compared to passive systems and also increased versatility. For these reasons active TPS is felt to warrant more detailed investigation.

CONCLUSIONS

ADVANTAGES OF ACTIVE TPS ARE:

- LOWEST WEIGHT REGARDLESS OF CROSSRANGE.
- REDUCED WEIGHT SENSITIVITY TO CROSSRANGE.
- ALLOWS FOR TPS INTEGRATION WITH ECS AND ORBIT THERMAL CONTROL.
- PROVIDES ABILITY TO REDUCE TPS WEIGHT FOR MISSIONS REQUIRING LESS THAN DESIGN CROSSRANGE.
- ELIMINATES LOW SPEED/GROUND STRUCTURAL COOLING REQUIREMENTS.

POTENTIAL DISADVANTAGES ARE:

- INCREASED COSTS
- DECREASED RELIABILITY

Figure 14

REFERENCE

1. Anthony, Frank M. and Huff, Roland D.: Analytical Evaluation of Actively Cooled Modified Monocoque Structural Concepts. AFFDL-TR-65-124, U.S. Air Force, July 1965.

ENVIRONMENTAL TESTING FOR EVALUATION OF SPACE SHUTTLE THERMAL PROTECTION MATERIALS AND SYSTEMS

By Howard K. Larson, Frank J. Centolanzi, Nick S. Vojvodich,
Howard Goldstein, M. Alan Covington, and Fred W. Matting
NASA Ames Research Center
Moffett Field, Calif.

INTRODUCTION

The Ames material evaluation and facility development program has been underway for more than a year. During this time a considerable amount of material thermal response data have been obtained. Analyses, which are based in part on interpretation of these data, have been developed and we have thereby achieved a better understanding of how to relate ground-based test results to flight performance. In addition, comparison of the results with the expected space shuttle environment has permitted a meaningful definition (and use) of facilities and test techniques. This in turn has resulted in the facilities under construction as well as the definition of the new facilities that have been proposed. It is the purpose of this paper to describe the results of the initial testing and analysis phase of the program and to show how these results have influenced the current program and formulation of future plans.

The first figure which follows will describe an overview of the problems of shuttle testing relative to our past experience.

ORDER OF MAGNITUDE ASSESSMENT OF SIMULATION REQUIREMENTS
(Figure 1)

This figure presents an "order-of-magnitude" view of the problem of environmental simulation of shuttle thermal protection materials and systems compared to our past experience. The problem of facility utilization relative to manpower and dollar resources can be appreciated by the product of exposure time and number of exposures. It can be seen that the shuttle problem is three orders of magnitude larger for each material or system under study. Facility power requirements for shuttle testing are dictated by the listed supersonic, turbulent boundary layer and large panel sizes. This was described in a paper by R. Howell of Langley at the Shuttle Conference in July 1970.* Finally, the accuracy of measurements of surface recession rates is important in laboratory measurements. It can be seen that four orders of magnitude separate our past experience from shuttle requirements.

The material evaluation program initiated a year or so ago dramatically revealed these problems to us. In our first test series we exposed single samples to a stream for 30 to 50 exposures of 1800 seconds each for a total of five sequences. This required 3 months elapsed time and on-line arc-jet operation time exceeding the six-year history of the arc-jet laboratory. It became very clear that material testing time and costs had to be reduced at least an order of magnitude. The results of this test program also demonstrated the importance of simulating the gas flow and associated parameters. This will be shown in the following figures.

---

*Howell, R. R.: Test Facilities for Space Shuttle Thermal Protection System. Space Transportation System Technology Symposium, NASA TM X-52876, Vol. III, 1970, pp. 229-238.

SPACE SHUTTLE THERMAL PROTECTION

ENVIRONMENTAL SIMULATION - MODERATE CROSSRANGE

PARAMETER	REQUIREMENT	MAIN BODY OF EXPERIENCE
HEAT TRANSFER RATE	1-100 W/cm^2	100-1000
LOCAL MACH NUMBER	0-10	0-1
BOUNDARY LAYER TYPE	TURBULENT	LAMINAR
EXPOSURE TO ENVIRONMENT	1000 sec/exp	100
NUMBER OF EXPOSURES	100	1
SURFACE RECESSION RATE	10^{-9} m/sec	10^{-5} m/sec
SURFACE MATERIALS	METALS, SILICA CARBON	POLYMERS, CARBON AND SILICA
SAMPLE SIZE	10 cm	1 cm

Figure 1

DEPENDENCE OF MASS LOSS ON TEST ENVIRONMENT OF TD-NiCr

(Figure 2)

In recent years, most of the research directed toward evaluating oxidation resistant alloys has been conducted in a static environment. Alloys tested in this manner tended to gain weight slowly with time. More recently, tests have been conducted on TD-nichrome in arc-jets which more closely simulate space shuttle entry conditions. In this environment, TD-nichrome loses weight steadily with time, an apparent contradiction with the static tests. The mass losses in the flowing environment are dependent upon temperature, pressure, and enthalpy. This figure shows the differences between arc-jet results obtained at Ames and static test results obtained by B. Stein of Langley and demonstrates that the extremely low mass loss rates can be determined with adequate accuracy. A theoretical treatment described in the next slide has satisfactorily explained the observed behavior.

DEPENDENCE OF MASS LOSS ON TEST
ENVIRONMENT OF TD-NiCr
T = 1480° K   CYCLE = 1800 sec

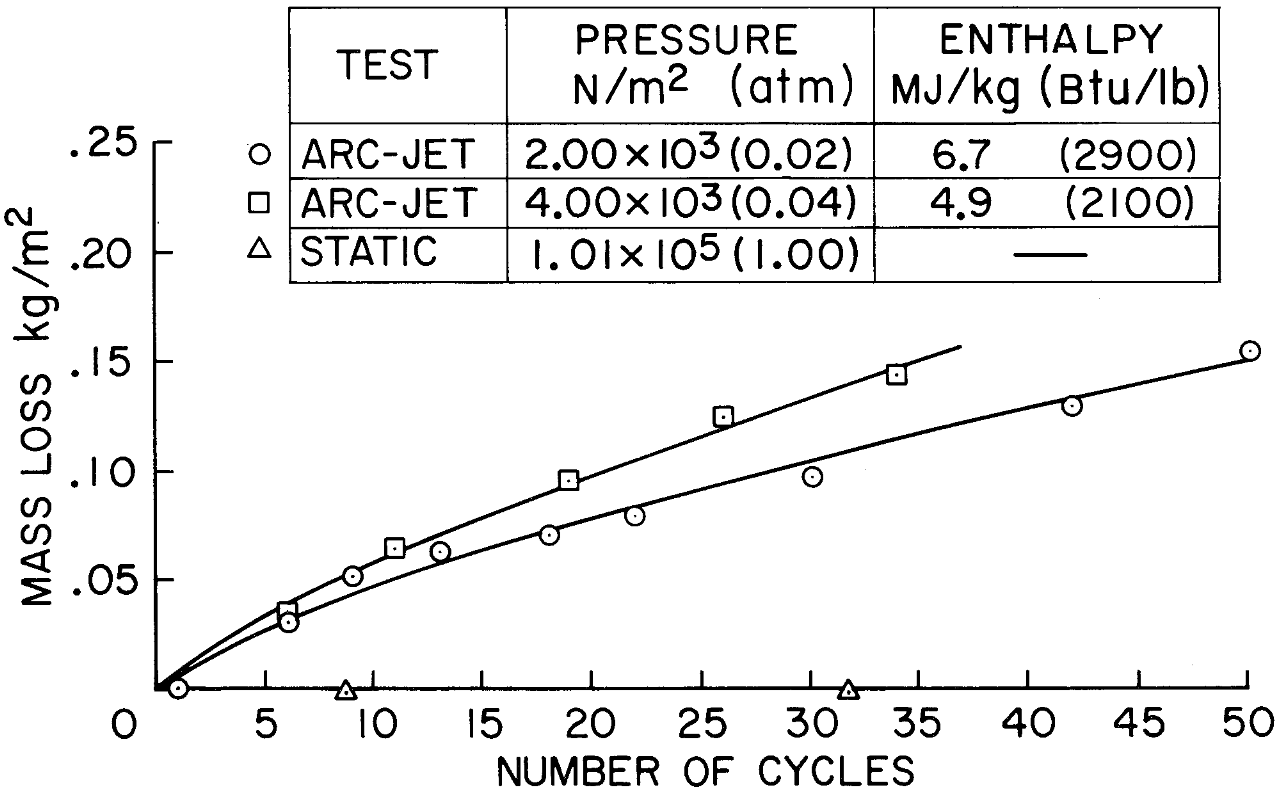

Figure 2

DIMENSIONLESS MASS LOSS RATE FOR TD-NiCr IN HYPERVELOCITY AIR FLOW
(Figure 3)

The weight loss of a metal in a flowing gas environment may result from spallation, sublimation, oxidation, etc. An analysis for TD-NiCr has shown that the measured weight loss in arc heated air can be predicted by an analytical model which accounts for boundary layer diffusion controlled oxidation and sublimation of the chromium oxide scale. A comparison of the dimensionless mass loss rate B'_w (i.e., mass loss rate divided by heat transfer coefficient) predicted by theory with the experimental data is shown in this figure. When the protective scale is removed the TD-NiCr alloy oxidizes and degrades much more rapidly than it would in static air. Therefore, static oxidation test data will indicate longer use life than is likely in flowing environments. An implication of the model for TD-NiCr is that many oxides such as MoO_3, V_2O_5, SiO_2 and Cr_2O_3 may be subject to increased, possibly excessive, volatilization in convective heating environments. This in turn would increase the metal loss and shorten use life. On the basis of these considerations convective heating tests of the candidate metallic heat shield materials are necessary

DIMENSIONLESS MASS LOSS RATE FOR TD-NiCr IN HYPERVELOCITY AIR FLOW

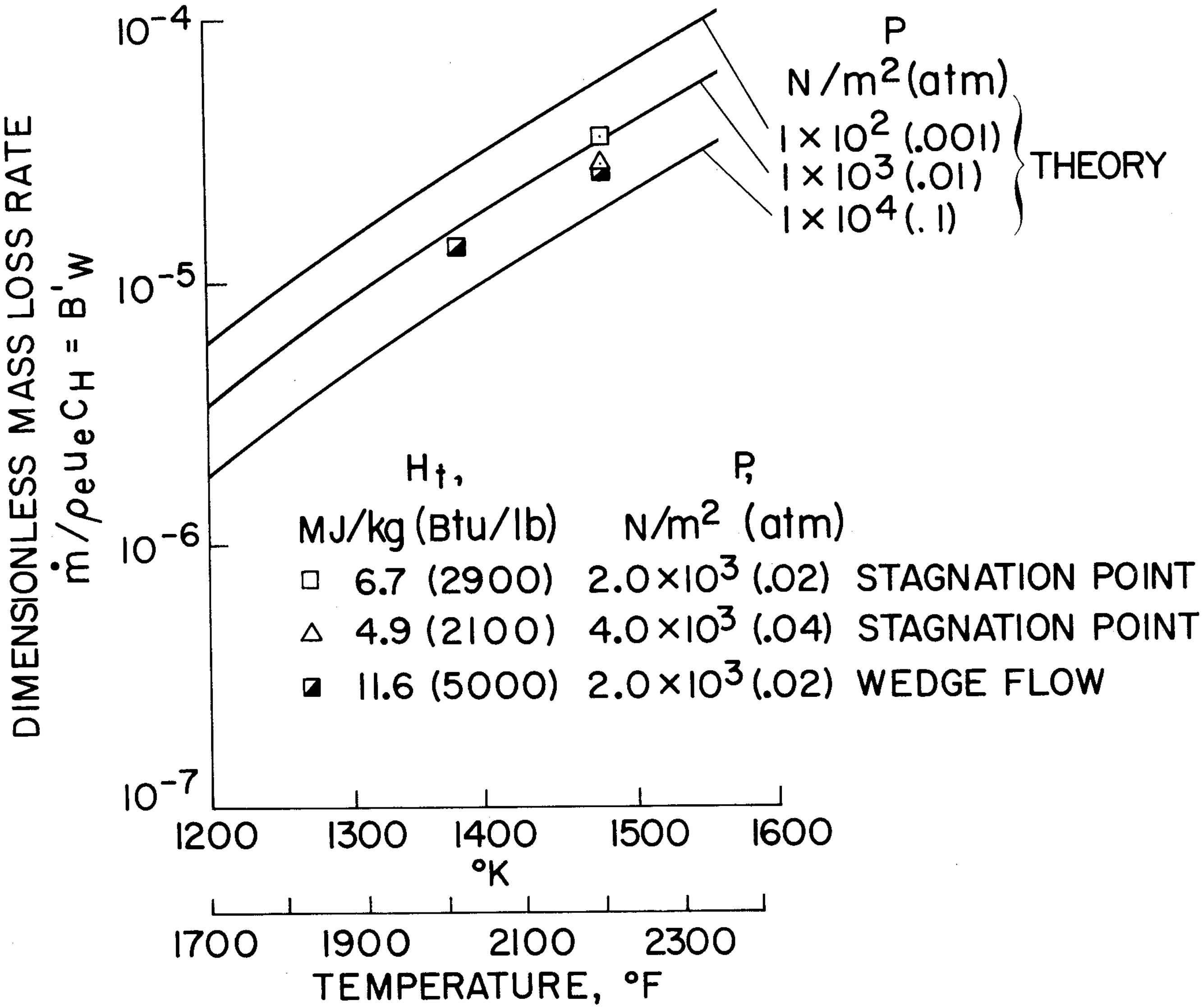

Figure 3

MULTIPLE SAMPLE STAGNATION TEST SUPPORT

(Figure 4)

Most of the early work in arc-jets directed toward evaluating metallic TPS* candidates was done with only one or two samples in the stream. In order to increase the efficiency of these tests a multiple sample support was constructed. This technique enables as many as eight materials to be tested simultaneously. Moreover, since the cold wall heating to each sample is about the same, the equilibrium temperature of each sample will be dependent upon its emissivity. Each sample is backed by Ames' low-density silica insulating material to reduce the rearward flow of heat. Temperatures are monitored with a thermocouple spotwelded to the rear of each specimen and by optical techniques through observation ports. A calorimeter mounted at the center of the support and pressure orifices distributed across the support provide direct measurements of heating rate and pressures during the test.

---

*TPS - thermal protection system.

MULTIPLE SAMPLE STAGNATION SUPPORT

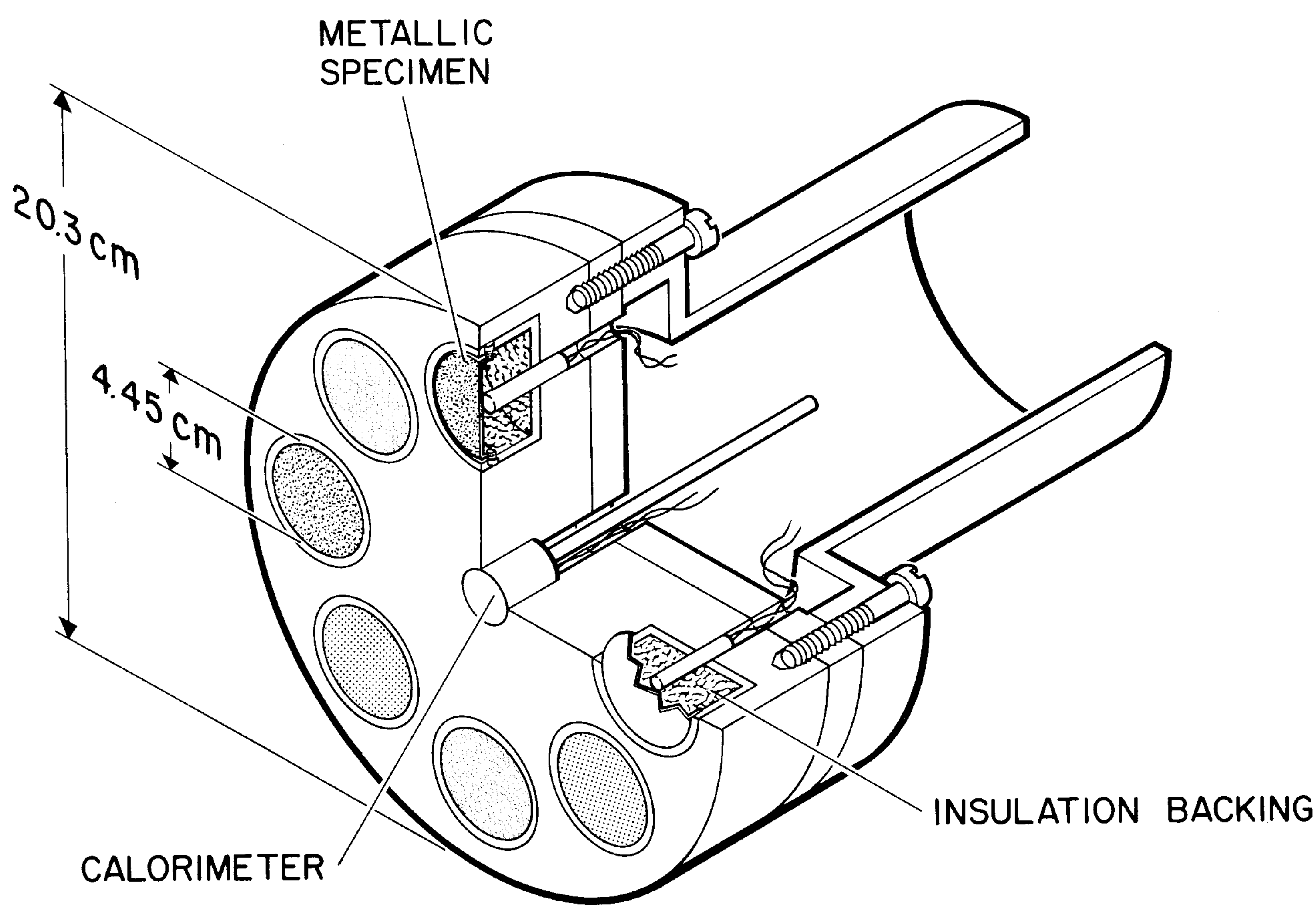

Figure 4

LAMINAR–FLOW ARC–JET TESTS USING MULTIPLE SAMPLE SUPPORT
(Figure 5)

A typical test run in the Ames Aerodynamic Test Facility using a multiple sample support is shown in the accompanying figure. The 20.3cm (8-inch) diameter sample support accommodates 8 samples. The nozzle exit shown is 61cm (24 inches) in diameter. A front surface mirror located at the edge of the nozzle is used for taking radiometric measurements during the run. Surface pressures and enthalpy during the test were maintained at about 9.3×10^2 N/m^2(.009 atm) and 9.3×10^6 J/kg (4000 Btu/lb), respectively. The equilibrium temperatures, which were dependent upon sample surface emissivity, ranged between 1366°K (2000°F) and 1444°K (2140°F). The composition of the materials located in the sample support are described in the next figure.

LAMINAR-FLOW ARC-JET TESTS USING MULTIPLE SAMPLE SUPPORT

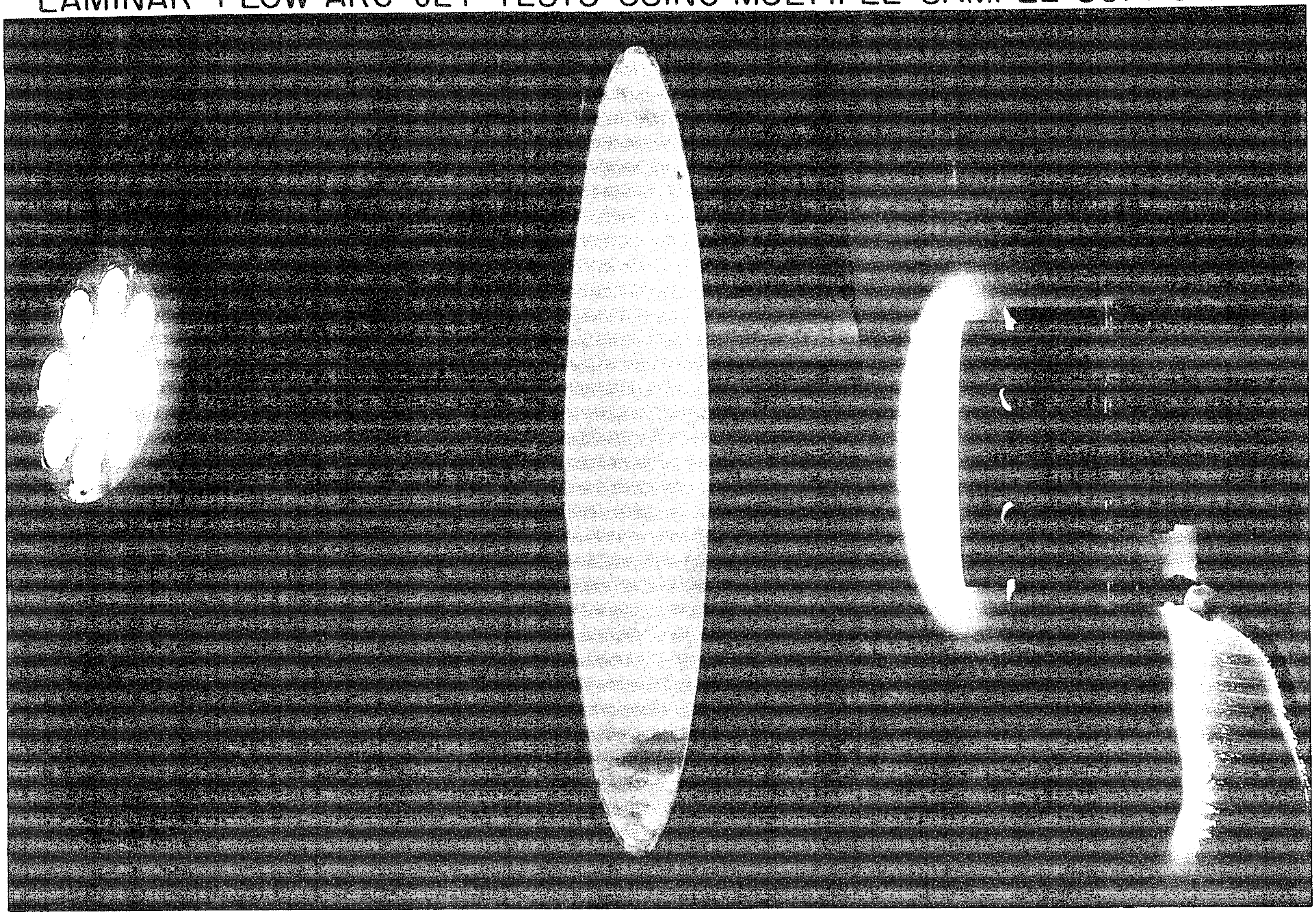

Figure 5

MULTIPLE SAMPLE TEST AFTER 50 CYCLES
(Figure 6)

A photograph of the multiple sample support after 50 test cycles of 1800 seconds duration is shown in this figure. The metallic specimens are identified clockwise starting from the top as follows:

1. TD-Ni-20Cr
2. HS-188
3. DS-Ni-20Cr
4. TD-Ni-16Cr-(x)Al-0.4Y(Proprietary) x >3.5
5. TD-Ni-20Cr-15Fe
6. TD-Ni-16Cr-3.5Al
7. TD-Ni-20Cr-3.5Al
8. TD-Ni

The color variation observed on some of the specimens is probably due to temperature gradients across the sample. The next figure contains a tabulation of the pertinent, preliminary results of these tests.

In this recent test series, eight samples of different alloys were exposed 50 times for periods of 1800 seconds. These tests were completed in less than three weeks and time and costs of exposing samples were reduced essentially an order of magnitude.

The observed differences in surface temperature and therefore in these tests at constant heating rate of similar alloys lead one to question the comparative evaluation of competing materials at equal wall temperatures since it is the aerodynamic heating rate that needs to be accommodated at various locations on the vehicles.

MULTIPLE SAMPLE TEST AFTER 50 CYCLES

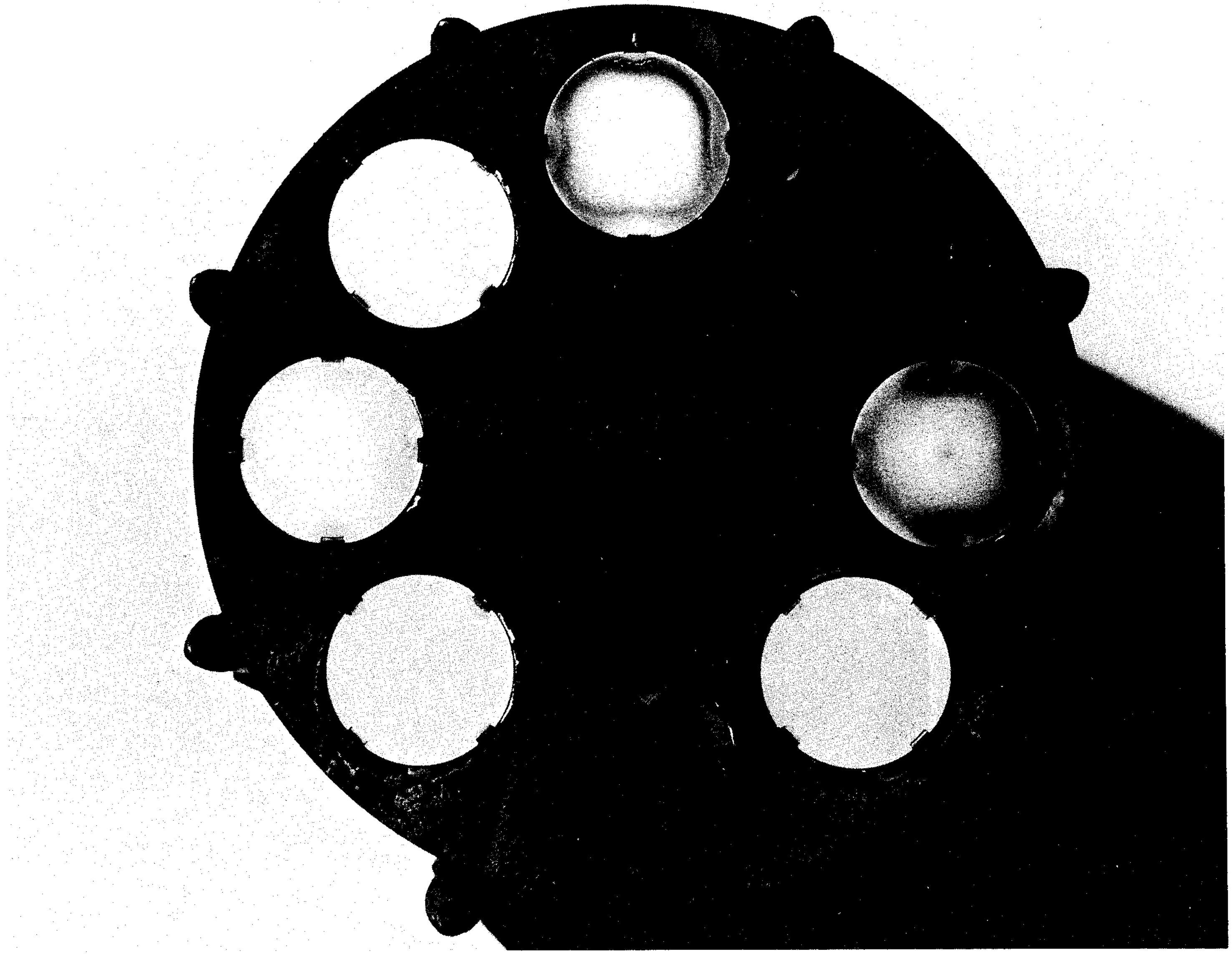

Figure 6

PRELIMINARY RESULTS OF MULTIPLE SAMPLE STAGNATION TESTS
(Figure 7)

Arc-jet tests have been performed on eight alloys of current interest in the space shuttle technology program and were described in the previous figure. The unique feature of these tests is that the samples were simultaneously exposed to the air stream. With this technique, the heating rates and surface pressures for each of the samples were nearly equal. During the first few cycles the temperatures varied considerably from sample to sample and also with time because of varying emissivities. However, as the samples developed stable oxides on their surfaces, the temperatures became essentially constant with time and are shown as nominal temperatures in the accompanying table. The resulting temperature differences between samples are due to varying emissivities. The emissivity difference between the hottest and the coldest sample is estimated to be about 0.2. The total weight changes for each sample are also shown. The samples are currently being sectioned and subjected to metallurgical examination.

PRELIMINARY RESULTS OF MULTIPLE SAMPLE STAGNATION TESTS

$P_w = 933\ N/m^2$ $H_t = 9.3\ MJ/kg$ 50 CYCLES

CYCLE = 1800 sec JANUARY, 1971

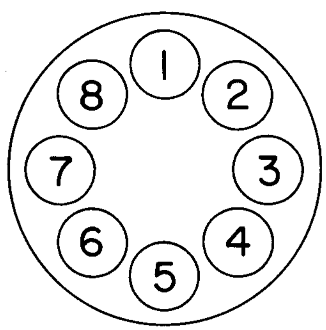

POSITION	MATERIAL	NOMINAL T_w °K (°F)	ΔM, mg
1	TD-Ni-20 Cr	1395 (2050)	− 30
2	HS-188	1365 (2000)	− 108
3	DS-Ni-20 Cr	1405 (2070)	− 50
4	TD-Ni-16 Cr-(X) Al-0.4 Y (PROPRIETARY) x >3.5	1365 (2000)	+ 10
5	TD-Ni-20 Cr-15 Fe	1400 (2060)	− 30
6	TD-Ni-16 Cr-3.5 Al	1400 (2060)	+ 3
7	TD-Ni-20 Cr 3.5 Al	1445 (2140)	− 45
8	TD-Ni	1430 (2110)	+121

Figure 7

AMES CONTRACT TEST PROGRAM FOR THERMAL SCREENING OF CANDIDATE SSV MATERIALS (Figure 8)

The first phase of procurement is now being negotiated. Approximately 667 hours of arc-jet tests will be conducted on materials in order to select those worthy of additional study and development. Six samples will be arranged on the front of two 11.4cm (4-1/2inch) diameter flat faced models which will be sequentially cycled in the test stream. In order to avoid some of the problems encountered at Ames and other test facilities with welded thermocouple joints the sample backface temperature will be measured with a high temperature spring-loaded Platinel thermocouple which will be an integral part of the test module and hence will provide a common basis for comparison of all test materials. Automatic scanning of the front face temperature will be provided since the temperature of the various samples will differ in the same environment due to differences in emissivity discussed previously. In addition, the temperature of the back-up insulation will be monitored at three in-depth positions. The environmental test philosophy is to duplicate the flight enthalpy, hot-wall heating rate, and heat transfer coefficient by testing at pressures lower than those expected on the full-scale vehicle. The various classes of materials will be tested over the following range of temperatures:

Metallics	1255 - 1477°K (1800 - 2200°F)
Surface Insulators	1477 - 1811°K (2200 - 2800°F)
Ablators	1477 - 1922°K (2200 - 3000°F)

AMES CONTRACT TEST PROGRAM FOR THERMAL SCREENING OF CANDIDATE SSV TPS MATERIALS

- PROVIDE LOW COST SCREENING TESTS OF
  1. METALLICS — LEWIS, MSFC
  2. SURFACE INSULATORS — MSC
  3. ABLATORS — LANGLEY

- TO DETERMINE:
  1. OXIDATIVE BEHAVIOR AS A FUNCTION OF TEMPERATURE IN A LAMINAR BOUNDARY LAYER
  2. INFLUENCE OF NUMBER OF CYCLES (30, 45, 90) AND CYCLE DURATION (30, 20, 10 min)
  3. EFFECT OF HEAT TRANSFER COEFFICIENT
  4. EMISSIVITY

- CONTRACTOR TASKS:
  1. DESIGN AND FABRICATE MODELS (MULTIPLE SAMPLES)
  2. PROVIDE CALIBRATED ARC-HEATED AIR STREAM
  3. CONDUCT TESTS AND MAKE APPROPRIATE MEASUREMENTS
  4. PROVIDE AMES WITH TESTED SAMPLES FOR ANALYSIS

Figure 8

REQUIREMENTS FOR TURBULENT FLOW SIMULATION
(Figure 9)

The requirements for turbulent flow simulation is, of course, related to the assessment of boundary-layer transition Reynolds number predictions. These predictions are uncertain and the most conservative criteria result in a prediction of supersonic turbulent flow on shuttle vehicles. The reason turbulent flow simulation is important is related to the higher pressures, shears, acoustic loads, and heat transfer coefficients of the turbulent flow at a given heat transfer rate as well as to the fundamental difference in interaction heating of flows over imperfect surfaces. By this, we mean panel joints, corrugations, thermal distortions, protuberances, etc.

Since the turbulent boundary layer is so thick due to large shuttle dimensions, one would anticipate the small dimensions shown in this figure to be of little concern. This figure shows a current panel joint design and its characteristic dimensions. A comparison of these dimensions should be made with the laminar sub-layer thickness calculations on the following figure.

RECENT COLUMBIUM TPS PANEL
JOINT DESIGN

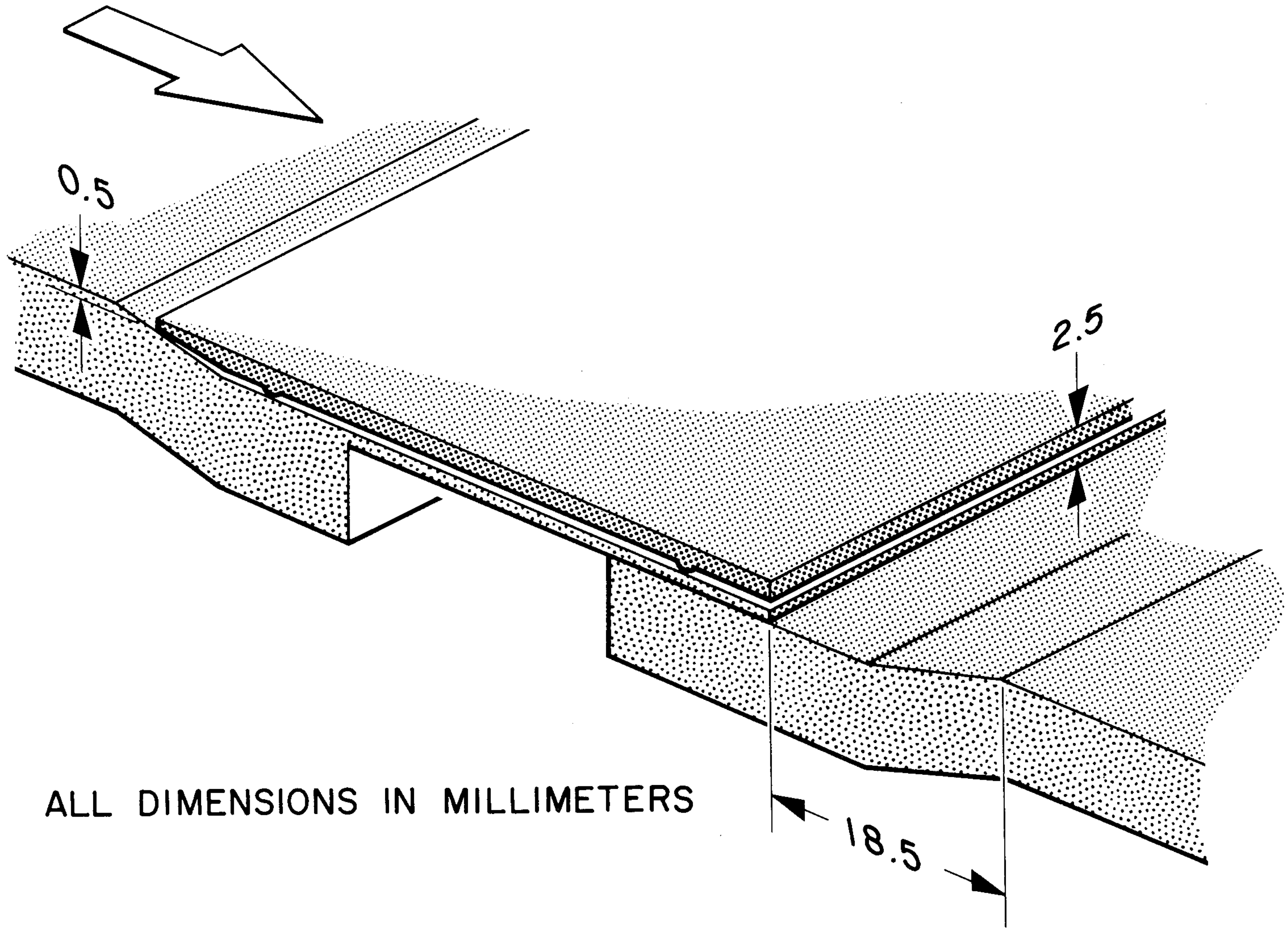

ALL DIMENSIONS IN MILLIMETERS

Figure 9

VARIATION OF CALCULATED LAMINAR SUB-LAYER THICKNESS WITH MACH NUMBER FOR TURBULENT FLOW
(Figure 10)

In order to assess the importance of the requirement of providing a turbulent-boundary-layer test flow, calculations were made of the laminar sub-layer thickness for a particular vehicle and trajectory. Although the results will be affected to a degree by the local edge conditions and hence trajectory details and configuration, it is believed that the calculations are representative of most shuttle entry modes. The figure shows that the sub-layer thicknesses are relatively small even though the boundary layer has had a relatively long run of 46 meters (150 feet). Accordingly, it can be concluded that considerable portions of the SSV* surface will be "effectively rough" because irregularities will exceed sub-layer thicknesses. Testing in turbulent ducts is needed, therefore, to determine the convective heating levels over both smooth and rough surfaces and at points of gross surface irregularity such as panel joints and protuberances. Present analytical techniques for predicting heat transfer in such situations are subject to great uncertainty. Furthermore, experiments are required to assess the influence of such non-uniformities in the geometry on TPS panel performance.

---

*SSV - space shuttle vehicle.

VARIATION OF CALCULATED LAMINAR SUB-LAYER THICKNESS WITH MACH NUMBER FOR TURBULENT FLOW

HIGH CROSS RANGE x = 45.7 m

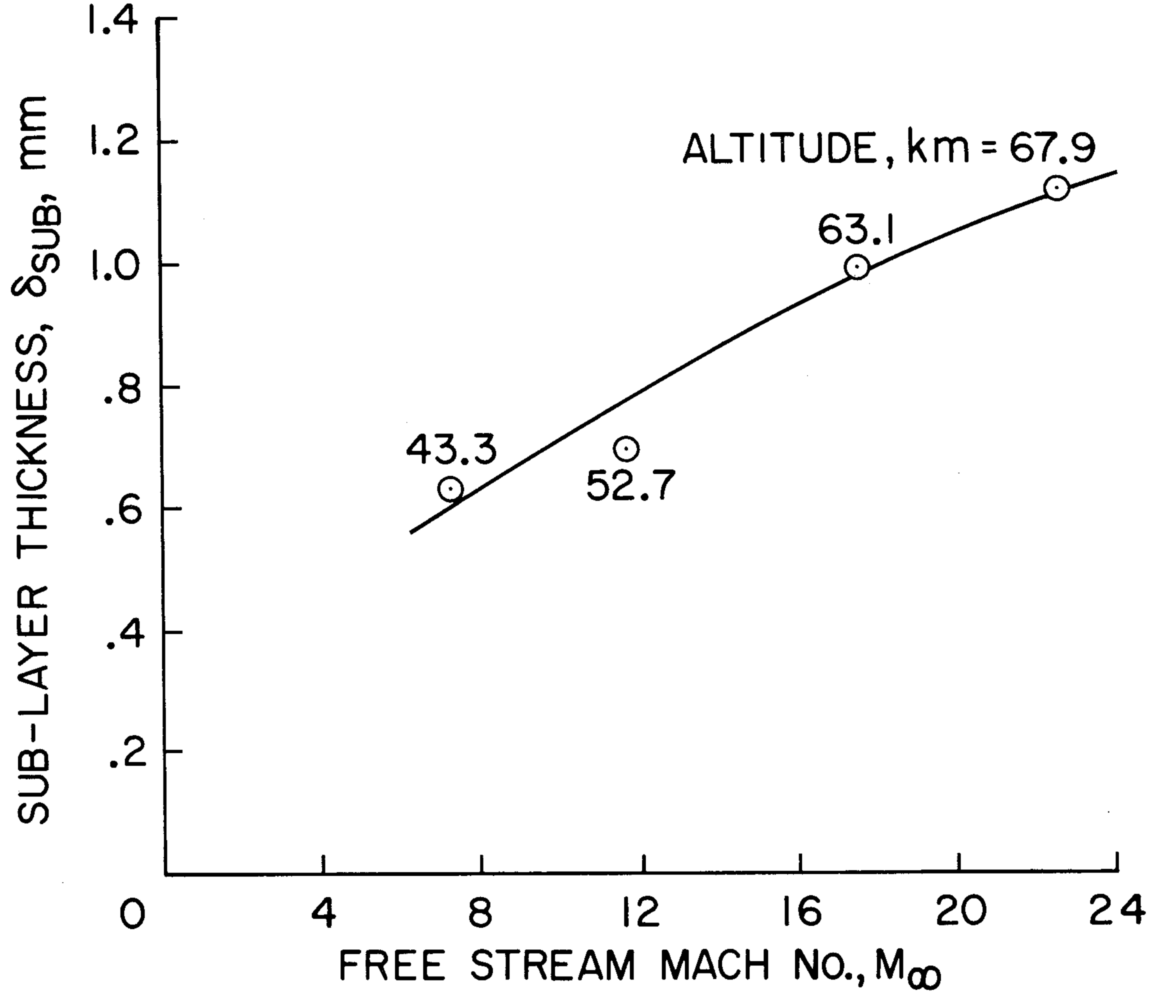

Figure 10

THE AMES RECTANGULAR TURBULENT-FLOW APPARATUS
(Figure 11)

In order to provide the continuous flow of turbulent, supersonic, high-temperature gas required for the thermal evaluation of relatively large flat test specimens of candidate TPS materials for the space shuttle, a water cooled nozzle-test section (Mach number 3.3) has been coupled to the Linde N-4000 arc heater. Operation at the highest possible local Reynolds numbers requires that the facility be run at high mass flow rates which, in turn, results in low total enthalpies. Two modes of heater operation were utilized to expand the range of attainable Reynolds numbers: In the first, all of the test gas flows through the arc; while in the second, dilutant gas (.38 of total) was added downstream of the arc to get higher mass flow rates. The range in pertinent facility operational parameters is as follows:

Total Pressure	$3.4 \times 10^5 - 43 \times 10^5 N/m^2$ (3.3 - 42atm)
Enthalpy	$1.2 \times 10^6 - 7 \times 10^6 J/kg$ (500 - 3000 Btu/lb)
Unit Reynolds Number	$25.6 \times 10^4 - 13.4 \times 10^6$ per m ($7.8 \times 10^4 - 4.1 \times 10^6$ per ft)
Total Power Input	$.4 \times 10^6 - 2.7 \times 10^6$ W
Mass Flow Rate	.068 - 1.36 kg/sec (.15 - 3.0 lb/sec)

A 10.2cm x 15.2cm (4 in. x 6 in.) cutout is provided in the lower tunnel wall to accommodate either the desired test specimens or a water-cooled calibration plate. Instrumentation mounted on the upper wall includes convective heat transfer gages, pressure orifices, and a total radiation pyrometer for measurement of test-sample surface-temperature history.

RECTANGULAR TURBULENT-FLOW APPARATUS

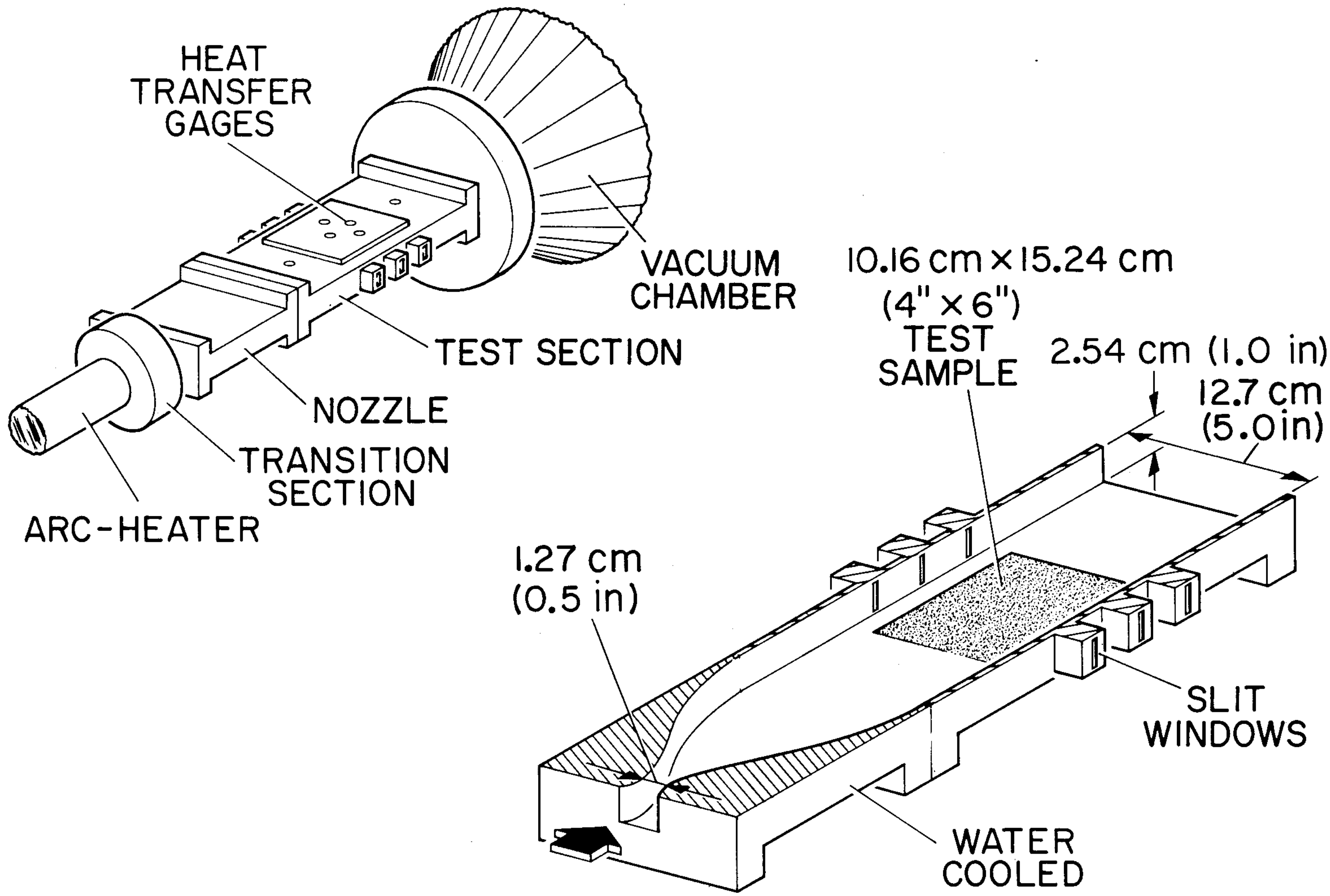

Figure 11

COMPARISON OF RECTANGULAR DUCT CONVECTIVE HEATING MEASUREMENTS WITH THEORY

(Figure 12)

The most direct method of assessing the nature of the boundary-layer flow is to compare the level and trend of the measured cold-wall heating rates with appropriate theory. The data which were measured with rapid response, water-cooled Gardon type gages represent the average obtained at the test section location. The laminar and turbulent predictions were performed as a function of enthalpy using the flat-plate theory of Dorrance for a wall to edge temperature ratio of 0.1. The data are divided with respect to total enthalpy. The agreement of the theory with the data at both levels of enthalpy satisfactorily demonstrates the existence of turbulent flow over the full range of pressure.

COMPARISON OF 1" × 5" DUCT HEAT TRANSFER DATA WITH THEORY

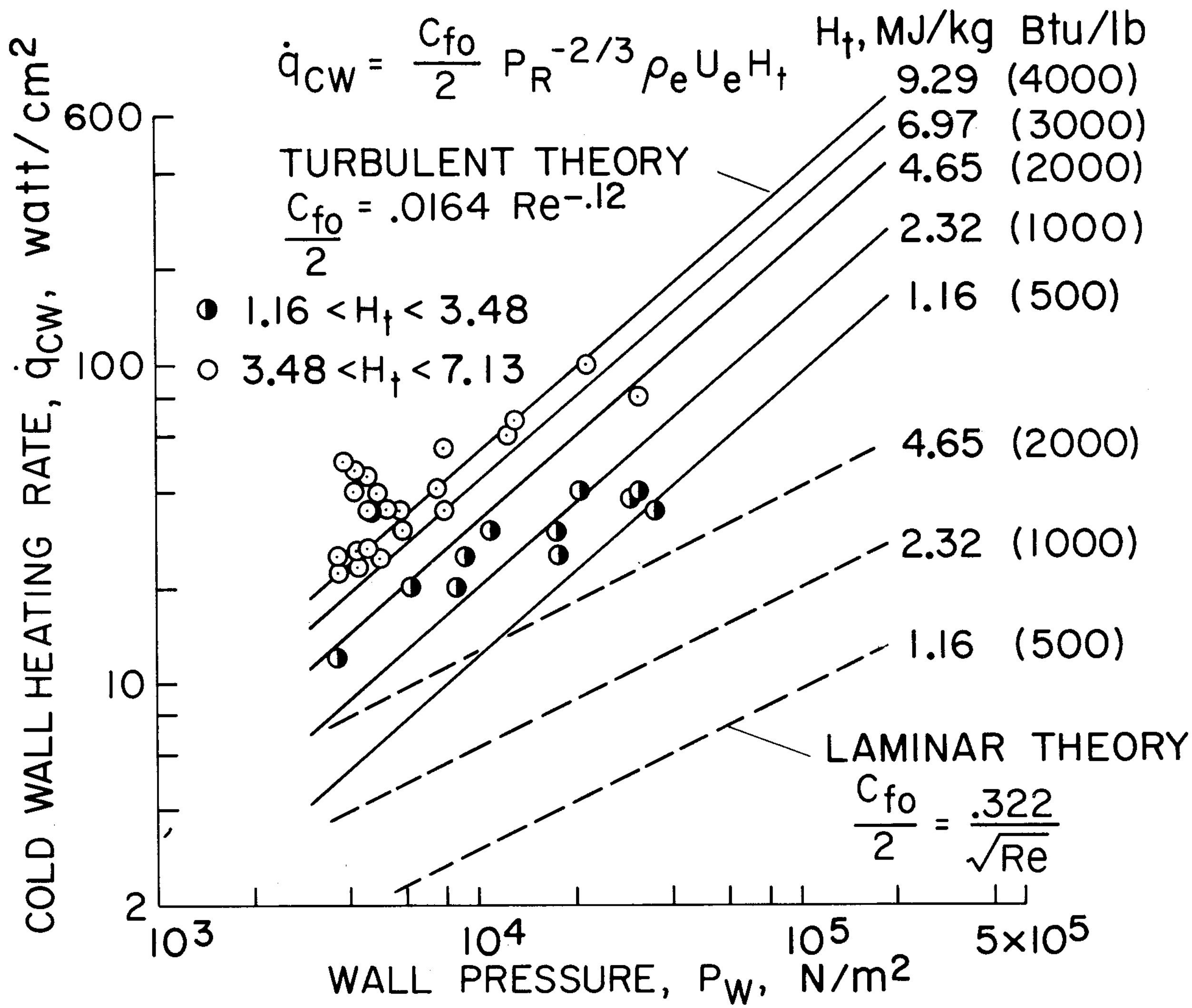

Figure 12

INFLUENCE OF STREAM TOTAL ENTHALPY ON HOT-WALL HEATING RATE AND WALL TEMPERATURE

(Figure 13)

One of the major consequences--in terms of facility simulation requirements--of testing at the low enthalpies associated with high Reynolds number flows is the reduction in the cold-wall heat transfer. The wall enthalpy at surface temperatures of interest for the shuttle TPS systems approaches the magnitude of the boundary-layer-edge value with the attendant effect on the resultant hot-wall heating. This effect was calculated for an assumed emissivity of .8 and a specific heat of .26 appropriate for air using an iterative program.

INFLUENCE OF TEST STREAM ENTHALPY ON HOT WALL HEATING RATE AND EQUILIBRIUM WALL TEMPERATURE

$$\dot{q}_{HW} = \dot{q}_{CW}\,\frac{(H_t - H_w)}{H_t} = \epsilon\sigma T_w^4 \qquad \epsilon = 0.8$$

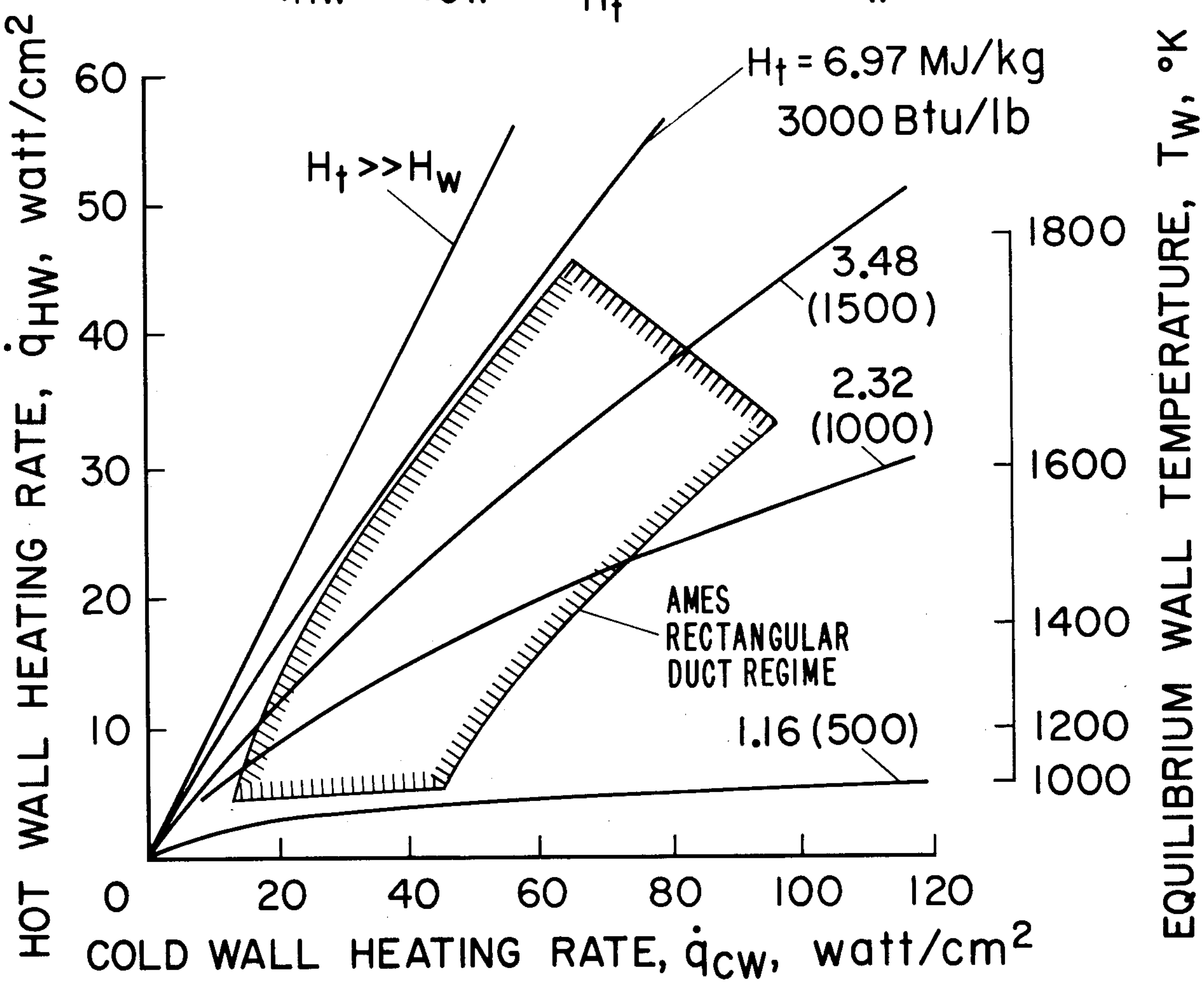

Figure 13

COMPARISON OF AMES TEST FACILITY HEATING PARAMETERS WITH EXPECTED SHUTTLE ENVIRONMENTS
(Figure 14)

The most important TPS simulation parameters for studying the surface thermochemical phenomena for the space shuttle vehicle are the hot wall heating rate, enthalpy level and the associated wall temperature. The range of laboratory conditions provided by the existing Ames laminar and turbulent flow facilities are shown to bracket the conditions calculated by H. Christensen of McDonnell Douglas for the lower fuselage surface of both the high and low cross range vehicle. Since the attitude of the vehicles will be continually modulated during entry the level of heat transfer will be within 85 percent of the values shown for the majority of the entry heating pulse (600 to 1300 seconds for the low and high cross range, respectively). In terms of laboratory simulation this means that step heat pulse tests will be adequate for the majority of material-evaluation tests. The higher enthalpies attainable in the laminar-flow facility account for the closer matching of the flight heat transfer coefficients. However, in either case, the laboratory tests at lower enthalpies may be considered to be conservative with respect to both heat transfer coefficient as well as nonequilibrium flow surface catalytic effects which become important at high enthalpies and low pressure. The latter may have an important bearing on trying to extrapolate very high enthalpy laboratory results to flight since it has been observed in tests of coated carbon-carbon composites at both McDonnell Douglas and MSC that at the same free-stream condition, the coating appears to act as a non-catalytic surface blocking recombination of the disassociated species at the wall with an attendant lower heat transfer and surface temperature.

COMPARISON OF AMES TEST FACILITY HEATING PARAMETERS WITH EXPECTED SHUTTLE ENVIRONMENTS

PARAMETER	TEST: LAMINAR STAG. POINT	TEST: TURBULENT DUCT	FLIGHT: LOW CR 325 km	FLIGHT: HIGH CR 3700 km
1. HOT WALL HEATING RATE $\dot{q}_{HW}$, W/cm^2	10-22	4.5-41	6-24	10-33
2. TOTAL ENTHALPY H_t, MJ/kg	4.64-11.6	1.62-9.06	11.6-26.7	11.6-25.5
3. WALL TEMPERATURE T_W, °K ($\epsilon = .8$)	1250-1475	975-1775	1080-1500	1260-1650
4. HEAT TRANSFER COEFFICIENT C_H, kg/m^2sec	$9.3\text{-}38.5 \times 10^{-3}$	$30\text{-}300 \times 10^{-3}$	$1.9\text{-}23 \times 10^{-3}$	$3.9\text{-}33.6 \times 10^{-3}$
5. WALL PRESSURE P_W, N/m^2	$1\text{-}4 \times 10^3$	$3.7\text{-}30 \times 10^3$	$.6\text{-}2.7 \times 10^3$	$.14\text{-}.28 \times 10^3$

Figure 14

RELATIVE ABLATIVE AND THERMAL PERFORMANCE OF TPS MATERIALS IN TURBULENT FLOW (Figure 15)

TPS material response data as a function of test exposure time was generated for a variety of ablators in the flow furnished by the rectangular duct facility. The purpose of the tests was to determine the degree of stream uniformity and to characterize the relative thermal performance of materials in a supersonic turbulent environment. The majority of the tests were devoted to obtaining data on a possible refurbishable heat shield concept--a PBI matrix impregnated with a gasifying polymer which, in principle, could be replenished after each flight or as required. The results, which were obtained with three impregnants (polyethylene, polymethylmethacralate, and polystyrene) showed no noticeable trend with type of impregnant and, as expected, an increase in mass loss rate above the unimpregnated matrix--about two to one. The additional mass--in the form of boundary-layer vapors--did not, however, appreciably alter the insulative performance as measured by the backface temperature rise of the various samples. This can be explained by the relatively poor efficiency of the boundary-layer blockage mechanism in turbulent flows at low enthalpies coupled with the high thermal conductivity of the PBI matrix. For reference purposes, some tests were also conducted at the same stream conditions on the Apollo heat shield material (AVCOAT 5026-39). The experimental degradation and temperature data were found to be in substantial agreement with the theoretical calculations of Matting.

RELATIVE ABLATIVE AND THERMAL PERFORMANCE OF TPS MATERIALS IN TURBULENT FLOW

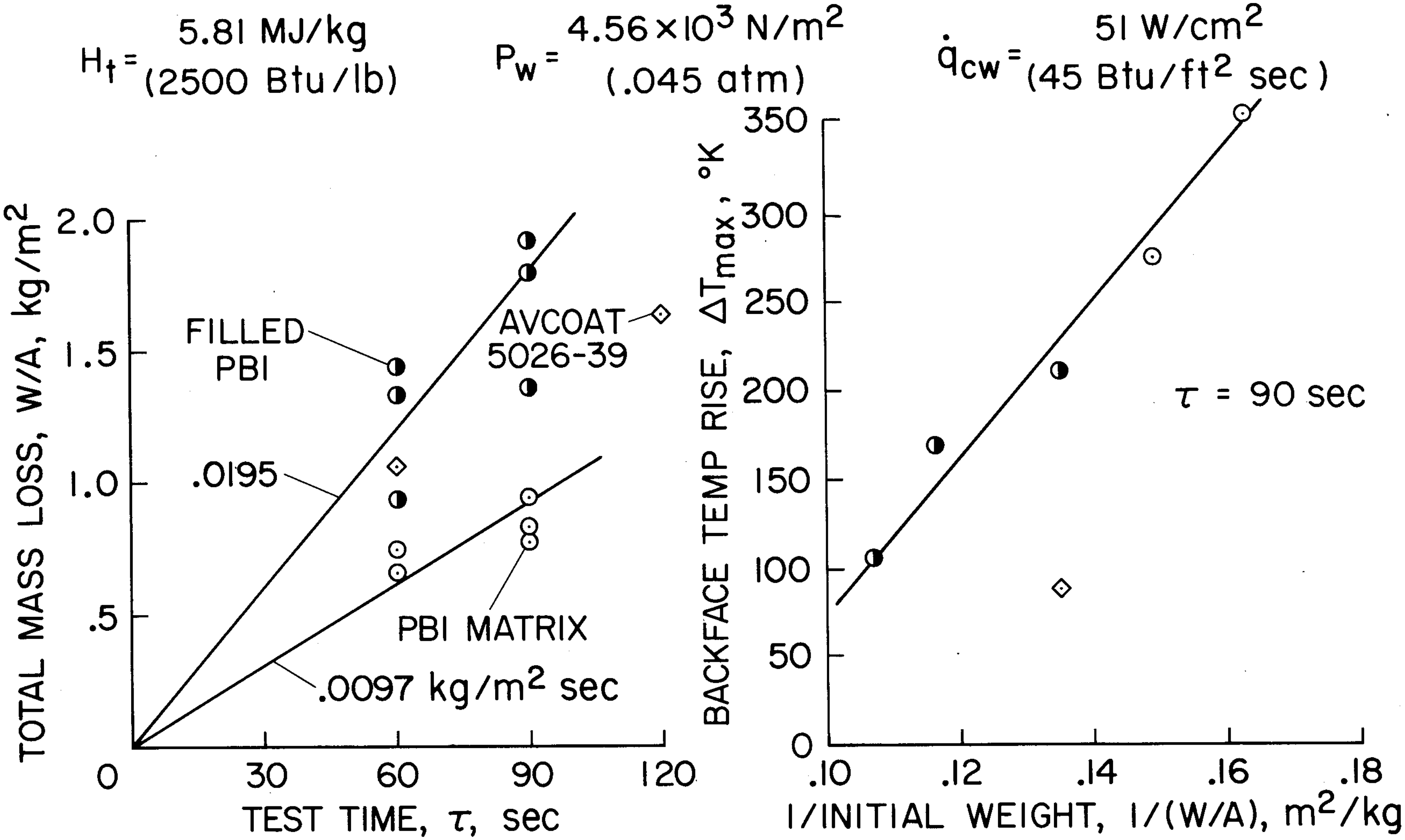

Figure 15

CONCLUSIONS

This paper has discussed the environmental simulation testing and evaluation of shuttle thermal protection materials and systems at the Ames Research Center. The conclusions reached as a result of this effort are listed below:

1. An order of magnitude reduction in time and costs compared to past experience was deemed necessary for this program. Most of this has been accomplished and additional reductions are in order.

2. Experimental data coupled with theoretical analysis have shown that appropriate flow simulation is necessary for evaluation of nickel-chromium alloys and extrapolation to flight conditions. This is expected to apply to other alloys also.

3. Simultaneous testing of eight different material samples at the same heating rate has disclosed a wide variation in surface temperature due to surface emissivities differing by as much as 0.2. This must be taken into consideration in the planning of tests, interpretation of data and application of the results to vehicle design.

4. A contract test program has been initiated for material screening and evaluation. The format of this program is based on our experiences regarding the need to reduce the time and cost of such tests and reflects the hoped for reductions.

5. The necessity for supersonic turbulent-boundary-layer simulation has been discussed; the

Ames small arc-heated duct and its performance have been described as well as some early data obtained in that facility. Based on the results of the small duct, a larger, by a factor of two, arc-heated turbulent-flow duct is under construction and will be operational in several months. It is in these facilities that larger size sample tests and interaction heating investigations will be performed.

COMMENTS ON THE NASA DESIGN CRITERIA DOCUMENT

By I. G. Hedrick
Grumman Aerospace Corporation
Bethpage, New York

PAPER 11

INTRODUCTION

(Slide 1)

Reference 1, which is the subject of these comments, is the result of work conducted by a combined industry/NASA/Air Force committee. The purpose of this design criteria document is to present general and mission-oriented structural criteria for the Space Shuttle. Thus, at the appropriate time, the document will provide information useful in drawing up contractual documents for Phases C and D of the Shuttle program.

In view of the many new and challenging problems associated with the Shuttle structure, the objectives of reference 1 are certainly valid and worthwhile. Those objectives are partially satisfied within the document, but considerable work remains to be done in some areas. In particular, four issues needing further investigation are discussed in the present paper.

INTRODUCTION

- UTILIZING PROBABILISTIC METHODS TO DETERMINE LIMIT LOADS & FACTORS OF SAFETY
- INFLUENCE OF FLAW GROWTH & FRACTURE MECHANICS CONSIDERATIONS ON SELECTING FACTORS OF SAFETY
- FAIL-SAFE/SAFE-LIFE DILEMMA
- THE POGO PROBLEM

Slide 1

PROBABILISTIC METHODS

(Slide 2)

A fundamental issue in all structural criteria is the definition of how limit loads are determined and what factors of safety are used with them. Reference 1 recognizes a growing interest in probabilistic methods for this purpose and emphasizes their possible use. Here are a few comments with respect to their application.

The determination of loads for the Shuttle depends, in large part, upon quantities that could be defined statistically - winds, gusts, turbulence, and variations in engine and control system performance, to name a few. Hence, statistical methods may be employed to describe the resulting variations in the loads to arrive at appropriate non-exceedence values for limit loads. Multiplying these by specified factors of safety results in design ultimate loads.

The problem in determining limit loads statistically is that many critical loads - for example, those encountered during ascent - are strongly influenced by variabilities in such items as engine and control system characteristics. Frequently, these variations are difficult to obtain until late in the design phase, and perhaps not until much of the flight test program is complete.

The next and more challenging step in the use of probabilistic methods centers about the fact that the strength of major structure is also statistical in nature and that it depends upon many factors: material property scatter, dimensional tolerances, variations in manufacturing and assembly procedures, and so forth.

Hypothetically, if both the applied load and strength distributions were completely known, they could be plotted as relative frequency of occurrence functions as shown in Slide 2. The separation of these two distributions would then determine probability of failure and, hence, the reliability.

APPLIED LOAD AND STRENGTH PROBABILITY DENSITY FUNCTIONS

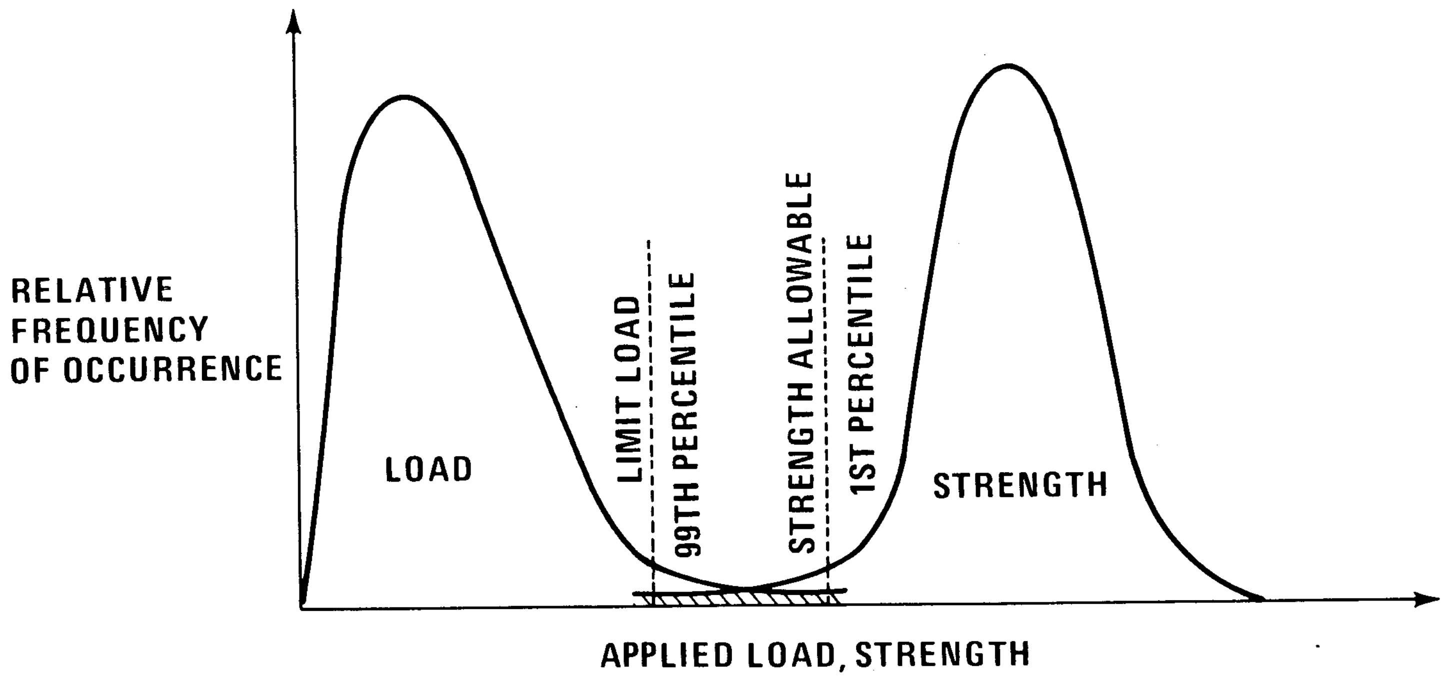

Slide 2

PROBABILISTIC METHODS – Concluded

(Slide 3)

Proponents of the probabilistic approach have adapted these notions to create generalized safety factor curves. For example, as shown in Slide 3 for a specified reliability, the result is a curve showing required factor of safety versus structural strength variation.

In theory, this approach is very appealing. The goal is now a specified structural reliability. In achieving this goal, scatter in structural strength, which of course exists, is accounted for in a logical manner. The corresponding factor of safety is introduced so that designers may use conventional procedures in carrying out their work of designing structure.

The essential shortcoming of this approach is that, to employ it, one needs an accurate picture of the variation of both the loading and strength of the structure being designed. In particular, the shape of the lower end of the strength scatter curve shown on the preceding slide is crucial. This kind of information can only be obtained accurately by large numbers of tests of nominally identical structural components. Unfortunately, there seems to be very little data of this nature available in the literature from past structural programs. Some data exist for 1940-vintage wings and tail surfaces, and a small amount of data is available on F-111 and on some foreign aircraft; however, these data are not nearly enough to perform a good statistical analysis. Even if there were extensive data on past aircraft, their applicability to modern advanced designs like the Shuttle would be extremely tenuous.

When statistical data already exist or will become available early in the design phase, use them. When they don't exist, however, the economics of obtaining them should be thoroughly assessed.

FACTOR OF SAFETY REQUIREMENTS

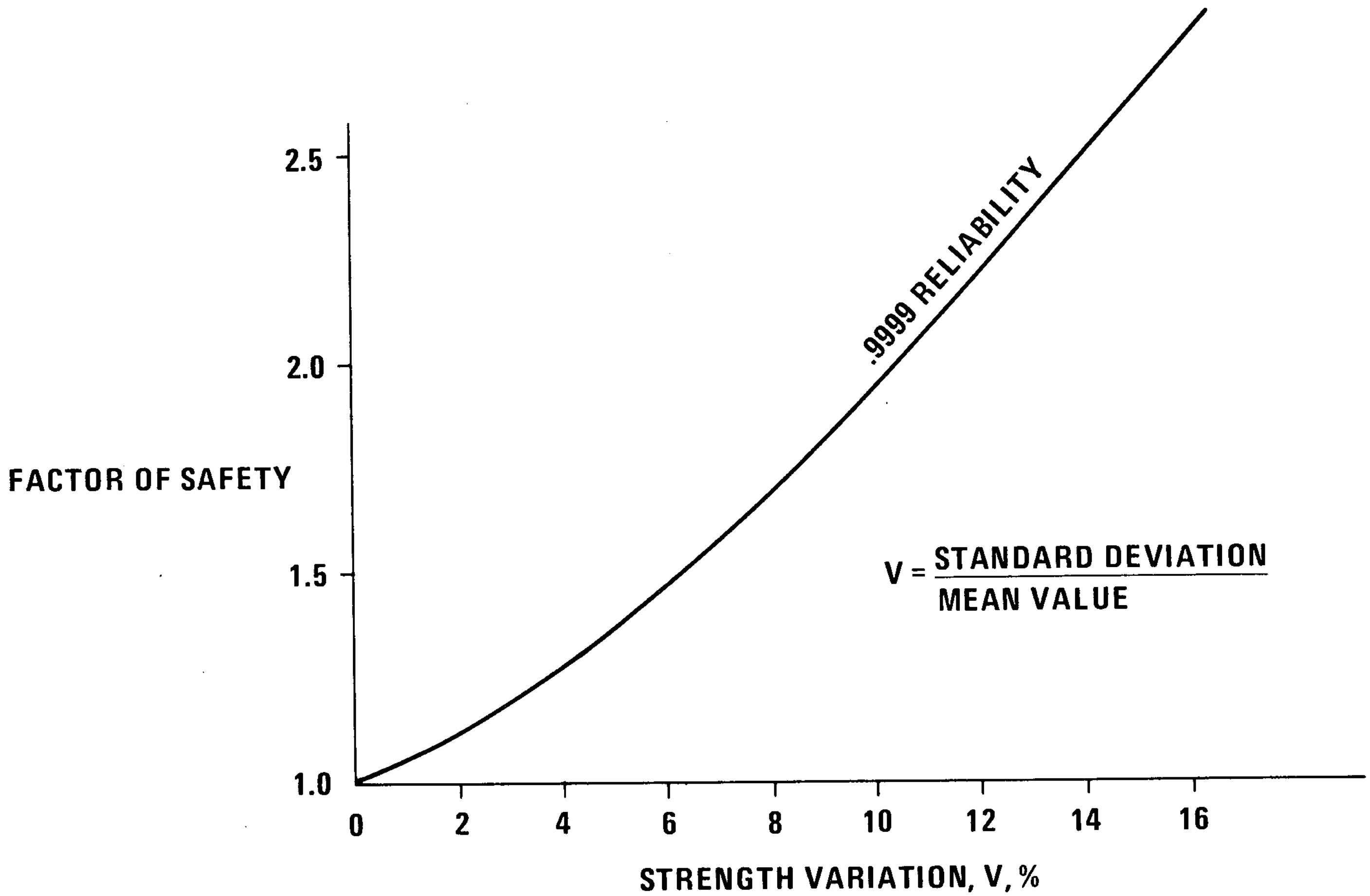

Slide 3

FLAW GROWTH CONSIDERATIONS

(Slide 4)

The next issue is fracture mechanics and the manner in which safety factors for main-propellant tankage are treated in reference 1. It appears that the proposed criteria fall short of defining an approach suitable for current tank design and weight estimates.

Reference 1 proposes three relevant criteria which are summarized in Slide 4.

Neither the safety factor of 1.4 nor a safety factor consistent with the use of a single proof test as a flaw screening device appears practical for tank design.

NASA DOCUMENT CRITERIA FOR TANK DESIGN

- RECOMMENDS A SAFETY FACTOR OF 1.4 AS STARTING POINT FOR THE DESIGN
- STATES THAT ". . . FOR METALLIC PRESSURE VESSELS NOT CARRYING VEHICLE LOADS, FLAW GROWTH SHALL BE ACCOUNTED FOR BY THE PRACTICES SET FORTH IN NASA SP-8040."
- "THE SAFE LIFE SHALL BE DETERMINED BY ANALYSIS AND TEST TO BE AT LEAST FOUR TIMES THE SPECIFIED SERVICE LIFE."

Slide 4

FLAW GROWTH CONSIDERATIONS - Continued

(Slide 5)

As an example, consider an orbiter configuration of current interest shown in Slide 5. This vehicle has a single oxygen tank located forward and two separate hydrogen tanks located aft. It is an example of orbiter configurations that have been studied at Grumman.

TYPICAL ORBITER CONFIGURATION

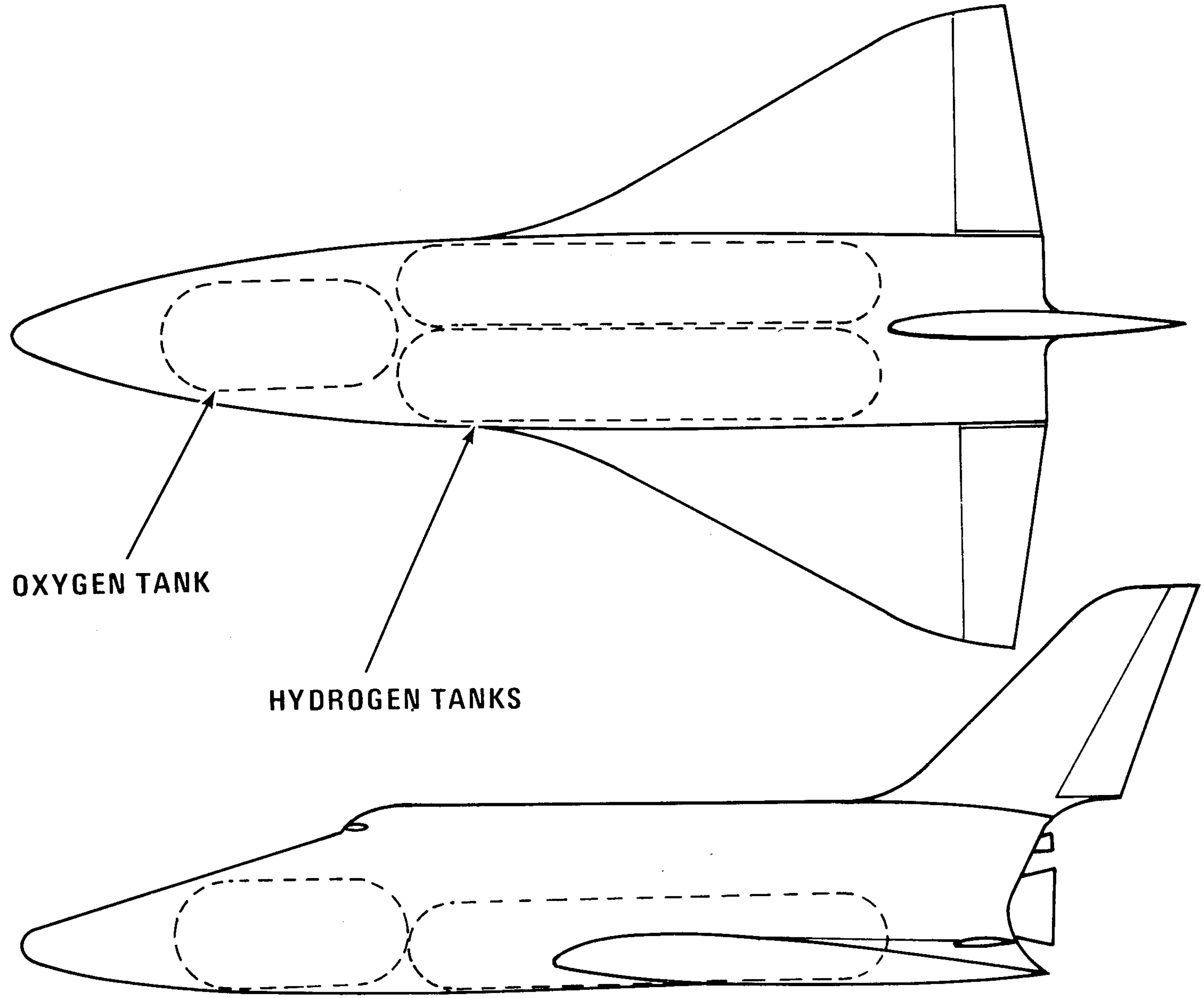

Slide 5

FLOW GROWTH CONSIDERATIONS – Concluded

(Slide 6)

Slide 6 gives the allowable limit stresses in the hoop direction for the orbiter tanks, using a safety factor of 1.4, or 1.75, or a safety factor based on the successful completion of a single proof test at liquid hydrogen temperature. Proof testing, although not necessarily at cryogenic temperature, is a requirement of NASA SP-8040 (ref. 2).

The tank material chosen here is 2219-T87 aluminum. The circular symbols show the allowable limit hoop stresses based on the successful completion of a single proof test at liquid hydrogen temperatures that would guarantee a life of 400 missions. The operating temperature of 89° K (-300° F) relates to the oxygen tank, while the temperatures of 111° K (-260° F) and 20° K (-423° F) correspond to two different hydrogen-tank insulation schemes, namely internal and external insulation.

Proof testing has been assumed at the coldest temperature (20° K (-423° F)) for each kind of tank. This may or may not be practical, but is used here for illustrative purposes. Suitable cyclic loadings have been used for each mission assuming the presence of an elongated surface flaw.

The results are in conflict and the difficulties are twofold, namely:

- For a tank with a factor of safety as low as 1.4, it does not appear possible by a single proof test to demonstrate that flaws will not propagate to disastrous dimensions during the life of the orbiter. Admittedly, though, it has not yet been possible to evaluate the effects of beneficial residual stresses that may be introduced at the flaw tips as a result of the proof test. These residual stresses may retard flaw growth to a very significant extent for a relatively short-lived vehicle such as the orbiter.

- To justify a safety factor as low as 1.4 requires that very small flaws be detected. Relying on non-destructive inspection techniques to do this leaves me with a rather uncomfortable feeling.

In view of these considerations, it can be concluded that:

- Some reasonable safety factor for design which represents an overall best judgment of the allowable stresses which might ultimately be established should be selected. Grumman and Boeing have considered a safety factor for tanks of 1.75 to be a "best guess" for current design. A safety factor of 1.4 looks low.

- A test program will be needed to establish limit stresses suitable for the Shuttle tanks. Pre-cracked specimens should be tested in the proper cryogenic environment and with proper load-temperature cycling including that which simulates the proof testing.

ALLOWABLE HOOP STRESSES FOR ORBITER TANKS USING VARIOUS CRITERIA

CALCULATED ALLOWABLES FOLLOWING NASA SP–8040 WITH SURFACE FLAW AND FOR DESIGN LIFE OF 400 MISSIONS

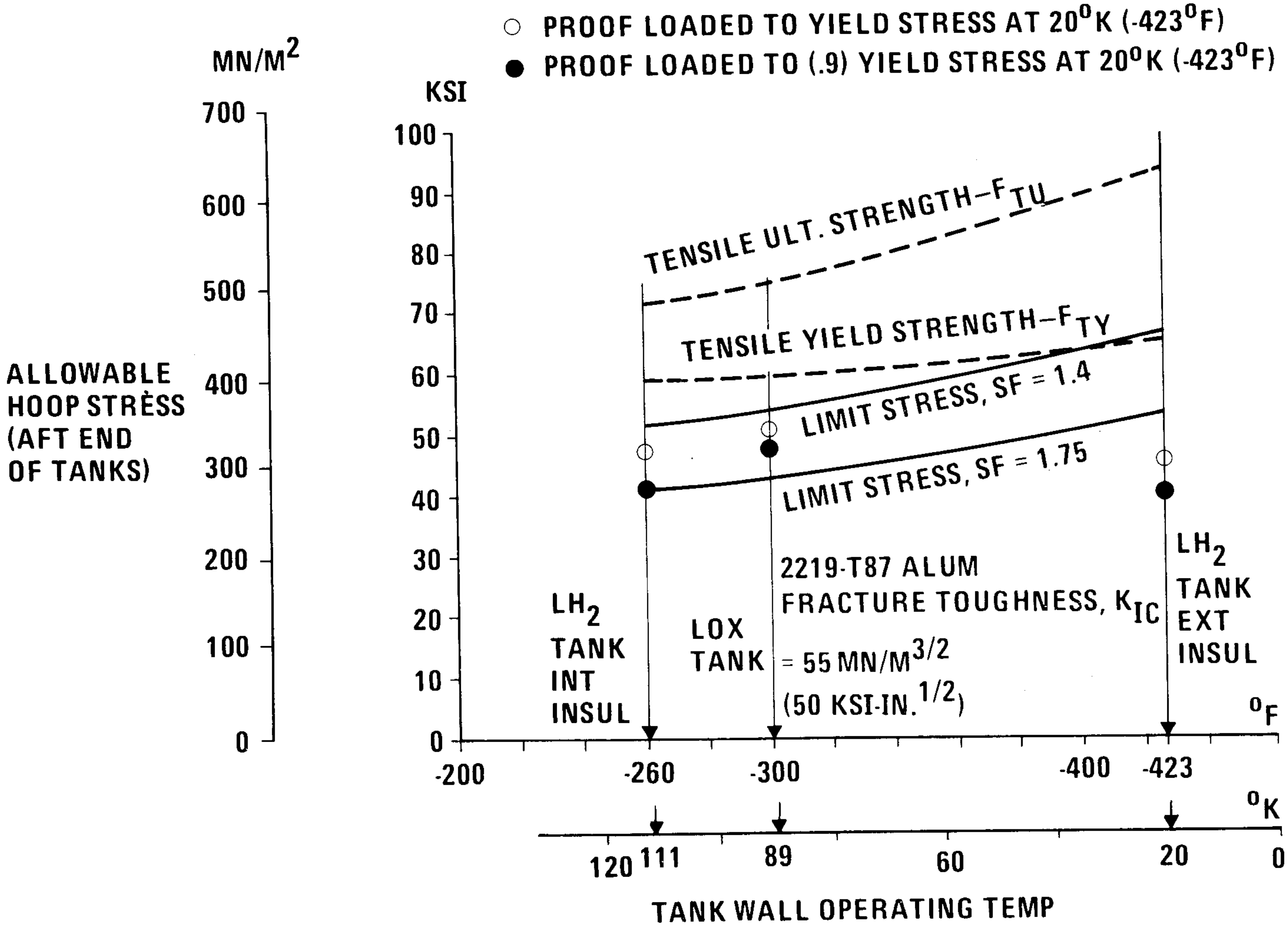

Slide 6

THE FAIL-SAFE/SAFE-LIFE DILEMMA

(Slide 7)

The choice between a fail-safe and a safe-life design approach is particularly difficult since one desires the safety of commercial transports (mostly fail-safe) and needs the performance of military aircraft (mostly safe-life). Where no significant weight penalty is involved, the fail-safe approach is the obvious choice. However, where the weight penalty is prohibitive, a safe-life design is the only choice. But, the following observation can be made: the weight penalty of a fail-safe design varies inversely with the effort and the imagination that went into the design.

For example, the fail-safe designs of current aircraft fuselages would be prohibitively heavy for the Shuttle. New concepts are needed to build structures that, if not fail-safe in the strict sense of current specifications, are at least more forgiving than a monolithic structure of high-strength material operating at a high stress level – that is, such materials as composites (boron, fiberglass, etc.), metal composite combinations (e.g., fiberglass overwrap on metallic tanks), and laminates (rolled laminated sheet with metallic interlayers).

Where a safe-life design approach is selected, a proof test should be considered. Proof tests are still employed on such vital structures as arresting hooks, hoisting slings, and pressure vessels – where each load application in service is expected to be close to design limit, where strength is sensitive to small variations in the manufacturing process, and especially where inspection cannot guarantee to separate the weak from the strong. While it is still too early to predict the advisability of proof testing any Shuttle components, it is worth noting that complete aircraft (F-111) and large booster propellant tanks (Saturn V) are still proof tested.

Of course, if proof testing is required on the Shuttle, then still another problem must be faced – that of post-proof-test inspection. Indeed, post-proof inspection is highly desirable where welded structure is involved. Present capabilities for a quick, thorough, and complete inspection of a large structure like the Shuttle leave much to be desired. This would seem to be fertile field for the expenditure of research funds.

THE FAIL—SAFE/SAFE—LIFE DILEMMA

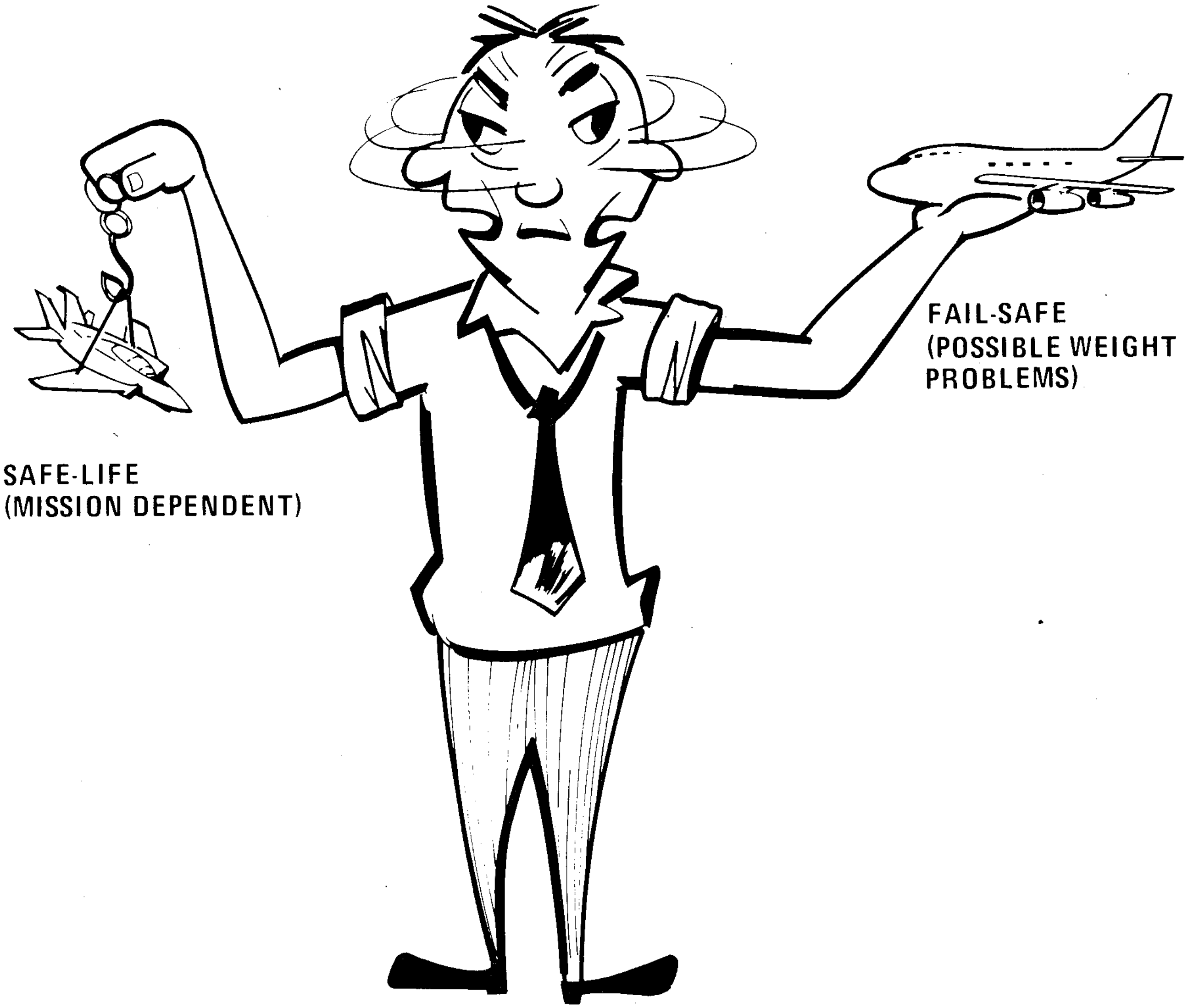

Slide 7

THE POGO PROBLEM
(Slide 8)

Shuttle design for the prevention of POGO is complicated by the offset orbiter which couples longitudinal and lateral motion. This coupling produces longitudinal modes of lower frequency than the Saturn V, and increases the number of combined modes in the low frequency range. Calculations of a typical offset orbiter configuration using 105 effective degrees of freedom reveal 6 modes which showed appreciable combined lateral and longitudinal motion increasing in frequency from 2.2 to 7 Hz. Three modes in the range of 4 to 7 Hz at booster burnout showed significant response at the engine. To evaluate the sensitivity of the design to POGO-type inputs, a 22-kN (5000-lb) oscillating force – which is about the limit permitted under current engine requirements - was applied to the 12 engines. This results in a 1/4 g acceleration at the engine, 2 g on the orbiter fin, and a 0.6 g lateral response in the orbiter crew compartment, assuming a structural damping of 1 percent of critical. (1 g = 9.8 m/sec^2 = 32.2 ft/sec^2.) The response in the crew compartment substantially exceeds the 1/4 g requirement established for the Gemini and Apollo programs. Slide 8 shows some of the calculated values at various locations on the booster and orbiter.

Based on data such as these, it would appear prudent to incorporate engine-induced loads as design requirements for structural integrity at oscillatory force levels larger than those specified for the engine output. Saturn V experience has demonstrated the necessity of providing such margins.

The current design criteria should provide for early attention to those analytical areas which have proven difficult in the past. These include the interfaces between the various components in the system, and rigorous and complete math-model simulations based on full-scale test data, where possible, for each component. The models should be good representations of the system elements away from resonances as well as at the peaks.

In view of the uncertainties inherent in the analysis, a conservative preliminary design margin for POGO prevention should be required in both gain and phase. A goal of 12 dB in gain and 30 degrees in phase is proposed. Provisions for suppression devices (i.e., helium-filled line accumulators) should be included in the basic Shuttle design.

RESPONSE TO 22 KN (5000 LBF) OSCILLATING FORCE AT 4.10 Hz

- BOOSTER BURNOUT CONFIGURATION
- RESPONSES SHOWN ARE MAXIMUM ACCELERATIONS IN g-UNITS (0 TO PEAK AMPLITUDE)
- STRUCTURAL DAMPING = 1% OF CRITICAL

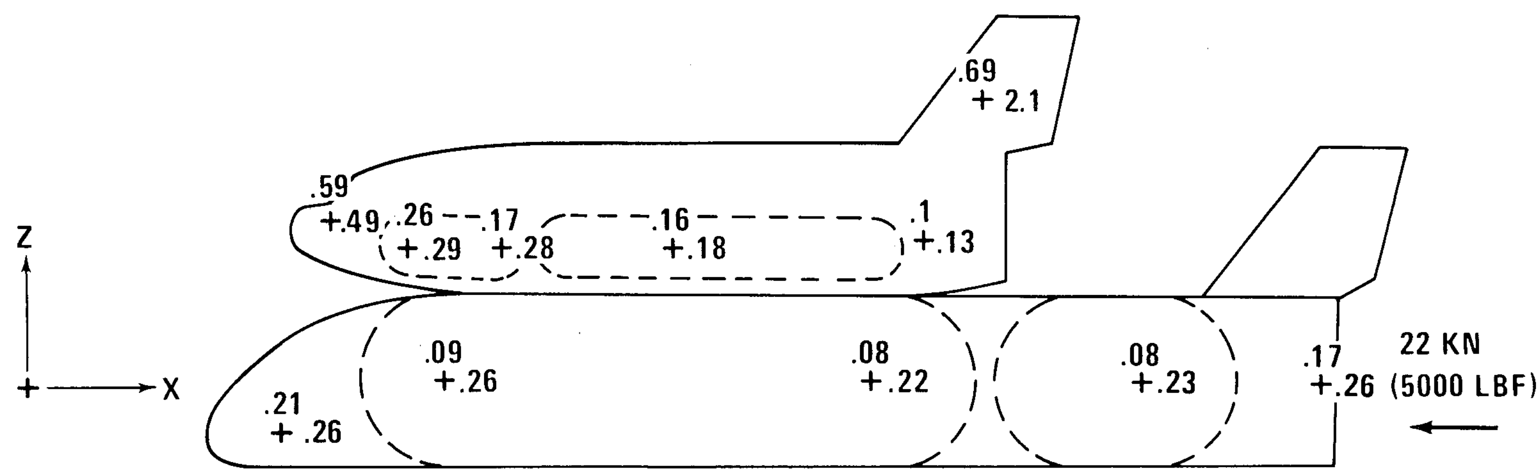

Slide 8

CONCLUSION

The work of preparing NASA SP-8057 seems quite worthwhile, both from the standpoint of pooling our knowledge and because it has focused attention on a vital aspect of Shuttle technology. It is hoped that the present comments will be useful in further refinement of the document.

REFERENCES

1. Anon.: Structural Design Criteria Applicable to a Space Shuttle. NASA SP-8057, Nov. 1970.
2. Anon.: Fracture Control of Metallic Pressure. NASA SP-8040, May 1970.

STRUCTURAL ANALYSIS AND AUTOMATED DESIGN

By Harvey G. McComb, Jr.
NASA Langley Research Center
Hampton, Virginia

PAPER 12

STRUCTURAL ANALYSIS AND AUTOMATED DESIGN

(Slide 1)

The present state-of-the-art in structural analysis and design is reviewed, the direction in which the technology is progressing is indicated, and applications to shuttle structures are discussed. Examples are drawn from aircraft and space vehicle structures technology to characterize the state-of-the-art. New results on shuttle-type structures are shown to illustrate applications of the latest technology. Certain specific computer programs are identified to clarify present and expected future capabilities. The programs mentioned are not necessarily unique nor are they necessarily the best of their type. They are simply representative examples that are known to the author.

The subjects on the slide are touched on in the order shown. There is a well developed capability to do structural analysis. Industry is particularly well tooled and government to a lesser extent - hundreds of computer programs are in existence. Programs to do automatic design of fixed structural configurations under fixed loading conditions have been developed and are beginning to be used in routine aircraft design. Finally, possibilities can be envisioned of computerized systems in which various technical disciplines are drawn together to perform certain design functions in an automated and integrated fashion.

STRUCTURAL ANALYSIS AND AUTOMATED DESIGN

ANALYSIS

- FINITE-ELEMENT METHODS
- FINITE-DIFFERENCE METHODS

AUTOMATED DESIGN

- FIXED STRUCTURE AND LOADING

INTEGRATED SYSTEMS

- COMBINED-DISCIPLINE ANALYSIS AND DESIGN

Slide 1

747 FINITE ELEMENT STRUCTURAL ANALYSES

(Slide 2)

The only aircraft in commercial operation which approaches the shuttle in size is the Boeing 747. It is 70.4 m (231 ft) long and 59.4 m (195 ft) in wingspan and has a takeoff gross weight in excess of 317,500 kg (700,000 lb). Large scale static structural analyses of this aircraft using finite element technology are illustrated on this slide. The two shaded portions of the 747 aircraft were analyzed in great detail with finite element computer programs. The wing-body intersection problem was the largest, and some indication is given as to the size of that calculation. This analysis was what Boeing called the -4 analysis and was the next to the last refinement of the finite element idealization. An indication of the effort required for the wing-body intersection problem is shown in the upper left.

747 FINITE - ELEMENT STRUCTURAL ANALYSES

WING-BODY INTERSECTION

10 MONTHS ELAPSED TIME
93 MAN-MONTHS PROFESSIONAL EFFORT
78 HOURS IN CDC 6600 CENTRAL PROCESSOR

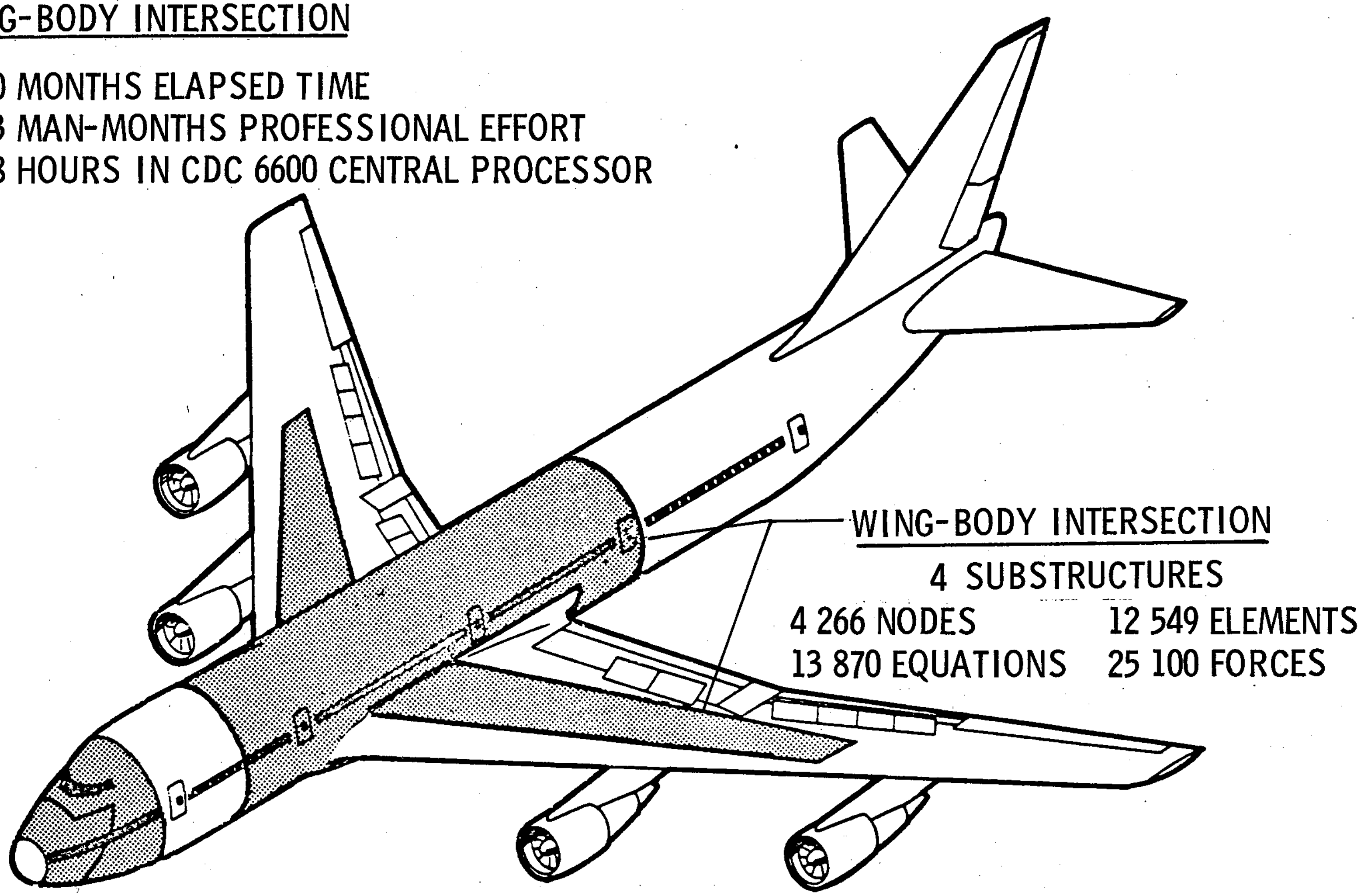

Slide 2

COMPARISON OF 747 AIRCRAFT ANALYSIS WITH TEST

(Slide 3)

Correlation between stresses calculated by the finite element analyses and experimental data from the 747 full-scale static tests are indicated on this slide. (This information was supplied by Ralph E. Miller, Jr., and Stanley D. Hansen of the Boeing Company.) The comparison is made for body station 1490, which is behind the body-mounted landing gear wells. A normalized axial stress in the fuselage shell wall is plotted as a function of water line or vertical distance on the fuselage. The -4 analysis is what was discussed on the preceding slide, and the -5 analysis is a somewhat more refined model. The symbols are data from strain gages mounted on the full-scale static test aircraft. The excellent agreement provides confidence in future large-scale finite element analyses.

COMPARISON OF 747 AIRCRAFT ANALYSIS WITH TEST

BODY STATION 1490; POSITIVE DIVE MANEUVER ULTIMATE CONDITION

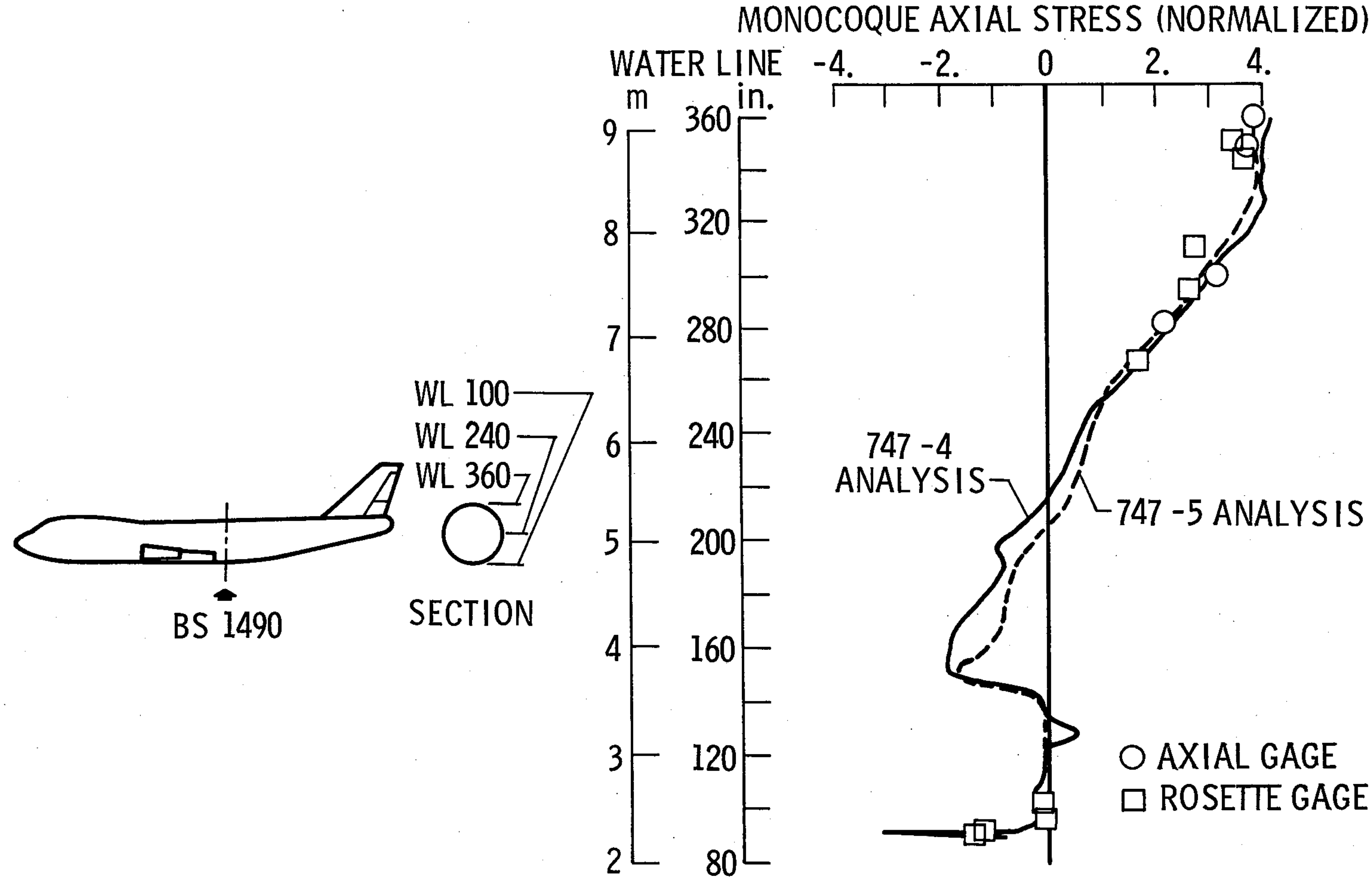

Slide 3

NASTRAN FINITE ELEMENT STRUCTURAL ANALYSIS COMPUTER PROGRAM

(Slide 4)

The basic finite element structural analysis computer program used at Langley is the NASTRAN system recently released by NASA. NASTRAN has an executive routine to manage the work of operational modules which perform the analysis tasks shown on the left of the slide. The executive routine calls the operational modules into core and brings in from the data base whatever information is required to perform the analysis. This mode of operation features simple, user-oriented instructions which make NASTRAN easily run by structural engineers who are not sophisticated computer programmers.

It is NASA's intention to maintain, update, and improve NASTRAN for use on a wide variety of structural problems. Some of the planned improvements are indicated at the bottom of the slide. The New Elements and Heat Transfer items are part of the shuttle structures technology activities and are intended to tool up NASTRAN with elements especially useful for analysis of shuttle structures. The last two planned improvement items are being pursued under the basic NASTRAN maintenance activity and should contribute to the program's overall usefulness for shuttle structures.

NASTRAN FINITE-ELEMENT STRUCTURAL ANALYSIS COMPUTER PROGRAM

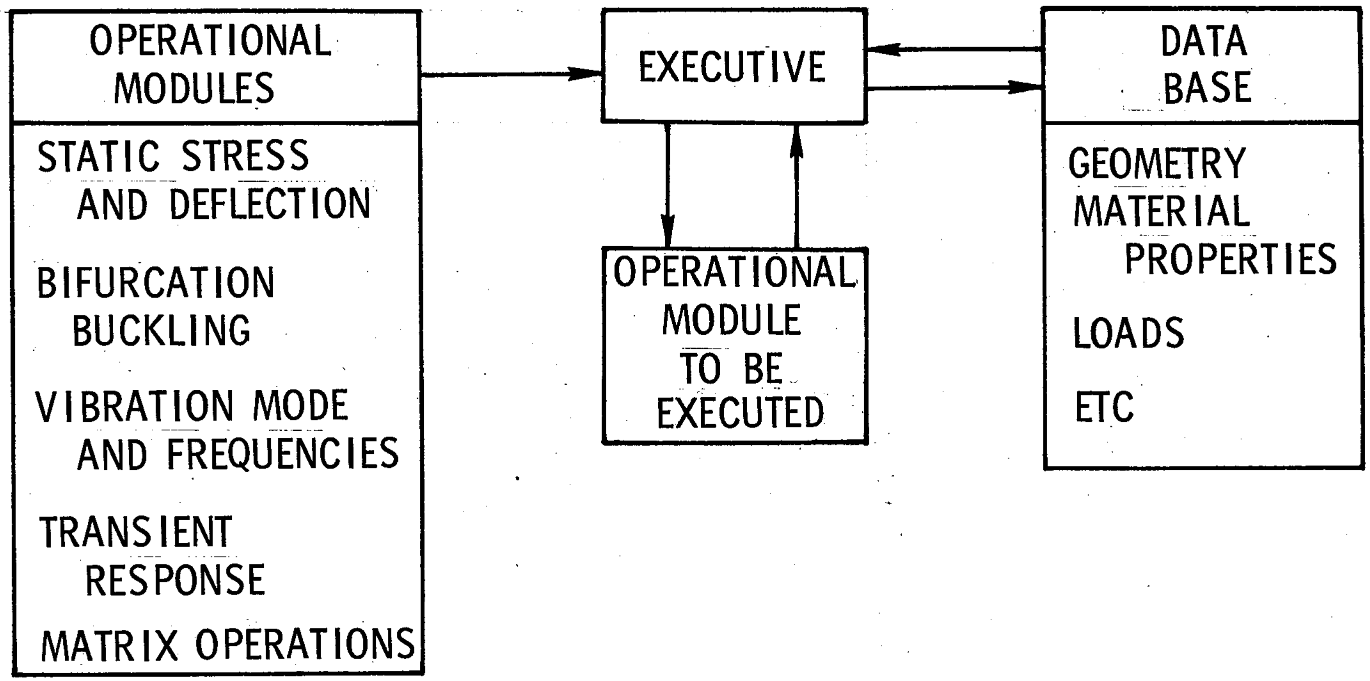

PLANNED IMPROVEMENTS

NEW ELEMENTS
HEAT TRANSFER
COMPUTATIONAL EFFICIENCY
SUBSTRUCTURING

Slide 4

APOLLO-SATURN SHORT STACK ANALYSIS

(Slide 5)

Although the finite element methods are very general and powerful, there are often excellent reasons to be interested in alternate approaches to analysis. One good example is the shell-of-revolution structure which can be analyzed much more efficiently with specialized programs than with the general finite element programs. Propellant tankage on shuttle vehicles may very well turn out to be shell-of-revolution structures. The Apollo-Saturn short stack is an example of a large structure of this type which has enough symmetry so that it was analyzed with the use of finite difference shell-of-revolution computer programs. The part of the vehicle termed the "short stack" consists of the Spacecraft Lunar-module Adapter (SLA), a relatively short Instrument Unit (IU), and the forward skirt of the S-IV B stage. The detailed wall configuration is shown and consists of a honeycomb sandwich conical shell (SLA), a short honeycomb sandwich cylinder (IU), and a ring and stringer stiffened cylindrical shell (S-IV B forward skirt). In order to obtain realistic results for buckling loads, for example, it is vital to model these details very accurately. The loading indicated is a condition at end-boost. Results for this end-boost condition are the meridional stresses in the shell wall at limit load, the meridional shape of the buckling mode (which has 7 waves around the circumference), and the magnitude of the buckling load for this load distribution (12.6 MN or 2.8×10^6 lb). The size of the calculating problem involved here is indicated by the number of stations and finite difference equations used, and an idea of the efficiency of calculations with shell-of-revolution programs (because the matrices are banded) is given by the fact that all these results for this one loading condition were obtained in less than two minutes CPU time on CDC equipment. (Ref. 1)

APOLLO-SATURN SHORT-STACK ANALYSIS

$P_{cr} = 12.6$ MN (2.8×10^6 lb)

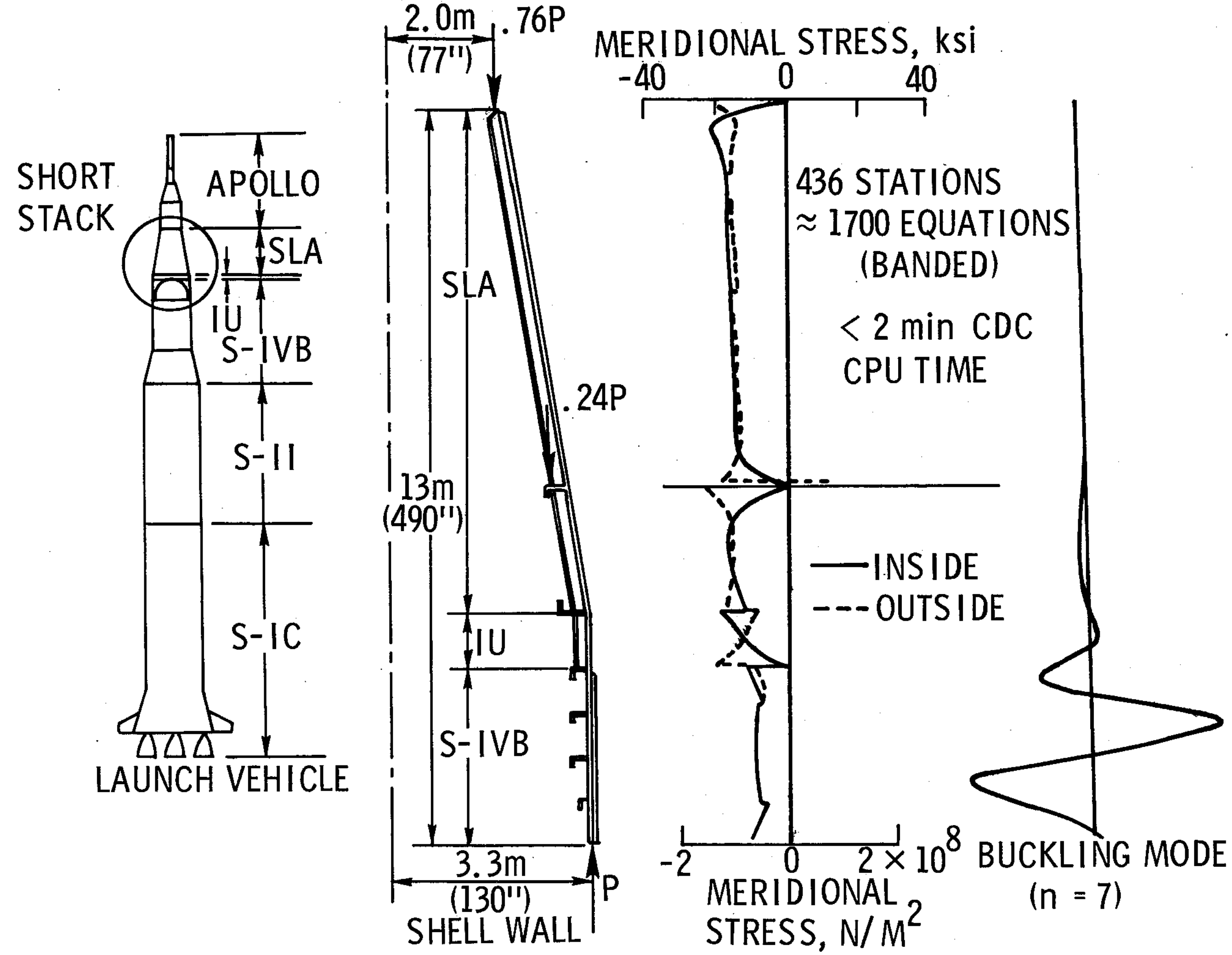

Slide 5

ANALYSIS WITH FINITE DIFFERENCE SHELL-OF-REVOLUTION COMPUTER PROGRAMS

(Slide 6)

Shell-of-revolution structures can be analyzed with finite difference or finite element programs. The finite difference approach is more common, however, and many such programs exist. Typical capabilities are shown here. Considerable generality in structural characteristics can be handled. The kinds of analyses and loadings that these programs can handle are also shown on the slide. The symmetry of shell-of-revolution structures leads to structural matrices which are banded (that is, the non-zero matrix elements cluster about the diagonal). Very efficient algorithms are available for the manipulation of these matrices on the computer, and this is the basic reason for the very short computation times required by these programs.

One especially good system of shell-of-revolution programs has been developed by Cohen (see, for example, refs. 2 and 3), and some improvements which are planned for this system are shown at the bottom. This type of program provides very rapid and accurate analysis capability for tankage structures in shuttle vehicles which might be circular cylindrical or conical or spherical shell structures.

ANALYSIS WITH FINITE - DIFFERENCE SHELL - OF - REVOLUTION COMPUTER PROGRAMS

CURRENT CAPABILITIES

STRUCTURAL CHARACTERISTICS

- GENERAL MERIDIONAL SHAPE
- VARIABLE PROPERTIES
- ORTHOTROPIC SHELL WALL
- STIFFENER ECCENTRICITIES
- DISCRETE RINGS
- SMEARED STRINGERS

ANALYSES

- STRESS
- VIBRATION (PRESTRESSED)
- BUCKLING (SYMMETRIC LINEAR AND NONLINEAR PREBUCKLING)
- TRANSIENT

LOADS

- MECHANICAL
- THERMAL
- DISTRIBUTED
- DISCRETE

PLANNED IMPROVEMENTS

BUCKLING UNDER ASYMMETRIC LINEAR PREBUCKLING

SHELL BRANCHING CAPABILITY

Slide 6

SHUTTLE STRUCTURE ANALYZED BY STAGS COMPUTER PROGRAM

(Slide 7)

Proposed shuttle configurations, on the other hand, are often highly asymmetric. An orbiter concept is shown on the slide, and a portion between adjacent frames might be modelled as a shell shown in the lower right. A program called STAGS is being developed by Lockheed Palo Alto Research Laboratories to analyze asymmetric shell structures like this. STAGS is intended to calculate the collapse strength of such a structure by following the growth of deformations from the start of loading and accounting for large lateral deflections of the shell wall which eventually bring about collapse.

SHUTTLE STRUCTURE ANALYZED BY STAGS COMPUTER PROGRAM

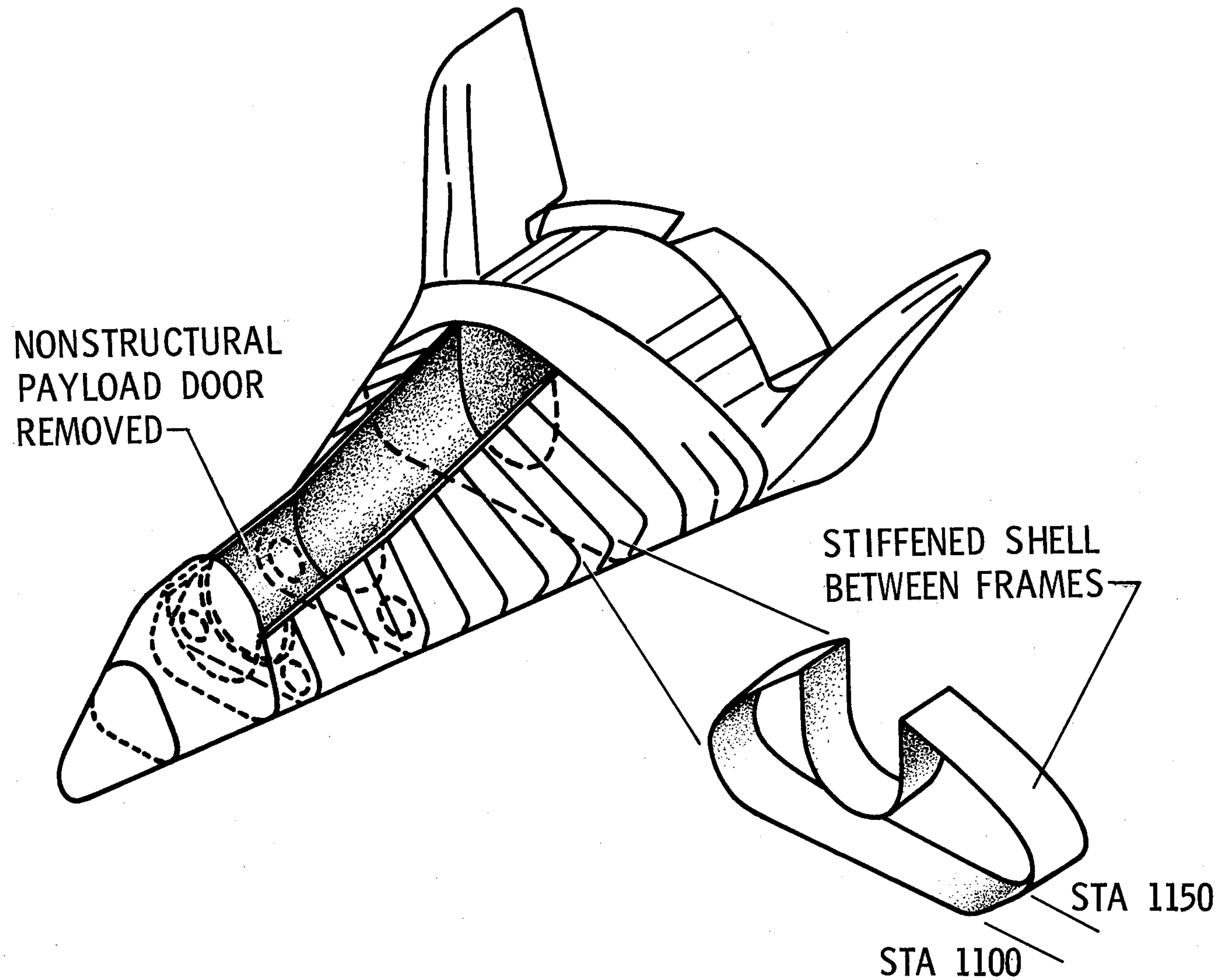

Slide 7

STAGS RESULTS FOR THE BEHAVIOR OF SHUTTLE STRUCTURE

(Slide 8)

Results are shown from a nonlinear analysis by STAGS of the component illustrated on the previous slide. (These data were supplied by Bo Almroth of Lockheed Palo Alto Research Laboratory.) A Z-stiffened shell configuration representative of orbiter structure was assumed and a combination end-shortening and relative rotation of the ends of the component was imposed. These applied displacements result in axial compression loads and bending moments representative of a maximum $q\alpha$ condition as indicated on sketch in the upper left. The end-shortening and relative rotation were imposed in a fixed ratio, and the magnitude of these displacements is characterized by the quantity λ . At the lower left is shown the lateral shell wall displacement at a location midway between the frame stations as a function of arc length around the perimeter for a particular value of λ . The arc length is measured around the perimeter starting at the bottom body center-line as indicated on the sketch. On the right are shown axial load, bending moment and a lateral displacement plotted as a function of λ . The lateral displacement (+ outward) plotted is for $s = 1310$ cm (515 in.) (located at the dot on the sketch) and represents one of the spikes in the chart at lower left. These particular calculations were not carried all the way to collapse because of excessive computer time requirements. Presumably, at collapse the curves of axial load and bending moment as a function of λ will become horizontal. With improvements in the program and refinement of the finite difference grid, it is believed that realistic estimates of collapse load can be obtained.

STAGS RESULTS FOR THE BEHAVIOR OF SHUTTLE STRUCTURE

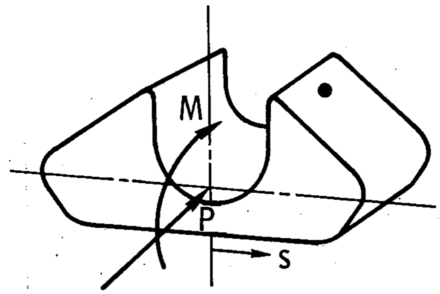

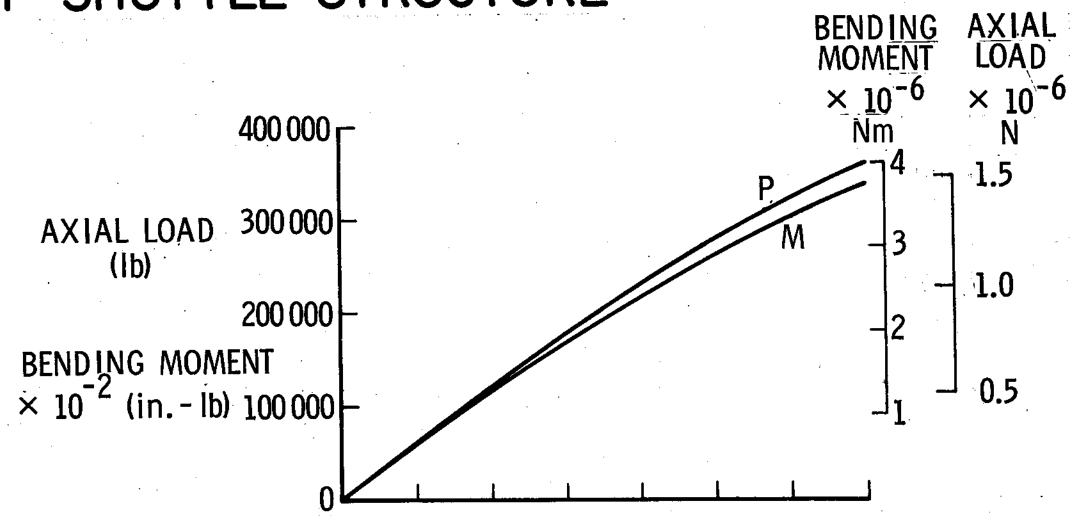

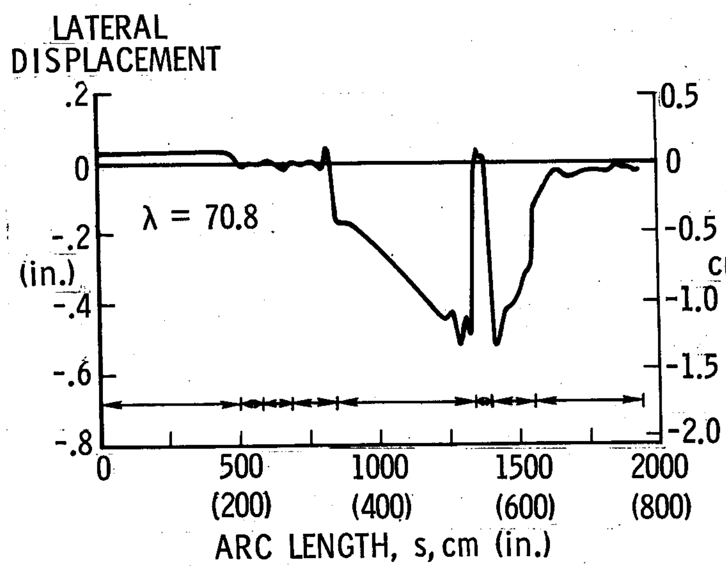

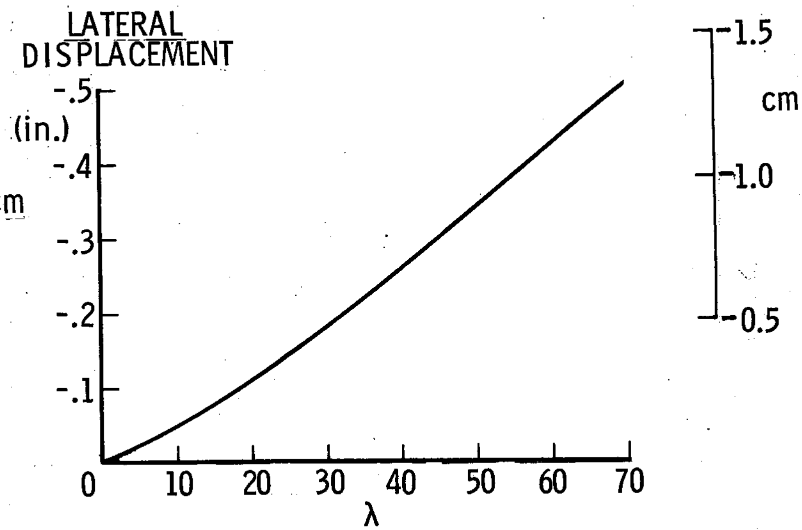

Slide 8

STRUCTURAL ANALYSIS OF GENERAL SHELLS (STAGS)

(Slide 9)

The STAGS program represents the next advancement in finite difference programs for the analysis of shell structures. The features of primary importance here are: (1) circumventing of the restriction to shell-of-revolution configurations and (2) focussing on nonlinear, or large deflection, analysis. For shell structures of general shape with little or no symmetry properties, failure is governed less by bifurcation buckling behavior and more by the nonlinear growth of deformation from the start of loading. It is vital, therefore, to be able to perform realistic nonlinear collapse analyses when dealing with shell structures which lack the geometric symmetry properties of a shell-of-revolution.

The STAGS program is already producing results, and under the shuttle structures technology development program improvements shown on the bottom of the slide are planned. The intention here is to make STAGS a user oriented analysis tool for the shuttle designer.

STRUCTURAL ANALYSIS OF GENERAL SHELLS (STAGS)

CURRENT CAPABILITIES

STRUCTURAL CHARACTERISTICS

- GENERAL SHELL SHAPE
- VARIABLE MATERIAL PROPERTIES
- ECCENTRIC STIFFENERS
- CUTOUTS BOUNDED BY COORDINATE LINES
- VARIABLE GRID

ANALYSES

- LINEAR STRESS
- NONLINEAR STRESS AND COLLAPSE
- BIFURCATION BUCKLING

LOADS

- MECHANICAL
- THERMAL
- DISTRIBUTED
- DISCRETE

PLANNED IMPROVEMENTS

- GENERAL CUTOUT IN SHELLS OF REVOLUTION
- ORTHOTROPIC SHELL WALL
- GENERAL GRID
- AUTOMATIC GRID GENERATION

Slide 9

AUTOMATED STRUCTURAL OPTIMIZATION PROGRAM (ASOP)
(Grumman Aerospace Corporation)

(Slide 10)

With highly computerized analysis tools in hand, it is natural to explore how these tools can be incorporated into automated design programs in which the computer is programmed to perform the more routine design decisions and clerical chores which are conventionally handled by engineers. Several programs are available which automatically size members in a structure having a fixed layout and subjected to prescribed loading conditions to obtain an approximate minimum-weight design. One example is a program developed by the Grumman Aerospace Corporation for the Air Force - characterized on this slide. The program has a finite element analysis routine built-in and includes a fairly extensive library of elements. It performs a so-called fully stressed design - that is, between analysis cycles the structural members are resized essentially to carry some prescribed allowable stress. After a limited number of analysis and redesign cycles the structural weight usually reaches a point where further changes cause only extremely small changes in weight, and the design is considered converged. It can be shown that for redundant structures the fully-stressed design is not necessarily the minimum-weight design, however, for practical structures it is usually not far off. In addition, this program has the feature of a deflection constraint algorithm. In this option structural members are further resized to meet prescribed deflection constraints at certain points on the structure. There are limitations on the size of structure this program can handle, but with 3000 elements and 6000 degrees-of-freedom fairly large structures can be modelled to a respectable degree of refinement. (Ref. 4)

AUTOMATED STRUCTURAL OPTIMIZATION PROGRAM (ASOP)
(GRUMMAN AEROSPACE CORP.)

FIXED STRUCTURAL LAYOUT AND LOADINGS

FINITE-ELEMENT STRUCTURAL ANALYSIS
- 3000 ELEMENTS
- 6000 DEGREES OF FREEDOM
- 20 LOADING CONDITIONS

AUTOMATED DESIGN
- FULLY STRESSED DESIGN
- DEFLECTION CONSTRAINTS

Slide 10

IDEALIZED ORBITER TANK STRUCTURE

(Slide 11)

Grumman engineers used ASOP to size elements of a very crude idealization of orbiter tankage structure as an initial exercise of the program for this kind of structure. The orbiter tanks were represented by a circular cylindrical shell structure. The structure was modelled with bars for stringers (axial stiffeners), beams for frames (circumferential stiffeners), and shear panels for skin. Heavy rings or bulkheads were located at each end of the structure. The number of elements and degrees of freedom are indicated on the slide. The structure was assumed to be loaded by the booster at end boost condition as shown on the slide (these loads are applied to one half of the shell structure). Inertia loads from the lox and liquid hydrogen tanks were introduced as indicated on the slide. No internal pressure loads were considered.

IDEALIZED ORBITER TANK STRUCTURE

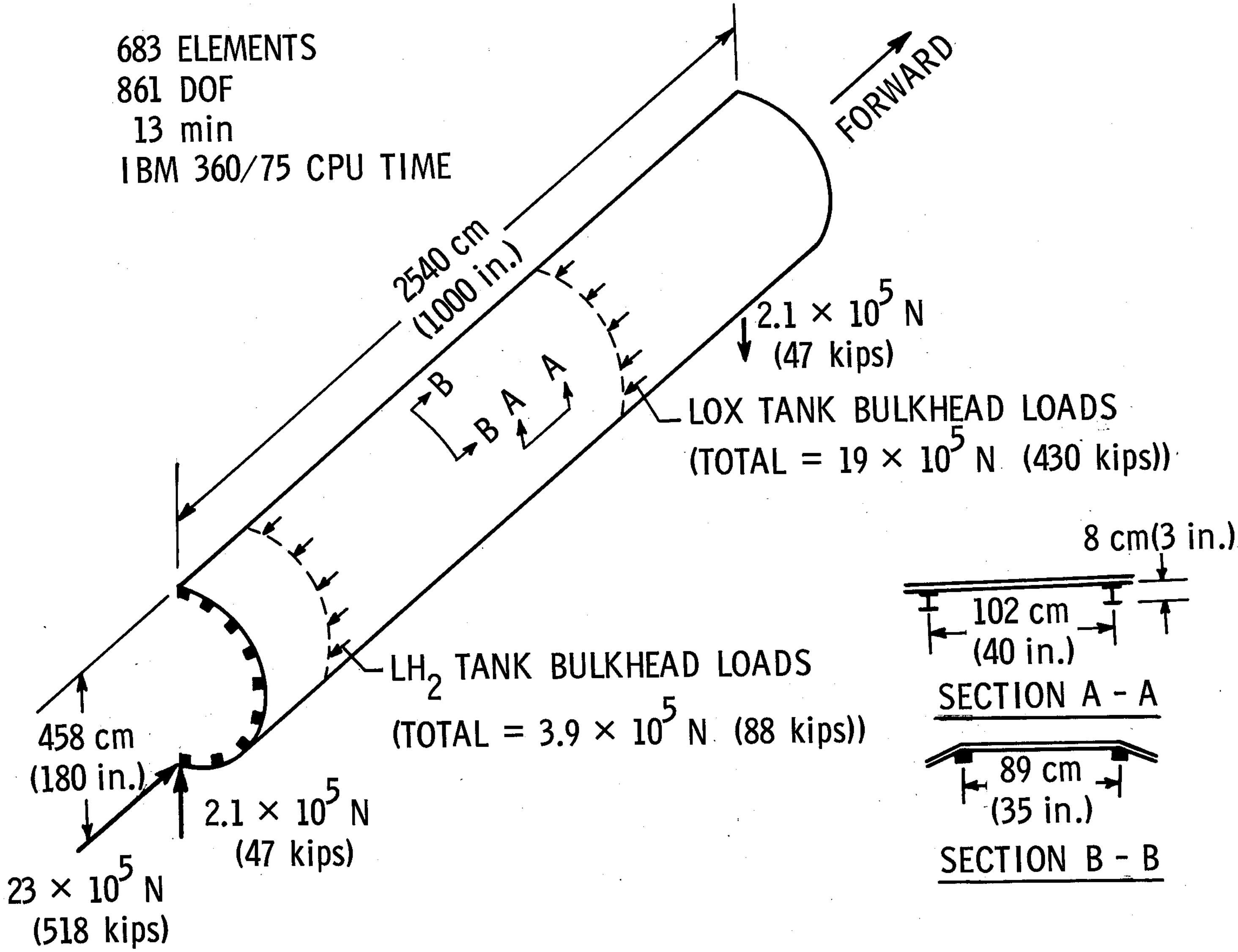

Slide 11

RESULTS FROM ASOP FOR ORBITER TANK STRUCTURE

(Slide 12)

Results from ASOP for the orbiter tankage structure are shown on the slide. Plotted are the equivalent thicknesses of smeared-out axial load carrying material as a function of axial distance from the aft end of the orbiter. Curves of thickness in the keel area, $22\frac{1}{2}^{\circ}$ away from the keel and then 45° away from the keel are shown. Forward of station 640 all material is minimum gage or 0.112 cm (0.044 in.) thick. For an initial design some very heavy gages and stiffener areas were chosen so that the initial structure weighed over 4,535 kg (10,000 lb). After the first design cycle, the weight was down to 2,450 kg (5,400 lb) and after four designs the final weight was 1,950 kg (4,300 lb) as indicated on the slide.

RESULTS FROM ASOP FOR ORBITER TANK STRUCTURE

1 st DESIGN	2450 kg (5400 lb)
4 th DESIGN	1950 kg (4300 lb)

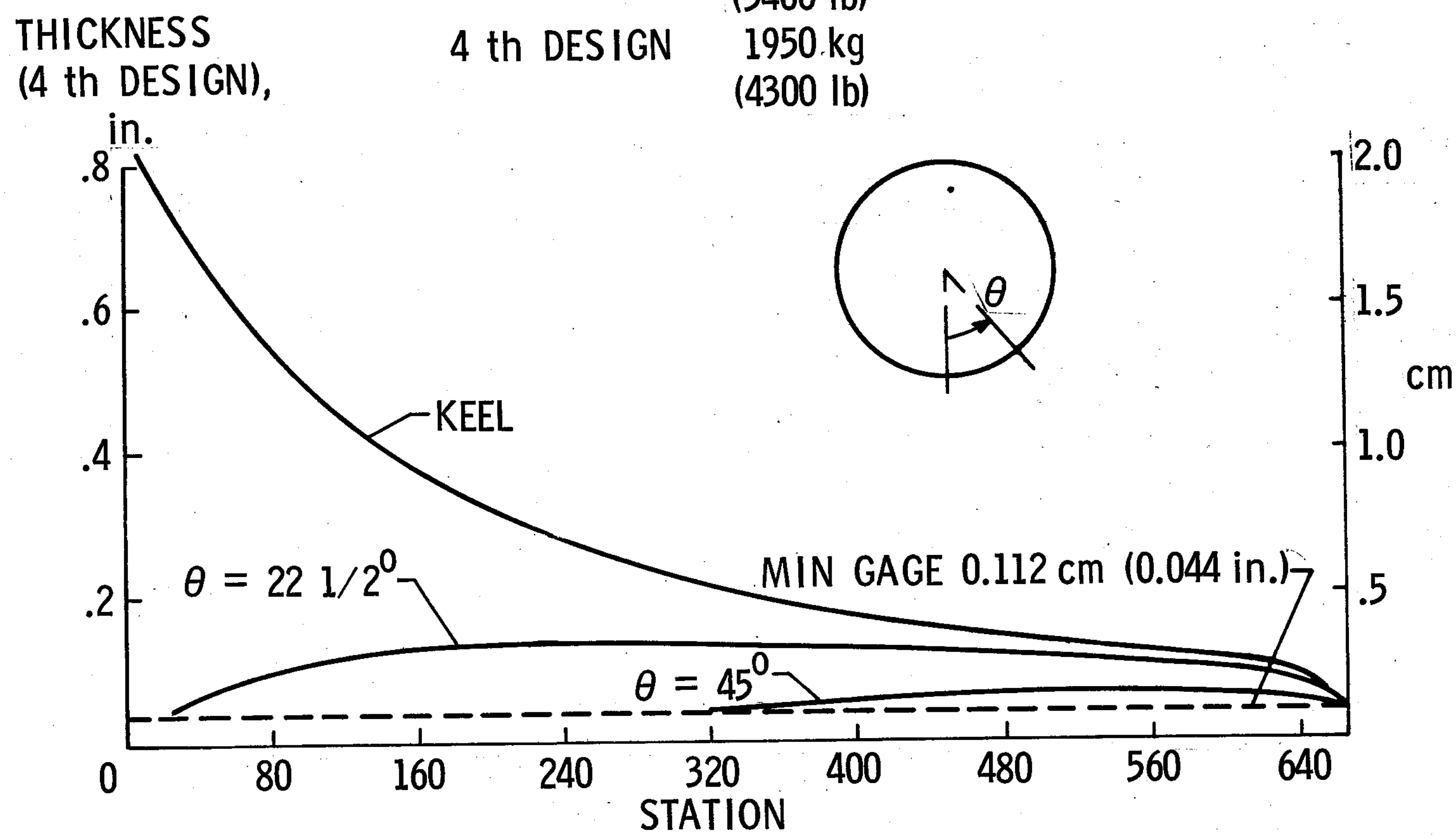

Slide 12

DAWNS - AUTOMATED STRUCTURAL DESIGN PROGRAM FOR WINGS

(Slide 13)

A pilot program has been developed at Langley in which structural and aerodynamic disciplines are integrated in an automated design function. This program is called DAWNS and is tailored for wing-type structures. The basic flow of the program is shown on the chart. The aerodynamic planform and geometric contours are input along with a relatively simple specification of the structural layout. An aerodynamic module then computes the pressure distribution on the wing, and fuel loads can be included. An initial structural sizing then provides inertia loads and feeds into a redundant structural analysis. The design cycle is a fully stressed design similar to that of the Grumman (ASOP) program. Allowables for wing cover panels account for buckling considerations automatically, and the cycling continues until a converged design results. The dashed lines refer to static aero-elastic and flutter modules which are not in DAWNS, but which are planned additions.

DAWNS - AUTOMATIC STRUCTURAL DESIGN PROGRAM FOR WINGS

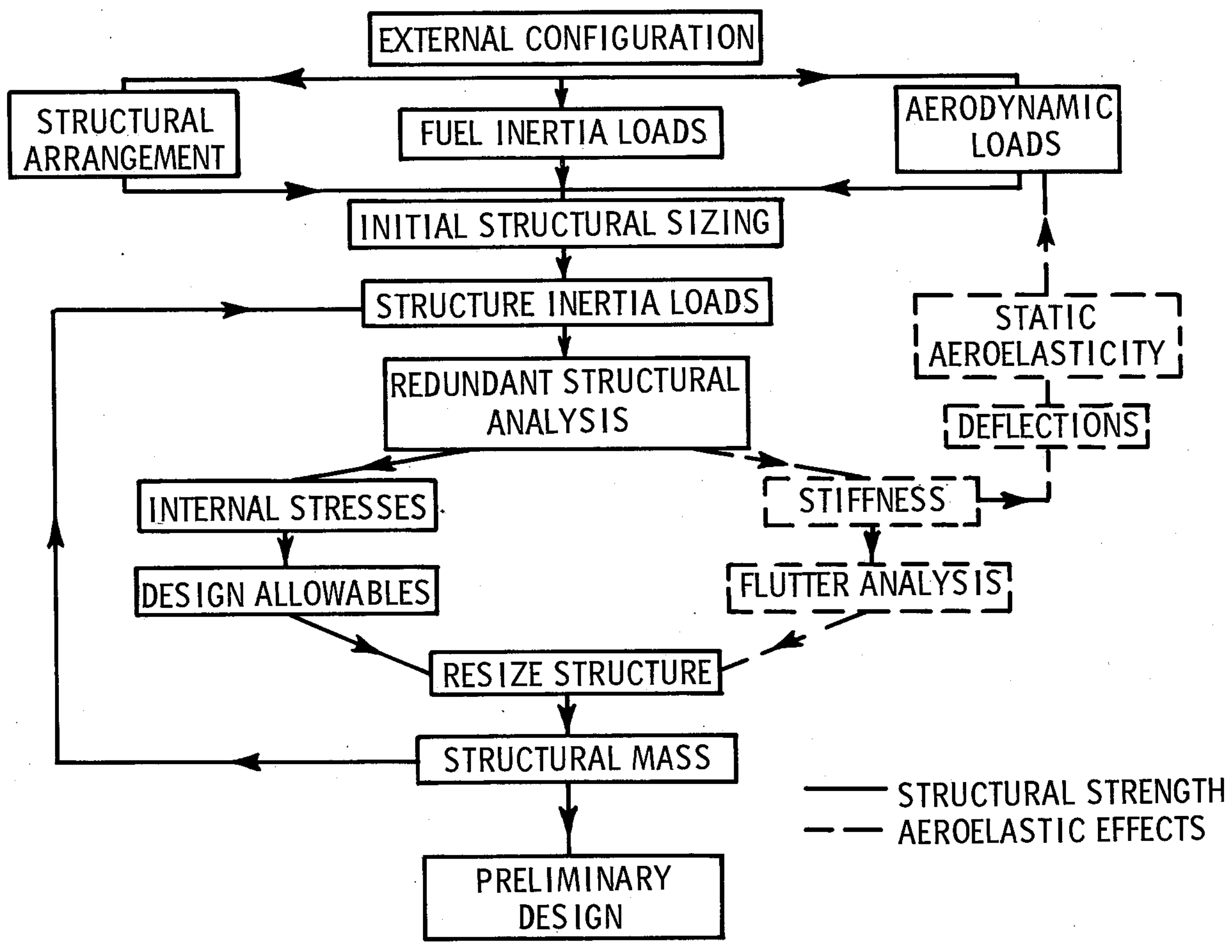

Slide 13

DESIGN OF SHUTTLE WING STRUCTURE WITH DAWNS

(Slide 14)

The operation of DAWNS is shown on this slide and the next. The wing shown is representative of a shuttle orbiter delta wing, and the loading condition considered is a maximum $q\alpha$ condition at a Mach number of 1.5. An ultimate factor of safety of 1.5 is included in the calculation, and the wing is assumed to be dry. The aerodynamic planform and thickness distribution and the structural layout are input. With relatively simple instructions, the program builds a finite element structural representation and prepares all geometry and nodal coordinate data for the structural analysis. The aerodynamic module in DAWNS is at present limited to supersonic flow, and the "Mach box" panelling and lifting pressure distribution are shown on the slide. The program then automatically lumps the aerodynamic pressures into concentrated loads at the node points of the structural idealization.

DESIGN OF SHUTTLE WING STRUCTURE WITH DAWNS

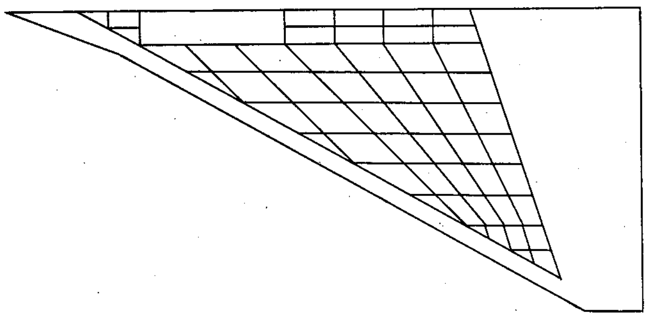

AERODYNAMIC PLANFORM
AND STRUCTURAL LAYOUT

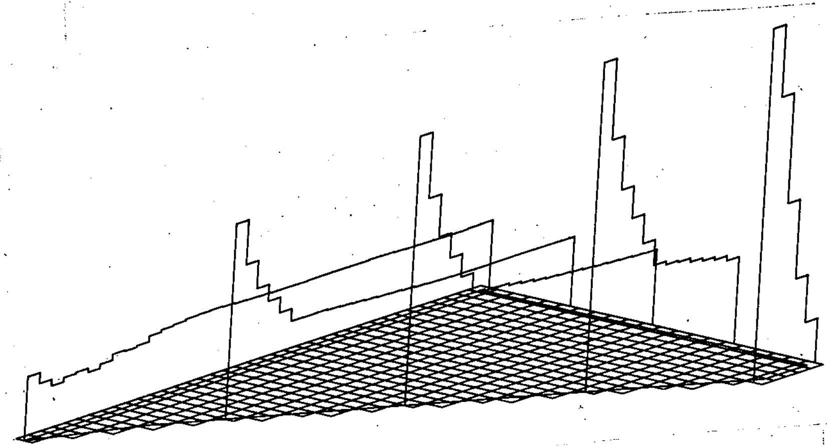

LIFTING PRESSURE DISTRIBUTION

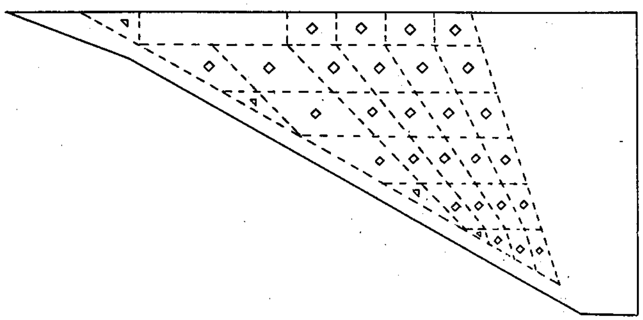

FINITE-ELEMENT IDEALIZATION

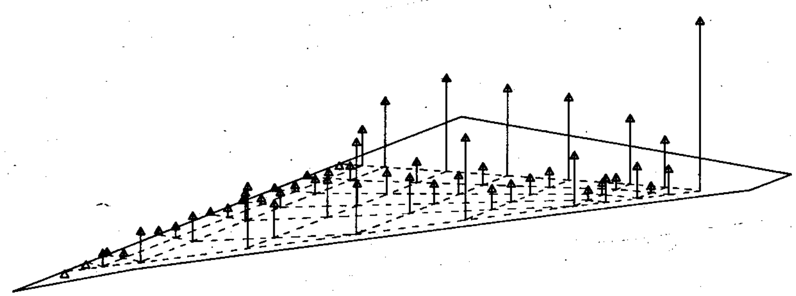

EQUIVALENT CONCENTRATED LOADS

Slide 14

DAWNS RESULTS AND DISPLAY CHOICES

(Slide 15)

Results of the fully stressed design are shown on this slide. The average cover plate thicknesses (or $\bar{t}$ quantities) are shown along with the deflected shape at ultimate load. The height of the boxes in the upper sketch represent the cover thicknesses, and the lateral deflection is to the same scale as the wing structure itself. DAWNS can be used in an interactive mode with a cathode ray tube display. All of the drawings shown on this slide and the previous one can be displayed on the CRT in addition to other input and output information including structural weights. The photo shows four alternate wing designs which are not associated with the orbiter wing, but simply to indicate that design changes can be introduced into the program through the CRT terminal, and their influence on the structural weights and sizings can be rapidly determined. These results for a structural model with about 130 elements and 135 degrees of freedom required about 6 redesign cycles and less than 4 minutes CPU time on the CDC 6600 computer.

DAWNS RESULTS AND DISPLAY CHOICES

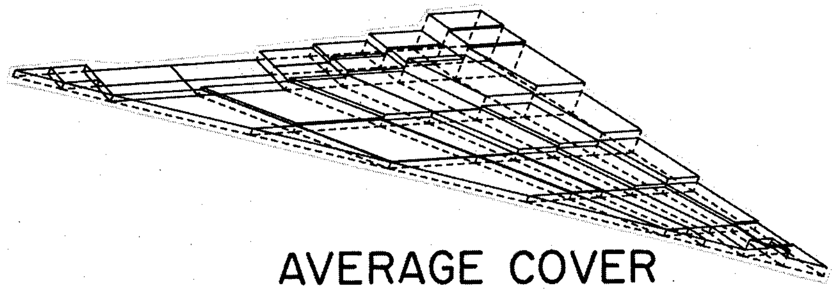

AVERAGE COVER
PANEL THICKNESSES

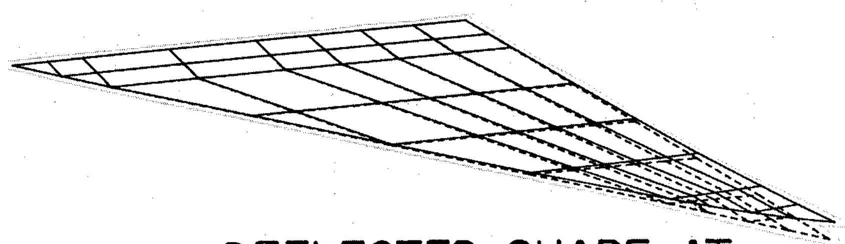

DEFLECTED SHAPE AT
ULTIMATE LOAD

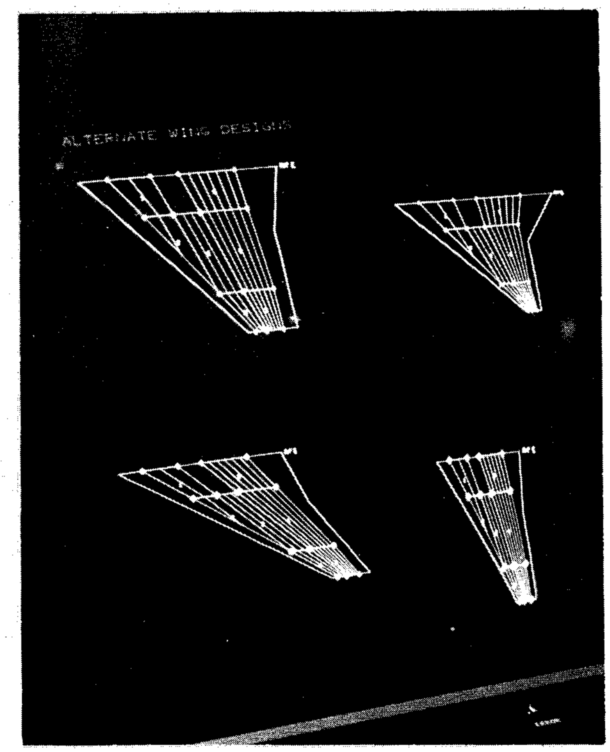

CRT DISPLAY OF
ALTERNATE WING DESIGNS

Slide 15

LANGLEY SHUTTLE STRUCTURAL DESIGN ACTIVITY

(Slide 16)

The DAWNS concept is just a faint glimmer of the potential for interdisciplinary integration in an automated design process which is possible with modern computing equipment. One of the long range research objectives of structures research at Langley is the building of an integrated system for aerospace vehicle design in which operational computer modules from the various disciplines would be brought under the control of an executive or monitor computer routine to manage the overall design process. The tremendous capacity and speed of the computer should be exploited as much as possible to perform the myriad of clerical and bookkeeping tasks and some of the routine design decisions now made by engineers. The culmination of these efforts, however, will probably be much too far into the future to have any impact on the shuttle program.

It is felt, on the other hand, that a computerized system can be built in the spirit of DAWNS which can be applied to shuttle structural problems. The tooling-up indicated at the top of the slide would have to be accomplished. About six months of work in-house is estimated to complete this development. At the completion of the tooling phase, studies could be made of optimum designs of components such as wings, bodies, tails, tankage; alternate arrangements which might be needed for reduced structural mass could be examined, and thermal and dynamic effects could be explored. Presumably, in six months the external geometric contours of the shuttle vehicles will be pretty well established, and these studies would have to be made within the confines of these contours.

LANGLEY SHUTTLE STRUCTURAL DESIGN ACTIVITY

PROGRAM DEVELOPMENT

- FUSELAGE TYPE GEOMETRY
- ADDITIONAL TYPES OF CONSTRUCTION
- IMPROVED AERODYNAMIC CAPABILITY
- MULTIPLE-LOAD CONDITIONS

SHUTTLE APPLICATIONS

- OPTIMUM DESIGN OF MAJOR STRUCTURAL COMPONENTS
- ALTERNATE STRUCTURAL ARRANGEMENTS FOR NEEDED MASS REDUCTION
- EXPLORE THERMAL AND DYNAMIC EFFECTS

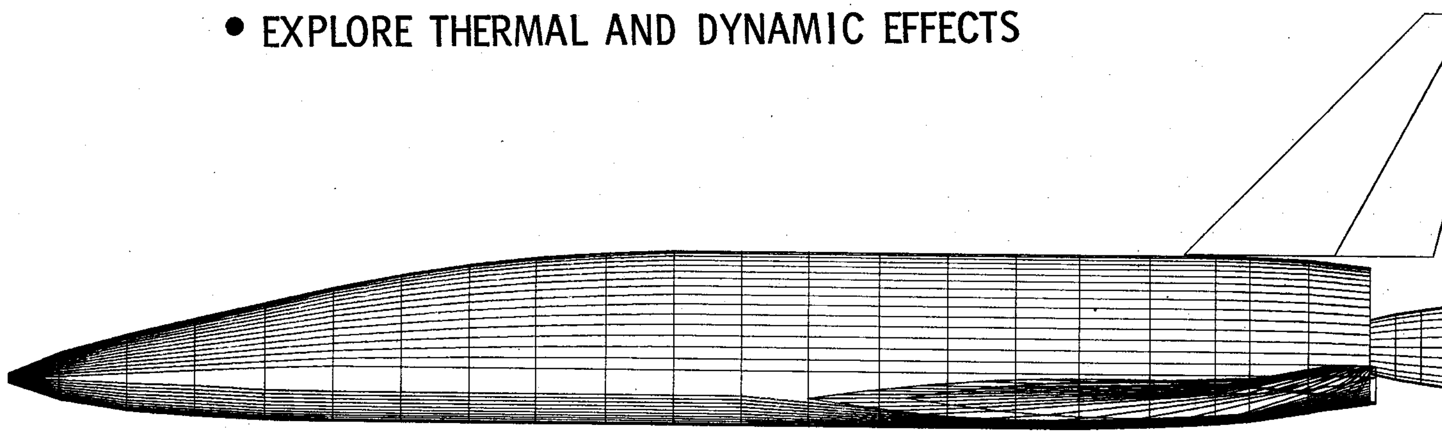

Slide 16

NUMERICAL DEFINITION OF ORBITER EXTERNAL GEOMETRY

(Slide 17)

These drawings of a representative orbiter configuration are computer generated and simply indicate that we have made some progress in development of the geometry routines needed for an automated design activity. In summary, the state-of-the-art in structural analysis is good. An extensive stable of finite element and finite difference computer programs is available throughout the nation to handle various aspects of this job. These tools have been characterized and the latest advances in the technology indicated. In addition, some of the latest developments in automated structural design have been characterized. Studies to date have indicated that the shuttle vehicle is extremely weight sensitive, and the opportunity should be grasped to exercise the very latest and best in computerized structural analysis and automated design tools to help arrive at the best vehicle the nation can build to meet the shuttle mission requirements.

NUMERICAL DEFINITION OF ORBITER EXTERNAL GEOMETRY

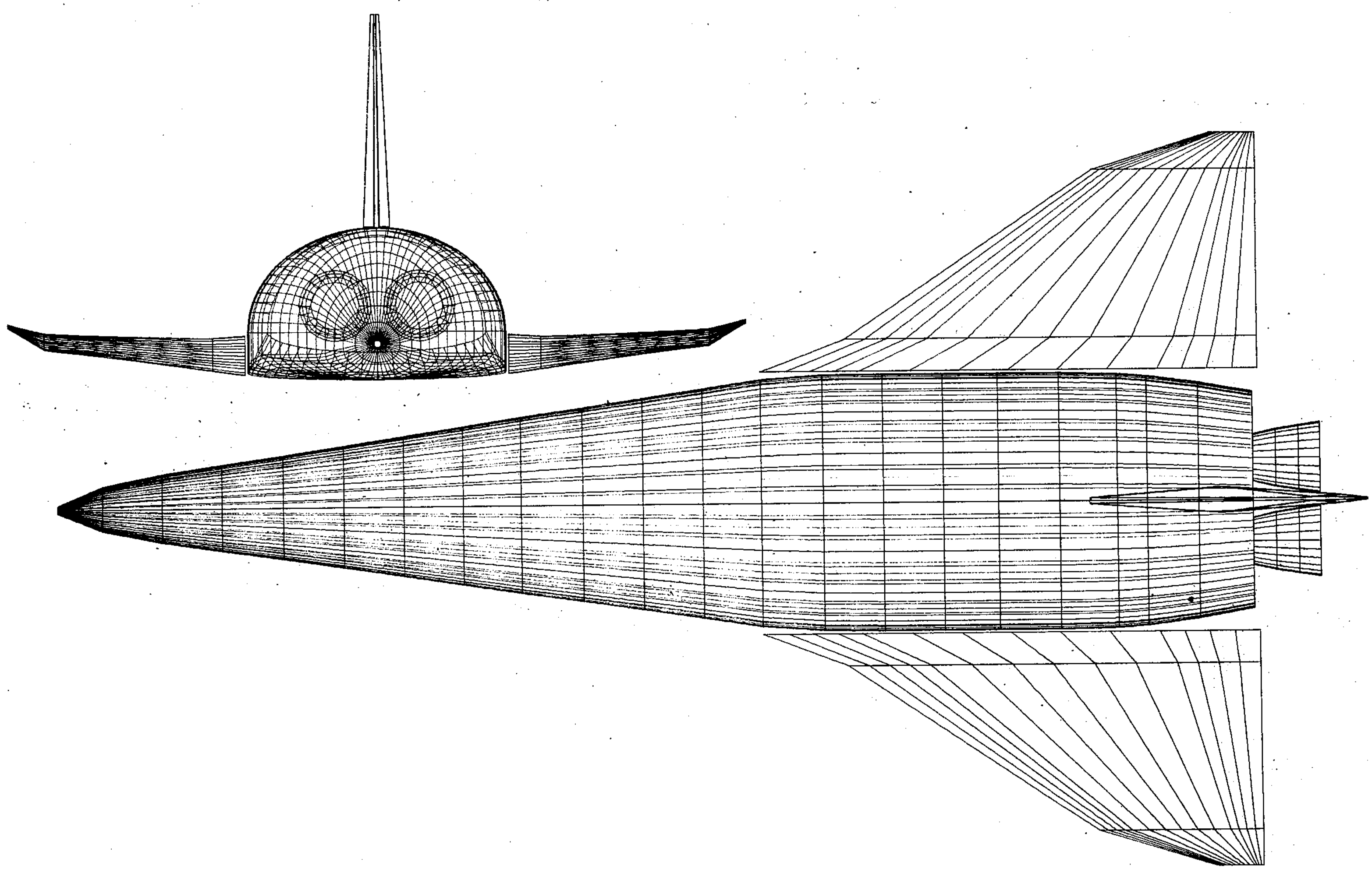

Slide 17

REFERENCES

1. Anderson, M. S.; Fulton, R. E.; Heard, W. L., Jr.; and Walz, J. E.: Stress, Buckling, and Vibration Analysis of Shells of Revolution. NASA paper presented at Conference on Computer Oriented Analysis of Shell Structures (Palo Alto, Calif.), Aug. 1970.
2. Cohen, Gerald A.: Computer Analysis of Asymmetrical Deformation of Orthotropic Shells of Revolution. AIAA J., vol. 2, no. 5, May 1964, pp. 932-934.
3. Cohen, Gerald A.: Computer Analysis of Asymmetric Free Vibrations of Ring-Stiffened Orthotropic Shells of Revolution. AIAA J., vol. 3, no. 12, Dec. 1965, pp. 2305-2312.
4. Lourenso, O.; and Dwyer, W.: Exploratory Study on Optimization Procedures for Fuselage Element Sizing. Note No. ADN 02-01-70.1, Grumman Aerosp. Corp., Nov. 1970.

CRITICAL STRUCTURAL DESIGN TRADE STUDIES SPACE SHUTTLE SYSTEM

BY T.P. BROOKS
MCDONNELL DOUGLAS CORPORATION
SAINT LOUIS, MISSOURI

INTRODUCTION

McDonnell Douglas has identified certain structural design trade studies to be particularly significant to the Phase B study because of the decisive influence their results have on shuttle vehicle configuration, cost, size, and weight. In each instance, these studies were pursued only to the depth necessary to assure that design concept selections could be made with confidence. This approach did not permit resolution of all problem areas, and some assumptions were made as to future technological state-of-art. Areas for technology and/or design development effort are identified in this presentation.

PAPER 13

CRITICAL STRUCTURAL DESIGN TRADE STUDIES

(FIGURE 1)

These trade studies were performed in the first six months of the Phase B study, when there were two baseline orbiters; straight wing low crossrange and delta wing high crossrange. Since January 1971 we have had only the delta wing orbiter. Integral vs. non-integral tanks and common vs. separate tank bulkheads trade studies were for the straight wing orbiter baseline. Recommendations of these studies have been incorporated in the design of the delta wing orbiter because the arrangement of delta orbiter body structure is similar to that of the straight wing orbiter studied. Comparison of forms of integral stiffening is based upon the baseline delta wing orbiter and single body canard booster; results of this study are directly applicable to the present baseline vehicles. Conventional materials were baselined for all shuttle structures. Composite material applications have been studied for the orbiter only; applications for the booster are being investigated. Aluminum alloy 2014-T6 was the selected baseline material for orbiter and booster main cryogenic propellant tanks; results of the 2219 vs. 2014 trade study are applicable to orbiter and booster.

Values of \$61.8K/kg (\$28K/lb) for the orbiter and \$12.37K/kg (\$5.6K/lb) for the booster were used to evaluate weight saving in terms of dollars. This dollar value for unit weight indicates the program cost for system resizing to maintain a fixed payload capability.

CRITICAL STRUCTURAL DESIGN TRADE STUDIES

MAIN CRYOGENIC PROPELLANT TANK DESIGN CONCEPTS:

- INTEGRAL VS NON–INTEGRAL TANKS
- COMMON VS SEPARATE TANK BULKHEADS
- COMPARISON OF FORMS OF INTEGRAL STIFFENING

MATERIALS:

- COMPOSITES VS CONVENTIONAL MATERIALS
- 2219 VS 2014 FOR MAIN CRYOGENIC PROPELLANT TANK MATERIAL

Figure 1

MAIN CRYOGENIC PROPELLANT TANK DESIGN CONCEPT
INTEGRAL VS. NON-INTEGRAL TANKS

(FIGURE 2)

Main propellant tanks must be designed to withstand internal operating pressures which include head pressures from ascent acceleration. The resulting structures have inherent potential for withstanding overall body bending and axial loadings with only additional stabilizing elements.

Without the need for an additional structural shell to carry overall loadings, walls of integral tanks can be brought closer to body moldlines and higher packaging efficiencies can result. Additional stiffening to stabilize the pressure wall to carry overall compressive loadings can be provided at considerably less weight than required for an additional, independent structural shell.

Non-integral tanks offer less tank structural and thermal complexity. Suspended within the body shell from statically determinate supports, non-integral tanks need carry only pressure loads and inertia loads from tank and contents. With fewer attachments, non-integral tanks have fewer heat shorts and are less likely to encounter significant thermal stresses and fatigue loadings.

This study evaluates these alternate design concepts for the orbiter vehicle.

MAIN CRYOGENIC PROPELLANT TANK DESIGN CONCEPT INTEGRAL VS. NON-INTEGRAL TANKS

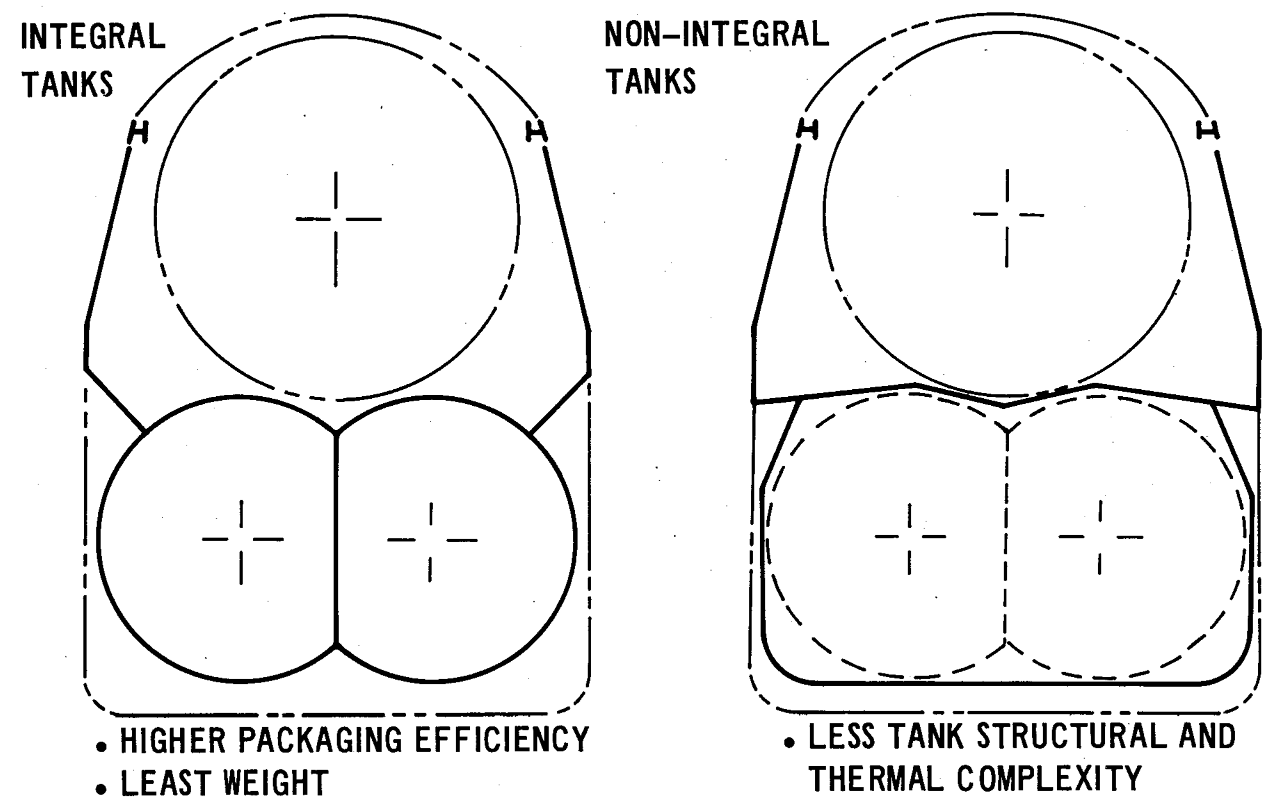

Figure 2

INTEGRAL VS. NON-INTEGRAL TANKS
STUDY METHODOLOGY

(FIGURE 3)

Baseline vehicle for this trade study was the straight wing orbiter, employing integral siamese propellant tanks with a common bulkhead between the oxygen and hydrogen tanks. These tanks extended for most of the vehicle length below the payload bay and crew compartment. Certain assumptions were made to fix overall vehicle geometry for purposes of this study.

Vehicle weight change resulting from the study would not be recycled; therefore, propellant tank geometry, vehicle length, and aerodynamic surfaces were not resized.

The body cross section was increased to accommodate the added body shell with non-integral tanks on the basis of assumed frame depth and moldline clearances.

Fuselage frame spacing of 508 mm (20 in.) was maintained for both configurations to be compatible with TPS support structure locations.

To normalize weight and cost factors in the decision process, the program cost of payload weight change of $61.8K/kg ($28K/lb) was used.

INTEGRAL VS. NON-INTEGRAL TANKS

Study Methodology

- TANK GEOMETRY AND VEHICLE LENGTH HELD CONSTANT
- AERODYNAMIC SURFACE GEOMETRY HELD CONSTANT
- AXIALLY STIFFENED SEMI–MONOCOQUE SHELL STRUCTURE WITH 152.4 MM (6.0 IN.) DEEP FRAMES AT 508.0 MM (20.0 IN.) SPACING
- 63.5 MM (2.5 IN.) MINIMUM ALLOWANCE FOR TPS BETWEEN OUTER MOLD LINE AND NEAREST STRUCTURAL ELEMENT
- RESIZE FOR CONSTANT PAYLOAD: $61.8 K/KG ($28 K/LB)

Figure 3

INTEGRAL VS. NON-INTEGRAL TANKS CONFIGURATION COMPARISON

(FIGURE 4)

Baseline vehicle body structure consists of integral siamese tanks with machined integral stiffening elements and mechanically attached rings and frames, side shear panels forming the upper body moldline, and upper longerons that share overall body loads with the tanks. Payload doors do not carry overall body loads, but stabilize the longerons against column buckling. TPS panels, forming lower side and bottom moldlines, are supported on posts and beams attached to external tank rings. TPS panels and their supports carry local pressure loadings only. A ground purge chamber is provided by a thin pressure wall around the outer flange of the tank rings.

With non-integral tanks, a lower body shell surrounds the tank in cross-section and replaces the integral tank for carrying overall body loads and providing TPS support. Non-integral tanks are suspended within this shell from statically determinate mounting points. A ground purge chamber is provided by the cavity between tank and body shell.

INTEGRAL VS. NON-INTEGRAL TANKS
Configuration Comparison

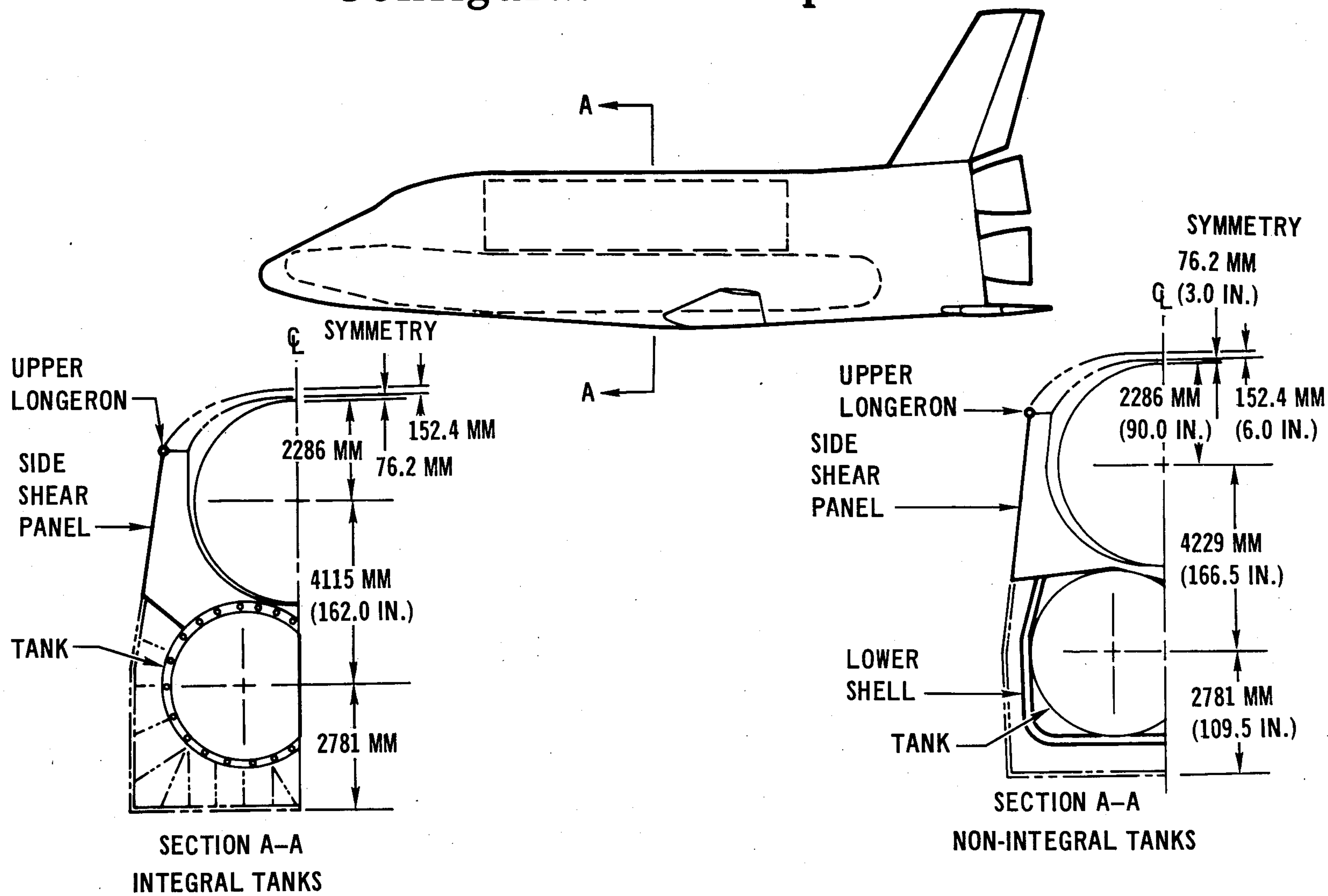

Figure 4

INTEGRAL VS. NON-INTEGRAL TANKS
WEIGHT DIFFERENCE

(FIGURE 5)

Non-integral tanks must withstand bending moments and axial loads from inertia of tanks and contents. These bending moments and axial loads are considerably less than the corresponding overall body forces, which are shared by integral tanks and upper body structure, but must be carried by the non-integral tank acting alone. Consequently, reductions in tank unit loading intensities (running compression and tension loads) were found to be small.

Little weight reduction is realized in tank structure since tank skins are sized for internal pressure and only the weight of stiffening elements can be reduced for reduced unit loads.

A separate liner to contain purge gas circulated around the tanks during prelaunch phase is not required with the non-integral tank; the purge liner function is served by the added body shell.

Body frames which support TPS panels must span the body width without benefit of intermediate support from the tank center web and, thus, incur a major weight penalty with non-integral tanks.

Bending loads carried by the non-integral tank effectively reduce the total bending moments that must be carried by the body structure, lower shell plus longerons. This reduction appears as reduced longeron weight with non-integral tanks.

The major structural weight increase from integral to non-integral tanks is the added weight of the lower body shell.

INTEGRAL VS NON-INTEGRAL TANKS
Weight Difference

ITEM	$\Delta W = W_{NI} - W_I$	REASON
TANK	−45 (−100)	REDUCED INTEGRAL STIFFENING
PURGE LINER	−499 (−1100)	NOT REQUIRED; STRUCTURAL SHELL PROVIDES PURGE WALL
FRAMES	+875 (+1930)	INCREASED SPAN OF LOWER BEAM
LONGERONS	−163 (−360)	REDUCED OVERALL BENDING LOADS
SHEAR PANELS	+45 (+100)	LOCALLY INCREASED SHEAR FLOWS FROM TANK SUPPORTS
LOWER SHELL	+3126 (+6890)	ADDED STRUCTURE
FUSELAGE AREA	+222 (+490)	PROVIDE TANK CLEARANCE
TPS	+76 (+167)	INCREASED FUSELAGE AREA REQUIRING TPS
TOTAL	+3637 KG (+8017 LB)	BASICALLY DUE TO EXTRA SHELL ADDED AROUND TANKS

W_{NI} = WEIGHT OF NON-INTEGRAL TANKS

W_I = WEIGHT OF INTEGRAL TANKS

SUMMARY: NON-INTEGRAL TANK DESIGN IS 3637 KG (8017 LB) HEAVIER THAN INTEGRAL TANK DESIGN FOR THE VEHICLE CONFIGURATION STUDIED

Figure 5

INTEGRAL VS. NON-INTEGRAL TANKS
SUMMARY
(FIGURE 6)

Increased weight with the non-integral tank design amounts to 3637 kg (8017 lb); nearly 90% of this weight is due to the structural shell added around the tank.

Thermal stresses in the propellant tank resulting from thermal gradients between warm upper body structure and cold tank were minimized by designing side panels to carry just shear loads. Tank thermal stresses are maximum at the top of the tank and do not exceed 103.4 MN/m^2 (15 KSI).

Requirements for periodic inspection were considered; consequently, access to the tank without its removal was judged necessary. Access to the integral tank is accomplished more easily (by removal of TPS panels plus purge liner) than access to the non-integral tank (by removal of TPS panels plus structural shell). Also, it was judged that repair of the tank while installed is less costly than tank removal and reinstallation. However, removability appears as an unquantifiable advantage for the non-integral tank.

Development plus investment cost for the orbiter with a non-integral tank was determined to be $48.8M higher than with an integral tank. This cost added to the cost for resizing the system to regain 3637 kg (8017 lb) of payload amounts to a total program cost increase of $273M for the non-integral design.

INTEGRAL VS. NON-INTEGRAL TANKS
Summary

ITEM	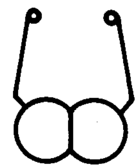 INTEGRAL TANKS	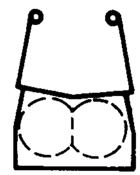 NON–INTEGRAL TANKS	REASON
FUSELAGE CHANGE: HEIGHT WETTED AREA VOLUME WEIGHT		+114.3 MM (+4.5 IN.) +15.5 M^2 (+167 FT^2) +0.436 M^3 (+15.4 FT^3) +3637 KG (+8017 LB)	PRIMARILY DUE TO EXTRA SHELL ADDED AROUND TANKS
TENSILE THERMAL STRESS (PROPELLANT TANK)	SMALL	NEGLIGIBLE	NON–INTEGRAL TANK ISOLATED FROM HOT STRUCTURE
TANK REMOVAL	NOT PRACTICAL	POSSIBLE	TANK REPAIR TECHNIQUES ON COMPLETE CONFIGURATION MAY BE ONLY PRACTICAL APPROACH
TOTAL PROGRAM COST CHANGE	–	\$273,000,000 MORE EXPENSIVE	PRIMARILY DUE TO DECREASED PAYLOAD WEIGHT

Figure 6

INTEGRAL VS. NON-INTEGRAL TANKS
STUDY CONCLUSIONS

(FIGURE 7)

Integral tanks save vehicle weight. Additional stiffening to stabilize the tank wall to withstand overall body loads is considerably lighter than addition of a complete independent body shell.

For the configuration studied, thermal stresses resulting from mutual constraints between cold integral tanks and warm body structure are reduced to acceptable levels by detail design techniques.

The present baseline delta wing orbiter has a body arrangement similar to the straight wing orbiter used for the trade study. Body shaping of the delta wing orbiter to reduce size has reduced outer mold-line to tank clearances below those shown for the study baseline orbiter. As a consequence, clearances for a body shell to permit non-integral tanks would require increase in body width and greater depth than considered in the study and an added weight penalty would result. On the other hand, body bending loads are considerably lower with the delta wing arrangement, and the weight penalty for an added lower shell would be significantly less. A weight penalty of from 2270 to 3630 kg (5000 to 8000 lb) is estimated for non-integral tanks on the present delta wing orbiter; therefore, integral tanks have been selected.

INTEGRAL VS. NON-INTEGRAL TANKS

Study Conclusions

- WITH INTEGRAL TANK DESIGN, THERMAL STRESSES DUE TO TEMPERATURE GRADIENTS THROUGH BODY SECTION ARE NOT PROHIBITIVE
- FOR THE VEHICLE CONFIGURATION STUDIED, INTEGRAL TANK DESIGN SAVES WEIGHT
- INTEGRAL TANK DESIGN HAS LOWER DEVELOPMENT, INVESTMENT, AND TOTAL PROGRAM COSTS

Figure 7

MAIN CRYOGENIC PROPELLANT TANK DESIGN CONCEPT
COMMON VS. SEPARATE TANK BULKHEADS

(FIGURE 8)

Common tank bulkheads were selected for the baseline straight wing orbiter and the baseline booster at the beginning of the Phase B study. Common bulkheads were selected on the basis of subjective evaluations that they would permit minimum vehicle length and total weight.

Separate bulkheads permit complete draining of propellants in the forward tank without running propellant lines from the forward tank through the aft tank. With either tension or compression common bulkheads the weight of residual propellants with LOX forward may exceed the weight saving in structure.

Common versus separate tank bulkheads trade study presented here deals with the common bulkhead in the orbiter siamese tank. Evaluation of common versus separate tank bulkheads for the booster is not covered in this presentation.

MAIN CRYOGENIC PROPELLANT TANK DESIGN CONCEPT
COMMON VS. SEPARATE TANK BULKHEADS

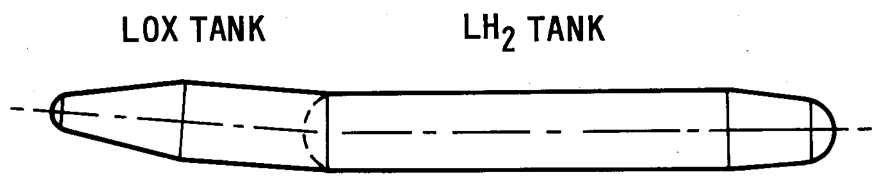

COMMON TANK BULKHEAD

- LEAST STRUCTURAL WEIGHT
- DECREASED FUSELAGE LENGTH AND VEHICLE TOTAL WETTED AREA

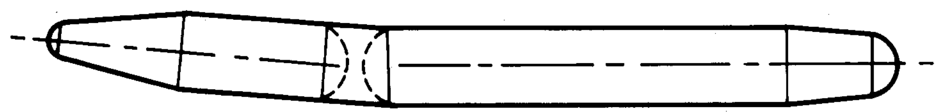

SEPARATE TANK BULKHEADS

- LEAST RESIDUAL LOX

Figure 8

COMMON VS. SEPARATE TANK BULKHEADS
STUDY METHODOLOGY

(FIGURE 9)

The baseline for this study was the straight wing orbiter employing integral siamese propellant tanks with a common bulkhead between the oxygen and hydrogen tanks. Minimum changes were made to incorporate separate bulkheads and orbiter weight was held constant.

With separate bulkheads, vehicle length is increased to accommodate separated tanks necessitating evaluation of additional structure and resizing of existing structure for increased loads.

Based on S-IVB experience, minimum separation distance between common bulkheads to accommodate the LOX tank sump was 635 mm (25 in.).

Methods of evaluating dropout propellants for the common bulkhead configuration were based on methods from NASA CR-59255, modified to account for tilt of liquid levels resulting from non-alignment of tank centerline and thrust vector.

Vertical and horizontal tail surfaces were resized to maintain aerodynamic stability with increased fuselage length, based on MIL-F-8785 short term frequency requirements. Tail weight change was calculated using empirical methods.

COMMON VS. SEPARATE TANK BULKHEADS

Study Methodology

- BODY STRUCTURE EVALUATED TO ACCOUNT FOR VEHICLE LENGTH CHANGE
- TANK SUMP CLEARANCE BASED ON S–IV B EXPERIENCE
- DROPOUT PROPELLANT WEIGHT PER NASA CR–59255
- HORIZONTAL AND VERTICAL TAIL SIZES ADJUSTED FOR VEHICLE LENGTH
- RESIZE FOR CONSTANT PAYLOAD: \$61.8 K/KG (\$28 K/LB)

Figure 9

COMMON VS. SEPARATE TANK BULKHEADS CONFIGURATION COMPARISON

(FIGURE 10)

This is the baseline straight wing orbiter and its modification used in this study.

Increased vehicle length with common bulkheads is partly due to allowance for the LOX tank sump between the bulkheads. With separate bulkheads the LOX tank aft dome is reversed, and the LOX and LH_2 volumes are no longer nested. Additional fuselage length is required to provide this volume.

The fuselage length is increased by adding structure in the inter-tank region; fuselage structure forward and aft of the tanks is not changed.

COMMON VS. SEPARATE TANK BULKHEADS
Configuration Comparison

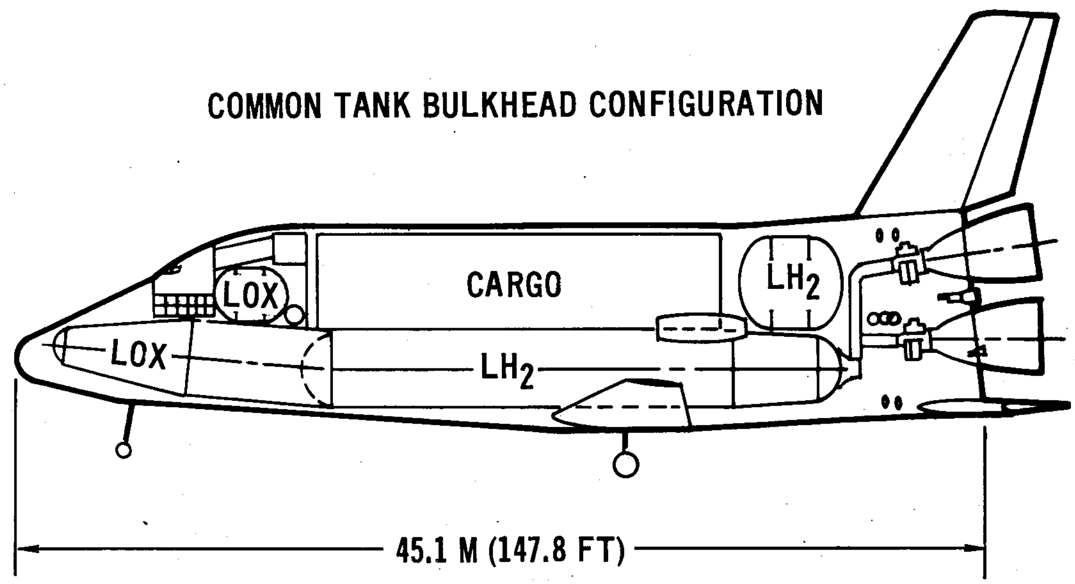

FUSELAGE CHANGES WITH SEPARATE TANK BULKHEADS:

LENGTH = +1321 MM (+52 IN.)

WETTED AREA = +40.69 M^2 (+438 FT^2)

VOLUME = +83.53 M^3 (+2950 FT^3)

Figure 10

COMMON VS. SEPARATE TANK BULKHEADS
BULKHEAD/TANK ASSEMBLY
(FIGURE 11)

A technique has been established for fabricating a common tank bulkhead. Our approach is to construct bulkhead domes of an integrally stiffened plate, formed to a spherical segment, rather than attempting the more complex honeycomb sandwich approach. The two domes are welded to the center forging which eventually is attached to the tank center web with mechanical fasteners. The "Y" ring is a welded assembly of forgings which is subsequently welded to the dome sub-assembly with a single continuous circumferential weld.

The bulkhead assembly is welded to the tank barrel section with a continuous circumferential weld.

COMMON VS. SEPARATE TANK BULKHEADS
Bulkhead/Tank Assembly

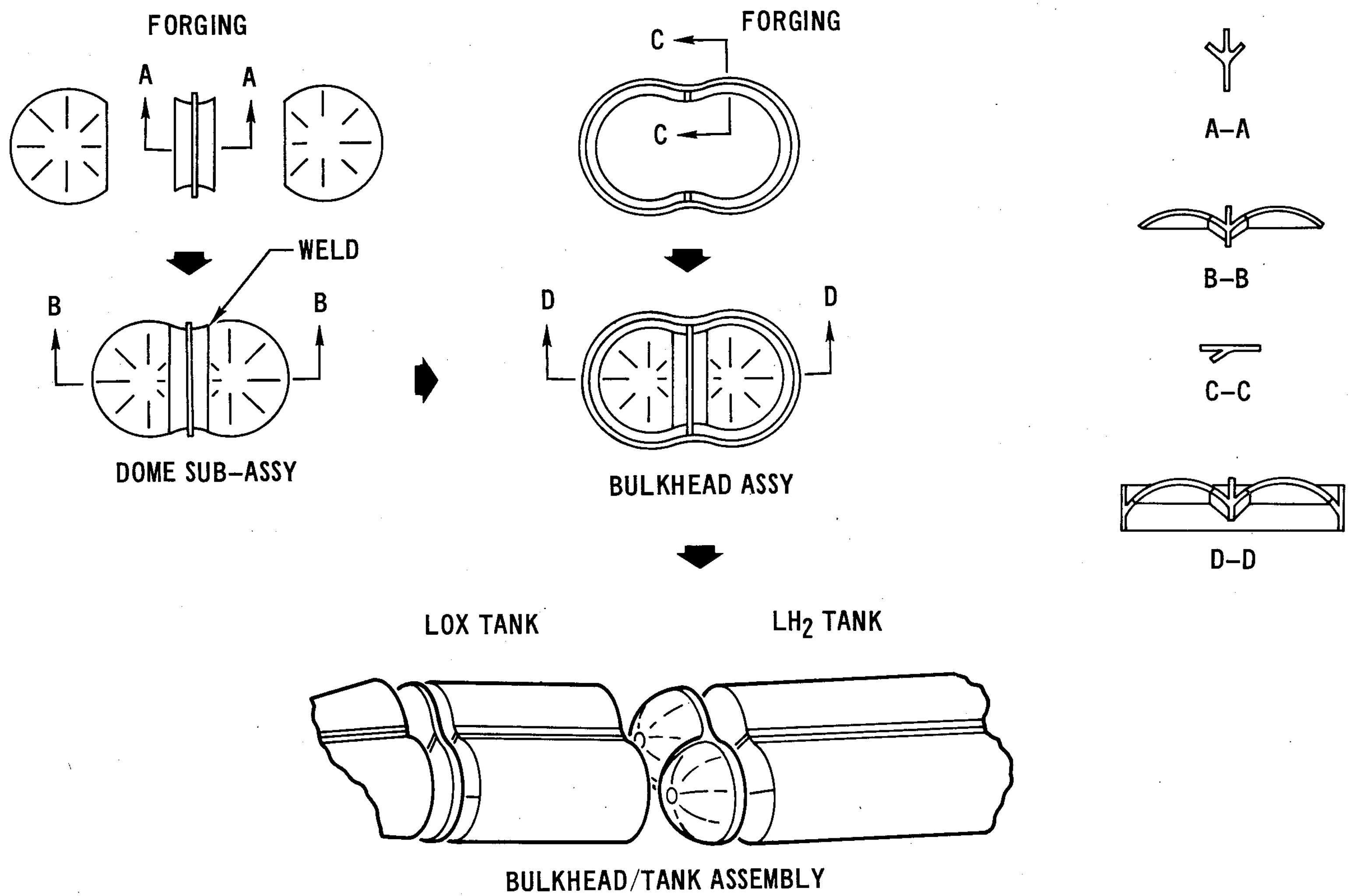

Figure 11

COMMON VS. SEPARATE TANK BULKHEADS
COMPARISON OF MANUFACTURING COMPLEXITY

(FIGURE 12)

Continuous, circumferential, automatic fusion welds are used to join the bulkhead dome sub-assembly to the "Y" ring, and to join the bulkhead assembly to the tank "barrel" section. To facilitate automatic welding across the cusp at the tank top and bottom centerlines, as typified by Section A-A, longitudinal transition sections are provided to allow a radius in the cusp as illustrated in Section B-B. This assembly technique will be employed for the common bulkhead (or separate bulkheads) and for tank end bulkheads.

It became evident that with the integrally stiffened bulkhead approach, the common bulkhead presents no more difficulty than separate bulkheads or end bulkheads, and in fact, was found to be less expensive to manufacture than two separate bulkheads plus inter-tank structure.

Bulkhead and tank assembly procedures are the same for either a tension or compression common bulkhead.

COMMON VS. SEPARATE TANK BULKHEADS

COMPARISON OF MANUFACTURING COMPLEXITY AT BULKHEAD/ CENTER WEB INTERSECTION

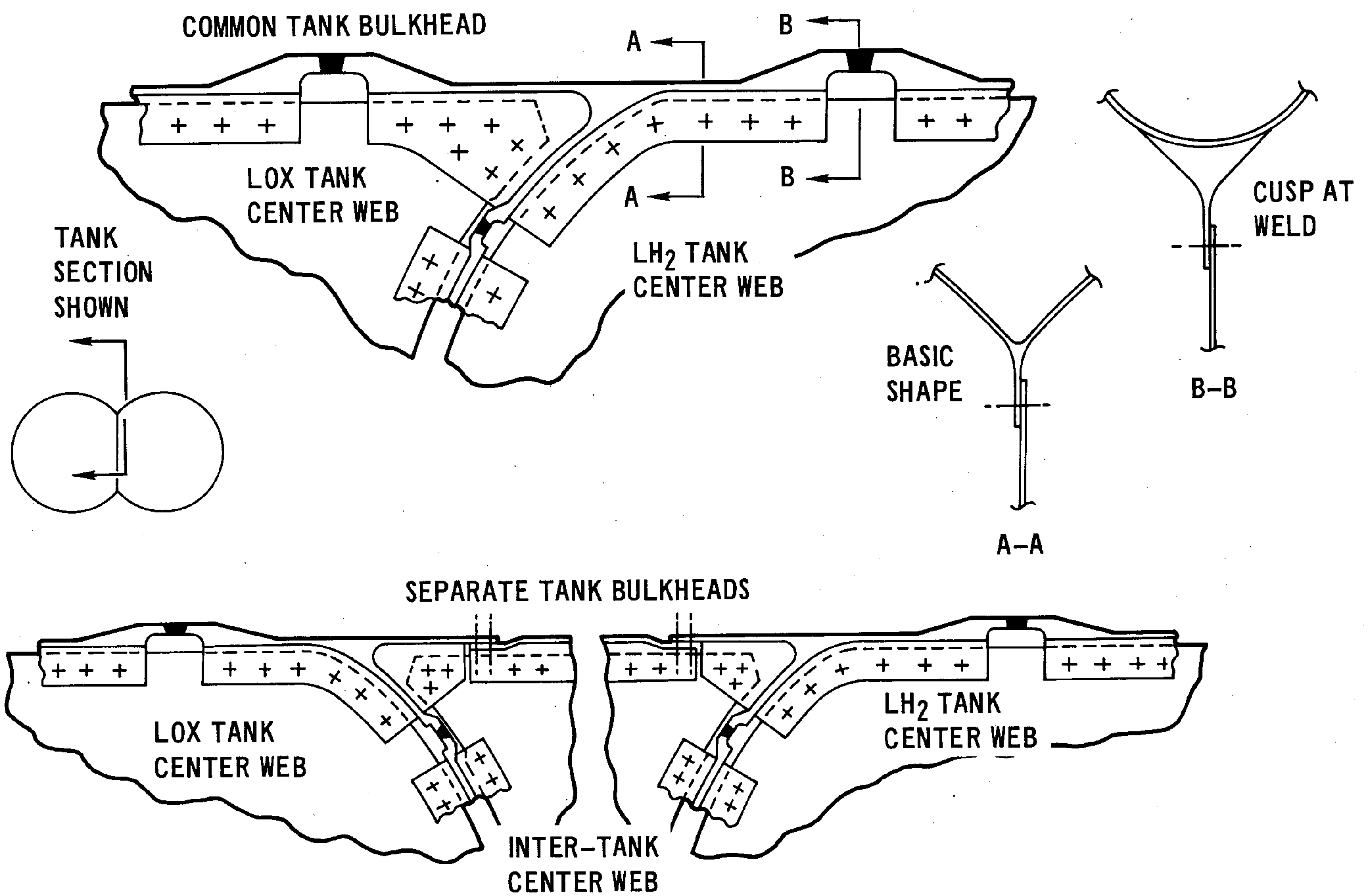

Figure 12

COMMON VS. SEPARATE TANK BULKHEADS WEIGHT DIFFERENCE

(FIGURE 13)

With separate tank bulkheads design there is a net increase of 680 kg (1499 lb) in vehicle inert weight. This consists of increases in weights of structure, TPS and LOX feed lines due to increased vehicle length, and of decreases in weights of bulkheads, LOX tank wall and aerodynamic surfaces.

The 340 kg (749 lb) saving in dropout propellant, possible with separate bulkheads, is relative to the use of a compression common bulkhead in the baseline vehicle.

As part of the trade study, various methods of reducing dropout propellant weight were investigated. Draining liquid oxygen from the bottom of a tension bulkhead by routing the LOX feed line through the LH_2 tank was rejected because of the LOX insulation requirements. Syphoning LOX from the bottom of a tension bulkhead without the formation of gaseous bubbles in the feed line is questionable; therefore, the compression bulkhead configuration was selected. Dropout propellant volume was computed using the method in NASA CR-59255, "Study of Terminal Draining." LOX feed lines were located to take advantage of the "tilt" of the tank centerline relative to the acceleration vector at end of burn. The included angle between the common bulkhead dome and LOX tank wall was established to be 15 degrees, as a minimum practical value for fabrication.

COMMON VS. SEPARATE TANK BULKHEADS

Weight Difference

ITEM	ΔWT* (KG)	ΔWT* (LB)	REASON FOR DIFFERENCE
STRUCTURE	(488)	(1076)	
BULKHEADS	−148	−327	TWO TENSION BULKHEADS WEIGH LESS THAN ONE COMMON COMPRESSION BULKHEAD
LOX TANK WALL	−198	−437	REDUCED LENGTH OF LOX TANK WALL WITH TENSION BULKHEAD
SKIRT	343	756	ADDITIONAL COMPONENT
RESIZED COMPONENTS	332	733	INCREASED LOADS DUE TO INCREASED VEHICLE LENGTH
UPPER FUSELAGE	115	253	ADDITIONAL VEHICLE LENGTH
CONTINGENCY (10%)	44	98	
THERMAL PROTECTION SYSTEM	(321)	(707)	
TPS MATERIAL	292	643	ADDITIONAL VEHICLE AREA
CONTINGENCY (10%)	29	64	
MAIN PROPULSION SYSTEM	(42)	(93)	
LOX FEED LINE	40	88	ADDITIONAL LENGTH OF LINE
CONTINGENCY (5%)	2	5	
AEROSURFACES	(−171)	(−377)	
HORIZONTAL TAIL	−64	−142	CG SHIFT
VERTICAL TAIL	−107	−235	CG SHIFT
DROPOUT PROPELLANT	−340	−749	BULKHEAD SHAPE & ORIENTATION
TOTAL =	+340	+750	

SUMMARY: SEPARATE TANK BULKHEADS ARE 340 KG (750 LB) HEAVIER THAN COMMON TANK BULKHEAD

*ΔWT = WEIGHT DIFFERENCE OF SEPARATE TANK BULKHEADS DESIGN COMPARED TO COMMON TANK BULKHEAD DESIGN

Figure 13

COMMON VS. SEPARATE TANK BULKHEADS
SUMMARY
(FIGURE 14)

Orbiter size and weight increase with separate tank bulkheads.

Program cost increase with separate bulkheads includes development and investment costs plus cost of resizing the system to regain 340 kg (750 lb) of payload at $61.8K/kg ($28K/lb).

COMMON VS. SEPARATE TANK BULKHEADS

Summary

ITEM	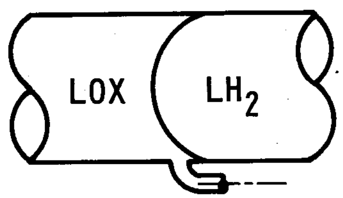 COMMON TANK BULKHEAD	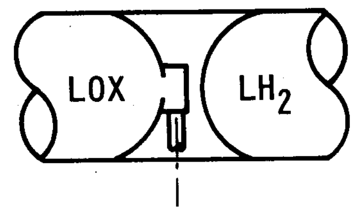 SEPARATE TANK BULKHEADS	REASON
FUSELAGE CHANGES: LENGTH WETTED AREA VOLUME WEIGHT	–	 +1321 MM (+52 IN.) +40.69 M^2 (+438 FT^2) +83.53 M^3 (+2950 FT^3) +340 KG (+750 LB)	PRIMARILY DUE TO INCREASED LENGTH OF FUSELAGE
TOTAL PROGRAM COST CHANGE	–	+ $30,950,000	PRIMARILY DUE TO DECREASED PAYLOAD WEIGHT

Figure 14

COMMON VS. SEPARATE TANK BULKHEADS
STUDY CONCLUSIONS

(FIGURE 15)

For the orbiter vehicle studied, the cost for fabricating one common bulkhead was found to be less than the cost for two separate bulkheads plus inter-tank structure; there are fewer parts, fewer welds and fewer pounds of structure.

Orbiter weight was less with the common tank bulkhead design; this results primarily from the fuselage having less length and less surface area.

Structural weight saving with the common tank bulkhead was halved by the weight of dropout propellant (LOX). Dropout propellant volume was computed using methods for cylindrical, non-tilted tanks; analytical corrections were applied for tank centerline to thrust line angularity.

Vehicle configuration changes will be monitored for effects on the selection of the common tank bulkhead design for the orbiter.

A similar study was made using the canard booster with LOX forward as a baseline. Small cost and weight savings were indicated for the common tank bulkhead approach; however, vehicle configurational considerations resulted in the selection of a separate bulkhead design for the booster. Current configuration studies of the booster are again addressing the question of common vs. separate tank bulkheads in conjunction with locating LOX aft.

COMMON VS. SEPARATE TANK BULKHEADS

Study Conclusions

- COMMON TANK BULKHEAD DESIGN COSTS LESS
- COMMON TANK BULKHEAD DESIGN WEIGHS LESS
- WEIGHT DIFFERENCE IS SENSITIVE TO DROPOUT PROPELLANT VOLUME
- CONCLUSIONS ARE HIGHLY SENSITIVE TO VEHICLE CONFIGURATION AS IT AFFECTS RESIDUAL PROPELLANT WEIGHT
- CONFIGURATION RELATED ADVANTAGES CAN JUSTIFY SELECTION OF EITHER DESIGN

Figure 15

COMPARISON OF FORMS OF INTEGRAL STIFFENING
REASONS FOR STUDY
(FIGURE 16)

Propellant tankage represents a significant portion of structural mass fraction. To achieve minimum weight tankage, stiffening arrangements with high resistance to buckling deformations required evaluation. Minimum tank penetrations for pressure adequacy dictated investigation of integral stiffening approaches.

Minimization of vehicle weight required evaluation of overall configuration effects on tank stiffening arrangement. Secondary loadings, such as result from support of the thermal protection system (TPS), and secondary structural functions, such as discrete rings integrating into adjacent structure, required study.

Evaluation of these considerations provides preliminary selection of stiffening arrangement for orbiter and booster main propellant tanks.

COMPARISON OF FORMS OF INTEGRAL STIFFENING
Reasons for Study

- MINIMUM WEIGHT REQUIRES STIFFENED STRUCTURE
- MINIMUM TANK PENETRATIONS DICTATE INTEGRAL STIFFENING
- OVERALL CONFIGURATION IMPACTS STIFFENING ARRANGEMENT
- IDENTIFY WEIGHT DIFFERENCES FOR SELECTED INTEGRAL STIFFENING APPROACHES.

Figure 16

COMPARISON OF FORMS OF INTEGRAL STIFFENING
DESCRIPTION OF CONCEPTS TRADED

(FIGURE 17)

Concepts evaluated were isogrid, 0° - 90° waffle, 0° - 90° waffle with discrete attached rings, and 45° waffle. Intrinsic stiffness associated with these approaches yields high buckling efficiencies.

When each candidate stiffening concept was sized to react just overall body loads, 0° - 90° waffle with discrete rings and isogrid both had greater residual capability to react circumferential bending load than either 0° - 90° waffle or 45° waffle. 0° - 90° waffle with deep, discrete stiffening rings accommodates circumferential bending loads (resulting from TPS support) with minimum weight. Isogrid, however, has a large number of potential attachment points (at the nodes) and thereby provides greater design flexibility to accommodate attachments to the tank.

While 0° - 90° waffle and 45° waffle stiffening concepts were competitive when sized to react just overall body loads, neither provided a mechanism as efficient as isogrid or 0° - 90° waffle with discrete rings for distributing point load introduction into the tank. Consequently, further investigation of these two forms of integral stiffening was not performed.

COMPARISON OF FORMS OF INTEGRAL STIFFENING

Description of Concepts Traded

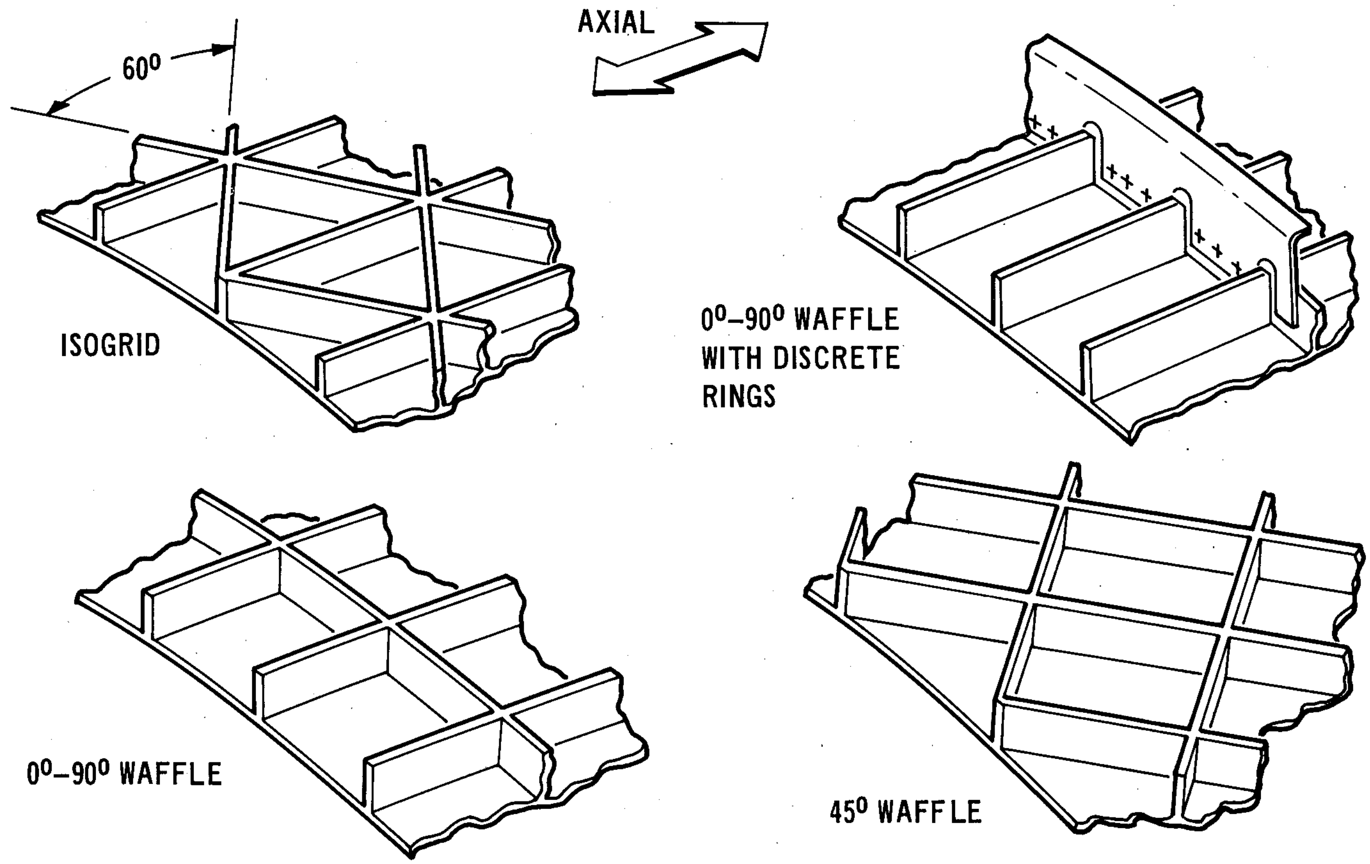

Figure 17

COMPARISON OF FORMS OF INTEGRAL STIFFENING
KEY FACTORS CONSIDERED
(FIGURE 18)

Material placement to match the maximum number of failure modes will generally result in minimum weight for buckling. Four primary failure modes were considered in this study: (1) general instability, (2) panel instability, (3) plate buckling, and (4) local crippling. Consideration of interaction between failure modes should be made in more refined design analyses to prevent premature overall instability failures precipitated by interacting with local failure modes. One approach to preventing this possibility with an insignificant weight penalty is to "design in" higher local failure mode allowables.

Integration of stiffening arrangement into the overall configuration requires consideration of external pressure load introduction into the tank and integration of the tank into the primary fuselage structure. The first consideration relates to both orbiter and booster, whereas the second relates primarily to the orbiter. For the orbiter, high unsymmetrical load introduction into the tanks results from support of TPS panels on a non-axisymmetric moldline. Deep, discrete rings can efficiently carry these loads and are easily integrated into the upper frames which stabilize longerons and support side shear panels.

Consideration of fabrication constraints/complexity unique to each concept is important. Minimum practical gage is judged to be 1 mm (0.04 in.). A typical 0° - 90° waffle geometry section for the orbiter was machined from representative plate stock and verified this judgement. It is felt that this is a reasonable value for the study concepts. Allowance for sufficient circumferential rib depth to accommodate ring attachment was made.

COMPARISON OF FORMS OF INTEGRAL STIFFENING

Key Factors Considered

- MATERIAL PLACEMENT TO MATCH MAXIMUM NUMBER OF FAILURE MODES
- INFLUENCE OF STIFFENING ARRANGEMENT ON OVERALL CONFIGURATION STRUCTURAL WEIGHT
- FABRICABILITY:
  - MINIMUM GAGE CONSTRAINTS
  - DISCRETE RING ATTACHMENT REQUIREMENTS

Figure 18

COMPARISON OF FORMS OF INTEGRAL STIFFENING
UNIT WEIGHT COMPARISON
ISOGRID VS. 0° - 90° WAFFLE (WITH DISCRETE RINGS) FOR ORBITER

(FIGURE 19)

Comparison of unit weight for axial compressive stability of representative orbiter main propellant tank material, geometry, and internal pressure indicated insignificant differences between isogrid and 0° - 90° waffle with discrete rings. The basic difference in load paths between these two approaches is that 0° - 90° waffle carries essentially all the hoop pressure load as hoop membrane load; whereas isogrid skin shares the hoop pressure loading with the integral ribs. Evaluation of hoop pressure load sharing for the 0° - 90° waffle geometry resulted in less than a 5% weight saving as some of the skin material had to be replaced in axial stiffening to keep the same axial compressive buckling failure mode allowables. This results in the skin thickness for 0° - 90° waffle being sized to carry all the hoop pressure load. This defines the minimum skin thickness which also resulted in minimum weight for axial compressive loading for the range of parameters considered.

Donnell type stability differential equations with bifurcation from a membrane prebuckled shape were used for general and panel instability allowables. Checks made with the full Flügge differential equations indicated that the higher order terms neglected by the Donnell equations had negligible effect for the study.

COMPARISON OF FORMS OF INTEGRAL STIFFENING
Unit Weight Comparison

ISOGRID VS 0°–90° WAFFLE (WITH DISCRETE RINGS) FOR ORBITER

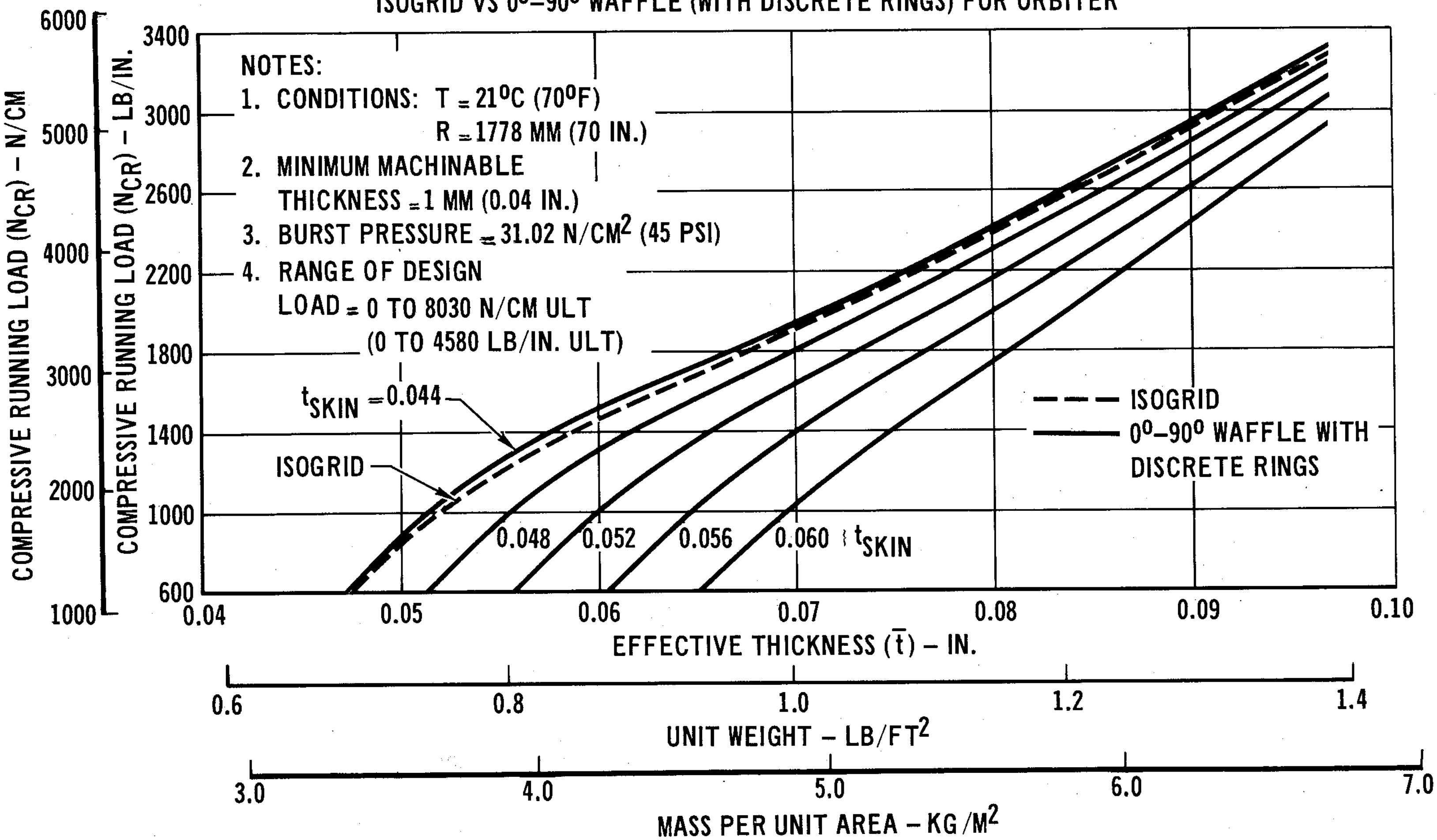

Figure 19

COMPARISON OF FORMS OF INTEGRAL STIFFENING
UNIT WEIGHT COMPARISON
ISOGRID VS. 0° - 90° WAFFLE (WITH DISCRETE RINGS) FOR BOOSTER

(FIGURE 20)

Similar conclusions result when the unit weights of these stiffening concepts are compared for booster application. Reduction in unit weight can be obtained for each concept by flanging the stiffeners; however, this results in an increase in manufacturing complexity.

COMPARISON OF FORMS OF INTEGRAL STIFFENING

Unit Weight Comparison

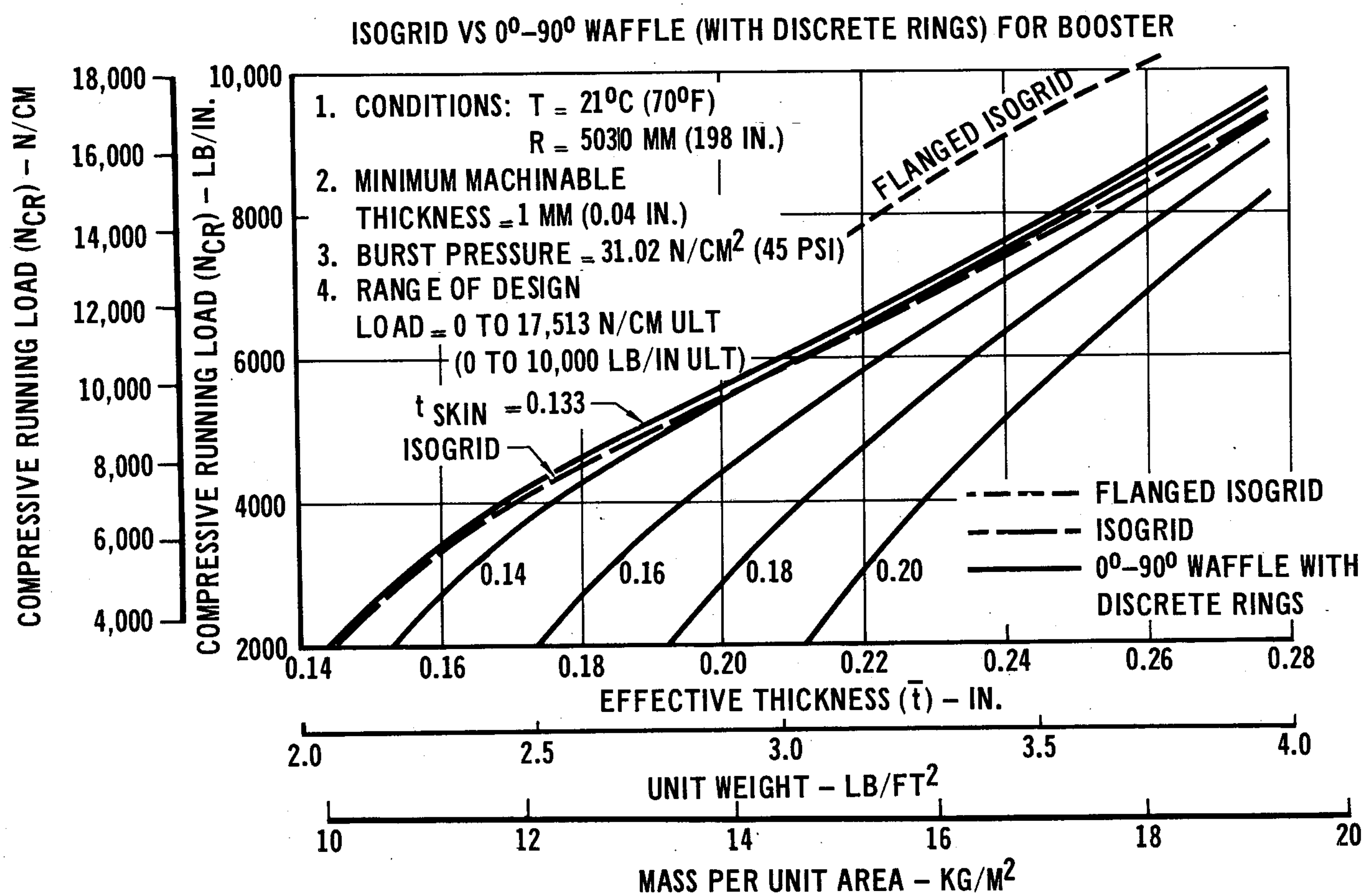

Figure 20

COMPARISON OF FORMS OF INTEGRAL STIFFENING
STUDY CONCLUSIONS
(FIGURE 21)

Weight penalty associated with reaction of secondary loads led to exclusion of 0° - 90° and 45° waffle designs without discrete rings from in-depth analysis.

Selection of stiffening concept between 0° - 90° waffle with discrete rings and isogrid is not conclusive if only tank structure is considered; the difference in unit weight and in fabrication cost is inconsequential (to the extent that assessment is accurate without fabrication of representative structure).

Secondary loadings and overall structural arrangement influenced stiffening concept selection for orbiter and booster. For the orbiter, selection of 0° - 90° waffle with discrete rings resulted in a 544 to 680 kg (1200 to 1500 lb) weight advantage over isogrid. Weight difference is primarily due to (1) reaction of high unsymmetrical loads with deep discrete rings; (2) circumferential variation of spacing of integral axial stiffeners to match circumferential changes in applied compressive running load due to bending moment predominance; (3) integration of discrete rings into fuselage upper frames for stabilization of longerons and support of side shear structure.

For the booster, selection of flanged isogrid was made for these reasons: (1) the combination of a near-axisymmetric aerodynamic fuselage moldline and an axisymmetric tank did not produce significant circumferential bending and thus eliminated an inherent weight advantage associated with deep rings; (2) predominance of axial loading resulted in small circumferential variation in running load and thus minimized the advantage of varying axial stiffener spacing.

COMPARISON OF FORMS OF INTEGRAL STIFFENING

Study Conclusions

- SELECTION OF INTEGRAL STIFFENING CONCEPT IS NOT CONCLUSIVE IF ONLY TANK STRUCTURE IS CONSIDERED:
  - SMALL WEIGHT DIFFERENCE
  - SMALL FABRICATION COST DIFFERENCE
- SELECTION OF INTEGRAL STIFFENING CONCEPT IS SENSITIVE TO SECONDARY LOADINGS AND OVERALL STRUCTURAL ARRANGEMENT

$\boxed{\text{FLANGED ISOGRID SELECTED FOR BOOSTER}}$

$\boxed{0^{\circ}\text{–}90^{\circ}\ \text{WAFFLE WITH DISCRETE RINGS SELECTED FOR ORBITER}}$

Figure 21

MATERIALS

COMPOSITES VS. CONVENTIONAL MATERIALS

(FIGURE 22)

Development of composite materials has progressed such that some composites can be used on shuttle vehicles without high risk. This study was performed to define potential weight and cost savings through use of composite materials on the orbiter; applications were limited to those requiring only minimum advancement of composites state-of-the-art.

Boron/epoxy and boron/aluminum were considered the most likely materials for low and moderate temperature applications in 1973.

MATERIALS
COMPOSITES VS. CONVENTIONAL MATERIALS

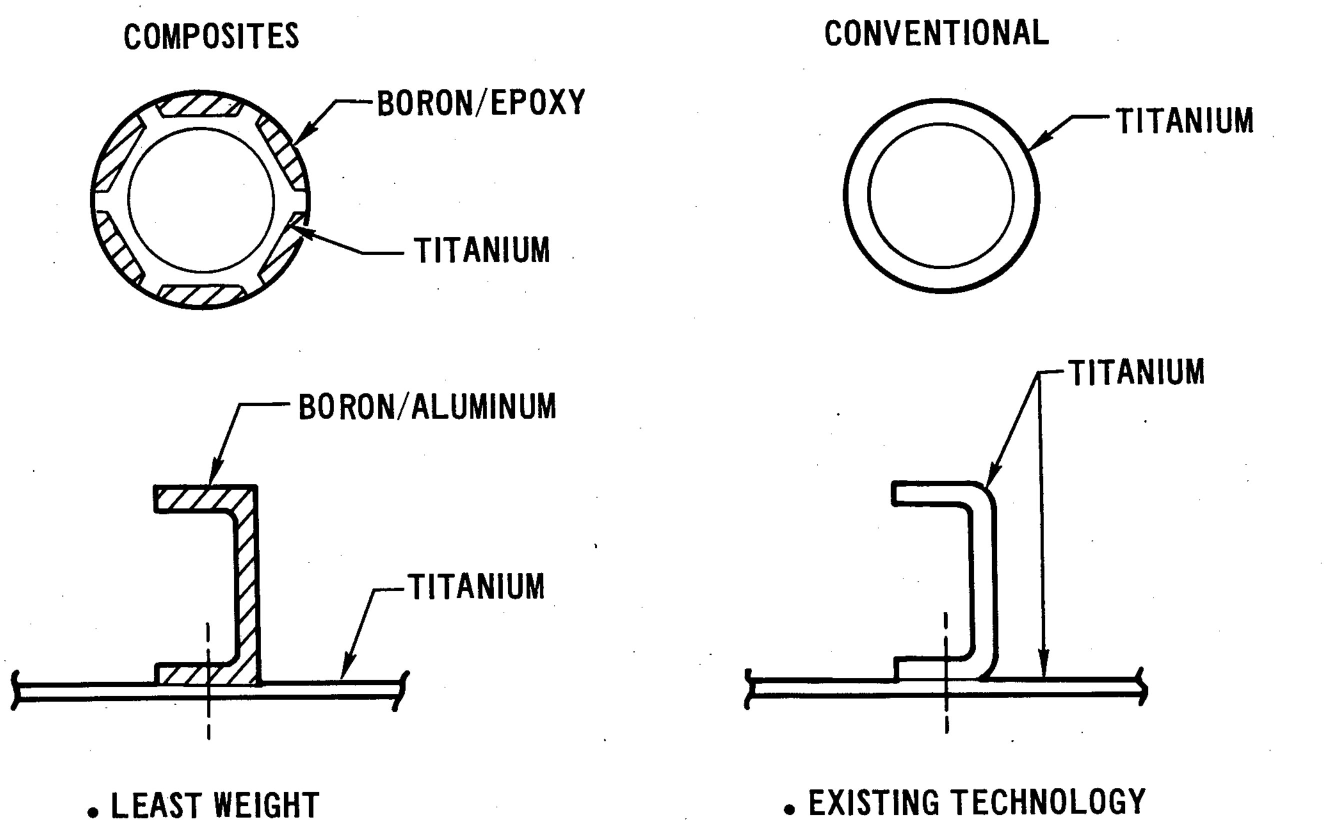

Figure 22

COMPOSITES VS. CONVENTIONAL MATERIALS
STUDY METHODOLOGY
(FIGURE 23)

Temperature limits indicated for boron/epoxy and boron/aluminum are expected 100 mission reuse temperatures.

To minimize risk of delay in technology development it was decided to limit composite elements to applications where metallic elements could be substituted if necessary. Straight, uniaxial elements were selected as the simplest to manufacture.

To facilitate replacement of composites with conventional metal elements and to minimize development requirements, all composite elements are mechanically attached to other structure.

It is assumed that SR&T recommended funding will assure the adequate development of composite technology by 1973.

COMPOSITES VS. CONVENTIONAL MATERIALS

Study Methodology

- MAXIMUM TEMPERATURE FOR REUSE: BORON/EPOXY 176^{o}C (350^{o}F); BORON/ALUMINUM 370^{o}C (700^{o}F)
- STRAIGHT UNIAXIAL STRUCTURAL ELEMENTS
- COMPOSITE STRUCTURAL ELEMENTS ARE MECHANICALLY ATTACHED AND DIRECTLY REPLACED WITH METALLIC COUNTERPARTS
- RESIZE FOR CONSTANT PAYLOAD: $61.8 K/KG ($28 K/LB)
- SR&T RECOMMENDED FUNDING WILL ASSURE COMPOSITE STRUCTURE TECHNOLOGY IN 1973

Figure 23

COMPOSITES VS. CONVENTIONAL MATERIALS
SELECTED COMPOSITE MATERIAL APPLICATIONS FOR ORBITER VEHICLE
(FIGURE 24)

Areas for composite applications are shown for the baseline delta orbiter.

Boron/epoxy was selected for thrust structure tubes. Temperatures in this region of the orbiter do not exceed 176°C (350°F) because of thermal protection requirements imposed by engine power heads and equipment items.

Boron/aluminum was selected for the remaining applications, which include stiffeners for wing skin panels, fuselage shear panels and payload doors, and caps for fuselage frames. In these applications, boron/aluminum elements are not exposed to temperature exceeding 370°C (700°F).

COMPOSITES VS. CONVENTIONAL MATERIALS

Selected Composite Material Applications for Orbiter Vehicle

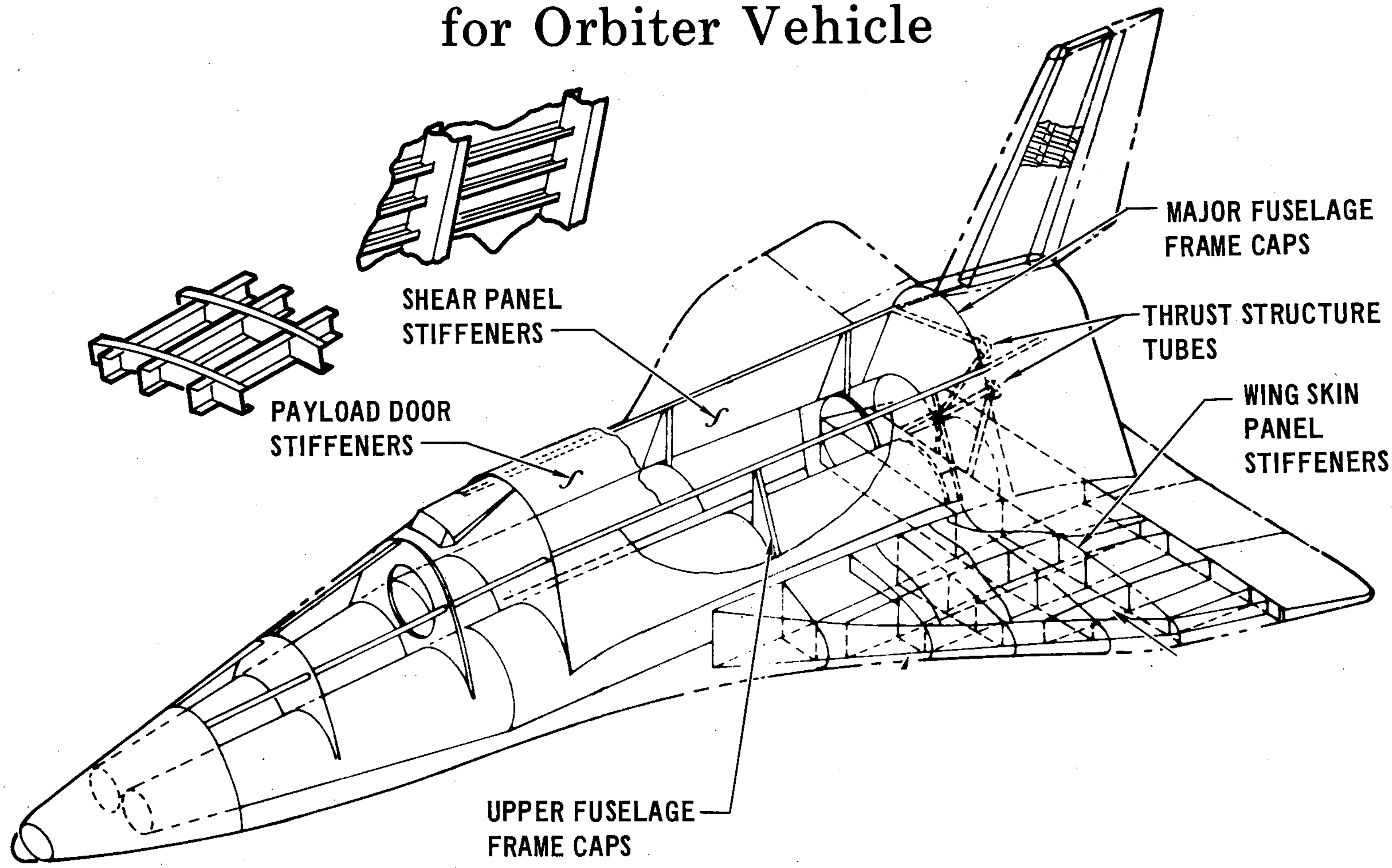

Figure 24

COMPOSITES VS. CONVENTIONAL MATERIALS
CROSS SECTIONS OF SELECTED COMPOSITE MATERIAL APPLICATIONS
(FIGURE 25)

Thrust structure tubes consist of uniaxial boron/epoxy composite overlay on titanium tubes. Tubes are 2.4 to 3.7 m (8 to 12 ft) in length, 254 to 305 mm (10 to 12 in.) in diameter, with 4.0 to 6.5 mm (.16 to .26 in.) thick boron/epoxy composite overlay.

Fuselage frame outer caps are boron/aluminum composite. The straight cap elements have 18 to 25 mm (.7 to 1.0 in.) flanges that are .61 to 2.54 mm (.024 to .100 in.) thick. The cap elements, which extend from the upper longerons to main cryogenic propellant tank rings, are up to 3.7 m (12 ft) in length.

Stiffeners for fuselage shear panels, payload door and wing skin panels are also boron/aluminum composite. Stiffeners for fuselage shear panels and payload door are 20.3 to 38.1 mm (.8 to 1.5 in.) in height, 0.61 to 1.00 mm (.024 to .040 in.) in thickness, and up to 1.01 m (3.33 ft) in length. Wing skin panel stiffeners are 20.3 to 63.5 mm (0.8 to 2.5 in.) in height, 0.61 to 5.10 mm (.024 to .200 in.) in thickness, and up to 12.2 m (40.0 ft) in length.

COMPOSITES VS. CONVENTIONAL MATERIALS

CROSS SECTIONS OF SELECTED COMPOSITE
MATERIAL APPLICATIONS

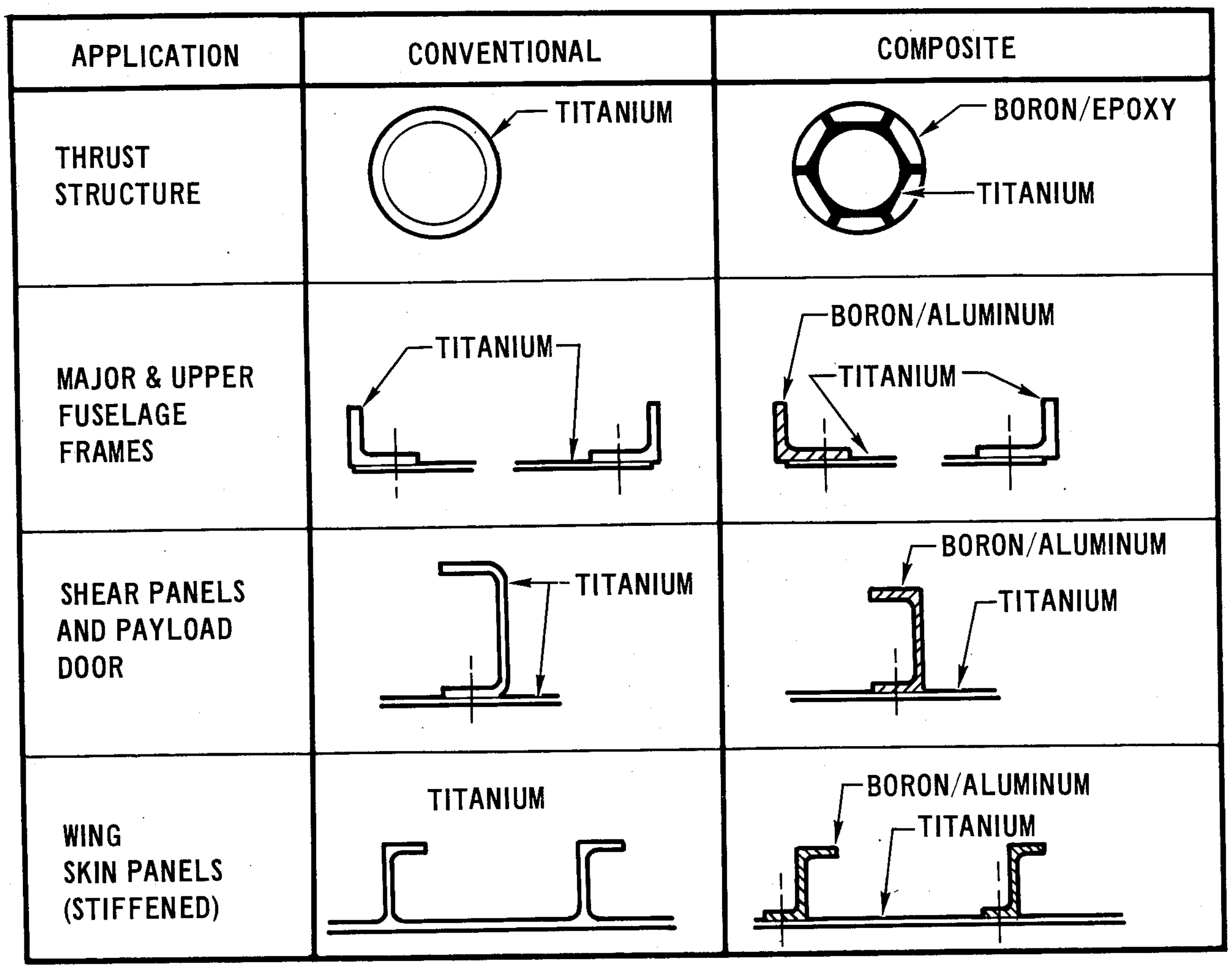

Figure 25

COMPOSITES VS. CONVENTIONAL MATERIALS
POTENTIAL WEIGHT SAVING WITH COMPOSITE MATERIALS

(FIGURE 26)

Through use of uniaxial, replaceable composite elements, a weight saving of 1323 kg (2916 lb) can be realized out of over 10,000 kg (22,000 lb) of structure considered in this study.

Baseline weight is the weight of the total baseline structure studied. The weight saving with composites is the net weight change from the baseline conventional metal structure to the structure employing composite elements together with conventional metal elements, and includes weight from resizing metallic elements where required.

COMPOSITES VS. CONVENTIONAL MATERIALS
Potential Weight Saving With Composite Materials

APPLICATION	DELTA WING ORBITER			
	BASELINE WEIGHT		WEIGHT SAVING WITH COMPOSITES	
	KG	LB	KG	LB
THRUST STRUCTURE UTILIZE BORON/EPOXY OVER TITANIUM THRUST TUBES	744	1640	184	406
PAYLOAD DOOR UTILIZE BORON/ALUMINUM STIFFENERS	887	1955	59	130
INTERMEDIATE FUSELAGE FRAMES UTILIZE BORON/ALUMINUM FRAME CAPS	1828	4030	186	410
SHEAR PANELS UTILIZE BORON/ALUMINUM STIFFENERS	1452	3200	170	374
WING SKIN/STIFFENERS UTILIZE BORON/ALUMINUM STIFFENERS	2116	4664	530	1168
MAJOR FUSELAGE FRAMES (WING ATTACH, INTERCONNECT TAIL SUPPORT FRAMES, ETC.) UTILIZE BORON/ALUMINUM FRAME CAPS	3166	6980	194	428
			TOTAL 1323 KG	TOTAL 2916 LB

Figure 26

COMPOSITES VS. CONVENTIONAL MATERIALS
POTENTIAL COST SAVING WITH COMPOSITE MATERIALS

(FIGURE 27)

The cost for boron/epoxy and boron/aluminum composite materials applications is $50.3 M and includes RDT&E, investment and operational costs. The dollar value of the 1323 kg (2916) lb) weight saving resulting from these applications is $81.5 M based upon resizing to maintain constant payload at $61.8 K/kg ($28 K/lb). The net program saving is $31.2 M and is the difference between the cost for composite materials application and the dollar value of the weight saving.

SR&T funding to assure adequate development of composite technology by 1973 is estimated to be $.5 M for boron/epoxy and $5.0 M for boron/aluminum.

COMPOSITES VS. CONVENTIONAL MATERIALS

Potential Cost Saving With Composite Materials

	DELTA WING ORBITER COMPOSITE MATERIAL APPLICATIONS	
	BORON/EPOXY THRUST STRUCTURE TUBES	BORON/ALUMINUM ELEMENTS
COST FOR COMPOSITE APPLICATION	$2.9 M	$47.4 M
WEIGHT SAVING	184 KG (406 LB)	1139 KG (2510 LB)
VALUE OF WEIGHT SAVING	$11.3 M	$70.2 M
NET PROGRAM SAVING	$8.4 M	$22.8 M

Figure 27

COMPOSITES VS. CONVENTIONAL MATERIALS
STUDY CONCLUSIONS

(FIGURE 28)

This trade study, which included technical and econometric analyses, has shown that a significant program cost saving can be realized through relatively limited use of boron/epoxy and boron/aluminum composites on the orbiter vehicle. This saving is possible with minimal technological advancement and risk, and can be obtained through applications that are less complex than experimental structures which have been fabricated for test.

Composites should be used in orbiter structures where total vehicle requirements can be met by composite elements of the type studied.

COMPOSITES VS. CONVENTIONAL MATERIALS

Study Conclusions

- BORON/EPOXY USED FOR THRUST STRUCTURE TUBES WILL SAVE PROGRAM COST
- BORON/ALUMINUM USED FOR STRAIGHT UNIAXIAL STIFFENERS AND FRAME CAPS WILL SAVE PROGRAM COST
- UTILIZE COMPOSITES FOR THE SELECTED APPLICATIONS AND FOR SIMILAR APPLICATIONS WHERE PROGRAM COST CAN BE SAVED WITH REPLACEABLE UNIAXIAL COMPOSITE STRUCTURAL ELEMENTS.

Figure 28

MATERIALS

2219 VS. 2014 FOR MAIN CRYOGENIC PROPELLANT TANK MATERIAL

(FIGURE 29)

Aluminum alloy 2014-T6 was baselined for orbiter and booster vehicles at outset of the Phase B study. Selection was based upon the fact that 2014 has higher ultimate and yield strength than 2219 and that a number of booster vehicles, e.g., the S-IVB, S-II and Titan series, have been constructed of 2014 alloy.

Aluminum alloy 2219-T87 was considered a rival candidate because of its superior stress corrosion resistance and its successful usage on the S-IC booster. This study was performed to compare 2219 with 2014 and to select the material which best meets shuttle requirements.

MATERIALS
2219 VS. 2014 FOR MAIN CRYOGENIC PROPELLANT TANK MATERIAL

ALUMINUM ALLOY 2219–T87

- SUPERIOR STRESS CORROSION RESISTANCE

ALUMINUM ALLOY 2014–T6

- HIGHER ULTIMATE AND YIELD STRENGTH
- EXTENSIVE USE IN BOOSTER APPLICATIONS

Figure 29

2219 VS. 2014 FOR MAIN CRYOGENIC PROPELLANT TANK MATERIAL
STUDY APPROACH

(FIGURE 30)

Comparison of 2219 with 2014 was based primarily on published data. Adequate data are available to evaluate weight based on factor of safety design, sensitivity to stress corrosion, and fabrication techniques. Adequate data are not available to assess with confidence tank weight based upon analyses to assure required tank life. Fracture strength and crack growth data for both 2219 and 2014 in thicknesses of interest are not found in the literature; therefore, tests are being performed during Phase B to provide these data for both parent metals and welds. These data will facilitate definition of allowable operating stresses, proof stresses, and NDE requirements to achieve a required tank life.

2219 VS. 2014 FOR MAIN CRYOGENIC PROPELLANT TANK MATERIAL

Study Approach

- USE AVAILABLE DATA
- PERFORM STATIC AND CYCLIC FRACTURE TESTS

Figure 30

2219 VS. 2014 FOR MAIN CRYOGENIC PROPELLANT TANK MATERIAL FACTORS CONSIDERED

(FIGURE 31)

Major factors influencing material selection are structural weight, susceptibility to stress corrosion, and fabrication considerations.

Tank weights for the factor of safety approach were based on MIL-HDBK-5 data. For the fracture mechanics approach, tank weights were based on published data that indicate flawed specimens of 2219 and 2014 have similar values for both static and cyclic strength. Results from Phase B testing generally agree with these published data.

The significance of stress corrosion threshold limits on material selection is influenced by the fabrication process and by methods used subsequently to minimize residual stress particularly in the short transverse grain direction.

2219 VS. 2014 FOR MAIN CRYOGENIC PROPELLANT TANK MATERIAL

Factors Considered

- TANK WEIGHT COMPARISONS BASED ON:
  - FACTOR OF SAFETY
  - FRACTURE MECHANICS
- STRESS CORROSION THRESHOLD:
  - PARENT MATERIAL
  - WELDMENTS
- FABRICABILITY:
  - FORMABILITY
  - WELDABILITY

Figure 31

2219 VS. 2014 FOR MAIN CRYOGENIC PROPELLANT TANK MATERIAL

TANK WEIGHT DIFFERENCE

(FIGURE 32)

The difference between weights of tanks made of 2219 and 2014 was computed for two cases: (1) design for a factor of safety (FS = 1.5) ultimate strength, and (2) design for a life of 1000 pressurizations.

With the factor of safety approach, booster tank weight is proportionally less sensitive to material selection than orbiter tank weight. For plates 63.5 mm (2.5 in.) in thickness as required for booster tanks, ultimate tensile strength of 2014 is just 6.9 MN/m^2 (1.0 KSI) greater than 2219. In addition, much of the booster LH_2 tank wall is sized for stability to withstand axial compressive loading rather than for tensile strength to withstand pressure. For plates 38.1 mm (1.5 in.) in thickness as required for orbiter tanks, ultimate tensile strength of 2014 is over 13 percent greater than 2219. Orbiter LOX and LH_2 tank wall gages are determined by pressure requirements; consequently, tank weight varies inversely with material tensile strength.

On the basis of fracture mechanics analyses, tensile yield rather than ultimate strength influences the weight of tankage designed for a life of 1000 pressurizations. The proof stress level to screen flaws was assumed to equal 0.9 F_{ty}. In both 63.5 and 38.1 mm (2.5 and 1.5 in.) plate material, 2014 has greater yield strength than 2219. At the reduced operating stresses to achieve a life of 1000 pressurizations, the booster LH_2 tank skin is sized to withstand pressure; consequently, the tank weight increase with 2219 material is more nearly in proportion to booster and orbiter tank weights.

Fracture mechanics analyses were based on published fracture strength and crack growth data for 2014 and 2219 specimens 15.2 to 22.9 mm (0.6 to 0.9 in.) in thickness. Shuttle tank wall thicknesses of 1.0 to 3.8 mm (0.04 to 0.15 in.) are considerably less than these specimen thicknesses; therefore, calculations made using these data are intended to indicate only a relative difference in tank weight. The published data indicated small differences between 2219 and 2014 for fracture strength and crack growth rate; the major factor accounting for the lesser weight of tanks made of 2014 is the greater yield strength of the material which allows greater proof and operating stresses.

2219 VS. 2014 FOR MAIN CRYOGENIC PROPELLANT TANK MATERIAL

Tank Weight Difference

TANK WEIGHT INCREASE WITH 2219 MATERIAL COMPARED TO 2014 MATERIAL

	FACTOR OF SAFETY	FRACTURE MECHANICS* 1000 PRESSURIZATIONS
BOOSTER	227 KG (500 LB)	3402 KG (7500 LB)
ORBITER	181 KG (400 LB)	680 KG (1500 LB)

*BASED ON AVAILABLE FRACTURE TEST DATA FOR THICK SPECIMENS.

Figure 32

2219 VS. 2014 FOR MAIN CRYOGENIC PROPELLANT TANK MATERIAL MECHANICAL PROPERTIES COMPARISON

(FIGURE 33)

Mechanical properties of 2014-T6 equal or exceed those of 2219-T87 for plate thicknesses required for booster and orbiter tanks.

MIL-HDBK-5 minimum guaranteed values have been multiplied by 1.07 to obtain "Guaranteed Typical" properties used in tank material sizing. Bracketed data are typical values from Phase B tests.

2219 VS. 2014 FOR MAIN CRYOGENIC PROPELLANT TANK MATERIAL

Mechanical Properties Comparison

NOTE: BRACKETED DATA ARE TYPICAL VALUES FROM PHASE B TESTS

		2014–T6		2219–T87	
		GUARANTEED TYPICAL	MIL–HDBK–5 "A" VALUES	GUARANTEED TYPICAL	MIL–HDBK–5 "A" VALUES
63.5 MM PLATE (2.5 IN. PLATE) BOOSTER TANK	F_{tu} (MN/M^2)	480 (492)	448	472 (494)	441
	(KSI)	69.6 (71.4)	65.0	68.5 (71.7)	64.0
	F_{ty} (MN/M^2)	427 (443)	400	376 (407)	352
	(KSI)	62.0 (64.2)	58.0	54.6 (59.0)	51.0
	ELONGATION (%)	(9)	4	(9)	6
38.1 MM PLATE (1.5 IN. PLATE) ORBITER TANK	F_{tu} (MN/M^2)	494	462	435	407
	(KSI)	71.6	67.0	63.1	59.0
	F_{ty} (MN/M^2)	465	434	376	352
	(KSI)	67.4	63.0	54.6	51.0
	ELONGATION (%)	–	6	–	6

Figure 33

2219 VS. 2014 FOR MAIN CRYOGENIC PROPELLANT TANK MATERIAL
STRESS CORROSION THRESHOLD VALUES

(FIGURE 34)

Resistance to stress corrosion is a major consideration. The stress corrosion threshold is clearly higher for 2219-T87, particularly in the short transverse direction.

For stress corrosion to occur there must be sustained or residual tension stresses on the surface exposed to a corrosive environment.

External integral stiffeners on both orbiter and booster tanks will require protection from corrosive environments. Short transverse grain will be exposed on machined flange surfaces. Residual stresses can result from machining, forming, or attachment to other structural members.

Difficulties in inspection of all external tank surfaces due to extensive removal of TPS, purge walls and access panels point up the risk of using a material susceptible to stress corrosion cracking.

2219 VS. 2014 FOR MAIN CRYOGENIC PROPELLANT TANK MATERIAL

Stress Corrosion Threshold Values

MATERIAL	GRAIN DIRECTION	PLATE		HAND FORGINGS	
		MN/M^2	KSI	MN/M^2	KSI
2014–T6	L	310	45	207	30
	LT	207	30	172	25
	ST	48	7	48	7
2219–T87	L	>276	>40	>262	>38
	LT	>262	>38	>262	>38
	ST	>262	>38	>262	>38

PARENT METAL AND FILLER WIRE	WELDMENTS (GAS TUNGSTEN ARC)				
	SHEET 2.03 TO 3.17 MM (0.08 TO 0.125 IN.)		PLATE 19.05 TO 25.4 MM (0.75 TO 1.0 IN.)		CONDITION
	MN/M^2	KSI	MN/M^2	KSI	
2014–T6/4043	212	30.7	>148	>21.4	AS WELDED
	203	29.4	>167	>24.2	AGED
2219–T87/2319	>172	>24.9	>107	>15.5	AS WELDED
	>225	>32.6	>165	>23.9	AGED

Figure 34

2219 VS. 2014 FOR MAIN CRYOGENIC PROPELLANT TANK MATERIAL PHASE B TEST DATA

(FIGURE 35)

Data obtained from our Phase B tests on 3.81 mm (0.15 in.) thick specimens show a slight but inconclusive advantage for 2014, particularly for low values of a/Q. At a/Q values of about 2.2 mm (0.09 in.), the two alloys appear to have equal strength; however, the trend indicates a possible strength advantage for 2219 at higher a/Q values. There also appears to be an increase in critical stress intensity factor, K_c with increasing flaw size for both materials.

A large reduction in fracture strength has been measured for some 2014 specimens with long, deep flaws. Because of the relative length of these flaws, both gross and net fracture stresses are shown. Comparative data for 2219 material are not yet available.

Relative fracture stress levels shown from these data are in substantial agreement with the relative fracture stresses obtained from published data for thick specimens and used for weight comparisons in this study.

2219 VS. 2014 FOR MAIN CRYOGENIC PROPELLANT TANK MATERIAL

Phase B Test Data

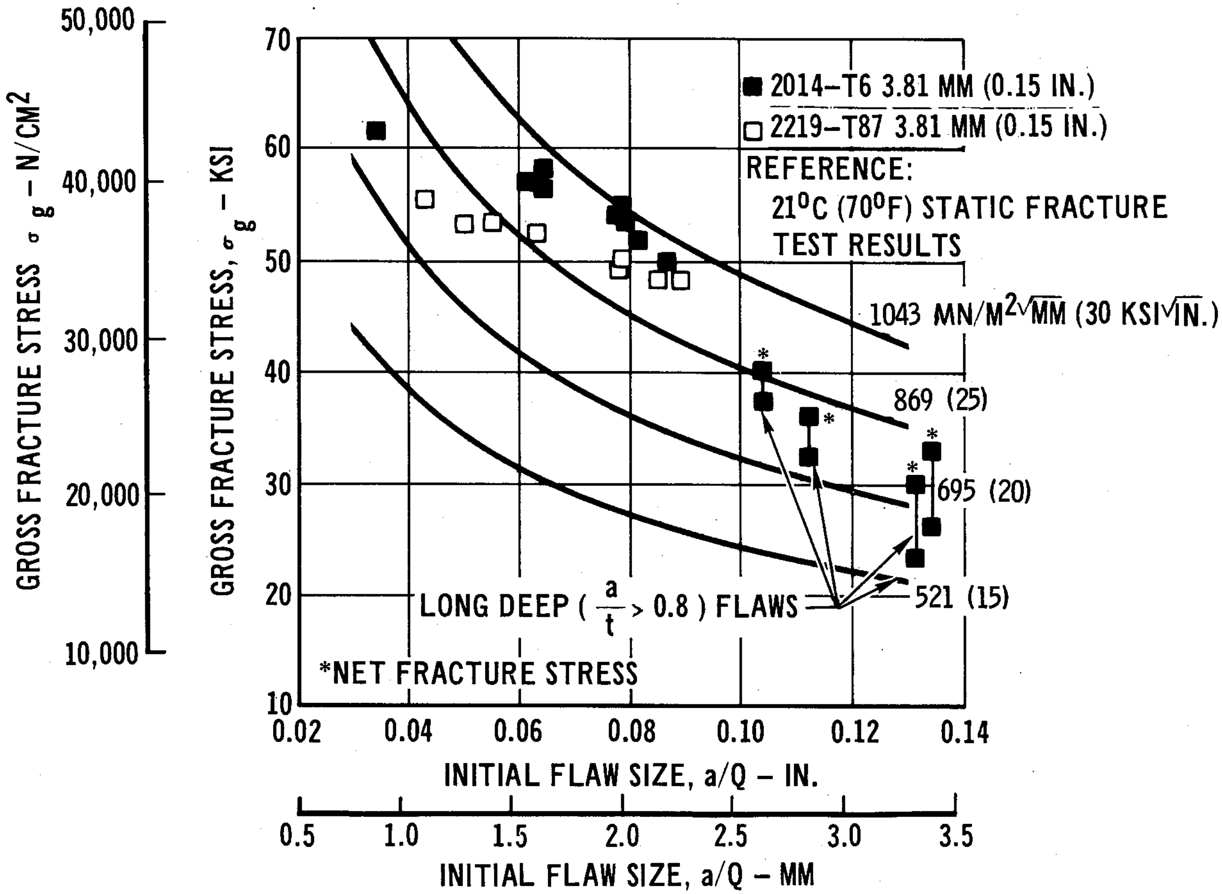

Figure 35

2219 VS. 2014 FOR MAIN CRYOGENIC PROPELLANT TANK MATERIAL
STUDY CONCLUSIONS

(FIGURE 36)

The advantages of 2219 are greatest in areas most difficult to quantify in cost or weight. Superiority of 2219 in resisting stress corrosion is well established. Superior elongation and area reduction characteristics of 2219 weldments have been verified in our Phase B tests and the better age forming and higher temperature limits of this material as well documented in the literature.

The weight advantage of 2014 on the basis of a factor of safety approach is clear. The apparent weight advantage of 2014 on the basis of fracture mechanics analyses is not certain. Proper material choice on the basis of fracture mechanics analyses will depend upon fracture strength data yet to be determined for thin gages and on definition of NDE capabilities which can be depended upon.

Our Phase B test program does not include stress corrosion, but the superiority of 2219 is not in doubt. Definition of the precise shuttle environments could minimize concern and analyses may show low residual stresses. Confidence in such analyses is low, however, and stress corrosion problems, if they occur, would be late in the program after commitment to the selected material.

It is important to resize the structure now and accept the weight penalty for selection of 2219. Because at this time there appears to be a significant weight saving by use of 2014, we believe there should be further testing of 2014 and 2219 such that if the weight saving potential is confirmed by test 2014 can be inserted in the program later.

2219 VS. 2014 FOR MAIN CRYOGENIC PROPELLANT TANK MATERIAL

Study Conclusions

2219–T87
- HIGHER STRESS CORROSION RESISTANCE
- BETTER WELD ELONGATION AND AREA REDUCTION
- BETTER AGE FORMING
- HIGHER MAXIMUM TEMPERATURE FOR REUSE

2014–T6
- WEIGHT ADVANTAGE BASED ON FACTOR OF SAFETY APPROACH
- APPARENT WEIGHT ADVANTAGE BASED ON FRACTURE MECHANICS APPROACH:
  - FRACTURE TOUGHNESS COMPARISON NOT CONCLUSIVE
  - CRACK GROWTH CHARACTERISTICS COMPARISON NOT CONCLUSIVE

2219–T87 APPEARS TO BE BEST CHOICE

Figure 3'6

RECOMMENDED TECHNOLOGY AND/OR DESIGN DEVELOPMENT EFFORT

(FIGURE 37)

Weight of dropout propellant is a significant factor in configuration trade studies. Existing data are applicable to ideal circular, vertical tanks. Tests should be performed on tilted siamese tanks to provide empirical data for more accurate evaluations of tank and propellant system designs.

In comparing forms of integral stiffening it was assumed that the same correlation (knock down) factor for general and panel instability applied to all concepts. Tests of the prime candidate integral stiffening designs, isogrid and 0° - 90° waffle with discrete rings, should be performed to determine accuracy of analytical predictions on this basis. Secondary benefits resulting from this effort are evaluation of fabrication techniques and determination of realistic non-optimum weight factors.

Composite technology development for even the modest applications selected should be underway to assure availability of established material processes, fabrication methodology and design techniques for the first shuttle vehicles. Tests should provide data for fail safe and safe life designs of boron/epoxy thrust tubes, and for fabrication, design and analysis of mechanically attached uniaxial boron/aluminum structural elements.

The need for thin gage fracture strength and crack growth rate data and for established reliable NDE capabilities is essential to the basic structural design approach to achieve system life. It appears unlikely that complete reliance can be placed upon a fracture mechanics approach in view of tank weight criticality and load spectrum complexity. Flightworthiness will have to be verified by inspection techniques to a considerable degree. Directly applicable fracture data should be obtained, however, to define NDE requirements and to form a basis for design criteria judgements.

RECOMMENDED TECHNOLOGY AND/OR DESIGN DEVELOPMENT EFFORT

- OBTAIN EMPIRICAL DATA FOR DROPOUT PROPELLANT VOLUME PREDICTIONS CONSIDERING SIAMESE TANK DESIGN AND TILT OF TANK CENTERLINE RELATIVE TO ACCELERATION VECTOR
- PERFORM COMPARATIVE TESTS TO DETERMINE COMPRESSIVE BUCKLING STABILITY OF INTEGRALLY STIFFENED SHELLS
- DEVELOP BORON/EPOXY TECHNOLOGY FOR THRUST STRUCTURE APPLICATION
- DEVELOP BORON/ALUMINUM TECHNOLOGY FOR UNIAXIAL, MECHANICALLY ATTACHED STRUCTURAL ELEMENTS
- DETERMINE STATIC AND CYCLIC FRACTURE STRENGTH AND CRACK GROWTH RATE DATA FOR 2219 AND 2014 PLATE MACHINED TO THICKNESSES REPRESENTATIVE OF MAIN PROPELLANT TANK WALLS
- IMPROVE FLAW DETECTION TECHNIQUES FOR MAIN PROPELLANT TANKS

Figure 37

APPLICATION OF BERYLLIUM TO ORBITER PRIMARY STRUCTURE

BY

T.J. Harvey and A.E. Trapp
Lockheed Missiles & Space Company
Sunnyvale, California

PAPER 14

INTRODUCTION

(Slide 1)

In seeking feasible and practical approaches to reduce overall program costs for a reusable space vehicle, the present attack is to examine alternate configurations to the two-stage reusable space shuttle. Lockheed, Grumman, Chrysler, and Boeing are participating in such activities. Lockheed cost studies have shown a significant advantage for the development of the stage-and-one-half concept.

Another approach is to examine the use of advanced materials and concepts for space shuttle application because of the potential for significant weight and cost savings.

Generally, in a material selection decision, conventional-material usage results in:

• Higher weight of structure/TPS	• Lower material costs
• Larger vehicle size	• Lower fabrication costs

while use of advanced materials results in:

• Reduced weight of structure/TPS	• Increased material cost
• Smaller vehicle size	• Increased fabrication costs

The costs referred to are, of course, those for structure/TPS materials and fabrication per unit weight. Weight savings due to the use of advanced materials, however, can equate to system benefits, such as reduced vehicle size, smaller number of engines, and lower propellant loads. These benefits have the appealing effect of actually reducing overall costs. It is not possible, therefore, to select materials properly without an evaluation of the effect on total program development and operational costs.

INTRODUCTION

THE COST EFFECTIVENESS OF ADVANCED-MATERIAL USAGE ON SPACE SHUTTLE VEHICLES CANNOT BE ASSESSED ON THE BASIS OF VEHICLE PERFORMANCE OR PAYLOAD IMPROVEMENT ALONE BECAUSE OF OVERALL SYSTEMS IMPLICATIONS.

IT IS LOCKHEED'S APPROACH, THEREFORE, THAT WITH FIXED PERFORMANCE PAYLOAD REQUIREMENTS, ADVANCED MATERIALS SHOULD BE USED TO:

- REDUCE VEHICLE SIZE, WHICH WILL
- REDUCE TOTAL PROGRAM COSTS

Slide 1

STIFFENED BERYLLIUM PANEL

(Slide 2)

A practical concept for structural panels is illustrated in slide 2. This is a photograph of a Z-stiffened beryllium structural panel constructed by Lockheed under Contract NAS 9-11222 for NASA/MSC. The total area of the panel is slightly greater than 4 ft^2 (0.4 m^2) and the weight is less than 2 lb (0.9 kg). This panel was designed as a heat-shield subpanel; however, its structural capability would qualify it for airframe structural applications.

STIFFENED BERYLLIUM PANEL

Slide 2

PRIMARY STRUCTURE MATERIALS

(Slide 3)

The apparent high material cost and complexity of design and fabrication have delayed the use of advanced materials in aircraft applications, thus far. Regular use of beryllium as a primary structural material has been achieved, however, for a non-reusable vehicle, the Agena, where proper engineering and manufacturing expertise have made possible the payload benefits. This is indicative of much greater benefits for a reusable vehicle, and the apparent payoff in a shuttle application warrants an effort to prove the feasibility and cost-effectiveness of advanced-material usage.

In its evaluation of the effects of advanced-material use, Lockheed chose beryllium for the structure on the basis of trade studies which indicate that this material results in the minimum-weight system. The high modulus-density ratio and the excellent elevated-temperature characteristics of beryllium permit maximum savings in lightly loaded structure and in thermal protection insulation thickness. Of the materials considered, beryllium was also found to be in the most advanced state of development, with a long record of successful space flight applications. In its studies, Lockheed has therefore considered beryllium as representative of a high level of structural efficiency; this level may be equalled or surpassed by other advanced materials or concept developments.

PRIMARY STRUCTURE MATERIALS

STRUCTURAL STABILITY WEIGHT INDEX VS. TEMPERATURE

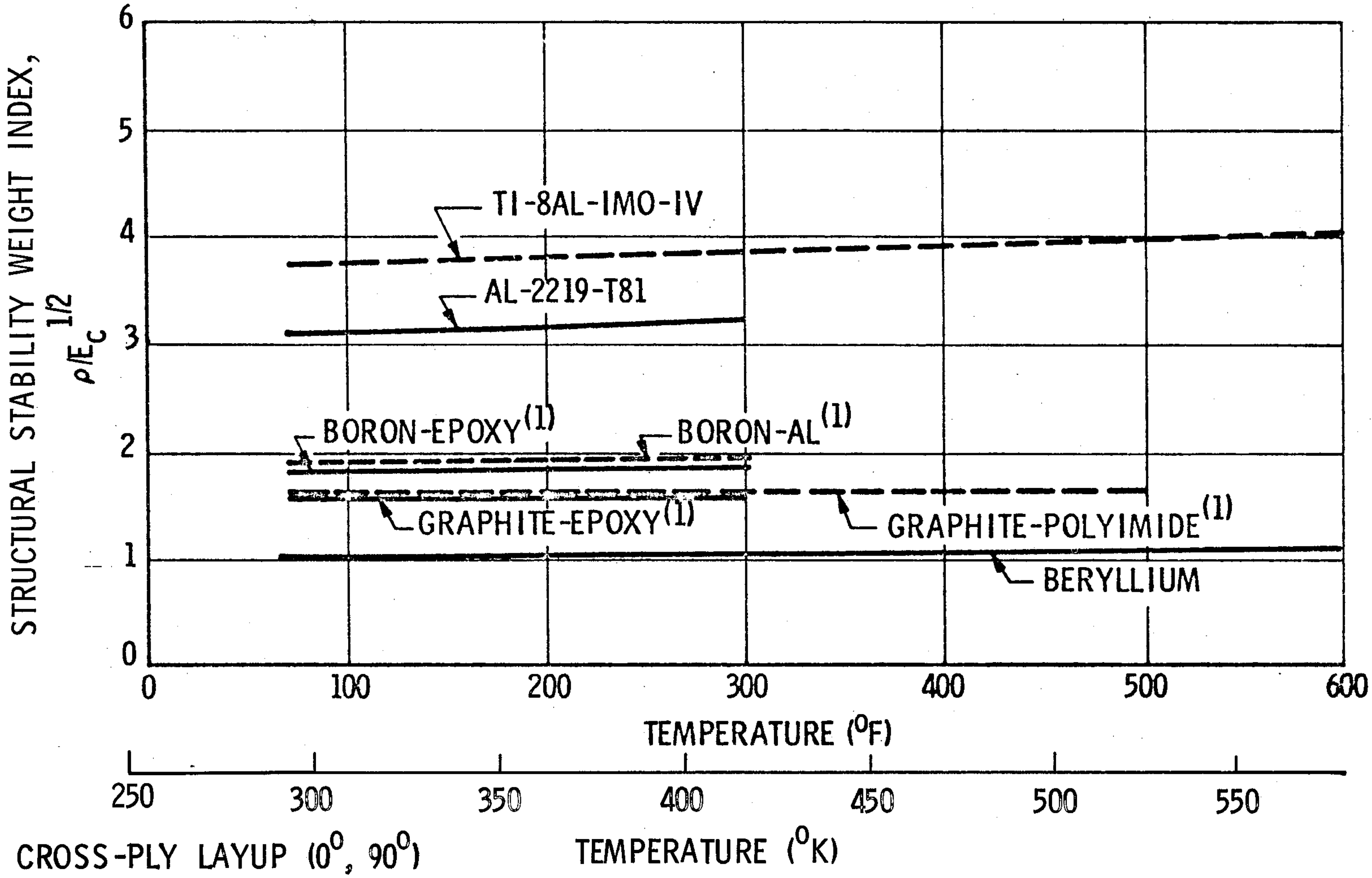

(1) CROSS-PLY LAYUP (0°, 90°)

Slide 3

COMPARATIVE SYSTEM PARAMETERS

(Slide 4)

To gain an understanding of the true value of the benefits of using advanced structural materials and/or concepts, two studies were conducted by Lockheed with the goal of reducing system size, weight, and complexity while fulfilling Phase B requirements. The approach taken in the first study was to design and perform a weight and cost analysis of systems containing conventional (aluminum/titanium) orbiters and also advanced-material orbiters which are compatible both with a conventional fully recoverable booster (two-stage concept) and with drop tanks (stage-and-one-half concept).

The second study addressed an orbiter configuration which, because of the restricted internal volume, is applicable only to the stage-and-one-half concept.

The remaining slides present the results of these studies for the two-stage and stage-and-one-half concepts. The cost data shown reveal the intrinsic value of reducing inert weight and provide a basis for establishing priorities for material or concept development.

The orbiter dry weight, which was 189,000 lb (85,700 kg) for Phase B with aluminum as the primary structure material, was reduced to 114,500 lb (52,000 kg), while launch weight dropped from 3,500,000 lb (1,590,000 kg) to 2,492,000 lb (1,130,000 kg). A comparative cost analysis showed a decline in Research, Development, Test, and Engineering (RDT&E) costs from $6,395 million to $5,686 million and in total program costs from $8,800 million to $7,756 million (see discussion of slide 11). From results of the second study, when the orbiter is designed to be only compatible with the stage-and-one-half concept, the weight is reduced to 107,000 lb (48,500 kg). Total program cost is further reduced to $5,214 million.

COMPARATIVE SYSTEM PARAMETERS
CONVENTIONAL VS ADVANCED MATERIALS

	TWO-STAGE		STAGE-AND-ONE-HALF (CONVERTIBLE TO TWO-STAGE)	
	CONV. MAT'LS	ADV. MAT'LS	CONV. MAT'LS	ADV. MAT'LS
• **ORBITER**				
SIZE: (FT)	153	121	153	121
(m)	47	37	47	37
DRY WEIGHT: (LB)	189,000	114,500	261,000	146,500
(kg)	85,700	52,000	118,000	66,500
ENGINE NUMBER	2	2	11	6
• **BOOSTER/DROPTANK**				
INERT WEIGHT: (LB)	518,000	387,300	126,000	63,000
(kg)	234,000	175,000	57,200	28,500
ENGINE NUMBER	11	8		
• **SYSTEM**				
GROSS LAUNCH WEIGHT: (LB)	3,500,000	2,492,000	3,500,000	1,920,000
(kg)	1,590,000	1,130,000	1,590,000	871,000
PROGRAM COST ($ MILLION)	8,800	7,756*	7,357	5,815*

*COMPLEXITY FACTOR = 1.5

Slide 4

DIMENSIONAL COMPARISON OF TWO ORBITER CONCEPTS

(Slide 5)

A dimensional comparison of the conventional- and advanced-material concepts for a two-stage vehicle reveals a 21% reduction in reference length and a similar reduction in aerodynamic surface size. This is possible primarily because of reduced propellant loadings even though mission requirements and parameters have been maintained. The reduction in propellant is such that the structural arrangement of the tanks can be chosen to allow an in-line concept which, for ascent, directs all axial inertia loading from the tanks directly into the thrust structure and aft attachment points. In addition, only cylindrical and spherical tank sections were utilized to reduce manufacturing complexity and expense.

DIMENSIONAL COMPARISON OF TWO ORBITER CONCEPTS

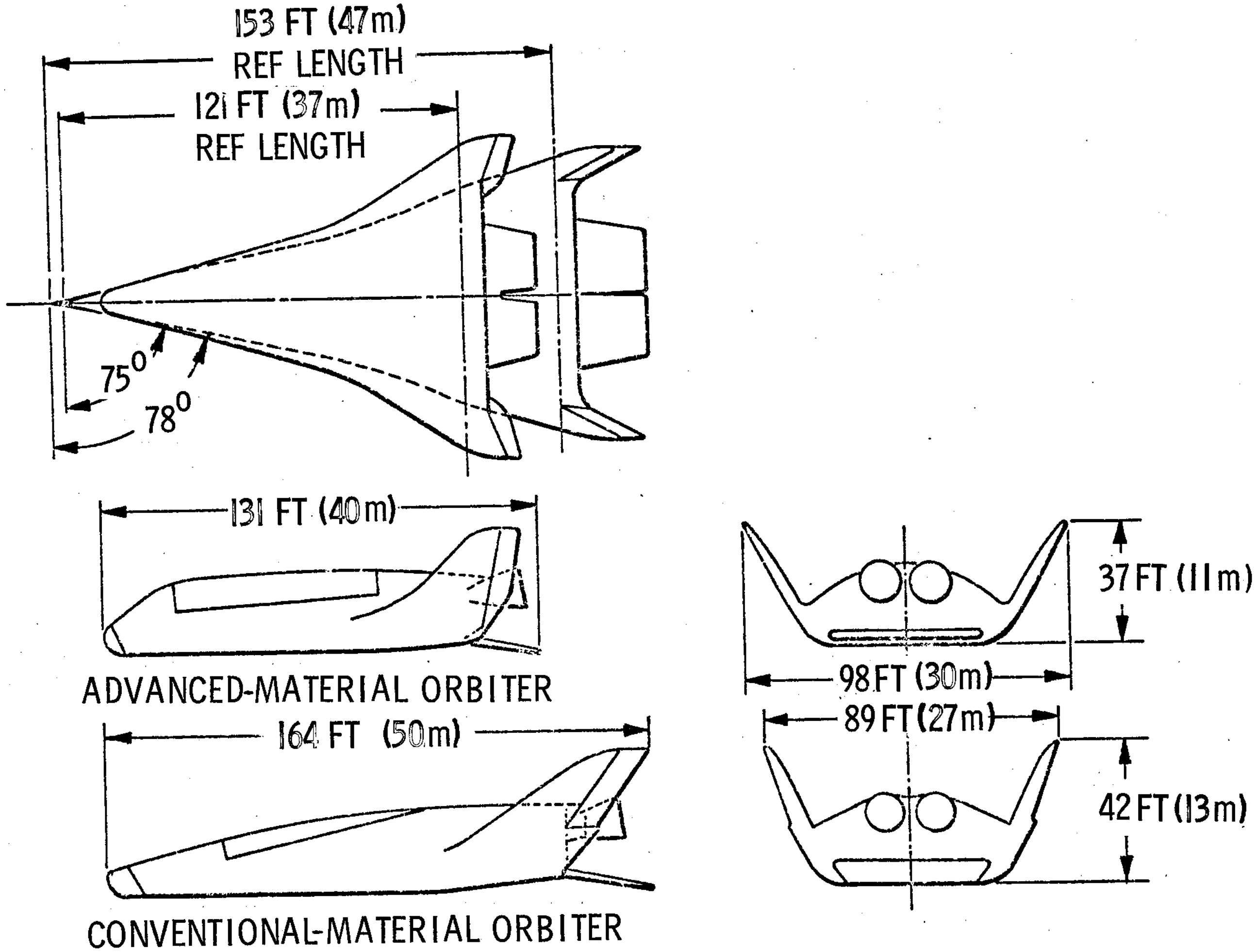

Slide 5

WEIGHT COMPARISON - TWO-STAGE DELTA-BODY ORBITERS
(Slide 6)

Weight analysis results for the advanced-material study are shown in the opposite slide. The Phase B conventional-material orbiter is seen to have a dry weight of 189,000 lb (85,700 kg) which can be reduced to 114,500 lb (52,000 kg) by application of advanced materials. The inherent efficiency of the selected structure/TPS concept results in a reduction of required propellant from 558,000 lb (253,000 kg) to 385,000 lb (175,000 kg). This reduction in required internal volume permitted the size decrease achieved. Since the orbiter launch weight decreases from 778,000 lb (353,000 kg) to 537,000 lb (244,000 kg), the booster inert weight is also smaller by 130,000 lb (59,000 kg), and the system launch weight is reduced by over 1,000,000 lb (454,000 kg) to 2,500,000 lb (1,134,000 kg) for the fully reusable booster application.

WEIGHT COMPARISON – TWO-STAGE DELTA-BODY ORBITERS

	CONVENTIONAL ORBITER WEIGHT		ADVANCED ORBITER WEIGHT	
	(LB)	(kg)	(LB)	(kg)
AERO SURFACES	17,104	7,760	7,600	3,450
BODY STRUCTURE	43,300	19,640	19,105	8,670
TPS (200 NM, LI-1500)	35,290	16,010	17,499	7,940
MAIN PROPULSION	35,650	16,170	26,376	11,960
OTHER	40,494	18,370	33,529	15,210
CONTINGENCY (10 PERCENT)	17,184	7,790	10,411	4,720
DRY WEIGHT	189,022	85,740	114,520	51,950
PERSONNEL	678	310	678	310
CARGO	23,551	10,680	30,000	13,610
RESIDUALS, RESERVES AND LOSSES	6,788	3,080	6,631	3,010
MAIN ENGINE IMPULSE PROPELLANT	557,961	253,090	385,423	174,830
LAUNCH WEIGHT	778,000	352,900	537,252	243,710
BOOSTER INERT AT SEPARATION	518,000	234,960	387,322	175,690
BOOSTER PROPELLANT	2,204,000	999,730	1,567,426	710,980
BOOSTER GROSS	2,722,000	1,234,690	1,954,748	886,670
TOTAL LAUNCH	3,500,000	1,587,590	2,492,000	1,130,380

Slide 6

DESIGN REQUIREMENTS

(Slide 7)

Application of the Phase B proposal ground rules to the design of a high-cross-range orbiter resulted in a delta-body orbiter having a dry weight of 197,600 lb (89,600 kg). Cargo capability for this vehicle was limited to 15,000 lb (6,800 kg) with the required system launch weight of 3,500,000 (1,590,000 kg). The resulting orbiter ignition weight was 778,000 lb (353,000 kg). Several factors led to these results:

- 3,500,000-lb (1,590,000-kg) launch weight requirement
- Use of metallic thermal protection system (TPS)
- Use of delta-body sweep of 78°
- Use of aluminum for structural body system
- 1500-NM cross-range requirement

A subsequent study was made to determine increased cargo capability with the substitution of LI-1500 for TPS and with the cross range at 200 NM without changing the basic vehicle. The dry weight reduced to 189,000 lb (86,000 kg) and the cargo capability increased to 23,500 lb (10,700 kg).

Given the alternate requirement of a 30,000-lb (13,600-kg) payload with variable launch weight raises the issue of reducing cost by reducing orbiter weight and composite vehicle launch weight, thereby reducing program costs. The study performed to consider alternate materials for the structural body system utilized the design ground rules shown in this slide.

DESIGN REQUIREMENTS

- 200-NM CROSS RANGE
- 30,000-LB (13,600-kg) PAYLOAD
- 9,000-FT/SEC (2,743-m/SEC) STAGING VELOCITY
- SUBSONIC L/D = 4.5; HYPERSONIC L/D HIGH AS POSSIBLE
- TWO-STAGE COMPATIBILITY WITH STAGE-AND-ONE-HALF SYSTEM
- PROPULSION SYSTEM (INCLUDING TANKAGE) DECOUPLED FROM BODY STRUCTURE

Slide 7

DESIGN FEATURES
(Slide 8)

Design features are summarized in the opposite slide. The most significant design features are:

- Reduce body sweep angle from 78° to 75°
- Delete TPS substructure and fasten the LI-1500 directly to the structural body, where temperature isotherms exceed $1000^{\circ}F$ ($810^{\circ}K$).

Reducing the body sweep angle while keeping base width constant results in reducing the reference body length from 153 ft (47 m) to 121 ft (37 m). Deleting the TPS substructure panels while permitting the unprotected body to heat up to $1000^{\circ}F$ ($810^{\circ}K$), and sizing the LI-1500 thickness on the basis of a maximum bondline temperature of $600^{\circ}F$ ($590^{\circ}K$), reduced TPS requirements quite significantly in comparison with those of the Phase B delta-body configuration (see slide 6).

Reducing the orbiter dry weight has the allied effect of reducing propellant loading required, thus resulting in a significant overall reduction in stage launch weight and composite vehicle liftoff weight (see slide 6).

DESIGN FEATURES

- REDUCED BODY SWEEP ANGLE: $78^0 \longrightarrow 75^0$
- SHORTER VEHICLE LENGTH: 153 FT (47m) ⟶ 121 FT (37m)
- BERYLLIUM USED FOR ALL PRIMARY STRUCTURE
  - (1) Z-STIFFENED PANELS: 30 IN. x 100 IN. (76 cm x 254 cm)
  - (2) FRAMES: AT 30-IN. (76-cm) INTERVALS
  - (3) LONGERONS: AT 100-IN. (254-cm) INTERVALS
  - (4) LANDING GEAR AND OTHER BULKHEADS
  - (5) PROPULSION FRAMING AND THRUST STRUCTURE
  - (6) PAYLOAD BAY DOOR
  - (7) AERODYNAMIC SURFACES
- ORBIT THRUST REACTED THROUGH ASCENT TANKAGE WITH LH_2 FORWARD/LOX AFT
- LI-1500 BONDED DIRECTLY TO BODY STRUCTURE, WHERE TEMPERATURE EXCEEDS 1000^0F (810^0K)
- LI-1500 THICKNESS SIZED TO LIMIT BONDLINE TEMPERATURE TO 600^0F (590^0K)
- RADIATION FOILS AND FIBROUS BATTING FOR TEMPERATURE-LIMITED COMPONENTS

Slide 8

COMPARISON OF ALUMINUM AND BERYLLIUM PRIMARY STRUCTURE

(Slide 9)

To minimize the structural weight of the Phase B orbiter, an open-faced trapezoidal corrugated shell, stiffened with frames, posts, and longerons, was chosen. The requirement of attaching LI-1500 directly to the skin led to the selection of a beryllium skin-stringer configuration. A configuration comprising sheet-metal Z-shaped stringers fastened to thin sheet was selected. This shape also lends itself better to conically shaped shells than integrally stiffened panels. The opposite slide presents the comparison of the Phase B structural approach and the present concept. It is noted that the Phase B approach uses a titanium trapezoidal-stiffened panel to which the LI-1500 is bonded. The panel is supported by the frames which, in turn, circumscribe the aluminum corrugated fuselage shell. The titanium subpanel is permitted to operate at 600°F (590°K), but insulation is required to limit the aluminum to 200°F (365°K). The current concept is very much simplified by eliminating the subpanels and the temperature limitation of 200°F (365°K) on the fuselage.

To account for the ever-present thermal stress problem, the structural fuselage was designed as follows: The panels to which LI-1500 are bonded will be axially load-carrying panels as shown in the slide. Along the fuselage sides, the bare beryllium panels will be mounted with shear clips. These panels will carry shear and aerodynamic pressures only. Preliminary analyses show this approach to have negligible thermal stresses when the lower panels are at 75°F (295°K) and the side panels reach 920°F (765°K) (at 200 sec of reentry). Materials used in the propulsion system are conventional. Main and orbit propellant tank weights are based on 2219-T87 aluminum.

COMPARISON OF ALUMINUM AND BERYLLIUM PRIMARY STRUCTURE

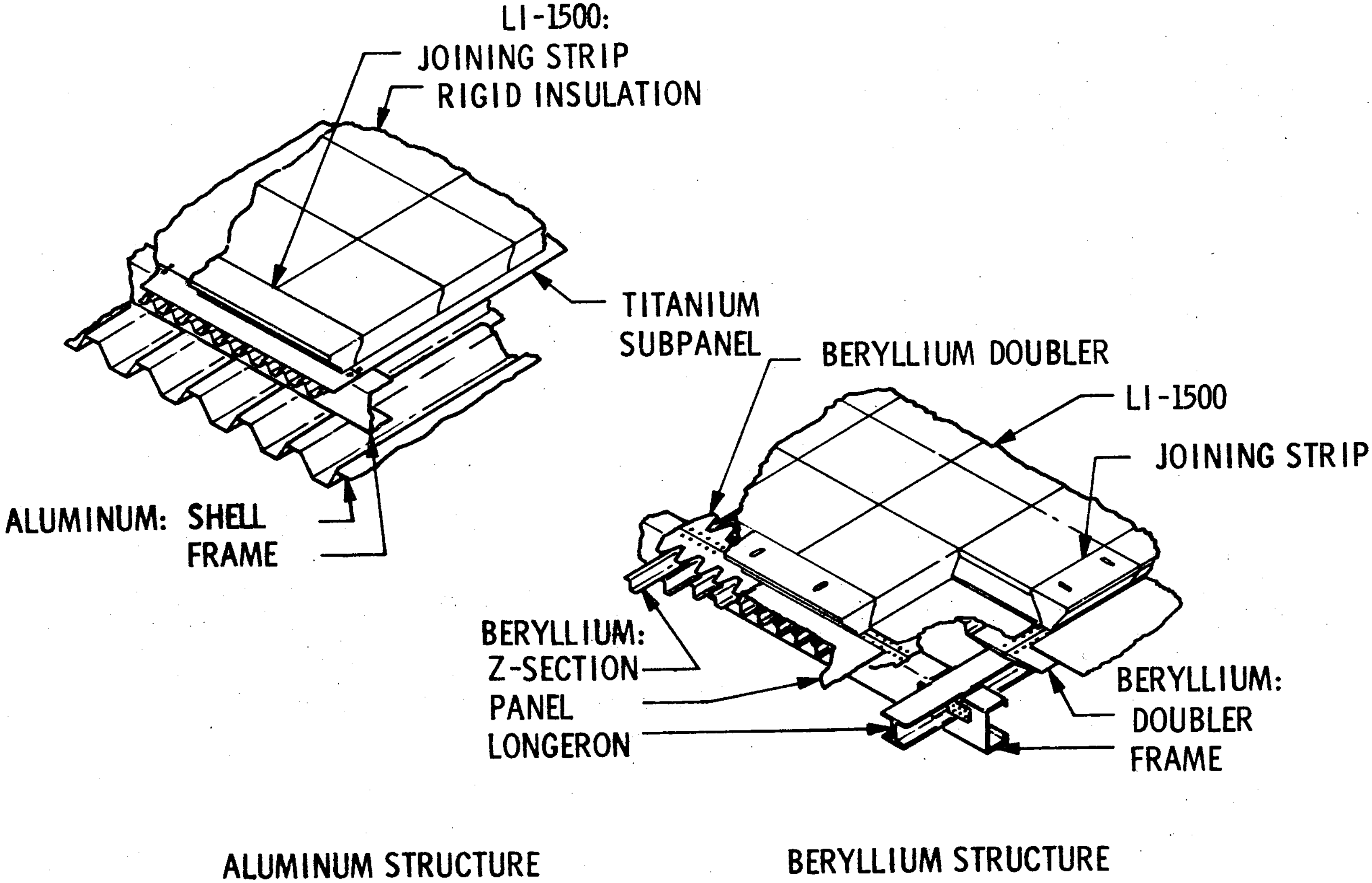

Slide 9

GROUND RULES FOR COST ESTIMATES OF ALTERNATE TWO-STAGE SHUTTLE SYSTEMS

(Slide 10)

The basic orbiter shown previously is the two-stage fully reusable orbiter. Booster costs for this system were obtained by scaling down from existing in-house Lockheed data. System costs for the conventional-material systems were also derived from similar data.

Costs were developed using the ground rules shown in the opposite slide. Although one may doubt the validity of the particular cost estimating relationship (CER) used, the techniques were applied consistently to all systems; hence relative costs were obtained in a known, impartial manner.

GROUND RULES FOR COST ESTIMATES OF ALTERNATE TWO-STAGE SHUTTLE SYSTEMS

- ALL COSTS GENERATED USING LOCKHEED CERs
- MISSION MODEL – 430 OPERATIONAL FLIGHTS
- OPERATIONAL FLEET: 5 ORBITERS AND 5 BOOSTERS PLUS 10 PERCENT INITIAL SPARES
- DEVELOPMENT TEST HARDWARE: EQUIVALENT OF 5 ORBITERS AND 5 BOOSTERS PLUS 20 PERCENT INITIAL SPARES
- LEARNING ASSUMED AT 90 PERCENT FOR PRODUCTION HARDWARE AND NO LEARNING FOR TEST HARDWARE
- ALL CASES ASSUME SAME COMMONALITY BETWEEN ORBITER AND BOOSTER SUBSYSTEMS
- OPERATIONAL TIME PERIOD IS 10 YEARS
- TWO OPERATIONAL LAUNCH BASES
- MATERIAL COMPLEXITY FACTORS FOR DEVELOPMENT WEIGHTED AT 20 PERCENT OF MANUFACTURING COMPLEXITY FACTOR

Slide 10

LOW-CROSS-RANGE DELTA-BODY ORBITER COSTS WITH LI-1500 TPS

(Slide 11)

The values obtained for the two-stage system are shown in the opposite slide. The two columns on the right indicate the effect of changing the manufacturing complexity factor from 1.5 to 3.0 to account for the increased fabrication costs of beryllium as compared to aluminum. The left-hand column shows costs for the conventional aluminum/titanium system. It can be seen that savings in RDT&E ($450 to $700 million) are achieved. This is the result of reduced system size which the CERs use as their basis. The data show that orbiter first-unit costs vary as follows with complexity factor:

Zp	Orbiter First-Unit Cost ($ Million)
1.0	74
1.5	82
2.0	88
2.5	94

Since the first-unit cost of the orbiter constructed of conventional materials is $88 million, a cross-over exists at Zp = 2.0. Considering orbiter RDT&E the cross-over occurs at Zp = 2.9.

LOW-CROSS-RANGE DELTA-BODY ORBITER COSTS WITH LI-1500 TPS

($ MILLIONS)

	CONVENTIONAL TWO-STAGE		NEW TWO-STAGE WITH Be STRUCTURE Zp for Be = 1.5		Zp for Be = 3.0	
RDT&E		6395		5686		5949
ORBITER	2216		2018		2227	
BOOSTER	2103		1867		1867	
SYSTEM COMMON	708		584		584	
SUPPORT AND MGMT	1368		1217		1271	
PRODUCTION HDWE		1258		1098		1191
OPERATIONS		1147		972		1011
TOTAL PROGRAM		8800		7756		8151

Slide 11

MINIMUM-ENVELOPE STAGE-AND-ONE-HALF ORBITER

(Slide 12)

From a structural standpoint, the delta-body configuration, being both wing and fuselage, offers the advantage of a large usable internal volume for the surface area. When payload dimensional requirements (15 x 60 ft (5 x 18 m)), the delta-body configuration, and the stage-and-one-half concept (which is desensitized from orbiter ascent propellant requirements) are combined, the shortest possible orbiter with the least possible surface area emerges. The decreased internal volume for propellants limits this approach to the stage-and-one-half system.

For this study, a minimum delta-body (78°-sweep) envelope was determined which would house the payload, thrust structure, sufficient ascent propellant to not significantly degrade system performance, and miscellaneous systems (jet engines and fuel, orbital tanks and propellant, landing gear, cabin, etc.). As noted in the slide, the reference length of this vehicle was determined to be 110 ft (34 m) and the span, 69.5 ft (21 m). For comparison purposes, it was decided to examine three structural materials systems: (1) all aluminum, (2) aluminum except for beryllium moveable aero surfaces, payload door, and TPS subpanels, and (3) all beryllium. Propellant tanks for all three remained aluminum and the thrust structure titanium.

Results of this study indicated that: (1) the all-aluminum vehicle was not feasible because the required number of engines was too great to fit within the base and wing loadings were too high for aerothermodynamic efficiency, (2) the aluminum/beryllium vehicle was marginal on both counts, but (3) the all-beryllium vehicle could easily house the engines in the base and had reasonable wing loadings.

MINIMUM - ENVELOPE STAGE-AND-ONE-HALF ORBITER

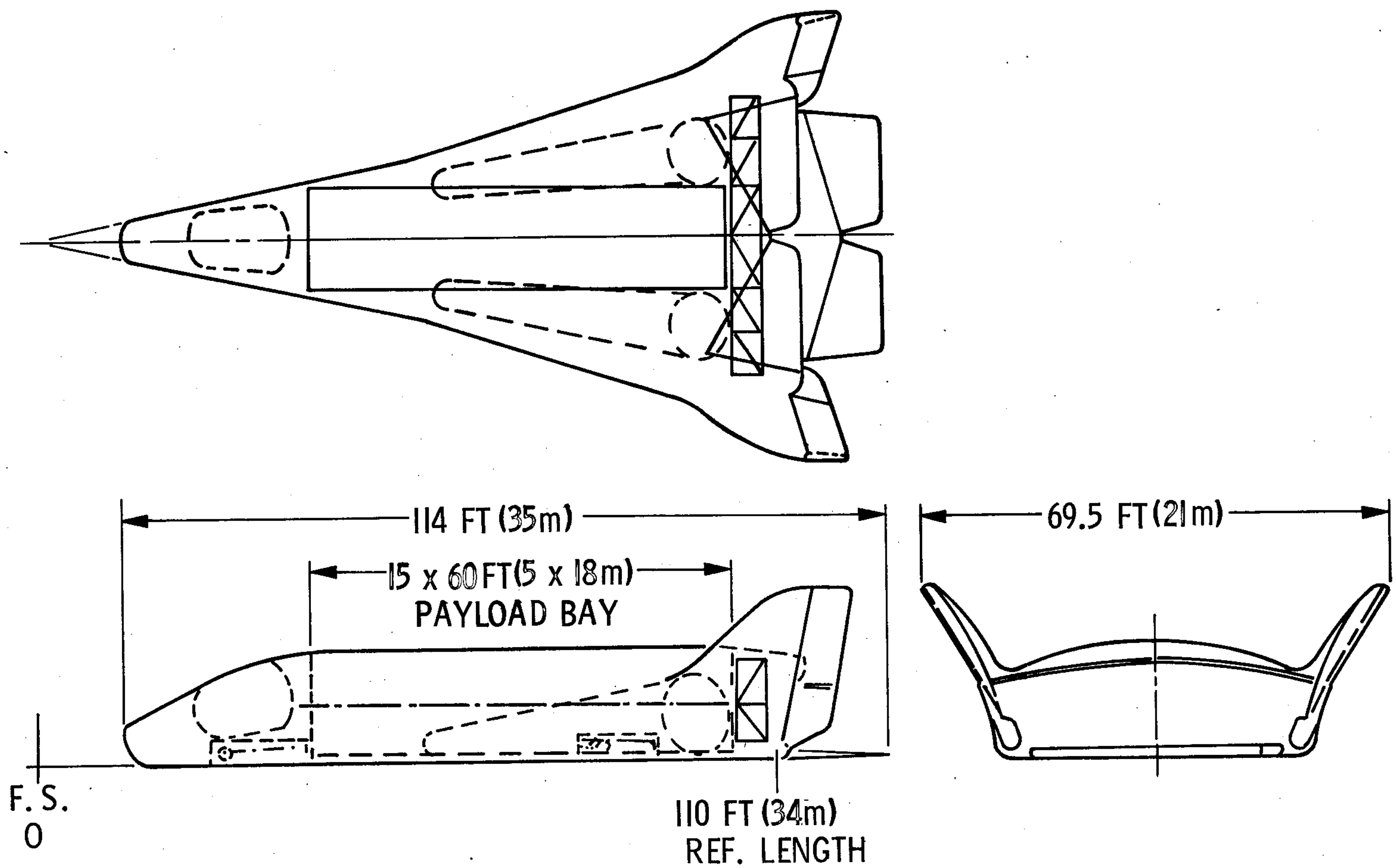

Slide 12

COMPARATIVE PARAMETERS FOR STAGE-AND-ONE-HALF MATERIALS
(Slide 13)

In addition to the technical parameters developed in this study, the opposite slide presents the results of a cost appraisal along with previously shown stage-and-one-half data for comparative purposes. The size effect of the extensive use of beryllium is shown as is the effect on complexity of the vehicle. The inert weights, the number of engines, and the gross liftoff weight are all reduced by more than 50%.

Even though a manufacturing complexity factor of 1.5 has been used for beryllium, total program costs are reduced on the order of 29%. Increasing the complexity factor to 3.0 would still yield a reduction of approximately 27%.

It is important to note that, in relation to the cost figures, NASA ground rules have changed since the original work was accomplished. These figures are consistent within themselves and, as totals, would represent the same relative standing as the most recent values.

COMPARATIVE PARAMETERS FOR STAGE-AND-ONE-HALF MATERIALS

		STAGE-AND-ONE-HALF (TWO-STAGE COMPATIBLE) CONV. MAT'LS	STAGE-AND-ONE-HALF (TWO-STAGE COMPATIBLE) ADV. MAT'LS	STAGE-AND-ONE-HALF (MINIMUM ENVELOPE) ADV. MAT'LS
• ORBITER LENGTH	(FT)	153	121	110
	(m)	47	37	34
DRY WEIGHT	(LB)	261,000	146,500	107,000
	(kg)	118,000	66,500	48,500
ENGINE NO.		11	6	5
• DROPTANK INERT WEIGHT:	(LB)	126,000	63,000	50,000
	(kg)	57,200	28,500	22,700
• SYSTEM: GLOW	(LB)	3,500,000	1,920,000	1,600,000
	(kg)	1,590,000	871,000	726,000
PROGRAM COST ($ MILLION)		7,357	5,815*	5,214*

*MANUFACTURING COMPLEXITY FACTOR = 1.5

Slide 13

STUDY CONCLUSIONS
(Slide 14)

Results of the study indicate that considerable cost savings may be possible by application of advanced materials, providing the cost estimating relationships are valid. These relationships obviously apply considerable emphasis to system size.

It is clear from the study that reduced system complexity will result because the large reduction in launch weight achieved immediately reduces the size and complexity of the propulsion system. Also, as structural weight is reduced, wing loading, reentry heating, landing speed, aerodynamic balance, and other benefits are achieved.

The study also shows that cost savings are a function of the system itself, with the stage-and-one-half system showing the greatest percentage reduction in total costs (29% as compared with 12% for the two-stage system). This further illustrates the need for the materials selection process to evaluate costs for the entire system.

STUDY CONCLUSIONS

- COMPARATIVE TOTAL PROGRAM COSTS SHOULD BE MATERIAL SELECTION CRITERION
- ADVANCED MATERIALS CAN PROVIDE MAJOR COST SAVINGS TO SPACE SHUTTLE PROGRAM
- REDUCED SYSTEM WEIGHT AND SIZE IS KEY TO COST SAVINGS ACHIEVED WITH ADVANCED MATERIALS

Slide 14

DESIGN, MANUFACTURE AND TESTING OF A TD NICKEL-CHROMIUM STRUCTURAL ASSEMBLY

By

Read Johnson, Jr.
McDonnell Douglas Astronautics Company-West
Huntington Beach, California

and

Charles L. Ramsey
Air Force Flight Dynamics Laboratory
Wright-Patterson AFB, Ohio

PAPER 15

SUMMARY

A milestone was reached in August 1970 when the vertical fin was delivered to the Air Force for structural testing. Another milestone will be reached upon completion of tests presently being conducted. Correlation of test results with previous stress analysis predictions will be made. Subsequently, a post structural test investigation will be conducted on the fin to determine material residual strength and microstructural changes. The work conducted during this program thus far has contributed significantly to an understanding of the material performance capabilities and manufacturing characteristics of TD NiCr. Also, the current series of ascent and reentry profile tests being conducted on the fin is providing a timely base of data to assess the performance of a large manufactured TD NiCr assembly and to establish a demonstrated capability to design with this class of materials.

INTRODUCTION

This presentation summarizes significant results of a current Air Force sponsored program to explore the potential use of dispersion-strengthened metals (DSM) in structures that will experience repeated elevated temperature service. The program was initiated in February 1967 by the Air Force Flight Dynamics Laboratory and specific interest was centered on second-generation dispersion-strengthened metals that had been developed with chromium as an alloying element to produce greater oxidation resistance. After initial material evaluation tests, TD NiCr (Ni-20Cr-2ThO_2) became the material of primary interest in the program because of its superior performance and because of its advanced development status compared to other second-generation dispersion-strengthened metals.

Early portions of the program were devoted to the determination of typical environments experienced by candidate structural components, material evaluation tests and experimental fabrication and testing of subscale structural components. Material properties were established in this phase of the program and sufficient fabrication experience was gained to provide a basis for in-depth evaluation of fabrication approaches to be used in the design of a structural test assembly. The detailed results of the first portion of the program are given in AFFDL-TR-68-130, Part I.

Efforts during the later portion of this program have been directed toward the design, analysis, manufacturing and testing of a major representative structural assembly utilizing TD NiCr. This presentation will report on this segment of the program.

Information generated under this program and the current tests being conducted on the TD NiCr fin at AFFDL provide timely contributions to related NASA sponsored efforts investigating the application of this material for space shuttle structures and thermal protection systems.

DSM STRUCTURAL TEST ASSEMBLY

(Slide 1)

The test assembly configuration selected was a full size vertical fin of the FDL-5A, a high lift-to-drag ratio reentry configuration developed in Air Force sponsored studies. The completed structural test assembly is approximately 2.4 m (8 ft.) in length at the base and 1 m (3-1/2 ft.) high at the trailing edge. The total surface area, including both sides of the fin, is approximately 2.8 m^2 (30 $ft.^2$). The structure, fabricated primarily from TD NiCr material, is currently undergoing simulated flight load and thermal tests at the AFFDL Structural Test Facility.

The overall design approach for the fin test assembly employed an internal load carrying hot structure made of TD NiCr formed sheet spars, ribs and diagonal members riveted together and covered with a total of 30 TD NiCr surface panels with overlapping edges. The surface panels were designed to carry only local loads, and are attached to the primary structure through machined fittings which permit all but one point on the panel to float, or move differentially with respect to the primary structure. The primary structure sustains all bending and shear loads, which are reacted at the base of the fin through a series of attach fittings that connect the TD NiCr fin to mating stainless steel frames which form a transition structure between the test assembly and the major test jig framework. The design approach of using discrete panels that are free to move relative to the primary structure was selected in an effort to diminish thermal stresses caused by temperature differences throughout the structure.

DSM STRUCTURAL TEST ASSEMBLY

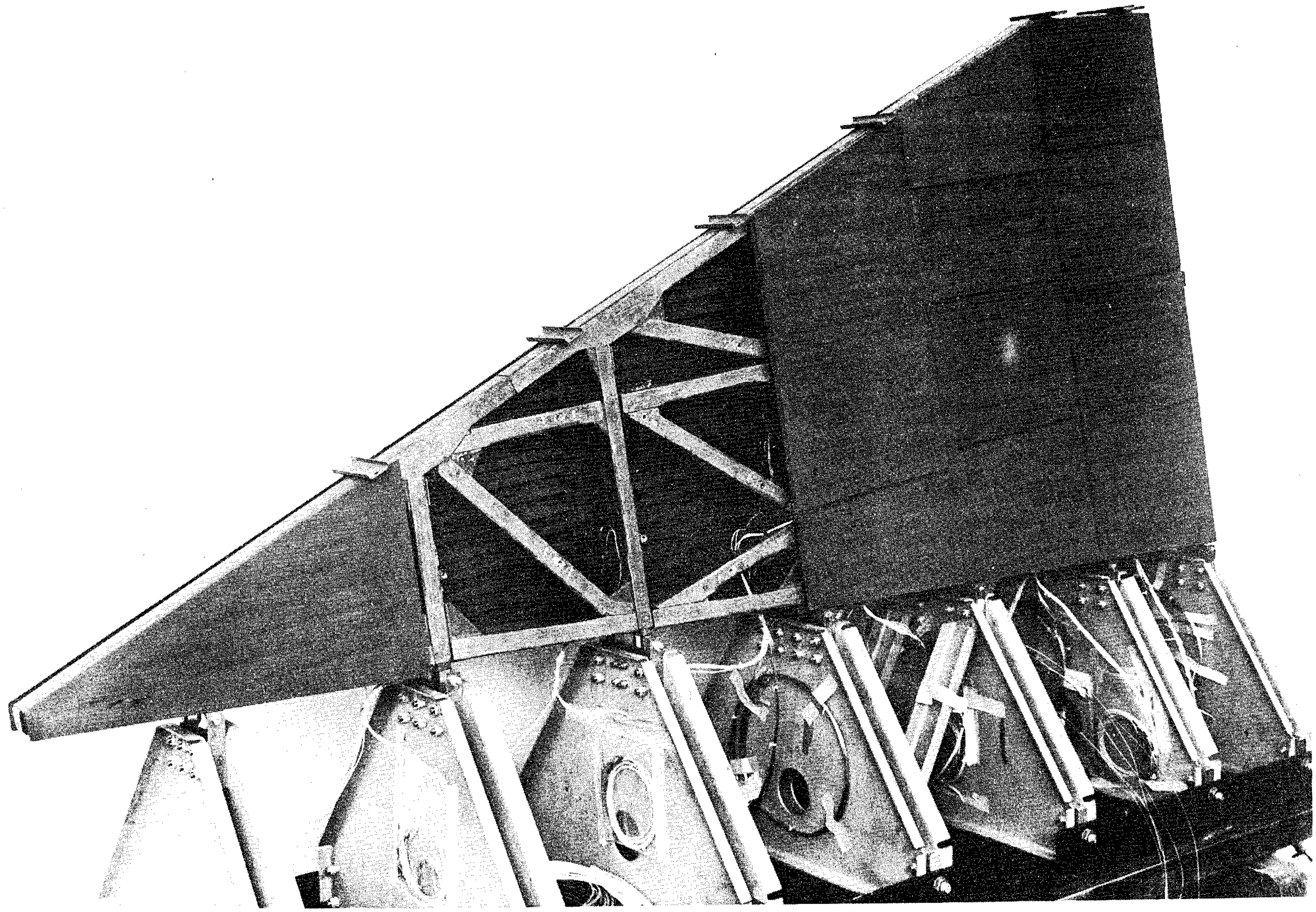

Slide 1

COMPLETED PRIMARY STRUCTURE IN ASSEMBLY JIG

(Slide 2)

The internal structure was assembled by standard jig assembly techniques used with sheet metal structures. This slide shows the completed primary structure in the assembly jig. The assembly was started by positioning the base rib and fin attach fittings in the jig, followed by mating the fittings to the spars. The leading edge members, ribs and diagonals were then positioned in the jig, drilled and riveted together. TD NiCr rivets were used in the temperature regions above 816°C (1,500°F), Hastelloy X fasteners were used in regions between 649°C (1,200°F) and 816°C (1,500°F), and A-286 fasteners were used at the base where temperatures are below 649°C (1,200°F). Approximately 500 TD NiCr rivets, 375 Hastelloy X and about 800 A-286 rivets were used in the primary structure. After completion of assembly operations, the structure was removed from the jig and given a stress relief anneal at 649°C (1,200°F). The limiting temperature for anneal was 649°C (1,200°F) due to the use of A-286 fasteners and fittings in the base region.

COMPLETED PRIMARY STRUCTURE IN ASSEMBLY JIG

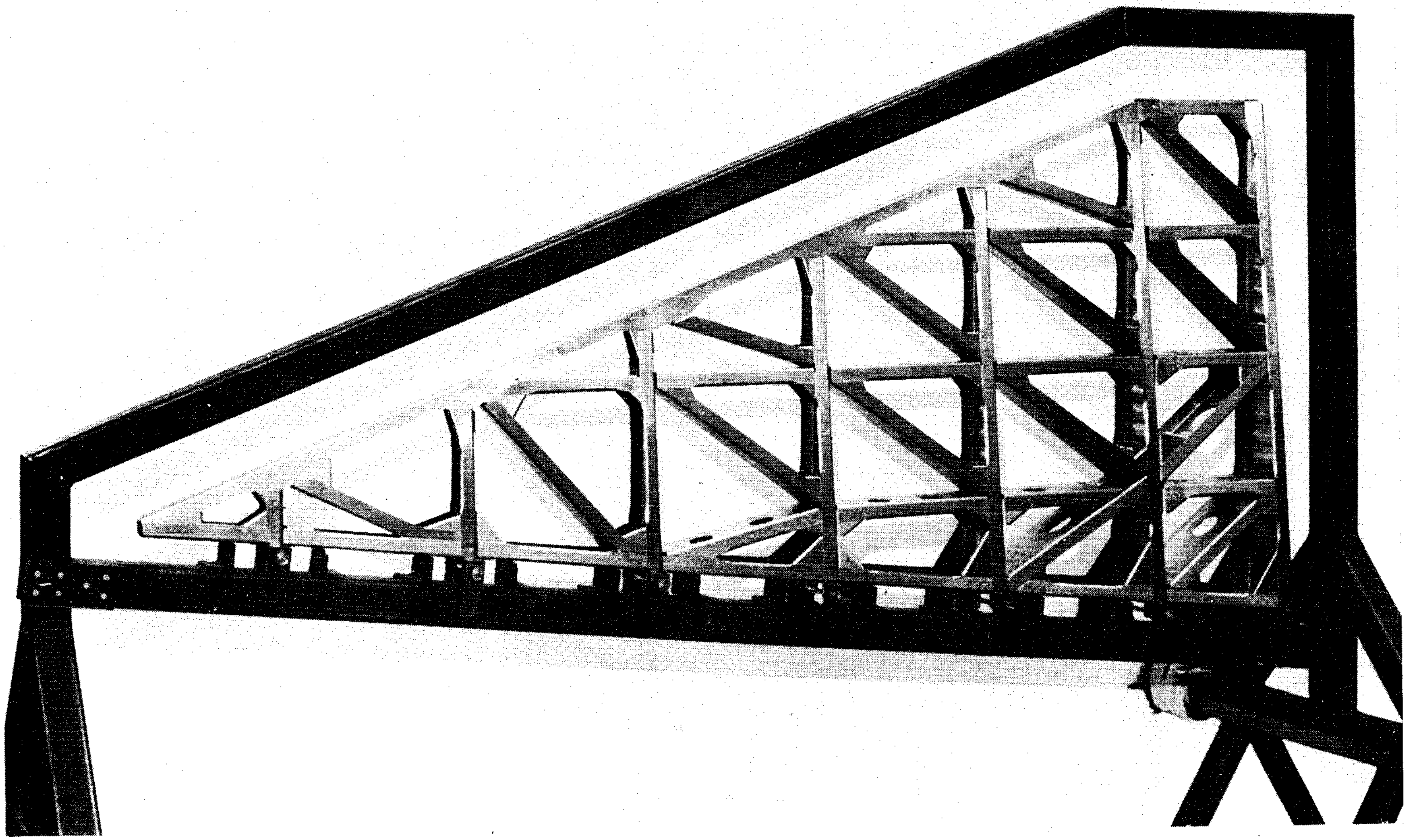

Slide 2

TD NICKEL-CHROMIUM WARM HEADED RIVETS

(Slide 3)

The development of TD NiCr fasteners involved studies of material microstructural changes that occurred during fabrication of rivets and threaded fasteners. One of the more serious problems encountered in the program was the change in grain size and subsequent loss of strength that resulted from excessive compressive deformation in forming the heads on fasteners. It should be noted that this strength loss due to a microstructural change has only been observed in material undergoing compressive deformation. From tests conducted up to this time the data obtained indicate that approximately 20% deformation is required to cause detrimental microstructural changes, and this amount is greater than the normal deformation at tensile failure of TD NiCr.

In normal fabrication of rivets, the heads are formed by upset forging either at room temperature or elevated temperatures. In the case of TD NiCr rivets, the deformation during heading coupled with subsequent exposure to temperatures in the range of 871°C (1,600°F) to 1,204°C (2,200°F) caused the microstructure in the head of the fastener to become fine-grained and untextured. This type of microstructure is typical of low strength TD NiCr.

Production of TD NiCr rivets was first tried by heading the rivets at 649°C (1,200°F) and subsequently annealing them at 1,300°C (2,370°F) for 1 hour in an inert environment. Slide 3 shows the rivets before and after annealing. Studies of the post-annealed rivet microstructures showed the first fabrication approach to be only partially successful in achieving a high strength condition, as the fine grained, low strength microstructure was still present to some extent in the head of the rivets after annealing.

TD NICKEL-CHROMIUM WARM HEADED RIVETS

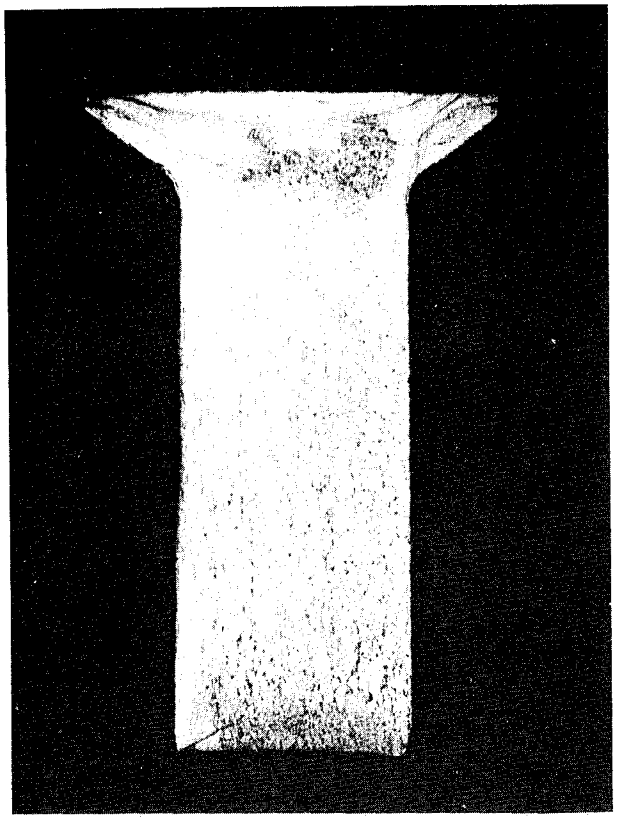

HEADED AT 649^{0} C (1,200^{0} F) FROM ANNEALED HIGH STRENGTH BAR

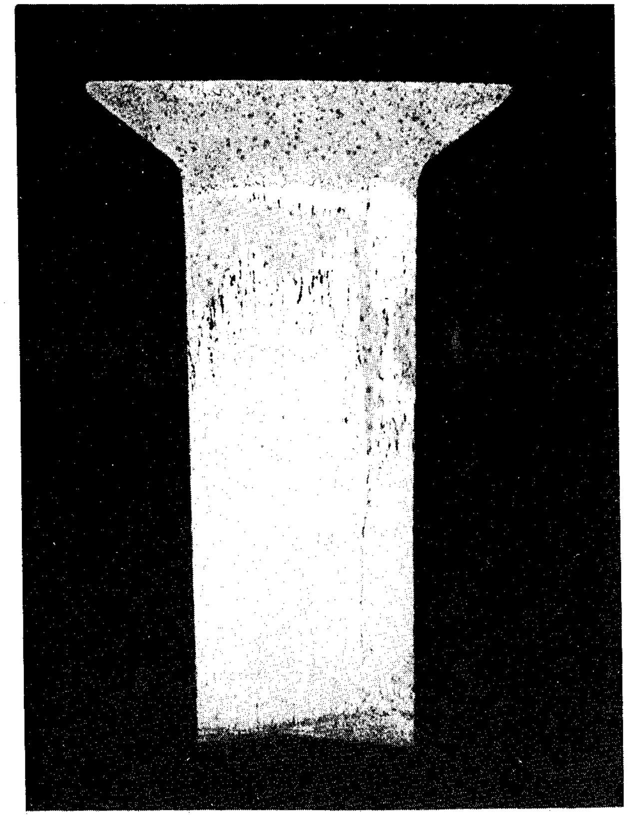

HEADED AT 649^{0} C (1,200^{0} F) PLUS ANNEALED 1 HR. AT 1,299^{0} C (2,370^{0} F) IN ARGON

Slide 3

TD NICKEL-CHROMIUM MACHINED RIVETS

(Slide 4)

This slide illustrates the second fabrication approach in which the rivets were machined from bar stock having a mixed grain size and then annealed at 1,300°C (2,370°F). The material microstructure achieved in this approach is typical of the large, axially elongated grains that are characteristic of the high strength TD NiCr. The second fabrication approach provided the best rivets, and, consequently, was used for all of the TD NiCr rivets in the test assembly.

All TD NiCr fasteners, both screws and rivets, were annealed at 1,300°C (2,370°F) for 1 hour in Argon. They were then preoxidized in the air furnace at 1,093°C (2,000°F) for 1 hour to provide an initial oxide coating. This oxide coating should help in preventing galling or seizing of the flush head panel attachment screws during high temperature exposures.

TD NICKEL-CHROMIUM MACHINED RIVETS

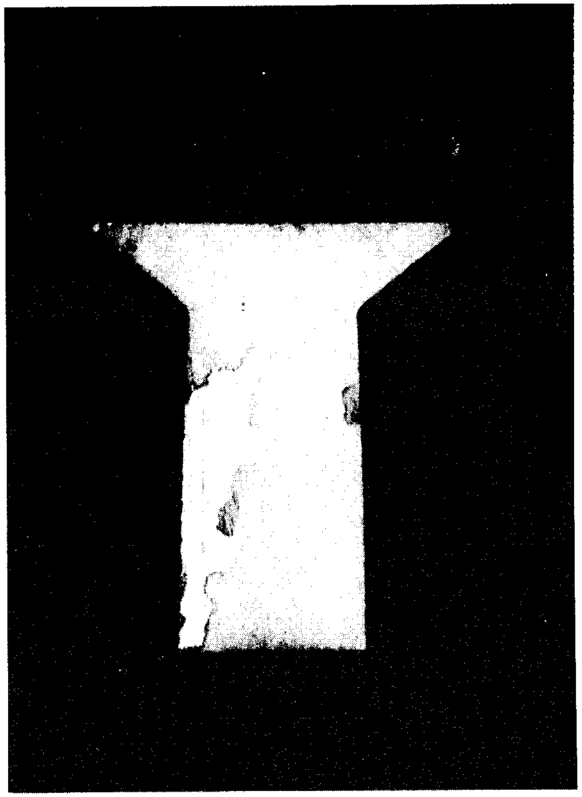

MACHINED FROM PARTIALLY RECRYSTALLIZED BAR

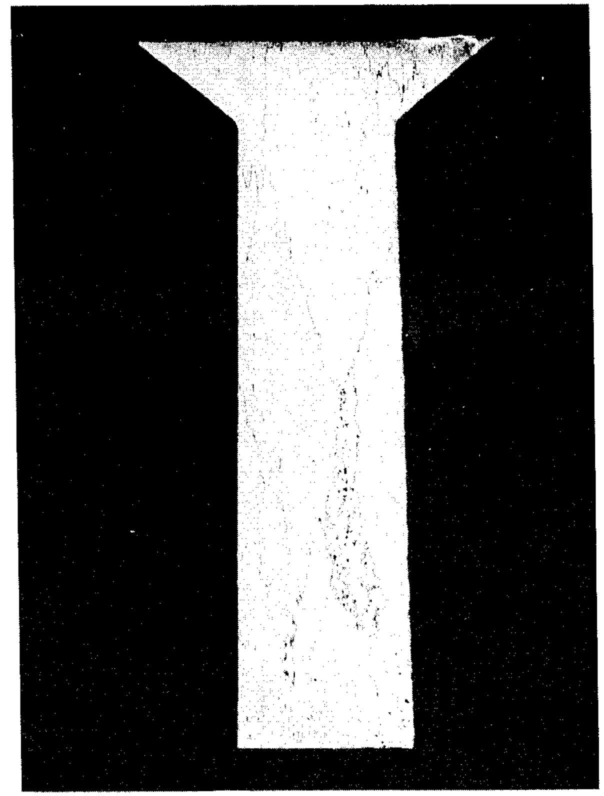

MACHINED PLUS ANNEALED 1 HR. AT 1,299^{0} C (2,370^{0} F) IN ARGON

Slide 4

TEST ASSEMBLY SURFACE PANEL

(Slide 5)

TD NiCr panels were used over the entire test assembly, a total of 30 panels being used to cover the fin primary structure. The panels used a single faced corrugation stiffened design in which the detail parts were assembled by spotwelding. Panel face sheets were made from 0.38-mm (0.015-in.) sheet, the corrugations were 0.25-mm (0.010-in.) material and the edge members were 0.51-mm (0.020-in.) gage TD NiCr. Assembly of the panels was accomplished by spotwelding the edge members and corrugations together initially, followed by spotwelding the face sheet to the sub-assembly of edge members and corrugation. After each panel was spotwelded it was then cleaned, grit blasted and preoxidized at 1,093°C (2,000°F) for 1 hour in an air furnace. The panel attach points were dimpled for the 6.35-mm (1/4-in.) diameter NAS 1221 configuration flush head screws that were used to attach the panels to the primary structure. The average weight for panels used on the test assembly was 8.2 kg/m^2 (1.68 lb./sq.ft.).

Several critical design areas were selected for preliminary test evaluation before final design stages were reached. One such component selected for tests was a typical surface panel. As shown in this slide, test panels were mounted on a TD NiCr riveted frame that simulated the fin primary structure and the test panel was then subjected to repeated 30 minute thermal cycles to evaluate the panel's ability to withstand repeated thermal exposures. Maximum panel face temperature reached in the test series was 1,227°C (2,240°F). Panel face sheet buckling occurred in the initial flat-faced panel designs and resulted in permanent deformation of the face sheets. The final panel design incorporated shallow beads in the face sheet, a design change which prevented buckling and provided a configuration capable of sustaining repeated thermal cycles. The final design sustained 30 test cycles without failure.

TD NiCr TEST HEAT SHIELD

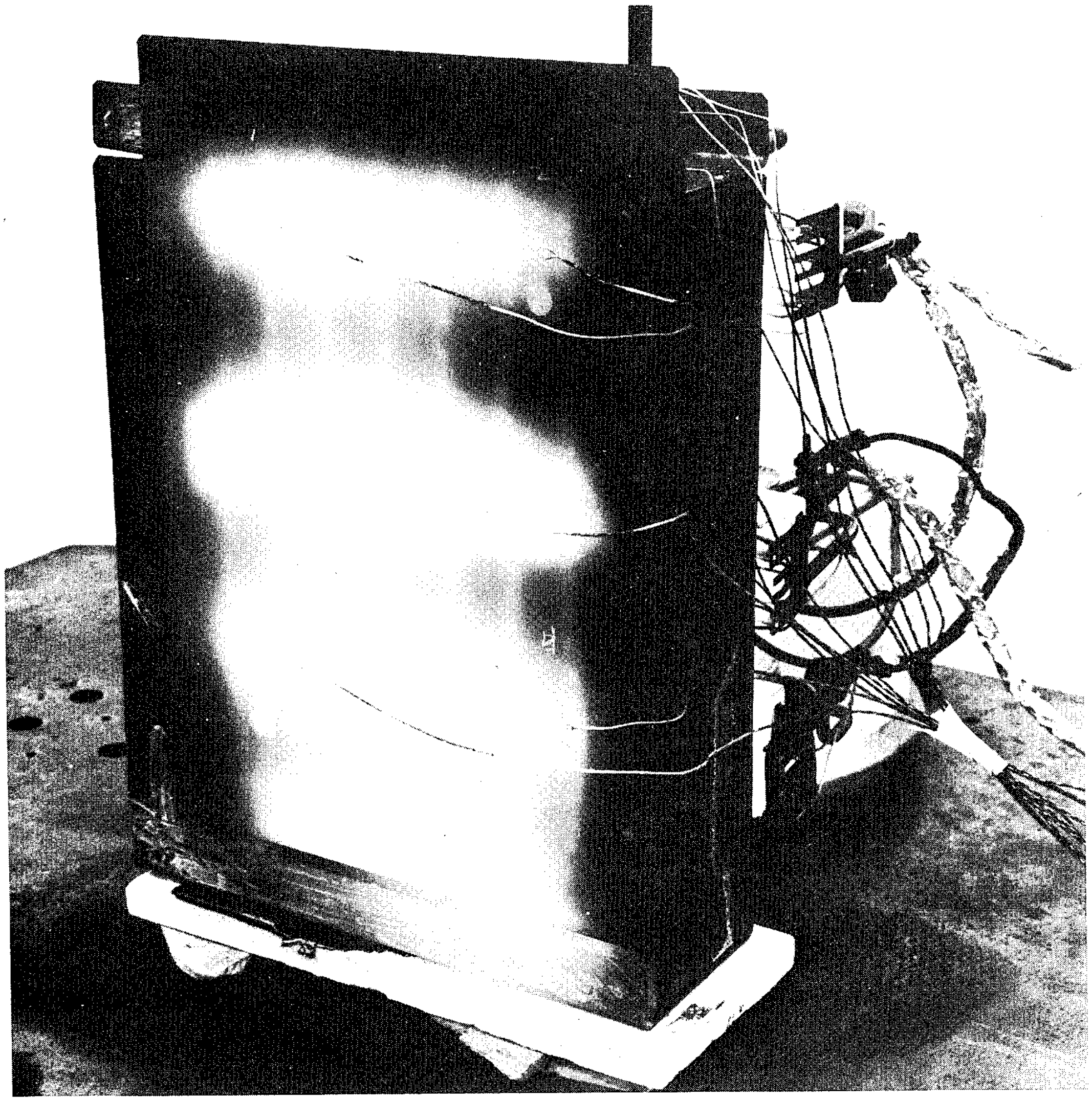

Slide 5

TEST LOADS AND TEMPERATURES FOR EXIT FLIGHT CONDITIONS

(Slides 6 and 7)

The operational mode of the FDL-5A was projected as that of a vertically boosted earth-orbital reentry vehicle having a nominal reentry time of 60 to 90 minutes. With such mission characteristics in mind, the two test conditions considered were exit and reentry flight load and temperature cycles.

Typical load and temperature profiles were developed for both flight conditions, and modifications were made to fit within simulation capabilities of the test facilities. Time-histories of the total fin loads and temperatures are shown in the next two slides for test conditions simulating exit flight. The relatively low temperatures during boost, coupled with the desire to protect strain gage instrumentation against damage from temperature overshoot, led to the selection of a constant temperature profile of 149°C (300°F) for exit flight simulation tests.

TEST LOAD NORMAL TO FIN SURFACE

EXIT FLIGHT CONDITION

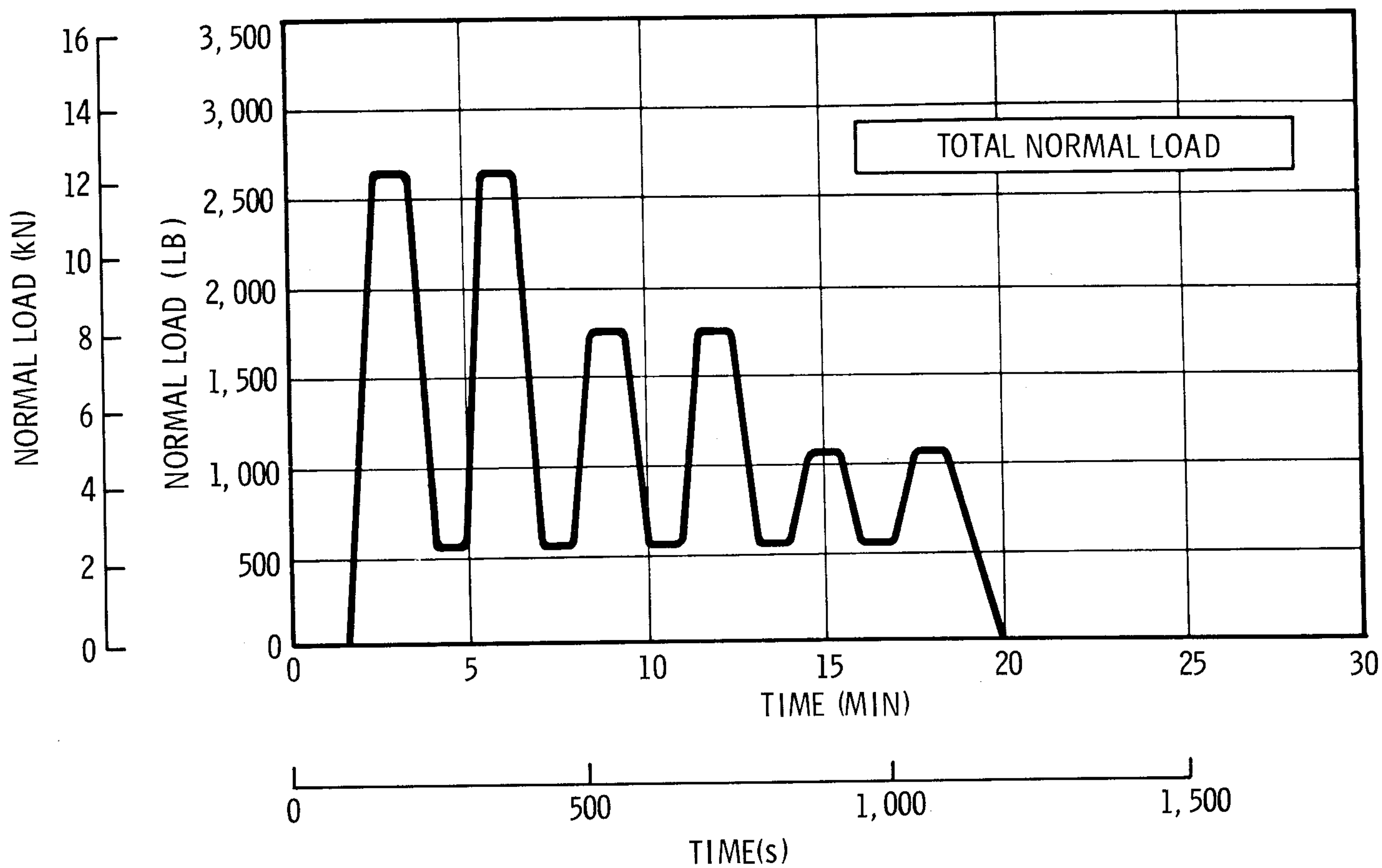

Slide 6

CHORDWISE TEST LOAD AND SURFACE TEMPERATURE

EXIT FLIGHT CONDITION

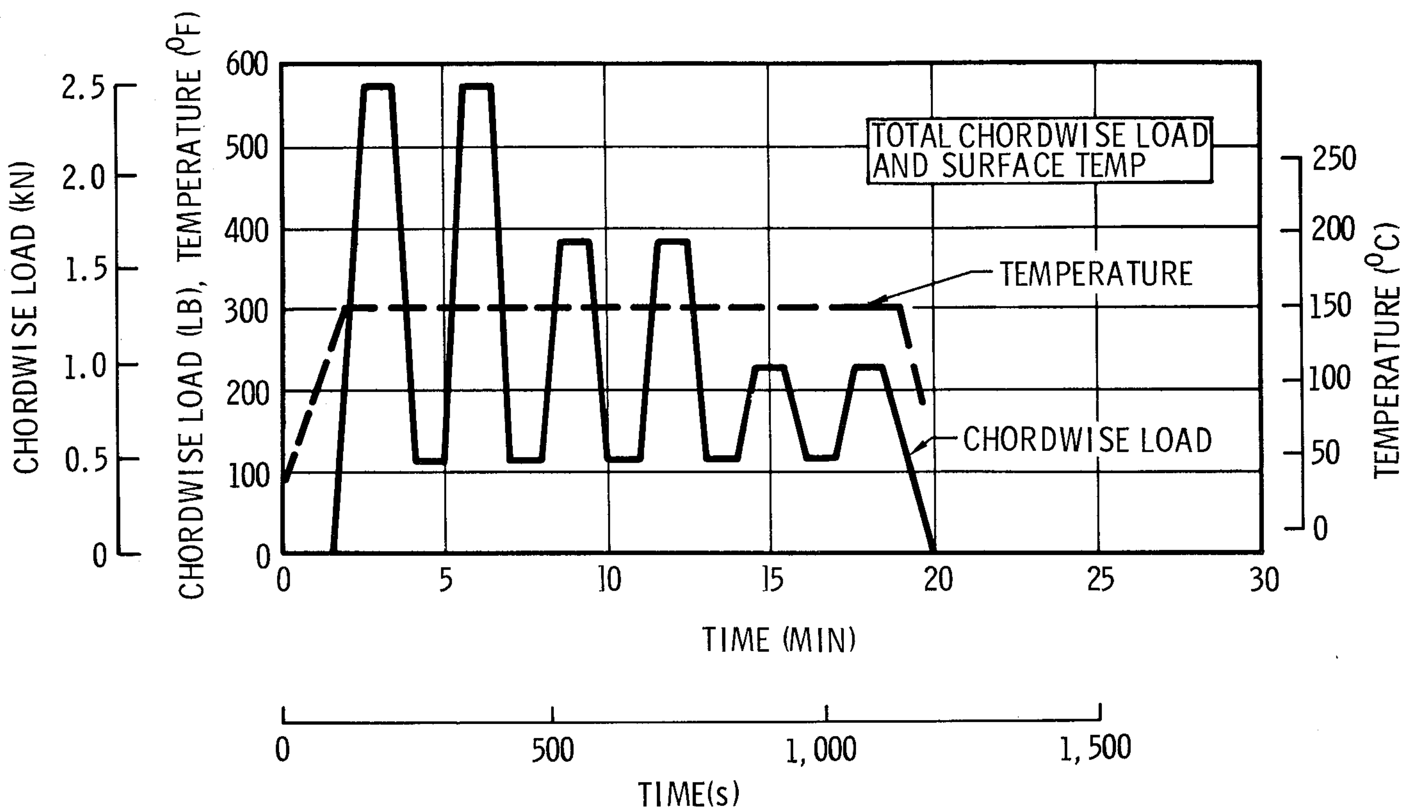

Slide 7

MAXIMUM REENTRY TEST TEMPERATURES

(Slides 8 and 9)

In reentry conditions the temperatures vary significantly across the surface of the fin and from one side of the fin to the other. The more complex temperature distributions for reentry were based upon available model test data that simulated the FDL-5A vertical fin surface. The selected distributions and the maximum temperatures associated with each isotherm are shown in Slide 8 for both sides of the test assembly. As shown here, a maximum test temperature of 1,204°C (2,200°F) is imposed near the leading edge.

Temperature time-histories used in tests simulating the reentry flight condition are shown in the following slide for the structural assembly areas sustaining the highest temperatures. The maximum temperature rise rate is 125°C (225°F) per min., which occurs in the hottest zone. Peak temperatures are held for 30 minutes, after which the temperature is dropped to approximately 80 percent of the maximum and held at that point for an additional 20 minutes. The total simulated reentry heating cycle has a duration of 90 minutes.

DISTRIBUTION OF MAXIMUM TEMPERATURES

REENTRY TESTS

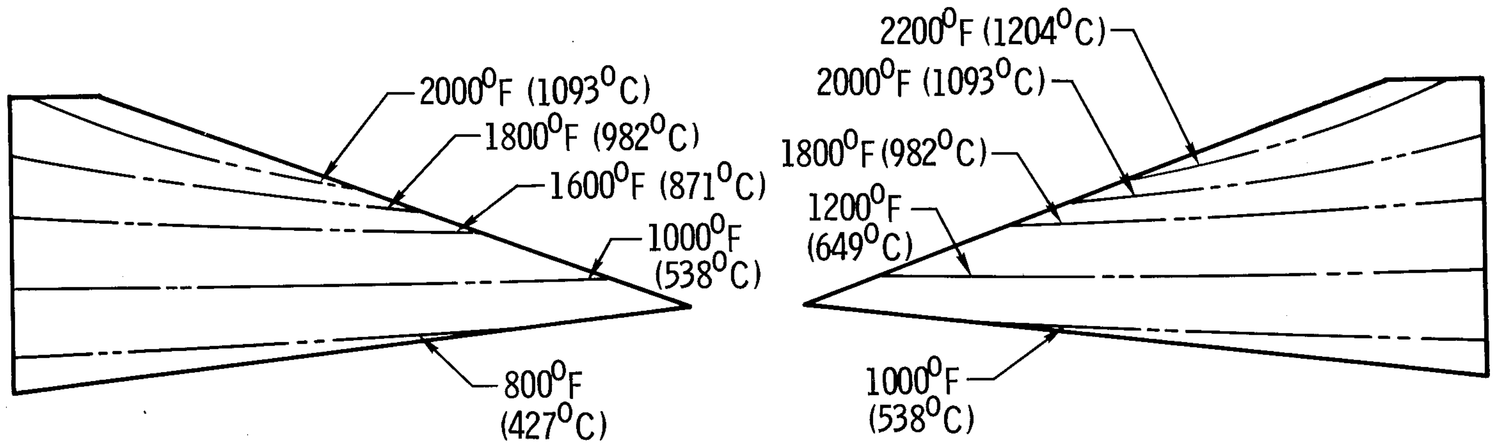

RIGHT HAND SIDE
(LOWER SIDE IN TEST POSITION)

LEFT HAND SIDE
(UPPER SIDE IN TEST POSITION)

Slide 8

TEST TEMPERATURE PROFILES

REENTRY FLIGHT CONDITION

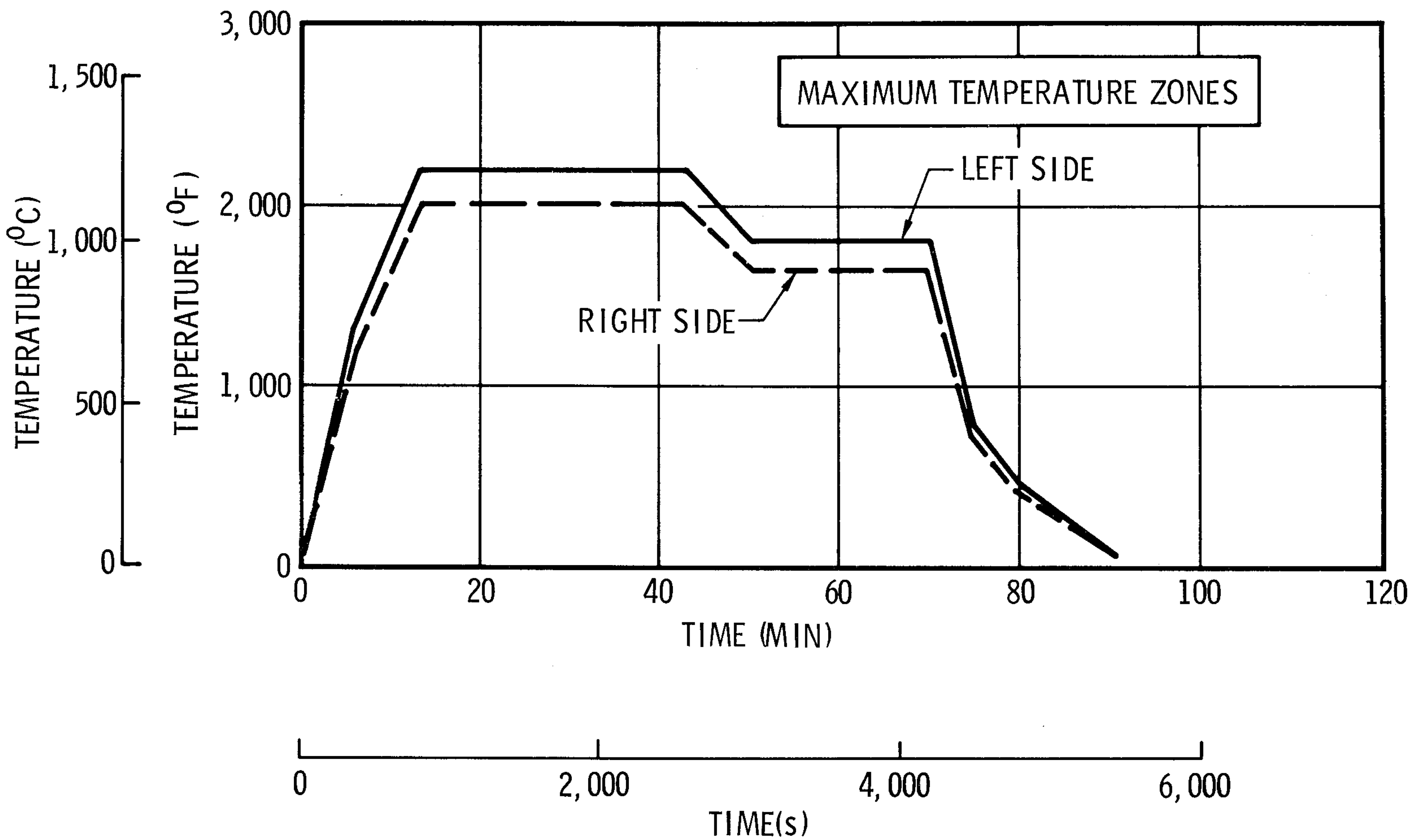

Slide 9

TEST LOADS FOR REENTRY FLIGHT CONDITIONS

(Slide 10)

The total fin loads are shown in this slide for the reentry test condition. Maximum cyclic loads are applied during the period of peak temperatures, with the loads decreasing to about 65 percent of the maximum during the period when a lower temperature plateau is applied. Minimum loads are 40 percent of the maximum loads for both exit and reentry conditions. The test loads shown in Slides 6 and 7, as well as this slide, are limit loads since a major test objective is to evaluate the effects on the structure of repeated applications of expected service loads and temperatures. The loads used for design of the structure were higher by a factor of 1.8 for exit conditions and by 1.5 for reentry conditions. The 1.8 ratio of ultimate to limit load used for exit conditions included a dynamic factor of 1.2.

TEST LOAD NORMAL TO FIN SURFACE

REENTRY FLIGHT CONDITION

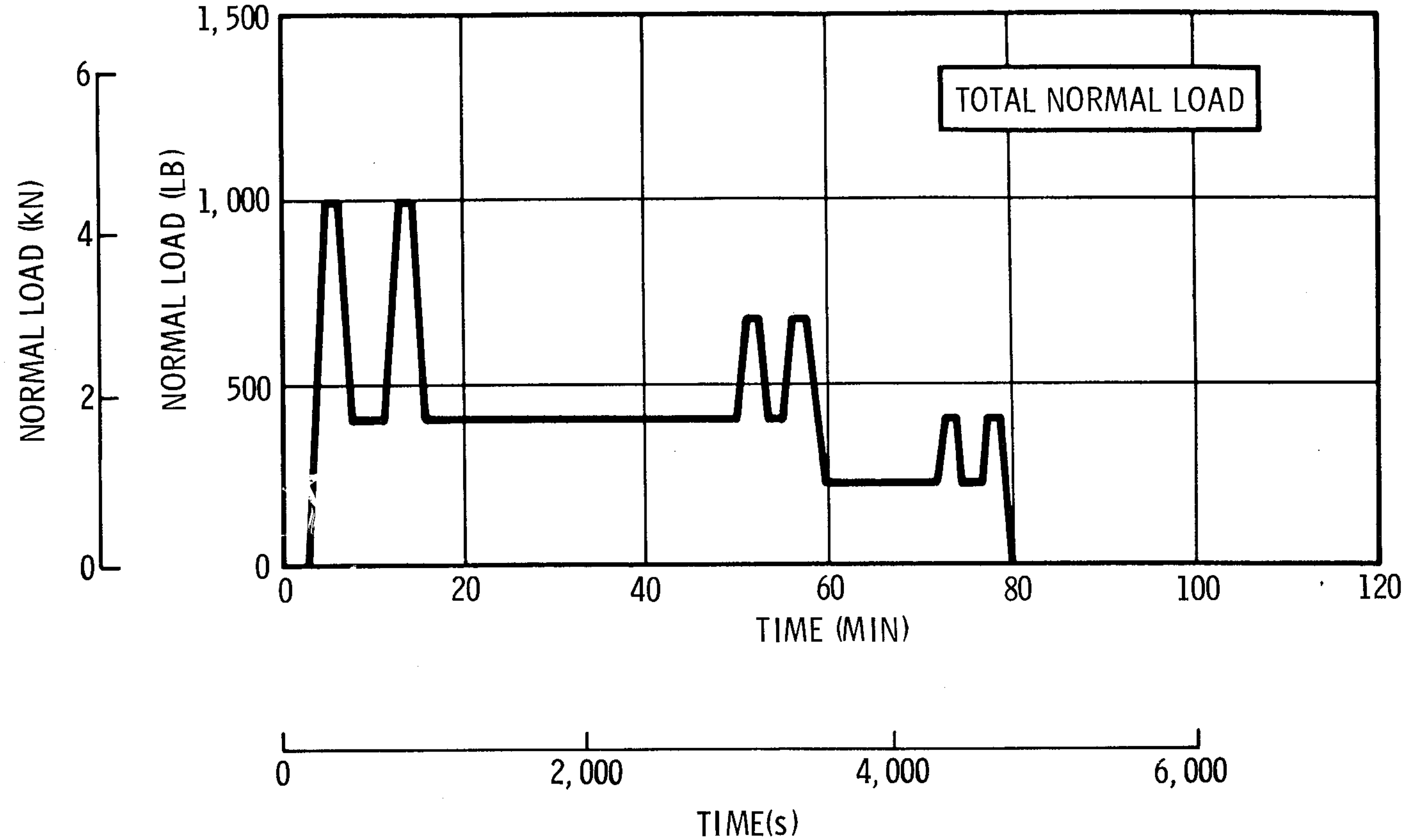

Slide 10

DSM FIN TEST SYSTEM

(Slide 11)

The overall test arrangement for the fin consists of a cantilevered horizontal attachment to a vertical test jig framework. Shown in this slide with the transition structure removed is the test setup consisting of load, thermal and data acquisition systems.

Programmed cyclic loads are applied to the structure through hydraulic load cylinders in response to signals from the Common Load/Heat Control Computer. Both normal and chordwise loads are applied, the normal loads being introduced at fittings near the tip of each spar and the chordwise loads being introduced at approximately the half-span position on the rear spar.

The heating system consists of heat lamp assemblies in position a few inches from each surface of the fin. The heat lamp assembly for each side is divided into 12 zones each controlled through the Heat Control Computer to provide the proper temperature profile.

Data acquisition is accomplished by the Transmitter Multiplexer Unit. Data signals are conditioned and transmitted to the CDC 1604 Digital Computer for Storage and/or processing.

Incorporated in the test system are automatic and manual abort procedures for temperature and load overshoot. The 1604 Digital Computer also controls an alarm display board which displays different colored lights for control and backup thermocouples for over and under programmed temperature conditions for each zone.

DSM FIN TEST SYSTEM

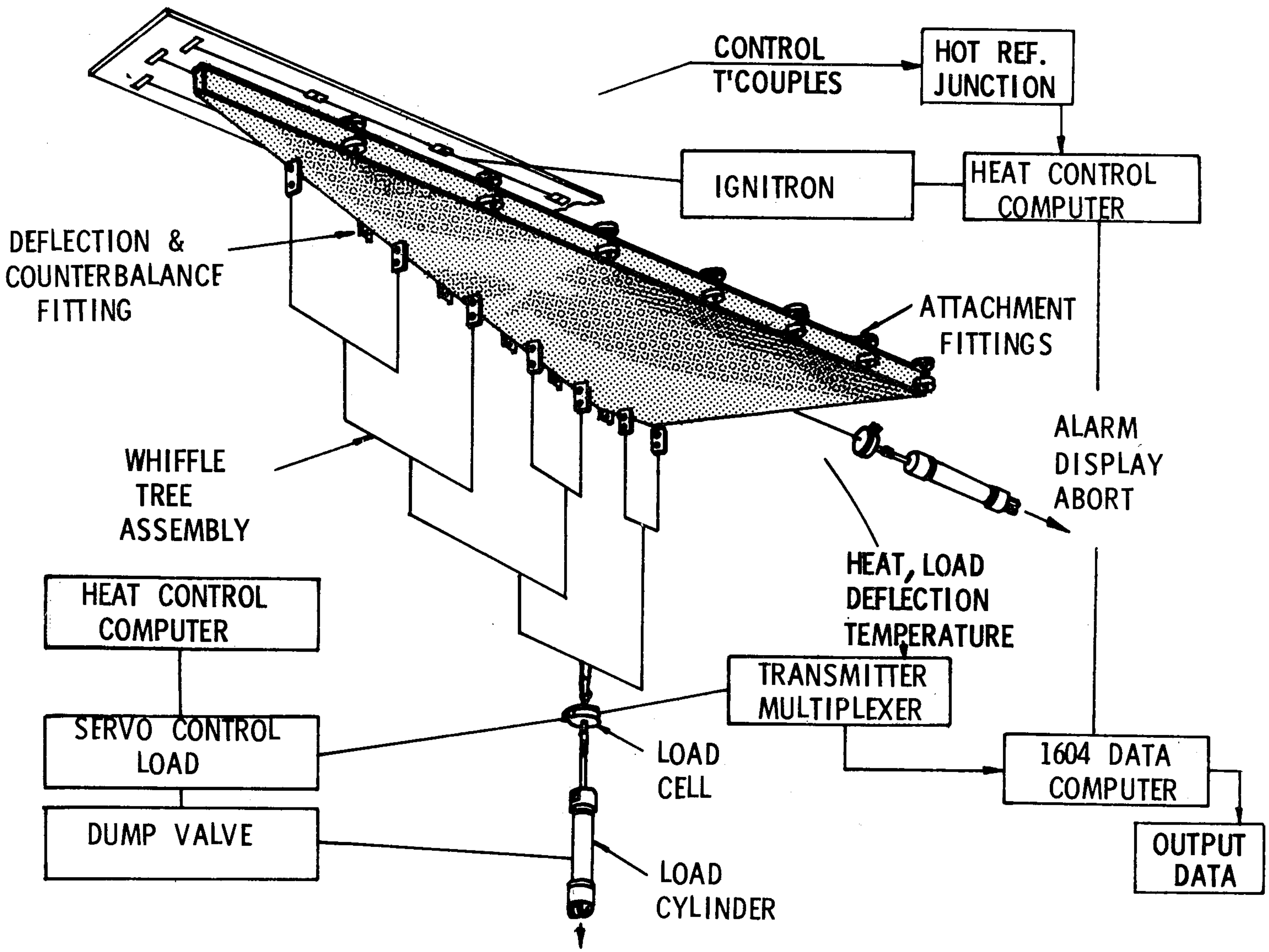

Slide 11

EXIT FLIGHT SIMULATION TEST

(Slide 12)

Basic test data to be recorded and reduced will be strains, temperatures and deflections. Strains, of course, can be measured only during exit flight profile tests because of temperature limits of available strain gages. A total of 41 strain gages and 61 thermocouples were used to instrument the primary structure and attach fittings, while the surface panels were instrumented with 59 thermocouples. This slide shows the fin during an exit profile test where 100% limit load is applied and surface temperatures are approximately 149°C (300°F). The view shown here is along the leading edge, forward (right) to aft (left) positions. Selected temperatures and stresses experienced by the primary structure are shown on the next slide.

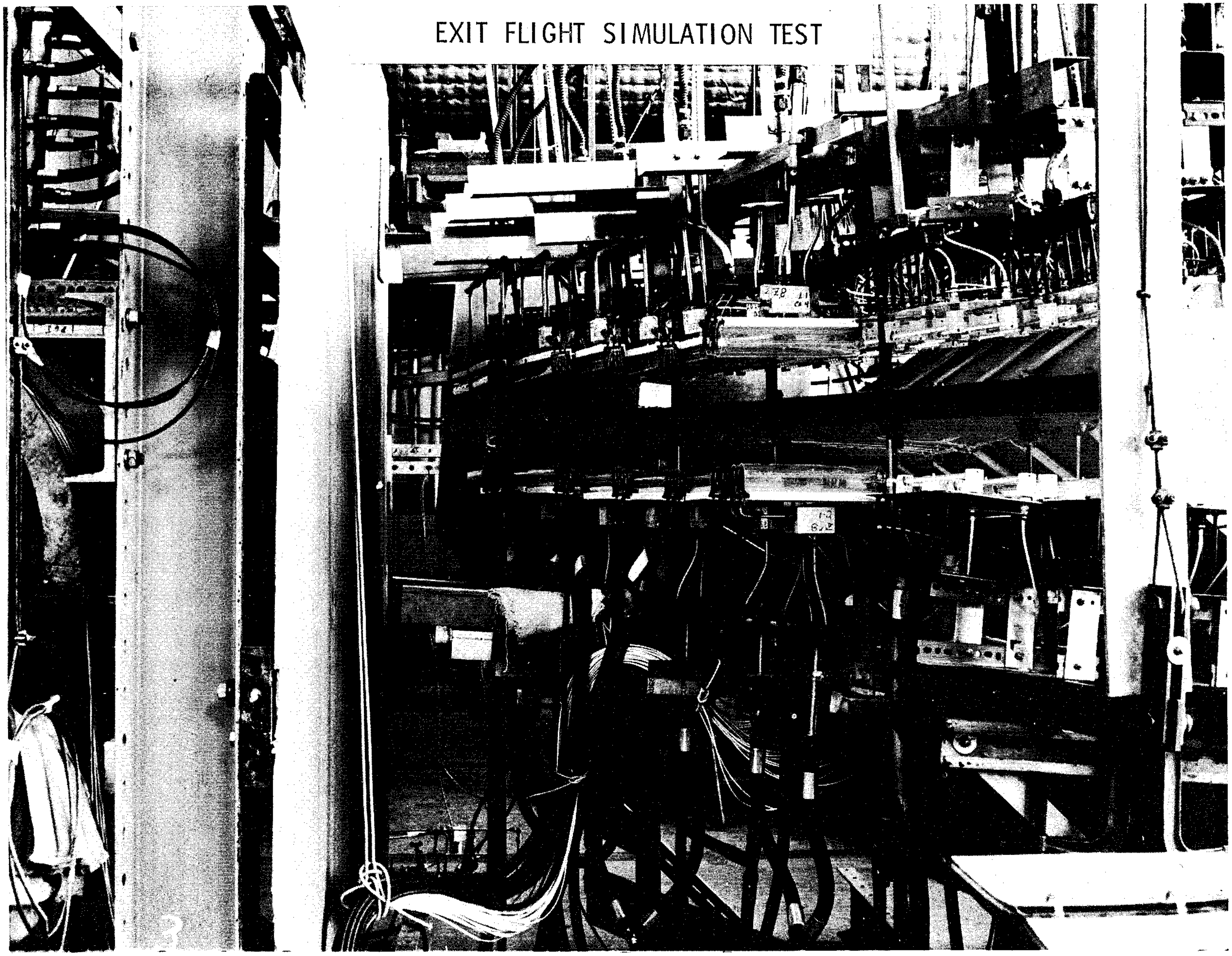

Slide 12

PRELIMINARY TEST RESULTS - EXIT FLIGHT CONDITION

(Slide 13)

Initial data results from the exit flight condition profile tests are shown on this slide. Selected stresses, tension and compression are indicated at various spar locations of the fin's primary structure as 100% limit load is applied. Temperatures shown are temperatures recorded at the time of maximum stress condition. Maximum external surface temperatures of the fin assembly ranged from 121°C (250°F) to 177°C (350°F) during the test run. Fifty repeated exit flight test runs are scheduled followed by a series of reentry test cycles.

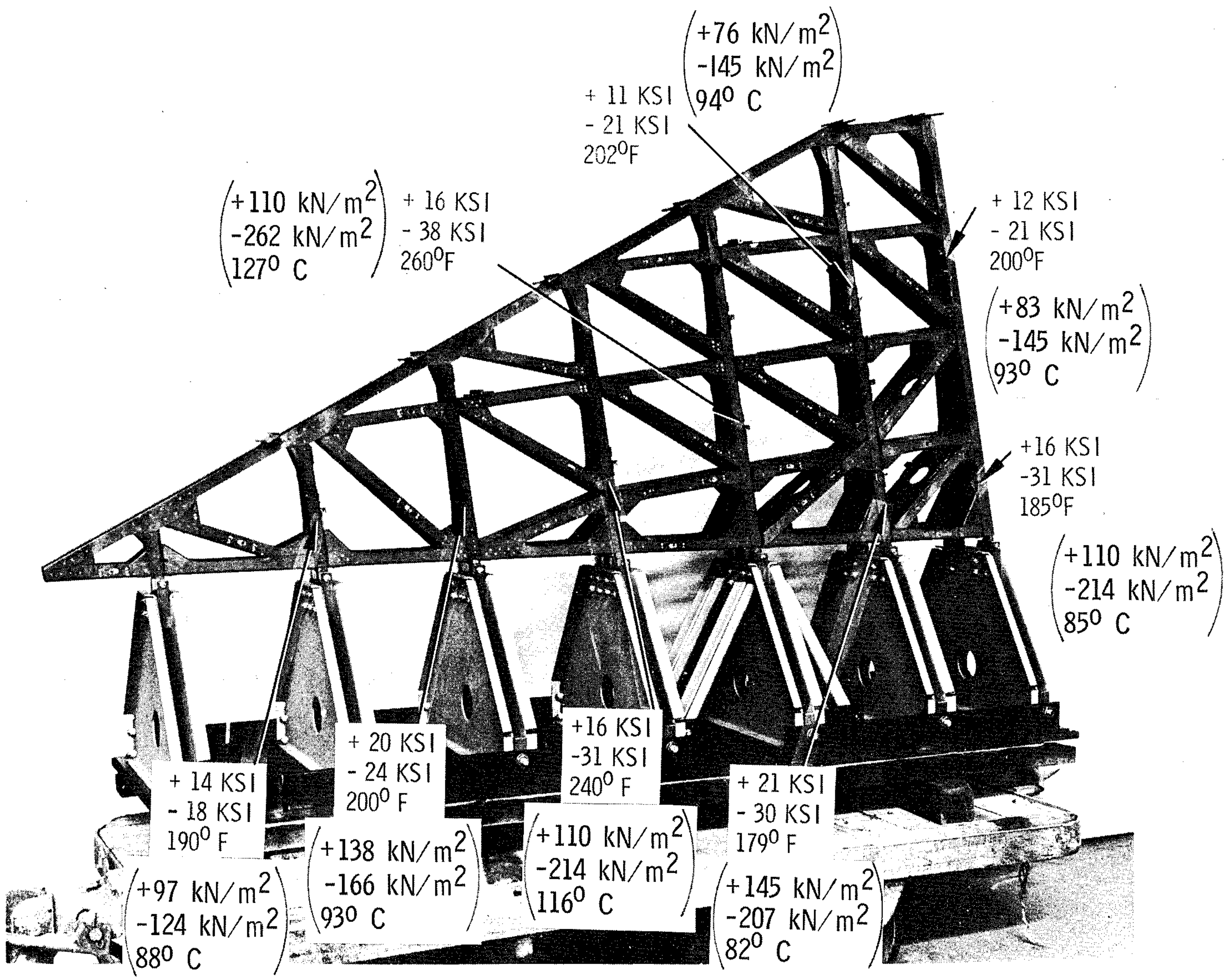

INITIAL TEST DATA - EXIT FLIGHT 100% L. LOAD

Slide 13

DESIGN AND TEST OF ADVANCED STRUCTURAL COMPONENTS AND ASSEMBLIES

By E. E. Engler and C. E. Cataldo
NASA George C. Marshall Space Flight Center
Marshall Space Flight Center, Ala.

In the development of structural concepts for planned new vehicle systems, such as the Space Shuttle, proof of concept through design, fabrication and test of large components and assemblies is an important link in the technology program. All areas of development, from material and analysis method research, advanced design, manufacturing technology, cost, NDI, and testing are combined into one program.

Two structural technology areas of special interest for the Space Shuttle are discussed in this report: Development of TPS/primary structure interaction and application of advanced composites for primary structures.

The two programs reported on have as goals the establishment of reliable TPS/primary structural design and the demonstration of the feasibility of the design by tests, and the determination of whether or not advanced composites have a defined place in the planned Space Shuttle stages. Several individual technology tasks are underway in these areas and considerable progress has been made, yet the work is far from completed. In general, the materials have been selected and the basic structural design concepts developed, but construction of test components, test facilities, and testing analyses have not progressed as well as originally anticipated. Details on the status of the programs and some results obtained to date are reported.

PAPER 16

TPS/Primary Structure

During the conceptual design of phase B Space Shuttle study, a number of metallic and non-metallic heat shield designs are being proposed. Shown on Figure 1 are the unit weights of some of the metallic designs, including the ones selected for test item No. 1 (Figure 2).

The spread in unit weight, depending on selection of design, material and environment, clearly indicates the need for the pursued program. An orbiter having a wetted area of approximately 2200 m^2 (20,000 ft^2) could experience a change in dry weight of 4540 kg (10,000 lb.), which is equivalent to payload weight, by having a unit weight change in the TPS of 2.44 kg/m^2 (0.5 lb/ft^2). Pressure and temperature predictions, material selection, applied factors of safety and design selection therefore are of upmost importance.

METALLIC HEAT SHIELD WEIGHTS AT TEMPERATURE

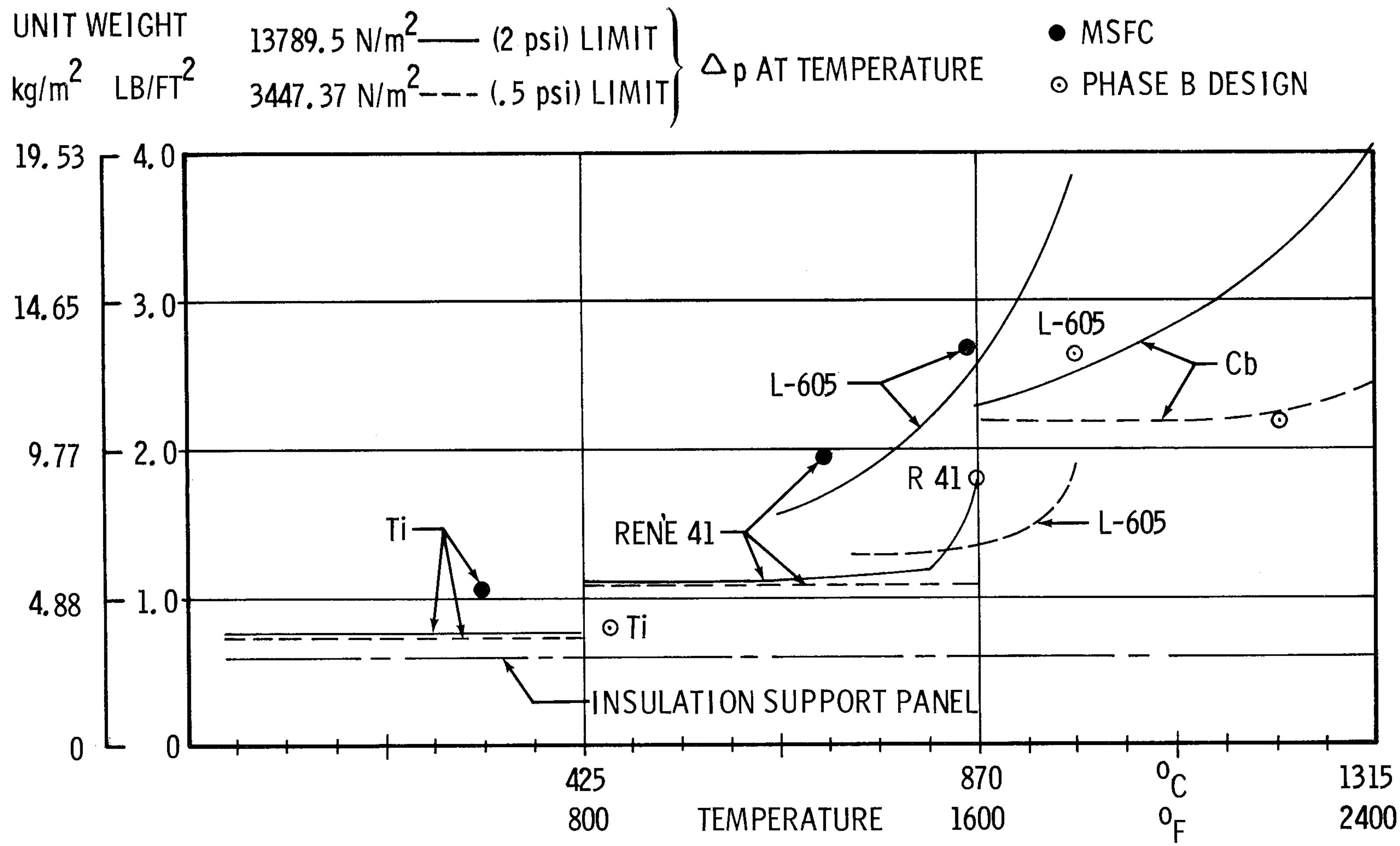

Figure 1

Detail design, thermal and structural analysis and preparation of test requirements for Test Item #1 are complete.

Hardware, including skins and bulkheads, is on hand for the liquid hydrogen tank. The welding process to be used has been verified and work orders issued for component fabrication, based on advanced information. A cleaning procedure is being developed and equipment fabricated to clean the tank after hydrostatic test preparatory to installing the internal insulation.

Process development for the materials to be used for the TPS Test Components and Test Item No. 1 continues. Machining, cleaning, forming and thermal treating processes have been established. Joining techniques are being established.

Materials are on hand for the additional process development required for Test Item No. 2. These are Haynes Alloy 188 and Columbium Alloys Cb 752, C 129Y, and FS 85. Manufacturing procedures are being developed.

Three metallic heat shield panels representing Test Item No. 1 configuration and materials are being fabricated.

TEST ITEM NO. 1 LH_2 TANK SECTION (BOOSTER)

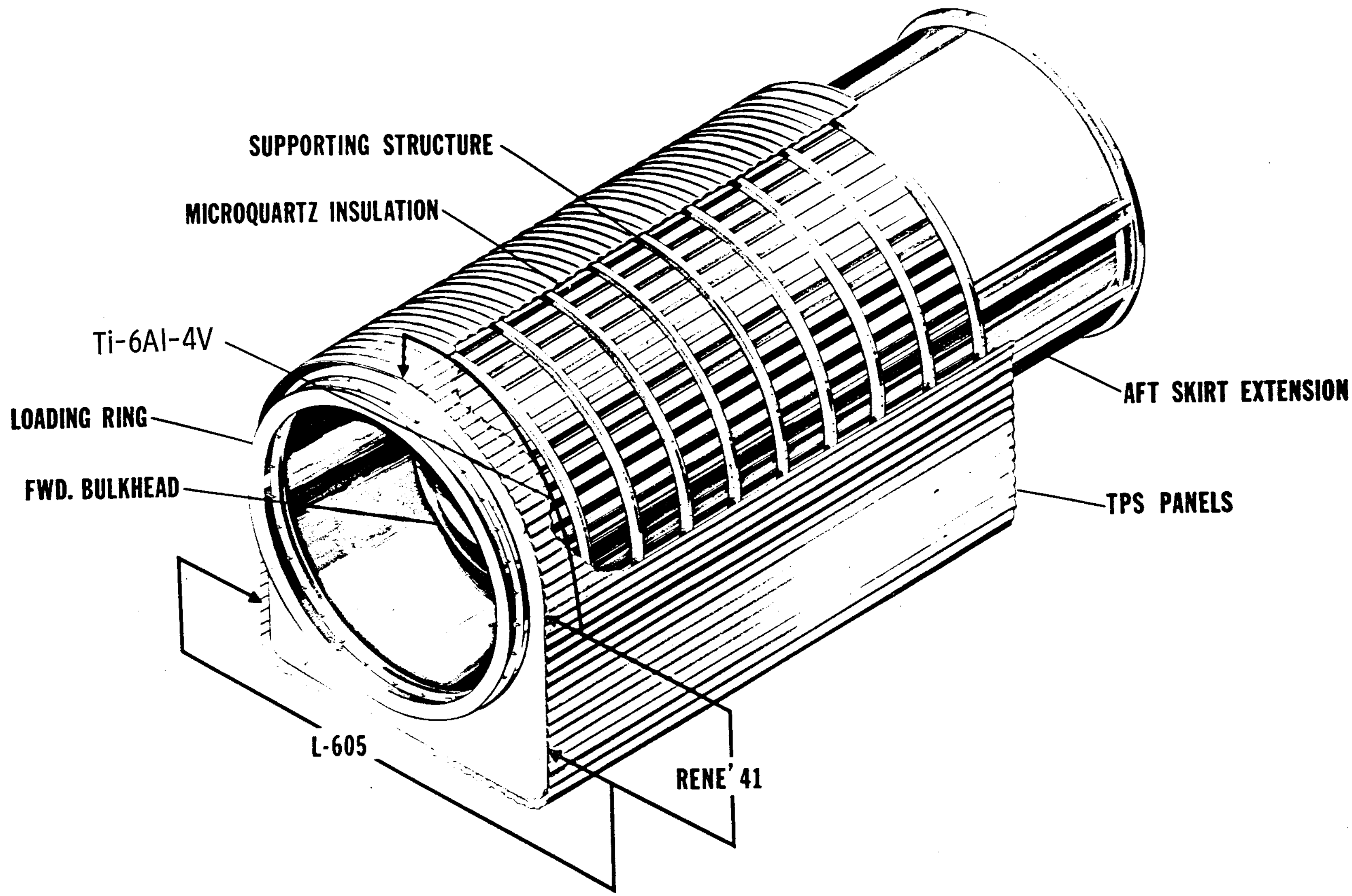

Figure 2

Material properties for design purposes were established for cobalt based superalloys L-605 and HS-188 and values are shown in Figure 3. Evaluation of TD nickel-chrome dispersion strengthened alloy and its fabricability and processing is in progress.

Stress corrosion tests on Inconel 718, Waspalloy, Rene' 41, A 286, L-605 and HS-188 were performed. All alloys passed room temperature requirements. High temperature stress corrosion effects and required test procedures are being determined.

MATERIAL PROPERTIES OF L-605 AND HS-188 COBALT BASE ALLOYS

TEST TEMP.	ALLOY	SPECIMEN CONDITION	SPECIMEN DIRECTION	SPECIMEN THICKNESS	F_{tu}		F_{ty}		ELONG. IN 50mm (2.0") (%)
					N/mm^2	KSI	N/mm^2	KSI	
24^{0}C (75^{0}F)	L-605	AS-REC.	T	1.6mm (.063")	952.2	138.1	461.3	66.9	52.5
	HS-188	AS-REC.	T	1.14mm (.045")	932.2	135.2	439.2	63.7	61.5
	HS-188	20% C.W.	T	0.91mm (.036")	1152.8	167.2	960.4	139.3	28.5
700^{0}C (1300^{0}F)	L-605	AS-REC.	T		652.9	94.7	255.8	37.1	34.5
	HS-188	AS-REC.	T		498.5	72.3	216.5	31.4	21.5
	HS-188	20% C.W.	T		808.1	117.2	648.8	94.1	8.5
870^{0}C (1600^{0}F)	L-605	AS-REC.	T		348.2	50.5	233.0	33.8	33.5
	HS-188	AS-REC.	T		355.1	51.5	220.0	32.2	25.0
	HS-188	20% C.W.	T		388.9	56.4	323.4	46.9	13.5
980^{0}C (1800^{0}F)	L-605	AS-REC.	T		168.2	24.4	133.1	19.3	35.0
	HS-188	AS-REC.	T		198.6	28.8	128.9	18.7	35.0
	HS-188	20% C.W.	T		189.6	27.5	126.2	18.3	18.0

Figure 3

During the material evaluation of HS 188, previously recommended for an upper use temperature of 1095^{o}C (2000^{o} F.), a loss of cold work strength and increase in creep were observed after repeated temperature cycling to levels shown (Figure 4). Resistance level is indicated at 980^{o} C. (1800^{o} F.)

HS-188 MATERIAL PROPERTIES AFTER TEMP. CYCLING (ROOM TEMP. VALUES)

EXPOSURE CONDITIONS	SPECIMEN CONDITION	SPEC. DIRECT.	SPECIMEN THICKNESS		F_{tu}		F_{ty} 0.2%		ELONG. IN 50mm - (2.0") (%)	C HARDNESS ROCKWELL
			mm	in	N/mm^2	KSI	N/mm^2	KSI		
NONE	AS REC.	T	1.14mm	.045"	926.7	134.4	415.1	60.2	62.5	13.5
NONE	20% CW	T	0.91mm	.036"	1157.9	167.5	924.5	136.7	30.0	34.0
1031.7^{0}C (1890 ^{0}F) } 15 min										
CYCLED 25 TIMES	AS REC.	L			883.2	128.1	392.3	56.9	36.5	16.0
" "	20% CW	L			993.5	144.1	444.0	64.4	46.5	24.0
1185^{0}C (2165^{0}F) } 30 min										
RAPID COOL	AS REC.	L			889.4	129.0	379.9	55.1	63.0	14.0
" "	20% CW	L			887.4	128.7	364.7	52.9	62.5	14.0

Figure 4

Test fixtures for metallic heat shield panel tests were designed and built. Figure 5 shows the heating fixture to be used in the 15-foot vacuum system. Cold wall simulation with LN_2, purge with GN_2, and temperature profiles up to 1370° C. (2500° F.) can be simulated in ambient and reduced pressure atmosphere. Panels up to 1m x 1m (36" x 36") can be tested.

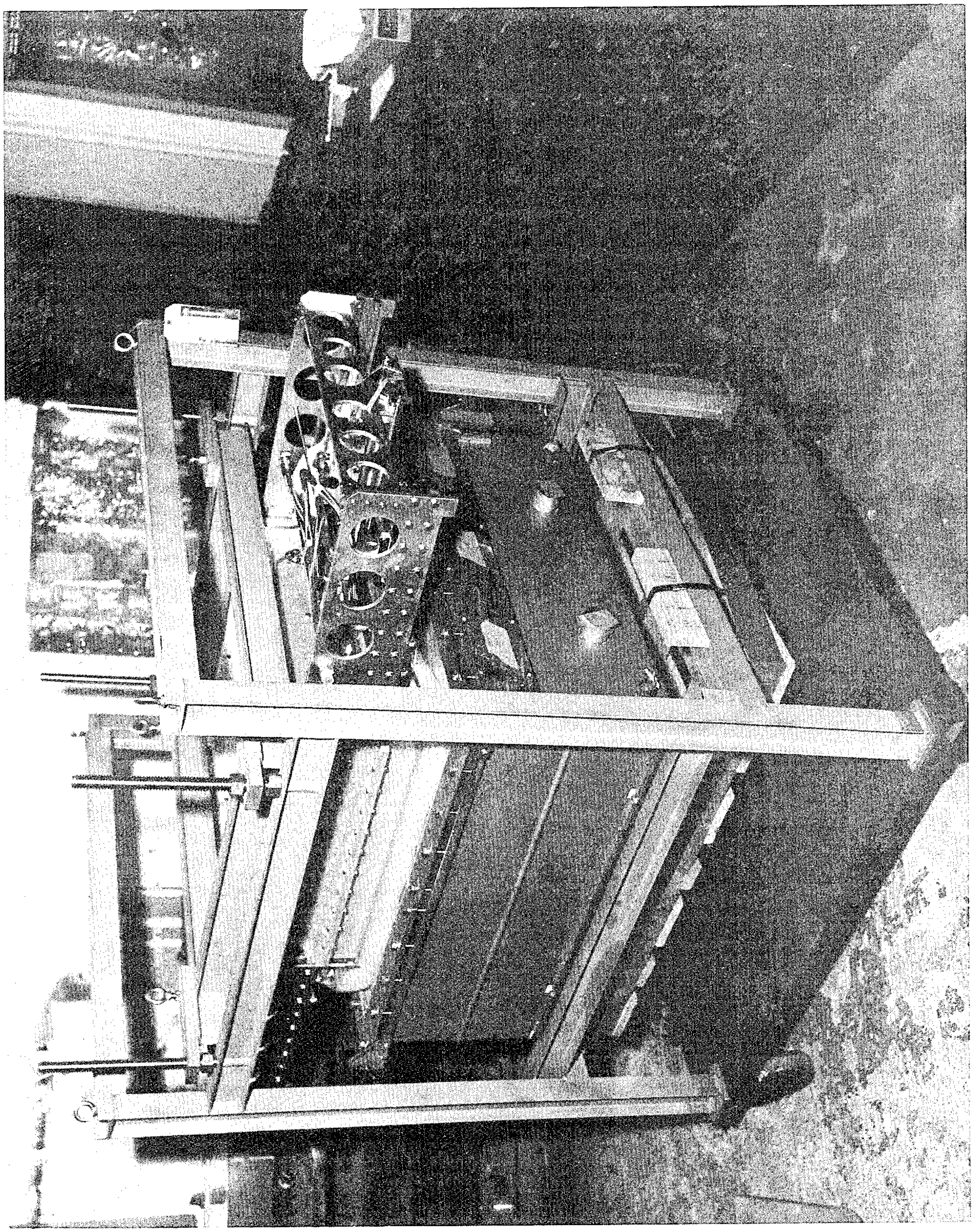

Figure 5

Thermal-acoustic tests will be conducted, using the test setup shown in Figure 6. The panel will be installed in an opening between the reverberation and anechoic chambers of the MSFC acoustic test facility, using the fixture. Heating and acoustic environment will be applied. Panels up to 1m x 1m (36" x 36") can be tested. Facility checkout and test concept demonstration are complete.

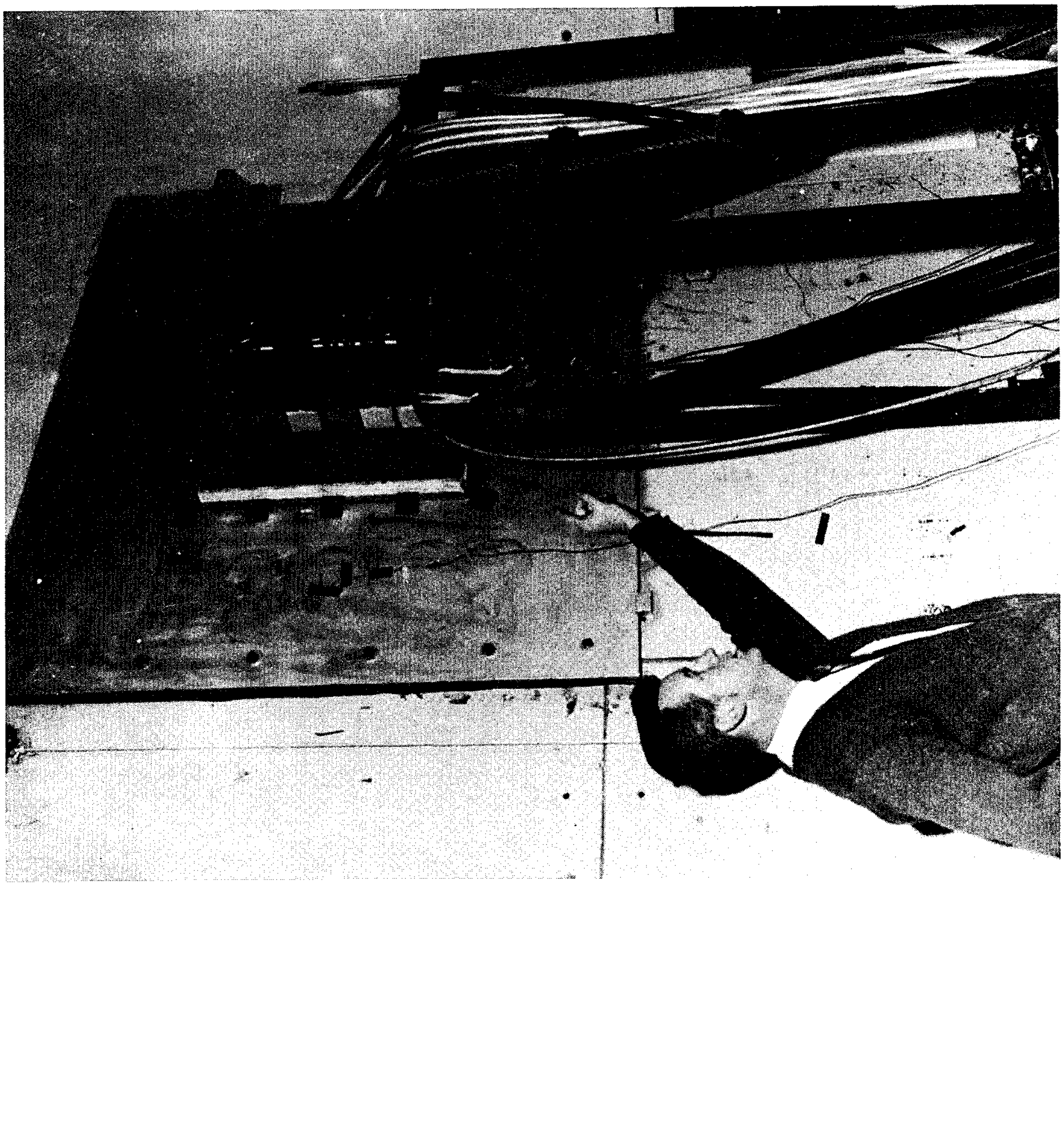

Figure 6

NDI (Nondestructive Inspection) Methods Development

Super Alloys:

Eddy current inspection using the Phasemaster Model D was selected since it does not require any special coupling media and the material does not have to be cleaned after use. The instrument basically responds to changes in electrical conductivity which makes it sensitive to surface cracks, material thickness and heat treat conditions. By observing rate of indication change, performing multi-frequency test, etc., these various changes can be distinguished from each other. Sensitivity to various conditions is as follows.

Coated Columbium:

In addition to the above type application, the Phasemaster will be used to measure coating thickness on coated Columbium alloys.

Stimulated electron emission radiography will be used during processing to assure homogeneity of coating chemistry. In test this technique will be evaluated as a possible monitor of coating condition.

Primary Structure:

Standard radiographic and dye penetrant inspection of tankage weldments will be performed to MSFC-SPEC-504. Delta Ultrasonic and Eddy Current Testing will also be performed on the welds to

NDI METHODS

TPS

TITANIUM AND SUPERALLOYS

EDDY CURRENT (PHASEMASTER MOD D)

SENSITIVITY:

- SURFACE CRACKS 0.025mm(0.001") DEEP
- THICKNESS 0.2%
- ELECTRICAL CONDUCTIVITY CHANGES 0.05%

COATED COLUMBIUM:

EDDY CURRENT

- SURFACE CRACKS THICKNESS AS ABOVE
- COATING THICKNESS 0.0025mm(0.0001")

STIMULATED ELECTRON EMISSION RADIOGRAPHY:

- COATING HOMOGENEITY DURING PROCESS

PRIMARY STRUCTURE

WELDMENT INSPECTION

RADIOGRAPHY, DYE PENETRANT — MSFC-SPEC-504

DELTA ULTRASONICS — LINEAR DEFECTS CRACKS, OXIDE INCLUSION

EDDY CURRENT (SURFACE CRACKS)

ACOUSTICAL EMISSION MONITORING (AEM)

- DURING HYDROSTAT (BASELINE)
- DURING STRUCTURAL & THERMAL TEST (MONITOR)

Figure 7

complement the X-ray and penetrant inspection. The delta ultrasonic technique will detect linear defects (crack, oxide inclusion, etc.) as small as 0.5 mm (0.020") deep x 0.75 mm (0.030") long and the Eddy Current technique will detect surface cracks as small as 0.025 mm (0.001") deep.

The feasibility of using acoustical emission monitoring (AEM) to monitor crack initiation and growth on a simulated flight item will be studied in this program. The structure will be instrumented with 16 sensors to provide AEM data during test. Baselining of the tankage structure, sans insulation and TPS, will be performed during tankage hydrotest. Repetition of the proof test will be performed in the test fixture with TPS and insulation installed to determine noise and/or interference due to TPS, insulation and test fixture. Continuous AEM will be performed throughout structural and thermal test; areas exhibiting high acoustical emission rates will be reinspected using the standard NDI techniques, X-ray, etc. A summary of proposed NDI methods is shown in Figure 7.

Preliminary design of Test Item No. 2, shown in Figure 8, has begun. The structure simulates a typical LH_2 tank section of an orbiter stage. The load carrying tank structure has a metallic heat shield and internal foam insulation.

TEST ITEM NO. 2

LH_2 TANK SECTION (ORBITER)

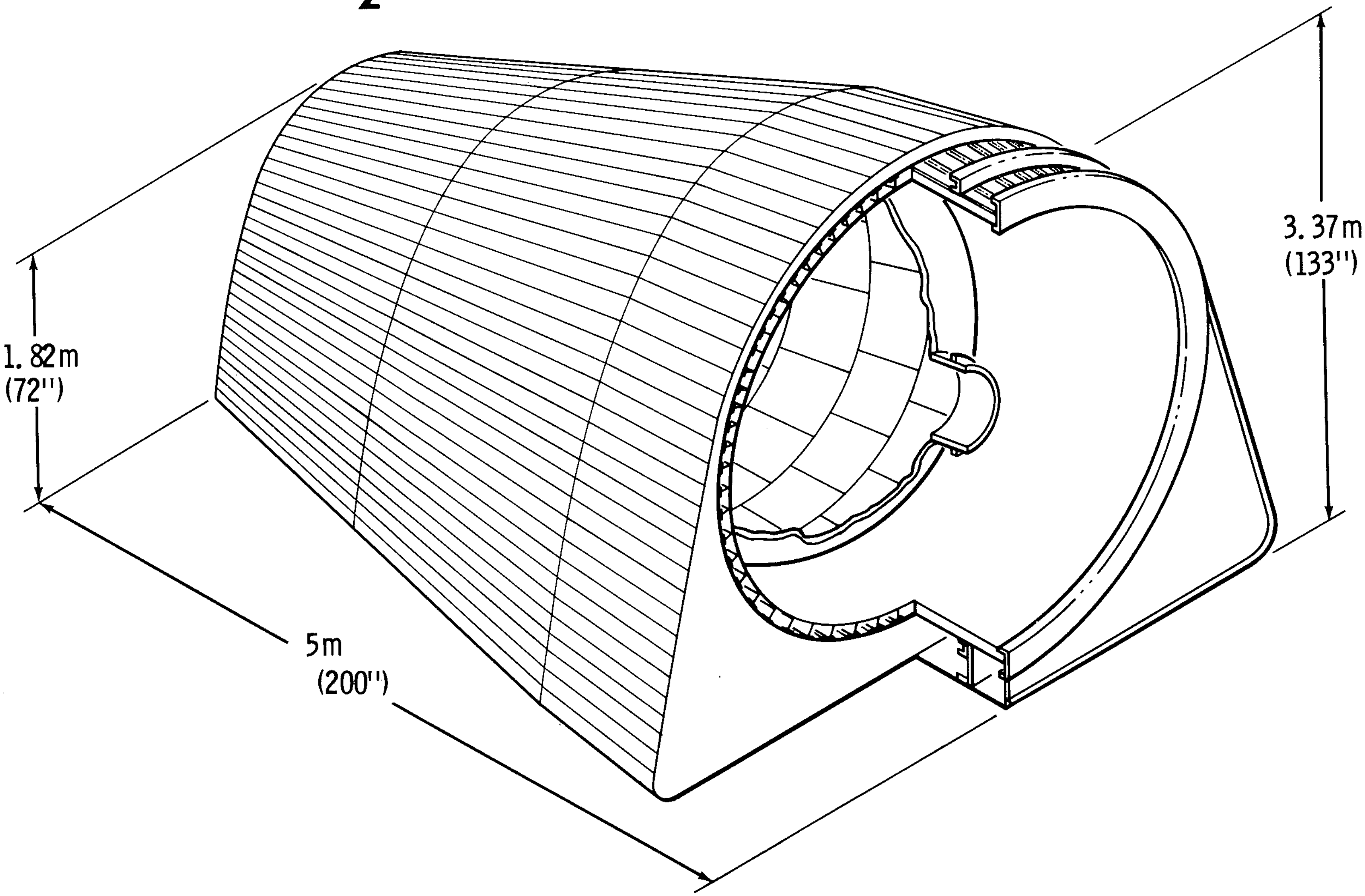

Figure 8

Figure 9 shows the selected heat shield temperatures. Materials for TPS are titanium and beryllium up to 426° C (800° F.), HS 188 up to 980° C (1800° F.) and coated columbium for up to 1260° C (2300° F.).

TEMPERATURE DISTRIBUTION
TEST ITEM #2

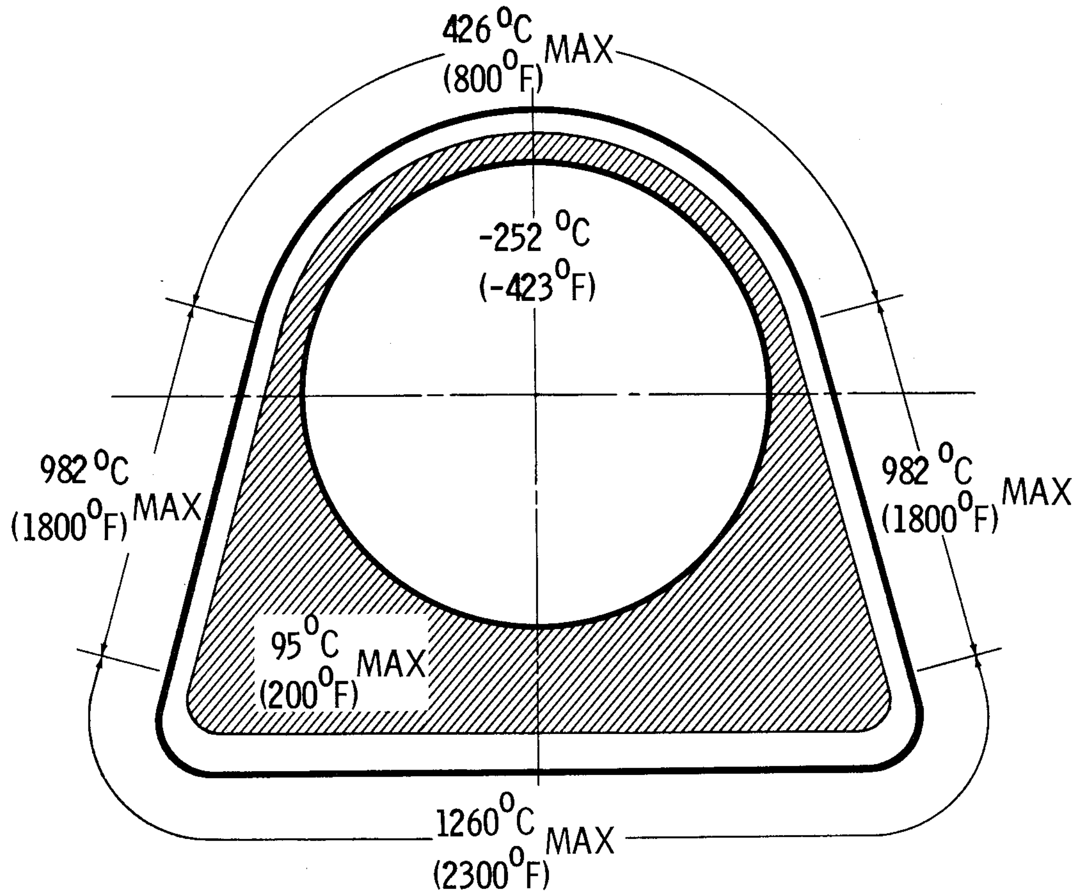

Figure 9

Application of Advanced Composites

The application of composites for primary Shuttle structures is depending on two main factors: demonstration of a reusable, reliable structure and definition of possible weight savings. The weight savings will also be assessed in relation to the additional cost of composites over conventional aircraft construction.

The evaluation of the composite systems for use in the 1/3 scale thrust structure (Figure 10) is conducted on two components: Engine support and compression panel.

The listed composite systems are used in the program:

Boron/Epoxy

Graphite/Epoxy

Boron/Aluminum

For weight and cost comparison, a baseline design and weight estimate of each component in either titanium or aluminum is established.

SUBSCALE THRUST STRUCTURE

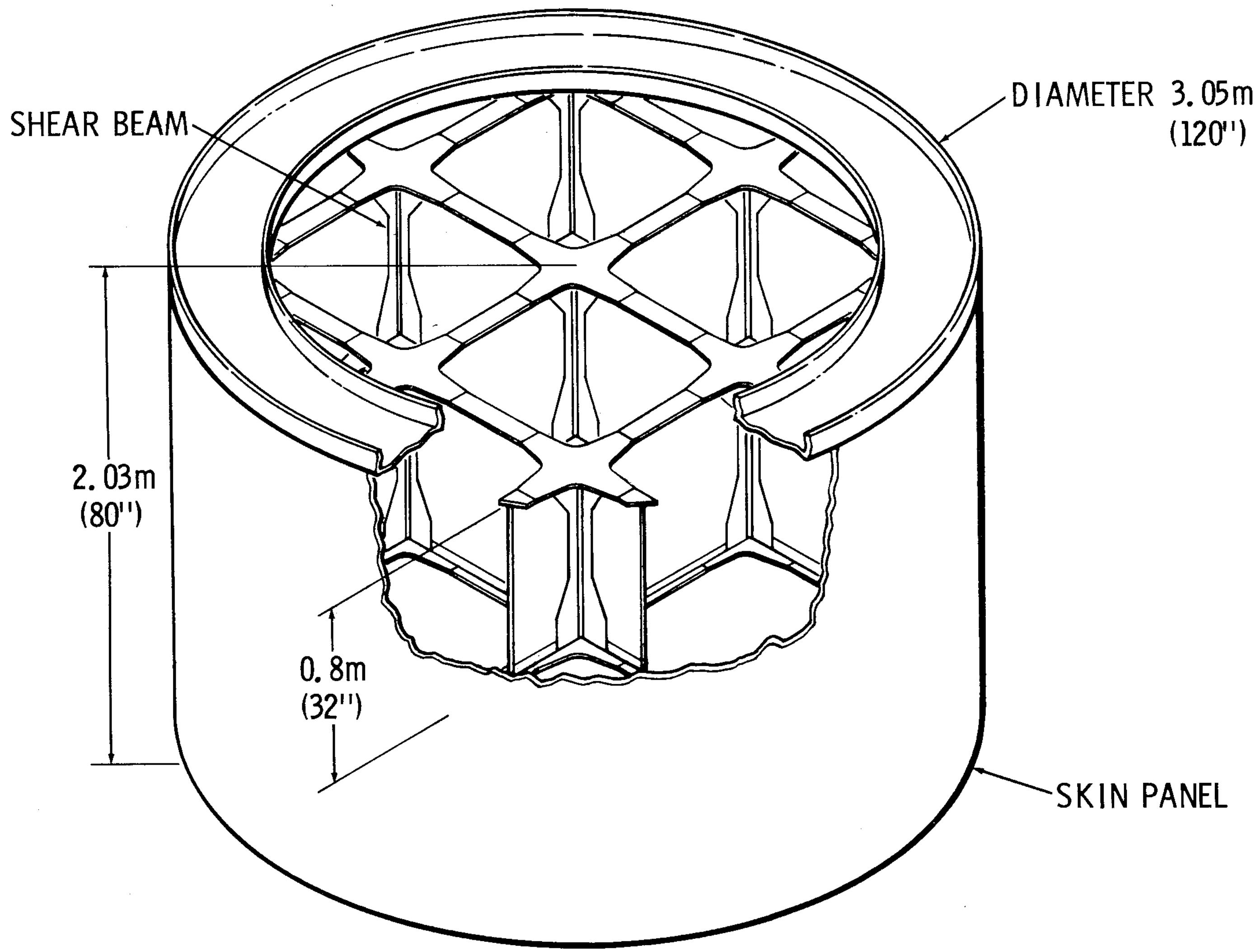

Figure 10

Design data for graphite/epoxy, graphite/polyimide and boron/aluminum composites are presently under investigation to supplement available information for boron/epoxy laminates.

Work under Contract NAS8-26198, "Development of Design Data for Graphite Reinforced Epoxy and Polyimide Composites," with General Dynamics/Convair Aerospace, has found that the 175° C. (350° F.) flexural strength of unidirectional graphite/epoxy laminates was adversely affected by ambient temperature aging. Typical degradation of longitudinal flexural strength is presented in Figure 11. This data shows degradation involving three different graphite fibers and three different epoxy resin systems. The HT-S fiber is Courtaulds high strength material marketed by Hercules. The X-904 resin is an epoxy system from Fiberite. This laminate showed a 44% decrease in strength after 20 weeks of aging. The same resin system with Celanese GY-70 high modulus fiber showed a 30% loss in 11 weeks. The HT-S fiber with Whittaker 1004 epoxy resin lost 21% strength in 16 weeks. The 1004 epoxy resin with Morganite Modmor II high strength fiber lost 27% in 21 weeks and 55% in 44 weeks. Hercules 3002 epoxy resin with the HT-S fiber lost 31% in 20 weeks.

Although only limited tests have been run, the data indicated that the room temperature longitudinal flexural strength has not been adversely affected by aging. On one system flexural strength loss was encountered at 82° C. (180° F.). Other data show a strength loss at 175° C. (350° F.) with the Narmco 5505 boron/epoxy system. Based on results obtained to date, absorption of moisture

DEGRADATION OF LONGITUDINAL FLEXURAL STRENGTH OF GRAPHITE/EPOXY LAMINATES (ROOM TEMPERATURE AGING)

LAMINATE		RT AGING	INITIAL STRENGTH		AGED STRENGTH		STRENGTH
FIBER	RESIN	WEEK	$175^{0}C$ - N/mm^2	$350^{0}F$ - KSI	$175^{0}C$ - N/mm^2	$350^{0}F$ - KSI	LOSS - %
HT - S[1]	X-904[2]	20	851.5	123.5	480,6	69.7	44
GY - 70[3]	X-904	11	477.1	69.2	335.1	48.6	30
HT - S	1004[4]	16	1046.6	151.8	828.7	120.2	21
MODMOR II[5]	1004	21	1110.1	161.0	808.8	117.3	27
MODMOR II	1004	44	682.6	99.0	310.3	45.0	55
HT - S	3002[6]	20	1274.2	184.8	890.1	129.1	31

1 COURTAULDS HIGH STRENGTH GRAPHITE FIBER

2 FIBERITE EPOXY RESIN

3 CELANESE HIGH MODULUS GRAPHITE FIBER

4 WHITTAKER EPOXY RESIN

5 MORGANITE HIGH STRENGTH GRAPHITE FIBER

6 HERCULES EPOXY RESIN

Figure 11

by the epoxy resin appears to be the main cause of strength degradation although other possible mechanisms have not been completely eliminated. The water appears to be acting mainly as a plasticizer. Some preliminary results indicate that the rate of degradation can be greatly decreased by a post cure at a somewhat higher temperature. Work on obtaining design data on graphite/epoxy laminates has been stopped, and the available effort will be devoted to solving this problem or used in other ways.

Test data to date shows no degradation of the 315° C. (600° F.) flexural strength on room temperature aging of the graphite/Monsanto RS 6234 polyimide laminates. Additional effort will be performed to insure that room temperature aging does not adversely affect the high temperature strength properties of graphite/polyimide laminates. Cure studies are in process on polyimide prepregs. Results obtained to date using hercules HT-S high strength graphite fibers and Monsanto RS 6234 polyimide resin are presented in Figure 12. When the results were normalized to 60 vol. % fiber, both the vacuum bag/press and vacuum bag/autoclave cures gave essentially the same flexural strength of about 1600 N/mm^2 (230,000 psi). When only a vacuum bag cure is used the flexural strength was somewhat lower at 1310 N/mm^2 (190,000 psi). The data also show that using the vacuum bag/press and vacuum bag/autoclave cures the minimum flexural strength should be 1172 N/mm^2 (170,000 psi); and for the vacuum bag cure 1034 N/mm^2 (150,000 psi).

PRELIMINARY LONGITUDINAL FLEXURAL STRENGTH OF GRAPHITE/POLYIMIDE LAMINATES
(DIFFERENT PROCESSES)

DATA	ROOM TEMPERATURE FLEXURAL STRENGTH					
	VACUUM BAG CURE		VACUUM BAG/PRESS CURE		VACUUM BAG/AUTOCLAVE CURE	
	N/mm^2	KSI	N/mm^2	KSI	N/mm^2	KSI
AVERAGE	1179.0	171	1330.7	193	1406.5	204
NORMALIZED 60 VOL. % FIBER	1310.0	190	1599.6	232	1592.7	231
MINIMUM EXPECTED	1034.2	150	1172.1	170	1172.1	170

Figure 12

Projected weight savings comparing the selected composite systems and design approaches with standard materials for the shear web beam are shown on Figure 13. The chart indicates the weight differences of basic structural elements and additional metallic parts required for joints and fittings.

ENGINE THRUST BEAM WEIGHTS

		SHEAR WEB BEAM					
MATERIAL		CAPS	WEB & STIFFENERS	THRUST POSTS	FITTINGS	REACTION POSTS	TOTAL
BORON/EPOXY	kg	15.1	21.6	27.5	75.4	8.0	147.5
	lbs	33.2	47.6	60.5(Ti)	166.0(Ti)	17.6(Ti)	324.9
GRAPHITE/EPOXY	kg	PRELIMINARY DATA, ALL BONDED DESIGN					111.2
	lbs						245.0
TITANIUM	kg	27.9	47.7	27.5	75.4	8.0	186.4
	lbs	61.4	105.0	60.5	166.0	17.6	410.5
BORON/EPOXY		0.56	0.45	1.0	1.0	1.0	.79
GRAPHITE EPOXY		PRELIMINARY DATA, ALL BONDED DESIGN					.60
TITANIUM		1.0	1.0	1.0	1.0	1.0	1.0

Figure 13

The shear web beam, shown in Figure 14, is designed with boron/epoxy composite. Shear webs, cap members, and web stiffeners are boron/epoxy multidirectional layup, connected by titanium fittings. Stiffeners and cap members are bonded to the web, titanium splices, and thrust post fittings are mechanically fastened. Component tests of joints, tension and compression caps and a simple shear beam section are in progress. Design and analysis are complete and hardware fabrication is under way. Material design data, established under U.S. Air Force Contract F 33615-68-C-1301 were used. Limit loads, used in the beam design, are indicated.

ENGINE THRUST BEAM
SHEAR WEB BEAM

	NEWTONS	KIPS
P_{1v}	481 980	108.36
P_{1H}	117 470	26.41
P_{2v}	351 300	78.98
P_{2H}	117 470	26.41

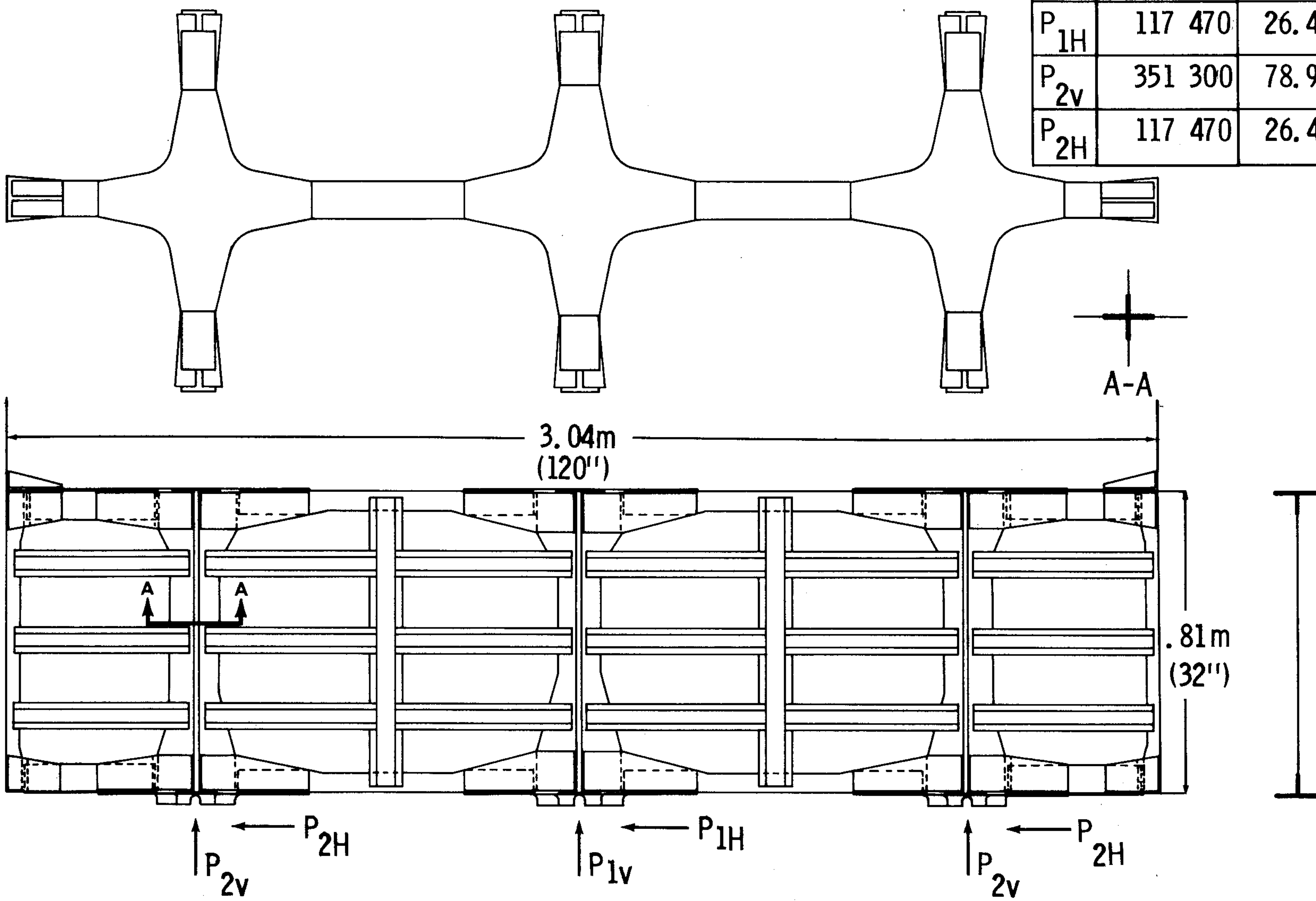

Figure 14

Figure 15 shows the component test sections being built and tested.

Components represent major parts of the shear web beam and test units will substantiate the selected design and analysis approach used in the beam design.

COMPONENT TEST SECTION
SHEAR WEB BEAM (BORON/EPOXY)

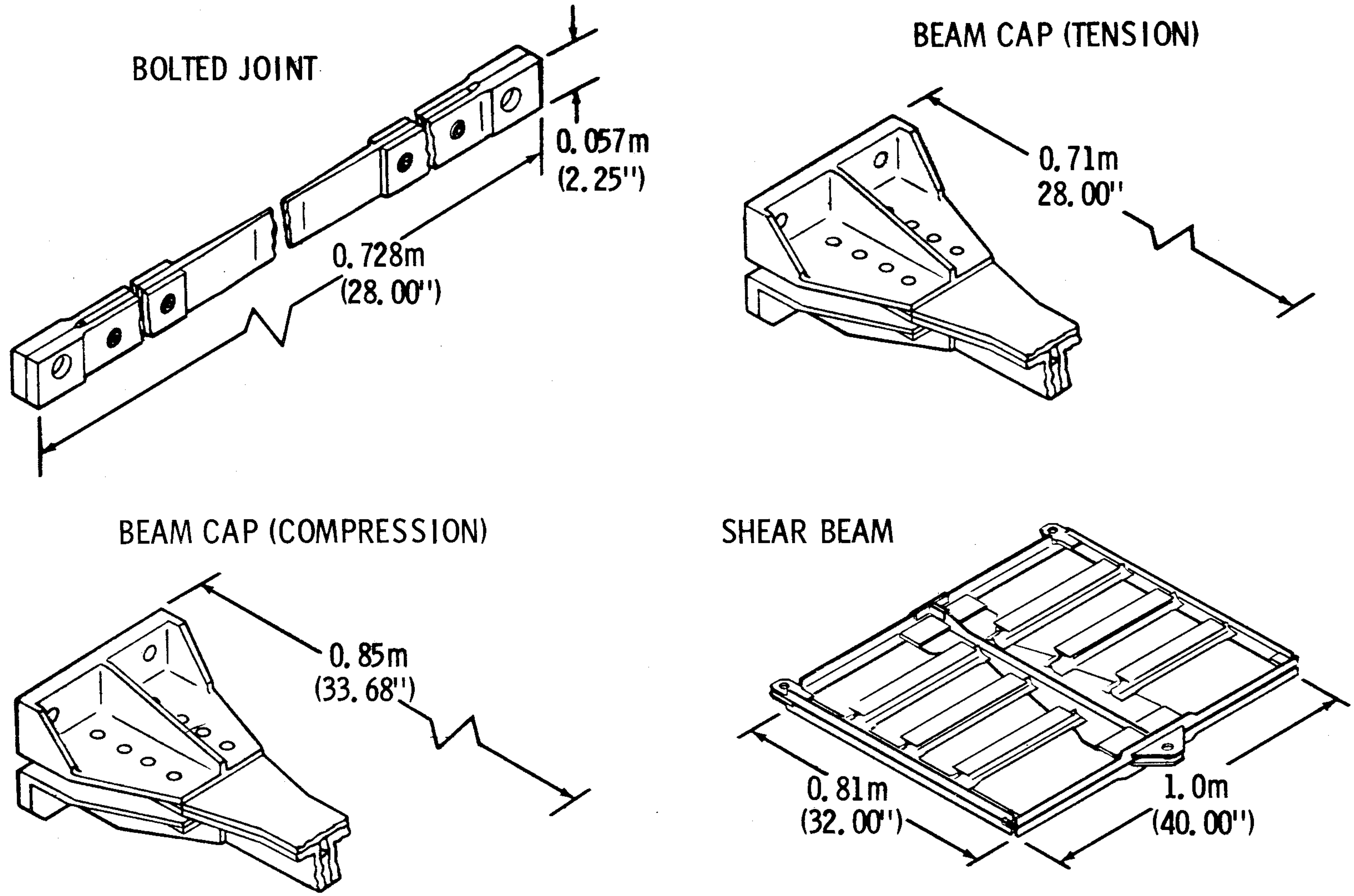

Figure 15

Projected weight savings comparing the selected composite systems and design approaches with standard material, are shown on Figure 16. The list indicates the weight differences of basic structural elements and additional metallic parts required for joints and fittings.

ENGINE THRUST BEAM WEIGHTS

MATERIAL		TRUSS BEAM TUB. MEMBERS	FITTINGS	REACTION POSTS	TOTAL
BORON/EPOXY	kg	34.2	70.4	22.7	127.3
	lbs	75.4	155.0	50.0	280.4
GRAPHITE/EPOXY	kg		(PRELIMINARY)		133.9
	lbs				295.0
TITANIUM	kg	46.3	84.4	22.7	153.5
	lbs	102.0	186.0	50.0	338.0
BORON/EPOXY		.74	0.80	1.0	0.83
GRAPHITE/EPOXY			(PRELIMINARY)		0.86
TITANIUM		1.0	1.0	1.0	1.0

Figure 16

The truss beam, shown in Figure 17, is designed with Boron/Epoxy composite. Tubular members are fabricated from a multidirectional layup, bonded to Titanium end fittings. A strut test program to verify the selected design approved, is in progress under contract NAS8-26675 with the Grumman Aerospace Corporation. Limit loads, used in the beam design, are indicated.

ENGINE THRUST BEAM
TRUSS BEAM

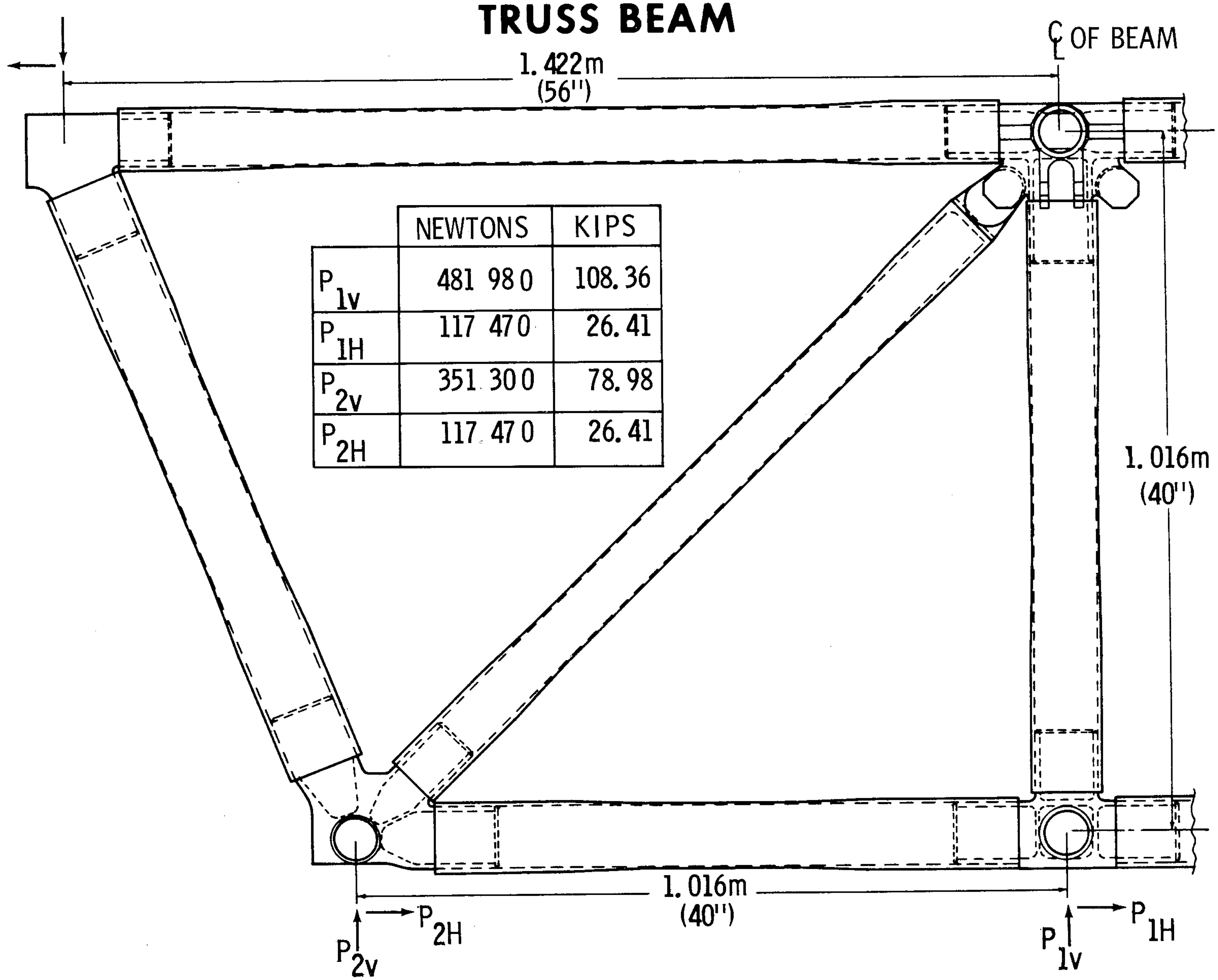

	NEWTONS	KIPS
P_{1v}	481 980	108.36
P_{1H}	117 470	26.41
P_{2v}	351 300	78.98
P_{2H}	117 470	26.41

Figure 17

The relative weights of Boron/Epoxy tubes, Boron/Epoxy tubes with Titanium fittings and Titanium tubes with fittings are shown on Figure 18.

TRUSS BEAM
COMPARATIVE TUBE WEIGHTS

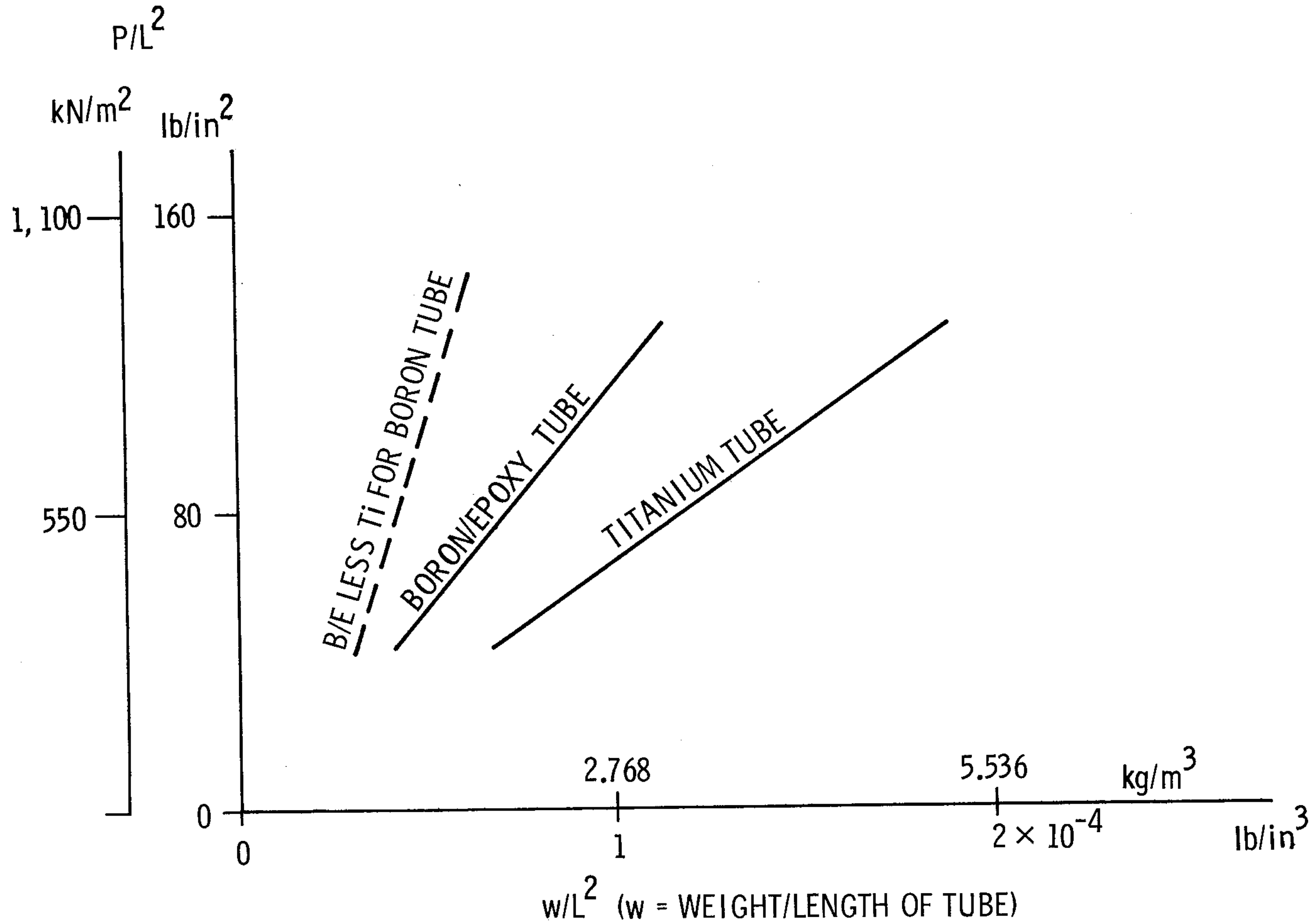

Figure 18

The design and fabrication method utilized in the boron/epoxy structure is indicated in Figure 19. The boron/epoxy tubes are capped at either end by semicircular, stepped titanium splice fittings, bonded within the laminate. The titanium splice fittings are initially split, to facilitate fabrication of the boron/epoxy tubes, which are laid-up undersize, and subsequently "blown-out" to a female mold form. After laminate cure, the split end fittings are joined by electron beam welding. Heat survey studies were performed to determine the minimum proximity of the electron beam weld to the boron laminate without exceeding a temperature of 140° C. (300° F.) at the titanium/adhesive-boron/epoxy interface. Results of the survey showed that 5 mm (0.200 inch) proximity could be achieved with proper application of chill bars; however, 13 mm (0.500 inch) was chosen as the design value to incorporate a safety factor.

TRUSS BEAM
TUBE JOINT DESIGN

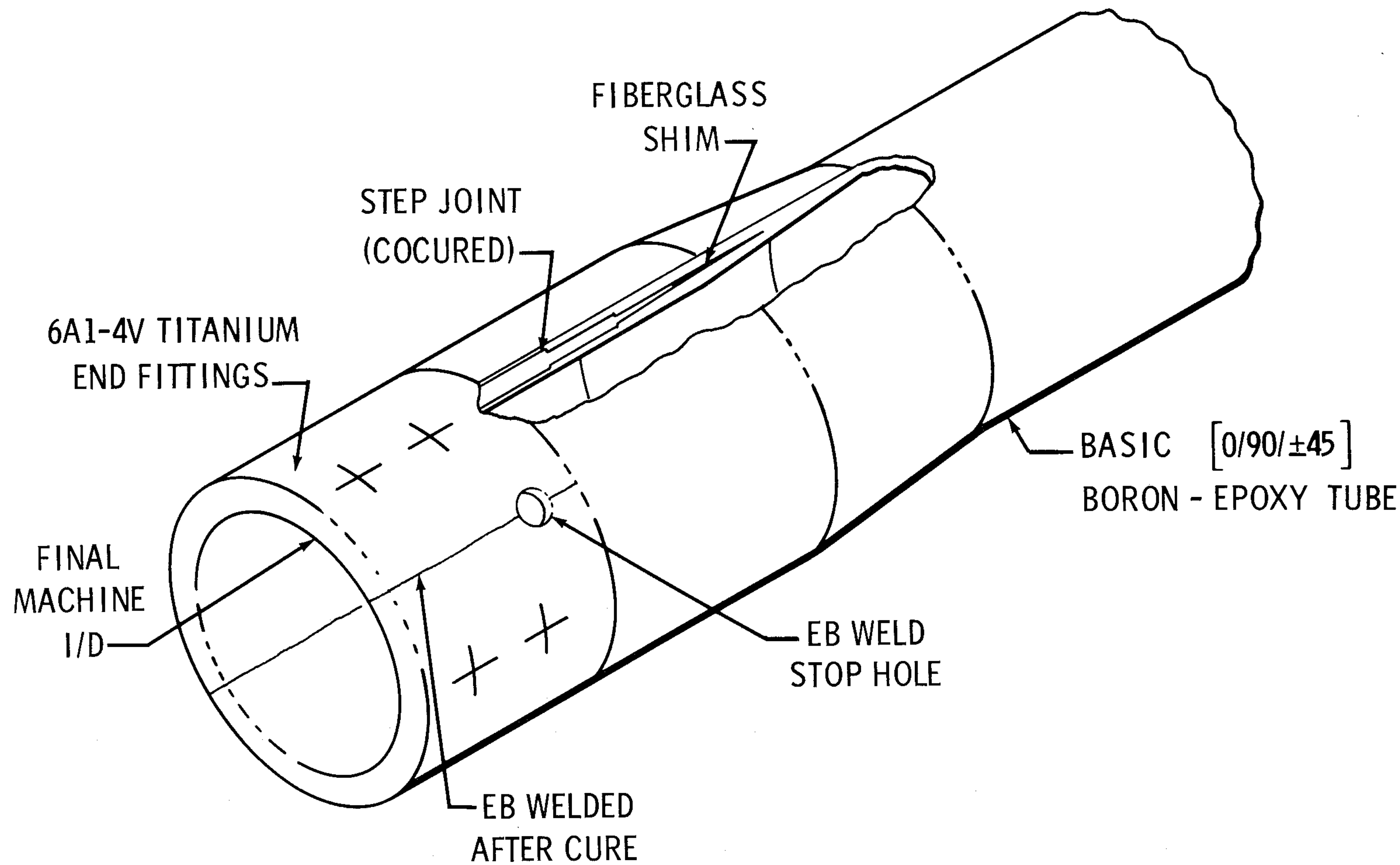

Figure 19

Compression panel weights, comparing three selected composite systems with high strength aluminum and titanium panel design, are shown in Figure 20. The chart indicates the weight differences of the basic panel element and the additional end fittings required.

COMPRESSION PANEL WEIGHTS .735m×2.03m (29"×80")

MATERIAL	BASIC PANEL		PANEL W/ END FTGS.		BASIC PANEL	PANEL W/ END FTGS.	STRESS LEVEL AT $\bar{t}$	
	kg	lbs	kg	lbs			N/mm^2	PSI
ALUMINUM	22.0	48.5	25.4	56.0	1.0	1.0	228.9	33,200
TITANIUM	24.3	53.6	27.7	61.1	1.11	1.09	379.22	55,000
GRAPHITE/EPOXY	12.0	26.5	18.7	41.1	.545	.735	238.6	34,600
BORON/EPOXY	11.2	24.7	18.0	39.6	.51	.707	337.8	49,000
BORON/ALUMINUM	10.9	~24.0			.48			

Figure 20

Figure 21 depicts the Boron/Epoxy compression panel, presently in development at MSFC. Stringers are laid up separately with a machined titanium fitting in each end. (Stringers laid up over fittings and matching mandrel.) Mechanical fasteners are added through the fittings on each end. The skin is laid up separately and stringer assemblies bonded to it. End angles and frame are mechanically attached. (Shims are required between stringer fittings and end angles.) Interleaved titanium foil 0.178 mm (.007 in.) is used in ends of stringers and skin for load transfer through mechanical fasteners. Limit loads, used for panel design, are indicated. Material Design data used were established under U.S. Air Force Contract F 33615-68-C-1301.

COMPRESSION PANEL (BORON/EPOXY)

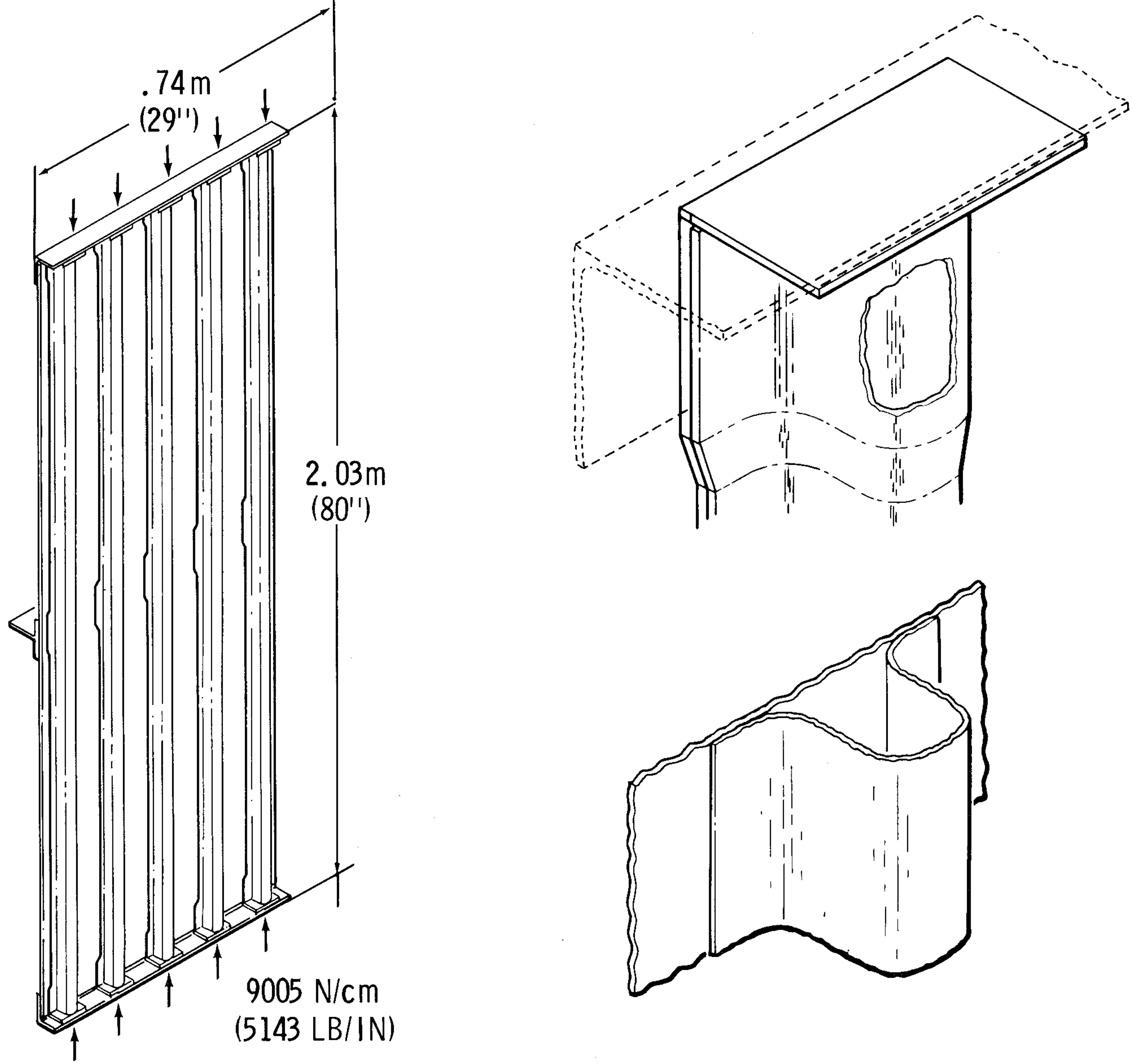

Figure 21

Figure 22 shows the component test sections being built and tested. Components represent major parts of the compression panel, and test results will substantiate the selected design and analysis approach used in the panel design.

COMPONENT TEST SECTION
COMPRESSION PANEL (BORON/EPOXY)

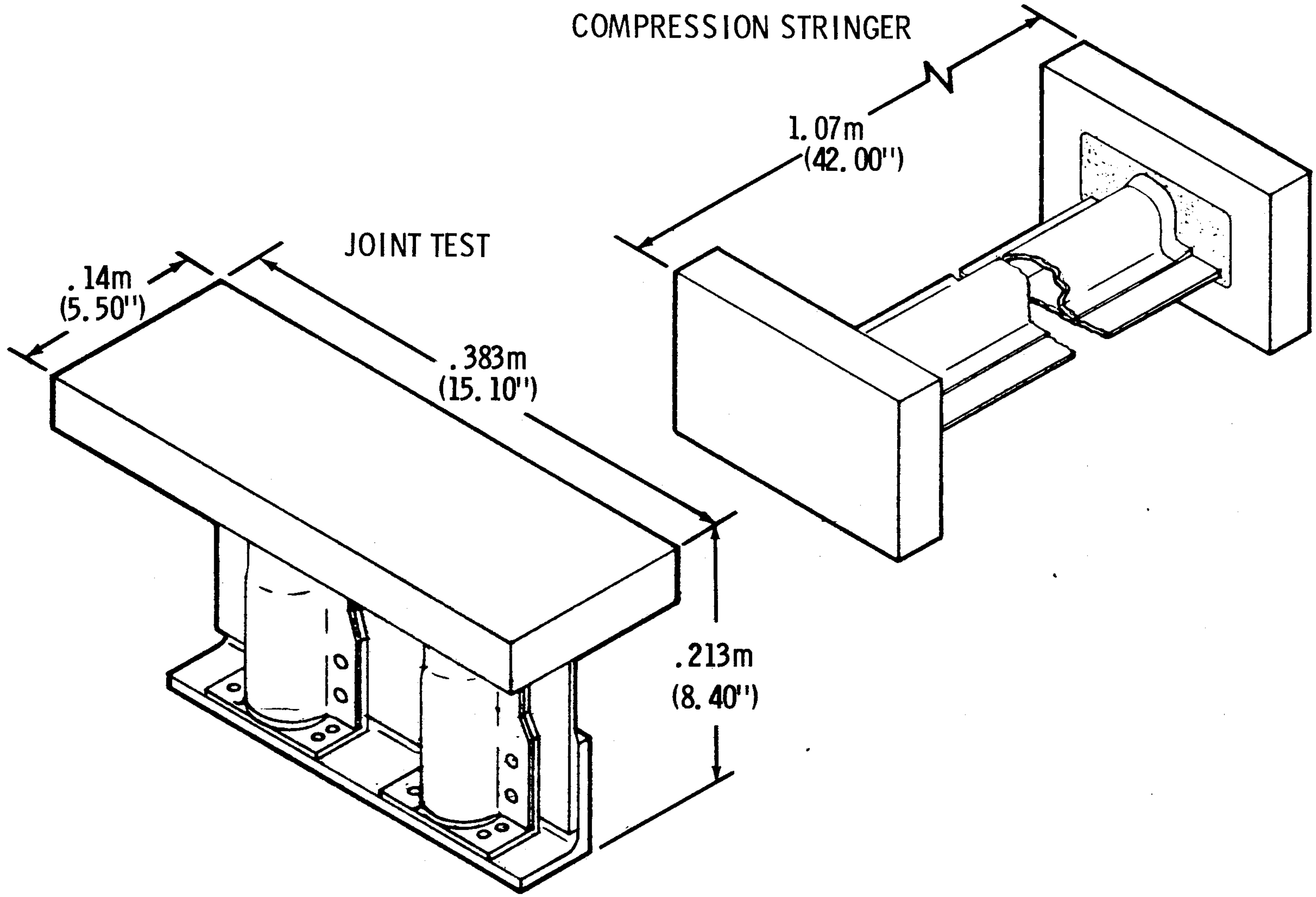

Figure 22

A 0.736 x 2.03 m (29 x 80 in.) graphite/epoxy panel (Figure 23) has been designed. The panel consists of a skin, five "hat" section stringers and one mid-panel frame. Laminated 1.22 x 0.304 m (48 x 12 in.) prepreg graphite/epoxy composite is used as the primary load carrying material with thin titanium shims sandwiched between graphite/epoxy plys at frame and end attachment areas for local reinforcement. The number, geometry and location of titanium shims have been determined so that the panel does not warp during the curing cycle and so that end load can be transferred entirely through bearing on attachment bolts. Shims terminate at various distances into the panel to eliminate stress concentrations. The panel contains 12.03 kg (26.5 lbs.) of graphite/epoxy and 1.98 kg (4.36 lbs.) of titanium shims. The graphite/epoxy panel program is under contract NAS8-26242 with Martin/Marietta Corporation, Denver Division.

COMPRESSION PANEL (GRAPHITE/EPOXY)

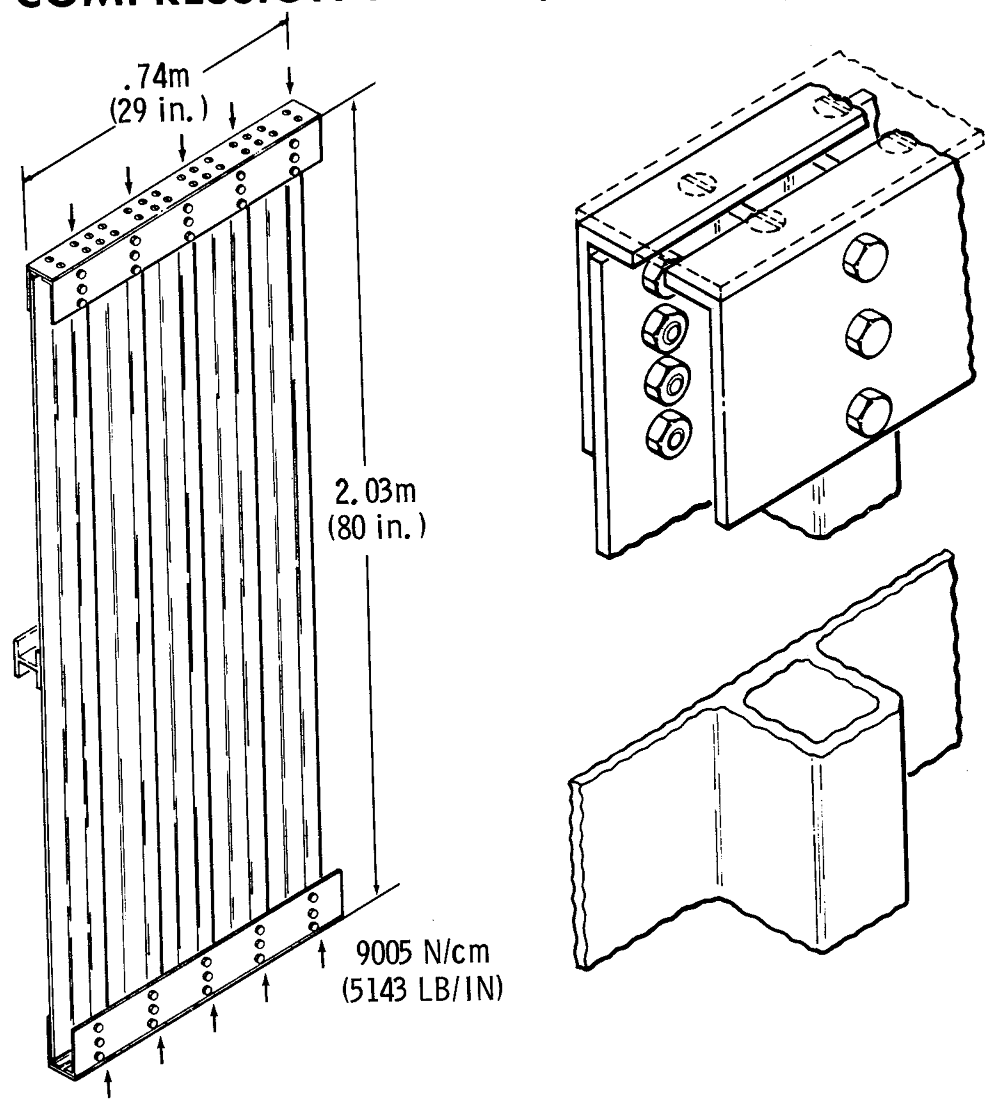

Figure 23

The analysis computer program used for panel design is formulated so that selected input values can be varied to determine their influence on panel weight (Figure 24). An input of high stress level results in panels with thin skin, many stringers and large stringer height to satisfy EI requirements. These designs are heavy due to the excessive amount of stringer web material. As the design stress level is reduced, skin thickness increases, stringer height is reduced, and fewer stringers are required. Stringer web weight reduction causes panel weight to reach a minimum. Selection of a panel stress level to be used depends upon minimum gage considerations, expected eccentricity of loading, initial curvature of the panel and strength factor of safety desired.

Curves were plotted for panel weight versus material with varying design stress levels. Minimum weight designs for high strength and high modulus fibers were approximately equal. The high strength fiber was chosen because of more consistent strength data exhibited and the inherent feeling that less problems would be encountered in designing for strength values selected.

PANEL DESIGN VARIATIONS

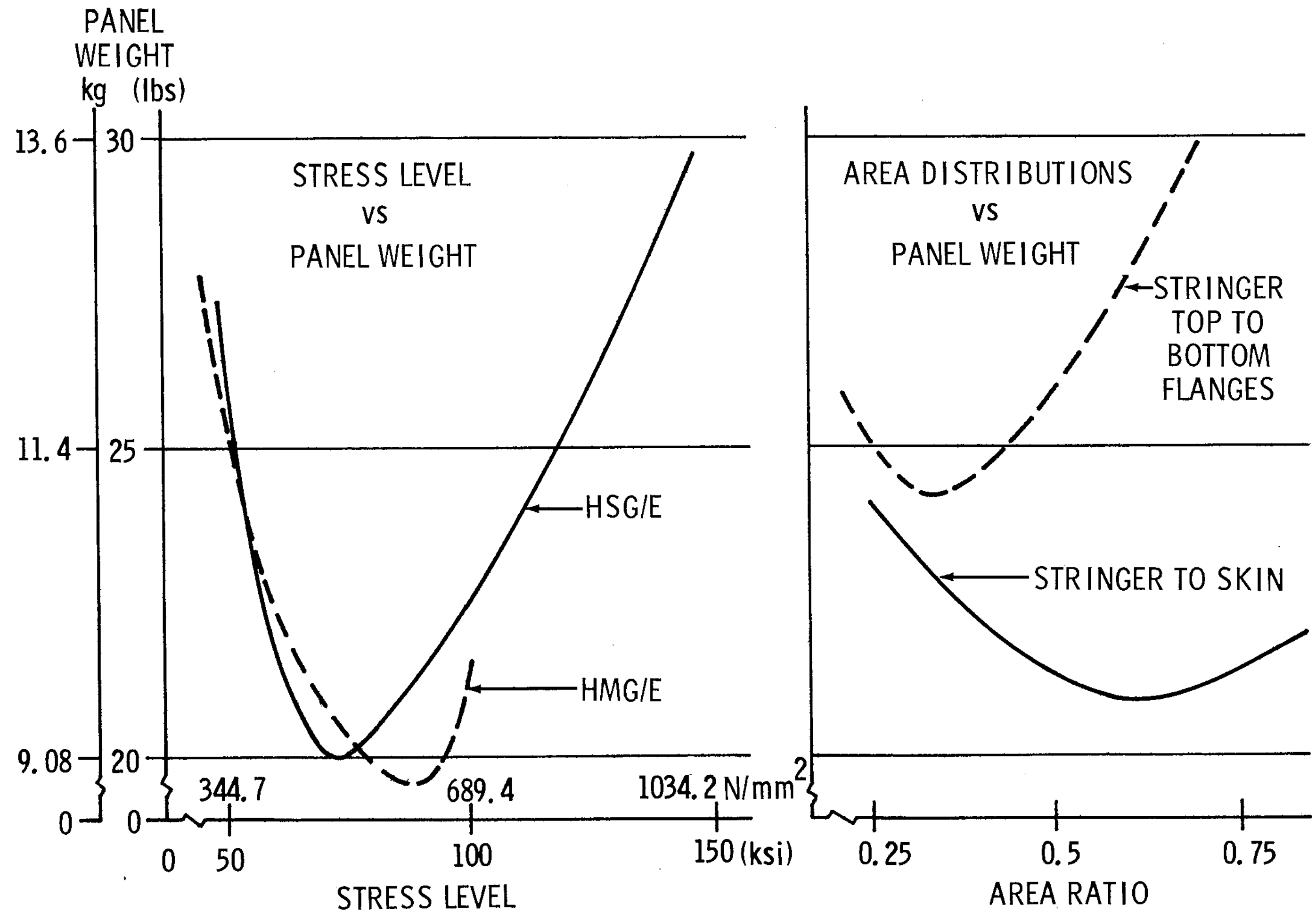

Figure 24

For a given overall panel stress level, redistribution of panel material will cause panel weight variations and will allow for movement of the panel neutral axis. Selection of proper material distribution will assure minimum panel weight with reduced eccentricity of loading.

$$\text{Area Ratio} = \frac{\text{Stringer Area}}{\text{Total Panel Area}}$$

$$\text{Area Ratio} = \frac{\text{Area of Stringer Top Flange}}{\text{Area of Stringer Top \& Bottom Flanges}}$$

Figure 25 shows the material properties of the two graphite fiber systems used in the evaluation and trade studies. The HS type fiber was selected for panel fabrication (Fiberite HY-E1311B prepreg tape).

MATERIAL PROPERTIES
OF
GRAPHITE/EPOXY COMPOSITES

PROPERTIES	HS TYPE (HIGH STRENGTH)		HM TYPE (HIGH MODULUS)	
	N/mm^2	KSI	N/mm^2	KSI
COMPRESSION MODULUS	137895	20000	172400	25000
COMPRESSION STRENGTH	1206.6	175.	689.5	100
INTERLAMINAR SHEAR STRENGTH	82.7	12	68.9	10
TRANSVERSE TENSILE MODULUS	6894.8	1000	6894.8	1000
TRANSVERSE TENSILE STRENGTH	68.9	10	68.9	10
FIBER VOLUME		0/0 - 60 +5 -3%		0/0 - 60 +5 -3%
TENSION STRENGTH	1241.1	180	758.4	110

Figure 25

A 1.22 m x 1.56 m (48 in. x 61.5 in.) compression panel fabricated from Boron/Aluminum is in development by McDonnell Douglas Corporation, St. Louis (Contract NAS8-26295). A unique fabrication process, eutectic bonding, developed by MDAC (patent pending) is used in joining monolayer boron/aluminum foils into laminated structural parts such as hat sections and skin panels. Panel configuration and loading are shown in Figure 26. Because of the potential high temperature capability of the composite, the panel is designed for a temperature limit of 260° C (500° F).

During the preliminary design of the panel, estimated material properties as shown on Figure 27 and Figure 28 were used. Layups, using proposed fabrication facilities and tools, were tested and properties are shown in comparison with previous estimates. Lower data are due to lower fiber volume of the monolayer boron/aluminum tape.

COMPRESSION PANEL BORON-ALUMINUM

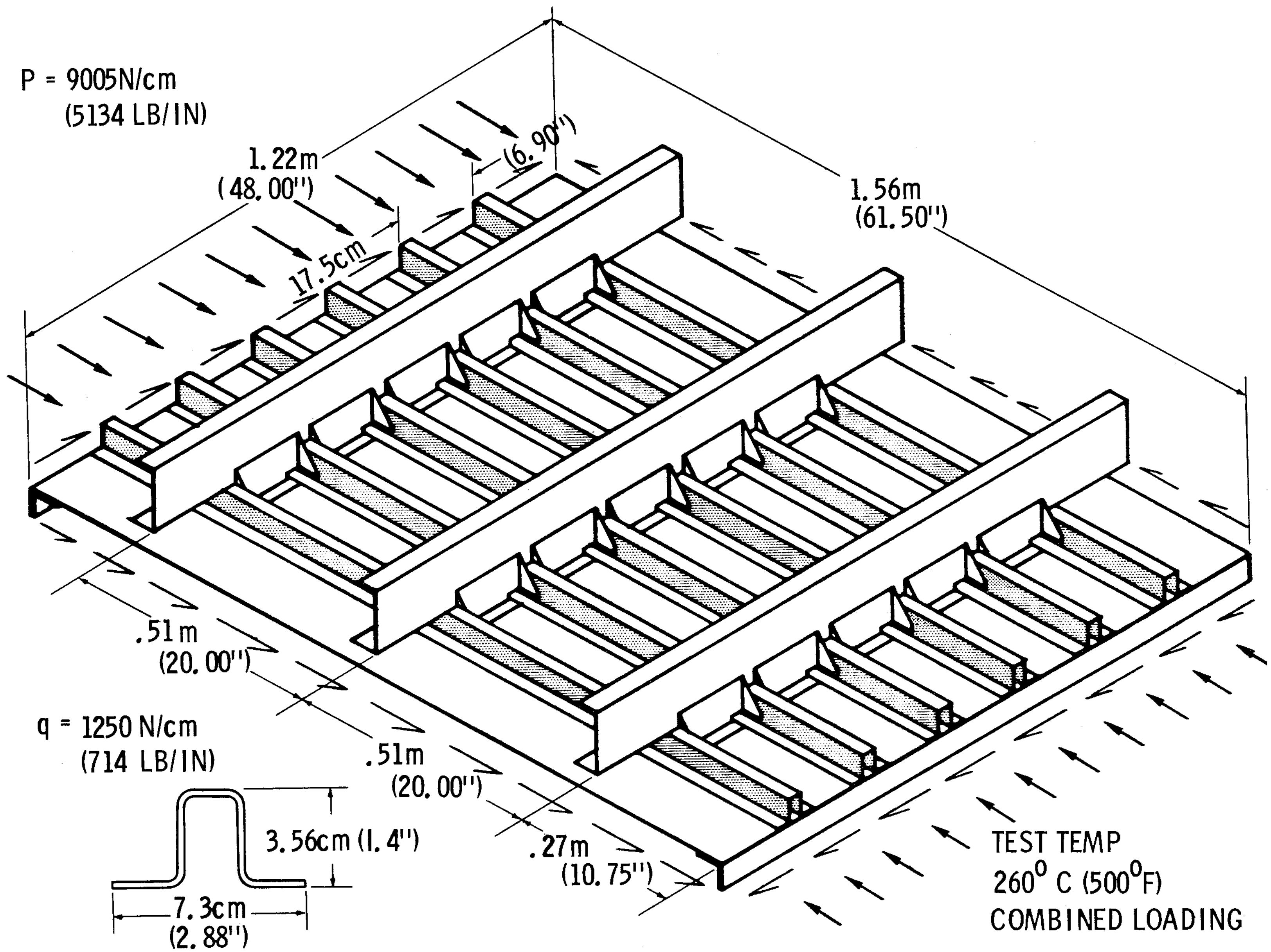

Figure 26

BORON-ALUMINUM MECHANICAL PROPERTIES ROOM TEMPERATURE

PROPERTY	PRELIMINARY ESTIMATE		TYPICAL TEST DATA	
FIBER V/O	45		40	
	N/mm^2	KSI	N/mm^2	KSI
MODULUS OF ELASTICITY				
E_L^c	220 630	32000	196 500	28 500
E_T^c	124 100	18000	115 141	16 700
G_{LT}	53 100	7 700	46 200	6700
STRENGTH				
F_T^{tu}	82.7	12.0	79.2	11.5
F_{LT}^s, $[0^0]ns$	79.2	11.5	64.8	9.4
F_{XY}^s, $[\pm 45^0]ns$	182.7	26.5	224.1	32.5
STRAIN				
ϵ_T^{tu}	0.14% 1400 μ IN/IN		0.5% 5000 μ IN/IN	
γ_{LT}, $[0^0$ ns$]$	0.127% 1270 μ IN/IN		> 0.7% > 7000 μ IN/IN	

Figure 27

BORON-ALUMINUM MECHANICAL PROPERTIES TEMPERATURE 260°C (500°F)

PROPERTY	PRELIMINARY ESTIMATE		TYPICAL TEST DATA	
FIBER V/O	45		40	
	N/mm^2	KSI	N/mm^2	KSI
MODULUS OF ELASTICITY				
E_L^c	199900	29000	169000	24600
E_T^c	102700	14900	78000	11400
G_{LT}	28300	4100	25000	3700
STRENGTH				
F_T^{tu}	41.4	6.0	52.4	7.5
F_{LT}^s, [0^0]	29.0	4.2	34.5	5.0
F_{XY}^s, [$\pm$ 45^0]	170.3	24.7	–	–
STRAIN				
ϵ_T^{tu}	.16% 1600 μ IN/IN		.149% 1490 μ IN/IN	
γ_{LT}, [0^0]	.6% 6000 μ IN/IN		> 1.4% > 14,000 μ IN/IN	

Figure 28

Conclusions:

The development programs reported are well in progress and results will be available in time for use in the planned phase C/D of the Space Shuttle development.

In detail, Test Item No. 1 (Mission Simulation Tests) will be fabricated by October 1971, and tests completed and reported by mid-1972. Test Item No. 2 will be completed by the first quarter of CY 72.

In the area of composite components, the composite panel program and the truss beam development will be concluded by December 1971.

Configuration, material selection and design for the 1/3 scale thrust structure will be performed as soon as test results from the above programs become available.

CONCLUSION

- **TECHNOLOGY PROGRAM INPUTS WILL BE AVAILABLE FOR PLANNED SPACE SHUTTLE PHASE C/D**

- **TEST ITEM #1** — FABRICATION COMPLETE - OCTOBER 71; TESTS COMPLETE - MID 72

- **TEST ITEM #2** — FABRICATION COMPLETE - MARCH 72

- **COMPOSITE PANEL PROGRAM**
  ENGINE THRUST BEAM PROGRAM — COMPLETE - DECEMBER 71

Figure 29

HIGH TEMPERATURE FASTENER TECHNOLOGY

By

Frank D. Boensch, AFFDL/AFSC
William H. Goesch, AFFDL/AFSC
Allan M. Norton, Martin Marietta Corp.

INTRODUCTION

The state-of-the-art in high temperature fastener technology has made significant progress since the days of the X-20, "Dyna Soar", and "ASSET" programs. Ramsey and Ingram (Ref. 1) provided an excellent summary of the achievements attained from 1960 to 1966. This paper is a brief summary of the achievements from 1966 to the present. These achievements are the result of two Air Force sponsored programs. The first program was the Advanced Structural Concepts Experimental Program, "ASCEP". This program was the first to make extensive use of second generation columbium alloys and coating systems in a structure of significant size. Approximately 2700 fasteners were used in the ASCEP structure. The second program was the Hypersonic Aerospace Structures Program, "HASP". This program provided extensive development of joint design concepts, design allowables, identification of service problems, and test data on fasteners subjected to realistic environment.

Ref. 1 Ramsey, C. L.; and Ingram, J. C.: Structural Fasteners for Extreme Temperature Utilization. SAE Paper N. 670887, Oct. 1967.

SHEAR FIXTURE

(Figure 1)

Biaxial, shear, and uniaxial load fixtures were used to develop fastener design allowable data. Shown in Figure 1 is the shear load fixture which consists of a picture frame assembly with pinned corners. This fixture was used to develop design allowable data for TDNiCr and tantalum fasteners during the HASP program. An L-605 shear frame was used in the TDNiCr tests, while a T-222 tantalum shear frame was used in the tantalum test. This fixture presented the biggest design problem because it had to be continuous in order to properly introduce the load into the test specimen. The primary concern was to match the $\alpha\Delta T$ characteristics of the test specimen and the picture frame. Both room and elevated temperature design allowables were developed. In the elevated temperature case, testing was conducted up to the following maximum operating temperatures:

a) HS-25 to 1600°F (871°C)

b) TDNiCr to 1900°F (1038°C)

c) Columbium to 2400°F (1316°C)

d) Tantalum to 3000°F (1649°C)

However, no design allowable data were developed for pure tension loading of the fastener.

SHEAR FIXTURE

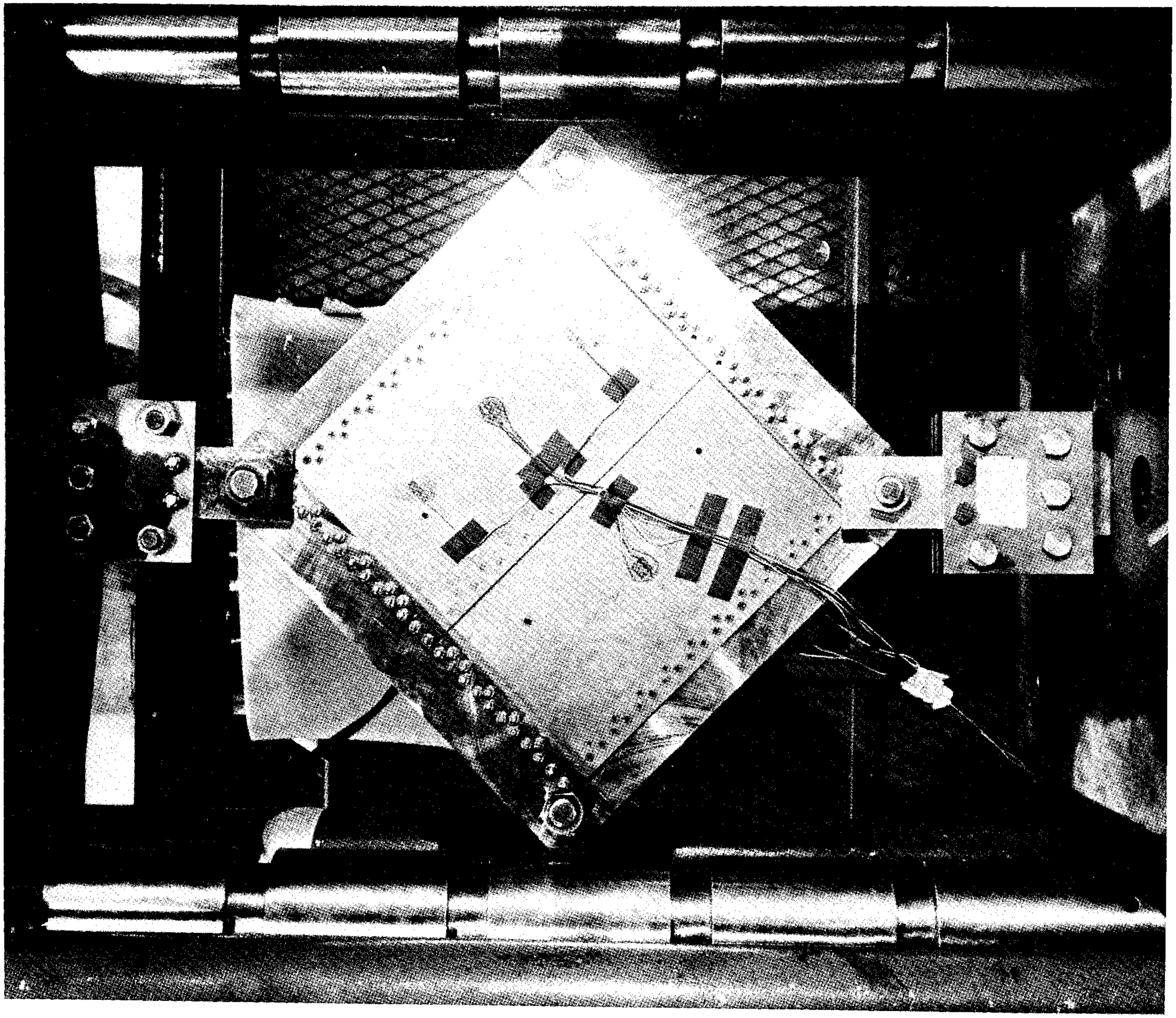

Figure 1

1/4" (0.64 cm) DIAMETER, SINGLE SHEAR FASTENER TEST RESULTS

(Figure 2)

A summary of the short time design allowable test results is shown in Figure 2. The results are from the single shear tests of 1/4" (0.64 cm) diameter fasteners. The failing load in pounds (newtons) is plotted on the ordinate and the test temperature in ^{o}F (^{o}C) is plotted on the abscissa. Both threaded fastener and rivet data are shown. The threshold or crossover point between uncoated and coated fasteners is clearly indicated at 1500^{o}F (816^{o}C). If the designer is forced to a coated fastener, then compatibility between the fastener and structural material is essential. For any coated application, a coated tantalum fastener using a coating system similar to that used on columbium is an attractive candidate up to a temperature of 2600^{o}F (1427^{o}C).

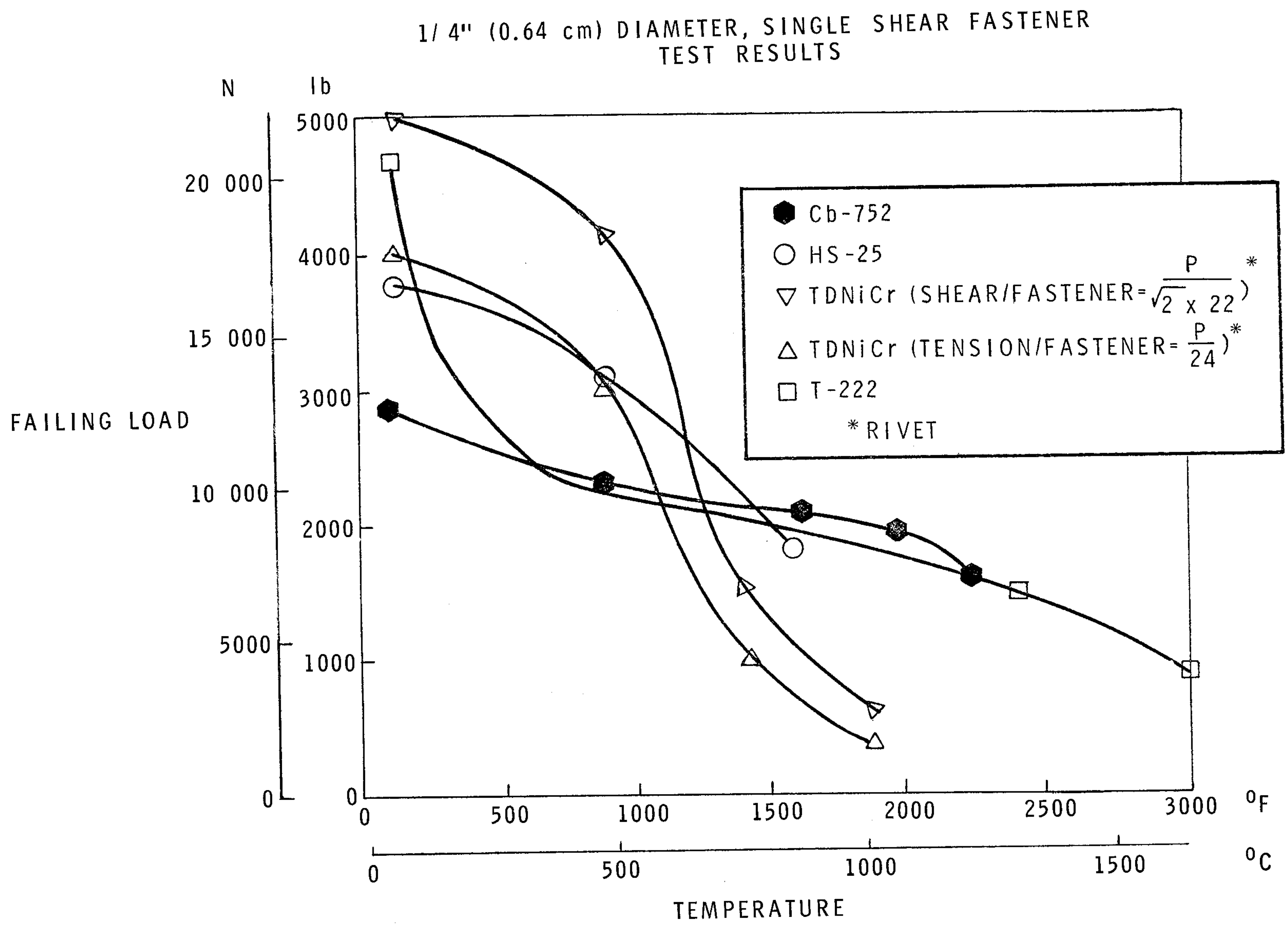
1/4" (0.64 cm) DIAMETER, SINGLE SHEAR FASTENER
TEST RESULTS
N
lb
FAILING LOAD
20 000
15 000
10 000
5000
0
5000
4000
3000
2000
1000
0
Cb-752
HS-25
TDNiCr (SHEAR/FASTENER= $\frac{P}{\sqrt{2} \times 22}$)*
TDNiCr (TENSION/FASTENER= $\frac{P}{24}$)*
T-222
* RIVET
0
500
1000
1500
2000
2500
3000
°F
0
500
1000
1500
°C
TEMPERATURE

Figure 2

TEMPERATURE AND LOAD CURVE SHAPE HISTORY OF TDNiCr JOINT LIFE TESTS

(Figure 3)

In addition to short time design allowable tests, flight-by-flight mission simulation tests were run to evaluate long time effects. The same fixtures were used as in the short time tests. Shown in Figure 3 are the temperature and load profiles used to conduct the TDNiCr joint life tests. The profiles shown simulate the entry of a high performance lifting re-entry vehicle. The upper curve denotes temperature, while the lower curve denotes the load. Load levels were established on the basis of short time test results. In the case of TDNiCr tests, the loads at temperature had to be reduced to 60 percent of the short time values. This was due to strain sensitivity characteristics of the material at high temperature.

TEMPERATURE AND LOAD CURVE SHAPE HISTORY OF TDNiCr JOINT LIFE TESTS

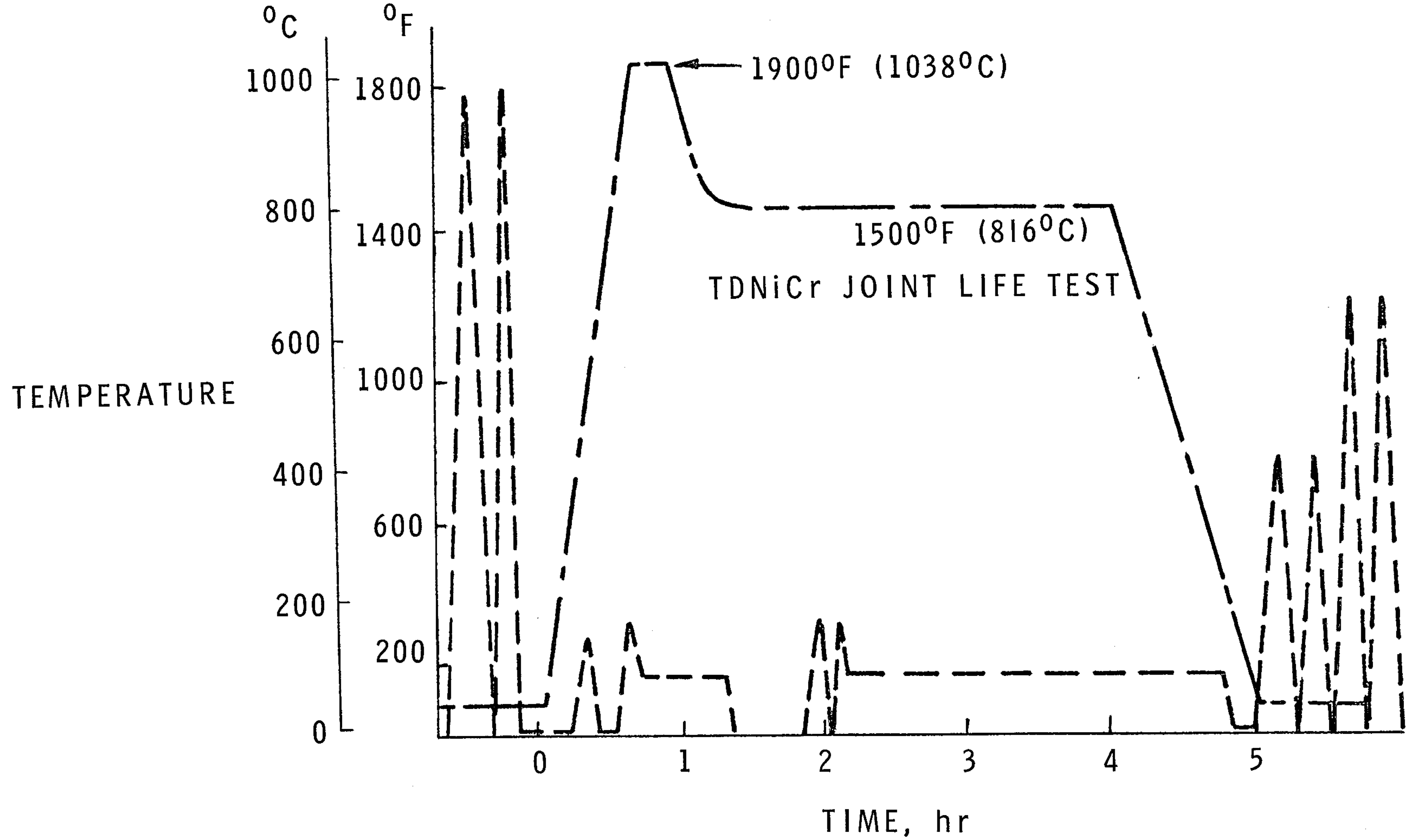

Figure 3

PHENOLIC TOOLS

(Figure 4)

Any discussion of high temperature fastener technology would not be complete without a few words on tooling needed to install or remove the fastener. A complete family of phenolic tools were designed and fabricated for use during the ASCEP program. They are shown in Figure 4. These tools were required for the nuts and bolts of both the HS-25 and coated columbium fasteners used on the ASCEP structure. The tools proved to be very satisfactory. The tools have large bearing surfaces and being fabricated of phenolic, a relatively soft material, do not damage the coated fasteners on which they are used.

Tools (not shown) for use on the internal wrenching fasteners were not as successful. The columbium coating tended to chip when the hex tool was inserted into the recess. To circumvent this difficulty, a new hi-torque slotted recess fastener was developed and used during the latter stages of the program.

PHENOLIC TOOLS

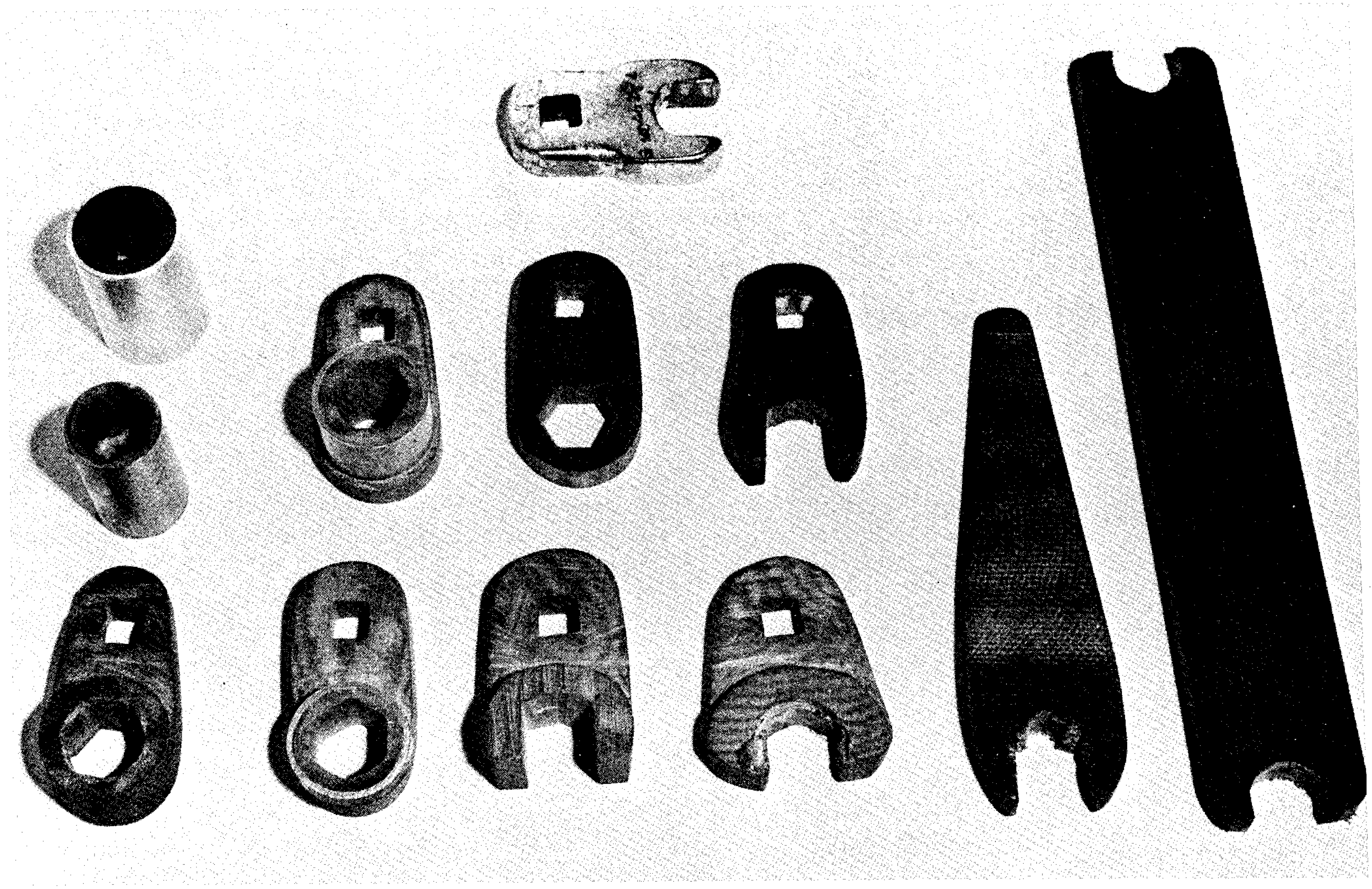

Figure 4

SUMMARY OF COATED C-129Y FASTENER TORQUE TESTS

(Figure 5)

Considerable experience was gained during both the ASCEP and HASP programs on installation and removal characteristics of superalloy, dispersion strengthened, and coated refractory metal fasteners. TZM, Cb-752, and C-129Y fasteners were evaluated during the ASCEP program, while L-605, TDNiCr, and T-222 fasteners were evaluated during the HASP program. A summary of torque test results is shown in Figure 5 where C-129Y fasteners have been pre-oxidized for 15 minutes at 2000°F (1093°C). As indicated by the results, the pre-oxidation cycle had a significant effect on the life of the fastener as well as on making installation and removal much easier. The average installation time for coated columbium fasteners on the ASCEP structure was 0.7 minutes per fastener, while the average removal time was 2 minutes per fastener. These values represent the average of 8 panels containing an average of 75 fasteners per panel.

The installation and removal of HS-25 superalloy fasteners on the ASCEP structure was not successful. The average installation time was 1.8 minutes per fastener, while removal time was 2 minutes per fastener. These figures are quite misleading, because approximately 30 percent of all the fasteners galled up and had to be drilled out at considerable time and expense.

SUMMARY OF COATED C-129Y FASTENER TORQUE TESTS

MATERIAL – COATING	SAMPLE NO.	TEST NO.	APPLIED TORQUE in.-lb (m-N)	REMARKS
C-129Y – TAPCO (OXIDIZED)	1	1	110 (12), LOOSENED AT 85 (10)	MINOR COATING DAMAGE TO THREADS
	--	2	150 (17), SLIPPED AT 85 (10)	MAJOR COATING DAMAGE TO THREADS
			LOOSENED AT 80 (9)	
	--	3	150 (17)	BOLT FAILED IN SHEAR AT ROOT OF THREAD
C-129Y – TAPCO (OXIDIZED)	2	1	60 (7)	MINOR COATING DAMAGE TO THREADS
C-129Y – TAPCO (OXIDIZED)	3	1	50 (6)	MINOR COATING DAMAGE TO THREADS
C-129Y – TAPCO (NOT OXIDIZED)	4	1	50 (6)	SEVERE COATING DAMAGE TO THREADS
C-129Y – TAPCO (NOT OXIDIZED)	5	1	155 (18)	BOLT FAILED IN SHEAR AT ROOT OF THREAD REMOVED FROM ALLEN RECESS

Figure 5

T-222 FASTENERS AFTER 3000°F (1649°C) EXPOSURE

(Figure 6)

Shown in Figure 6 are the results of exposing coated tantalum fasteners to 3000°F (1649°C) for approximately 5 minutes during a tantalum panel test. As indicated, extensive oxidation of the fasteners has taken place. Under any combination of load and temperature that was experienced in these tests, the coating on both the nut and bolt threads would break down and the nut and bolt would seize together. Above 3000°F (1649°C), nothing attempted would prevent bonding of the nut to the bolt; however, below 2600°F (1427°C) no failures were experienced.

T-222 FASTENERS AFTER 3000°F (1649°C) EXPOSURE

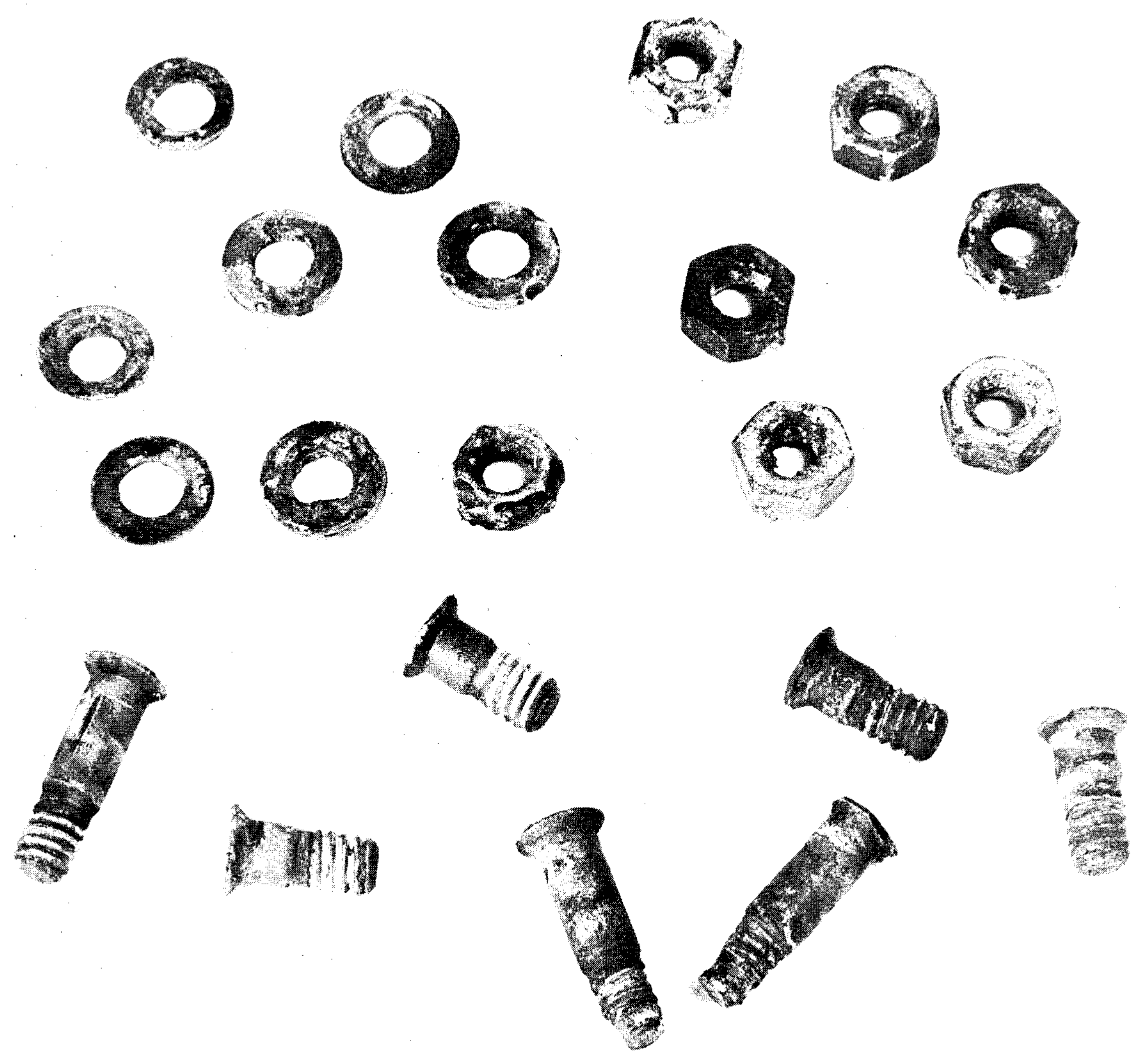

Figure 6

CONCLUSIONS

(Figure 7)

In conclusion, it can be stated that:

1. Reusable fastener technology is ready for engineering development at temperatures up to 2600°F (1427°C). Superalloy and coated columbium fasteners have been developed and ground tested. Dry film lubricant development appears needed to prevent extensive galling and seizure of superalloy fasteners.

2. Integration of the total fastener system is required; that is, compatibility of the fastener material, coating system, and structure to be fastened must be insured.

3. The total fastener environment must be evaluated before a commitment can be made. It is not enough to select a fastener based on any one property or characteristic; one must evaluate the fastener over the entire use spectrum before a given material or even a fastener configuration is selected.

CONCLUSIONS

- REUSABLE FASTENER TECHNOLOGY IS READY FOR ENGINEERING DEVELOPMENT FOR TEMPERATURES BELOW $2600^{\circ}F$ ($1427^{\circ}C$)
- INTEGRATION OF THE TOTAL FASTENER SYSTEM IS REQUIRED
- THE TOTAL FASTENER ENVIRONMENT MUST BE EVALUATED BEFORE A COMMITMENT CAN BE MADE

Figure 7

BEARINGS, LUBRICANTS, AND SEALS FOR ACTUATORS AND MECHANISMS

by Robert L. Johnson, William R. Loomis,
and Lawrence P. Ludwig
NASA Lewis Research Center, Cleveland, Ohio

ABSTRACT

Lubricated and hydraulic components for the shuttle vehicle with high temperature and vacuum operating capabilities are under investigation. A review of C-ethers as potential hydraulic fluids and lubricants indicates important advantages of increased thermal stability, high bulk modulus, high surface tension, and low vapor pressure. Good progress is reported in resolving lubricant-coolant deficiencies of the base fluid by formulation. Actuator rod seals with polyimide chevron sealing elements and molecular flow impedance are described. Problems of rotating shaft seals are discussed and the design concept is presented of spiral groove for liquids and helical groove molecular flow pumping seals for low density vapor. Vibration as well as high temperature is suggested as an airframe bearing problem. Calcium-fluoride lubricated porous metal composites and mechanical carbons are indicated to have the advantage of good damping capacity in addition to useful friction behavior.

BEARINGS, LUBRICANTS, AND SEALS FOR AUTUATORS AND MECHANISMS

by Robert L. Johnson, William R. Loomis,
and Lawrence P. Ludwig
NASA Lewis Research Center, Cleveland, Ohio

INTRODUCTION

Lubrication problems in the shuttle vehicle are very much dependent on mission and design details that remain to be defined. Critical problems for airframe bearings and hydraulic system components are associated with high temperatures as well as with exposure to vacuum. Much consideration is being given to thermal protection of the vehicle in general. Thermal protection of lubricated components and hydraulics must be achieved in critical circumstances. A reasonable concept for design of such components, however, would be to provide for them to operate at the most extreme conditions that will give an acceptable confidence level and thereby minimize the thermal protection problem.

Airframe bearings of aerodynamic control surfaces will see very high temperatures (e.g., to 1600° F or 1144 K) for relatively short periods of time, as well as high loads and severe vibration. "Acoustic vibration" of airframe bearings has severely limited the operation of one large supersonic flight vehicle so that it is well to provide damping capacity in the bearing materials or designs.

The hydraulic systems under consideration by potential contractors are basically the so-called Type II aircraft hydraulic systems. Such systems are intended to operate at <275° F (<408 K) and with no consideration for vacuum exposure or operation. There are very pertinent

considerations for both rotating shaft seals and linear actuator seals as well as hydraulic fluids that need greater attention.

The combination of operation at high temperatures in air and more nominal temperatures in vacuum imposes a complication for lubricated components not found in either aircraft or spacecraft. Fortunately, however, it appears that some of the advanced capabilities shown in recent research programs (ref. 1) of the Lewis Research Center can be adapted for requirements of the shuttle.

The objective of this paper is to present a discussion of Lewis Research Center studies and backgrounds that are pointing to solutions of potential problems in the shuttle. The present discussion will be limited to airframe bearings and hydraulic system seals and fluids and supplements reference 1.

AIRFRAME BEARINGS

Previously reported information (refs. 1 and 2) showed that CaF_2 lubricated ball bearings have been run with meaningful loads (93,000 psi or 64,000 N/cm^2 Hz) and unidirectional motion at 1200° and 1500° F (922 and 1089 K) for time periods greater than 100 hours. Airframe bearings are most commonly of the plain spherical configuration as shown in figure 1 but both ball bearings and concave roller bearings have areas of application. Because weight is a critical factor, airframe bearings are usually designed to operate at high stress levels. (See ref. 3.) Most commonly, such bearings have the inner surface of the outer race lined with 0.007- to 0.008-inch thick (0.018- to 0.020-cm) reinforced

TYPES OF SELF-ALIGNING AIRFRAME BEARINGS

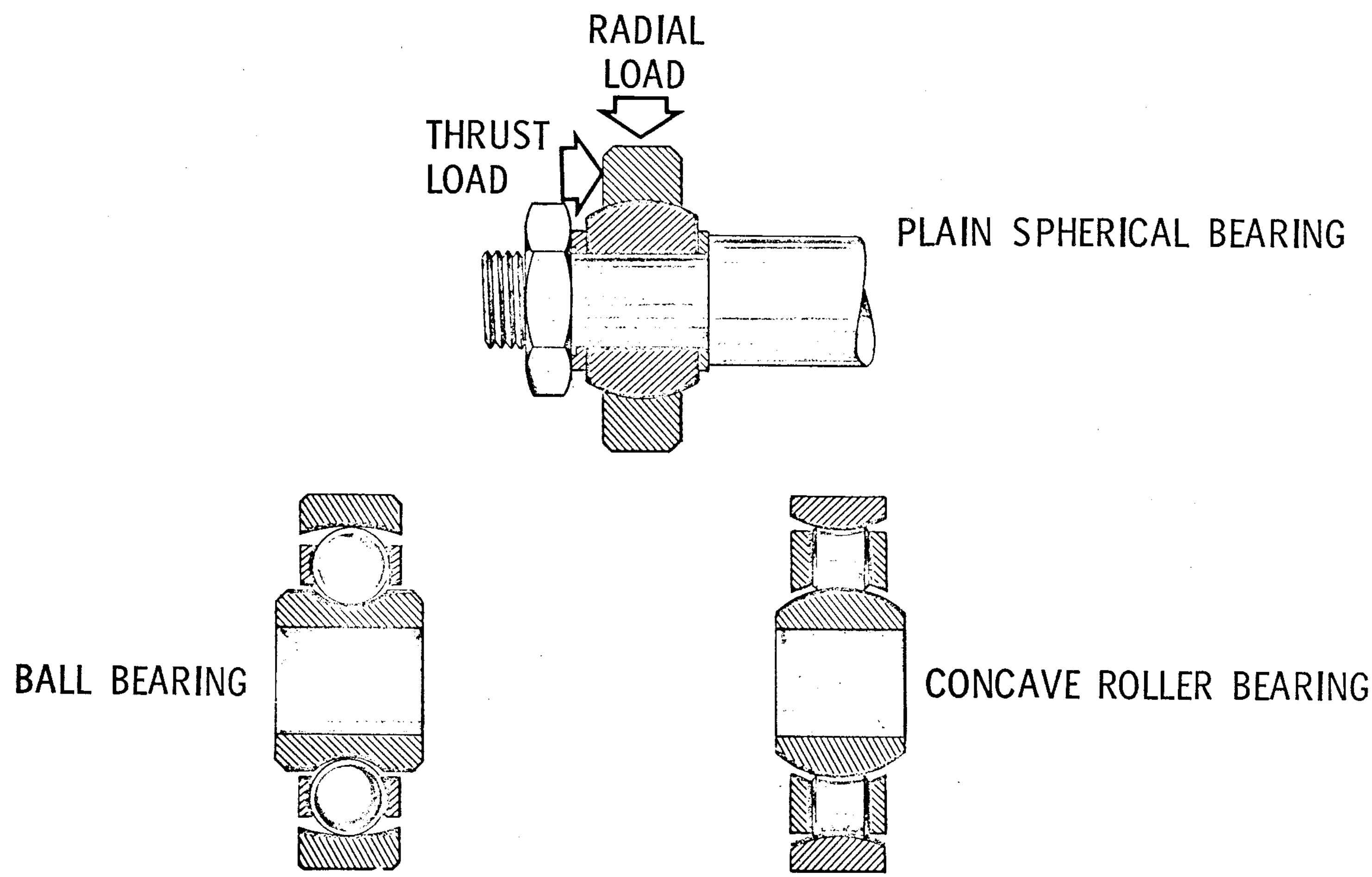

Figure 1

polytetrafluoroethylene (PTFE) fabric. The temperature limitations of PTFE will prevent its use on the shuttle. Both the Concorde and the Boeing SST use fabric-reinforced PTFE compositions for airframe bearings. In relatively short duration supersonic flights of the Concorde, at least one of the PTFE compositions has shown prohibitive deformation and wear as a result of vibration. Thus, it is important to provide damping capacity or elasticity that can minimize fretting and impact damage by vibration.

The early experience reported for CaF_2 (ref. 1) lubricated high-temperature bearings used a fused thin film of a CaF_2 plus BaF_2 eutectic on ball-bearing retainer surfaces. The lubricant transferred to other bearing parts to provide a thin lubricating film. The bearing performed well at the conditions discussed previously; but it is important to note that no vibration, oscillating motion, or variable loading was imposed.

Greases or oils provide effective damping media for bearings subject to vibration. Because of high temperature and vacuum exposure, the use of organic lubricants does not appear to be feasible. Thus, solid lubricating materials with resilience or damping ability are of greater interest. Figure 2 shows sliding friction data over a range of temperatures for the CaF_2-BaF_2 eutectic fused film. In 204-size ball bearings, that film gives friction torque of 2 to 4 inch-ounces (0.0142 to 0.0283 m-N) with a 30-pound (133 N) axial load. Additional data for two other materials offering improved damping are also presented. The sintered nickel-chromium metal composite was infiltrated with a ceramic oxidation inhibitor (NBS A418 modified) and then coated with a CaF_2-BaF_2 eutectic

FRICTION OF SOLID LUBRICATING MATERIALS IN AIR AT HIGH TEMPERATURES

NOTE: 5% OXIDATION LIMIT FOR MECHANICAL CARBONS

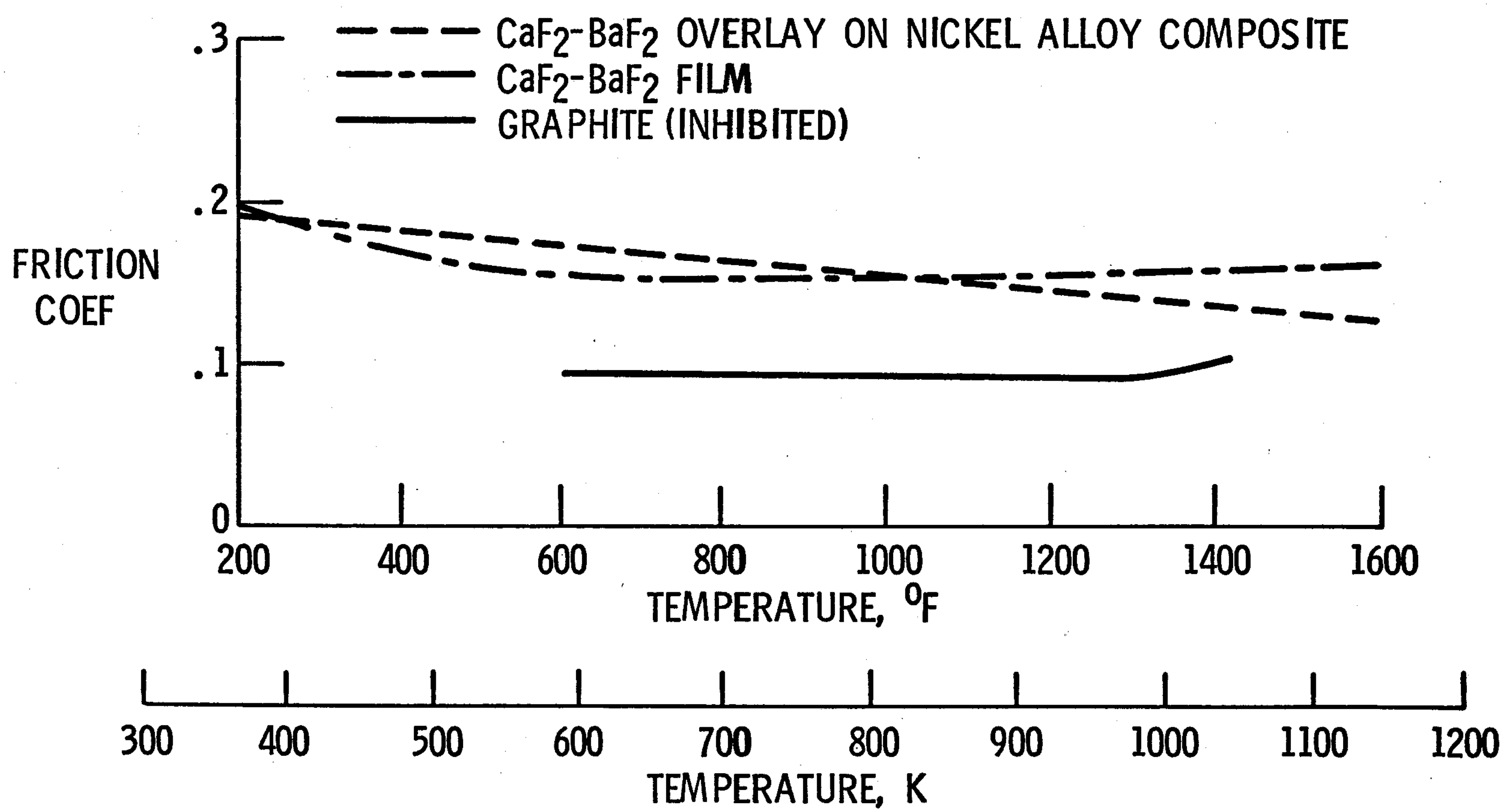

Figure 2

overlay. This composite material gave similar friction performance to the fused film lubricated surface. The composite remains somewhat porous and would offer improved damping capacity as well as extended life compared with the use of thin solid films.

Mechanical carbon-graphite materials have been very useful in both primary and secondary seals of aircraft turbines where vibration instability is common. The best of oxidation-inhibited commercial carbon materials have friction behavior similar to that in figure 2. That material has substantially lower friction than the CaF_2 lubricated surfaces. Although the carbon bodies include oxidation inhibitors, they are subject to rapid oxidation above 1200° F (922 K) and, in fact, the high temperature wear mechanism is primarily one of oxidation. Mechanical carbons are considered useful to the limit of 5-percent oxidation by weight. A shielded bearing configuration to restrict dissipation of the gaseous products of oxidation can greatly reduce the oxidation problem and may make it tolerable in view of the short times at extreme temperatures. In addition, the new materials made under NASA contract NAS 3-13497 for seals have one-tenth the oxidation rate of commercial materials at 1300° F (978 K). (See ref. 4.) It is also anticipated that carbon fiber or cloth-reinforced bodies such as those developed for brakes can be useful compositions.

SEALS

Dynamic seals for the vehicle structure are mostly associated with the hydraulic system. The use of linear and rotating seals with local extreme temperatures and exposure to vacuum must be anticipated.

Actuator Seals

A significant background of work on dynamic seals for advanced aircraft such as the SST has led to the use of materials and configurations (e.g., PTFE foot seal) for actuator seals that are limited to about 400° F (478 K). The metallic seals used in the B-70 had high temperature capability and worked under laboratory conditions but may be inadequate for operational use; matched surfaces are required and tolerance to misalinement, wear, and contamination are questionable.

A more appealing approach to the high-temperature actuator seal problem is the use of advanced polymers such as polyimides in chevron configurations with needed sealing force provided by pressure and metal springs. (See fig. 3.) Such seals have been successful under severe duty cycles to 500° F (533 K). (See ref. 5.) Lubrication studies in vacuum (ref. 6) show polyimides to have excellent self-lubricating properties and have no measurable deterioration in vacuum until temperatures of about 700° F (644 K) are reached.

Vacuum exposure is the primary difference between experience to date with the actuator seal design and shuttle requirements. The sealing mechanism varies with change in state from the viscous liquid continuum to transition (slip) and finally molecular flow. Vaporization of residual liquid adhering on actuator rods exposed to vacuum can accelerate leakage. Thus, vapor pressure and surface energies of the fluid are important. Fortunately, design provisions to impede molecular flow can be relatively simple. The Knudsen number λ/L which controls the flow regimes can be altered. That can be done by varying a characteristic flow-field dimension L such as the annular clearance and length of the leakage path. The main free path λ which varies with pressure is a function

ACTUATOR ROD SEAL

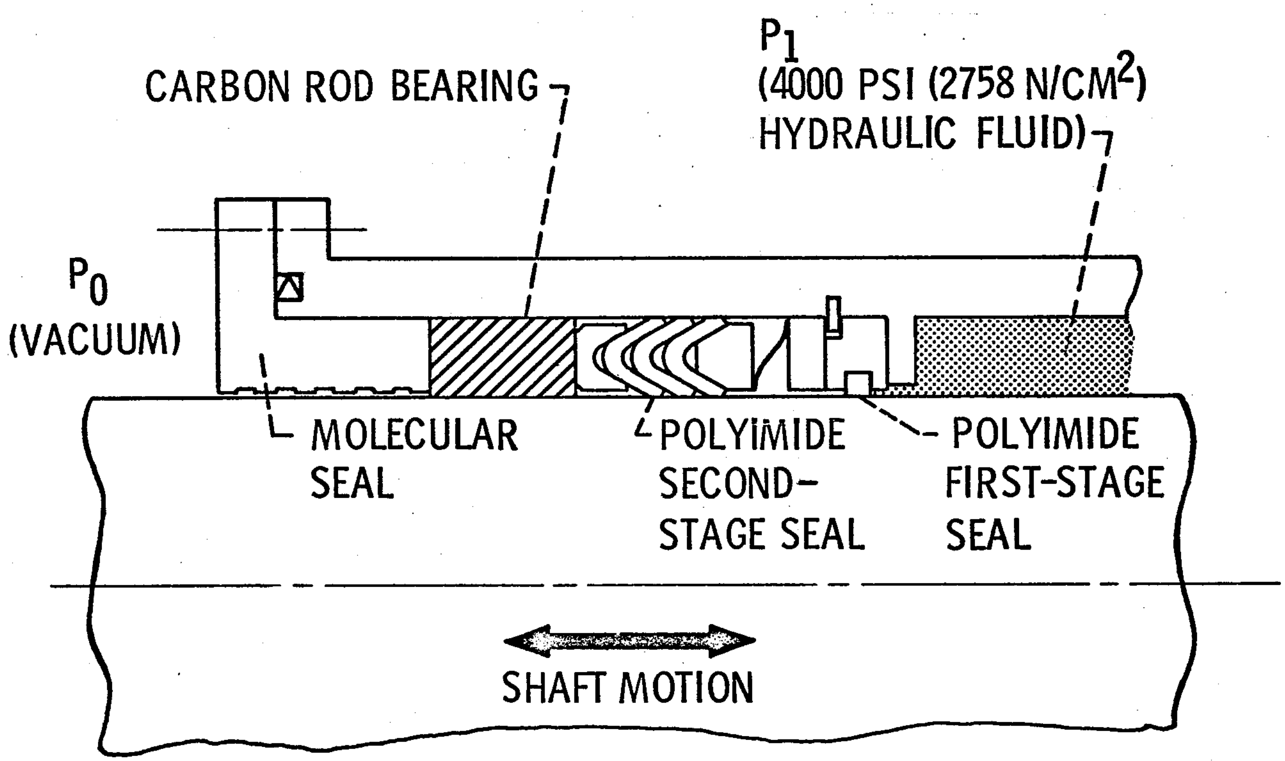

Figure 3

of the material. The geometries of the boundary surfaces can also be important to the molecular collision process for impeding leakage flow.

An experimental measurement of weight loss for the ester di (2-ethylhexyl) silicate (Octoil S) from a simulated bearing cavity including a stationary walled housing annulus has been reported with reference to the Helios antenna despin mechanism (ref. 7). It was found that the oil loss rates were much greater than those calculated by theory for free molecular flow. Further, it was indicated the loss rate result was greatly influenced by surface migration phenomena. Surface migration is dependent on surface energy relationships and suggests that higher surface tension of the fluid would deter loss. Further lower vapor pressure of the fluid would have been advantageous both in establishing a less critical flow regime through the annulus and in reducing the fluid vaporization of the surface migrated fluid. Factors important to evaporation loss are summarized in reference 8.

The design considerations to restrict molecular leakage to vacuum are shown in figure 3 to be rather simple changes for the polyimide chevron seal assembly that continues to be studied. The external guide bushing also serves a sealing function. In atmosphere the useful temperature for the seal material can be from -400° to 600° F (33 to 589 K) for extended operation and higher (e.g., 900° F or 755 K) for short periods. In simulated aircraft flight cycle experiments at 500° F (533 K) sealing a 4000 psi (2760 N/cm^2) silicone fluid from atmosphere, the leakage rate for over 1000 hours of operation was <0.02 cc per hour (ref. 5).

Rotating Shaft Seals

Aircraft hydraulic motors for severe service are usually equipped with face-type seals as shown in figure 4. Laboratory visual studies at Lewis and by others (ref. 9) show that sealed fluid-film vaporization occurs in the sealing interface so that only part of that surface is wet by liquid and the leakage is vapor with various liquids reaching their characteristic boiling points at the interface. The boundary between the liquid and vapor phases is stable but moves with changed operating conditions (e.g., speed or pressure). The presence of two phases and the liquid at its boiling point provides a sufficiently high pressure regime for viscous or transition (slip) flow of the vapor. The relatively rapid leakage through the seal to vacuum would be further accelerated by surface migration and subsequent evaporation.

Figure 5 shows a conventional rotating shaft face seal assembly as used on hydraulic motors in aircraft but not originally intended for exposure to vacuum. This type of seal would have the two-phase interface film described in both atmosphere and vacuum. An improved seal design for vacuum is suggested in figure 6. This design utilizes a spiral groove radially outward pumping face seal with interface liquid feed to remove heat generated in shear of the thin (100 to 200 microinch or 2.5 to 5.1 μm) film. Further, a helical groove molecular flow vapor seal with low surface energy barrier films is provided to contain leakage past the spiral groove liquid seal. The barrier film should not be wet by the sealed liquid.

LUBRICATION MECHANISM FOR CONVENTIONAL SEALS

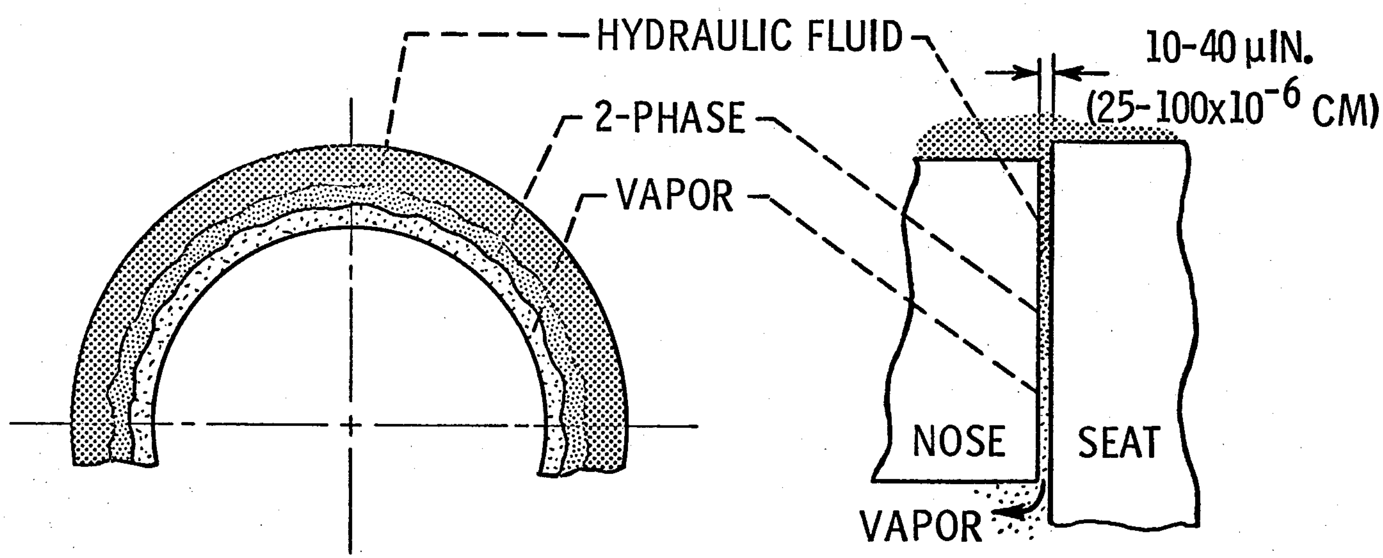

Figure 4

CONVENTIONAL ROTATING SHAFT FACE SEAL

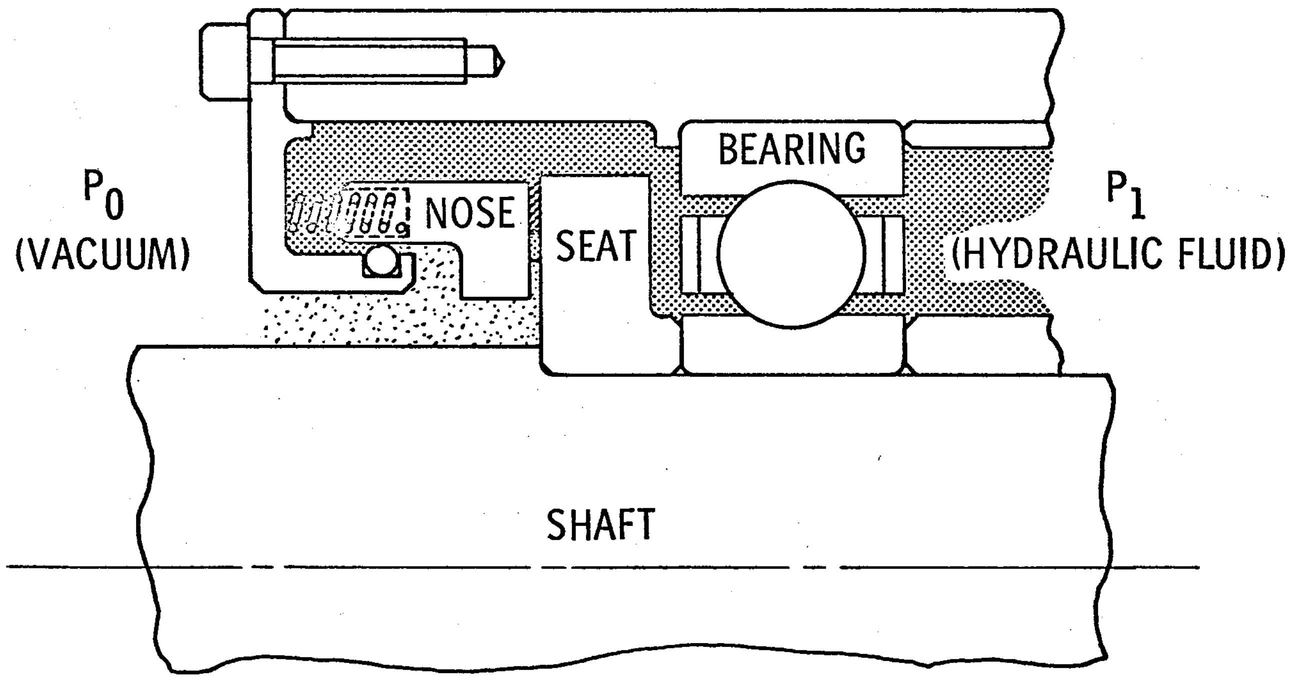

Figure 5

SPIRAL PUMPING

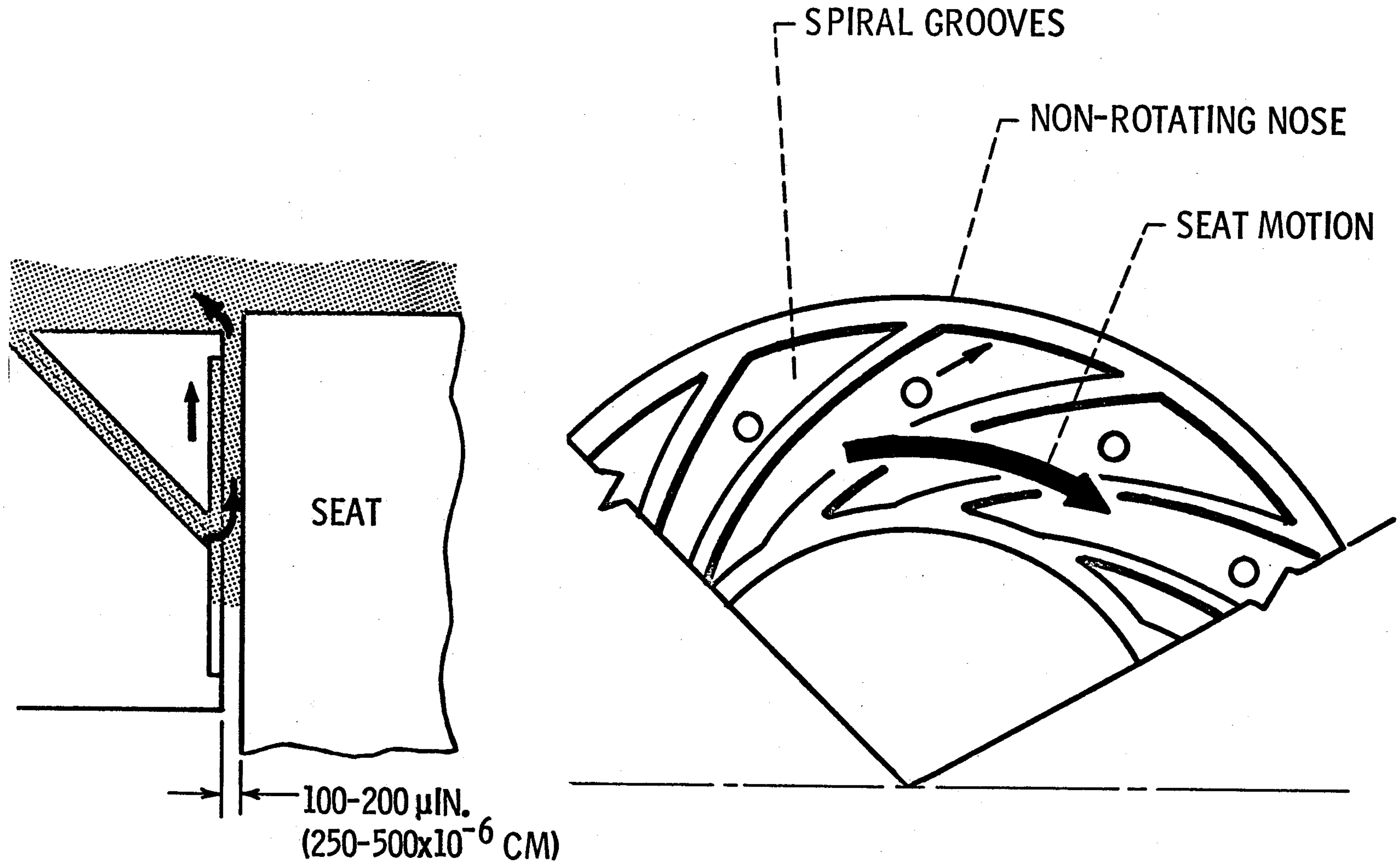

Figure 6(a)

ROTATING SHAFT SEAL TO VACUUM

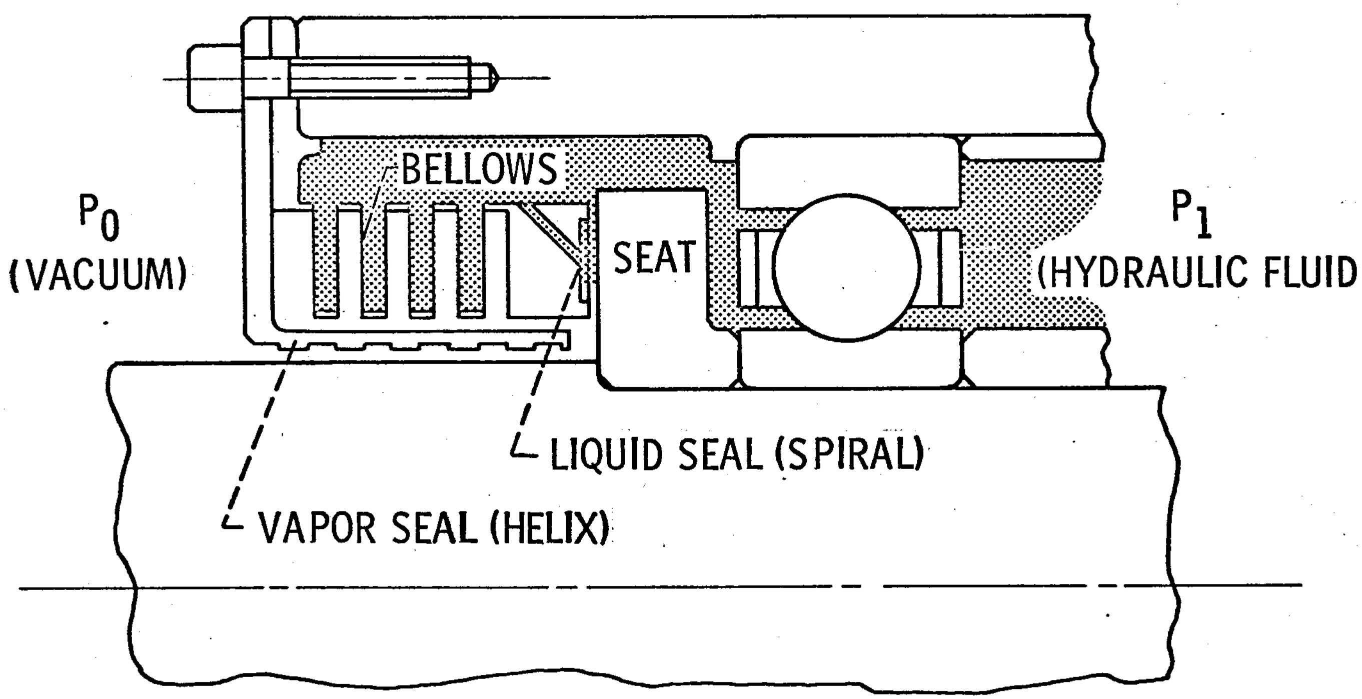

Figure 6(b)

These sealing concepts to vacuum have been explored in studies for space power-generating systems. The spiral groove concept was used to provide a no-leakage seal for liquid sodium and oil (ref. 10) and has been incorporated in recent experimental mainshaft seals for aircraft. Studies of a rotating helical molecular flow seal combined with a visco seal for organic fluids (4P3E polyphenyl ether) at modest pressures gave leakage rates to vacuum (10^{-7} torr) of 0.7 to 2.6 kilograms in 10 000 hours (ref. 11). That seal also had low-surface-energy films of PTFE in the molecular flow section to eliminate liquid migration. Several of these concepts were combined to provide the suggested advanced space power system seal reported in reference 12. Consideration of the design requirements for the space shuttle suggested that the seal concepts of figure 6(b) should be applicable to hydraulic motors capable of operating in air or vacuum.

HYDRAULIC FLUIDS

The preceding discussion has mentioned several properties of fluids that can reduce the seal problems of hydraulic systems that must operate in vacuum as well as in air. In particular, surface tension should be high and vapor pressure low for the liquid. Figure 7 is a table showing those and several additional properties (important to hydraulic systems) for four fluids. The fluids identified as MIL-H-5606 (petroleum) and M2-V (disiloxane) are considered as phase B fluids by present shuttle contractors. The so-called SST ester is the advanced polyol ester fluid currently planned for the Boeing supersonic transport. Also listed is a C-ether (modified polyphenyl ether) that we are currently working with

PROPERTIES OF POTENTIAL HYDRAULIC FLUIDS

		MIL-H-5606	M2-V	SST ESTER	C-ETHER
FLUIDITY	VIS, CS (OR 10^{-6} m^2/SEC)				
	AT 210^0 F (372 K)	5.2	5.4	4.3	4.2
	AT 400^0 F (478 K)	2.0	1.6	1.4	1.1
	POUR PT, ^{0}F (K)	-75 (214)	-110 (194)	-75 (214)	-20 (244)
VAPOR PRESSURE, mmHg					
AT 400^0 F (478 K)		220	0.6	145	0.3
AT 600^0 F (589 K)		---------	70	323	30
SURFACE TENSION, DYNE/cm (OR 10^{-5} N/cm) AT 75^0 F (297 K)		30	27	30	50
ISOTHERM SECANT BULK MODULUS AT 4000 PSI, PSI (N/cm^2)					
AT 100^0 F (311 K)		212 000 (146 000)	195 000 (134 000)	296 000 (202 000)	340 000 (234 000)
AT 350^0 F (450 K)		106 000 (73 000)	100 000 (69 000)	156 000 (107 000)	235 000 (162 000)
FIRE RESIST; A. I. T., ^{0}F (K)		470 (516)	760 (678)	755 (675)	940 (778)
THERMAL STAB, ^{0}F (K)		550 (561)	610 (594)	660 (622)	740 (666)

Figure 7

to improve its already substantial credentials as a hydraulic fluid and air-breathing engine lubricant for the space shuttle. The only inadequacy of C-ethers shown by this tabulation is that of pour point; pour point requirements for the shuttle are not clear.

Figure 8 shows that the pour point can be substantially reduced by utilizing the lower molecular weight less viscous polymers of the same chemical structure. As shown, the primary penalty of using the less viscous polymer is that of increased vapor pressure. Even the least viscous fluid has vapor pressure no greater than the present shuttle hydraulic fluid candidates. There is technology for achieving reduced pour points including blending varied isomers, changing molecular weight distributions and additive effects. Such approaches have not yet been fully explored. Also, as already practiced for both high- and low-temperature systems, a constantly circulating fluid system can avoid thermal problems of the operating environment. A clear definition of the low-temperature requirements on the shuttle hydraulic system is, however, needed.

Figure 9 indicates the effects of temperature on vapor pressure for the original fluids described. Also, the high temperature terminal point for these curves is the limit of thermal stability shown by isoteniscope data. The C-ether offers substantial improvement over the other fluids in figure 9.

One of the more critical uses of hydraulics for the shuttle will be the flight-control system. The physical size of the system, its response characteristics and stability are directly dependent on the bulk modulus

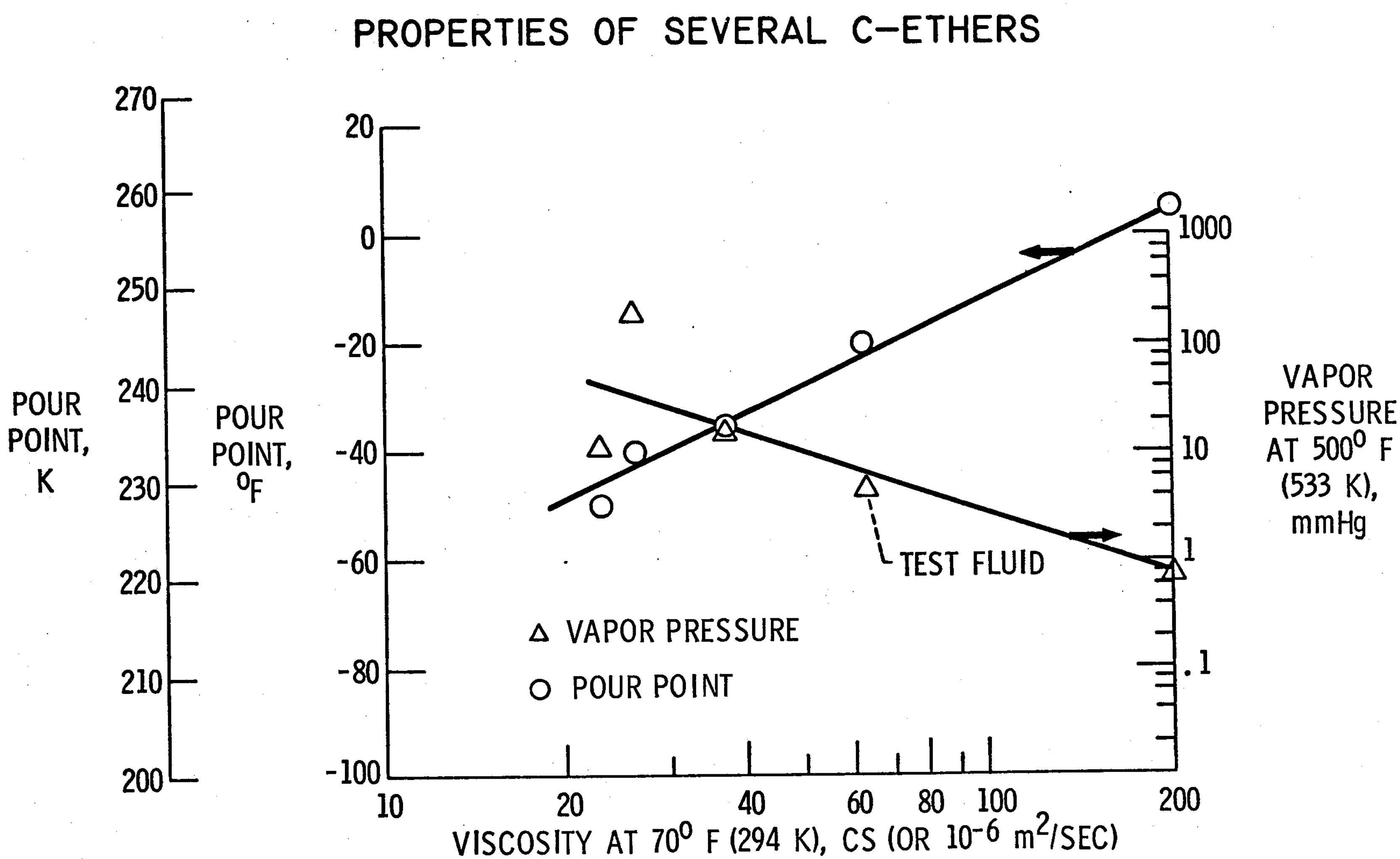
PROPERTIES OF SEVERAL C–ETHERS
POUR POINT, K
270
260
250
240
230
220
210
200
POUR POINT, °F
20
0
-20
-40
-60
-80
-100
VAPOR PRESSURE AT 500° F (533 K), mmHg
1000
100
10
1
.1
TEST FLUID
Δ VAPOR PRESSURE
○ POUR POINT
10
20
40
60
80
100
200
VISCOSITY AT 70° F (294 K), CS (OR 10⁻⁶ m²/SEC)

Figure 8

VAPOR PRESSURE OF HYDRAULIC FLUIDS

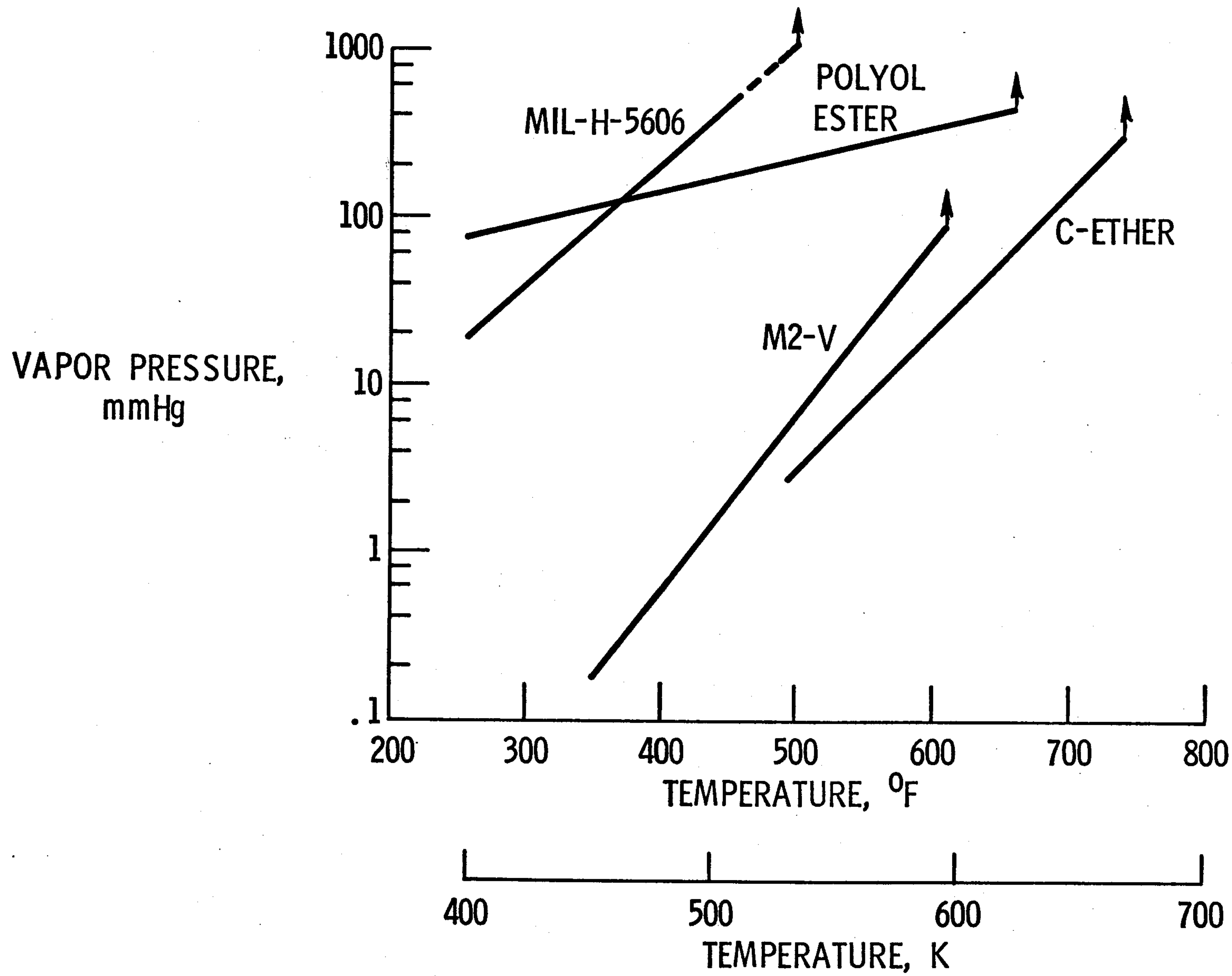

Figure 9

(compressibility) of the hydraulic fluid. Actuation system response is especially critical for supersonic flight and for large systems. Figure 10 shows the isothermal secant bulk modulus data given at 4000 psi (2760 N/cm^2) as a function of temperature for the fluids previously described. Included on this figure is the requirement for the SST (converted from adiabatic values) that has been very carefully developed by Boeing. While no similar criterion has been suggested for the shuttle, the requirements are not likely to be less stringent than for the SST; both 5606 and M2-V may be inadequate. The high bulk modulus that is characteristic of aromatic compounds makes the C-ethers very attractive for the shuttle hydraulic system.

The C-ethers are not a new class of fluids but have been subject to both cursory and detailed investigation by several organizations. Initial concern was for their lubricating ability since this is an apparent inadequacy of conventional polyphenyl ethers. The C-ethers and polyphenyl ethers are closely related. Modest changes in chemistry have, however, given the C-ethers some improved lubricating ability and low-temperature fluidity at the expense of a reduction in thermal stability. Reference 13 is a synopsis of much of the early data obtained by the manufacturer. The world's major engine builders including Pratt and Whitney Aircraft (ref. 14), General Electric Company, Rolls Royce Limited (ref. 15) and SNECMA* have performed limited work with C-ethers and the problems observed can most likely be resolved. Certainly, an engine can be designed to run well with this fluid.

---

*Société Nationale d'Étude Engine et de Construction de Moteurs d'Aviation

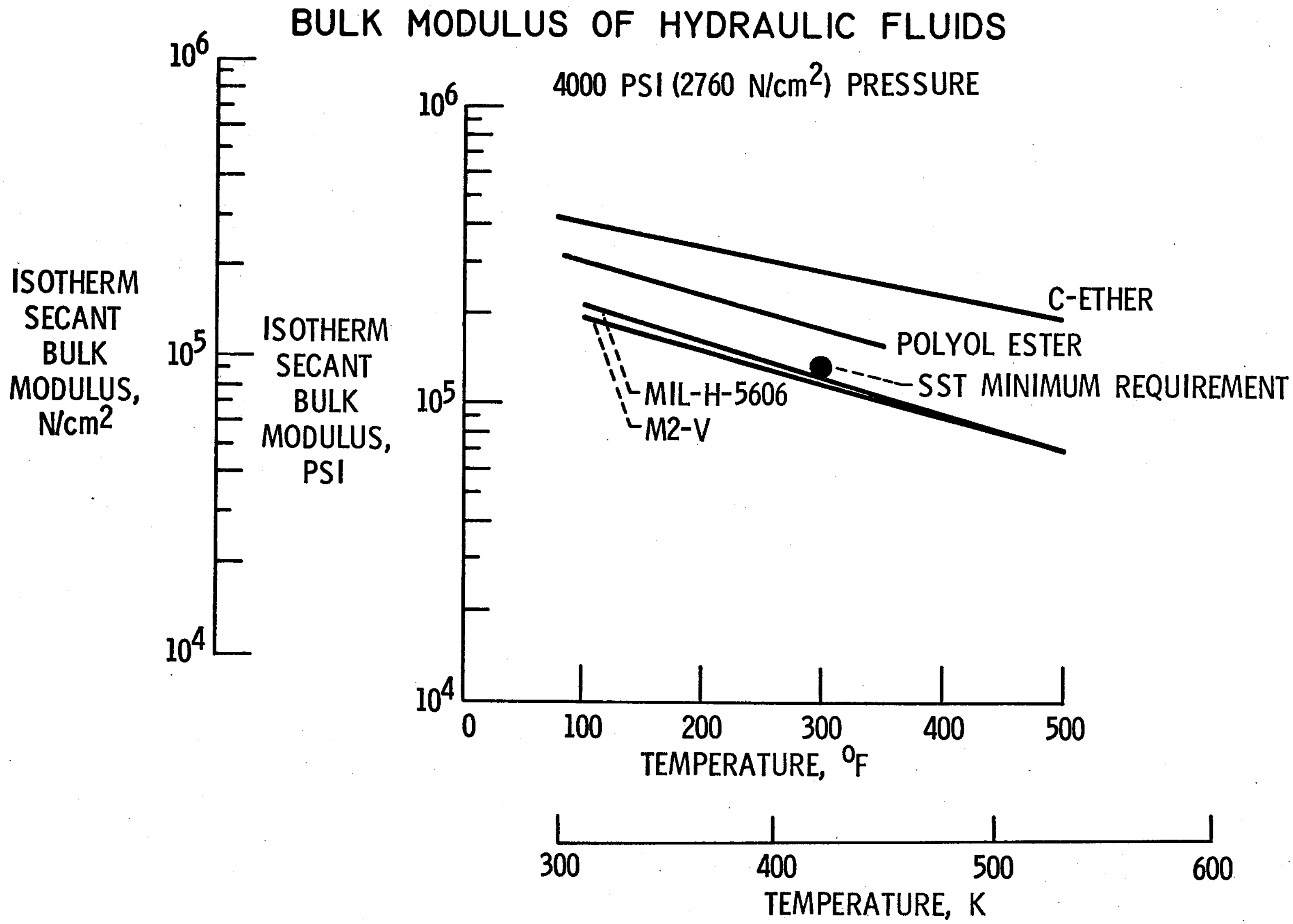

BULK MODULUS OF HYDRAULIC FLUIDS
4000 PSI (2760 N/cm2) PRESSURE
ISOTHERM SECANT BULK MODULUS, N/cm2
ISOTHERM SECANT BULK MODULUS, PSI
10^6
10^5
10^4
C-ETHER
POLYOL ESTER
SST MINIMUM REQUIREMENT
MIL-H-5606
M2-V
0
100
200
300
400
500
TEMPERATURE, °F
300
400
500
600
TEMPERATURE, K

Figure 10

Reference 14 suggests that the C-ethers will provide at least as good bearing life as the best advanced esters. It is significant that the bearing life comparison testing was done with the C-ether lubricant at 50° F (28 K) higher temperature than the esters. The higher temperature would result in the C-ether functioning at much lower viscosity levels than the esters at the respective test conditions and makes the favorable bearing life data especially noteworthy. Reference 16 also indicates that the thin film (boundary) lubrication performance of the C-ethers does not deteriorate with higher temperatures as is usually found for organic lubricants. It is suggested that a very thin film of a high molecular weight analog of the C-ether fluid (e.g., friction polymer) forms on the wetted metal surfaces of the lubricated parts. The presence of similarly developed films has been identified for other fluids by several investigators.

The C-ether fluid has been used for several full-scale engine tests as well as in numerous bench studies, bearing tests, and hydraulic pump systems. Except for the bearing endurance runs of reference 14, the experience has been of short duration. <u>Apparent</u> lubrication failures have occurred that had a common pattern.

Following successful short-time full-scale engine operation, Pratt and Whitney Aircraft twice found wear and scoring in aluminum bearings run with a steel shaft of a gear-type lubricant scavenge pump. An example of such failure as duplicated in laboratory tests is shown in figure 11. In an earlier engine run, no problem had been encountered and it was found the gear box scavenge pump was a different model with lower bearing loads and more massive housings.

SCAVENGE PUMP PARTS FROM JT3D-3B ENGINE RUN WITH C-ETHER BASE FLUID

CHROME ANODIZED ALUMINUM JOURNALS

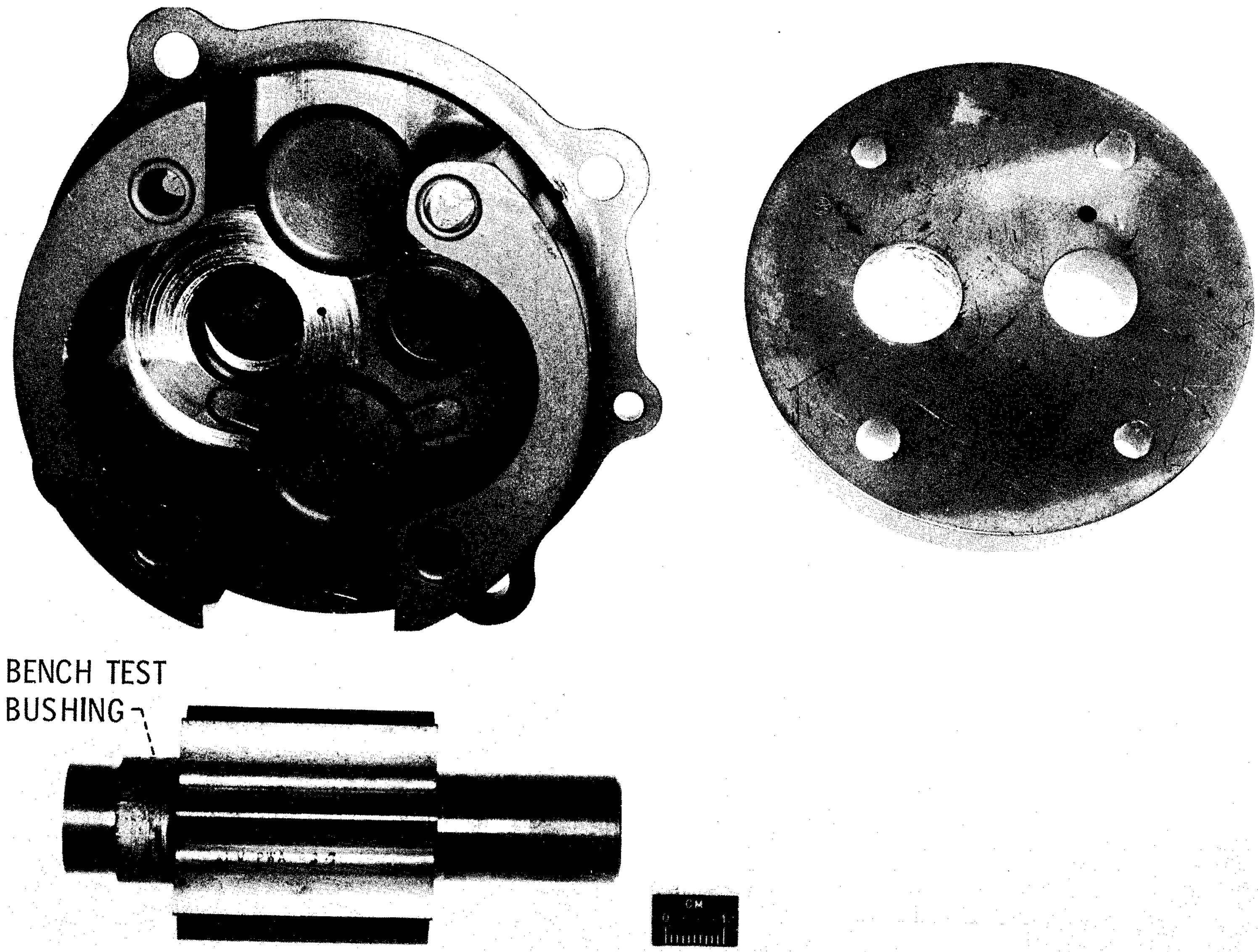

Figure 11

Vane pump operation with M-50 steel vanes and housings (ref. 17) gave higher wear with the C-ether and conventional polyphenyl ethers than with mineral oils. Piston-pump operation of the C-ether in a simple hydraulic loop (ref. 16) resulted in surface smearing of the S-Monel thrust bearings on the M-2 tool steel swash plate. Experience with both 25-mm and 125-mm ball bearings under severe temperature conditions (refs. 18 and 19) indicated inadequacies. These varied experiences of unsatisfactory operation had a common pattern: (1) There were frequently problems in achieving temperature stability for bearing parts during operation and (2) Following operation, the surfaces showed wear and smearing of the surface metal.

Lubricants for most mechanisms must serve the dual role of acting as both a lubricant and a coolant. Enough of the early data showed C-ethers to be good lubricants under a variety of conditions that it was clear the coolant function of the fluid needed consideration in evaluating the failures that had occurred.

Examination of pump and bearing parts from the varied experimental operations described showed a significant common characteristic. The test fluid would not spread (wet) on the surfaces of the used parts. If it is assumed that these surfaces have a film of a high molecular weight analog of the base fluid, the lack of wetting can be explained. Aromatic compounds show a decrease in surface tension with increased molecular weight (ref. 20). Consequently, the higher surface tension liquid is unable to spread on the lower surface tension film covering the metal part. The vapor phase occupies much of the volume in the lubricant

immediately following concentrated contacts like a ball on a bearing race. When the vapor phase is a substantial part of the volume, good wetting of the lubricant is needed to provide a continuous coolant film. If wetting is inadequate, cooling may be ineffective and there is potential for temperature increases and instability.

Based on the premise that inadequate cooling by the C-ether was the reason for the several apparent lubrication failures, formulation to improve wetting was recommended to the fluid manufacturer. The concepts of reference 20 were suggested for guidance. A formulation was made available for evaluation that had improved wetting. It is also likely, however, that the fractional percentage of additive could have other surface chemical effects in addition to improved wetting.

The results from this modest formulation effort by the fluid manufacturer were very encouraging. The formulation completed a 100-hour run with two of six 25-mm ball bearings operating at 600° F (589 K) and 44 000 rpm (ref. 21) and the other four bearings were run at least 40 hours. Earlier operation of the C-ether base fluid resulted in failures in a few minutes. The formulation also provided satisfactory performance in bench tests of the engine gear box scavenge pump described earlier. Figure 12 is a photograph of the originally described pump housing with a distressed bearing and a similar housing of a pump showing appearance after operation with the C-ether containing additives that improve wetting. The bearing surfaces of the second housing show no distress.

Another observation for the C-ethers, but more common to conventional polyphenyl ethers, is the formation of sludge that can plug fine filters.

SCAVENGE PUMP HOUSINGS FROM JT3D-3B ENGINES AFTER RUNS WITH C-ETHER

CHROME ANODIZED ALUMINUM JOURNALS

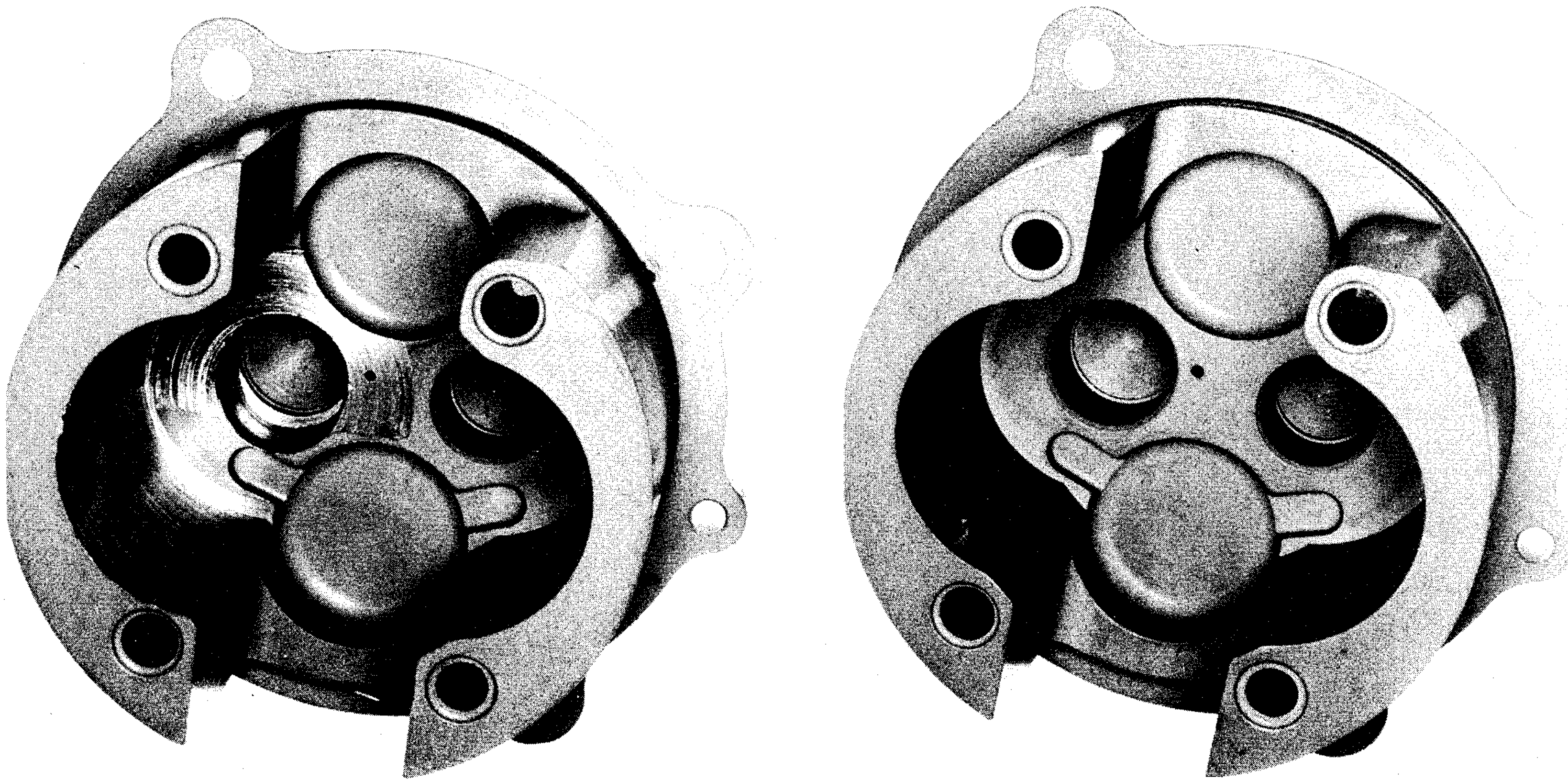

BASE FLUID

FLUID WITH ADDITIVE

Figure 12

Such deposits have been shown to contain high metallic content and are most likely from wear debris that is not expected with the formulated C-ethers.

The C-ethers have promise as hydraulic fluids (and air-breathing engine lubricants) for the shuttle vehicle. Initial results in compensating for deficiencies have been successful. A contract program of further formulation and evaluation studies with Monsanto is proceeding.

CONCLUDING REMARKS

Lubrication programs at the Lewis Research Center and by contractors for aeronautics and space-power systems provide design information applicable to the shuttle. Allowing such lubricated components as airframe bearings and hydraulic devices to operate at increased temperature levels and with capability for direct exposure to vacuum can significantly reduce thermal protection problems.

C-ethers are important candidates to replace presently proposed hydraulic fluids and allow higher temperature operation. Greater thermal stability, bulk modulus, surface tension and fire resistance as well as reduced vapor pressure are real advantages. Low-temperature fluidity and questionable lubricant-coolant performance are problem areas for which reasonable solutions are anticipated from present programs.

Hydraulic system seal designs for linear and rotating actuators with capability for the vacuum problem are suggested but remain to be evaluated. Surface-tension and vapor-pressure properties of the hydraulic fluid are important to the sealing problem.

Airframe bearings lubricated with CaF_2 base eutectic solid materials in metal composites should be effective to >1600° F (1144 K). Oxidation inhibited mechanical carbons may have promise of lower friction. Metal composites and mechanical carbons have damping ability considered to be advantageous for vibration problems of high-speed flight.

REFERENCES

1. Sliney, H.E.: Bearings, Lubricants, Seals for The Space Shuttle. Vol. III, pp. 289-296, Proceedings Space Transportation System Technology Symposium, NASA-Lewis Research Center, Cleveland, Ohio July 15-17, 1970, NASA TM X-52876.
2. Sliney, H.E. and Johnson, R.L.: Preliminary Evaluation of Greases to 600° F and Solid Lubricants to 1500° F in Ball Bearings. ASLE Trans., Jan. 1969.
3. Craig, W.D., Jr.: Predicting Spherical Bearing Life in Airplane Control Systems. Lubrication Engineering, Jan. 1962, pp. 25-29.
4. Fechter, N.J. and Petrunich, P.S.: Development of Seal Ring Carbon-Graphite Materials. NASA Contract NAS3-13211, Union Carbide Corp., NASA CR-72799, 1971.
5. Loomis, W.R., Johnson, R.L. and Lee, J.: High-Temperature Polyimide Hydraulic Actuator Rod Seals for Advanced Aircraft. NASA TM X-52889. Paper presented to Society of Automotive Engineers, Los Angeles, California, Oct. 5-8, 1970.
6. Buckley, D.H.: Friction and Wear Characteristics of Polyimide and Filled Polyimide Compositions in Vacuum (10^{-10} mm Hg). NASA TN D-3261, 1966.
7. Wilkens, W.: Contamination Threats by Oil Lubricated Ball Bearings in Spacecrafts. Deutsche Forschungs-Und Versuchsanstalt für Luft-Und Raumfahrt (DFVLR) Institut F, Bericht FC 7001, Nov. 1970.

8. Johnson, R.L. and Buckley, D.H.: Lubrication and Wear Fundamentals for High Vacuum Applications. Proceedings Institution of Mechanical Engineers, 1967-68, vol. 182, pt. 3A, pp. 479-490.

9. Orcut, F.K.: An Investigation of the Operation and Failure of Mechanical Face Seals. The Fourth International Conference on Fluid Sealing. Preprint no. 22, ASLE, 838 Busse Highway, Park Ridge, Illinois 60068.

10. Strom, T.N.; Ludwig, L.P.; Allen, G.P. and Johnson, R.L.: Spiral Groove Face Seal Concepts: Comparison to Conventional Face Contact Seals in Sealing Liquid Sodium (400 to 1000° F). ASME Trans., Jl. of Lub. Tech., ser. F, vol. 90, no. 2, April 1968, pp. 450-462.

11. Hudelson, J.C. and Ludwig, L.P.: Screw-Seal Performance in Vacuum Environment. NASA TN D-3842, Feb. 1967.

12. Orsino, A.J.; Findlay, J. and Sneck, H.J.: Spiral Groove Face Seal Development for SNAP-8, NASA Contract NAS3-11824, Final Report. General Electric Research Development Center, Schenectady, New York, CR-72826, 1971.

13. McHugh, Kenneth L. and Stark, Louis, R.: Properties of a New Class of Polyaromatics for Use as High-Temperature Lubricants and Functional Fluids. ASLE Trans., vol. 9, no. 1, Jan. 1966, pp. 13-23.

14. Miner, John R.: Advanced Lubricating Fluids for Turbojet Engines. Paper presented at 1970 Air Force Materials Symposium, Session on Fluids and Lubricants, May 19, 1970, Miami Beach, Florida.

15. Edge, R.G. and Squires, A.T.B.D.: Lubricant Evaluation and Systems Design for Aircraft Gas Turbine Engines. SAE paper 69D424, presented at National Air Transportation Meeting, New York, N.Y., April 21-24, 1969.

16. Damasco, F.: Evaluation of Hydraulic Fluids for Use in Advanced Supersonic Aircraft. Contract NAS3-7263, Republic Aviation Div., Fairchild Hiller, NASA CR-72372, Nov. 1967.

17. Jones, W.R., Jr.; Hady, W.F. and Swikert, M.A.: Lubrication with Some Polyphenyl Ethers and Superrefined Mineral Oils in a 600° F (316 C) Inerted Vane Pump Loop. NASA TN D-5096, March 1969.

18. Wachendorfer, C.J. and Sibley, L.B.: Bearing-Lubricant Endurance Characteristics at High Speeds and High Temperatures. Contract NASw-492, SKF Industries, Inc., NASA CR-74097, 1965.

19. Rhoads, W.L. and Sibley, L.B.: Supersonic Transport Lubrication System Investigation. Contract NAS3-6267, SKF Industries, Inc., NASA CR-54662, Sept. 18, 1967.

20. Bascom, W.D.; Cottinton, R.L. and Singleterry, C.R.: Dynamic Surface Phenomena in the Spontaneous Spreading of Oils on Solids. Contact Angle, Wettability andAdhesion Advances in Chemistry Series, no. 43, pp. 355-379, American Chemical Society, Washington, D.C. 1964.

21. Peacock, L.A. and Rhoads, W.L.: High-Temperature Lubricant Screening Tests. Final Report contract NAS3-11171, SKF Industries, Inc., NASA CR-72615, Sept. 26, 1969.

NASA-Langley, 1971 — 17 L-7738

NATIONAL AERONAUTICS AND SPACE ADMINISTRATION
WASHINGTON, D. C. 20546

OFFICIAL BUSINESS
PENALTY FOR PRIVATE USE $300

FIRST CLASS MAIL

POSTAGE AND FEES PAID
NATIONAL AERONAUTICS A
SPACE ADMINISTRATION

National Aeronautics and Space Administration
WASHINGTON, D. C. 20546

OFFICIAL BUSINESS

Penalty For Private Use, $300.00

POSTAGE AND FEES PAID
NATIONAL AERONAUTICS AND
SPACE ADMINISTRATION

03C 001 42 50 3DS 71118 00942
PICATINNY ARSENAL
PLASTICS TECHNICAL EVALUATION CENTER
DOVER, NEW JERSEY 07801

ATT SMUPA-VP3

POSTMASTER: If Undeliverable (Section 1
Postal Manual) Do Not Ret

hall be conducted so as to contribute ... to the expansion of ... knowledge of phenomena in the atmosphere and space. The Administration shall provide for the widest practicable and appropriate dissemination of information concerning its activities and the results thereof."

—NATIONAL AERONAUTICS AND SPACE ACT OF 1958

NASA SCIENTIFIC AND TECHNICAL PUBLICATIONS

TECHNICAL REPORTS: Scientific and technical information considered important, complete, and a lasting contribution to existing knowledge.

TECHNICAL NOTES: Information less broad in scope but nevertheless of importance as a contribution to existing knowledge.

TECHNICAL MEMORANDUMS: Information receiving limited distribution because of preliminary data, security classification, or other reasons.

CONTRACTOR REPORTS: Scientific and technical information generated under a NASA contract or grant and considered an important contribution to existing knowledge.

TECHNICAL TRANSLATIONS: Information published in a foreign language considered to merit NASA distribution in English.

SPECIAL PUBLICATIONS: Information derived from or of value to NASA activities. Publications include conference proceedings, monographs, data compilations, handbooks, sourcebooks, and special bibliographies.

TECHNOLOGY UTILIZATION PUBLICATIONS: Information on technology used by NASA that may be of particular interest in commercial and other non-aerospace applications. Publications include Tech Briefs, Technology Utilization Reports and Technology Surveys.

Details on the availability of these publications may be obtained from:

SCIENTIFIC AND TECHNICAL INFORMATION OFFICE

NATIONAL AERONAUTICS AND SPACE ADMINISTRATION

Washington, D.C. 20546